27
5/19/77
25 to NTIS

ORNL/TM-5715

Precision Rectifier Detectors for AC Resistance Bridge Measurements with Application to Temperature Control Systems for Irradiation Creep Experiments

Michael Gary Duncan

MASTER

MASTER

OAK RIDGE NATIONAL LABORATORY
OPERATED BY UNION CARBIDE CORPORATION FOR THE ENERGY RESEARCH AND DEVELOPMENT ADMINISTRATION

Printed in the United States of America. Available from
National Technical Information Service
U.S. Department of Commerce
5285 Port Royal Road, Springfield, Virginia 22161
Price: Printed Copy $10.50; Microfiche $3.00

ORNL/TM-5715

Contract No. W-7405-eng-26

METALS AND CERAMICS DIVISION

PRECISION RECTIFIER DETECTORS FOR AC RESISTANCE BRIDGE MEASUREMENTS WITH APPLICATION TO TEMPERATURE CONTROL SYSTEMS FOR IRRADIATION CREEP EXPERIMENTS

Michael Gary Duncan

A thesis presented to the faculty of the graduate school of the University of Tennessee in partial fulfillment of the requirements for the degree of Doctor of Philosophy.

Date Published: May 1977

OAK RIDGE NATIONAL LABORATORY
Oak Ridge, Tennessee 37830
operated by
UNION CARBIDE CORPORATION
for the
ENERGY RESEARCH AND DEVELOPMENT ADMINISTRATION

THIS PAGE

WAS INTENTIONALLY

LEFT BLANK

ACKNOWLEDGMENTS

Financial support for this study was provided by the Energy Research and Development Agency through the Metals and Ceramics Division of the Oak Ridge National Laboratory operated by the Union Carbide Corporation and through contract with the University of Tennessee.

The author wishes to express his appreciation to Dr. J. M. Googe for the opportunity to undertake this study. Also, his initial suggestions were most helpful. Many thanks also go to Dr. M. O. Pace for his support and encouragement. In addition, thanks go to Dr. D. Rosenberg for his encouragement and help. The author also wishes to thank Dr. T. V. Blalock for lectures and comments on electronics. Thanks go to Dr. G. W. Hoffman for his counseling. The comments of Dr. T. C. Reiley of the Oak Ridge National Laboratory were greatly appreciated. Dr. H. T. Mathews's lectures on calculus were also appreciated. The author would also like to express his thanks to Dr. J. D. Tillman and Dr. R. E. Bodenhiemer.

The author would like to extend his gratitude to his parents for their continuing encouragement and faith in him.

THIS PAGE

WAS INTENTIONALLY

LEFT BLANK

ABSTRACT

The suitability of several temperature measurement schemes for an irradiation creep experiment is examined. It is found that the specimen resistance can be used to measure and control the sample temperature if compensated for resistance drift due to radiation and annealing effects. A modified Kelvin bridge is presented that allows compensation for resistance drift by periodically checking the sample resistance at a controlled ambient temperature.

A new phase-insensitive method for detecting the bridge error signals is presented. The phase-insensitive detector is formed by averaging the magnitude of two bridge voltages. Although this method is substantially less sensitive to stray reactances in the bridge than conventional phase-sensitive detectors, it is sensitive to gain stability and linearity of the rectifier circuits. Accuracy limitations of rectifier circuits are examined both theoretically and experimentally in great detail. Both hand analyses and computer simulations of rectifier errors are presented.

Finally, the design of a temperature control system based on sample resistance measurement is presented. The prototype system is shown to control a 316 stainless steel sample to within a 0.15 °C short term (10 sec) and a 0.03 °C long term (10 min) standard deviation at temperatures between 150 and 700 °C. The phase-insensitive detector typically contributes less than 10 ppm peak resistance measurement error (0.04 °C at 700 C for 316 stainless steel or 0.005 °C at 150 °C for zirconium).

THIS PAGE

WAS INTENTIONALLY

LEFT BLANK

TABLE OF CONTENTS

LIST OF FIGURES

FIGURE PAGE

FIGURE PAGE

FIGURE PAGE

CHAPTER I

INTRODUCTION

I. GOAL OF DISSERTATION

In the past many methods of measuring temperature have been devised including gas, ultrasonic, noise, thermocouple, mercury, radiation, and resistance thermometers.[1] One of the most accurate thermometers is the platinum resistance thermometer in which the resistance is measured by balancing a bridge. AC bridges have the advantage of insensitivity to thermoelectric voltages, but they are sensitive to phase shift due to stray reactances. Typically complex phase compensating techniques are employed together with very low AC frequency to help correct this problem. A novel detector employing precision rectifiers as error detectors is presented that minimizes sensitivity to phase shift. The detector allows high-frequency operation (1 KHz) thereby making fast temperature measurement and control possible.

The accuracy limitation of this detector is the linearity of the rectifier. A thorough literature search reveals that a complete analysis of rectifier error is not available. Therefore, a complete error analysis is given in this dissertation for precision rectifier circuits, in which diodes or transistors are placed in the feedback path of an opamp.

This detector was developed for use in a temperature control system for a radiation creep experiment. Background information on the creep experiment will be given next.

II. BACKGROUND INFORMATION ON RADIATION CREEP

Recent concern over future energy shortages has resulted in intense search for energy sources. Nuclear energy is becoming an important source of energy because of its low cost and abundant fuel resources. Unfortunately, some of the properties of materials in or near the core of nuclear reactors change due to exposure to nuclear radiation.[2] At present, the understanding of these changes is critical to the proper design of nuclear reactors, especially breeder and thermonuclear reactors. The economic costs associated with an incomplete understanding of radiation damage for light-water, breeder, and thermonuclear reactors are very large (approximately half a billion dollars per year increasing to six billion dollars by the year 2000).[2]

In breeder reactors, fast-neutron fluxes of the order of 10^{16} neutrons/cm^2-sec are expected. This is three orders of magnitude higher than encountered in existing thermal light-water reactors.[2] This high fast-neutron flux will accelerate radiation damage and will give rise to new problems. The two most serious of these problems are swelling, caused by the formation of voids, and radiation-enhanced creep. Radiation-enhanced creep is the elongation of a stressed sample, while swelling is the increase in sample volume independent of stress. Swelling of up to a 20 percent increase in volume has been observed,[2] while creep rates may be increased by up to several orders of magnitude due to radiation effects.[3] Both swelling and radiation creep require reactor design compromises which may adversely affect reactor efficiency; e.g., a breeder reactor with a heavy internal support structure (necessitated by swelling or irradiation creep behavior) may not breed.

The radiation effect with which this dissertation is concerned is radiation-enhanced creep. This is defined as the excess time-dependent deformation of stressed material due to nuclear irradiation and contains deformation associated entirely with swelling.[4,5] An overview of the present state of the effect of radiation on materials is given in Reference 6. The experimental features associated with irradiation creep are given in References 4, 7, and 8.

In the past, irradiation creep testing has been accomplished by placing samples in reactors, monitoring sample temperature and radiation levels, and periodically removing samples from the reactor to measure changes in sample length. Disadvantages of this technique are as follows. Since only discrete data points are produced, fine detail of the sample creep history is lost. In particular, transient behavior is lost. Since samples must be removed from the reactor and placed in controlled equilibrium temperature environments, the sample recovery behavior may introduce error. If continuous creep data is desired, the cost of required equipment is very large (of the order of a million dollars per specimen as opposed to only a few thousand dollars for the discrete method).

It has recently been shown that irradiation creep due to neutrons can be simulated by light ion irradiation such as alpha particles, deuterons, and protons.[2,4] Charged particle testing has several advantages.

1. Sources of high energy ions are readily available such as cyclotrons and Van de Graff accelerators.

2. The cost of testing thin samples with ions is low (of the order of a few thousand dollars).
3. In tests conducted out of reactor, tight tolerances on sample test conditions can be achieved making continuous creep measurement possible. Hence transient and recovery characteristics can be studied.

The irradiation creep experiment to be conducted at Oak Ridge National Laboratory by the Metals and Ceramics Division includes measurement of the change in length with time of metal foil samples while they are bombarded by high energy (approximately 60 MeV) alpha particles at current densities up to 10 $\mu A/cm^2$ from the Oak Ridge Isochronous Cyclotron. At this current density, the specimen displacement rate will match that at the core of planned breeder reactors uniformly through the sample.

A description of the experimental apparatus as shown in Figures 1 and 2 is given below.

1. Specimens having gauge dimension of 0.0076 x 0.2 x 2.0 cm are attached by hydraulic grips to two pullrods. Capacitance extensometers ASL Model 1072 (resolution better than 250 Å) sit on two sides of the specimen between the grips, as illustrated in Figure 2, thereby eliminating errors associated with remote strain measurement. Sample thickness can be increased up to 0.0127 cm for creep tests at temperatures above approximately 250 °C.
2. Stress is applied via a motor-driven spring (the spring is of the ring type to prevent any twisting tendencies) to enable

ORNL DWG 75-8127

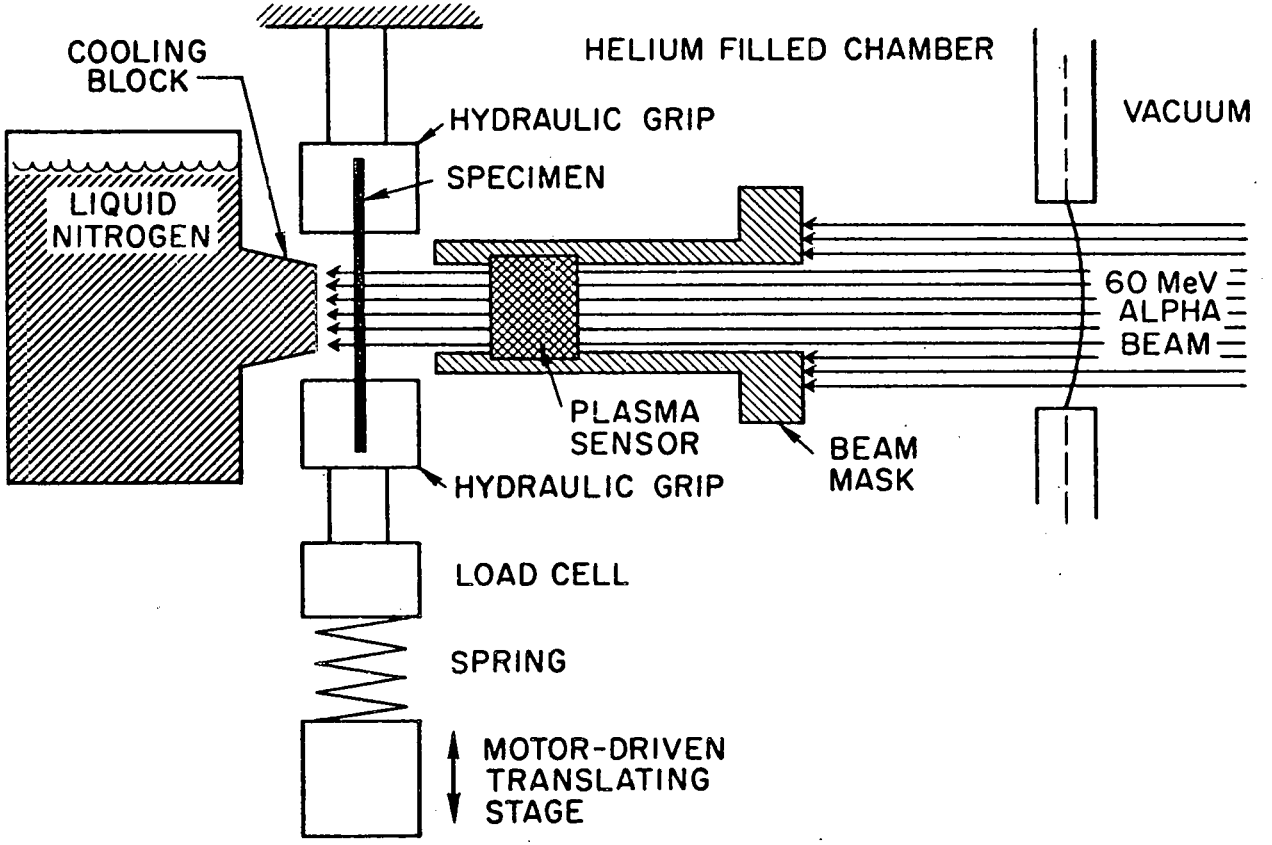

Figure 1. Schematic diagram of irradiation creep apparatus.

ORNL DWG 75-8128

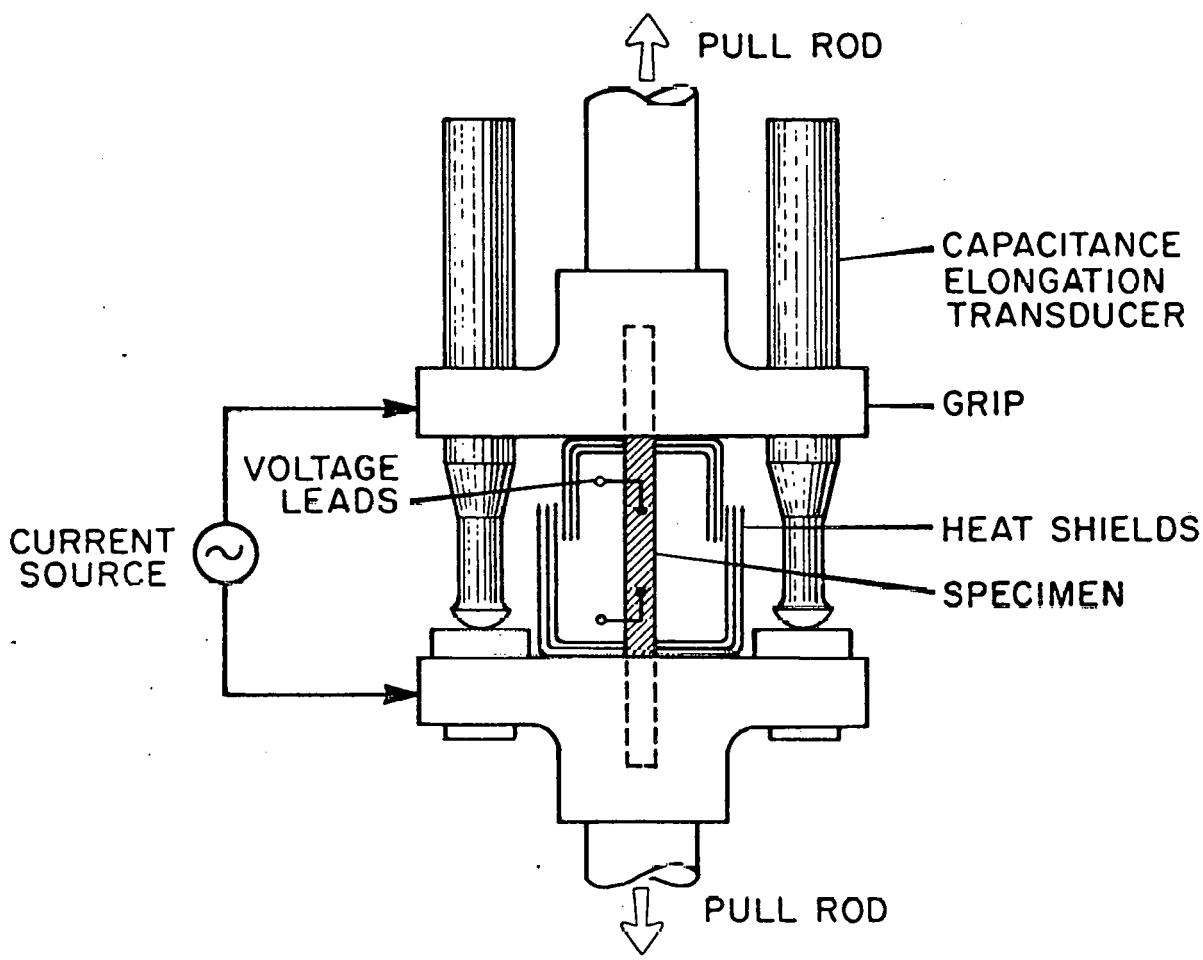

Figure 2. Schematic diagram of grip section showing spatial relationship of specimen and elongation transducers.

rapid variation of stress up to 580 MPa (MN/m^2). A load cell provides monitoring of stress (0.22 N resolution).

3. A liquid nitrogen-filled heat sink provides constant sample cooling by heat conduction through circulated helium (1/3 to 1 atm at 26.7 ± 0.5 °C).
4. Temperature control and monitoring are based on the variation of sample resistance with temperature. Ohmic heating current is supplied by the control system to control sample temperature over a range from about 150 °C to 700 °C. An infrared pyrometer, Raytek Thermalert Model S/L-300 B (2.8 °C repeatability) monitors the temperature profile along the sample. Nisil/Nicrosil and/or Pt/Pt-10%Rh thermocouples are provided to monitor sample temperature under equilibrium room temperature conditions to enable compensation of the control system for bulk resistivity changes. Ambient temperature control of the apparatus is provided by circulating water through structural members and by circulating helium in the test chamber. The short specimen thermal time constant (approximately 0.4 sec) enables rapid variations in sample temperature to be made.
5. Alpha-beam monitoring will be accomplished via a flat-plate Langmuir probe mounted on the beam mask and by monitoring the ohmic heating current. To maintain a uniform beam profile on the sample, the beam can be wobbled.

This project has several objectives. The steady-state and transient creep behavior in pure metals and alloys will be examined. Creep will be studied as a function of temperature, fluence, and stress. This will

be facilitated by the equipment which allows rapid variation of temperature, stress, and atomic displacement rate. Candidate reactor construction materials to be tested for use in breeder, thermonuclear, and conventional thermal reactors include both established alloys as well as developmental ones. Test materials will be preirradiated to varying fluences in EBR-II (Experimental Breeder Reactor-II) and other reactors to avoid long-term structural transients and to study creep as a function of fluence (neutrons/cm^2). Structural coupling between stress and radiation damage will be studied by preirradiating some samples in the stressed condition.

III. SCOPE OF DISSERTATION

The subject of this dissertation is the sample temperature control system for the irradiation creep experiment. In Chapter II, the importance of precision temperature control to the experiment is stressed. Methods of temperature measurement and control are discussed. Reasons for choosing sample resistance as a measure of average sample temperature are given. Advantages of AC bridges over DC bridges are enumerated. Finally, a bridge that allows compensation for changes in bulk resistivity due to radiation damage is developed. Results of computer programs are presented in Appendix A, in which polynomial equations for thermal expansion and resistance change with temperature are used to calculate the temperature and resistance control necessary for 1 ppm strain resolution.

In Chapter III, methods for measuring the error signal from AC bridges are discussed. A new method employing precision rectifiers is

developed. The chief advantage of this method is the insensitivity to stray phase shifts in the practical bridge. This method allows very long cables to be employed in the bridge without causing significant error. However, the linearity of the rectifier is shown to be of utmost importance.

Error analyses of some precision rectifier circuits are presented in Chapter IV. Hand analyses, utilizing both piecewise-linear and exponential diode models, and elaborate CSMP (IBM Computer System Modeling Program) computer analyses are given. Accuracy as affected by gain, offset voltages, input bias current, slew rate limitations, exponential characteristics of PN junctions, H_{FE} fluctuation with collector current, and stray capacitance is investigated. A discussion of difficulties in experimental verification of theoretical results is also presented.

The final control system for the irradiation creep experiment is described in Chapter V in terms of experimental data and an equivalent system model. Results and suggestions for further study are given in Chapter VI.

CHAPTER II

TEMPERATURE CONTROL CONSIDERATIONS

I. TEMPERATURE CONTROL REQUIREMENTS FOR IRRADIATION CREEP EXPERIMENTS

The Need for Temperature Control

One of the most important aspects of the experiment is temperature control and measurement since thermal expansion cannot be distinguished from mechanically induced length changes. The importance of temperature control is clear, given expected irradiation creep rates during these experiments of 50 ppm/24 hr. If the temperature averaged along the length of the specimen varies by approximately 2 °C, the corresponding thermal expansion is approximately the same as the creep occurring in a day! To allow testing under conditions of low stress and displacement rate, a strain measurement accuracy of one microstrain (1 ppm) is desired. This is substantially better than most previous experiments. For instance, for the experiments recently reported, strain measurement accuracies range from 50 ppm,[9] to 5 ppm.[10] The required temperature control for 1 ppm thermal expansion ranges from 0.043 °C at 700 °C for 316 stainless steel to 0.403 °C at 700 °C for zirconium as shown in Table 1. The data presented in Table 1 were calculated via two computer programs. The first program was employed to fit a polynomial equation to thermal expansion data obtained from References 11 and 12. A second program calculated the temperature control (ΔT) using the following equation:

TABLE 1

THE CHANGE IN TEMPERATURE CAUSING A 1 PPM CHANGE IN SAMPLE LENGTH FOR SEVERAL METALS

Metal	Temperature Change (°C) at a Temperature (°C) of					
	0.00	26.66	150.00	300.00	500.00	700.00
Hastelloy F	0.074	0.073	0.068	0.063	0.058	0.053
Nickel	0.075	0.074	0.070	0.065	0.060	0.056
Niobium	0.123	0.123	0.123	0.123	0.123	0.123
316 Stainless Steel	0.065	0.064	0.058	0.053	0.047	0.043
Zirconium	0.242	0.233	0.249	0.291	0.347	0.403

$$\Delta T = L(T)\ 1.0(10^{-6})/L'(T)\ , \tag{1}$$

where L(T) is sample length as a function of temperature. For more information on these programs, see Appendix A.

Another reason for temperature control is the reproducibility or repeatability of experimental results. Although radiation creep is only slightly temperature dependent,[4,5] conventional thermal creep is highly temperature dependent.[4] Thermal creep (whether governed by dislocation motion or by diffusional mechanisms) has a thermal dependence which is normally that of self-diffusion; e.g.,

$$\dot{e} = f(\sigma)\ D_v\ ,^{4} \tag{2}$$

where $\dot{e}$ is the diffusion creep rate, $D_v = D_o \exp(-Q/RT)$, D_v is the self-diffusion coefficient, $f(\sigma)$ is a function of stress related to the creep mechanism, Q is the activation energy for self-diffusion (typically tens of Kcal/mole), D_o is a constant, and R is the gas constant. Wolfer et al. have shown that the radiation-induced creep rate is empirically given by

$$\dot{e} = \frac{1}{3}\,\delta_{ij}\,(\frac{\Delta\dot{V}}{V}) + (C + D(\frac{\Delta\dot{V}}{V}))\,\frac{3}{2}\,S_{ij}\ ,^{5} \tag{3}$$

where $\Delta\dot{V}/V$ is the swelling rate, S_{ij} is the deviatoric stress, δ_{ij} is the Kronecker delta, and C and D are constants of the material. Also, thermal creep is usually dominant at very high temperatures, while radiation creep dominates at low temperatures as shown in Figure 3.

Alternatively temperature measurement could be employed instead of temperature control. If temperature and creep were measured

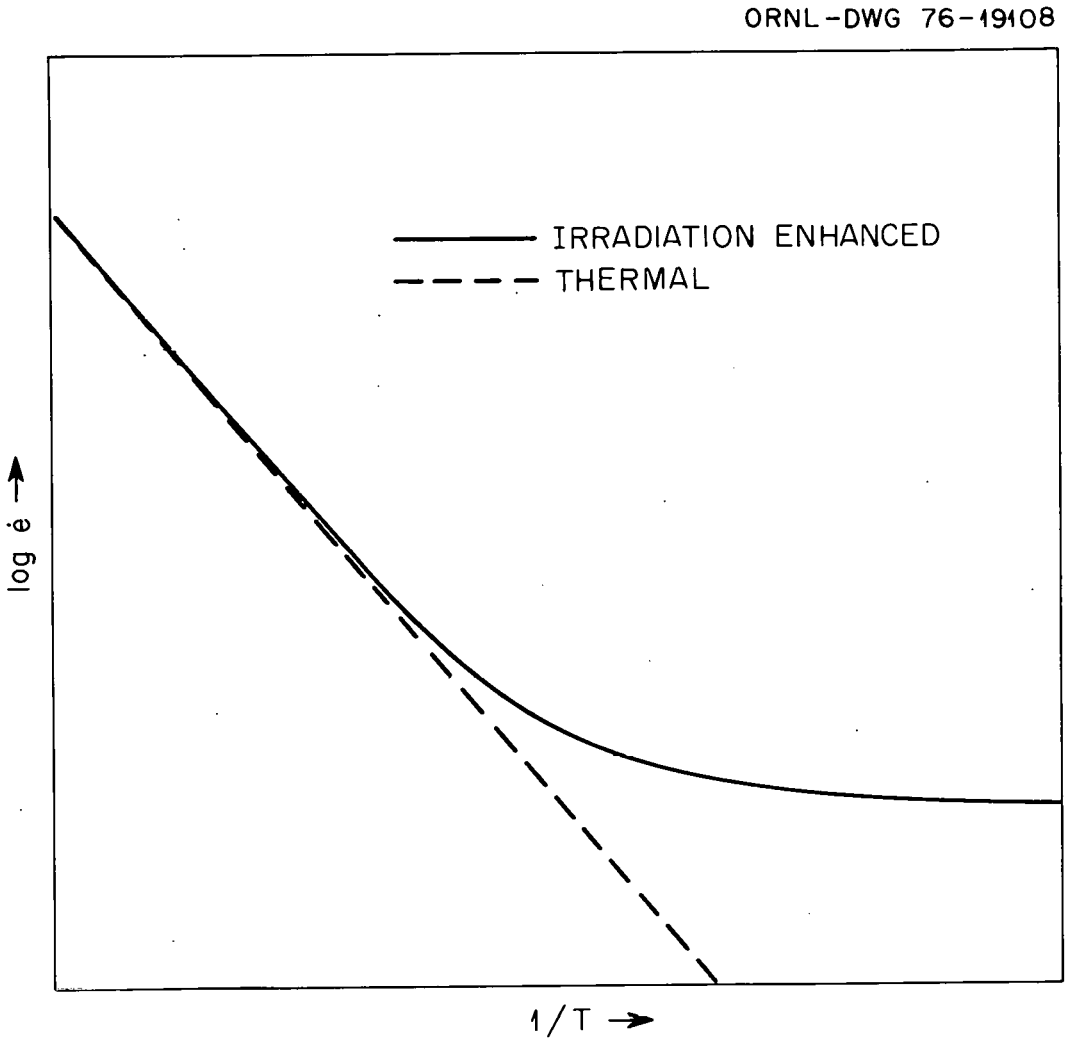

Figure 3. Creep rate versus temperature.

simultaneously, it would be possible to correct the creep data for temperature fluctuations. The shortcoming of this method results from transient response limitations of the equipment. Without temperature control, the sample temperature undergoes random, rapid fluctuations of the order of degrees due to beam power fluctuations and turbulent flow of helium in the chamber. Also, the cyclotron is prone to failure, resulting in loss of beam and large temperature changes of the sample unless temperature control is employed. See Chapter V. In addition, reproducibility of results at high sample temperatures would be poor due to the large temperature dependence of thermal creep. Hence, temperature control is preferable to temperature measurement.

Experimental Considerations

Because of the importance of specimen temperature control, temperature control should be given special consideration in design of the creep apparatus. Dissipation of beam power, sample temperature profile, and measurement and control of the mean sample temperature are three areas of utmost importance. With a full beam power density of 300 W/cm^2, the net incident beam power on the sample is 120 W. Approximately 10 percent of this power is absorbed by the foil sample. Power loss, due to radiation and conduction of heat to the grips, is inadequate to prevent excessive specimen temperatures. Therefore, conduction of heat via circulating helium to a cryogenically cooled heat sink was chosen for this experiment as the method of heat removal. This allows sample temperatures below 250 °C with full beam power. Sample temperatures of 250 to 700 °C are obtained via AC ohmic heating current furnished by the control system.

Of particular concern is the temperature profile across the length and width of the sample. Some computed temperature profiles are shown in Figure 4. The importance of a uniform temperature profile is illustrated by the following example. Suppose that the length of a specimen at uniform temperature (T) is given by the following quadratic equation.

$$L(T) = L_o \ (1 + \alpha T + \beta T^2) \ .$$

Breaking the sample into infinitesimal lengths (dZ), the length of the sample is given by

$$L = \int_0^L dZ = \int_0^{L_o} (1 + \alpha T + \beta T^2) \ dZ_o$$

$$= L_o \ (1 + \alpha \overline{T} + \beta \overline{T^2}) \ . \qquad (4)$$

Hence control of the average temperature along the length of the sample ($\overline{T}$) does not necessarily eliminate changes in length due to thermal expansion since the mean square temperature ($\overline{T^2}$) must also be held constant. (All of the metals in Table 1 (page 11) have quadratic expressions for L(T), except for niobium which has a linear L(T)).

A nonuniform lateral temperature profile will result in nonuniform stress across the width of the specimen. For example, Chipley[13] has calculated a lateral temperature differential, from the center line to the outside edge, of 3.73 and 6.51 °C at mean sample temperatures of 327 and 651 °C, respectively. These lateral temperature differentials will create differential stresses of 13.34 and 23.28 MN/m^2, respectively. In addition, a nonuniform temperature profile will cause nonuniform

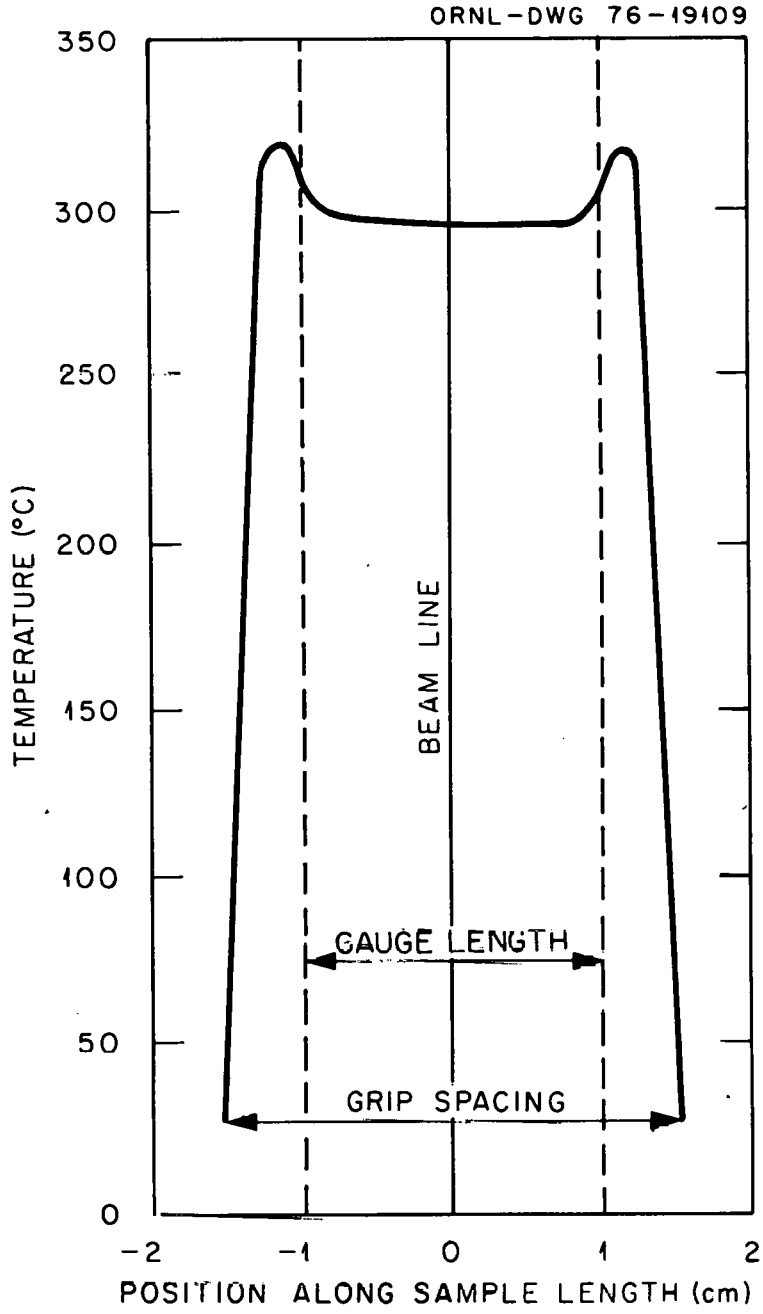

(a) Temperature profile with 12 W absorbed beam power in the gauge length and a 3.16 grip spacing. No heat generation in grips.

Figure 4. Computed temperature profiles of a specimen having a 2 cm gauge length; 4.35 W ohmic heating applied to sample.

Source: K. K. Chipley, Oak Ridge National Laboratory, Experimental Engineering Division, Intralaboratory Correspondence. (Unpublished.)

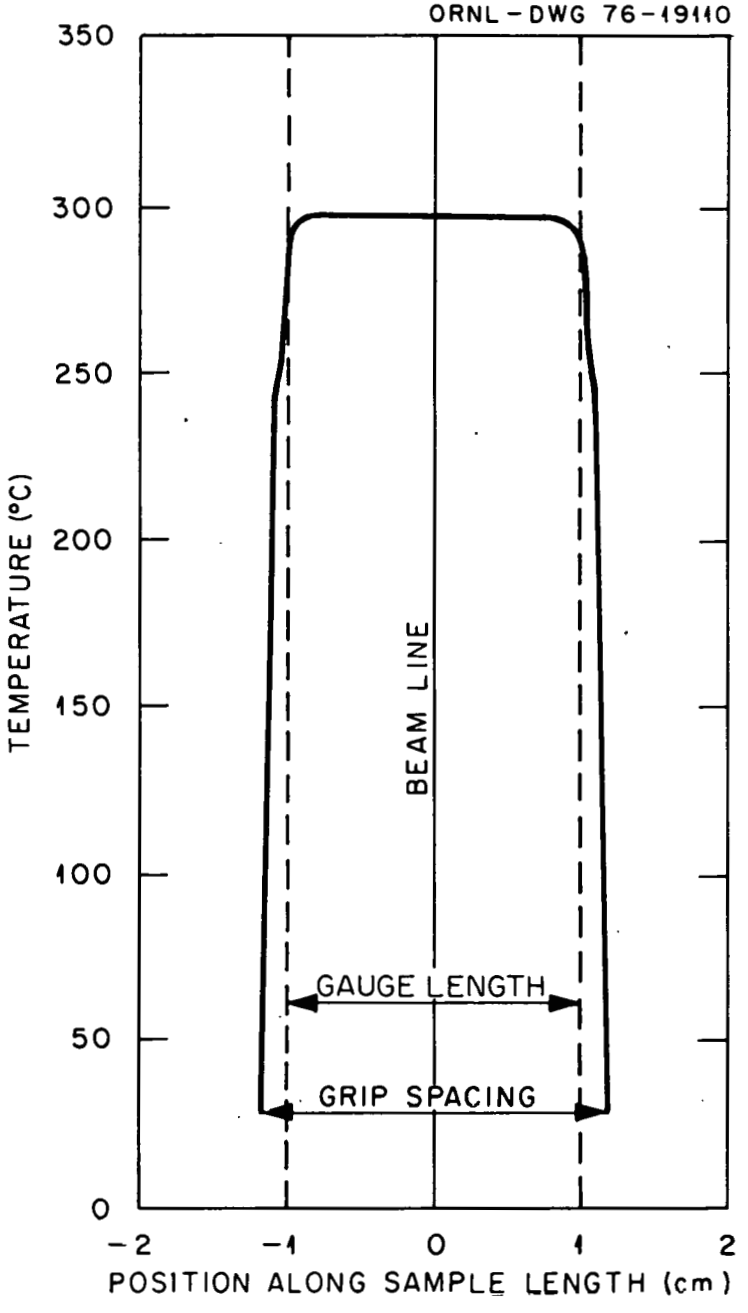

(b) Temperature profile with 12 W absorbed beam power in the gage length and 2.762 cm grip spacing. Heat generation in grips = 1426 W/cm^3.

Figure 4 (continued)

thermal creep resulting in an increase in nonuniformity of stress and strain throughout the sample.

Several methods are currently being used in irradiation creep experiments to control temperature. At Harwell, McElroy et al.[10] place a foil sample in a helium atmosphere and measure the sample temperature using an infrared pyrometer. This pyrometer can scan the sample to measure and control the temperature at any small spot on the sample, using DC ohmic heating for control. Beam wobbling is utilized to attempt to maintain uniform irradiation and temperature. (See discussion of pyrometry on page 24.) On the other hand, Hendrick et al.[4] attempt to maintain a constant temperature profile in the irradiation creep experiments at the Naval Research Lab by placing a sample in direct contact with a heat sink. The general location of the heat sink, pullrods, sample, and beam are similar to those shown in Figure 1 on page 5. Sample temperature is monitored by thermocouples inside the heat sink, and by a three-part thermocouple formed by two wires and the sample. (See discussion on thermocouples on page 19.) Specimen temperature control is provided by the beam, heaters and cooling coils inside the heat sink, and pullrod heaters. There are several limitations to this latter approach. First, changes in beam power would not cause equal changes in sample and heat sink temperatures if the beam directly heats both. Also, close thermal coupling between heaters and thermocouples requires careful tuning of the control system to minimize interaction. Finally, the transient response of the system must be slow due to the heat sink's thermal inertia.

In the experiments at ORNL, direct sample heating and temperature measurement was chosen to allow fast response to beam perturbations. The temperature profile can be adjusted by varying the spacing between heat sink and sample, the helium pressure, the pullrod temperature, the ohmic heating current, and the beam power.[13] Thus the temperature profile may be shaped by several techniques.

II. TEMPERATURE MEASUREMENT METHODS

Several methods of measuring temperature were considered for temperature monitoring and control including the following: thermocouples, infrared pyrometers, Johnson noise thermometers, and resistance thermometers. The suitability of each of these schemes to the measurement of sample temperature will now be examined.

Thermocouples

Thermocouples consist of two metals having different Seebeck coefficients that are joined together at a point. The potential difference between the open ends is

$$E = - \int_L S \, \vec{\nabla} T \quad d\vec{L} \, ,^{14} \tag{5}$$

where E is the thermal emf in μV, S is the Seebeck coefficient as a function of the path along the thermocouple wire in μV/°C, $\vec{\nabla} T$ is the temperature gradient in °C/cm, $d\vec{L}$ is the position vector in cm, and L is path. See Figure 5(a). If S_a and S_b are the Seebeck coefficients of wires A and B, respectively, then E is given by

$$E = \int_{T_1}^{T_2} (S_a - S_b) dT \, . \tag{6}$$

ORNL-DWG 76-19111

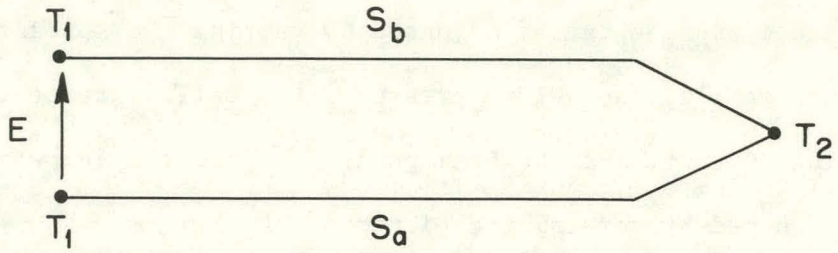

(a) Sample thermocouple.

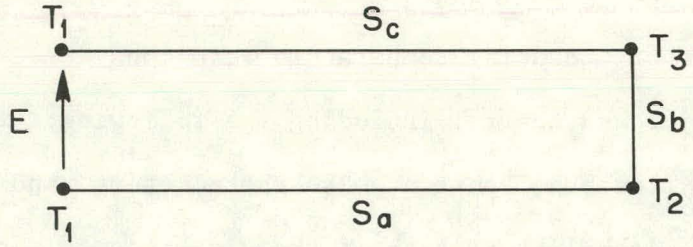

(b) Three part thermocouple.

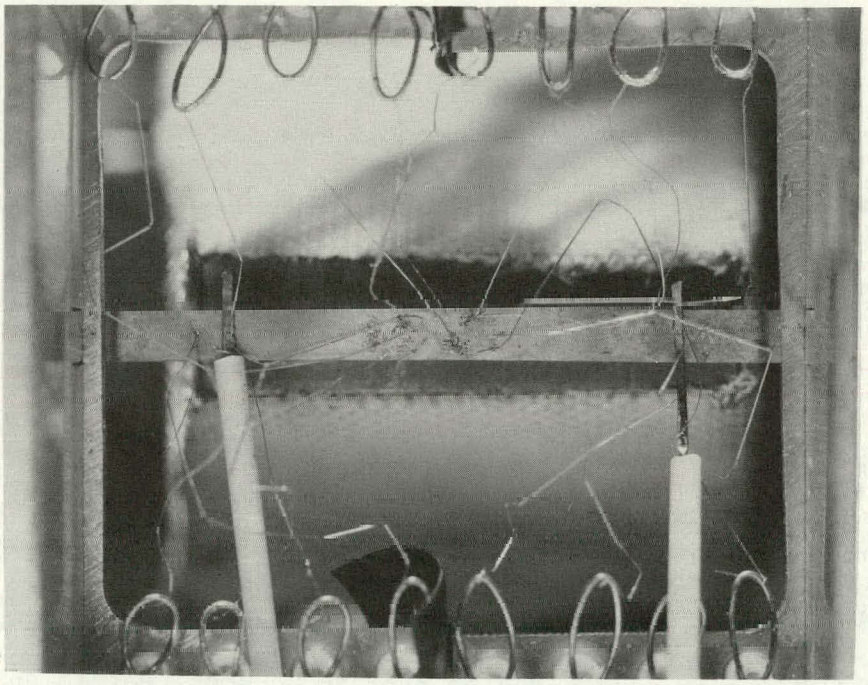

(c) Several thermocouples attached to specimen.

Figure 5. Thermocouples.

If a third wire is added to the thermocouple with a Seebeck coefficient of S_c with junction temperatures of T_2 and T_3 as shown in Figure 5(b), the thermoelectric voltage becomes

$$E = \int_{T_1}^{T_2} S_a \, dT + \int_{T_2}^{T_3} S_b \, dT + \int_{T_3}^{T_1} S_c \, dT$$

$$= \int_{T_1}^{T_o} (S_a - S_c) \, dT + \int_{T_o}^{T_o - T_d} S_a \, dT + \int_{T_o - T_d}^{T_o + T_d} S_b \, dT + \int_{T_o + T_d}^{T_o} S_c \, dT \, , \tag{7}$$

where $T_d = (T_3 - T_2)/2$ and $T_o = (T_3 + T_2)/2$.

There are several reasons why thermocouples would be a poor choice as the primary temperature measurement device for this experiment.

1. A major problem is thermal shunting. Since thermocouple wires are generally good thermal conductors, they can act as localized heat sinks at the points of contact with the sample. Because of low thermal inertia of the foil sample, temperatures would tend to be lower at the points of contact than they would be without the thermocouples.
2. Also, if thermocouples are exposed to the beam (as they must be to allow direct temperature measurement of the irradiated specimen), beam heating can create large temperature gradients along the wires. These gradients can cause error if the thermocouple wires are inhomogeneous or if the thermocouple is composed of more than two wires as illustrated by Figure 5(b)

and Equation (7); i.e., the thermoelectric emf depends on T_1, T_2, and T_3 or T_1, T_o, and T_d. Hence, unless the temperature profile along the wires is known, the voltage is difficult to interpret.

3. Electrical shunting can also be a problem. Shunting effects due to finite resistance of wire insulation can cause errors. While helium gas would normally be a good insulator, the alpha beam will tend to ionize the gas, reducing its resistance. Hence, insulated wires must be employed. However, radiation can also cause ionization in the wires and insulation resulting in leakage.

4. Thermocouples lose calibration due to structural changes occurring at high temperatures. Decalibration characteristics vary drastically with thermocouple material; type K thermocouples decalibrate 11 °C while Nicrosil/Nisil thermocouples change less than 0.5 °C when exposed to 1100 C for 700 hours.[14] Both type S and Nicrosil/Nisil are good choices for this experiment because of their stability.

5. Radiation also causes decalibration of thermocouples over long periods of exposure.[15] Decalibration can result from radiation-induced structural changes and transmutation of the elements that combine to form the thermocouple wires. Radiation can also create parasitic currents in the thermocouple wires.

6. An additional problem is possible error due to AC voltages caused by the heating current. This problem is solved by reading the thermal emf with voltmeters having very high common and normal mode rejection ratios.

7. To measure the average sample temperature, several thermocouples are required since temperature can only be determined at discrete points. The average of these temperatures is taken as the average sample temperature.
8. Problems also occur in attaching thermocouples to the specimen. First, insulating and connecting small wire is very tedious, and the wires break easily. Secondly, spot welding many wires to thin metal samples is likely to damage the specimen enough to affect creep measurements due to localized annealing, changes in thickness, etc.

As an example of the magnitude of errors that can occur, errors of over 10 °C were encountered when a beam current density of 3 $\mu A/cm^2$ at 60 MeV and an ohmic heating current were applied to a specimen at temperatures between 150 and 500 °C. Nicrosil/Nisil thermocouples of 2.54×10^{-3} cm diameter were used; the fine wire reduced the conductance of heat along the wire and to the helium gas. Quartz tubing of 7.60×10^{-3} cm diameter were utilized to both electrically and thermally insulate the thermocouple wire. As illustrated in Figure 5(c) (page 20), thermocouples were attached to the sample by laser spot welding Nicrosil and Nisil wires separately to the 316 stainless steel sample, forming a three-part thermocouple. Furthermore, the thermocouple wires were exposed to the beam, which may have caused large temperature gradients along parts of the thermocouple wires. In some cases, two wires of a thermocouple were spaced longitudinally on the sample so that AC voltages of up to 0.1 volt appeared across the thermocouple wires. Nicrosil/Nisil has a typical output of 30 $\mu V/°C$; therefore, in order to

measure the thermal emf to within 0.05 °C, a voltmeter with a normal-mode rejection of approximately 30 dB would be required.

Infrared Pyrometry

Pyrometers can be used to measure the electromagnetic radiation emitted from the sample to determine its temperature. The Stefan-Boltzmann equation gives the radiant exitance or flux emitted per unit area as follows:

$$M = \varepsilon(2\pi,\overline{\lambda})\sigma T^4 \text{ ,}^{16} \tag{8}$$

where $\varepsilon(2\pi,\overline{\lambda})$ is the hemispherical total emittance of the specimen at the absolute temperature (T), and σ is the Stefan-Boltzmann constant (5.6697×10^{-8} W/m^2). For a blackbody (i.e., one that absorbs all incident radiant energy and emits the maximum possible spectral exitance for any wavelength (λ) for its T), $\varepsilon(2\pi,\lambda) = 1$. The spectral exitance is given by Plank's law as

$$M_\lambda = \varepsilon(2\pi,\lambda)\ C_1\ \lambda^{-5}\ (\exp(C_2/\lambda T) - 1)^{-1} \text{ ,} \tag{9}$$

where

$$C_1 = 2\ C_o^{\ 2}\ h = 3.7415 \times 10^{-8}\ \text{W/m}^2 \text{ ,}$$

$$C_2 = C_o h/k = 1.43879 \times 10^{-2}\ \text{m-K} \text{ ,}$$

C_o is the speed of light in the environment of the specimen, h is Plank's constant, and $\varepsilon(2\pi,\lambda)$ is the hemispherical spectral emittance. Note that M_λ may be written in terms of frequency (f) as follows:

$$M_f = \varepsilon(2\pi, \frac{C_o}{f})\ 2hf^3/(C_o^{\ 2}\ (\exp(hf/kT) - 1)) \tag{10}$$

so that

$$M = \int_0^\infty M_f \, df = \int_0^\infty M_\lambda \, d\lambda \ . \tag{11}$$

The spectral exitance is employed to calculate the energy emitted over a finite spectral bandwidth by integrating M_λ over that bandwidth. Generally, a detector can measure M over a small angle as illustrated in Figure 6(a). In this case, the spectral radiance, the flux propagated in a given direction per unit solid angle about that direction and per unit area normal to that direction, is given by

$$L_\theta = \varepsilon(\theta,\overline{\lambda})\sigma T^4/\pi \tag{12}$$

and the directional spectral emittance of the specimen is

$$L_{\theta,\lambda} = \varepsilon(\theta,\lambda)C_1/(\pi\lambda^5(\exp(C_2/\lambda T) - 1)) \ , \tag{13}$$

where $\varepsilon(\theta,\overline{\lambda})$ is the total directional emittance and $\varepsilon(\theta,\lambda)$ is the directional spectral emittance of the sample. Solving Equation (13) for T, one obtains

$$T = \frac{C_2}{\lambda} \left(\ln\left(\frac{\varepsilon(\theta,\lambda)C_1}{\pi\lambda^5 \, L_{\theta,\lambda}} + 1\right)\right)^{-1} \ . \tag{14}$$

For $\lambda T < 2898$ m-°K the number one can be omitted with less than 1 percent error in the measured T. This approximation, known as Wien's law, yields the following simplification:

$$T \simeq \left(\frac{1}{T_a} + \frac{\lambda}{C_2} \ln \varepsilon(\theta,\lambda)\right)^{-1} \ , \tag{15}$$

where T_a, the apparent temperature, is the temperature given by Equation (14) with $\varepsilon(\theta,\lambda) = 1$.

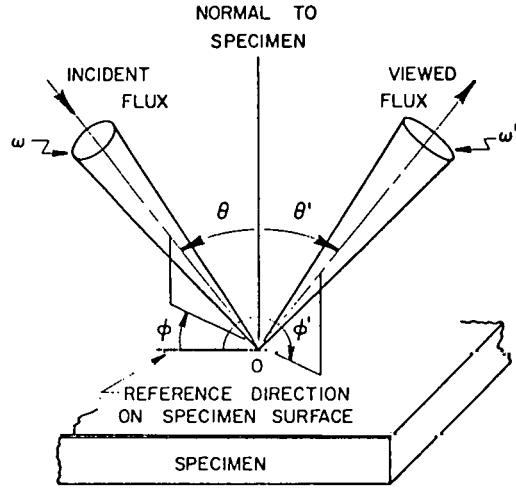

(a) Geometric parameters descriptive of reflection from a surface. θ is the zenith angle, or co-latitude, in degrees; φ is the azimuthal angle, or longitude, in degrees; ω is the beam solid angle, in steradians; and the symbol ′ refers to viewing conditions.

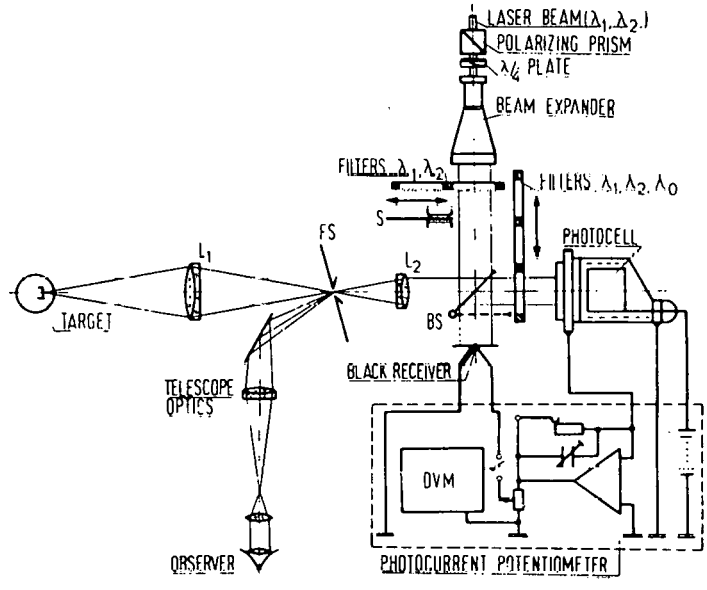

(b) Schematic of apparatus for surface temperature measurement by the radiance ratio method showing the arrangement for determining the spectral absorptance ratio by spectral heating.

Figure 6. Radiation pyrometers.

Source: H. H. Plumb, Temperature, Its Control and Measurement in Science and Industry (Pittsburgh: Instrument Society of America, 1972), pp. 460, 603, and 620.

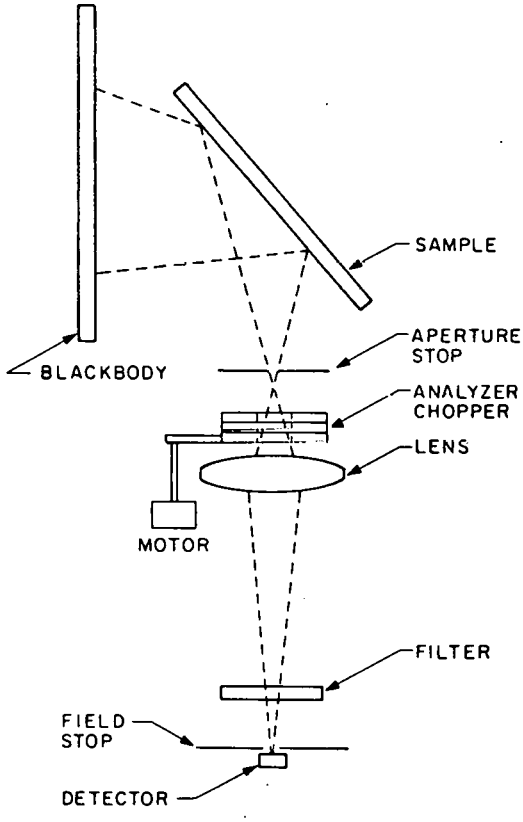

(c) Schematic of polaradiometer.

Figure 6 (continued)

Since the reflectance of a material is equal to one minus the emittance for an opaque sample, many pyrometers measure the reflected radiation of a source from the sample. At least one pyrometer utilizes a laser as the source.[17] While a detailed discussion of pyrometry is beyond the scope of this dissertation, an excellent treatise on pyrometry containing both theoretical analysis, measurement techniques, and radiation properties of materials is given by Touloukia et al.[16]

Infrared pyrometry has both advantages and disadvantages. Its chief advantage is that no contact to the sample is necessary. A big problem is the determination of the emittance or reflectance of the sample. This is influenced by not only the material from which the sample is constructed, but also the surface conditions; i.e., geometry of the object, surface coating and smoothness, angle of measurement with respect to the surface, and measurement wavelength. Thus, oxidation of the sample surface and accumulation of oil (such as that produced by diffusion pumps) on the sample's surface can cause error. Furthermore, the transmittance of the sample's atmosphere and viewing windows must be considered. Moreover, typical accuracy of infrared pyrometers is 6 °C between 250 and 500 °C.

Despite these problems, McElroy et al.[10] at Harwell claim temperature control accuracy of 0.2 °C at 500 °C with an infrared pyrometry control system. To achieve this accuracy, the specimen was preoxidized to reduce emittance drift during the experiment. There are, however, several indications that creep behavior, especially for thin specimens, may be effected by a surface oxide.[18]

It should be mentioned that several techniques may be employed to minimize pyrometer sensitivity to emittance drift. In one technique,

Kunz's ratio method,[19] the thermal radiation is measured at two wavelengths. Utilizing the Wien approximation to Equation (14), T is as follows:

$$T \approx \left(\frac{1}{T_r} + \frac{\ln(\varepsilon(\theta,\lambda_1)/\varepsilon(\theta,\lambda_2))}{C_2(\lambda_1^{-1} + \lambda_2^{-1})}\right)^{-1} ,$$

where $T_r = \left(\frac{1}{\lambda_1 T_{s1}} - \frac{1}{\lambda_2 T_{s2}}\right)/\left(\frac{1}{\lambda_1} - \frac{1}{\lambda_2}\right)$, and T_{s1} and T_{s2} are the spectral radiation temperatures at λ_1 and λ_2, respectively. If the gray body assumption is made (i.e., $\varepsilon(\theta,\lambda_1) = \varepsilon(\theta,\lambda_2)$), T equals T_r. The validity of the gray body assumption depends on both the specimen and the wavelengths. In another method, Murray's polarized radiation technique,[20] the polarization of the sum of radiation emitted by a blackbody source and reflected from the test surface and the radiation emitted by the surface determines the sample temperature. As pictured in Figure 6(b) (page 27), a rotating analyzer chopper examines the polarity of the radiation. While the blackbody source emits unpolarized radiation, the radiation emitted from the specimen is predominantly polarized in the plane of incidence (E_{11}). Assuming Kirchoff's law holds for each component (i.e., the incident energy equals the sum of the reflected and emitted energy), the reflected radiation is predominantly polarized perpendicular to the plane of incidence. The sum of the reflected and emitted intensity is given by

$$I = 0.25\ (E_{br}^2 + (\varepsilon_p + \varepsilon_s)(E_{bs}^2 - E_{br}^2) + (\varepsilon_p - \varepsilon_s)(E_{bs}^2 - E_{br}^2)\cos 2\phi) , \qquad (17)$$

where E_{br} and E_{bs} are the amplitude of the emitted radiation of the

blackbody and sample, respectively. Only the term involving cos 2 ϕ is utilized by the instrument. The orientation of the analyzer can be adjusted so that as the transmission axis passes through the plane of incidence, a reference signal is generated. If the maximum transmitted signal is in phase with the reference signal, the blackbody is cooler than the specimen, while if the transmitted signal is out of phase with the reference signal, the blackbody is hotter than the sample. Sample emittance can vary from 0.05 to 0.65 with less than 2 percent temperature error over a range of 150 to 450 °C without compensation for emittance value. This technique could potentially yield results accurate to 0.05 °C if the sample emittance is known to within a few percent. Theoretically, the system could be made to yield results independent of sample emittance or reflectivity.

The temperature profile can also affect the accuracy of the thermal measurement. As discussed on page 15, to make the thermal expansion error equal to zero, either the temperature profile of the sample must be constant, or the temperature averaging must be weighted so that the sample temperature measured by the pyrometer is equivalent to thermal expansion. There are several approaches to temperature profile measurement that can be taken with pyrometers. The pyrometer can be focused on a spot on the sample, and this spot can be moved along the sample. The location of the spot and its temperature can be fed to a computer to calculate the weighted average temperature of the sample. Alternately, a cylindrical lens can be employed to shape the spot so that it just covers all of the sample. This method would yield an unweighted average temperature if a polarizing pyrometer were employed, but would yield a logarithmically

weighted temperature if a pyrometer operated on Wien's law. Finally, if the temperature profile were constant, temperature control at one spot on the sample would be sufficient, although the likelihood of a constant profile throughout the duration of an experiment is small due to beam perturbation. However, because there is no physical contact with the specimen, measurement flexibility is large, and accuracy is good. Infrared pyrometry is a potential candidate for temperature measurement in radiation creep experiments.

Johnson Noise Thermometry

The thermal noise of a resistor can be utilized to measure its mean temperature.[21] This is accomplished by measuring the rms noise voltage and current of a resistor through amplifiers having known noise bandwidths. The product of the rms noise voltage and noise current is proportional to the mean absolute temperature of the resistor.

The scale factor of a noise thermometer can be derived from Nyquist's formula for the equivalent noise voltage of a resistor. The noise voltage, as shown in Figure 7(a), is given by

$$\overline{e_n^2} = 4hfR/(\exp(hf/kT) - 1) \ , \tag{18}$$

where $\overline{e_n^2}$ is the noise voltage spectrum in V^2/Hz, h is Plank's constant, k is Boltzmann's constant, T is absolute temperature in °K, f is frequency in Hz, and R is resistance in ohms. If $f \ll kT/h (= 20.8\ GHzT/°K)$, then Equation (18) becomes

$$\overline{e_n^2} = 4kTR \ , \tag{19}$$

which is independent of resistor material. The Norton equivalent circuit

ORNL-DWG 76-19112

(a) Equivalent noise circuits of a resistor.

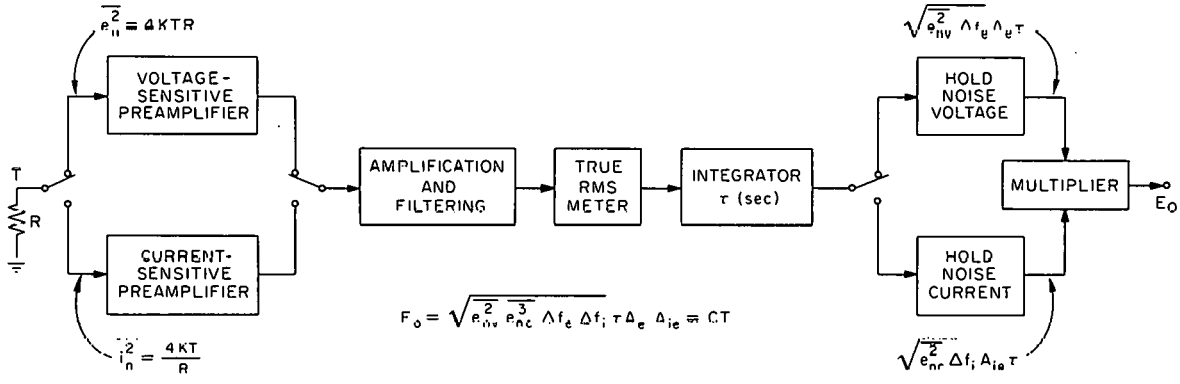

(b) A system for measuring thermal noise power.

Figure 7. Johnson noise thermometer.

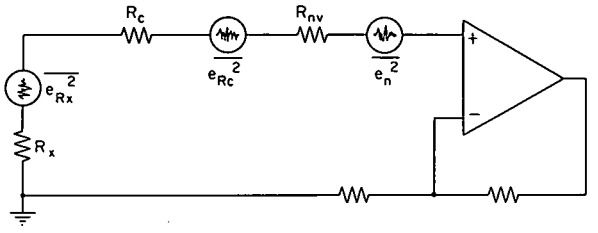

(c) Cable and amplifier noise for a charge sensitive amplifier.

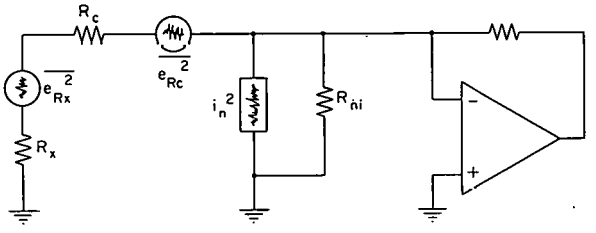

(d) Cable and amplifier noise for a current sensitive amplifier.

Figure 7 (continued)

gives a noise current spectrum in A^2Hz as

$$\overline{i_n^2} = 4kTR \ . \tag{20}$$

Note that the noise power spectral density is given by

$$P_n = ((\overline{e_n^2})(\overline{i_n^2}))^{1/2} = 4kT \ , \tag{21}$$

which gives an absolute, linear temperature scale independent of resistance.

A noise thermometer operates in the following manner. First the noise voltage is measured with a voltage sensitive amplifier having a very large input impedance and a gain of A_e. As shown in Figure 7(b), the rms output of this amplifier is integrated for a period of time (τ). Next, the noise current is measured with a current sensitive amplifier having very low input impedance and a gain of A_{ie}. The rms output of the current amplifier is also integrated for the same period of time. The product of the integrated outputs is

$$E_o = C\ T \ , \tag{22}$$

where $C = A_e\ A_{ie} 4\ k\ (\Delta f_e \Delta f_i)^{1/2}\ \tau^2$ and Δf_e and Δf_i are the noise bandwidths of the voltage and current amplifiers, respectively. See References 22 and 23 for information on noise bandwidth.

The chief advantage of this system is that the calibration is independent of any resistance changes. However, the system has several faults: sensitivity to external noise sources such as cable noise resistance and amplifier noise, sensitivity to gain stability and nonlinearity of amplifiers, sensitivity to amplifier impedance, and slow response time.

The noise sensitivity of the system is a big problem. If the voltage amplifier has an equivalent noise resistance of R_{nv} measured at room temperature (T_a) and if the cable resistance is R_c at a mean cable temperature of T_c, then the output of the noise voltage integrator will be

$$V_{ne} = A_e(4kT_xR_x\Delta f_e)^{1/2}C_e\ \tau\ , \tag{23}$$

where

$$C_e = (1 + \frac{R_{nv}T_a + R_cT_c}{R_xT_x})^{1/2}\ , \tag{24}$$

and R_x and T_x are the sample resistance and temperature, respectively, as illustrated in Figure 7(c). If the equivalent noise resistance of the current sensitive amplifier is R_{ni} as shown in Figure 7(d), then the output of the current integrator will be

$$V_{ni} = A_{ie}(\frac{4KT_x\Delta f_i}{R_x})^{1/2}C_i\ \tau\ , \tag{25}$$

where

$$C_i = (B^2(1 + \frac{R_cT_c}{R_xT_x}) + \frac{R_xT_a}{R_{ni}T_x})^{1/2} \tag{26}$$

and

$$B = R_x/(R_x + R_c)\ . \tag{27}$$

Hence, the product of V_{ne} and V_{ni} gives

$$P_{nr} = A_eA_{ie}\tau^2(\Delta f_e\Delta f_i)^{1/2}\ C_eC_i4KT_x\ . \tag{28}$$

Thus, the cable and amplifier noise makes the temperature scale nonlinearly dependent on R_x and T_x. Borkowoski and Blalock have shown

that with R_x of approximately 300 ohms, the external noise causes increasing error as T_x decreases as predicted by the preceding equations.[21] By using similar equations to correct the data, they were able to reduce error to about 0.5 °C at 273.2 °K. Unfortunately, the error would be much worse in the creep experiment since R_x can be below 8.0 mΩ; i.e., small R_x increases sensitivity to cable noise and requires the use of transformers to optimize S/N. Also, the alpha beam will creat noise due to random fluctuation of the beam current and ionization of the helium atmosphere.

Since the measured temperature is multiplied by A_e and A_{ie}, the stability and nonlinearity of the amplifiers and rms converters are of the utmost importance. To measure a T_x of 700 °C (973.2 °K) to within 0.05 °C requires gain accuracies of better than 30 ppm. The accuracy by which the noise bandwidths are known and deviations of the noise spectra from white noise are also important. The errors caused by clipping and slewing of amplifiers are difficult to predict. For instance, high frequency overload problems can sometimes cause out-of-band noise due to intermodulation distortion to be as large as the in-band noise.[24] The effects of nonzero input impedance of the current sensitive amplifier and less than infinite input impedance of the voltage sensitive amplifier also cause scale factor errors due to current and voltage division, respectively.

Because Johnson noise is random, long integration times are necessary to reduce the standard deviation of the measurements to 0.05 °C at 1000 °K. If the response time of the rms converter is much shorter than τ and if $\Delta f_i = \Delta f_e = \Delta f << f_c$, where f_c is the center

frequency of the filters used to measure the noise, the percent error is

$$P_\sigma = 100\% \ (\Delta f \ \tau)^{-1/2} \ .^{21} \tag{29}$$

Note that τ would have to be 4000 sec for Δf of 100 KHz if a measurement accuracy of 0.05 °C at 1000 °K is desired. Hence, a total measurement time of 8000 sec is required. Thus, noise thermometry is substantially too slow.

Resistance Thermometry

Resistance thermometry measures the change in resistance due to temperature change. Platinum resistance thermometers achieving accuracies of up to 0.0001 °C have been reported.[25] Unfortunately, in the creep experiments, metals other than platinum are to be tested. Resistance size, temperature coefficients of resistance, resistance change due to strain, resistance change due to radiation damage, and electrical shunting can limit the accuracy of temperature measurement.

The resistance measurement accuracy required for 1 ppm strain accuracy was determined for several metals by the computer programs in Appendix A. The results are presented along with resistance versus temperature in Table 2. One program fitted polynomial equations to resistance data obtained from References 11, 12, 26, and 27. Another program calculated the resistance control accuracy necessary for 1 ppm strain accuracy using the following equation:

$$\Delta R_x = R_x'(T)\Delta T \ , \tag{30}$$

where ΔT is given by Equation (1) on page 12. It is evident that there

TABLE 2

THE RESISTANCE, R_x(mΩ), AND THE CHANGE IN RESISTANCE, ΔR_x (μΩ), OF A 0.00762 x 0.2 x 2 CM^3 SPECIMEN TO THE TEMPERATURE CHANGE NECESSARY TO CAUSE A LENGTH CHANGE OF 1 PPM FOR SEVERAL METALS

Metal	Sample Temperature in °C					
	0.00	26.66	150.00	300.00	500.00	700.00
Hastelloy F						
R_x	150.	151.	155.	158.	162.	164.
ΔR_x	2.50	2.37	1.72	1.59	0.642	0.415
Nickel						
R_x	8.37	9.71	17.2	30.2	35.1	37.8
ΔR_x	3.60	3.87	4.87	7.19	1.70	1.45
Niobium						
R_x	18.9	20.5	27.9	36.4	46.9	56.4
ΔR_x	7.66	7.58	7.21	6.76	6.16	5.55
316 Stainless Steel						
R_x	97.1	99.7	111.	123.	136.	145.
ΔR_x	6.42	6.15	5.02	3.86	2.61	1.61
Zirconium						
R_x	59.1	65.4	92.5	121.	150.	169.
ΔR_x	58.3	54.8	41.2	29.1	17.5	9.09

is a wide spread of resistance values ranging from a low of 8.37 mΩ for Nickel at 0 °C and a high of 160 mΩ for Zirconium at 700 °C. Note that Hastelloy F provides the worst case resistance measurement problem for 1 ppm strain resolution of 0.415 μΩ out of 164 mΩ (or 2.5 ppm) at 700 °C. The next worst case is 316 stainless steel with a required resistance measurement of 1.61 μΩ out of 145 mΩ (or 11 ppm) at 700 °C. The difficulty of this measurement accuracy is illustrated by the following: if a 1 amp measuring current is employed, Hastelloy F and 316 stainless steel require that the potential drop across the sample is measured to within 0.415 μV and 1.61 μV in the high noise environment of the cyclotron.

The resistance change due to creep will affect the temperature measurement. The sample strain (e) will cause a change in sample resistance due to the change in sample length and cross section; i.e., resistance is given by

$$R_x = \frac{\rho L}{A} , \tag{31}$$

where R_x is the sample resistance, ρ is the resistivity of the sample in ohm-cm, L is the length of the specimen, and A is its cross section. Assuming elastic strain, A can be found in terms of A_o, the initial value of A, by

$$A = A_o(1 - \nu e)^2 , \tag{32}$$

where ν is Poisson's ratio. Thus R_x is related to e by

$$R_x = \frac{\rho L_o(1 + e)}{A_o(1 - \nu e)^2} . \tag{33}$$

Differentiating Equation (33) with respect to e, one obtains

$$R_x' = \frac{\rho L_o}{A_o} \left(\frac{1 + 2\nu + \nu e}{(1 - \nu e)^3}\right) . \tag{34}$$

If e << 1, then the sensitivity of R_x to ε is

$$\frac{R_x'}{R_x} = S_{R_{x_e}} \simeq 1 + 2\nu . \tag{35}$$

Since ν typically lies between 0.25 and 0.5, $S_{R_{x_e}}$ lies between 1.5 and 2.0. However, a temperature control, based solely on sample resistance measurement, will try to maintain a constant R_x; i.e.,

$$dR_x = \frac{\partial R_x}{\partial T} dT + \frac{\partial R_x}{\partial e} de = 0 . \tag{36}$$

Hence, the change in temperature due to strain is

$$dT = -\left(\frac{\partial R_x}{\partial e} de\right) / \left(\frac{\partial R_x}{\partial T}\right) = -R_x S_{R_{x_e}} de / \left(\frac{\partial R_x}{\partial T}\right) . \tag{37}$$

But a change in sample temperature will cause a change in sample length as was illustrated earlier on page 12 in Equation (1). Thus the measured elongation of the sample will be

$$dL_m = L'(T)\, dT + L(T)\, de ,$$

or

$$dL_m = \left(-R_x S_{R_{x_e}} L'(T) / \left(\frac{\partial R_x}{\partial T}\right) + L(T)\right) de . \tag{38}$$

In other words, the percent error in the measure[illegible] ifferential strain is

$$P_e = ((-R_x \, S_{R_{x_e}} \, L'(T)/(L \frac{\partial R_x}{\partial T})) \, 100\% \, . \tag{39}$$

$L'(T)/(L \frac{\partial R_x}{\partial T})$ may be found from Table 2, page 38, via Equations (1) and (30). Hence, P_e is given by

$$P_e = -S_{R_{x_e}} \, 10^{-4}\%/(\Delta R_x/R_x) \, , \tag{40}$$

where ΔR_x is the change in R_x corresponding to the temperature change necessary to cause a change in length of 1 ppm. Taking worst case conditions for Hastelloy F and 316 stainless steel, $\Delta R_x/R_x$ is 2.5×10^{-6} and 11.0×10^{-6}, respectively. Hence P_e lies between -60% and -80% for Hastelloy F and -14% and -18% for 316 stainless steel, both at 700 °C. Note, however, that this error is easily compensated. Typically, P_e will be much smaller. For instance, P_e will be between -2.4% and -3.2% for stainless steel at 150 °C.

Changes in the bulk resistivity of a specimen can also occur due to annealing and radiation damage. To find the error due to annealing, four cold worked 304 stainless steel samples were ohmically heated to temperatures of 415, 442, 490, and 660 °C for 24, 24, 1, and 1.25 hrs, respectively. The respective changes in resistance at 25 °C were -4.59%, -4.63%, -4.77%, and -4.40%. This indicates that most of the resistance annealing effects occur within the first few minutes of heating at the above test temperatures. Although radiation induced resistivity changes are approximately proportional to the fluence at low defect concentrations, the resistivity increase associated with an increase of point defects due to the irradiation is greatly reduced by annealing effects.

Furthermore, the resistivity change due to irradiation is very small for most metals, particularly at the high irradiation temperatures to be employed in this experiment.[28] Fortunately, the resistance changes due to nuclear irradiation and annealing during the creep test are expected to be small for the preirradiated specimens. It may be assumed that small changes in resistivity will amount to constant ΔR_x shifts in the resistance versus temperature curve (Mathieson's rule) as illustrated in Figure 8.[27,28,29] Hence, resistance drift may be compensated by periodically measuring R_x at a fixed temperature. A detailed discussion of the compensation technique employed in the ORNL experiment is given in the next section.

The additional temperature control error due to changes in sample resistivity can be found by including resistivity effects into Equation (36) as follows:

$$dR_x = \frac{\partial R_x}{\partial T} dT + \frac{\partial R_x}{\partial e} de + \frac{\partial R_x}{\partial \rho} d\rho = 0 \ , \tag{41}$$

where

$$\frac{\partial R_x}{\partial \rho} = \frac{L(T)}{A(T)} \tag{42}$$

and A(T) is the cross sectional area of the specimen. Hence the change in temperature due to resistivity drift is

$$dT = -\left(\frac{L(T)}{A(T)} d\rho\right) / \left(\frac{\partial R_x}{\partial T}\right) \ . \tag{43}$$

The dT given by the above equation may be added to that given by Equation (37) on page 40 to find the total temperature error.

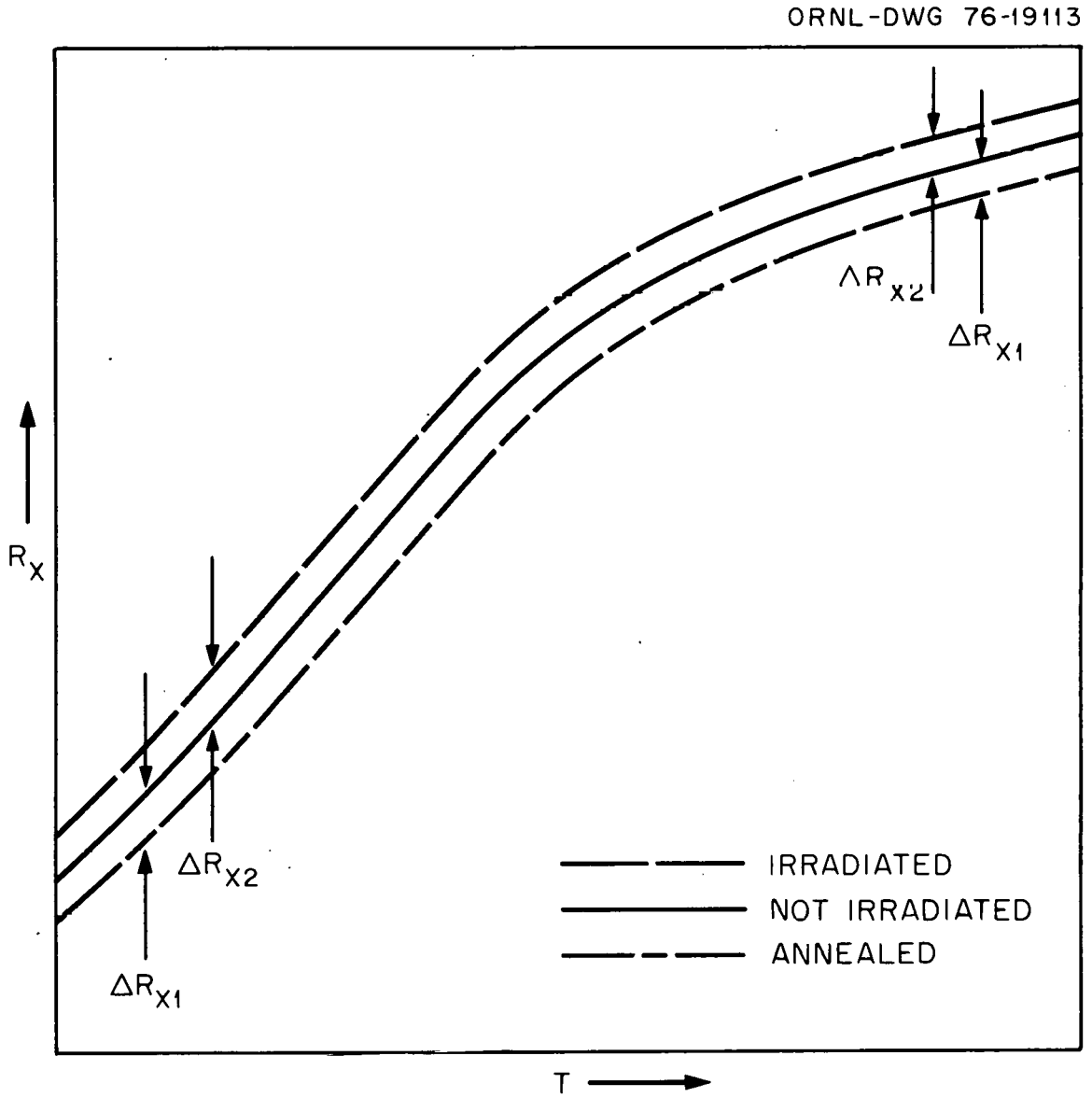

Figure 8. Effects of radiation or annealing on sample resistance.

Electrical shunting could also affect results. The impedance of the helium plasma would be in parallel with R_x. The effect of the plasma resistance is minimized by the low resistance of R_x. For 316 stainless steel at 700 °C, a 11 ppm drop in the measured resistance would be caused by an effective shunting resistance of 13 KΩ.

The type of plasma is dependent on beam current. Without beam, a one component plasma is formed by electrons thermionically emitted from the sample. The electron space charge forms a poor conductive path between the sample grips. An estimation of plasma resistance (R_p) can be easily obtained by modeling the sample grips as two parallel, flat, perfectly conducting surfaces as shown in Figure 9. The maximum current due to a one component plasma is given by the Langmuir-Child law as

$$I = -\frac{4\varepsilon}{9d^2}\left(\frac{2qV_o}{M_e}\right)^{1/2} A_o V_o \,, \quad 30^* \tag{44}$$

where ε is the permittivity of helium (8.85×10^{-12} F/m), A_o is the area of either plate in m^2, d is spacing between the plates in m, q is the magnitude of the electron charge (1.6×10^{-19}C), M_e is the electron mass (9.11×10^{-31} Kg), and V_o is the potential difference between the plates in V. Hence the minimum plasma resistance is

$$R_p = \frac{V_o}{I} = \frac{9\, d^2}{4\varepsilon\, A_o}\left(\frac{M_e}{2\, q\, V_o}\right)^{1/2} = 4.29 \times 10^5 \frac{d^2}{A_o V_o^{1/2}} \,. \tag{45}$$

If d is 2.5×10^{-2} m and A_o is 5.0×10^{-4} m^2, then R_p is

---

*Note that in Reference 30, Equation 44 is given in esu units, but it is given here in MKS units.

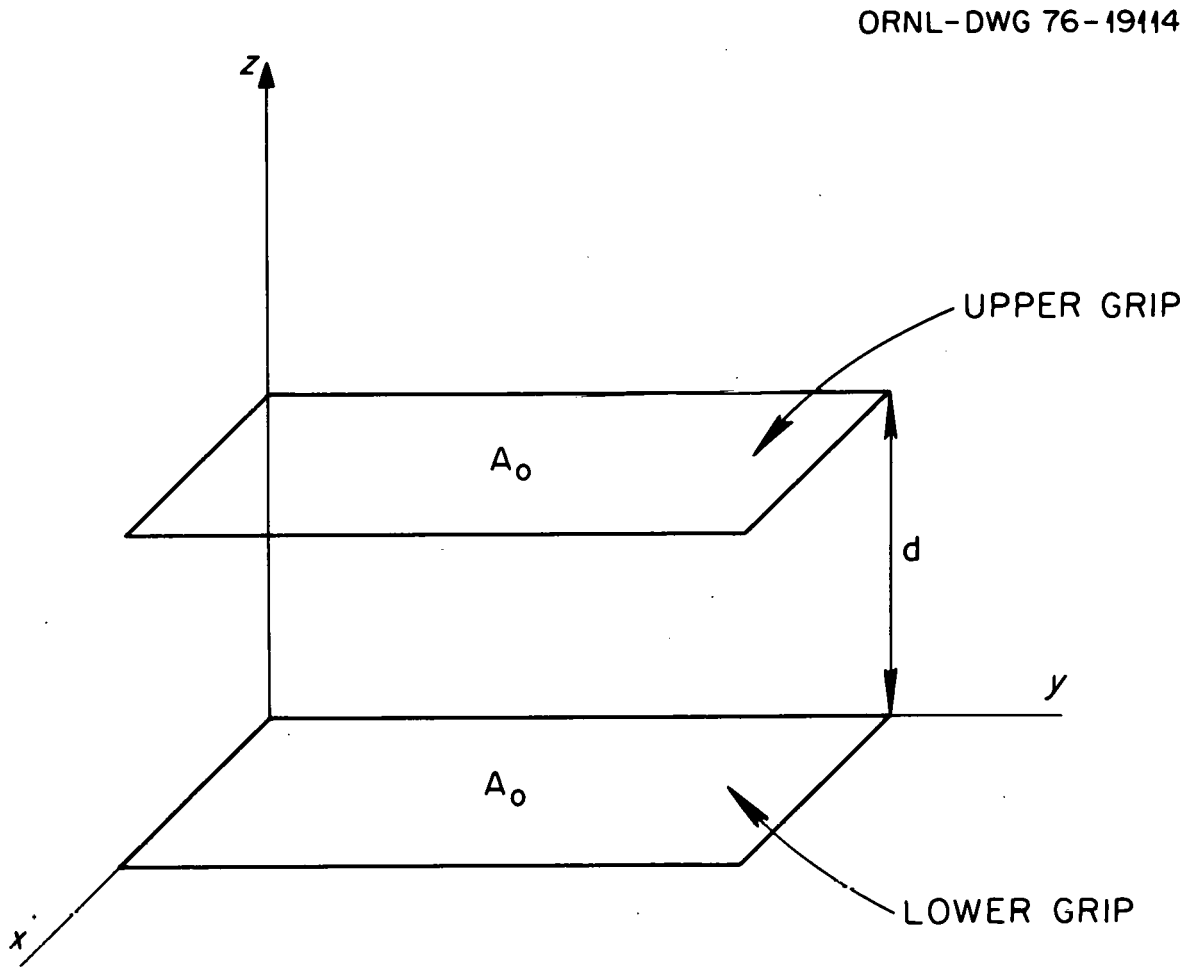

Figure 9. Simplified model of specimen grips used to estimate plasma resistance.

$5.36 \times 10^5/V_o^{1/2}$ Ω. Since V_o is always less than 2 V, R_p is much greater than 13 KΩ when the beam is off.

To calculate R_p due to ionization, the electron density (n) and the mobility of electrons in helium gas (μ_n) must be known. Neglecting the current due to helium ions, R_p is given by

$$R_p = \frac{d}{A_o\ q\ n\ \mu_n} = \frac{V_o}{A_o\ q\ n\ w}\ , \tag{46}$$

where w is the drift velocity of electrons in helium. If the gas pressure is 1 atmosphere at 300 °K, d is 2.5 cm, and V_o is 2 V, then w is 8×10^3 cm/sec.[31] If A_o is 5.0 cm^2, R_p is

$$R_p = 3 \times 10^{14}/n\ . \tag{47}$$

If the gas were completely ionized, R_p would be 6×10^{-6} Ω. Clearly, this is unacceptably low. Fortunately, R_p, as measured via the plasma sensor, is 1.5 MΩ when V_o is 50 v and beam current is 15 μA. (The plasma sensor, consisting of two plates as shown in Figure 1, page 5, and Figure 9, page 45, is employed to measure beam current.) Because of the large area of the plates (≈ 10 cm^2), the close spacing (≈ 1 cm), and the high voltage, 1.5 Mμ is a conservative estimate; therefore R_p should have a negligible effect on the measured value of R_x.

The sample temperature profile can also cause errors. Controlling the sample resistance will not necessarily eliminate thermal expansion errors, nor will control of the average sample temperature. Although sample resistance could be measured in small segments in a method similar to that for thermocouples (see page 23) or that suggested for pyrometers (see page 30), this is not necessary as long as the

temperature profile is fairly uniform. Reasons for having a uniform profile were discussed previously on page 15. Ideally, the equation for $R_x'(T)$ should be proportional to that for $L'(T)$ to enable perfect control of thermal expansion by resistance control; i.e.,

$$L'(T) \propto R_x'(T) \ . \tag{48}$$

From Table 2 on page 38, it is obvious that Equation (48) is not generally satisfied. For the metals in Table 2, the resistance control (ΔR_x) monotonically decreases as T increases. For small deviations from a flat temperature profile or for large deviations over a small portion of the gauge length, this decrease has negligible effect on the system error. For example, since the resistance of the sample is given by

$$R_x = \int_0^L \frac{\rho}{A_o} \, dZ \ , \tag{49}$$

assume a temperature profile as given in Figure 10(a). If the sample has uniform cross section, then

$$R_x = \frac{1}{A_o} \left(a_1\rho(T_1) + a_2\rho(T_2) + a_3\rho(T_3)\right) L_o \ , \tag{50}$$

where the sample temperature is T_1, T_2, and T_3 over sample lengths of $a_1 L_o$, $a_2 L_o$, and $a_3 L_o$, respectively, such that the sample gauge length is

$$L = L_o(a_1 + a_2 + a_2) \ . \tag{51}$$

If $\Delta\rho$ is the deviation of ρ from the mean value (ρ_o), and Δa is the deviation from that at the mean temperature (a_o), then

ORNL-DWG 76-19115

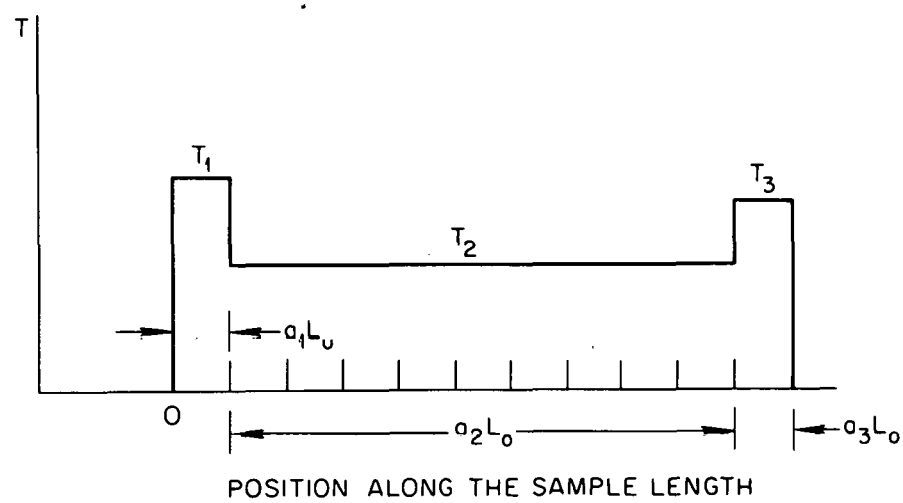

(a) Temperature profile along the gauge length (L_o) where $a_1 + a_2 + a_3 = 1$.

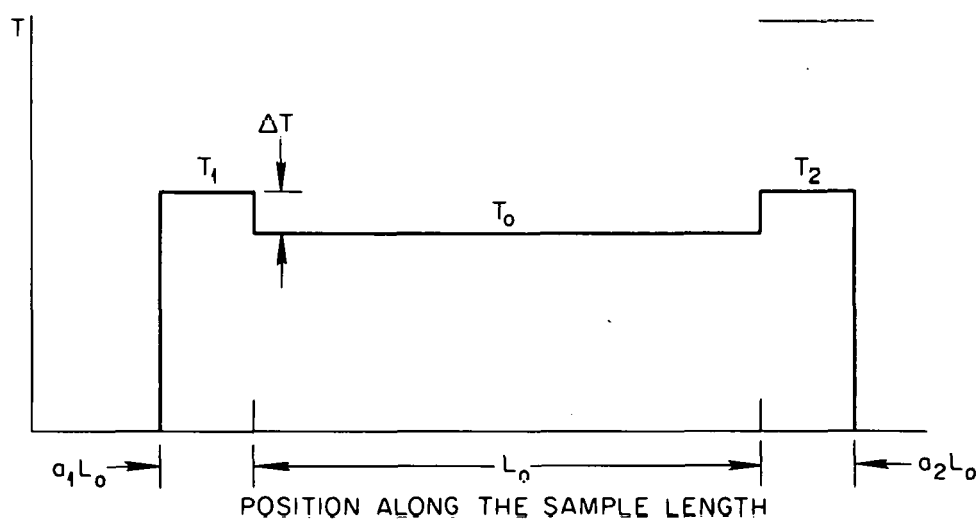

(b) Temperature profile between the grips, where L_o is the gauge length and $L_o(1 + a_1 + a_2)$ is the distance between the grips.

Figure 10. Sample temperature profile models.

$$R_x \simeq \frac{\rho_o}{A_o} L_o \left(1 + \frac{a_{o1}\Delta\rho_1 + a_{o2}\Delta\rho_2 + a_{o3}\Delta\rho_3}{\rho_o}\right) \tag{52}$$

and

$$L = L_o \left(1 + \Delta a_1 + \Delta a_2 + \Delta a_3\right) . \tag{53}$$

If a zirconium sample has $a_{o1} = a_{o3} = 0.1$ with

$$\frac{R_x(T)}{R_x(0)} = 1.0 + 4.084092 \times 10^{-3}\ T - 2.030671 \times 10^{-6}\ T^2 \tag{54}$$

and

$$\frac{L(T)}{L(0)} = 1.0 + 4.136880 \times 10^{-6}\ T + 2.803955 \times 10^{-5}\ T^2 , \tag{55}$$

where T is in °C, then it can be shown that R_x does not change if the temperature changes from a uniform 300 °C to $T_1 = T_3 = 325$ °C and $T_2 =$ 293.89 °C. However, this change in temperature profile will cause an increase in gauge length of only 1.1 ppm and an increase in the average sample temperature of only 0.11 °C. Since the temperature profile across the gauge length is expected to deviate no more than 6 °C from a uniform profile, and since zirconium is generally more sensitive to temperature profile than the other metals in Table 2, page 38, the error should be negligible.

Another source of error is the thermal expansion between the sample grips, but outside the gauge length over which the sample is irradiated and R_x is measured. Unfortunately, the sample length is measured at the grips (see Figures 1 and 2, pages 5 and 6) in the ORNL experiment. If the sample length outside the gauge length is 1/3 that of the gauge

length, if the thermal expansion coefficient of the specimen is 20 ppm/°C, and if the temperature profile is as shown in Figure 10(b), then a change in T_1 and T_3 with respect to T_2 of only 0.15 °C will cause a 1 ppm error in the measured gauge length. Several techniques can be employed to minimize this error.

1. The resistance can be measured beyond the gauge length.
2. Pyrometers can be employed to measure the temperature beyond the gauge length. The pyrometer outputs can then be used to control heating at the grips or beam wobbling to maintain uniform beam profile.
3. The length between the grips and the gauge length can be minimized, but only if the grips are heated.
4. Optical techniques could possibly be employed to measure the gauge length directly.

Finally, it should be mentioned that if R_x is employed to set operating temperature, it is important to know $R_x(T)$ accurately. Care should be exercised in using data on $\rho(T)$, i.e.,

$$R_x(T) - \rho(T)\ L(T)/A(T)\ . \tag{56}$$

See References 25, 32, 33, 34, and 35 for methods of measuring $R_x(T)$.

Temperature Measurement System Employed in the Experiment

From the preceding discussion, it is evident that no temperature system is perfect, but that resistance measurement offers the best potential accuracy. In addition, resistance measurement offers nearly instantaneous measurement of sample temperature. But resistance

measurement cannot easily measure temperature profiles. For this purpose, an infrared pyrometer will be utilized. Nisil/Nicrosil and/or type S thermocouples will be employed to measure temperature when beam current is zero and ohmic heating power is very small; i.e., when the sample temperature is near room temperature. Thermocouples will have excellent accuracy when the entire apparatus is at uniform equilibrium temperature. Under these conditions, the sample can be monitored for bulk resistivity changes. A bridge allowing compensation for bulk resistivity changes will be presented next.

CHAPTER III

RESISTANCE BRIDGES AND ERROR DETECTORS

I. BRIDGE TOPOLOGY

The first resistance bridge was developed by Sir Charles Wheatstone in 1843 and was based on ideals presented by S. H. Christie ten years earlier.[36] In the Wheatstone bridge shown in Figure 11(a), the error voltage (V_e) is zero (i.e., the bridge is balanced if

$$R_x = R_s \, R_A/R_B \; . \tag{57}$$

Unfortunately, the resistance of the wire, connecting R_x and R_s to the bridge, will effectively be added to either or both the standard resistor (R_s) and the sample resistance (R_x), thereby causing error. This can be particularly troublesome with low resistance standards and samples.

An improved bridge, known as the Kelvin double bridge, corrects for cable loss and is widely employed in platinum resistance thermometers.[25] As shown in Figure 11(b),

$$V_e = V_s - V_R \; , \tag{58}$$

where

$$V_s = \frac{\left[R_x + \dfrac{r_y \, (R_a + r_a)}{r_y + R_{ab}}\right] V_g}{R_x + R_s + r_y \| R_{ab}} \; , \tag{59}$$

$$V_R = \frac{(R_A + r_A) \, V_g}{R_{ab}} \; , \tag{60}$$

ORNL-DWG 76-19116

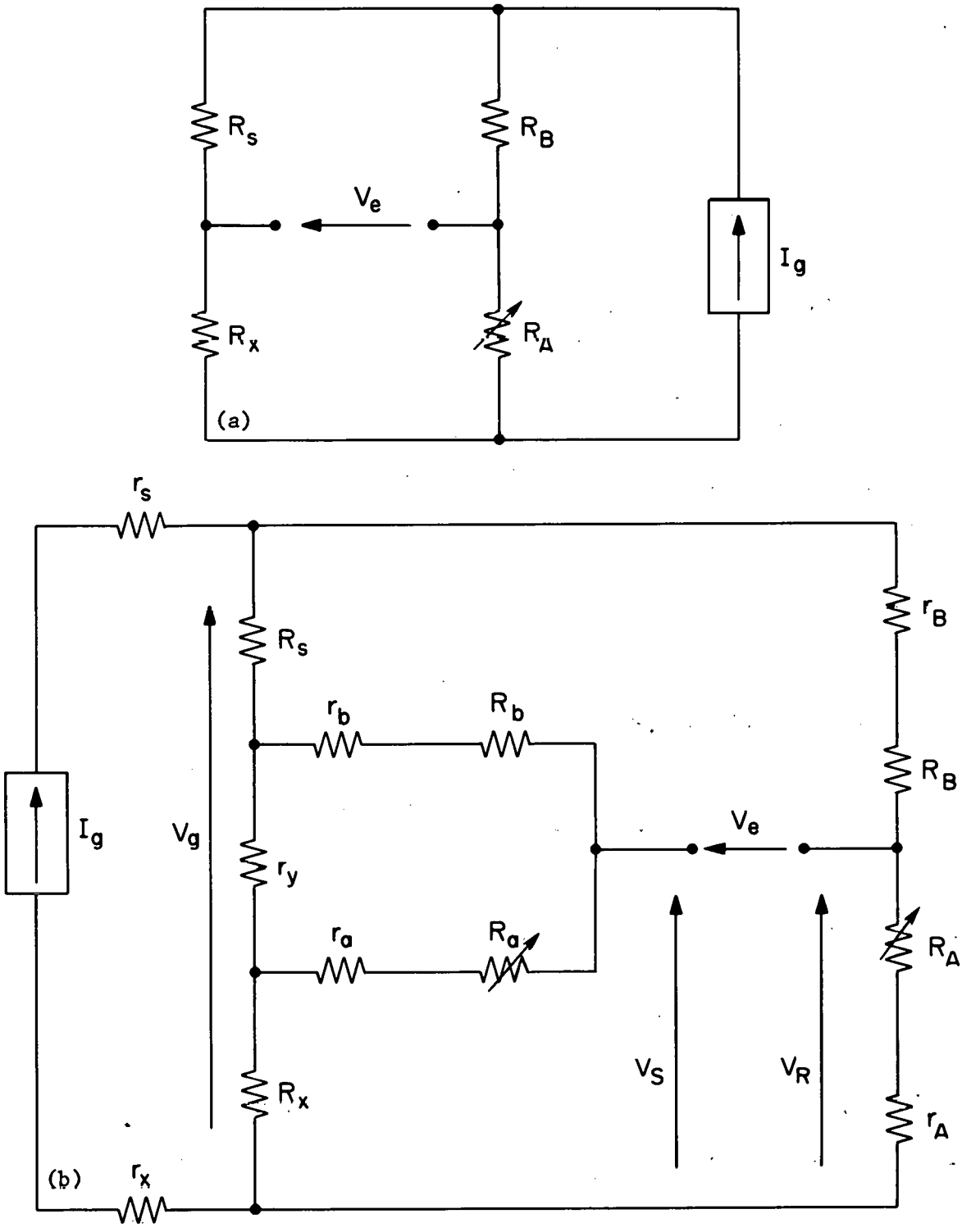

Figure 11. Circuit diagram of (a) Wheatstone and (b) Kelvin bridges.

$$V_g = I_g[(R_x + R_s + r_y||R_{ab})||R_{AB}] \ , \tag{61}$$

$$R_{ab} = R_a + R_b + r_a + r_b, \text{ and } R_{AB} = R_A + R_B + r_A + r_B \ .$$

If $R_{AB} >> R_x + R_s$ and $R_{ab} >> r_y$, Equation (61) becomes

$$V_g \simeq I_g(R_x + R_s + r_y) \ . \tag{62}$$

Plugging Equations (59) and (66) into Equation (58) gives

$$\frac{V_e}{V_g} = \frac{R_x(R_B+r_B)-R_s(R_A+r_A)+\dfrac{r_y[(R_a+r_a)(R_B+r_B)-(R_b+r_b)(R_A+r_A)]}{r_y + R_{AB}}}{(R_x+R_s+r_y||R_{ab})\ R_{AB}} \ . \tag{63}$$

Note that if

$$(R_a + r_a)(R_B + r_B) = (R_b + r_b)(R_A + r_A) \tag{64}$$

and if V_g is approximated by Equation (62), then Equation (63) becomes

$$V_e \simeq \frac{(R_x\ (R_B + r_B) - R_s\ (R_A + r_A))}{R_{AB}}\ I_g \ , \tag{65}$$

which indicates that the bridge balance condition given by

$$R_x = R_s\ (R_A + r_A)/(R_B + r_B) \tag{66}$$

is independent of r_y. Effects of r_B and r_a on bridge calibration are minimized by making $r_B << R_B$ and $r_A << R_A$, or by making $r_A/r_B = R_A/R_B$. Hence, the Kelvin double bridge is suitable for use in this experiment since it eliminates errors due to r_y.

Figure 12 shows the bridge developed for use in the ORNL radiation creep experiment. The bridge is essentially a Kelvin double bridge with some important special features. R_a is the series combination of a 2.5KΩ resistor and two precision potentiometers; COR1 (3.35KΩ) and CP1 (33.5KΩ). R_A is formed by the series combination of another 2.5KΩ resistor and two precision potentiometers: COR2 (3.35KΩ) and CP2 (33.5KΩ). R_b and R_B are both 25KΩ resistors. Note that the bridge can be balanced for two different values of R_x since CP1 and CP2 have two sliders each, either of which may be used to balance the bridge depending on the position of switch S2. Since the correction potentiometers COR1 and COR2 are in the bridge, regardless of S2, they may be employed to compensate for drift in the bulk resistivity of R_x in the following manner: With S2 in position M, the bridge is balanced at the start of the experiment with the sample at a carefully controlled ambient temperature (T_a). T_a can be measured with thermocouples attached to the sample. Then with S2 in position R, the bridge is set for balance at operating temperature without disturbing either correction potentiometer. Whenever a check on resistivity drift is desired, S2 is returned to position M and the sample temperature is set to T_a. Then the bridge is rebalanced, if necessary, by utilizing only the correction potentiometers. This automatically compensates the bridge for a fixed ΔR_x shift regardless of S2. This becomes obvious when Equation (66) is rewritten as follows:

$$R_x + \Delta R_x = \frac{R_s}{R_B + r_B} (R_{A_o} + R_{cp} + R_{cor} + \Delta R_{cor}) , \qquad (67)$$

where

ORNL-DWG 76-19117

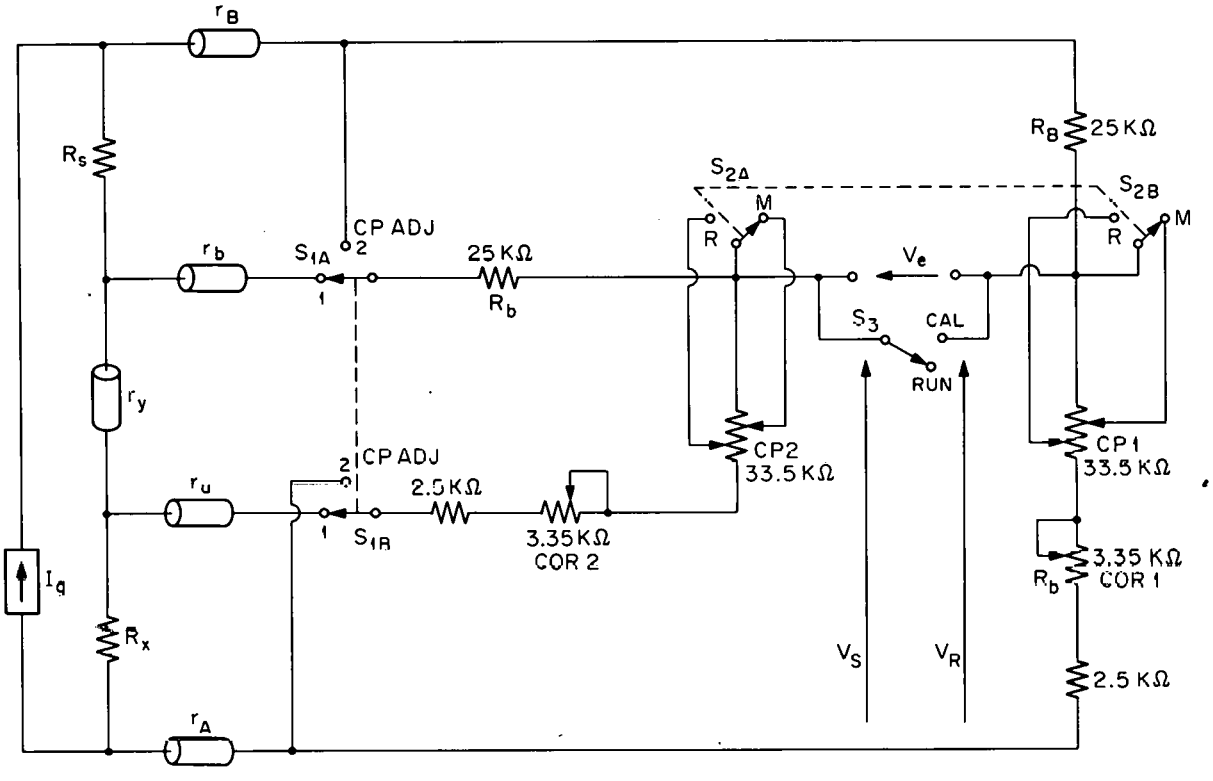

Figure 12. Circuit diagram of a Kelvin double bridge that allows two balance conditions for R_x and compensation for R_x drift.

$$\Delta R_x = \frac{R_3}{R_B + r_B} \Delta R_{cor} , \tag{68}$$

R_{cor} is the initial value of the correction pot resistance, ΔR_{cor} is the change in the correction pot resistance to correct for ΔR_x, and R_{cp} is the resistance of the CP1 pot corresponding to the initial sample resistance for either T_a or operating temperature. Equation (64) is satisfied by adjusting CP2 and COR2 to balance the bridge when S1 is in position CP2 adj. With S1 in this position, R_A acts as a sample resistor and R_B as a standard resistor in a Wheatstone bridge. Since r_b, r_a, and R_b are set equal to r_B, r_A and R_B, respectively, both Equations (64) and (57) are satisfied by setting $R_a = R_A$.

II. AC/DC BRIDGE CONSIDERATIONS

The frequency of the measurement current (I_g) is an important consideration. There are two reasons why a DC measurement and heating current should not be employed in the Oak Ridge experiment. First, a DC current will preclude the use of thermocouples on the sample since the DC voltage across the thermocouple wires due to the DC current can not be readily distinguished from the thermoelectric potential difference; i.e., the emf induced into the thermocouple by a DC heating current can be orders of magnitude higher than the thermoelectric emf (see page 23). Secondly, to cancel errors due to thermoelectric voltages, two balances must be made with opposite polarities of I_g. In other words, a single polarity measurement current should not be employed.

The frequency of I_g must be chosen with care. A low frequency I_g will adversely affect the response time of the control system; i.e., a

10 Hz I_g will allow only ten temperature measurements per sec or, equivalently, a system response time much longer than 100 msec. Moreover, a high frequency I_g can cause errors due to stray reactances. For this reason, only a sinusoidal I_g should be employed in resistance bridges. Thermal expansion determines the lower frequency limit. Since the increase in temperature due to ohmic heating is approximately proportional to the mean-square current times the sample resistance, the temperature ripple is determined by the frequency and the sample thermal time constant (T_t). Duncan et al.[23] have shown that the output of a mean-square circuit with single pole averaging is given by

$$T - T_o = \frac{H_t R_x I_o^2}{2} \left(1 + \frac{\cos(2\omega_1 t + \theta)}{(1 + (2\omega_1 T_t)^2)^{1/2}}\right) , \qquad (69)$$

where

$$\theta = \tan^{-1}(-2\omega_1 T_t) ,$$

the current through the sample is

$$I(t) = I_o \sin\omega_1 t ,$$

H_t is the DC value of the thermal transfer function, and is a function of the mean specimen temperature, T_o is the sample temperature without ohmic heating, and the frequency is sufficiently high so that R_x is constant; i.e., the temperature ripple is small.[23] The temperature ripple is given by

$$T(t) = \frac{H_t R_x I_o^2 \cos(2\omega_1 t + \theta)}{2\,(1 + (2\omega_1 T_t)^2)^{1/2}} , \qquad (69)$$

while the average temperature is given by

$$\overline{T} = \frac{H_t R_x I_o^2}{2} + T_o \ . \tag{70}$$

To analyze the effect of this temperature ripple, the effective moving mass attached to the sample (the mass of the lower pullrod and grip), the compliance of the spring attached to the lower pullrod, and the compliance of the sample must be considered. A simplified equivalent mechanical system and its electrical analog circuit are shown in Figure 13. (For information on electrical analogs, see References 37 and 38.) $\dot{X}_o$ is the rate of change in length of the sample due to temperature ripple if sample were perfectly rigid, $\dot{X}_1$ is the actual rate of change in length of the sample assuming the upper pullrod is stationary, M is the moving mass of the lower pullrod, K_1 is the compliance of the spring attached to the lower pullrod, and K_2 is the compliance of the sample. In the equivalent electrical circuit, voltage, current, inductance, and capacitance represent force, velocity, mass, and compliance, respectively. Hence the AC analysis yields

$$\dot{X}_1 = I_1 = I_o \ C_1 / [(C_1 + C_2)(1 - \frac{LC_1C_2\omega^2}{C_1 + C_2})] \tag{71}$$

and

$$F_2 = V_2 = \frac{I_o(1 - LC_1\omega^2)}{(1 - \frac{LC_1C_2\omega^2}{C_1 + C_2})(C_1 + C_2)j\omega} \tag{72}$$

where $\omega = 2\omega_1$, the sample's compliance is given by

$$K_2 = C_2 = L_o/(A_oE) \ , \tag{73}$$

ORNL-DWG 76-19118

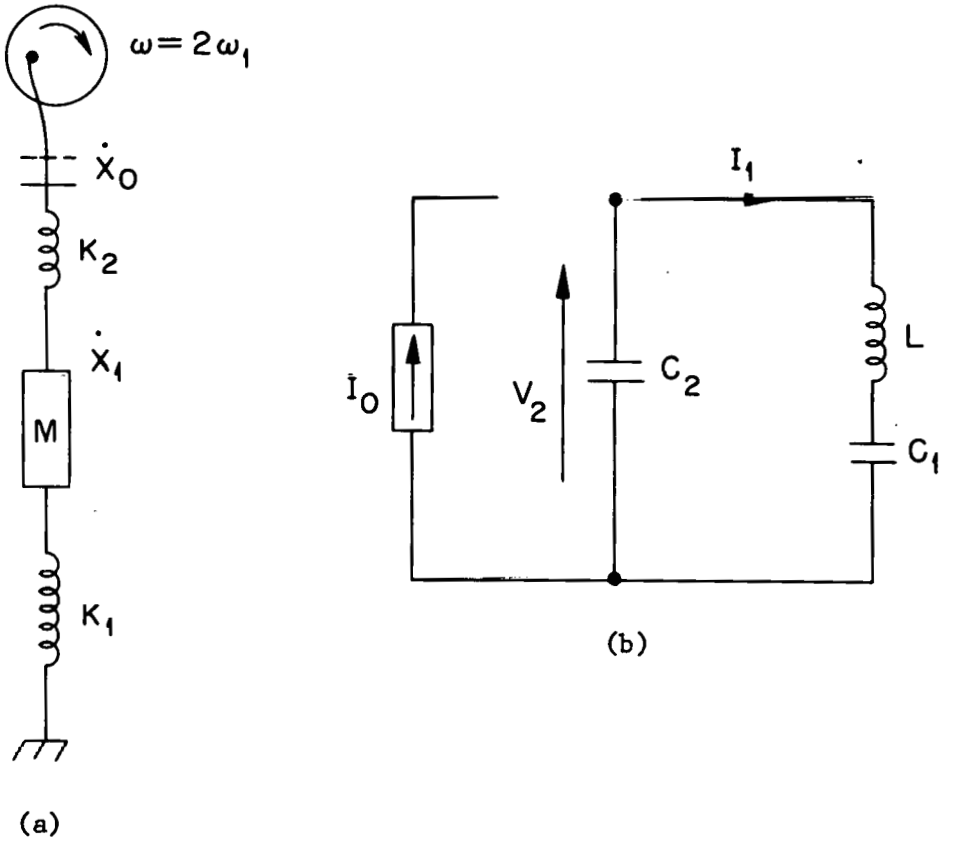

Figure 13. The mechanical system and the AC electric analog of the spring, pullrod, and sample.

E is the specimen's Young's modulus, L_o is the distance between the grips, and A_o is the sample cross sectional area. Since $C_2 << C_1$, Equations (71) and (72) reduce to

$$I_1 \simeq I_o/(1 - L\ C_2\ 4\omega_1^{\ 2}) \tag{74}$$

and

$$V_1 \simeq I_o\ jL\ 2\omega_1/(1 - L\ C_2\ 4\omega_1^{\ 2})\ . \tag{75}$$

By rewriting Equations (74) and (75) in terms of their mechanical counterparts, using the fact that the peak value of $\dot{x}$ is $X_{1p}2\omega_1$, $\sigma = F/A_o$, and $X_{op} = L_o\ \alpha_t\ T_p(\omega)$, one obtains

$$X_{1p} \simeq \frac{L_o \alpha_t H_t R_x I_o^{\ 2} \underline{/\theta}}{2(1 + (2\omega_1\ T_t)^2)^{1/2}(1 - M\ K_2\ (2\omega_1)^2)} \tag{76}$$

and

$$\sigma_{2p} \simeq \frac{L_o \alpha_t H_t R_x I_o^{\ 2}(1 - M\ K_1(2\omega_1)^2)\underline{/\theta}}{2(1 + (2\omega_1 T_t)^2)^{1/2}(1 - M\ K_2\ (2\omega_1)^2)A_o\ K_1} \tag{77}$$

where α_t is coefficient of thermal expansion of the specimen. Note that Equations (76) and (77) indicate if the radian frequency of I_g is close to $(4MK_2)^{-1/2}$, very large AC fluctuations in sample length and stress could result. Not only would this make strain measurement difficult, but also sample fracture would be likely. Since M is approximately 1.5 Kg and K_2 ranges from 0.47 to 2.4 μm/Nt for the five metals in Tables 1 and 2 on pages 11 and 38, respectively, with L_o = 2.5 cm, A_o ranging from 0.15 to 0.26 sq mm, and E ranging from 60 to 210 GNt/sq m, the resonant frequency ranges from 40 to 95 Hz. If α_t = 20 ppm/°C, $\overline{T}$ is 700 °C, T_o is

150 °C, T_t is 0.4 sec, and the resonant frequency is 95 Hz, then the minimum frequency of I_g for less than 250 Å peak length ripple is given by Equation (76) as approximately 270 Hz. If A_o is 0.15 sq mm and K_1 is 70 μm/Nt, the minimum frequency for less than 35 M Nt/sq m peak stress ripple is given by Equation (77) as 130 Hz. Hence, the lower frequency limit determined by the strain ripple is 270 Hz.

Another resonant mode is that of transverse vibration of the sample. If the sample is assumed perfectly elastic and the pullrods stationary, the resonant frequencies are determined by the tension ($A_o\sigma$), and the line density of the specimen ($A_o\rho$) as

$$f_n = \frac{n}{2L_o} \left(\frac{A_o\sigma}{A_o\rho}\right)^{1/2} = \frac{n}{2L_o} \left(\frac{\sigma}{\rho}\right)^{1/2} . \tag{78}$$

If the maximum density of the five metals in Table 2 on page 38 is 8902 Kg/m^3, and L_o is 2.5 cm, and A_o is 0.15 mm^2, then the mimimum resonant frequency is

$$f_1 = 212\sigma^{1/2} \text{ Hz}/(\text{MNt/m}^2)^{1/2} . \tag{79}$$

For an expected minimum applied stress of 35 MNt/m^2, the upper limit on frequency is 1.3 KHz. The severity of this resonant mode is minimized by the fact that the primary means of excitation by the heating current is via the magnetic field caused by the current flow. Because there are no close ferromagnetic materials to the sample, the magnetic force on the sample is small. Moreover, no vibration problems have been observed in an experimental mockup with a 1 KHz heating current frequency. A frequency of 1 KHz was chosen due to noise considerations: it is far

enough from the 1.92 KHz noise due to the capacitance extensometers and the 360 Hz noise of the cyclotron environment to allow filtering of these noise frequencies from the 1 KHz signal. The effects of stray reactances on system accuracy will be discussed in greater detail next.

III. BRIDGE DETECTORS

Conventional Phase-Sensitive Detectors

To utilize a bridge in a control system, a DC signal must be derived so that the signal is zero if the bridge is balanced, one polarity if R_x is larger than balance value, and the opposite polarity if R_x is below balance value. Usually, this is accomplished with a phase-sensitive detector (PSD) as shown in Figure 14. PSD's operate on the principal that the DC component of the product of two sinusoids at the same frequency is proportional to the product of their amplitudes and the cosine of their phase difference; i.e.,

$$v_{psd}(t) = V_e V_d \sin(\omega_o t + \theta_e) \sin(\omega_o t + \theta_d)$$

$$v_{psd}(t) = \frac{V_e V_d}{2} (\cos(\theta_e - \theta_d) - \cos(2\omega_o t + \theta_e + \theta_d)) \quad (80)$$

[22,39]

The double frequency component can easily be suppressed with a lowpass filter or an integrator. When $v_e(t)$ is in phase with $v_g(t)$, $V_{psd} = V_e V_d/2$, but when they are out of phase, $V_{psd} = -V_e V_d/2$. When V_e is zero, so is V_{psd}, regardless of the relative phase. This means that a small relative phase shift will not affect the balance condition if $V_e = 0$. Unfortunately, V_e will usually not be zero due to stray reactances in the bridge. For instance, if Equations (59) and (60) are rewritten in terms of impedances

ORNL-DWG 76-19119

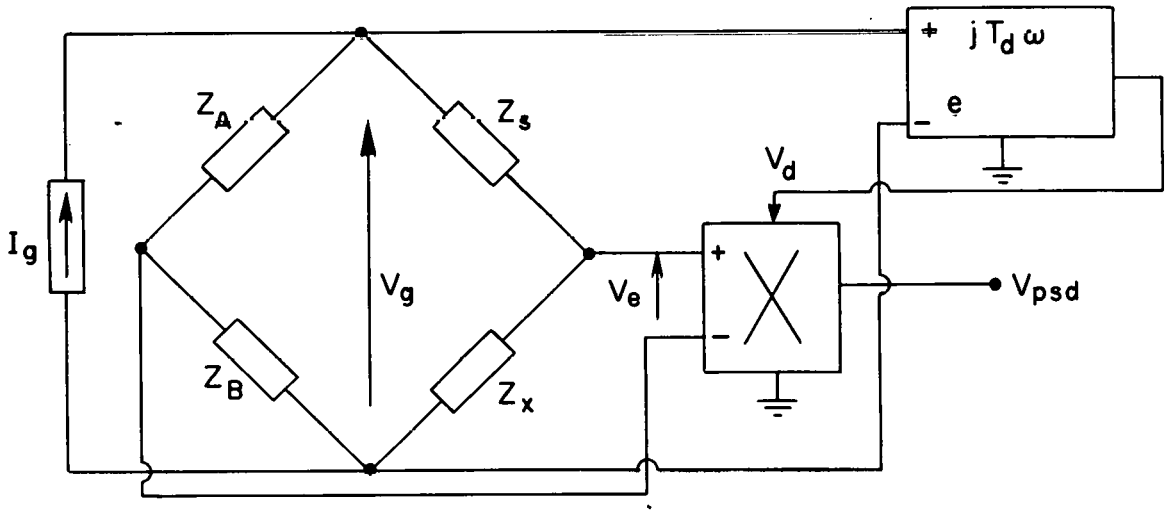

Figure 14. Phase-sensitive detector.

having nonzero reactances, then phase shifts may result as follows:

$$V_s = V_g\ A_s(\omega_o)\underline{/\theta_s} = V_g\ (\mathrm{Re}\ A_s(\omega_o) + j\ \mathrm{Im}\ A_s(\omega_o)) \tag{81}$$

and

$$V_R = V_g\ A_R(\omega_o)\underline{/\theta_R} = V_g\ (\mathrm{Re}\ A_R(\omega_o) + j\ \mathrm{Im}\ A_R(\omega_o))\ . \tag{82}$$

Thus V_e becomes

$$V_e = V_g\ (\mathrm{Re}\ (A_s(\omega_o) - A_R(\omega_o)) + j\ \mathrm{Im}(A_s(\omega_o) - A_R(\omega_o)))\ . \tag{83}$$

If the phase shifts are very small, then the bridge is approximately balanced when $\mathrm{Re}(A_s(\omega_o)) = \mathrm{Re}(A_R(\omega_o))$. Thus, V_e is

$$V_e = jV_g\mathrm{Im}(A_s(\omega_o) - A_R(\omega_o))\ . \tag{84}$$

But a phase-sensitive detector will indicate balance if and only if $\cos(\theta_e - \theta_d) = 0$. Hence, θ_d is very critical for proper balance. Furthermore, the proper value for θ_d will change significantly for different values of R_x. Substantial phase shifts will be introduced by the 30 m cables in the bridge.

It should be mentioned that techniques can be employed to compensate automatically for phase shift error. One technique, shown in Figure 15(a) largely stabilizes phase shift dependence in R_x by keeping the ratio of R_s:R_x constant. In this method, R_A and R_B are fixed, and R_s is the potentiometer employed to balance the bridge.[40] Unfortunately, this technique would be prohibitively costly because of the very low values of R_x. While this technique is normally employed with R_x's in the tens of kiloohm range, R_x in this experiment can be less than 10 mΩ. This

ORNL-DWG 76-19120

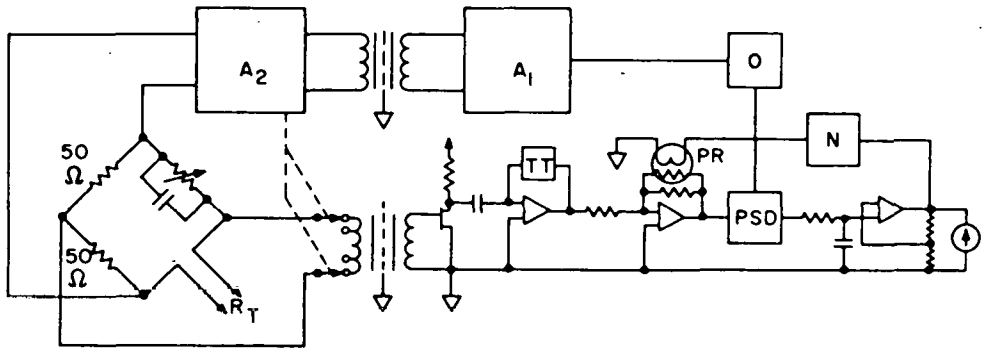

(a) RC phase shift compensation where O is the oscillator, A_1 and A_2 are attenuators, R_T is the specimen resistance, TT is a twin tee filter in the feedback path of an opamp to form a band-pass filter, PR is a photo resistor acting as a voltage controlled amplifier, PSD is the phase-sensitive detector, and N is the frequency compensation.

Source: W. Weyhman, "Thermometry at Ultralow Temperatures," in Methods of Experimental Physics: Solid State Physics, eds. L. Marton and R. V. Coleman (New York: Academic Press, 1974), p. 500.

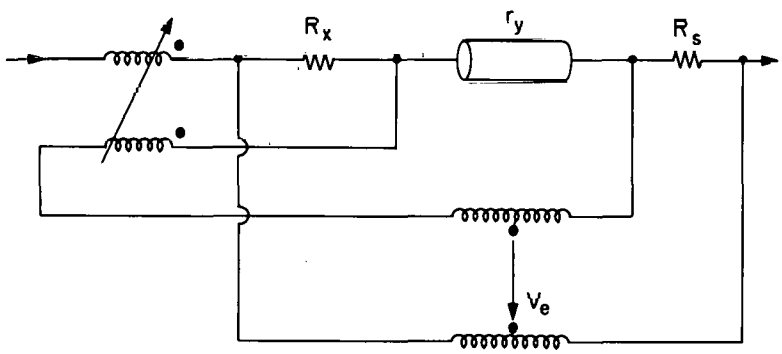

(b) Inductive phase compensation.

Source: J. J. Hill, "Platinum-Resistance Thermometry Using an AC Inductive Ratio Bridge," ISA Trans., Vol. 7, p. 105, 1968.

Figure 15. Manual phase compensation techniques for phase-sensitive detector.

causes two problems: for equivalent voltages the power dissipation in R_x and R_s is greatly increased, and due to contact resistance problems, potentiometers accurate to 0.4 μΩ (as required by Hastelloy F specimens) would be very bulky and expensive. Inductive phase shift compensation has been employed in platinum resistance thermometers (25 ohms at 25 °C) as shown in Figure 15(b).[25] An automatic quadrature detector can be added to PSD's as pictured in Figure 16. However, alignment of the compensator is critical.[41]

Despite the severe phase problem, PSD's have excellent noise rejection properties. If the noise component of the error signal is n(t), then the output of the PSD is

$$v_{psd}(t) = \frac{V_e V_d}{2} (\cos(\theta_e - \theta_d) - \cos(2\omega_o t + \theta_e + \theta_d))$$

$$+ V_d\, n(t) \cos(\omega_o t + \theta_d) \ . \qquad (85)$$

Hence, a PSD acts as a DSBSC (double sideband, suppressed carrier) AM modulator in which the modulating signal is $v_e(t) + n(t)$. Therefore, the noise power spectral density ($N(\omega)$) is translated in frequency space by $\pm\omega_o$; i.e., the modulated noise power spectral density is

$$N_{psd}(\omega) = \frac{V_d^2}{2} (N(\omega - \omega_o) + N(\omega + \omega_o)) \ .^{22} \qquad (86)$$

The implication of this is that the noise can be suppressed if a band-pass filter centered about ω_o with a bandwidth less than half that of the low pass filter is employed to filter $v_e(t)$ as illustrated in Figure 14 on page 64.

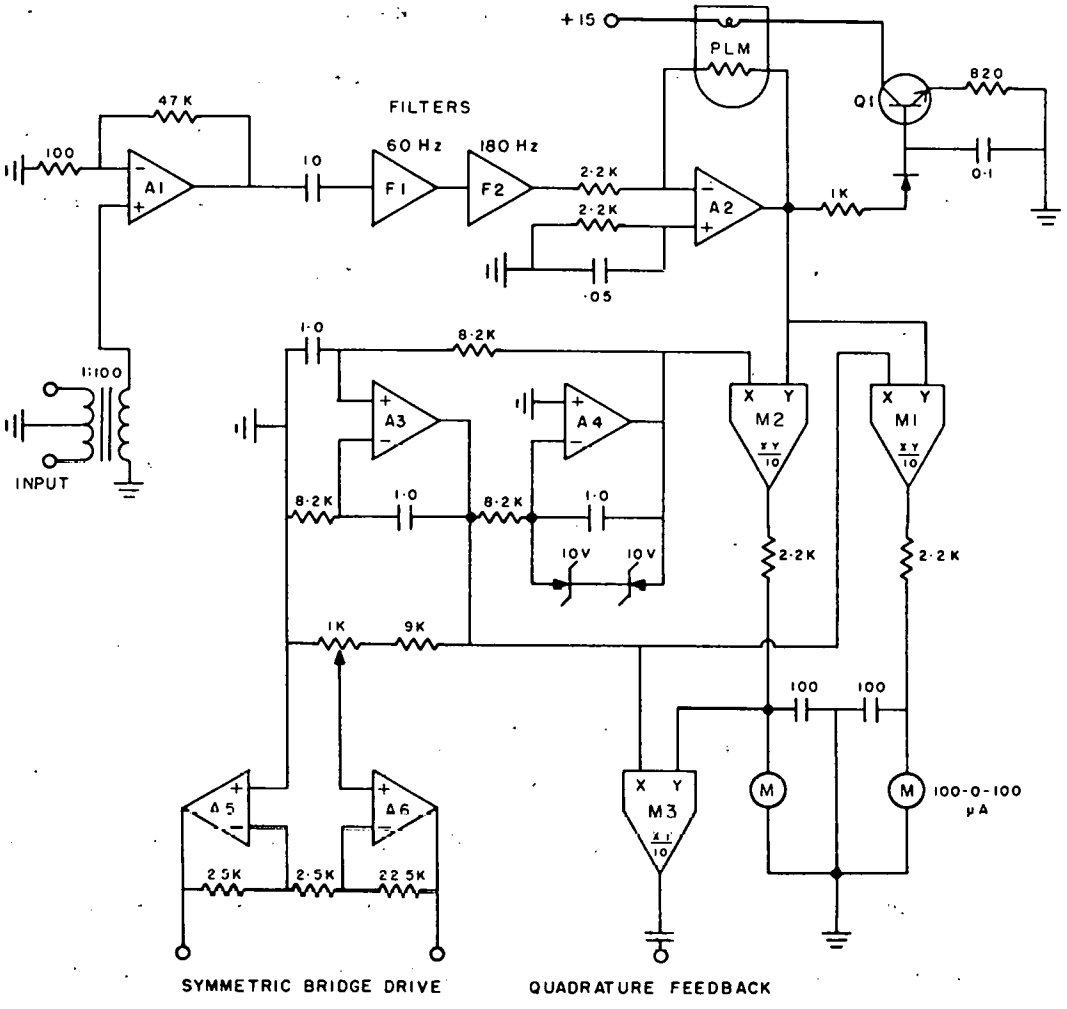

Figure 16. A phase-sensitive detector with quadrature detection.

Source: C. G. Kirby, "The Use of Operational Amplifiers to Generate Precise Current Ratios for Platinum Resistance Thermometry," in Temperature, Its Measurement and Control in Science and Industry, ed. H. H. Plumb (Pittsburg: Instrument Society of America, 1972), p. 1518.

Another approach used to suppress noise in PSD's is to integrate rather than filter $v_{psd}(t)$. This technique makes use of the orthogonal properties of sinusoids; that is to say, frequency components of $v_e(t)$ will yield stationary outputs if they are equal to those of $v_d(t)$. Thus, the output of a PSD is given by

$$V_{psd} = \frac{V_e V_d}{T} \int_t^{t+T} \sin(\omega_e t + \theta_e) \sin(\omega_d t + \theta_d) dt$$

$$V_{psd} = \left. \frac{V_e V_d \sin((\omega_e + \omega_d)t + \theta_e + \theta_d)}{T\ (\omega_e + \omega_d)} \right|_t^{t+T} \tag{85}$$

$$+ \left. \frac{V_e V_d \sin((\omega_e - \omega_d)t + \theta_e - \theta_d)}{T\ (\omega_e - \omega_d)} \right|_t^{t+T} ;$$

therefore,

$$\lim_{T\to\infty} V_{psd} = \begin{cases} \frac{V_e V_d}{2} \cos(\theta_e - \theta_d), & \text{if } \omega_e = \omega_d \\ 0, & \text{if } \omega_e \neq \omega_d \end{cases} . \tag{86}$$

Thus, noise rejection is excellent if the averaging time is much longer than the period of waveform. A potential problem with PSD's is that distortion in V_g or distortion due to the practical multipliers can cause a PSD to lock onto harmonics of the waveform. Hence, filtering is normally employed to insure that the noise components at the harmonics are much less than the fundamental signal.[40,41,42]

Another fundamental limitation of PSD's is the accuracy of the multipliers. Circuits employed in multipliers and their limitations are discussed in Reference 43. Typical four-quadrant multipliers have low

frequency errors of about 1% full scale including feedthrough and nonlinearity, although an order of magnitude better accuracy can be obtained with multipliers operating on the pulse modulation principle. Unfortunately, vector errors typically reach 0.5° for frequencies above a few kilohertz, and pulse type multipliers have much poorer performance. Moreover, multipliers are generally very noisy devices: typical noise level is approximately 500 μV with state-of-the-art devices achieving 50 μV rms noise over a noise bandwidth of 5 Hz to 10 KHz. Thus, for 1 KHz operation the error signal must be greatly amplified, and phase errors in the bridge must be minimized to make the performance of PSD's acceptable. To ensure a large input signal to the multiplier, an AGC amplifier is normally placed ahead of the multiplier as pictured in Figures 15 and 16 on pages 66 and 68, respectively. However, this necessitates the use of a tracking expander following the PSD to ensure stability of the control system. Expanders and AGC amplifiers are discussed in great detail by Duncan et al.[22,23]

Phase-Insensitive Detector

A thorough literature search revealed that PSD's were always employed to detect V_e in AC resistance bridges. However, a technique for measuring V_e that is independent of phase shift introduced by stray reactances in the bridge, would be highly desirable. A sum or difference of two AC signals independent of their phase or frequency is accomplished by first converting them to equivalent DC signals before addition or subtraction.[23] Hence, instead of detecting V_e directly, V_R and V_s are detected separately and are each converted to a DC signal by either average-magnitude, peak or rms detection as illustrated in Figure 17.

ORNL-DWG 76-19121

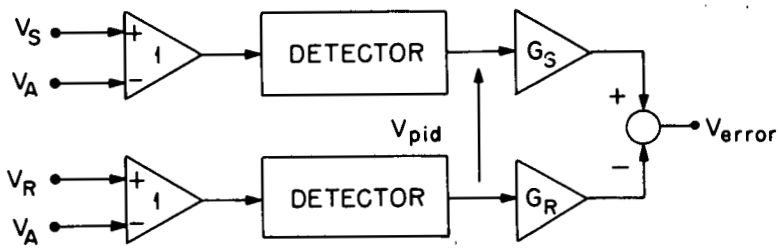

(a) Phase-insensitive bridge detector.

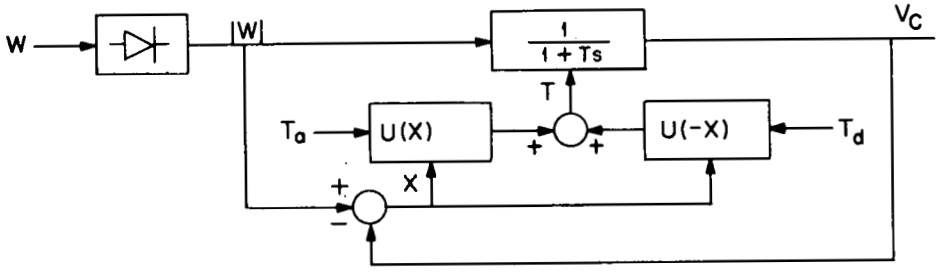

(b) Peak detector.

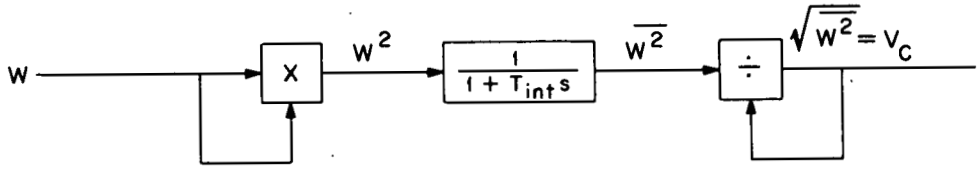

(c) RMS detector.

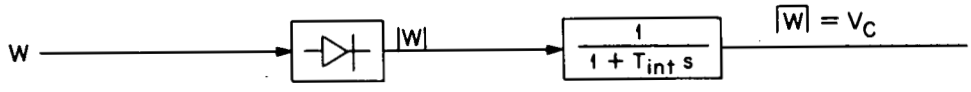

(d) Average magnitude detector.

Figure 17. Three types of detectors for use in a phase-insensitive bridge detector.

Source [parts (b), (c), and (d)]: M. G. Duncan, D. Rosenberg, and G. W. Hoffman, "Design Criteria of a Universal Compandor for the Elimination of Audible Noise in Tape, Disc, and Broadcast Systems," Jour. Aud. Eng. Soc., Vol. 23, p. 614, Oct. 1975.

The importance of phase insensitivity is illustrated by effects of cable and detector input capacitance on the bridge employed in the ORNL experiment. In Figure 18, the four 30 m cables connecting nodes 1 through 4 to 1' through 4', respectively, are modeled as 1Ω resistors shunted to ground by capacitors. The capacitances shown in Figure 18 are based on a cable capacitance of 66 pf/m and amplifier input capacitances of 20 pf. In Appendix B, equations were derived for V_s, V_R, and V_A in terms of V_{cm} and V_g. Taking component values as shown in Figure 18 with the frequency of V_d and V_{cm} of 1 KHz, V_s, V_R and V_A are given as follows:

$$V_s = V_{cm}(0.999990086 - j3.15572 \times 10^{-3}$$

$$- V_g(0.166664997 - j5.25.951 \times 10^{-4}) \ , \qquad (87)$$

$$V_R = V_{cm}(0.999982401 - j4.20145 \times 10^{-3})$$

$$- V_g(0.166663734 - j7.00242 \times 10^{-4}) \ , \qquad (88)$$

and

$$V_A = V_{cm}(0.999999999 - j1.2902 \times 10^{-5}$$

$$- V_g(0.499973334 - j6.338 \times 10^{-6}) \ . \qquad (89)$$

Since the values of $\bar{R}_A$ and $\bar{R}_a$ where determined from Equations (65) and (66) on page 54, the bridge will be perfectly balanced at DC. Hence, any errors are due to reactances in the bridge. For the phase-sensitive detector, V_e is given by

ORNL-DWG 76-19122

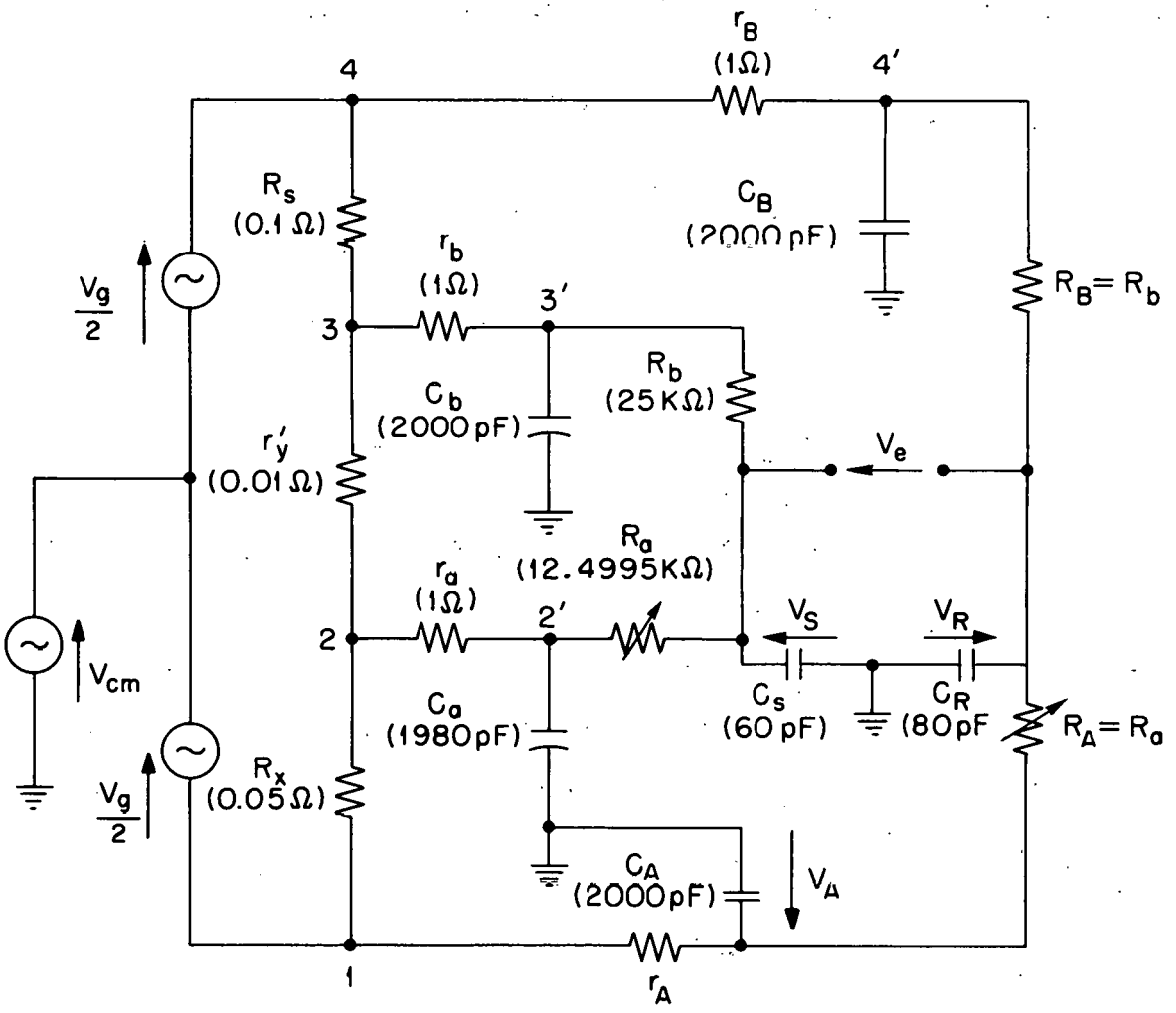

Figure 18. Kelvin bridge circuit used to calculate the error due to stray capacitances.

$$V_e = V_s - V_R = V_{cm}(7.6849 \times 10^{-6} + j1.045727 \times 10^{-3})$$

$$- V_g(1.2634 \times 10^{-6} + j1.74290 \times 10^{-4}) \ , \qquad (90)$$

while for a phase-insensitive detector, the error voltage is

$$V_{pid} = |V_S - V_A| - |V_R - V_A|$$

$$= |-V_{cm}(9.913 \times 10^{-6} + j3.142822 \times 10^{-3})$$

$$+ V_g(0.333308337 + j5.32289 \times 10^{-4})|$$

$$- |-V_{cm}(1.7598 \times 10^{-5} + j4.188548 \times 10^{-3})$$

$$+ V_g(0.333309601 + j7.06580 \times 10^{-4})| \ . \qquad (91)$$

Specific values for V_g, V_d, and V_{cm} may be used to clarify the difference in performance between PSD's and PID's. For example, if $V_{cm} = 0$, $V_d = 2$, and $\theta_g = 0$, then the filtered output of the PSD as given by Equation (80) on page 63 is

$$V_{psd} = -V_g \ 1.74295 \times 10^{-4} \cos 89.5847° = -1.263 \times 10^{-6} \ V_g \ ,$$

while V_{pid} is given by Equation (91) as

$$V_{pid} = -1.588 \times 10^{-6} \ V_g \ .$$

The apparent deviation of R_x from set point (R_{xs}) is given by Equations (62), (65), and (66) on page 54 as

$$\frac{\Delta R_x}{R_{xs}} = \frac{V_e(R_{xs} + R_s)(R_x + R_s + r_y)}{V_g \ R_{xs} R_s} = 4.8 \ \frac{V_e}{V_g} \ . \qquad (92)$$

Thus, the error in R_x is -6.064 and -7.622 ppm for PSD and PID, respectively. For R_x to be accurate to 7.622 ppm, θ_d must be between -0.9373° and 0.1067°. However, results are dependent on V_{cm}. For instance,

$$V_{psd} = +V_g \; 3.48583 \times 10^{-4} \cos(89.5761°) = +2.579 \times 10^{-6} \; V_g$$

and

$$V_{pid} = 1.310 \times 10^{-6} \; V_g$$

for $V_{cm} = V_g/2$, while for $V_{cm} = -V_g/2$

$$V_{psd} = -V_g \; 6.97172 \times 10^{-4} \cos 89.5804° = -5.106 \times 10^{-6} \; V_g$$

$$V_{pid} = -10.235 \times 10^{-6} \; V_g \; .$$

To make the accuracy of R_x as measured by a PSD equal to that measured by a PID, θ_d must lie between -0.6306° and -0.2000° for $V_{cm} = V_g/2$ and -1.2608° and 0.4216°. While this phase accuracy is not impossible to obtain, the calibration of θ_d is somewhat complex. However, calibration of PID's is very simple.

The fundamental calibrations for PID's are gain matching between the two AC/DC converters and DC offset. Calibration is readily accomplished in situ by throwing switch S_3, in Figure 12 on page 56, to position cal. This forces V_e to be zero; hence, V_{error} should also be zero when the PID is perfectly calibrated. Hence, gain matching is easily obtained by adjusting for zero V_{error} with a large V_g, while DC offset is easily adjusted by setting V_{error} to zero with a zero or small V_g.

However, since PID gains must be matched, linearity of the AC to DC converters is of the utmost importance. The effect of gain mismatching is illustrated by the following equation:

$$V_{error} = |V_s - V_A|\, G_s - |V_R - V_A|\, G_R$$

or if the bridge is balanced, (93)

$$V_{error} = |V_s - V_A|\, G_s \frac{\Delta G_s}{G_s} = \frac{R_A\, G_s\, (\Delta G_s/G_s)\, V_g}{R_A + R_B + r_A + r_B},$$

where $\frac{\Delta G_s 100\%}{G_s} = \frac{(G_s - G_R)100\%}{G_s}$ = the percent mismatch in gain and in non-linearity between the two detectors. Since the apparent V_e is V_{error}/G_s, the apparent $\Delta R_x/R_x$ as given by Equation (92) is

$$\frac{\Delta R_x}{R_x} \simeq \frac{(R_x + R_s + r_y)}{R_s} \frac{\Delta G_s}{G_s}. \tag{94}$$

If R_x/R_s lies between 0.1 and 1.574 (as in the Oak Ridge experiment) and r_y/R_s is 0.1, then the sensitivity of $\Delta R_x/R_x$ to $\Delta G_s/G_s$ ranges from 1.2 to 2.674. Thus, for R_x control accuracy of 10 ppm, the two detector gains must track each other to within 5 ppm for the duration of a test. Note, however, that a magnitude of $\Delta G_s/G_s$ substantially larger than 5 ppm can be allowed since the temperature set point need only be known to an accuracy of about a degree for adequate repeatability as discussed in Chapter II. $\Delta G_s/G_s$ need only remain constant to within 5 ppm during the test. For example, for a 316 stainless steel specimen at 700 °C with $R_x = R_s$, a constant gain offset of 123 ppm will cause the control system to maintain an average specimen resistance that differs from the

desired set point by 258 ppm; i.e., the sample temperature will be off set point by a stationary 1 °C. But if the gain offset drifts 5 ppm, then the sample temperature will drift by 0.04 °C. The limitations of $\Delta G_s/G_s$ will be discussed in Chapters IV and V.

The type of detector influences the noise rejection properties of the PID. The peak detector may be analyzed as an envelope demodulator. Narrow-band noise can be represented by the following expression:

$$n(t) = n_c(t)\cos\omega_1 t - n_s(t)\sin\omega_1 t \ .^{22} \tag{95}$$

If the signal (s(t)) is represented by $A(t)\cos\omega_1 t$, then the signal plus noise is given by

$$s(t) + n(t) = A_n(t)\cos(\omega_1 t + \theta) \ , \tag{96}$$

where

$$A_n(t) = (A^2(t) + 2A(t)n_c(t) + n_c^2(t) + n_s^2(t))^{1/2}$$

and $\theta = \tan^{-1}\left(\frac{-n_s(t)}{A(t) + n_c(t)}\right)$. Since $A_n(t)$ is the envelope of the noisy signal, the noisy output of the PID will be

$$V_{pidp}(t) = (A^2(t) + 2A(t)n_{cs}(t) + n_{cs}^2(t) + n_{ss}^2(t))^{1/2}$$

$$- (A^2(t) + 2A(t)n_{cR}(t) + n_{cR}^2(t) + n_{sR}^2(t))^{1/2} \ , \tag{97}$$

where $A(t) = A_s(t) = A_R(t)$, and the s and R suffixes indicate components of V_s and V_R respectively. Using the first two terms of the Maclaurin series expansion for $(1 + x)^{1/2}$, Equation (97) may be rewritten as

$$V_{pidp}(t) \simeq \frac{A(t)}{2}\left[\frac{2n_{cs}(t) - 2n_{cR}(t)}{A(t)} + \frac{n_{cs}^2(t)+n_{ss}^2(t)-n_{cR}^2(t)-n_{sR}^2(t)}{A^2(t)}\right]. \tag{98}$$

Equation (98) is valid if the noise voltages are much less than the signal voltages. Assuming that $n_e = n_s - n_R$,

$$V_{pidp}(t) \simeq n_{ce}(t) + \frac{n_{cR}(t)n_{ce}(t) + n_{sR}(t)n_{se}(t) + n_{ce}^2(t) + n_{se}^2(t)}{A(t)} . \tag{99}$$

Since the noise voltages are much smaller than A(t),

$$V_{pidp}(t) \simeq n_{ce}(t) . \tag{100}$$

Since $\overline{n_e^2(t)} = \overline{n_{ce}^2(t)} + \overline{n_{se}^2(t)} = \overline{2n_{ce}^2(t)}$ for random noise,

$$\overline{V_{pid}^2(t)} \simeq \overline{n_e^2(t)}/2 ; \tag{101}$$

that is, the signal-to-noise improvement is 3 dB for random noise.

The noise rejection properties of PID's employing rms detection is easily analyzed. By definition, the rms sum of signal and noise is

$$\left[\overline{(s(t) + n(t))^2}\right]^{1/2} = \left[\overline{s^2(t) + n^2(t)}\right]^{1/2} \tag{102}$$

if signal and noise are uncorrelated. Therefore, the output of the rms PID is

$$V_{pidr}(t) = \left[\overline{s^2(t) + n_s^2(t)}\right]^{1/2} - \left[\overline{s^2(t) + n_R^2(t)}\right]^{1/2} . \tag{103}$$

Again assuming large signal-to-noise ratios, the first two terms of the Maclaurin series expansion for $(1 + x)^{1/2}$ can be used to approximate $V_{pidr}(t)$ as

$$V_{pidr}(t) \simeq \frac{N_s^2 - N_R^2}{2S} , \tag{104}$$

where N_s and N_R are the rms values of $n_s(t)$ and $n_R(t)$, respectively. Assuming that $N_e = N_s - N_R$, the noise output of the rms PID is

$$V_{pidr}(t) \simeq \frac{N_R}{S} N_e + \frac{N_e^2}{2S} = (N_R + \frac{N_e}{2}) \frac{N_e}{S} . \tag{105}$$

Hence, for a rms PID, the signal to noise improvement depends on the common mode noise. Since N_R will normally be much less than S, the noise improvement can be substantial.

Analysis of noise performance of a PID employing average magnitude detection is somewhat involved. Fortunately, analysis becomes manageable if the narrow-band assumption is made; i.e., noise is given by Equation (95) and A(t) is slowly varying with respect to $\cos\omega_1 t$. Assuming a large signal-to-noise ratio, $A_n(t)$ as given in Equation (96) reduces to $A(t) + n_c(t)$, while θ can be approximated by $n_s(t)/A(t)$. Therefore, the full-wave rectified signal plus noise is

$$s(t) + n(t) \simeq (A(t) + n_c(t)) \cos(\omega_1 t + \theta) . \tag{106}$$

The average magnitude of signal plus noise is

$$\begin{aligned} \overline{|s(t) + n(t)|} &\simeq \frac{1}{\pi} \int_{-\frac{\pi}{2} - \theta}^{\frac{\pi}{2} - \theta} (A(t) + n_c(t)) \cos(\phi + \theta) d\phi \\ &\simeq \frac{(A(t) + n_c(t))}{\pi} \int_{-\frac{\pi}{2} - \theta}^{\frac{\pi}{2} - \theta} \cos(\phi + \theta) d\phi \simeq \frac{2(A(t) + n_c(t))}{\pi} . \end{aligned} \tag{107}$$

Hence, the output noise of an average-magnitude PID is

$$V_{pida} = 2n_{ce}(t)/\pi \ . \tag{108}$$

Since the signal is also multiplied by $2/\pi$, the S/N of the average-magnitude detector is essentially the same as the S/N of a peak detector. S/N would of course be the same for a half-wave detector since both signal and noise would be half that for a full-wave rectifier.

The type of detector affects both accuracy and transient response of PID's. Root-mean-square converters are principally two types: computing and thermal. Computing rms detectors operate by calculating the rms value directly: analog multipliers are employed to square the signal which is then passed through an averaging low-pass filter, then the square root is taken to yield the rms value. Computing detectors are generally limited to accuracies greater than 0.1%.[43] Duncan et al. have shown that ripple attenuation characteristics of the low-pass filter can substantially affect the accuracy.[23] Although the ripple component does not affect the accuracy of mean square signal, the square root operation causes the ripple to have a DC component. Hence, further filtering of the ripple after the rms detector cannot eliminate ripple error. Thermal converters, on the other hand, achieving accuracies of 0.001 ppm from 40 Hz to 10 KHz increasing to 100 ppm at 10 MHz have been reported.[44] Unfortunately, thermal converters are slow: rise times are greater than 100 msec and fall times are greater than 300 msec.[45] Incidentally, all rms detectors have slower fall times than rise times.[45,46] Thermal detectors sense the temperature of a resistor that is ohmically heated by the signal.

Theoretically, peak and average detectors can yield accurate results if the waveform is known. While rms detectors are insensitive to the phase of harmonics, average and peak detectors are sensitive, peak detectors being more sensitive to phase than average detectors. If the nth harmonic is in phase with the fundamental (that is, the fundamental's zero points coincide with zero points of the harmonic) and the amplitude of the harmonic is less than 1/n times the fundamental's amplitude, then the output of the average detector is

$$V_a = \frac{A}{\pi}\int_0^{\pi} (\sin\theta \pm B \sin n\theta)d\theta \ , \ |B| < 1/n$$

$$= \begin{cases} \frac{2A}{\pi}(1 \pm \frac{B}{n}), & n \text{ is odd} \\ \frac{2A}{\pi} \quad , & n \text{ is even} . \end{cases} \tag{109}$$

If either of the above assumptions is not valid, then computation of V_a becomes very complex since the zero points of the composite waveform must be known. However, Equation (109) gives a good estimate of the V_a for very small B. The range of V_a for various harmonics is given in Reference 47. By inspection, the range of a peak detector output is

$$V_p = A(1 \pm B), \ |B| << 1 . \tag{110}$$

Maximum and minimum values of V_p occur when the maximum values of the fundamental occur simultaneously with that of the harmonic. However, the output of the rms detector is

$$V_{rms} = A(\frac{1 + B^2}{2})^{1/2} . \tag{111}$$

This indicates if severe phase shift occurs during a test, the error voltage could drift by ±AB/n, ±AB, ±0 for average, peak, and rms PID's, respectively. However, phase shift drifts in the bridge are very small. The principal phase shift drifts would be expected to come from the bandpass filters employed to suppress noise and harmonics. These phase shift drifts should be due primarily to drifts in the center frequency of the filter. For instance, if a second order bandpass filter is employed, the transfer function is

$$H(j\omega) = \frac{H_o j\omega}{1 + \frac{jT\omega}{Q} - T^2\omega^2} \cdot \tag{112}$$

The sensitivity of H(j) to T is

$$\frac{\frac{\partial |H(j\omega)|}{\partial T}}{|H(j\omega)} = \frac{(1 - T^2\omega^2)(1 + T^2\omega^2)}{T[(1 - T^2\omega^2)^2 + (\frac{T\omega}{Q})^2]} \cdot \tag{113}$$

From Equation (112), the normalized attenuation of the second and third harmonics is -14.65 and -19.55 dB, respectively, where Q = 3.54, and the fundamental (ω_1) is $\omega_o = T^{-1}$. But the sensitivity at the first, second and third harmonics is 0, $\frac{-1.610}{T}$, and $\frac{-1.236}{T}$, respectively. Hence, T stability is not very critical. In fact, a change in T of ±50 ppm will cause a change in $|H(j\omega_1)|$ of only -6.27 ppm. Since the rate of phase change with respect to T change is

$$\frac{\partial\theta}{\partial T} = - \frac{\omega(T^2\omega^2 + 1)}{Q((1 - T^2\omega^2)^2 + \frac{T^2\omega^2}{Q^2})} , \tag{114}$$

the phase change rate for first, second, and third harmonics is $\frac{-405.65°}{T}$, $\frac{-17.37°}{T}$, and $\frac{-7.50°}{T}$, respectively. If T increases 1.7 ppm, the shift in phase of second and third harmonics with respect to the fundamental would be -0.00066° and -0.00068°. Such small changes in phase are inconsequential compared to the amplitude changes. Because of the lower sensitivity of harmonics to changes in T and the low phase shift sensitivity, harmonic distortion does not substantially affect the accuracy of the PID regardless of the type detector.

In conclusion, PID's are viable alternatives to PSD's for use as bridge detectors. PID's achieve phase insensitivity in exchange for gain sensitivity. Both types of detectors require filtering of the bridge signals to reduce the effects of noise and distortion on performance. A rms detector is the best candidate for use as a PID if fast response is not important. This is because of its superior noise rejection properties, waveform insensitivity, and accuracy. Where fast response is desirable, an average detector should be used.

Accuracy limitations of practical rectifier circuits will be analyzed next. Root-mean-square detectors are discussed in References 44, 45, 46, and 48.

CHAPTER IV

PERFORMANCE OF PRACTICAL RECTIFIER CIRCUITS

I. RECTIFIER CIRCUITS

Physical Diode Models

The ideal diode would have characteristics as shown in Figure 19(a). Such a diode would make a perfect rectifier. Unfortunately, practical diodes have characteristics as pictured in Figure 19(c). The PN junction diode characteristic can be approximated by

$$I_D + I_s(\exp(q\ V_D/m\ k\ T) - 1)\ , \tag{115}$$

where I_D and I_s are the diode current and reverse saturation current, respectively, V_D is the voltage across the diode, k is Boltzman's constant, T is the absolute temperature of the PN junction, q is the magnitude of the charge of an electron, and m is an empirical factor ranging between 1 and 2.[43,49] As Figure 20(b) illustrates, m = 1 for moderate currents where I_D is dominated by diffusion current, but m = 2 at very low and very high currents due to recombination current and high injection effects.[49] For an introduction to semiconductor theory, the book by Pierce and Paulus is highly recommended.[50]

Bipolar transistors can also be employed as rectifiers. The collector current of a transistor can be approximated by

$$I_c = I_s(\exp(q\ V_{BE}/m\ k\ T) - 1)\alpha + I_{CBO}\ , \tag{116}$$

where I_s and I_{CBO} are the emitter and collector reverse current,

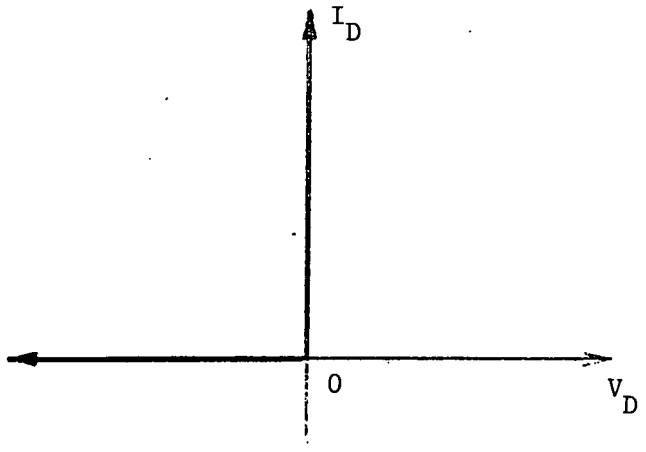

(a) Ideal diode.

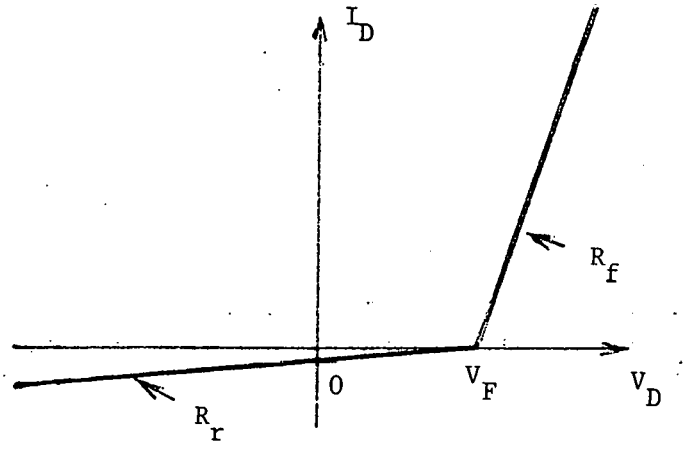

(b) Third order piece-wise linear diode model.

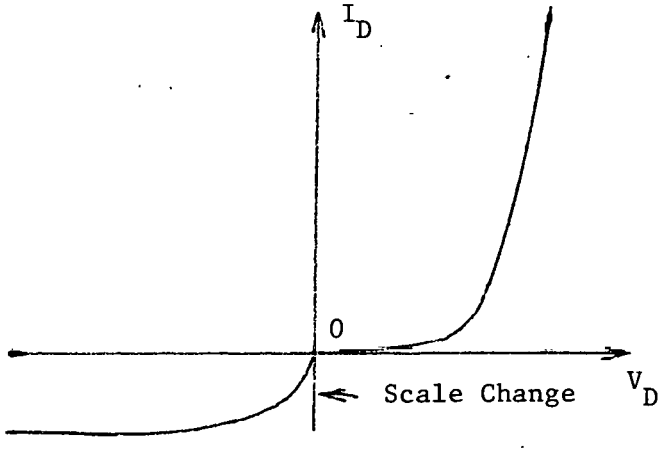

(c) Real diode.

Figure 19. Diode models.

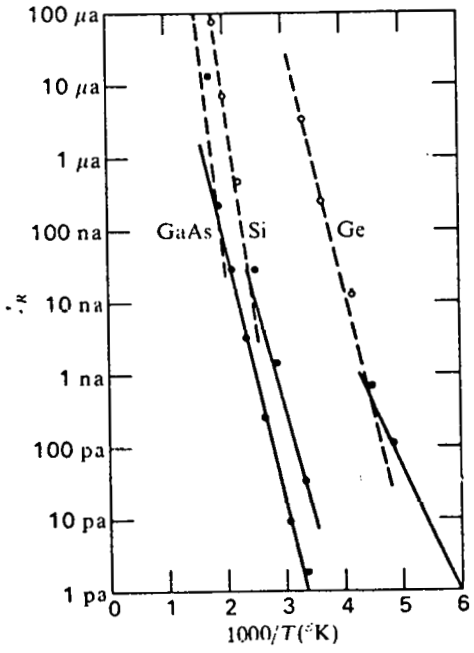

(a) Reverse current at V_R = 1 V as a function of temperature. Dots designate primarily generation-current type, circles designate primarily diffusion-current type current-voltage characteristics. Dashed lines represent temperature dependence of n_i^2; solid lines that of n_i.

Figure 20. Current-voltage characteristics of practical diodes and transistors.

Source: A. S. Grove, Physics and Technology of Semiconductor Devices (New York: John Wiley and Sons, Inc., 1967), pp. 179, 190, and 221.

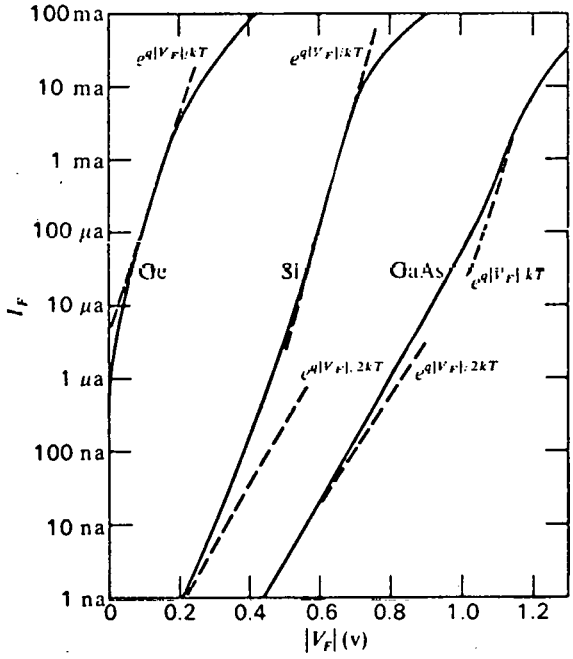

(b) Comparison of the forward current-voltage characteristics of the germanium, silicon, and gallium arsenide diodes at 25°C. Dashed lines indicate slopes of $e^{\eta|V_F|/kT}$ and $e^{q|V_F|/2kT}$ dependences.

Figure 20 (continued)

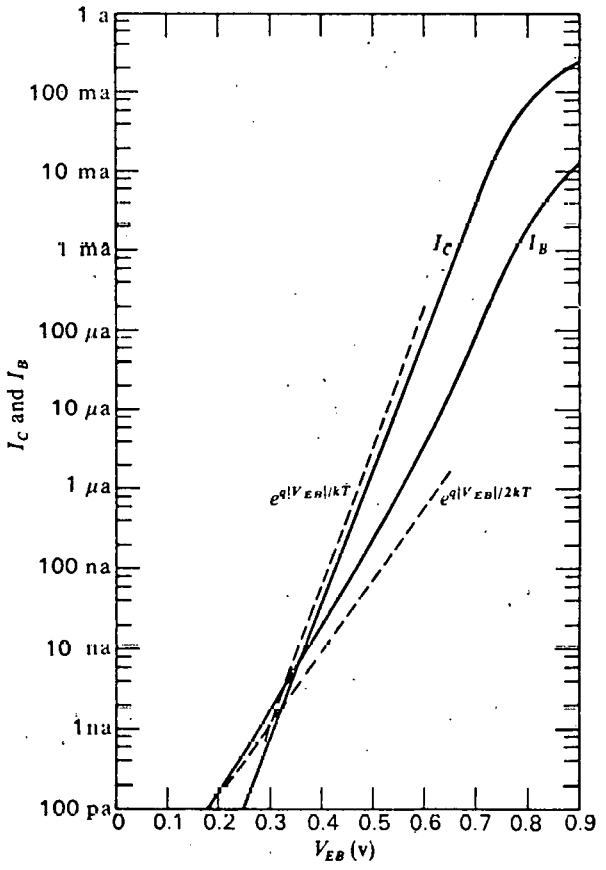

(c) Collector and base currents as a function of emitter-base forward bias for the pnp transistor. (V_{CB} = 0)

Figure 20 (continued)

respectively, V_{BE} is the base-emitter voltage, and α is the common-base short-circuit current gain.[49,50,51]

It is evident that neither diodes nor transistors have sufficient accuracy as rectifiers for use as bridge detectors in this experiment if they are driven by voltage sources. However, if they are driven by current sources as shown in Figure 21(a) accuracy is dramatically improved. In this case, the diode current is readily calculated if matched diodes are assumed; i.e., $I_s = I_{s1} = I_{s2}$ and $V_T = m\ k\ T/q = V_{T1} = V_{T2}$. Therefore

$$I_{in} = I_{D1} - I_{D2} = 2\ I_s\ \sinh(V_{D1}/V_T)\ , \tag{117}$$

where

$$I_{D1} = I_s(\exp(V_{D1}/V_T) - 1) \tag{118}$$

and

$$I_{D2} = I_s(\exp(-V_{D1}/V_T) - 1)\ . \tag{119}$$

V_{D1} is obtained from Equation (117) as

$$V_{D1} = V_T\ \sinh^{-1}(I_{in}/2\ I_s)\ . \tag{120}$$

Using the identity $\sinh^{-1}x = \ln(x + (x^2 + 1)^{1/2})$ obtained from Reference 52, Equations (120) and (118) yield

$$I_{D1} = I_s\ \left(\frac{I_{in}}{2I_s} + \left[\left(\frac{I_{in}}{2I_s}\right)^2 + 1\right]^{1/2} - 1\right)\ . \tag{121}$$

The average value of I_{D1} can be computed, assuming that I_{in} is $I_s 2B\cos\omega t$ as follows:

ORNL-DWG 76-19123

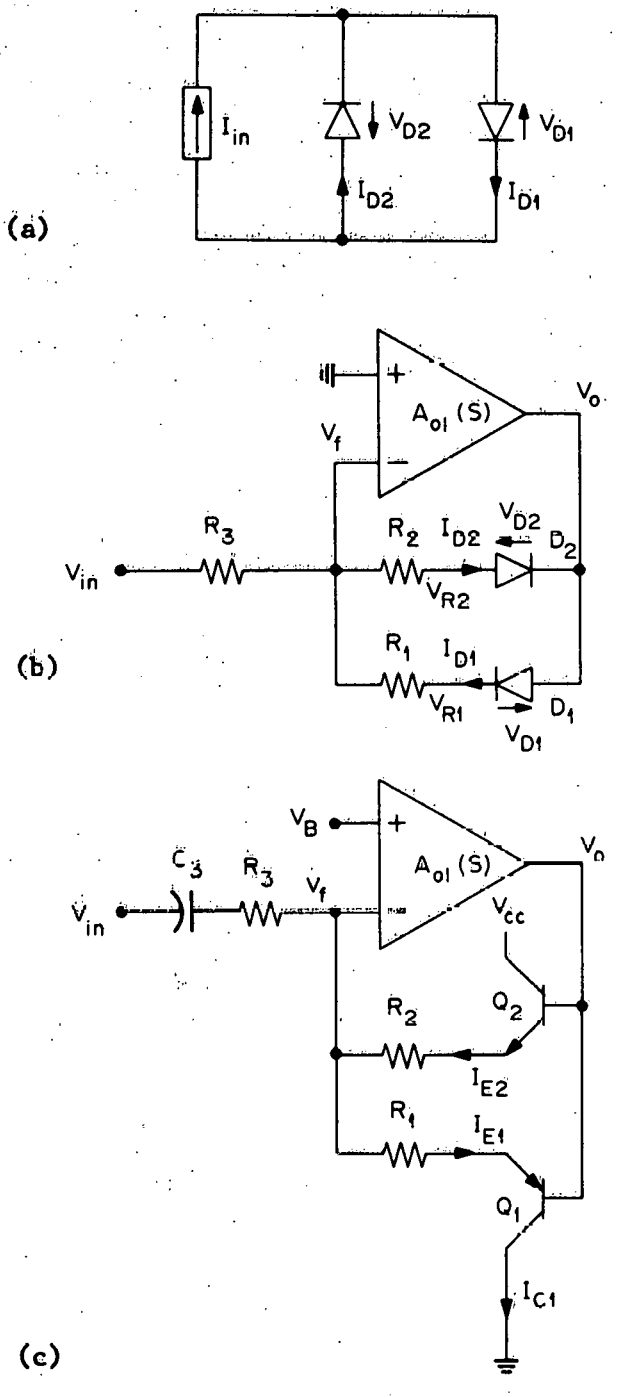

Figure 21. Precision rectifier circuits.

ORNL-DWG 76-19124

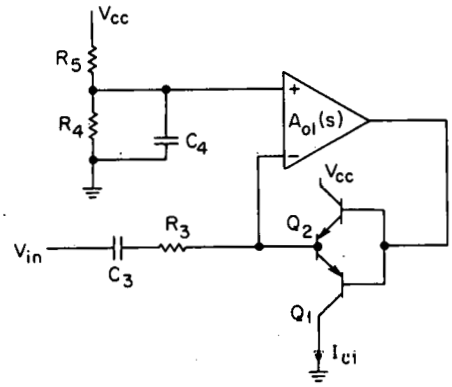

(d)

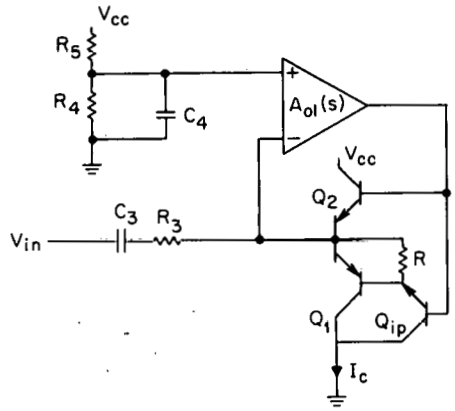

(e)

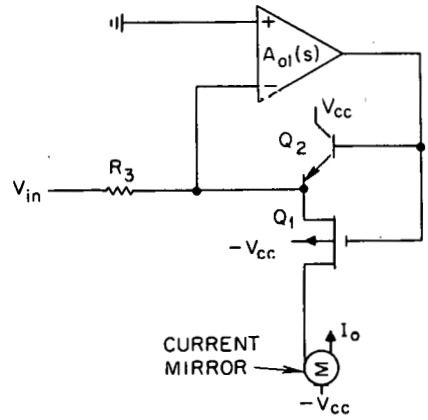

(f)

Figure 21 (continued)

$$\overline{I_{D1}} = \frac{1}{2\pi}\int_0^{2\pi} I_{D1}\, d\theta = \frac{I_s}{2\pi}\int_0^{2\pi} (B\cos\theta + (1 + B^2\cos^2\theta)^{1/2} - 1)d\theta$$

$$= \frac{I_s}{2\pi}\left[4(1 + B^2)^{1/2}\int_0^{\pi/2} (1 - \frac{B^2}{1 + B^2}\sin^2\theta)^{1/2}d\theta - 2\pi\right]$$

$$= \frac{I_s}{2\pi}\left[4(1 + B^2)^{1/2}\, E(B^2/(1 + B^2)) - 2\pi\right] , \qquad (122)$$

where $\theta = \omega t$, $E(m)$ is the complete elliptic integral of the second kind, and $m = B^2/(1 + B^2)$. Because m is very close to 1 for reasonable signal levels, it is convenient to define a new variable $m_1 = 1 - m = (B^2 + 1)^{-1}$. From the NBS math tables,[52] $E(m)$ can be written as follows:

$$E(m) = 1 + \sum_{n=1}^{4} (a_n\, m_1^{\,n} - b_n\, m_1^{\,n} \ln(m_1)) + \varepsilon(m) , \qquad (123)$$

where $|\varepsilon(m)| \leq 2 \times 10^{-8}$ for $0 \leq m \leq 1$ with $\lim_{m\uparrow 1} \varepsilon(m) = 0$. Neglecting terms where $n>1$, $E(m)$ becomes

$$E(B^2/(1 + B^2)) \simeq 1 + (B^2 + 1)^{-1}(a_1 + b_1 \ln (1 + B^2)) , \qquad (124)$$

where a_1 and b_1 are 0.44325 and 0.24998, respectively. Using the first two terms of the Maclaurin series expansion for $(1 + X)^{1/2}$, the average diode current is approximately

$$I_{D1} \simeq \frac{I_s\, 2\,|B|}{\pi}\left(\left[1 + \frac{1}{2\,B^2}\right]\left[1 + \frac{a_1 + b_2 \ln (1 + B^2)}{(1 + B^2)}\right] - \frac{1}{2|B|}\right) . \qquad (125)$$

Since $\lim_{u\to\infty} \left(\frac{a_1 + b_1 \ln u}{u}\right) = \lim_{r\to\infty} \left(\frac{b_1}{u}\right)$ by l'Hospital's rule, the percent

error of I_{D1} referred to the ideal half-wave rectifier output ($I_s\ 2|B|/\pi$) may be given by

$$P_e \simeq P_{dc} + P_{nl} \tag{126}$$

$$\simeq P_{dc}, \text{ for very large } B,$$

where

$$P_{dc} \simeq -50\%/B \tag{127}$$

and

$$P_{nl} \simeq 100\% \left(\frac{1}{2\ B^2} + \frac{a_1 + b_1 \ln (1 + B^2)}{(1 + B^2)}\right)$$

$$\simeq 100\% \ (0.5 + 0.44325 + 0.49996 \ln B)/B^2 \ . \tag{128}$$

Note that P_{dc} amounts to an error due to a DC offset, while P_{nl} is a nonlinear error. Since P_{dc} may be cancelled with a DC offset adjustment, only P_{nl} is important. For a very small signal level of $B = 10^4$, P_{nl} is only $6.7 \times 10^{-8}\%$. Therefore, the theoretical limit to accuracy of rectification via PN junction diodes is very low, indeed.

Unfortunately, this limit is unattainable since ideal current sources cannot be built and stray capacitances were neglected in the calculation. The performance of practical precision rectifiers will be examined next.

Practical Precision Rectifier Circuits

In the previous section, it was shown that driving diodes or transistors with a current source results in a precision rectifier. One method of achieving current drive is to place the diodes or

transistors in the negative feedback loop of an opamp as illustrated in Figures 21(b) and 21(c) on page 90. To illustrate how this achieves current drive, consider the circuit shown in Figure 22(a). Here, the rectifying PN junctions (diodes D1 and D2 or the base-emitter junctions of transistors Q1 and Q2) and their series resistors (R_1 and R_2) are represented by an equivalent nonlinear feedback impedance (Z_F). Using the equivalent circuit shown in Figure 22(b), the loop equations are

$$V_o = (Z_{ineq} + Z_f)\, I_f + Z_{ineq}\, I_{in}$$

$$V_o = -\left(\frac{A_{o1}\, Z_{ineq}\, Z_{leq}}{Z_o} + Z_{leq}\right) I_f - \frac{A_{o1} Z_{ineq}\, Z_{leq}\, I_{in}}{Z_o}\,, \tag{129}$$

where $Z_{ineq} = Z_{in}||Z_3$ and $Z_{leq} = Z_L||Z_o$. Solving the loop equations for I_f, one obtains the following expression:

$$I_f = \frac{-Z_{ineq}\,(1 + A_{o1}\, Z_{leq}/Z_o)\, I_{in}}{Z_{leq} + Z_f + Z_{ineq}\,(1 + A_{o1}\, Z_{leq}/Z_o)}\,. \tag{130}$$

Note that Equation (130) is that of current division between two impedances as shown in Figure 22(c). This indicates that the effective impedance of the source (Z'_{in}) is $Z_{ineq}\,(1 + A_{o1}\, Z_{leq}/Z_o)$. Since $Z_L >> Z_o$ and $Z_{in} >> Z_3$, Equation (130) simplifies to

$$I_f = \frac{-I_{in}\, Z'_{in}}{Z'_{in} + Z_o + Z_f}\,, \tag{131}$$

where $Z'_{in} = Z_3\ (1 + A_{o1})$. Hence, by making the opamp gain (A_{o1}) very large, Z'_{in} is also made very large. For instance, if $Z_{in} = 2K\Omega$ and A_{o1} is 1000, Z'_{in} becomes $2M\Omega$. Therefore as A_{o1} increases, the accuracy

ORNL-DWG 76-19125

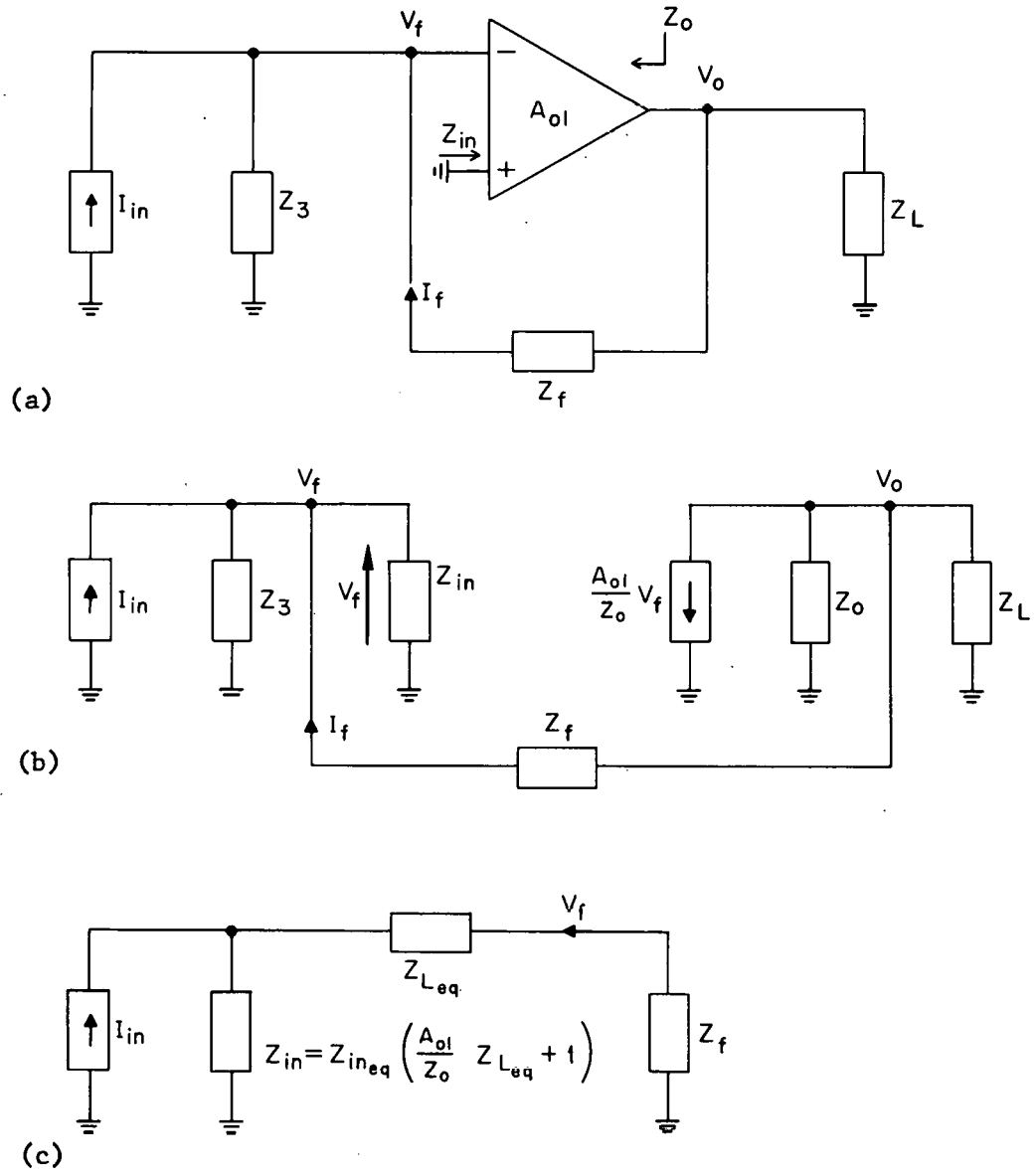

Figure 22. Equivalent circuits of a shunt feedback rectifier.

of the rectifier increases. Factors that cause additional errors and error analysis will be presented next.

II. ERROR ANALYSIS OF PRECISION RECTIFIER CIRCUITS

Approximate Piecewise-Linear Analysis

A substantial simplification in the analysis of a precision rectifier circuit can be made by employing piecewise-linear, third-order or second-order diode models as shown in Figure 19(b) on page 85. The second-order model (i.e., $R_r \to \infty$) has been employed by Thomason to analyze a precision rectifier.[53] However, the more general approach of a third-order diode will be utilized here. Equivalent circuits of a general piecewise-linear rectifier is shown in Figure 23(a). Furthermore, let A_{o1} be independent of frequency. Then the node equations of the circuits are

$$I_{in} + I_e + I_{D1} - I_{D2} = 0 \ , \tag{132}$$

where

$$I_{in} = V_{in}/R_3, \quad I_e = (V_o - V_f)/Z'_{in} \ ,$$

$$I_{D1} = \frac{(V_o - V_f - V_F)}{R_1 + R_{D1}} \ ,$$

and (133)

$$I_{D2} = \frac{(V_f - V_o - V_F)}{R_2 + R_{D2}} \ ,$$

where $R_{D1} = R_{f1}$ and $R_{D2} = R_{f2}$ if I_{D1} and I_{D2} are greater than zero, respectively; otherwise R_{D1} and R_{D2} are equal to R_{r1} and R_{r2},

ORNL-DWG 76-19126

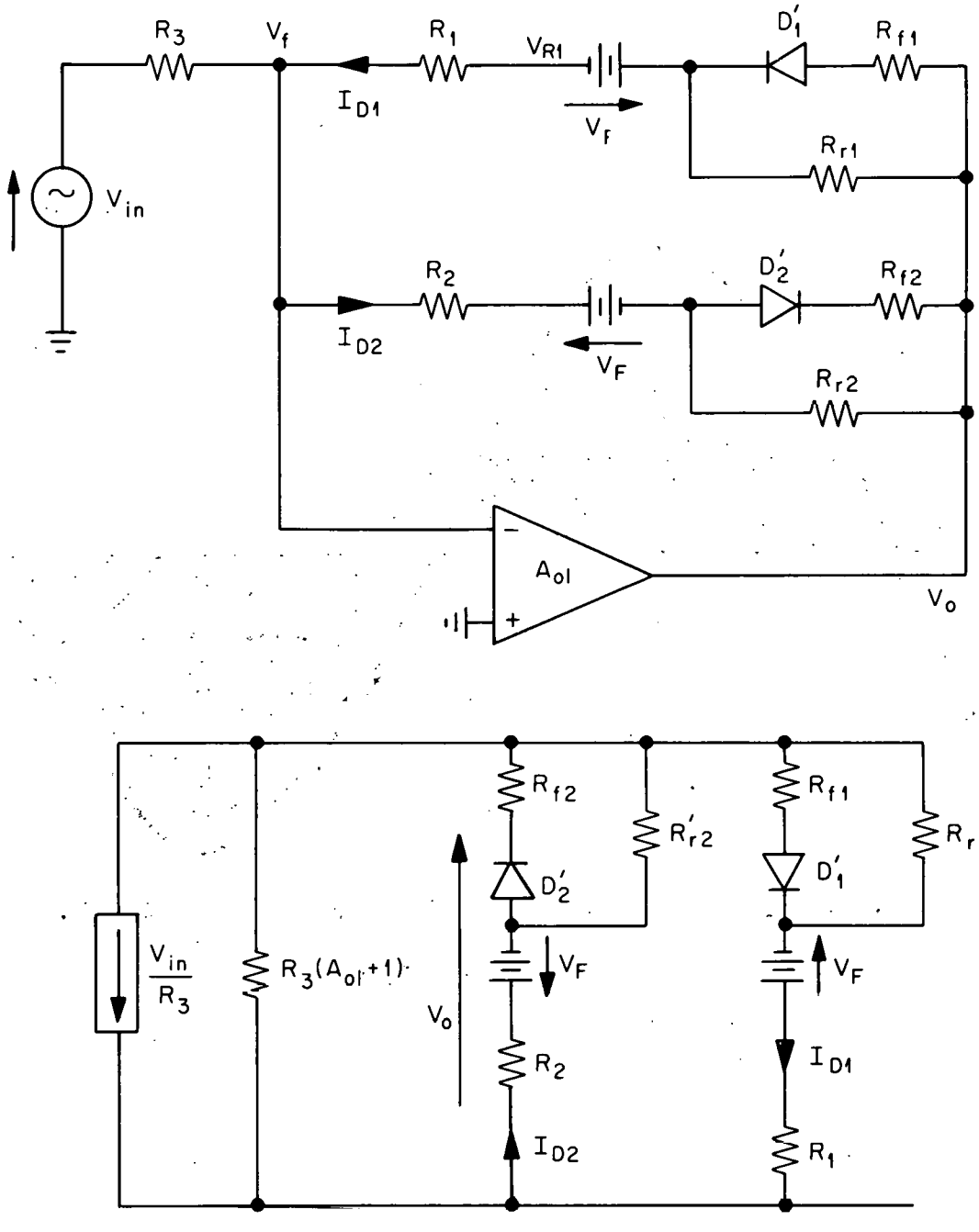

(a) Equivalent circuits of piecewise-linear rectifier circuit where $R_{f1} = R_{f2}$, $R_{r1} = R_{r2}$, and D_1' and D_2' are ideal diodes.

Figure 23. Circuits used for piecewise-linear analysis of rectifier.

ORNL-DWG 76-19127

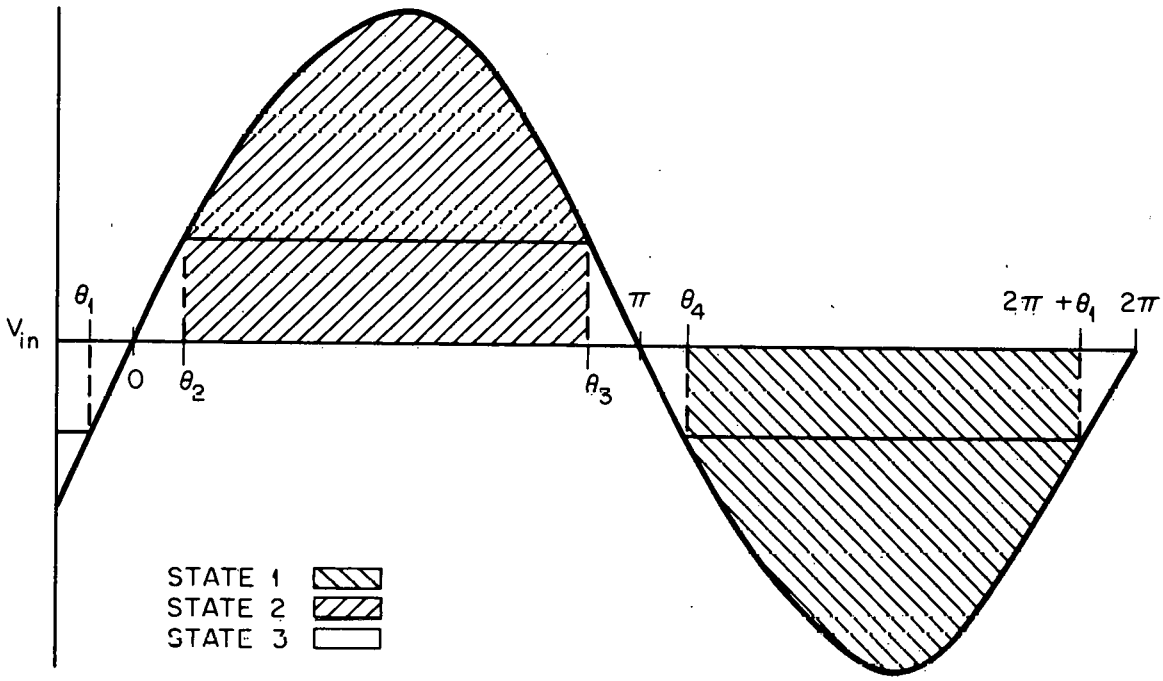

(b) Input voltage showing the various states of the circuit.

Figure 23 (continued)

respectively. Solving Equations (132) and (133) for I_{D1} and I_{D2}, one obtains

$$I_{D1} = \frac{-[\frac{V_{in}}{R_3} + V_F\,(\frac{2}{R_2 + R_{D2}} + \frac{1}{R_3\,(A_{o1} + 1)})]R_P}{(R_1 + R_{D1})} \tag{134}$$

and

$$I_{D2} = \frac{[\frac{V_{in}}{R_3} - V_F\,(\frac{2}{R_1 + R_{D1}} + \frac{1}{R_3\,(A_{o1} + 1)})]R_P}{(R_2 + R_{D2})} , \tag{135}$$

where $R_P = (R_1 + R_{D1})||(R_2 + R_{D2})||(R_3(A_{o1} + 1))$. There are three states in the circuit: (1) D1 on and D2 off, (2) D1 off and D2 on, and (3) D1 and D2 off. From Equation (134) D1 is on ($I_{D1} > 0$) when

$$V_{in} < V_{inc1} = - V_F(\frac{2\,R_3}{R_2 + R_{r2}} + \frac{R_3}{R_3\,(A_{o1} + 1)}) . \tag{136}$$

Likewise, from Equation (135), D2 is on when

$$V_{in} > V_{inc2} = V_F(\frac{2\,R_3}{R_1 + R_{r1}} + \frac{R_3}{R_3\,(A_{o1} + 1)}) . \tag{137}$$

State (3) occurs when $V_{in}\ \varepsilon(V_{inc1}, V_{inc2})$.

It is important to note the difference between a voltage output rectifier of the type shown in Figure 21(b) on page 90 and a current output rectifier as illustrated by Figure 21(c) through 21(e) on pages 90 and 91. In a current rectifier, the output is a function (ideally linear) of I_D, I_E, or I_S. However, the output of a voltage rectifier (V_{R1}) is given by

$$V_{R1} = V_f + R_1\,I_{D1} . \tag{138}$$

As will be shown, the current rectifier has better performance than a voltage rectifier as a peak detector or, if the diodes are not matched,

as an average detector. For instance, the peak value of I_{D1} can be obtained directly from Equation (134). Since the ideal value of I_{D1} is $-V_{in}/R_3$ for $V_{in} \leq 0$, the instantaneous or peak error is

$$P_{cp} = P_{csfp} + P_{cdcp}$$

where

$$P_{csfp} = \frac{-R_p \; 100\%}{(R_3 \; (A_{o1} + 1)) || (R_{r2} + R_2)}$$

and (139)

$$P_{cdcp} = \frac{R_3 \; R_p \; V_F \; 100\%}{[(R_{D1} + R_1)(R_3(A_{o1} + 1)) || (\frac{R_{r2} + R_2}{2})]V_{in}} .$$

V_f is found from Equations (132) and (133) to be

$$V_f = \frac{(\frac{V_{in}}{R_3} + V_F \; (\frac{1}{R_2 + R_{D2}} - \frac{1}{R_1 + R_{D1}})) \; R_p}{A_{o1} + 1} \tag{140}$$

by using the identity $V_o = -A_{o1} \; V_f$. Since the ideal voltage output is $V_{R1} = -R_1 \; V_{in}/R_3$, the instantaneous or peak error is given by

$$P_{vp} = P_{vsfp} + P_{vdcp}$$

where

$$P_{vsfp} = \frac{(R_3 \; (A_{o1} + 1)) || (R_{r2} + R_2)}{R_1 \; (A_{o1} + 1)} + 1) \; P_{csfp}$$

and (141)

$$P_{vdcp} = (\frac{(R_2 + R_{r2} - R_1 - R_{D1}) \; R_3}{R_1 \; (2R_3(A_{o1} + 1) \; + R_2 + R_{r2})} + 1) \; P_{cdcp} .$$

Note that while the scale factor error of a voltage output rectifier is greater than that of a current output rectifier, the DC errors can be identical only in state (3) where the error is high. In state (1), the region of good rectification, $R_{D2} = R_{r2} >> R_{D1} + R_1 = R_{f1} + R_1$; therefore,

$$|P_{vdcp}| > |P_{cdcp}| .$$

The errors calculated from Equations (139) and (141) are graphed in Figure 24(a), (b), and (c). V_F and R_f equal to 0.525 V and 160 ohms, respectively, were chosen as appropriate values for simulating silicon diodes and transistors; $R_f = 160\Omega$ is the dynamic forward resistance of an exponential diode at a quiescent current of 0.16 mA with V_T = 26 mV. These graphs show that the second-order diode model yields increasingly lower error values than the third-order model as A_{o1} increases. Note that as $R_1 + R_{D1}$ approaches zero, the scale factor and DC errors for the current rectifier approach zero and

$$\frac{V_F \; 200\% \; (R_3(A_{o1} + 1) + \frac{R_{r2} + R_2}{2})}{(A_{o1} + 1)(R_{r2} + R_2)}$$

respectively. $R_1 = 0$ can only be utilized in current output rectifiers since Equation (138) shows that V_{r1} would equal V_f if $R_1 = 0$. Figure 24(a) and 24(c) show that the current rectifier has better accuracy as a peak detector for identical component values, while Figure 24(b) shows that the performance of the current rectifier is substantially improved by setting R_1 to zero particularly at high input voltage levels. Finally, the graphs show that increasing A_{o1} improves accuracy, particularly if R_{r2} is very large.

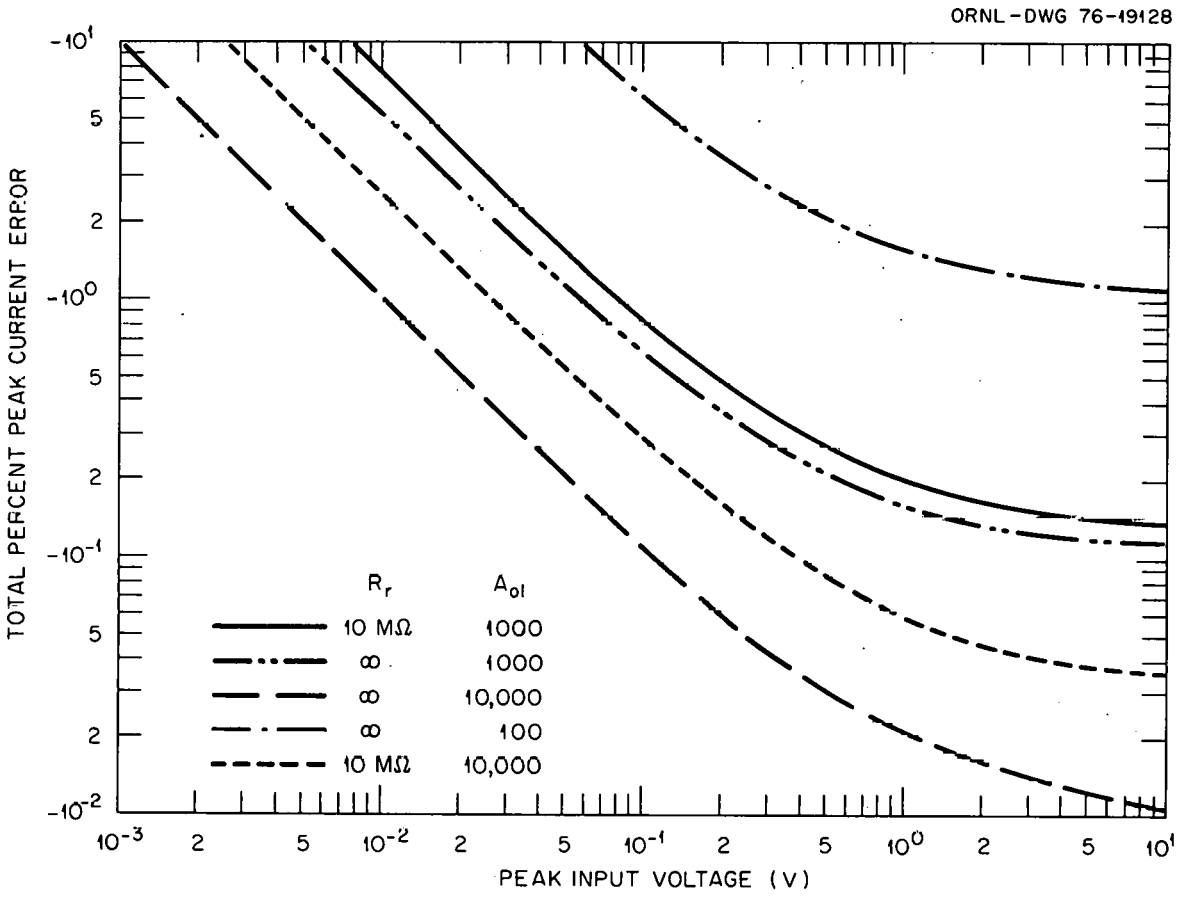

(a) Peak error of current output rectifier with $R_1 = R_2 = 2K\Omega$.

Figure 24. Error analysis of precision rectifier via piecewise-linear method.

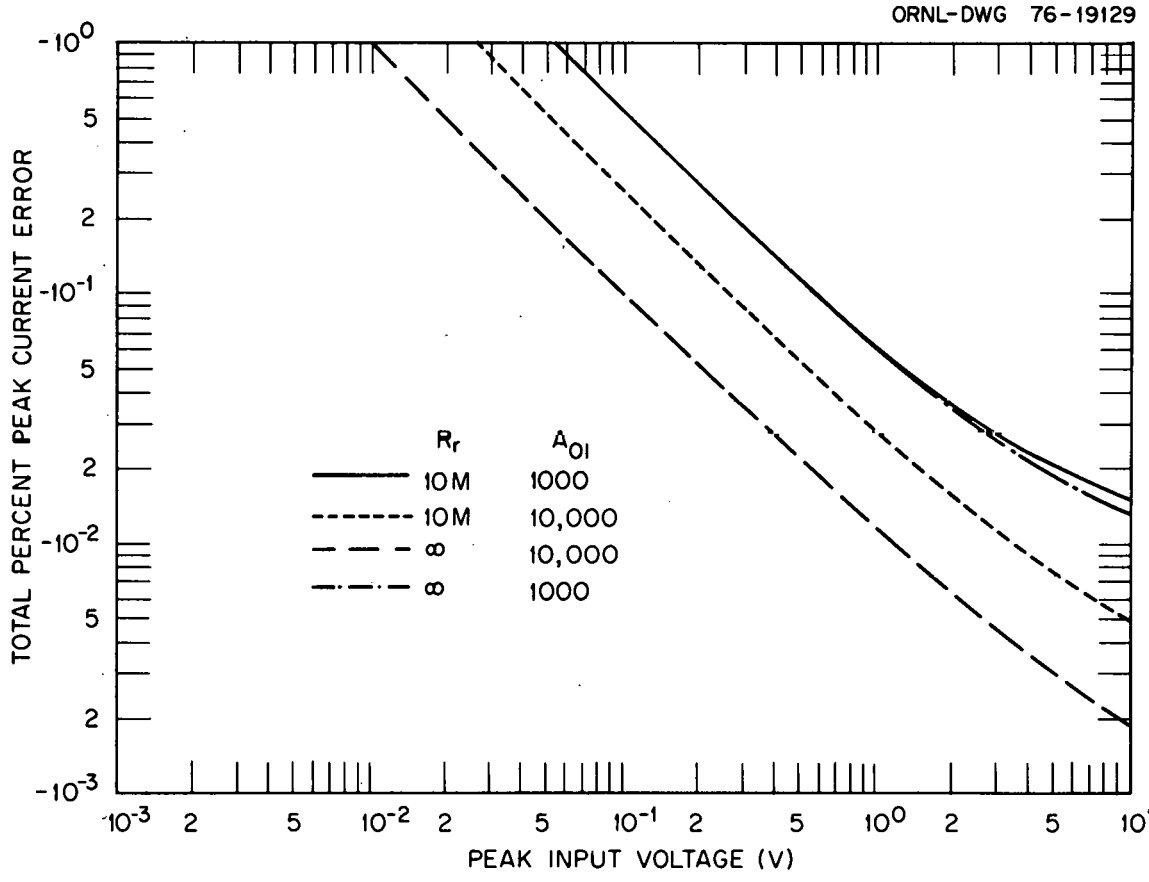

(b) Peak error of current output rectifier with $R_1 = R_2 = 0\Omega$.

Figure 24 (continued)

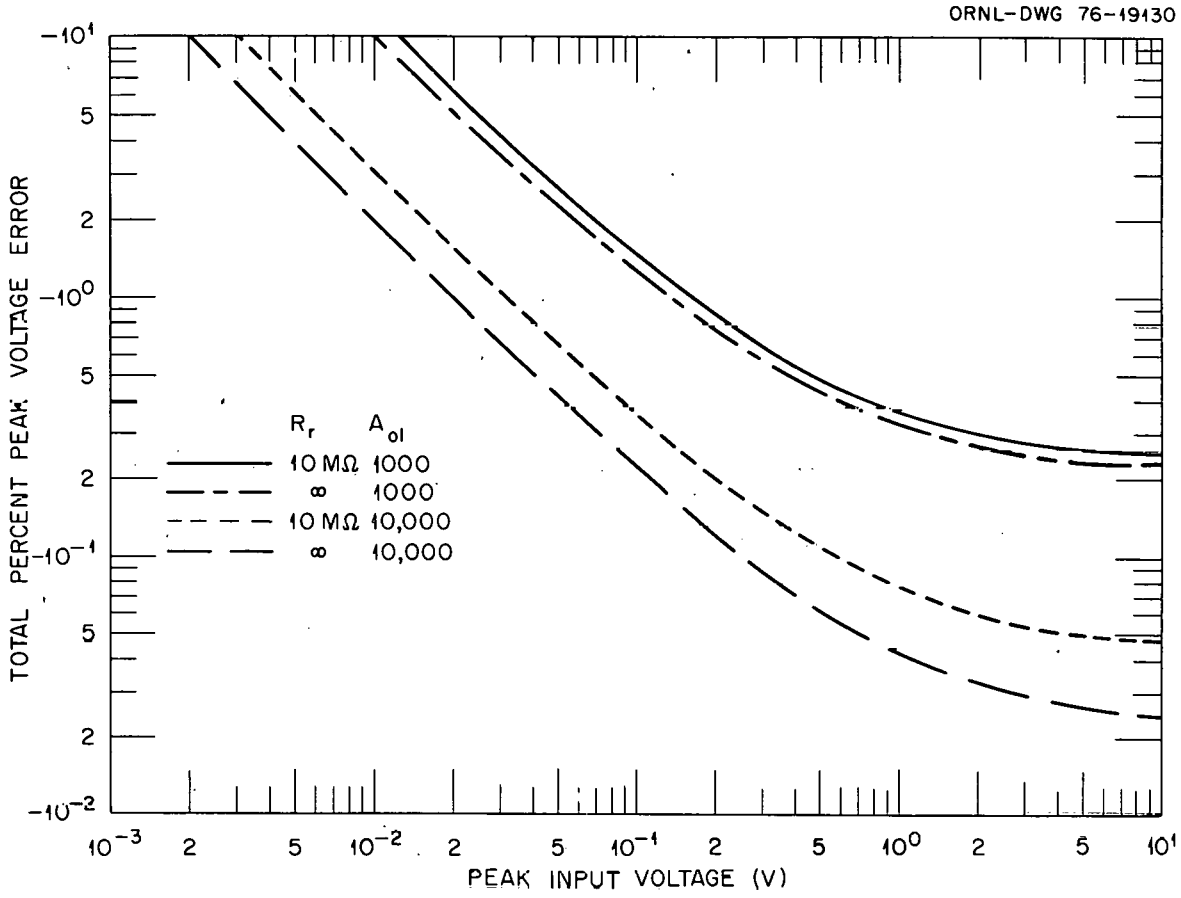

(c) Peak error of voltage output rectifier with $R_1 = R_2 = 2K\Omega$.

Figure 24 (continued)

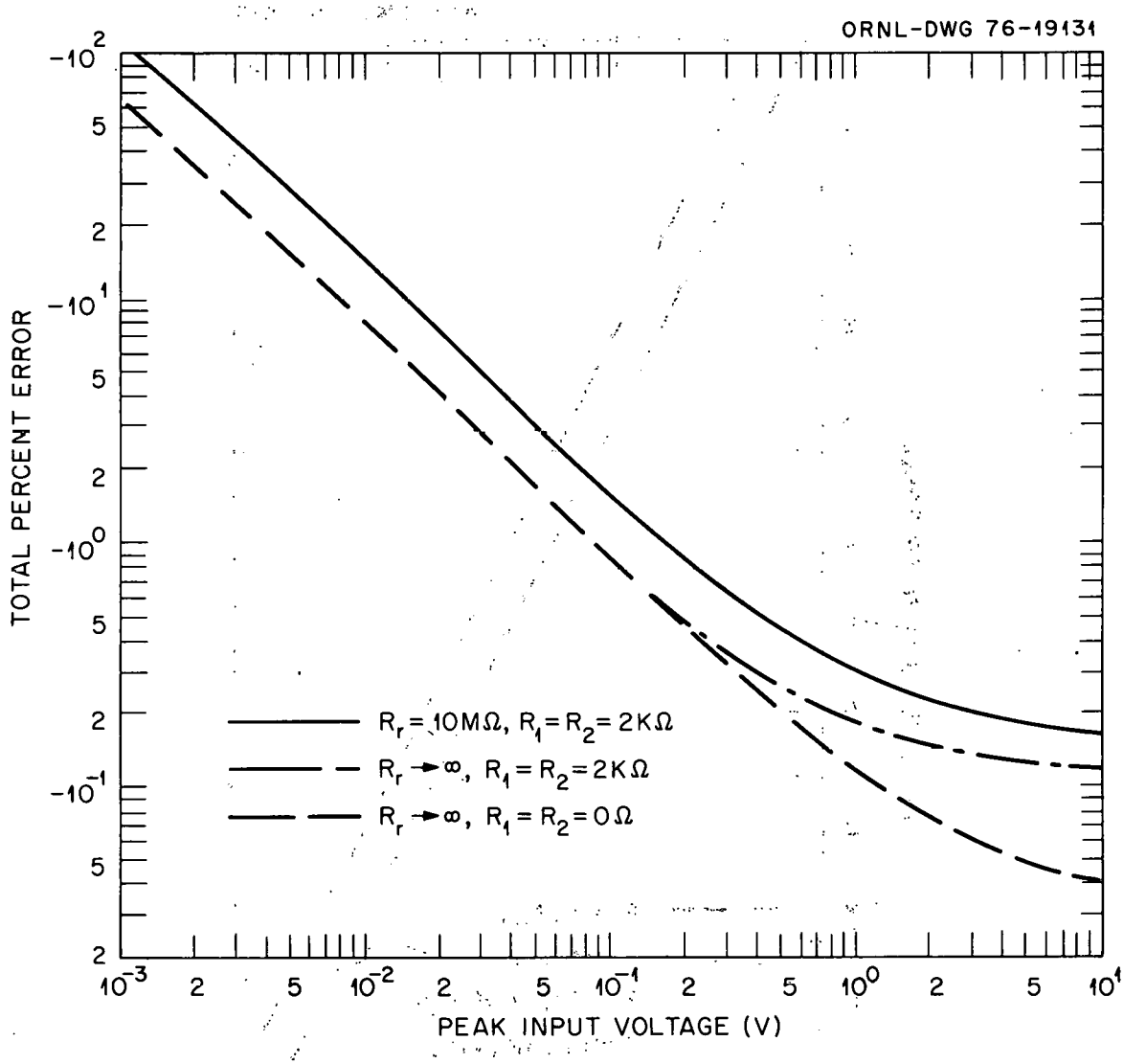

(d) Average error for both current and voltage output rectifiers with $A_{ol} = 1000$.

Figure 24 (continued)

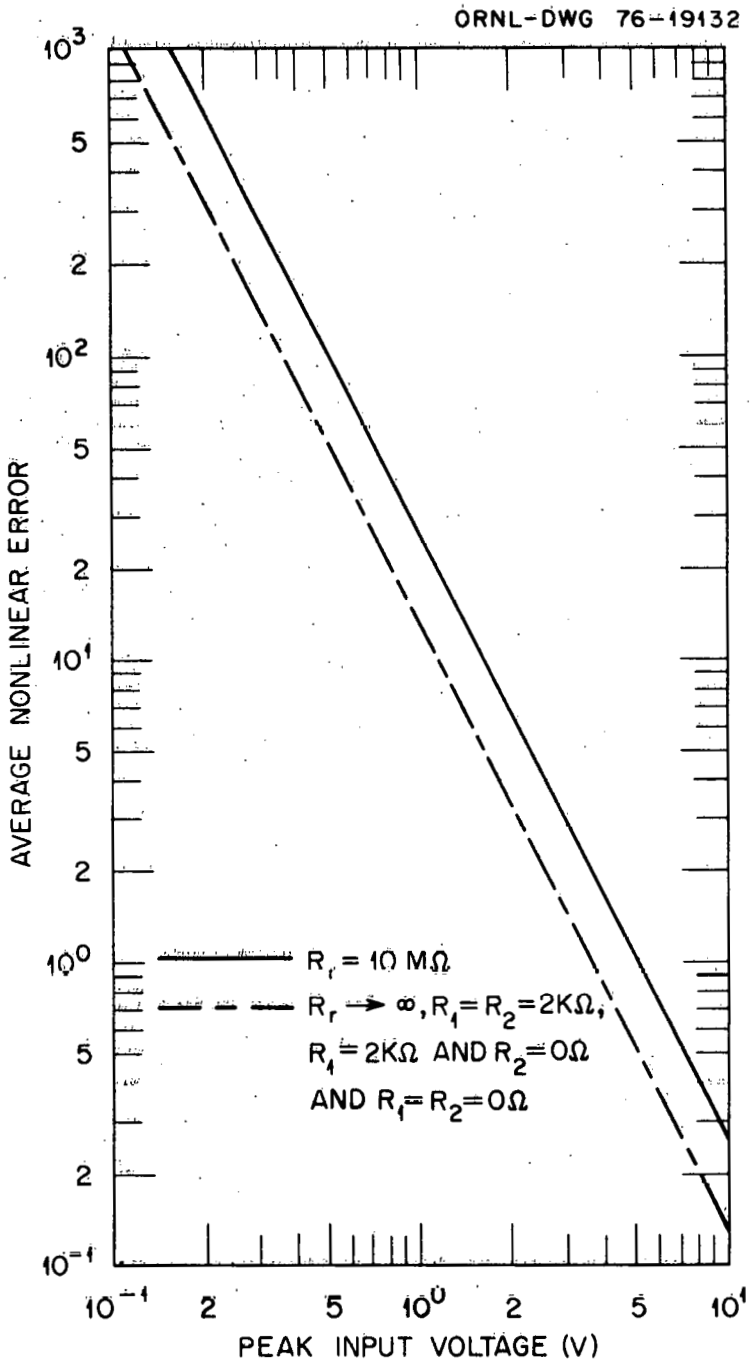

(e) Average nonlinear error (ppm) for both current and voltage output rectifiers with A_{ol} = 1000.

Figure 24 (continued)

In analyzing the average error of the rectifier, all three states must be considered. The average output current is

$$\overline{I_{D1}} = \frac{1}{2\pi} \int_{\theta_1}^{\theta_1+2} I_{D1}\, d\phi = \frac{I_{13} + I_{22} + I_{33} + \quad 41}{2\pi} , \tag{142}$$

where I_{ij} is the integral of I_{D1} over the interval $[\theta_i, \theta_{i+1}]$ in which the circuit is in state j, $\theta_5 = \theta_1 + 2\pi$, and $V_{in} = V_{inp} \sin\phi$ (see Figure 23(b) on page 98. I_{ij} is given by the following equation:

$$I_{ij} = \int_{\theta_i}^{\theta_{i+1}} I_{D1}\, d\phi$$

$$= \frac{R_p[\frac{V_{inp} \cos \phi}{R_3} - V_F (\frac{2}{R_2 + R_{D2}} + \frac{1}{R_3 (A_{o1} + 1)}) \phi]}{(R_1 + R_{D1})} \Bigg|_{\theta_i}^{\theta_{i+1}} , \tag{143}$$

where θ_i is given by the following expressions:

$$\theta_1 = \sin^{-1}(V_{inc1}/V_{inp}) ,$$

$$\theta_2 = \sin^{-1}(V_{inc2}/V_{inp}) , \tag{144}$$

$$\theta_3 = -\sin^{-1}(V_{inc2}/V_{inp}) + \pi = -\theta_2 + \pi,$$

and

$$\theta_4 = -\sin^{-1}(V_{inc1}/V_{inp}) + \pi = -\theta_1 + \pi.$$

Therefore $\overline{I_{D1}}$ is given by the following expression:

$$\overline{I_{D1}} = \frac{1}{2\pi}\left[-V_F\left(\frac{2\,\frac{R_{p3}}{R_{pp3}}(\theta_2-\theta_1)+\frac{R_{p2}}{R_{pp2}}(\pi-2\theta_2)}{R_1+R_{r1}}+\frac{R_{p1}(\pi-2\theta_1)}{R_{pp1}(R_1+R_{f1})}\right)\right.$$

$$\left.+\frac{2V_{inp}}{R_3}\left(\frac{R_{p1}\cos\theta_1}{R_1+R_{f1}}-\frac{R_{p2}\cos\theta_2+R_{p3}(\cos\theta_1-\cos\theta_2)}{R_1+R_{r1}}\right)\right] \qquad (145)$$

where $R_{pi} = R_p$ and $R_{ppi} = (R_3\,(A_{o1}+1))\,||\,(\frac{R_2+R_{D2}}{2})$ in the ith state. Using the small angle approximations, $\theta \simeq \sin\theta$ and $\cos\theta \simeq 1-\theta^2/2$, Equation (145) may be simplified as follows:

$$\overline{I_{D1}} \simeq \frac{V_{inp}}{R_3\pi}\left[\frac{R_{p1}}{R_1+R_{f1}}-\frac{R_{p2}}{R_1+R_{r1}}-\frac{V_F\pi R_3}{2V_{inp}}\left(\frac{R_{p2}}{R_{pp2}(R_1+R_{r1})}+\frac{R_{p1}}{R_{pp1}(R_1\ R_{f1})}\right)\right.$$

$$-\left(\frac{V_{inc1}}{V_{inp}}\right)^2\frac{1}{2}\left(\frac{R_{p1}}{R_1+R_{f1}}-\frac{R_{p3}}{R_1+R_{r1}}\right)-\left(\frac{V_{inc2}}{V_{inp}}\right)^2\frac{1}{2}\left(\frac{R_{p3}-R_{p2}}{R_1+R_{r1}}\right)$$

$$+\frac{V_F\,V_{inc1}\,R_3}{V_{inp}^{\ 2}\,R_{pp3}}\left(\frac{R_{p3}}{R_1+R_{r1}}-\frac{R_{p1}}{R_1+R_{f1}}\right)$$

$$\left.-\frac{V_F\,V_{inc2}\,R_3}{V_{inp}^{\ 2}(R_1+R_{r1})}\left(\frac{R_{p3}}{R_{pp3}}-\frac{R_{p2}}{R_{pp2}}\right)\right]. \qquad (146)$$

Since the ideal value of $\overline{I_{D1}}$ is $V_{inp}/(R_3\pi)$, the error is composed of three parts:

$$P_{ce} = P_{csfe} + P_{cdce} + P_{cnle}\ , \qquad (147)$$

where the scale factor error is

$$P_{csfe} \simeq \left(\frac{R_{p1}}{R_1+R_{f1}}-\frac{R_{p2}}{R_1+R_{r1}}-1\right)100\%\ ,$$

the DC error is

$$P_{cdce} \simeq -\frac{V_F \pi R_3}{V_{inp}} \left[\frac{R_{p2}}{R_{pp2}(R_1 + R_{r1})} + \frac{R_{p1}}{R_{pp1}(R_1 + R_{f1})}\right] 50\%$$

and the nonlinearity error is

$$P_{cnle} \simeq -\frac{V_{inc1}}{V_{inp}^2} \left[\frac{R_{p1}}{R_1 + R_{f1}} - \frac{R_{p3}}{R_1 + R_{r1}}\right] \left[\frac{V_F R_3}{R_{pp3}} + \frac{V_{inc1}}{2}\right] 100\%$$

$$+ \frac{V_{inc2}}{V_{inp}^2} \left[\frac{V_F R_3}{R_1 + R_{r1}} \left(\frac{R_{p2}}{R_{pp2}} - \frac{R_{p3}}{R_{pp3}}\right) + \frac{V_{inc2}(R_{p2} - R_{p3})}{2(R_1 + R_{r1})}\right] 100\% .$$

Substituting for V_{inc1} and V_{inc2} the equivalent expressions given by Equations (136) and (137) on page 99, P_{cnle} may be simplified to

$$P_{cnle} \simeq \frac{V_F^2 R_3^2 \, 100\%}{V_{inp}^2} \left[\frac{1}{2R_{pp3}^2} \left(\frac{R_{p1}}{R_1 + R_{f1}} - \frac{R_{p3}}{R_1 + R_{r1}}\right)\right.$$

$$\left. + \frac{1}{R_{pq3}(R_1 + R_{r1})} \left[R_{p2} \left(\frac{1}{R_{pp2}} + \frac{1}{2R_{pq3}}\right) - R_{p3} \left(\frac{1}{R_{pp3}} + \frac{1}{2R_{pq3}}\right)\right]\right] \tag{148}$$

where $R_{pq3} = \left(\frac{R_1 + R_{r1}}{2}\right) || (R_3(A_{o1} + 1))$.

Note that if the second-order diode assumption is made, the error terms reduce to

$$P_{csfe} \simeq \frac{(B_1 - 1)100\%}{(1 + A_{o1} B_1)} ,$$

$$P_{cdce} \simeq \frac{-V_F \pi B_1 \, 50\%}{V_{inp}(1 + A_{o1} B_1)} , \tag{149}$$

$$P_{cnle} \simeq \frac{V_F^{\,2}\, B_1\, 100\%}{V_{inp}^{\,2}(A_{o1} + 1)2(1 + A_{o1}\, B_1)} ,$$

where the voltage feedback ratio in state (1), B_1, is $R_3/(R_1 + R_{f1} + R_3)$.

To calculate the average error of V_{R1}, the mean value of V_f must be known. Integrating V_f in a manner similar to that used for I_{D1}, $\overline{V_f}$ becomes

$$\overline{V_f} = \frac{2V_F}{(A_{o1} + 1)} \left\{ \theta_1 \left[R_{p1}\left(\frac{1}{R_2 + R_{f2}} - \frac{1}{R_1 + R_{f1}}\right) + R_{p3}\left(\frac{1}{R_1 + R_{r1}} - \frac{1}{R_2 + R_{r2}}\right)\right] \right.$$

$$+ \theta_2 \left[R_{p2}\left(\frac{1}{R_1 + R_{r1}} - \frac{1}{R_2 + R_{f2}}\right) + R_{p3}\left(\frac{1}{R_2 + R_{r2}} - \frac{1}{R_1 + R_{r1}}\right)\right]$$

$$\left. + \frac{\pi}{2} \left[R_{p1}\left(\frac{1}{R_2 + R_{r2}} - \frac{1}{R_1 + R_{f1}}\right) - R_{p2}\left(\frac{1}{R_2 + R_{f2}} - \frac{1}{R_1 + R_{r1}}\right)\right]\right\} . \quad (150)$$

Using the small angle approximation where $\theta_1 \simeq V_{inc1}/V_{inp}$ and $\theta_2 \simeq V_{inc2}/V_{inp}$, expression (149) can be rewritten as

$$\overline{V_F} \simeq \frac{V_{inp}\, V_F}{\pi(A_{o1} + 1)} \left\{ \frac{V_{inc1}}{V_{inp}^{\,2}} \left[R_{p1}\left(\frac{1}{R_2 + R_{f2}} - \frac{1}{R_1 + R_{f1}}\right) + R_{p3}\left(\frac{1}{R_1 + R_{r1}} - \frac{1}{R_2 + R_{r2}}\right)\right] \right.$$

$$+ \frac{V_{inc2}}{V_{inp}^{\,2}} \left[R_{p2}\left(\frac{1}{R_1 + R_{r1}} - \frac{1}{R_2 + R_{f2}}\right) + R_{p3}\left(\frac{1}{R_2 + R_{r2}} - \frac{1}{R_1 + R_{f1}}\right)\right]$$

$$\left. + \frac{\pi}{2V_{inp}} \left[R_{p1}\left(\frac{1}{R_2 + R_{r2}} - \frac{1}{R_1 + R_{p1}}\right) - R_{p2}\left(\frac{1}{R_2 + R_{f2}} - \frac{1}{R_1 + R_{r1}}\right)\right]\right\} .$$

(151)

Since the ideal value of $\overline{V_{R1}}$ is V_{inp}/π, the total average error is

$$P_{ve} = P_{vsfe} + P_{vdce} + P_{vnle} ,$$

where

$$P_{vsfe} \simeq P_{csfe} ,$$

$$P_{vdce} \simeq P_{cdce} - \frac{\pi\ 100\%\ V_F}{2(A_{o1} + 1)V_{inp}} \left[R_{p1}\left(\frac{1}{R_1 + R_{f1}} - \frac{1}{R_2 + R_{r2}}\right) + R_{p2}\left(\frac{1}{R_1 + R_{r1}} - \frac{1}{R_2 + R_{f2}}\right)\right] ,$$

and

$$P_{vnle} \simeq P_{cnle} + \frac{V_F\ 100\%}{(A_{o1} + 1)V_{inp}^{\ 2}} \left[V_{inc1}\left[R_{p1}\left(\frac{1}{R_2 + R_{r2}} - \frac{1}{R_1 + R_{f1}}\right) + R_{p3}\left(\frac{1}{R_1 + R_{r1}} - \frac{1}{R_2 + R_{r2}}\right)\right] + V_{inc2}\left[R_{p2}\left(\frac{1}{R_1 + R_{r1}} - \frac{1}{R_2 + R_{f2}}\right) + R_{p3}\left(\frac{1}{R_2 + R_{r2}} - \frac{1}{R_1 + R_{r1}}\right)\right]\right] . \tag{152}$$

Since $R_{fi} << R_{ri}$ where i is 1 or 2, the magnitude of P_{vdce} and P_{vsfe} is larger than that for P_{cdce} and P_{csfe}, respectively, but the magnitude of P_{vnle} may be either less than, equal to, or greater than that for P_{cnle}. If the second-order diode assumption is made, the error components become

$$P_{vsfe} \simeq P_{csfe} ,$$

$$P_{vdce} \simeq P_{cdce}[1 + \frac{B_1 - B_2}{B_1(1 + A_{o1}B_2)}] ,$$

and

$$P_{vnle} \simeq P_{cnle}[1 + \frac{2(B_1 - B_2)}{B_1(1 + A_{o1}B_2)}] , \tag{153}$$

where B_2, the voltage feedback ratio in state (2), is $R_3/(R_2 + R_{f2} + R_3)$.

Figure 24(d) and (e), pages 105 and 106, graphically represent the average error calculated via Equations (148), (149), (152) and (153). These graphs illustrate that as long as $R_1 = R_2$ and the diodes are matched, the performance in an averaging circuit of both current and voltage rectifiers is identical. However, as readily illustrated in Equation (149), letting $R_1 + R_{f1}$ approach zero implies that B_1 approaches unity; therefore, P_{csfe} goes to zero. As illustrated by Figure 24(d), letting R_1 approach zero significantly improves the performance only at high voltages. In fact, Figure 24(e) shows essentially no improvement in nonlinearity error with reduction of R_1. However, the overall improvement is significant since the sensitivity of the output to A_{o1} is reduced at high input voltages. This is of particular significance since the input voltage in the Oak Ridge controller was chosen to be above 1 V to minimize error. Note also for input voltages above 1 volt, the nonlinearity is of the order of a few ppm. Since A_{o1} is 20,000 at 1 KHz in the Oak Ridge experiment while Figure 24(d) and (e) are for $A_{o1} = 1000$, the total error can be up to twenty times lower than predicted in the graphs, while the nonlinearity can be 400 times lower. Note, furthermore, that the second-order model yields higher estimates of rectifier accuracy. Finally, setting $R_2 + R_{f2} \neq R_1 + R_{f1}$ results in a

very slight change in the error of voltage output rectifiers over that with $R_2 = 2K\Omega$. This change in error is caused by a nonzero DC component of V_f due to the asymmetry of the circuit. Thus, the change is directly dependent on A_{o1}. This change is readily observed from Equation (153) since B_1 and B_2 are dependent on R_1, R_{f1}, R_2, and R_{f2}, respectively. With $R_1 + R_{f1} = 2.16\ K\Omega$ and $R_2 + R_{f2} = 160\Omega$, expression (153) gives a change in P_{vdce} and P_{vnle} of $-9.99 \times 10^{-4}\ P_{cdce}$ and $-2.00 \times 10^{-3}\ P_{cnle}$, respectively, if $A_{o1} = 1000$. Since the relative change increases as A_{o1} decreases, a 10% relative change would occur if A_{o1} were reduced to approximately 10 for the above B_1 and B_2.

Unfortunately, the piecewise-linear analysis as presented here can give poor estimates of rectifier accuracy. One reason for poor results is the omission of frequency dependence of the opamp gain and stray capacitances in the diodes. Note that $A_{o1}(j\omega)$ may not be directly substituted into the error expressions because of the nonlinearity of the circuit. To include frequency dependence substantially increases the complexity of the piecewise-linear analysis. For more information on piecewise-linear analysis of nonlinear systems References 54, 55, 56, 57, 58, and 59 are recommended. Frequency dependence will be examined later.

Another limitation of the above analysis is the assumption of ideal transistors with $\alpha = 1$. Since $\alpha = H_{FE}/(H_{FE} + 1)$, a constant α can be had only if H_{FE} is very large or independent of current and temperature. Unfortunately, since H_{FE} normally decreases at low currents and very high currents, and increases with increasing temperature, a device having very large H_{FE} at low currents is mandatory for high

accuracy. The peak error can be estimated by evaluating α at the currents of interest; that is, the additional peak error due to α is $P_{\alpha p} = (\alpha - 1)\ 100\%$. Since the average error depends on I_D which ranges from its minimum to its peak value, α will have a larger effect on the accuracy of average detectors.

An estimate of the range of error due to α can be made by assuming that the error is a uniform DC error:

$$P_{\alpha DCp} = \frac{I_o \varepsilon}{I}\ 100\% \ , \tag{154}$$

where $I_o\varepsilon$ is the effective DC error current, I is the instantaneous emitter current of Q_1, and I_o is an arbitrary reference current. If H_{FEo} and α_o are evaluated at I_o, then combining Equations (153) and (154) yields the following result:

$$\alpha = 1 + (P_{sfp} + P_{DCp})/100\% \ , \tag{155}$$

where $P_{\alpha sfp} = (\alpha_o - 1 - \varepsilon)100\%$. From the above equation,

$$\frac{H_{FE}}{H_{FEo}} = \frac{1 + U}{1 - H_{FEo}\ U} \ , \tag{156}$$

where

$$U = (\frac{P_{\alpha DCp}}{100\%} - \varepsilon)/\alpha_o = (\frac{I_o}{I} - 1)\varepsilon/\alpha_o \ .$$

Note that U may also be defined in terms of the average DC error, if the rectifier input is sinusoidal, by substituting $P_{\alpha DCp} = P_{\alpha DCe}/\pi$. Figure 25 illustrates the limits on H_{FE}/H_{FEo} versus $(|U|\pi)^{-1}$. Note that the lower limit is given by $U \in (-1,0)$, while the upper limit is designated by $U \in (0,1/H_{FEo})$. $U \in (-1, \frac{1}{H_{FEo}})$ results in negative values for H_{FE}, which

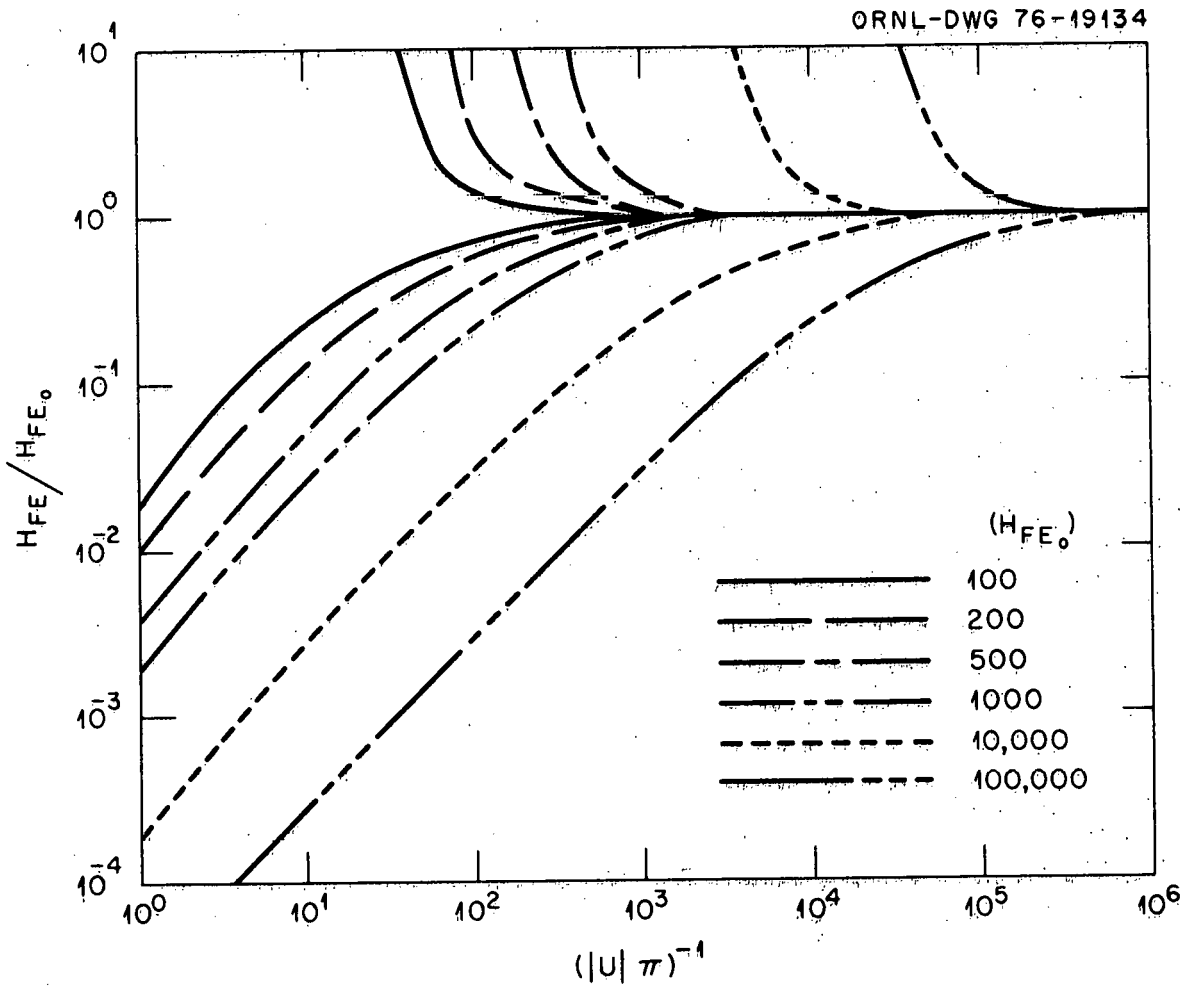

Figure 25. Limits on H_{FE}/H_{FE_o} as a function of $\alpha_o|(I/\pi)/[(I_o - I)\varepsilon]| = (|U|\pi)^{-1}$ where the effective DC error current is $I_o\varepsilon$.

are physically unrealizable. Equivalently, $I/I_o \in (\varepsilon/(\varepsilon - \alpha_o), 1)$ and $I/I_o \in (1, \varepsilon/(\varepsilon + (H_{FEo} + 1)^{-1}))$ are the ranges of I/I_o for the lower and upper limits, respectively.

Figure 25 can be utilized in at least two ways. First, for a specified H_{FEo}, the change in H_{FE} that will cause a given error can be found. The graph shows that a larger relative change in H_{FE} is allowed for a given error limit for larger H_{FEo} or for larger error limits given H_{FEo}. Secondly, the limits of the variation of H_{FE} versus current for specified H_{FEo} and $I_o|\varepsilon|$ can be found. For instance, if I_o is chosen as the maximum current and $P_{\alpha DCe}$ is assumed to be better than 0.001% for peak sinusoidal signals from 0.1 I_o to I_o, then $|\varepsilon|\pi \leq 1 \times 10^{-5}$. Thus $(|U|\pi)^{-1} = 10^5\ \alpha_o\ I/(I_o - I)$. Therefore, if $H_{FEo} = 500$, H_{FE}/H_{FEo} must not fall below 0.984, 0.862, 0.385, 5.72×10^{-2}, and 4.26×10^{-3} at 0.111, 0.0101, 0.00100, 1.00×10^{-4}, and $1.00 \times 10^{-5}\ I_o$. Transistors having this uniform H_{FE} would have to be hand selected. Fortunately, higher H_{FE} devices such as Darlington transistor arrays allow much higher variation of H_{FE}/H_{FEo} as illustrated in Figure 25. Furthermore, this graph illustrates a maximum current dependence of H_{FE} which is approximately proportional to current. Fortunately, most transistors exhibit a H_{FE} current dependence at low currents of I^N, where $0 \leq N \leq 1$. (See discussion of Darlington rectifier circuit on page 180.)

Other sources of error that were neglected in this analysis include the nonlinearity of the amplifier. The severity of the error these approximations cause will become evident in the more exact analysis that follows.

Iterative Technique with Exponential Diode Model

A significant improvement in the analysis of a precision rectifier circuit can be made by employing the exponential diode model as pictured in Figure 19(c) on page 85. The equivalent circuit of a general precision rectifier is illustrated in Figure 26(a). Unfortunately, the characteristic equation for an exponential diode in series with a resistor is transcendental:

$$I_{D1} = I_{s1} \left(\exp\left(\frac{V_o - V_{R1}}{V_{T1}}\right) - 1\right) , \tag{157}$$

and

$$I_{D2} = I_{s2} \left(\exp\left(\frac{V_{R2} - V_o}{V_{T2}}\right) - 1\right) ,$$

where $V_{R1} = V_f + I_{D1} R_1$ and $V_{R2} = V_f - I_{D2} R_2$. Even if the circuit is modified to eliminate the series resistance as illustrated in Figure 26(c), the equivalent parallel impedance also results in a transcendental equation:

$$\frac{V_{in} Z_{in}'}{R_3(Z_{in}' + R_1)} = \frac{V_{D1}}{R_1 + Z_{in}'} + I_{s1}\left(\exp\left(\frac{V_{D1}}{V_{T1}}\right)-1\right) - I_{s2}\left(\exp\left(\frac{V_{D1}}{V_{T2}}\right)-1\right) , \tag{158}$$

or for matched diodes

$$= \frac{V_{D1}}{R_1 + Z_{in}'} + 2\, I_s \sinh\left(\frac{V_{D1}}{V_T}\right) .$$

Such equations may be solved by series approximation. Schafer among others has employed this technique to determine the harmonic distortion in transistor and diode circuits.[60,61,62] While this technique works well in the calculation of distortion products, it is an extremely

ORNL-DWG 76-19133

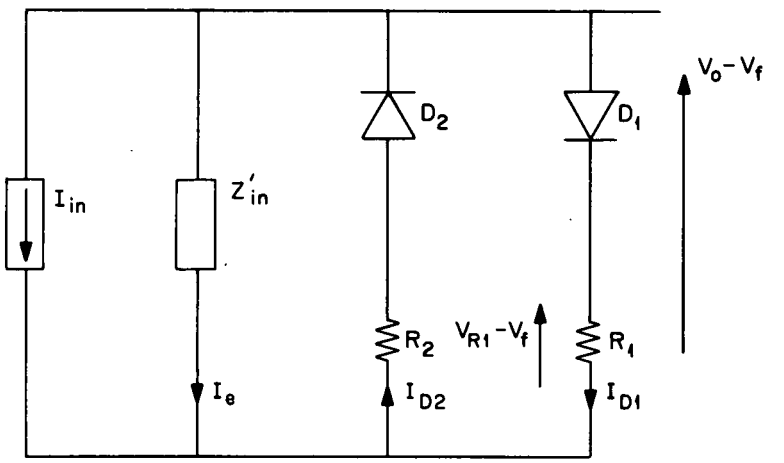

(a) Equivalent circuit of precision rectifier.

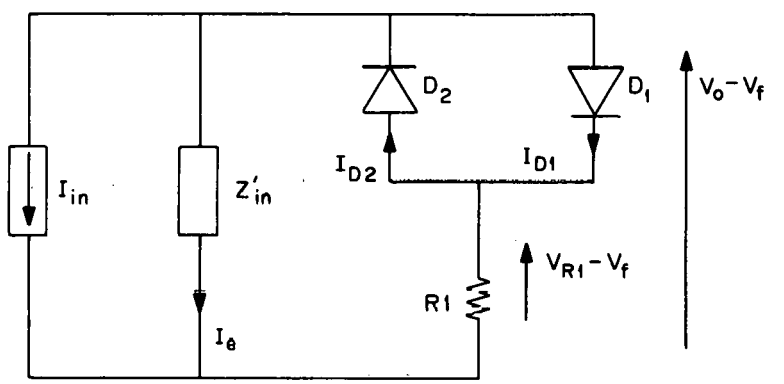

(b) Approximate equivalent circuit of precision rectifier.

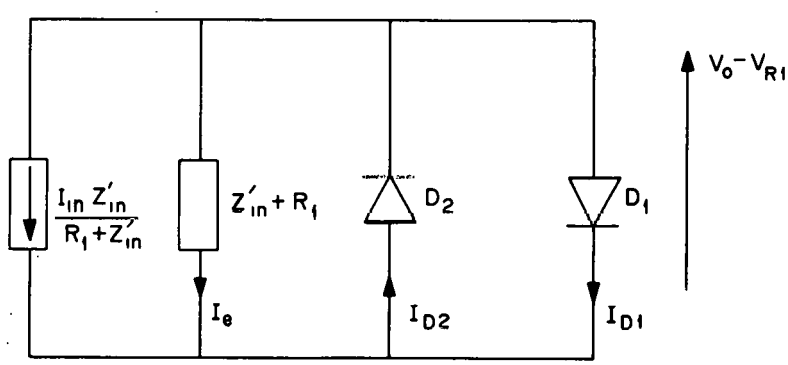

(c) Circuit B simplified by Norton equivalent source.

Figure 26. A, B, and C circuits used for iterative analysis of rectifier.

cumbersome technique to calculate the DC term (average value to the waveform) or the peak value of the waveform from a series. For instance, if a Taylor series expansion is employed, every even power term will contribute to the DC term, hence many terms will have to be evaluated. Note that one should not neglect the fact that $\cos^n\theta$ is equal to a sum of sinusoidal terms $n\theta$, $(n-2)\theta$, $(n-4)\theta$, ... to DC or θ. For example, $\cos^2\theta = (1 + \cos 2\theta)/2$ while $\cos^3\theta = (3 \cos \theta + \cos 3\theta)/4$.

Another method of solving transcendental equations is iteration. In this method, assumed values for I_{D1} and I_{D2} are utilized to calculate an error current. This error current is employed to improve the estimates of I_{D1} and I_{D2}. The process is repeated until the error current is sufficiently small. This method is easily applied to precision rectifier analysis where A_{o1} is independent of frequency, as will be assumed here.

As a further simplification, reverse bias diode currents will be neglected. For the range of signals considered here and for silicon diodes, this assumption will cause negligible error (see page 89). Moreover, assume that the circuit is symmetrical; i.e., $R_1 = R_2$, $I_{s1} = I_{s2} = I_s$, and $V_{T1} = V_{T2} = V_T$. With the above assumptions R_1 and R_2 may be replaced with one resistor as illustrated in Figure 26(c). An equivalent Norton current source makes the calculations much simpler. For this circuit, the node equation is

$$-I_{in} = \frac{-V_{in} B_1(A_{o1} + 1)}{(A_{o1} B_1 + 1)R_3} = I_e + I_{D1} - I_{D2} , \qquad (159)$$

where $B_1 = R_3/(R_1 + R_3)$ and

$$I_e = \frac{V_o - V_{R1}}{R_1 + R_3\,(A_{o1} + 1)} \; .$$

If I_{D2} is zero,

$$I_e = \frac{V_T}{R_1 + R_3\,(A_{o1} + 1)} \ln\left(1 + \frac{I_{D1}}{I_{s1}}\right) \; . \tag{160}$$

The above equations now can be used in an iteration technique to compute I_{D1}. Initially assume that $I_e = 0$, then $I_{D1} = -I_{in}$. Using Equation (160), a second estimate of I_e can be made (${}^2I_e$). Using ${}^2I_e$ in Equation (159) results in a second estimate for I_{D1} (${}^2I_{D1}$). An estimate of the accuracy of ${}^2I_{D1}$ may be obtained by computing ${}^3I_e$ by using ${}^2I_{D2}$ in Equation (160). For instance, assuming $A_{o1} = 1000$, $R_1 = R_3 = 2\ K\Omega$, $I_s = 10$ pA, and $V_T = 26$ mV, the convergence of the iteration method is shown in Table 3. Note that the second estimate for I_{D1} is an excellent approximation of the real diode current for $V_{in} \leq -0.001$ V. Since $I_e > 0$, ${}^1I_{D1}$ is larger than I_{D1}. This results in ${}^2I_e > I_e$ and causes ${}^2I_{D1} < I_{D1}$. The ratio of I_e to I_{D1} increases as I_{D1} decreases, until ${}^1I_e > {}^1I_{D1}$ causes ${}^2I_{D1}$ to go negative, which is counter to the assumption that D1 is on. Note that I_{D1} cannot be less than $-I_s$. When the estimated I_e becomes larger than half of $-I_{in}$, an initial assumption of ${}^1I_e = -I_{in}$ and ${}^1I_{D1} = 0$ will yield better results. With the above assumption, $V_o - V_{R1} = V_{D1}$ is determined from Equation (159), then ${}^2I_{D1}$ may be computed from Equation (157). Next, Equation (159) is employed to calculate ${}^2I_e$. The process is repeated until adequate accuracy has been obtained. The excellent convergence of this

TABLE 3

CONVERGENCE OF ITERATIVE TECHNIQUE FOR ANALYSIS OF PRECISION RECTIFIER CIRCUITS

Currents (A)	Input Voltage (-V) 10	1	0.1	0.01	0.001	0.0001	0.0001
$^{1}I_{e}$	0	0	0	0	0	0	4.995×10^{-8}
$^{1}I_{D1}$	4.995×10^{-3}	4.995×10^{-4}	4.995×10^{-5}	4.995×10^{-6}	4.995×10^{-7}	4.995×10^{-8}	0
$^{2}I_{e}$	2.599×10^{-7}	2.300×10^{-7}	2.001×10^{-7}	1.702×10^{-7}	1.404×10^{-7}	1.106×10^{-7}	4.949×10^{-8}
$^{2}I_{D1}$	4.995×10^{-3}	4.993×10^{-4}	4.975×10^{-5}	4.825×10^{-6}	3.591×10^{-7}	-6.065×10^{-8}	4.599×10^{-10}
$^{3}I_{e}$	2.599×10^{-7}	2.300×10^{-7}	2.003×10^{-7}	1.698×10^{-7}	1.361×10^{-7}	*	4.951×10^{-8}
$(^{3}I_{e}-^{2}I_{e})/^{2}I_{e}$	-2.598×10^{-6}	-2.598×19^{-5}	-2.603×10^{-4}	-2.643×10^{-3}	-3.049×10^{-2}	*	3.307×10^{-4}
$^{3}I_{D1}$	4.995×10^{-3}	4.993×10^{-4}	4.975×10^{-5}	4.825×10^{-6}	3.634×10^{-7}	*	4.436×10^{-10}
$(^{3}I_{D1}-^{2}I_{D1})/^{2}I_{D1}$	$2.\quad\times10^{-10}$	$1.2\quad\times10^{-8}$	1.047×10^{-6}	9.324×10^{-5}	1.192×10^{-2}	*	-3.559×10^{-2}

*Negative $^{2}I_{D1}$ is counter to the assumption that D1 is on and yields a false value for $^{3}I_{e}$.

approach for a -0.0001V input is tabulated in Table 3. However, for input voltages where $I_{D1} \sim I_e$ (-4.993×10^{-4}V for $I_{D1} = I_e$) the former iteration method converges faster than the latter method. In fact, the former method will converge for input voltages less than -0.25 mV.

Having established that ${}^2I_{D1}$ for the former method has sufficient accuracy for input voltages less than -1 mV, ${}^2I_{D2}$ may be utilized to compute the peak error of a precision rectifier. ${}^2I_{D1}$ is given by the following expression:

$$ {}^2I_{D1} = -I_{in} - {}^2I_e = -I_{in} - \frac{V_T \ln(1 - I_{in}/I_s)}{R_1 + R_3 (A_{o1} + 1)} \tag{161} $$

$$ = \frac{-V_{in} B_1 (A_{o1} + 1)}{R_3 (A_{o1} B_1 + 1)} - \frac{V_T \ln\left[1 - \frac{V_{in} B_1 (A_{o1} + 1)}{R_3 (A_{o1} B_1 + 1) I_s}\right]}{R_1 + R_3 (A_{o1} + 1)} . $$

Since the peak value of $-I_{in}$ is much greater than I_s for $V_{inp} > 1$ mV, the argument of the ln term can be approximated by $-I_{in}/I_s$. Hence the peak error is

$$ P_{cp} = P_{csfp} + P_{cdcp} + P_{cnlp} , \tag{162} $$

where

$$ P_{csfp} \simeq \frac{(B_1 - 1)\ 100\%}{(A_{o1} B_1 + 1)} , $$

$$ P_{cdcp} \simeq \frac{-V_T B_1\ 100\%}{(A_{o1} B_1 + 1) V_{inp}} \ln\left(\frac{B_1 (A_{o1} + 1)}{I_s R_3 (A_{o1} B_1 + 1)}\right) , $$

$$ P_{cnlp} \simeq \frac{-V_T B_1\ 100\%}{((A_{o1} B_1 + 1) V_{inp}} \ln(V_{inp}) , $$

and V_{inp} is the magnitude of the negative peak of the input voltage. P_{cp} and P_{cnlp} are graphed in Figure 27(a) and (c), respectively, for $B_1 = 0.5$ and 1.0. Comparing these graphs with those for the piecewise-linear diode model shown in Figure 24(a), (b), and (e), pages 102, 103, and 106, shows that piecewise-linear analysis poorly estimated the rectifier error. At high input voltages, the earlier analysis gave a good prediction of total error for $B_1 = 0.5$ where the scale factor error is dominant. Unfortunately, the piecewise model gives a highly conservative estimate of the DC error (approximately three times too large), while the nonlinear error estimate has little resemblance to the nonlinear error computed by the iterative method.

The poor results of the piecewise-linear analysis can be explained in the following manner. The piecewise-linear rectifier does not rectify until the voltage exceeds the turn on voltage. But an exponential diode will rectify at any voltage (although the rectification of low voltages is poor) due to the round knee of the current-voltage characteristics. Hence, the piecewise-linear model predicts excessive error. However, the approximate diode model does predict general trends (see Figure 24 on pages 102-106). For example, it correctly predicts that increasing B will reduce the scale factor error.

The iterative technique may also be employed to compute the error of a voltage output rectifier. By using the fact that $V_o = -A_{o1} V_f$ along with Equation (138) on page 99 and Equation (159), V_{R1} is obtained as follows:

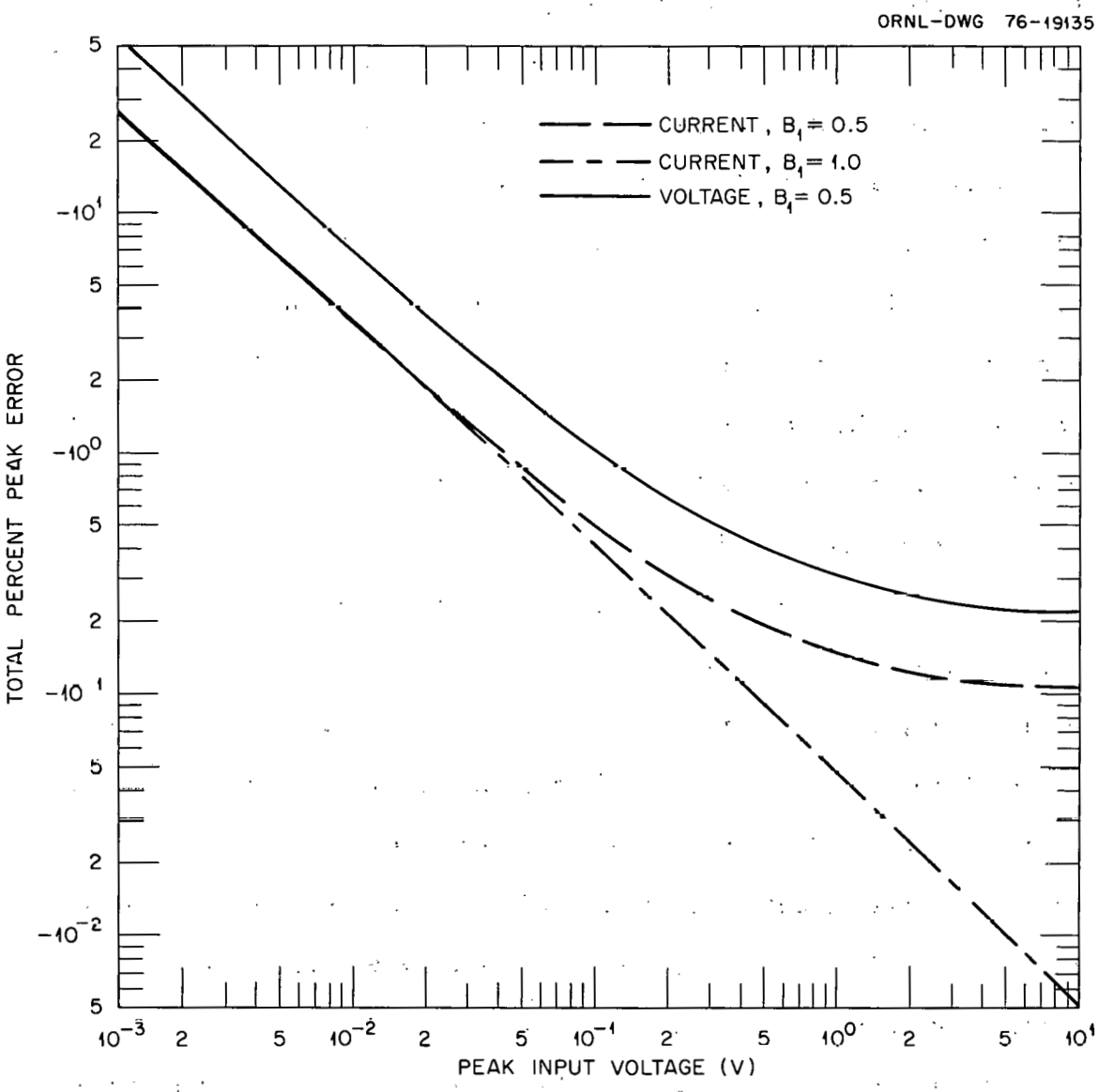

(a) Peak error with A_{o1} = 1000.

Figure 27. Error analysis of precision rectifier by iterative technique.

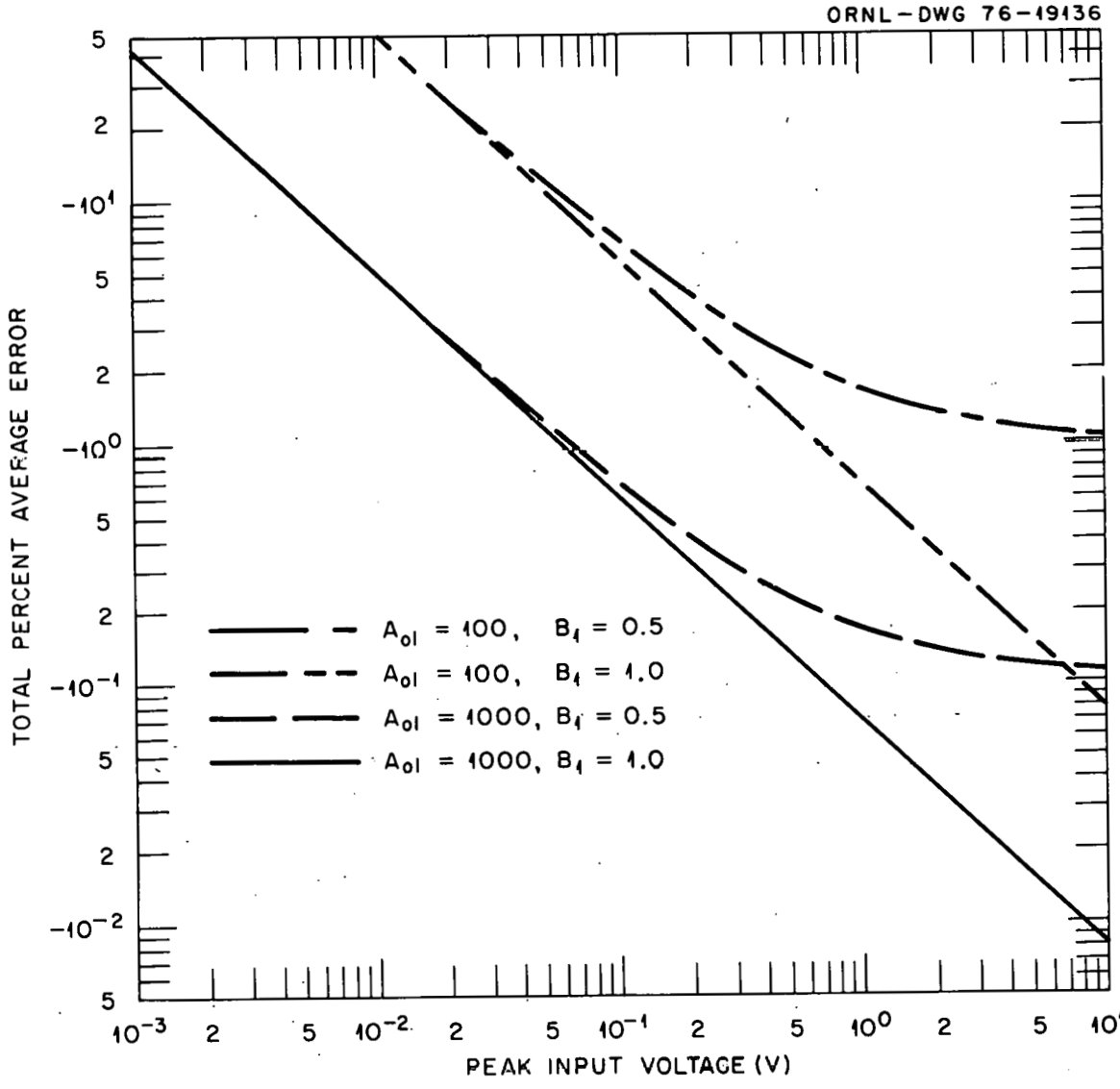

(b) Average error.

Figure 27 (continued)

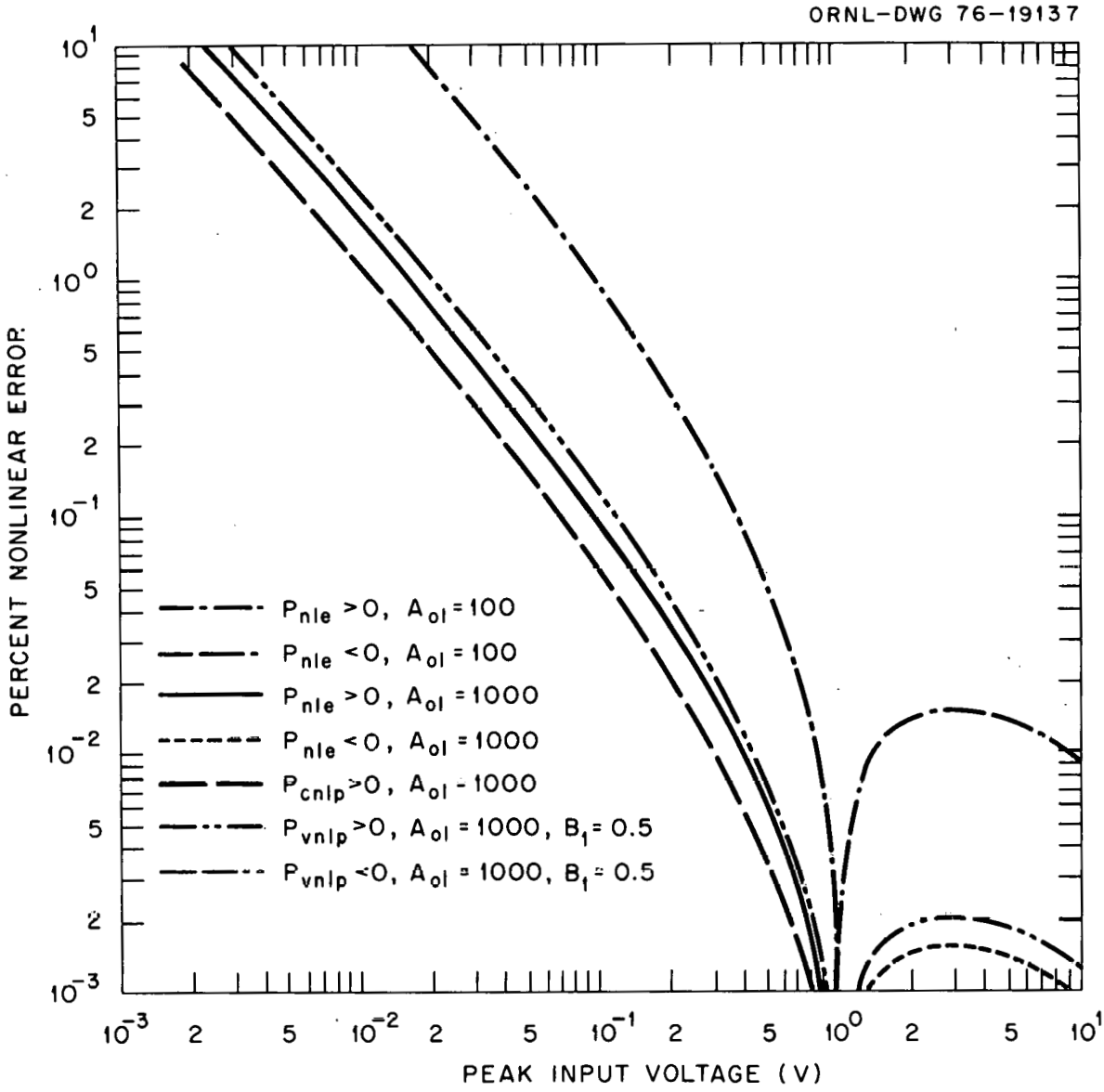

(c) Nonlinear error for both current and voltage output rectifiers.

Figure 27 (continued)

$$V_{R1} = -\frac{I_{in}\, A_{o1}\, R_1}{1 + A_{o1}} - I_e\,(R_1 + R_3)$$

$$= \frac{-V_{in}\, A_{o1}\, B_1\, R_1}{(A_{o1}\, B_1 + 1)R_3} - I_e\,(R_1 + R_3)\ . \tag{163}$$

Substituting ^2I_e for I_e, the error is

$$P_{vp} = P_{vsfp} + P_{vdcp} + P_{vnlp}\ ,$$

where

$$P_{vsfp} = \frac{-100\%}{A_{o1}\, B_1 + 1}\ ,$$

$$P_{vdcp} = \frac{P_{cdcp}}{1 - B_1}\ , \tag{164}$$

$$P_{vnlp} = \frac{P_{cnlp}}{1 - B_1}\ .$$

The total error and P_{vnlp} are graphed in Figure 27(b) and (c). Comparing these graphs with Figure 24(c) and (e) on pages 104 and 106 again shows good agreement between the second-order piecewise-linear model at high voltages but about three times too much error for the piecewise-linear model at low voltages on the total error. The nonlinear error has little resemblance to that of the exponential diode analysis. However, the piecewise-linear model correctly predicts that the voltage error is approximately twice the current error for $B_1 = 0.5$.

The iteration method may also be used to compute the average rectifier error as follows:

$$\overline{I_{D1}} = \frac{1}{2} \int_{\pi}^{2\pi} I_{D1}\, d\phi = \frac{1}{2\pi} \int_{\pi}^{2\pi} -I_{in} - I_e\, d\phi \ , \tag{165}$$

where $V_{in} = V_{inp} \sin \phi$ and $V_{inp} > 0$. Note that the integral is only over $[\pi, 2\pi]$ since I_{D1} is zero by assumption over the interval $[0,\pi]$. While computing the integral of I_{in} is straightforward, the integral of I_e must be treated with caution. Recall from Table 3 on page 121 that ${}^2I_e$ is good approximation of I_e only for voltages above 1 mV. Since $V_{in} = 0$ at both π and 2π, it is desirable to break the integration interval into parts as follows:

$$2\pi \overline{|I_e|} = \int_{\pi}^{2\pi} I_e\, d\phi = -2 \int_{0}^{\pi/2} I_e\, d\phi = 2(I_1 + I_2)$$

where

$$I_1 = \int_{0}^{\theta_c} -I_e\, d\phi \leq \int_{0}^{\theta_c} I_{in}\, d\phi \ , \tag{166}$$

$$I_2 = \int_{\theta_c}^{\pi/2} -I_e\, d\theta \leq \int_{\theta_c}^{\pi/2} -I_e\, d\phi \ ,$$

and the interval $[0,\theta_c]$ is that over which ${}^2I_e$ is not a good approximation of I_e. Substituting an equivalent expression for ${}^2I_e$ from Equation (161) on page 122, I_2 becomes

$$I_2 \leq \int_{\theta_c}^{\pi/2} K_1 \ln\left(1 + \frac{I_{inp} \sin\phi}{I_s}\right) d\phi \ , \tag{167}$$

where $K_1 = V_T/(R_1 + R_3\ (A_{o1} + 1))$. Unfortunately, the value of the above integral could not be located in integral tables; however, $\int_{0}^{\pi/2} \ln \sin \phi\, d\phi$

was found to be equal to $-\frac{\pi}{2}\ln 2$.[52] Assuming that $I_{inp}\sin\theta_c/I_s >> 1$ and $\theta_c \simeq \sin\theta_c$, Equation (167) may be rewritten as follows:

$$I_2 \simeq K_1((\frac{\pi}{2} - \theta_c)\ln(\frac{I_{inp}}{I_s}) + \int_0^{\pi/2} \ln\sin\phi\, d\phi - \int_0^{\theta_c} \ln\sin\phi\, d\phi)$$

$$\simeq K_1((\frac{\pi}{2} - \theta_c)\ln(\frac{I_{inp}}{I_s}) - \frac{\pi}{2}\ln 2 - \int_0^{\theta_c} \ln\phi\, d\phi) , \qquad (168)$$

where $\int_0^{\theta_c} \ln\phi\, d\phi = \theta_c(\ln(\theta_c) - 1) - \lim_{\varepsilon\downarrow 0}(\frac{\ln(\varepsilon) - 1}{\varepsilon^{-1}})$. By l'Hospital's rule,

$$\lim_{\varepsilon\downarrow 0}(\frac{\ln(\varepsilon) - 1}{\varepsilon^{-1}}) = \lim_{\varepsilon\downarrow 0}(\varepsilon^{-1}/(-\varepsilon^{-2}) = \lim_{\varepsilon\downarrow 0} -\varepsilon = 0 .$$

For $A_{o1} = 1000$, $R_1 = R_3 = 2K\Omega$, and $V_T = 26$ mV, $I_{inc}/I_s = 1.3 \times 10^4$ gives an ${}^2I_e$ within 20% of I_e. For other values of A_{o1} and the same accuracy ${}^2I_e$, I_{inc}/I_s is roughly inversely proportional to A_{o1}. Letting $\theta_c \simeq \sin\theta_c = I_{inc}/I_{inp}$, Equation (165) becomes

$$\overline{I_{D1}} \simeq \frac{1}{\pi}(I_{inp} - \frac{I_{inc}^2}{2I_{inp}} + K_1\left[\frac{\pi}{2}\ln(\frac{I_{inp}}{2I_s}) + \frac{I_{inc}}{I_{inp}}\left(1 - \ln(\frac{I_{inc}}{I_{inp}})\right)\right] . \qquad (169)$$

One may estimate the relative sizes of the terms of the above equation using the above circuit parameters along with $I_s = 10$ pA. If $I_{inp}/I_{inc} = 4$, then $I_{inp} = 5.2 \times 10^{-7}$ A, $\frac{K_1\pi}{2}\ln(\frac{I_{inp}}{2I_s}) = 2.1 \times 10^{-7}$, $\frac{I_{inc}}{I_{inp}}\left[K_1(1 - \ln(\frac{I_{inc}}{I_{inp}}) - \frac{I_{inc}}{2}\right] = -8.5 \times 10^{-9}$. This indicates that neglecting the terms involving I_{inc} results in less than 4.1% additional error in the estimation of the rectifier accuracy at input currents greater than $4I_{inc}$; thus, $\overline{I_{D1}}$ is approximately

$$\overline{I_{D1}} \simeq \frac{B_1 V_{inp}}{R_3 (A_{o1} B_1 + 1)\pi} \left[A_{o1} - 1 - \frac{\pi V_T}{2 V_{inp}} (\ln V_{inp} + \ln \left(\frac{B_1 (A_{o1} + 1)}{R_3 (A_{o1} B_1 + 1) 2 I_s} \right) \right] . \tag{170}$$

Hence the error is

$$P_{ce} = P_{csfe} + P_{cdce} + P_{cnle} ,$$

where

$$P_{csfe} \simeq \frac{(B_1 - 1)\ 100\%}{(A_{o1} B_1 + 1)} ,$$

$$P_{cdce} \simeq \frac{-\pi B_1 V_T\ 50\%}{(A_{o1} B_1 + 1) V_{inp}} \ln \left(\frac{B_1 (A_{o1} + 1)}{R_3 (A_{o1} B_1 + 1) 2 I_s} \right)$$

$$P_{cnle} \simeq \frac{-\pi B_1 V_T\ 50\% \ln V_{inp}}{(A_{o1} B_1 + 1) V_{inp}} .$$

Since the circuit is symmetrical, V_f has a zero mean value, hence the average voltage output error is equal to that of the current output.

Figure 27(b) and (c) on pages 125 and 126 graph the average errors as given by Equation (170). Comparison of results with those of the piecewise-linear model as illustrated in Figure 24(d) on page 105 again show the latter total error estimates to be about three times too large at low input voltages. However, the accuracy improves as the input voltage increases. Again the approximate linear analysis correctly predicts that increasing B_1 will reduce the scale factor error. In addition, the piecewise linear model gives a very poor estimate of the nonlinear error.

Although the preceding analysis considered only a symmetrical circuit, the technique is also applicable to nonsymmetrical circuits. As long as the reverse biased diode current can be neglected, only one diode and its associated series resistor need be considered at any given time. Thus, the peak error Equations (162) and (164) on pages 122 and 127 are also valid for nonsymmetrical circuits. Additionally, expression (170) for the average error of a current rectifier is also valid for nonsymmetrical circuits; however, the mean value of V_f must be computed to find the average voltage error of a nonsymmetrical rectifier. Using the identities $V_{R1} = R_1 I_{D1} + V_f$ and $V_{R2} = -R_2 I_{D2} + V_f$ with Equation (159) on page 119, where R_2 is substituted for R_1 when D_1 is off, V_f is found to be

$$V_{fi} = \frac{R_i B_i V_{in}}{(A_{o1} B_i + 1) R_3} - R_3 I_{ei} , \tag{171}$$

where

$$I_{ei} = \frac{V_{Ti}(-1)^i}{R_i + R_3 (A_{o1} + 1)} \ln \left(1 + \frac{I_{Di}}{I_{si}}\right) ,$$

$B_i = R_3/(R_i + R_3)$, and D_i is on ($i = 1$ or 2).

Thus, the average value of V_f is given by the following equation:

$$2\pi\overline{V_f} = -\left(\int_0^{\pi} I_{e2} d\phi + \int_{\pi}^{2\pi} I_{e1} d\phi\right) R_3 + \frac{R_2 B_2 V_{inp}}{R_3(A_{o1}B_2+1)} \int_0^{\pi} \sin\phi d\phi + \frac{R_1 B_1 V_{inp}}{R_3(A_{o1}B_1+1)} \int_{\pi}^{2\pi} \sin\phi d\phi$$

$$\approx -\left(\int_0^{\pi} 2 I_{e2} d\psi + \int_{\pi}^{2\pi} 2 I_{e1} d\psi\right) R_3 + 2V_{inp}\left(\frac{R_2 B_2}{R_3(A_{o1}B_2+1)} - \frac{R_1 B_1}{R_3(A_{o1}B_1+1)}\right) , \tag{172}$$

where

$$\int_0^{\pi} 2I_{e2}\, d\phi \simeq \frac{-V_{T2}\, B_2 \pi}{R_3(A_{o1}B_2+1)} \left(\ln\left(\frac{V_{inp}B_2(A_{o1}+1)}{2R_3(A_{o1}B_2+1)I_{s2}}\right)\right)$$

and

$$\int_{\pi}^{2\pi} 2I_{e1}\, d\phi \simeq \frac{V_{T1}\, B_1 \pi}{R_3(A_{o1}B_1+1)} \left(\ln\left(\frac{V_{inp}B_1(A_{o1}+1)}{2R_3(A_{o1}B_1+1)I_{s1}}\right)\right) .$$

Therefore, the voltage error for a nonsymmetrical rectifier circuit is

$$P_{ve} = P_{vsfe} + P_{vdce} + P_{vnle} ,$$

where

$$P_{vsfe} \simeq P_{csfe} + \frac{R_2\, B_2\, 100\%}{R_3(A_{o1}B_2+1)} - \frac{R_1\, B_1\, 100\%}{R_3(A_{o1}B_1+1)} ,$$

$$P_{vdce} \simeq 2P_{cdce} + \frac{\pi B_2 V_{T2}\, 50\%}{(A_{o1}B_2+1)V_{inp}} \ln\left(\frac{B_2(A_{o1}+1)}{R_3(A_{o1}B_2+1)2I_{s2}}\right) , \tag{173}$$

$$P_{vnle} \simeq 2P_{cnle} + \frac{\pi B_2 V_{T2}\, 50\%}{(A_{o1}B_2+1)V_{inp}} \ln(V_{inp}) ,$$

and P_{csfe}, P_{cdce}, and P_{cnle} are evaluated with $V_T = V_{T1}$ and $I_s = I_{s1}$. Note that the above equation indicates that all three error terms are dependent on the degree of asymmetry of the circuit. However, the piecewise-linear analysis predicted that P_{vsfe} is independent of the asymmetry of the rectifier circuit.

While the iteration method yields results of superior accuracy to that of the piecewise-linear technique, the computations are surprisingly simple for the former method. Unfortunately, frequency dependent

parameters are not readily handled by either method. In order to incorporate frequency dependence and additional nonlinearities, computer analysis methods will be discussed next.

Computer Simulation by Delay Method

Although the iterative method gives accurate results, it is still limited to frequency independent parameters. Frequency dependence can be handled in a computer analysis of the rectifier circuits. Two canned computer programs were considered: PCAP (Princeton Circuit Analysis Program) and CSMP (Computer System Modeling Program).[63,64,65] PCAP has the advantage of directly analyzing electronic circuits; however, its flexibility is rather limited. The PCAP diode model is the third-order piecewise-linear model. Although an exponential dependent current source is available, when attempts were made to use it in a diode configuration, the current would increase to a value many orders beyond the correct value. Moreover, PCAP does not allow general Fortran statements. CSMP, on the other hand, allows general Fortran statements. CSMP does not directly handle circuits, but handles system transfer functions. Additionally, many more options are available for integration methods with CSMP. Unfortunately, CSMP cannot solve the transcendental Equations (157 and (158) on page 117. However, the circuit can be modified to allow a CSMP solution.

An equivalent system block diagram of a precision rectifier circuit is pictured in Figure 28. As in the earlier two analyses, the opamp input and output impedances are assumed to be infinite and zero, respectively. However, the opamp slew rate limit and frequency response is included. Although a single pole opamp frequency response is shown,

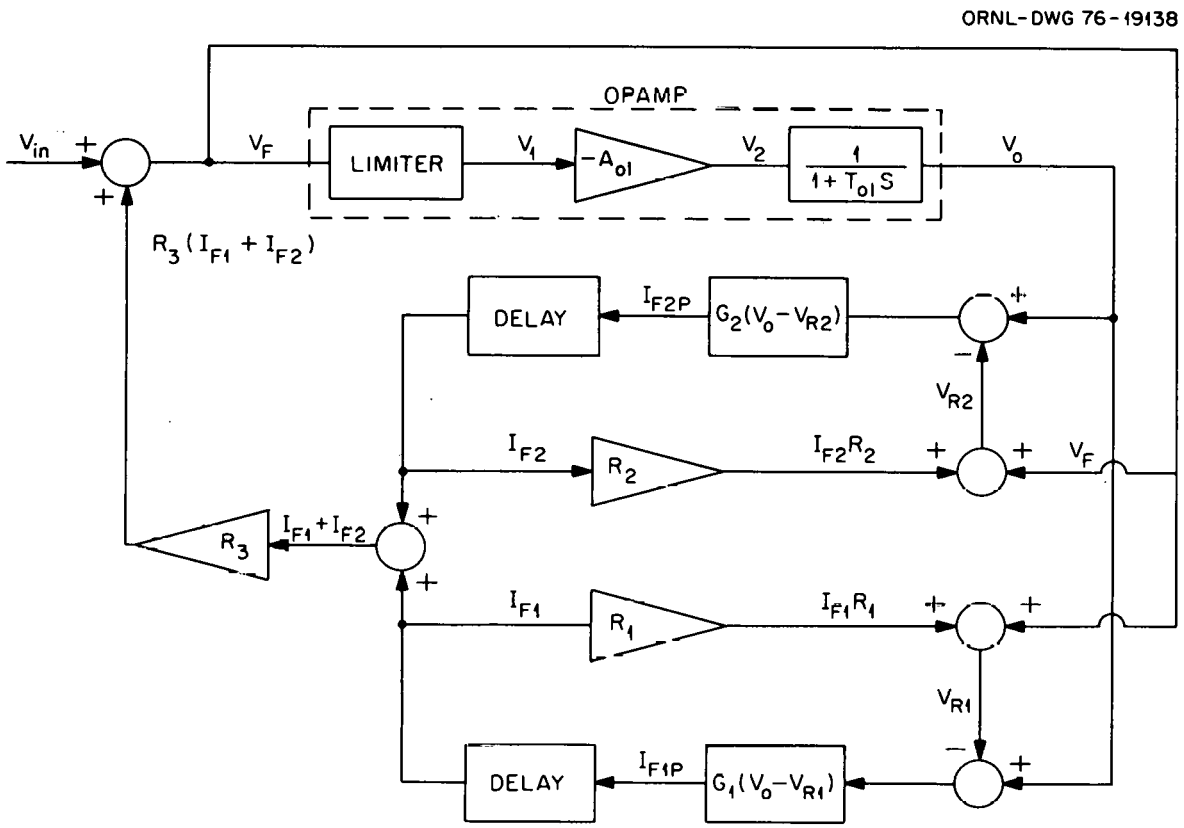

Figure 28. Block diagram of system representing precision rectifier.

any physically realizable frequency response can be handled in CSMP. The slew rate limitation is represented by the limiter. G_2 and G_1 represent the conductance of diodes D2 and D1, respectively. G_2 and G_1 can be any function, but exponential diodes will be considered here. The blocks marked delay are inserted into the system model to allow a solution and can be any function having memory such as a delay, a real pole, or an integrator. This is necessary since CSMP requires at least one memory function in each feedback loop.[64,65]

The CSMP program is listed in Appendix C. In this program several parameters may be set by the programmer. VINPK and FINPUT represent the negative peak amplitude (V) and the frequency (Hz) of the sinusoidal input voltage. IS1, IS2, VT1, and VT2 represent I_{s1}, I_{s2}, V_{T1}, and V_{T2}, respectively. AOL, GBWP, SRRISE, and SRFALL represent the open-loop DC opamp gain, the gain-bandwidth-product (Hz), and the magnitude of the positive and negative slew rate limits (V/sec) of the opamp, respectively. By definition, the time constant of the single pole opamp (TOL) is AOL/(2πGBWP). Since the application of a step function of height=SR TOL/AOL to the input of the opamp will result in an initial rate of change in V_o of -SR, the maximum and minimum values of V1 will determine SRFALL and SRRISE, respectively. Two types of errors are computed by the program: instantaneous and average. VERORT and IERORT are the instantaneous errors of the voltage and current output rectifiers:

$$\text{VERORT} = \frac{(\text{VR1RF} - \text{VOIDEL})\ 100\%}{\text{VOIDLA}}$$

and (174)

$$\text{IERORT} = \frac{(\text{VIF1RF} - \text{VOIDEL})\ 100\%}{\text{VOIDLA}} ,$$

where VR1RF = VR1 R3/R1, VIF1RF = IF1 R3, VOIDLA = -VINPK/π, and VOIDEL (the ideal output of the rectifier referred to the input) is given by

$$\text{VOIDEL} = -\text{VINPK VIND U}(-\text{VIND}) \tag{175}$$

where VIND = sin (2πFINPUT t + PHASE), U(X) is the unit step function, and PHASE is an estimate of the phase shift of the rectifier output due to the finite bandwidth of the opamp. PHASE is computed by estimating the closed-loop bandwidth of the circuit (FCL) by the following expression:

$$\text{PHASE} = \tan^{-1}(-\text{FINPUT/FCL}) \ , \tag{176}$$

where FCL = (AOL B_2 + 1)/(2 TOL), B_2 = R3/(R2 + R3 + $\frac{\text{VT2}}{\text{IF2IC1}}$), and IF2IC1 is an estimate of the initial value of IF2. It is assumed that D1 and D2 are initially off and on, respectively. After PHASE has been computed, a new estimate of IF2IC1 is made (IF2IC) by -VINPK sin (PHASE)/R3 (VINPK is assumed negative). This new estimate is compared with the old estimate to form the convergence criteria of an iterative loop. The initial value of VO is assumed equal to -VT2 ln(1.0 - IF2IC/IS2). The initial value of IF1 is assumed to be -IS1. Good estimates of initial conditions are important in the computation of VERORA and IERORA for small input signals. VERORA and IERORA (the average error of voltage and current output rectifiers, respectively) are given by the following equations:

$$\text{VERORA} = (\text{VOA} - \text{VOIDLA})\ 100\%/\text{VOIDLA}$$

and (177)

$$\text{IERORA} = (\text{IOA} - \text{VOIDLA})\ 100\%/\text{VOIDLA} \ ,$$

where VOA and IOA are the average values of VR1RF and VIF1RF over one period of the input waveform.

In the simulation of exponential diodes, the diode conductance is given by

$$G_i(VO - VRi) = \frac{IFiP}{VO-VRi} = \frac{ISi\ (EXP\ (\frac{VO - VRi}{VTi(-1)^{i+1}}) - 1)}{(VO - VRi)(-1)^{i+1}}\ , \tag{178}$$

where VRi = VF + Ri IFi and i is 1 or 2. The memory function relating IFiP to IFi must be chosen with care. For example if a delay function is chosen, then the delay time must be chosen small enough to prevent instability of the circuit and insure an accurate representation of the rectifier circuit. Unfortunately, a delay function can cause instability of the diode feedback loops since these loops do not have any poles. For instance, the small signal loop transmission of a diode loop is

$$T_{Di} = \frac{Ri(IFiP\ (-1)^{i+1} + ISi)}{VTi}\ DELAY\ . \tag{179}$$

For DELAY equal to a delay function, the phase of T_{Di} is

$$\underline{/T_{Di}} = -\ TDELAY\ 2\pi f\ , \tag{180}$$

where TDELAY is the delay time. Hence, if $|T_{Di}| = 1$, the system will be unstable. Since IFiP must go to zero for a sinusoidal input signal, IFiP must be less than $\frac{VTi}{Ri}$ - ISi if the loop is to be stable. For R1 = R2 = R3 and VTi = 26 mV, this restricts Vinp to less than 26 mV. If DELAY is a real pole instead of a delay, the diode loop will be stable since the maximum phase of T_{Di} is -90°. If the pole's time constant is TDELAY, then the close-loop small-signal diode transfer function is

$$G_i(S) = \frac{IFi}{VO - Vf} = ((R_{Fi} + Ri)(\frac{R_{Fi}\ TDELAY}{R_{Fi} + Ri} S + 1))^{-1} , \tag{181}$$

where $R_{Fi} = VTi/(IFi\ (-1)^{i+1} + ISi)$. Neglecting reverse diode currents, the rectifier circuit's small-signal loop transmission with Di on is

$$T_{ckt}(S) = \frac{AOL\ B_o}{(T_2\ S + 1)(TOL\ S + 1)} , \tag{182}$$

where $B_o = R3/(Ri + R3 + R_{Fi})$ and $T_2 = \frac{R_{Fi}\ TDELAY}{Ri + R3 + R_{Fi}}$. According to Pierce and Paulus,[50] the phase margin of a second-order system is

$$PM \simeq \tan^{-1} (\frac{4\xi^2}{(4\xi^4 + 1)^{1/2} - 2\xi^2})^{1/2} ,$$

where

$$\xi = \frac{T_2 + TOL}{2(T_2\ TOL\ (1 + AOL\ B_o))^{1/2}} .\ ^{49} \tag{183}$$

Since PM is minimum when ξ is minimum, the worst case condition for stability with a given value of TDELAY is when ξ is minimized with respect to R_{Fi}. Setting the derivative of ξ with respect to R_{Fi} equal to zero, the critical value of R_{Fi} is found to be

$$R_{Fic} = \frac{(Ri + R3)(1 + \frac{AOL\ R3}{Ri + R3})}{\frac{(TDELAY + TOL)}{TOL}(1 + \frac{AOL\ R3}{Ri + R3}) - 2} . \tag{184}$$

or if $AOL\ R3/(Ri + R3) >> 2$, then

$$R_{Fic} \simeq \frac{TOL\ (Ri + R3)}{TDELAY + TOL} .$$

Computing ξ for R_{Fi} equal to, greater than, and less than R_{Fic} shows that ξ is minimum at R_{Fic}. Thus, the minimum ξ is

$$\xi_{min} \simeq \left(\frac{(TDELAY + TOL)(Ri + R3)}{TDELAY\ R3\ AOL}\right)^{1/2}$$

$$\simeq \left(\frac{(TDELAY + TOL)(Ri + R3)}{TOL\ TDELAY\ GBWP\ 2\pi\ R3}\right)^{1/2}, \tag{185}$$

where AOL R3/(Ri + R3) >> 2. Solving Equation (180) for ξ in terms of PM, and assuming that TOL >> TDELAY, TDELAY is given for a specified PM or ξ by the following expression:

$$TDELAY \simeq \frac{(Ri + R3)}{R3\ GBWP\ 2\pi\ \xi_{min}}$$

$$\simeq \frac{(Ri + R3)(1 + \tan^2 PM)^{1/4}}{R3\ GBWP\ \pi\ \tan PM}. \tag{186}$$

To insure accurate representation, $\xi_{min} \gtrsim 1$ or PM $\gtrsim 76.35°$. For instance, if GBWP = 1 MHz and Ri = R3, then TDELAY $\lesssim$ 0.318 μs, but if Ri = 0Ω, then TDELAY $\lesssim$ 0.159 μs.

Figure 29 graphs the results of CSMP simulations of rectifier circuits with R1 = R2 = R3 = 2 KΩ and matched diodes with IS = 10 pA and VT = 26 mV. Figure 29(a) shows that the total average error is approximately inversely proportional to opamp gain and proportional to input frequency in the region of the 20 dB per decade roll off of the opamp gain for low input voltages. Also, this figure illustrates that a slew rate of 0.5 V/usec has little effect on the average error for 1 KHz input signals above 0.08 V peak and no effect below 0.08 V peak. The threshold input voltage for slew limiting can be estimated

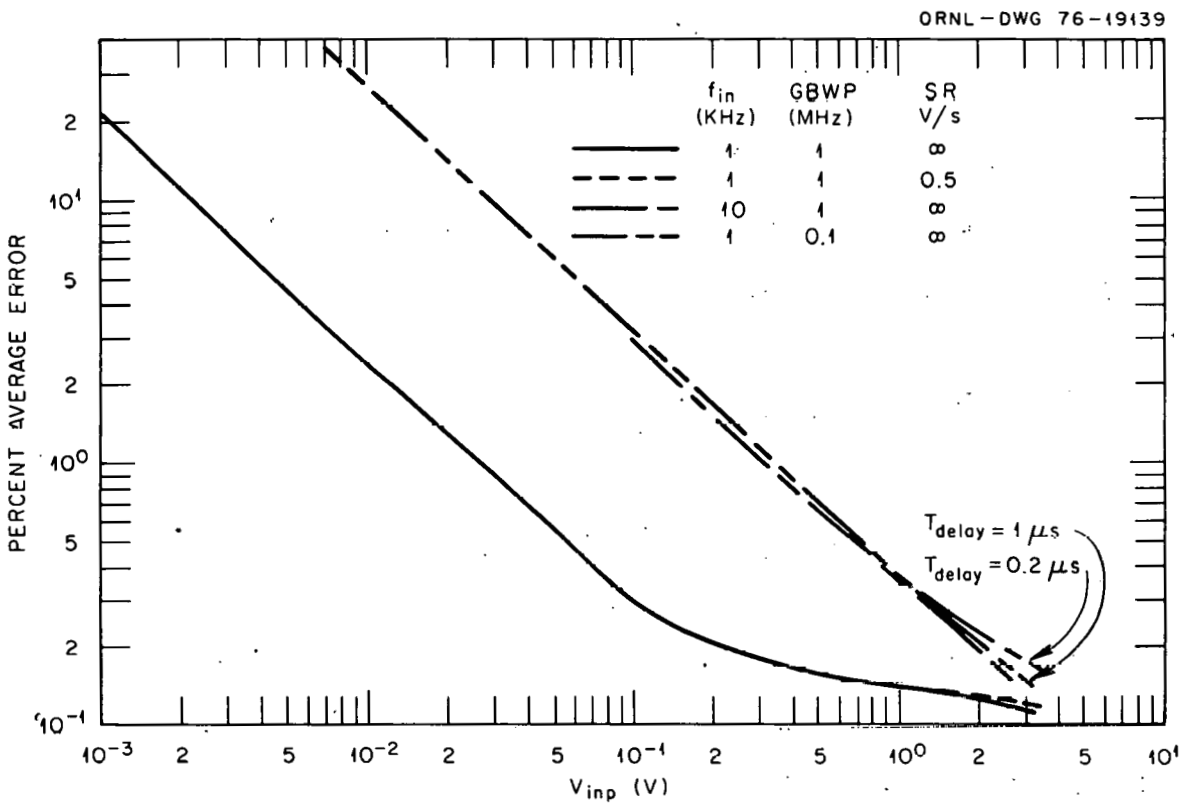

(a) Computed average error.

Figure 29. Error analysis, by delay method, of precision rectifier with $A_{o1} = 2 \times 10^5$, $R_1 = R_2 = R_3 = 2K\Omega$, and matched diodes having I_s = 10 pA, and V_T = 26 mV.

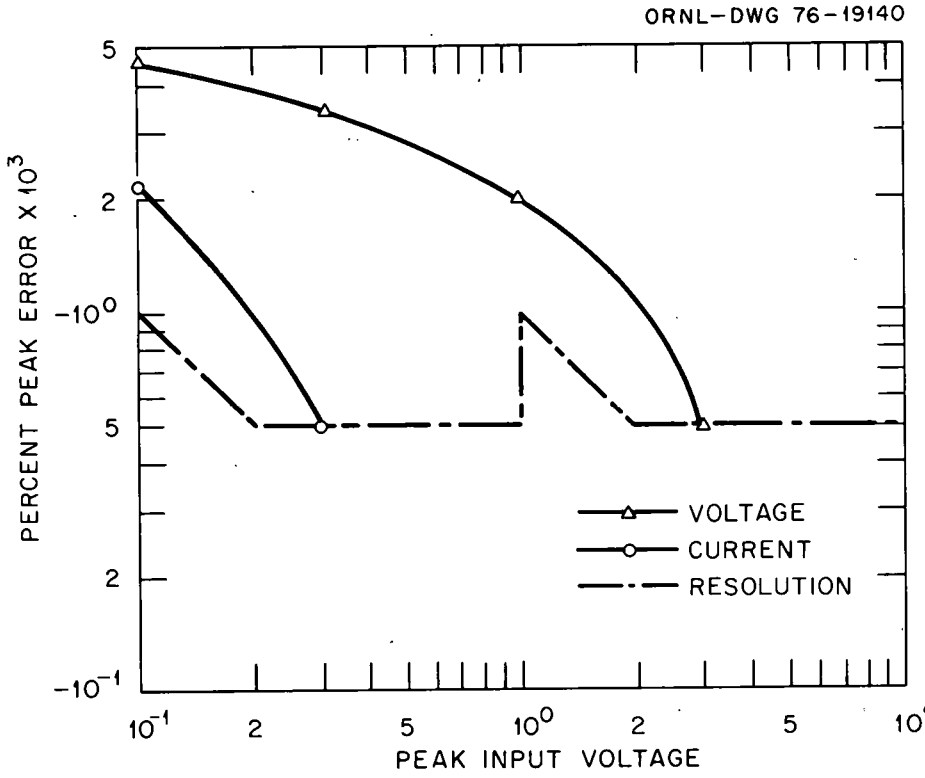

(b) Computed 1 KHz peak error with GBWP = 1 MHz and SR = 0.5 V/μs.

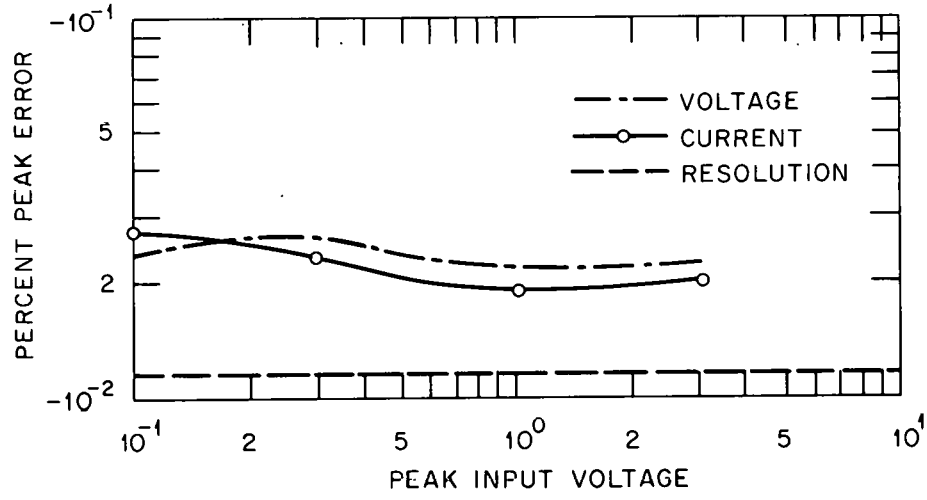

(c) Computed 10 KHz peak error with GBWP = 1 MHz.

Figure 29 (continued)

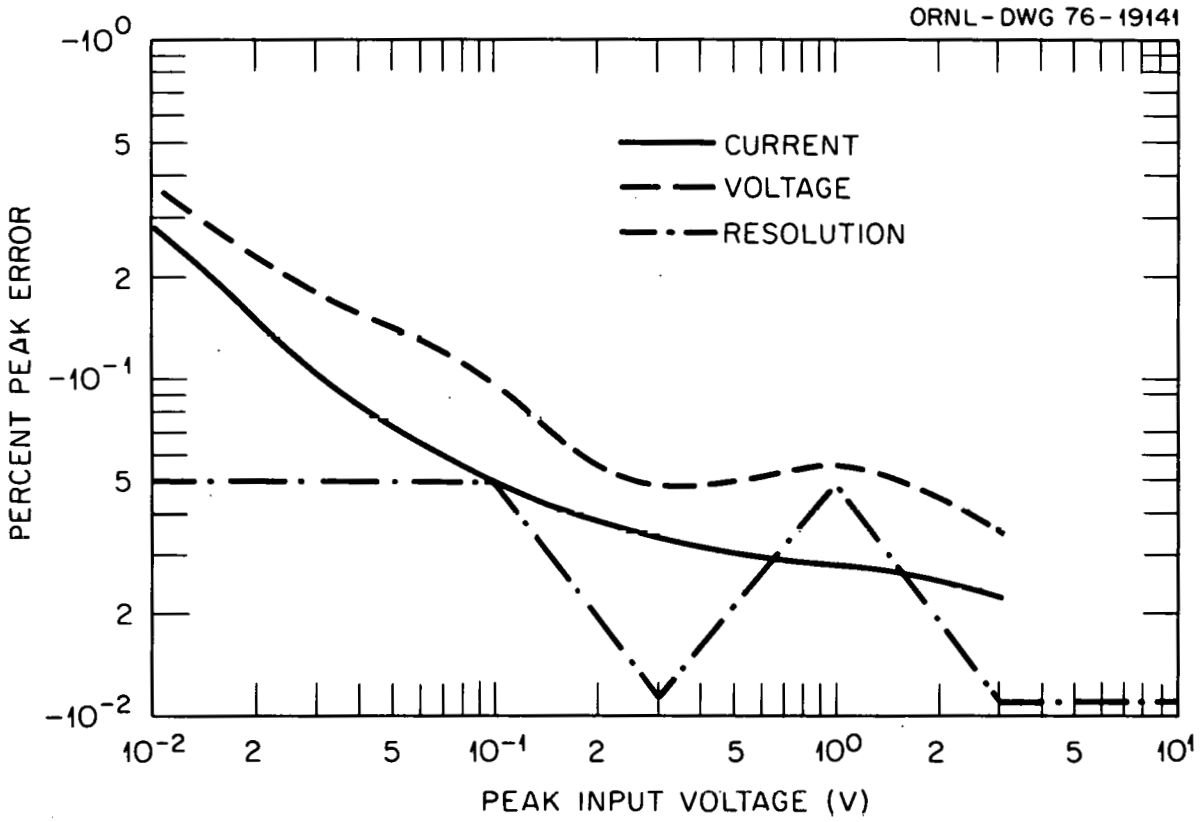

(d) Computed 1 KHz peak error with GBWP = 100 KHz.

Figure 29 (continued)

by assuming a second-order piecewise-linear diode. Then when both diodes are off, there is no negative feedback. If the input signal is sinusoidal, then

$$\dot{V}_{in}(t) = \omega_o V_{in}(t) = \dot{VF} = \frac{\dot{VO}\ (1 + jTOL\ \omega_o)}{AOL}$$

or (187)

$$VINPK_s = \frac{SR\ (1 + TOL^2\ \omega_o{}^2)^{1/2}}{AOL} ,$$

where ω_o is the radian input frequency, SR is the slew rate limit, and $VINPK_s$ is the maximum peak input voltage without slew limit. Note that for ω_o TOL >> 1, $VINPK_s \simeq SR\ TOL/AOL = SR/(2\pi\ GBWP)$. Thus, for an opamp having a GBWP of 1 MHz and a SR of 0.5 V/μsec, $VINPK_s \simeq 0.0796$ V. Since real diodes always conduct to some extent either due to reverse saturation current or junction capacitance, expression (187) gives a conservative estimate for $VINPK_s$. The effect of slewing on rectifier waveforms is shown in Figure 30. If a second-order piecewise-linear diode is assumed, the time required to turn D1 on and D2 off is

$$T_{SR} \simeq (V_{F1} + V_{F2} + V_{f1} - V_{f2})/SR ,$$

or if ω_o TOL >> 1 and ω_o << 2π FCL, then (188)

$$T_{SR} \simeq (V_{F1} + V_{F2})(\frac{1}{SR} - \frac{1}{V_{in}(t_o)}) ,$$

where $V_{f1} = V_{f2} = V_{in}$ when D1 and D2 turn on and off, respectively, while $V_{in}(t_o)$ is the mean rate of change in $V_{in}(t)$ during the time when D2 turns off and D1 turns on. While T_{SR} can be used to estimate the error due to slew rate limiting, the estimate may be optimistic unless

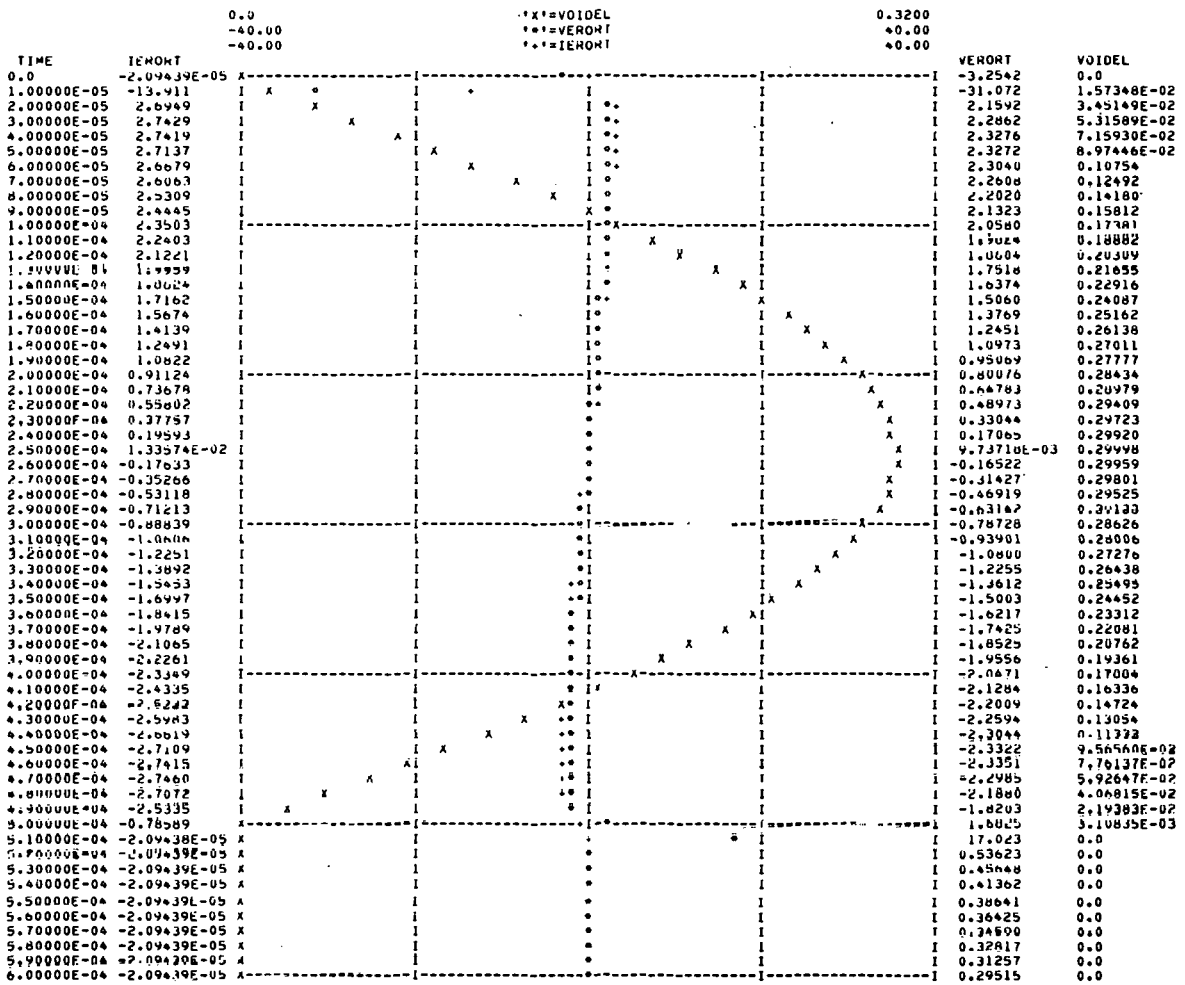

TIME	IERORT	VERORT	VOIDEL
0.0	-2.09439E-05	-3.2542	0.0
1.00000E-05	-13.911	-31.072	1.57348E-02
2.00000E-05	2.6949	2.1592	3.45149E-02
3.00000E-05	2.7429	2.2862	5.31589E-02
4.00000E-05	2.7419	2.3276	7.15930E-02
5.00000E-05	2.7137	2.3272	8.97446E-02
6.00000E-05	2.6679	2.3040	0.10754
7.00000E-05	2.6063	2.2608	0.12492
8.00000E-05	2.5309	2.2020	0.14180
9.00000E-05	2.4445	2.1323	0.15812
1.00000E-04	2.3503	2.0580	0.17381
1.10000E-04	2.2403	1.9024	0.18882
1.20000E-04	2.1221	1.8604	0.20309
1.30000E-04	1.9959	1.7518	0.21655
1.40000E-04	1.8624	1.6374	0.22916
1.50000E-04	1.7162	1.5060	0.24087
1.60000E-04	1.5674	1.3769	0.25162
1.70000E-04	1.4139	1.2451	0.26138
1.80000E-04	1.2491	1.0973	0.27011
1.90000E-04	1.0822	0.95069	0.27777
2.00000E-04	0.91124	0.80076	0.28434
2.10000E-04	0.73678	0.64783	0.28979
2.20000E-04	0.55802	0.48973	0.29409
2.30000E-04	0.37757	0.33044	0.29723
2.40000E-04	0.19593	0.17065	0.29920
2.50000E-04	1.33574E-02	9.73710E-03	0.29998
2.60000E-04	-0.17633	-0.16522	0.29959
2.70000E-04	-0.35266	-0.31427	0.29801
2.80000E-04	-0.53118	-0.46919	0.29525
2.90000E-04	-0.71213	-0.63162	0.29133
3.00000E-04	-0.88839	-0.78728	0.28626
3.10000E-04	-1.0808	-0.93901	0.28006
3.20000E-04	-1.2251	-1.0800	0.27276
3.30000E-04	-1.3892	-1.2255	0.26438
3.40000E-04	-1.5453	-1.3612	0.25495
3.50000E-04	-1.6997	-1.5003	0.24452
3.60000E-04	-1.8415	-1.6217	0.23312
3.70000E-04	-1.9789	-1.7425	0.22081
3.80000E-04	-2.1065	-1.8525	0.20762
3.90000E-04	-2.2261	-1.9556	0.19361
4.00000E-04	-2.3349	-2.0471	0.17004
4.10000E-04	-2.4335	-2.1284	0.16336
4.20000E-04	-2.5242	-2.2009	0.14724
4.30000E-04	-2.5983	-2.2594	0.13054
4.40000E-04	-2.6619	-2.3044	0.11372
4.50000E-04	-2.7109	-2.3322	9.56560E-02
4.60000E-04	-2.7415	-2.3351	7.76137E-02
4.70000E-04	-2.7460	-2.2985	5.92647E-02
4.80000E-04	-2.7072	-2.1880	4.06815E-02
4.90000E-04	-2.5335	-1.8203	2.19383E-02
5.00000E-04	-0.78589	1.6825	3.10835E-03
5.10000E-04	-2.09438E-05	17.023	0.0
5.20000E-04	-2.09439E-05	0.53623	0.0
5.30000E-04	-2.09439E-05	0.45848	0.0
5.40000E-04	-2.09439E-05	0.41362	0.0
5.50000E-04	-2.09439E-05	0.38641	0.0
5.60000E-04	-2.09439E-05	0.36425	0.0
5.70000E-04	-2.09439E-05	0.34690	0.0
5.80000E-04	-2.09439E-05	0.32817	0.0
5.90000E-04	-2.09439E-05	0.31257	0.0
6.00000E-04	-2.09439E-05	0.29515	0.0

(a) VOIDEL, VERORT, and IERORT with no slew limit.

Figure 30. One KHz performance, computed by delay method, of precision rectifiers with and without SR limits, $A_{01} = 2 \times 10^5$, GBWP = 1 MHz, $R_1 = R_2 = R_3 = 2K\Omega$, and matched diodes.

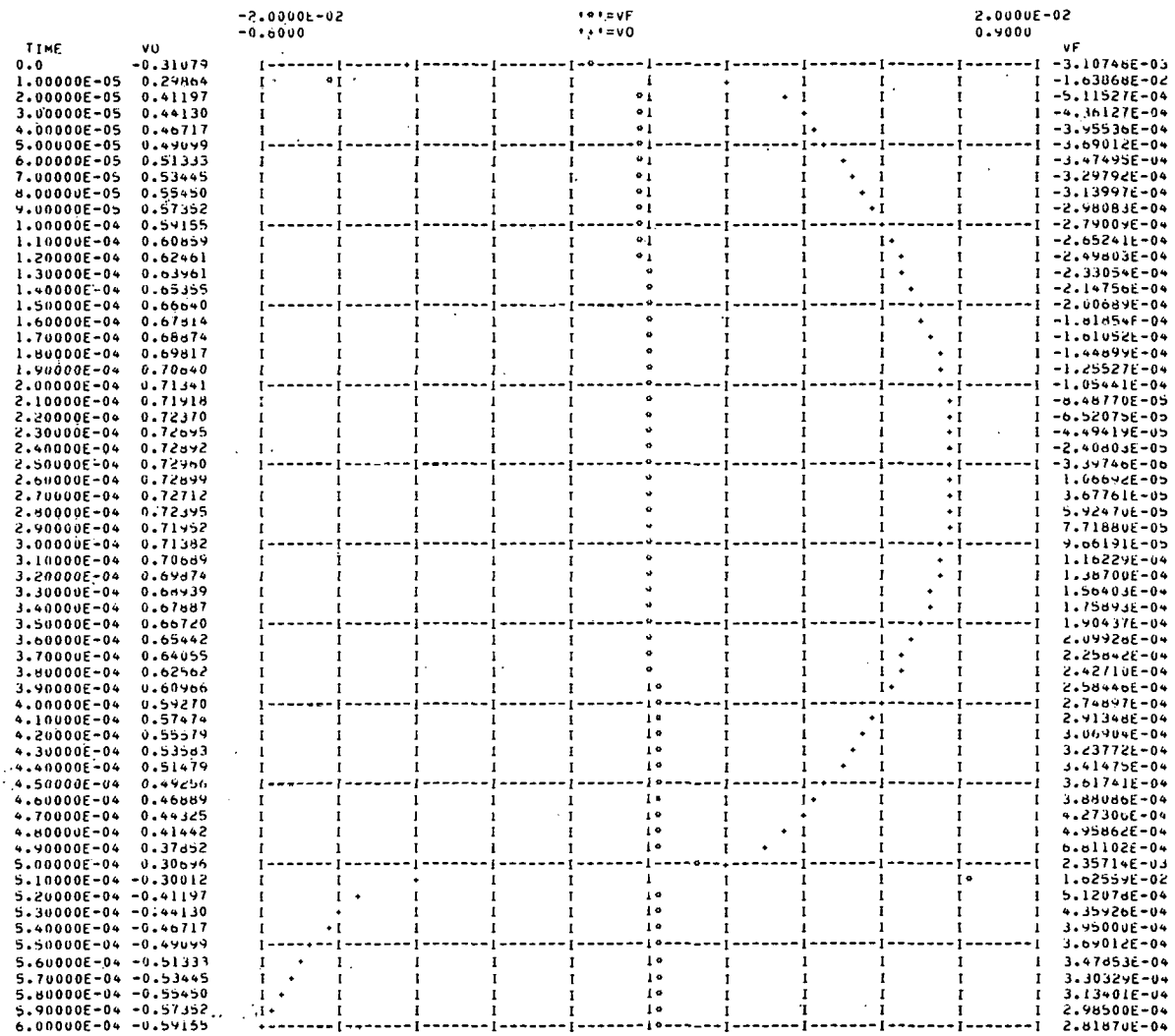

TIME	VO	VF
0.0	-0.31079	-3.10746E-03
1.00000E-05	0.29864	-1.63868E-02
2.00000E-05	0.41197	-5.11527E-04
3.00000E-05	0.44130	-4.36127E-04
4.00000E-05	0.46717	-3.95536E-04
5.00000E-05	0.49099	-3.69012E-04
6.00000E-05	0.51333	-3.47495E-04
7.00000E-05	0.53445	-3.29792E-04
8.00000E-05	0.55450	-3.13997E-04
9.00000E-05	0.57352	-2.98083E-04
1.00000E-04	0.59155	-2.79009E-04
1.10000E-04	0.60859	-2.65241E-04
1.20000E-04	0.62461	-2.49803E-04
1.30000E-04	0.63961	-2.33054E-04
1.40000E-04	0.65355	-2.14756E-04
1.50000E-04	0.66640	-2.00689E-04
1.60000E-04	0.67814	-1.81854E-04
1.70000E-04	0.68874	-1.61052E-04
1.80000E-04	0.69817	-1.44899E-04
1.90000E-04	0.70640	-1.25527E-04
2.00000E-04	0.71341	-1.05441E-04
2.10000E-04	0.71918	-8.48770E-05
2.20000E-04	0.72370	-6.52075E-05
2.30000E-04	0.72695	-4.49419E-05
2.40000E-04	0.72892	-2.40803E-05
2.50000E-04	0.72960	-3.39746E-06
2.60000E-04	0.72899	1.66692E-05
2.70000E-04	0.72712	3.67761E-05
2.80000E-04	0.72395	5.92470E-05
2.90000E-04	0.71952	7.71880E-05
3.00000E-04	0.71382	9.66191E-05
3.10000E-04	0.70689	1.16229E-04
3.20000E-04	0.69874	1.38700E-04
3.30000E-04	0.68939	1.56403E-04
3.40000E-04	0.67887	1.75893E-04
3.50000E-04	0.66720	1.90437E-04
3.60000E-04	0.65442	2.09926E-04
3.70000E-04	0.64055	2.25842E-04
3.80000E-04	0.62562	2.42710E-04
3.90000E-04	0.60966	2.58446E-04
4.00000E-04	0.59270	2.74897E-04
4.10000E-04	0.57474	2.91348E-04
4.20000E-04	0.55579	3.06906E-04
4.30000E-04	0.53583	3.23772E-04
4.40000E-04	0.51479	3.41475E-04
4.50000E-04	0.49256	3.61741E-04
4.60000E-04	0.46889	3.88086E-04
4.70000E-04	0.44325	4.27306E-04
4.80000E-04	0.41442	4.95862E-04
4.90000E-04	0.37852	6.81102E-04
5.00000E-04	0.30696	2.35714E-03
5.10000E-04	-0.30012	1.62559E-02
5.20000E-04	-0.41197	5.12078E-04
5.30000E-04	-0.44130	4.35926E-04
5.40000E-04	-0.46717	3.95000E-04
5.50000E-04	-0.49099	3.69012E-04
5.60000E-04	-0.51333	3.47853E-04
5.70000E-04	-0.53445	3.30329E-04
5.80000E-04	-0.55450	3.13401E-04
5.90000E-04	-0.57352	2.98500E-04
6.00000E-04	-0.59155	2.81870E-04

(b) VF and VO with no slew limit.

Figure 30 (continued)

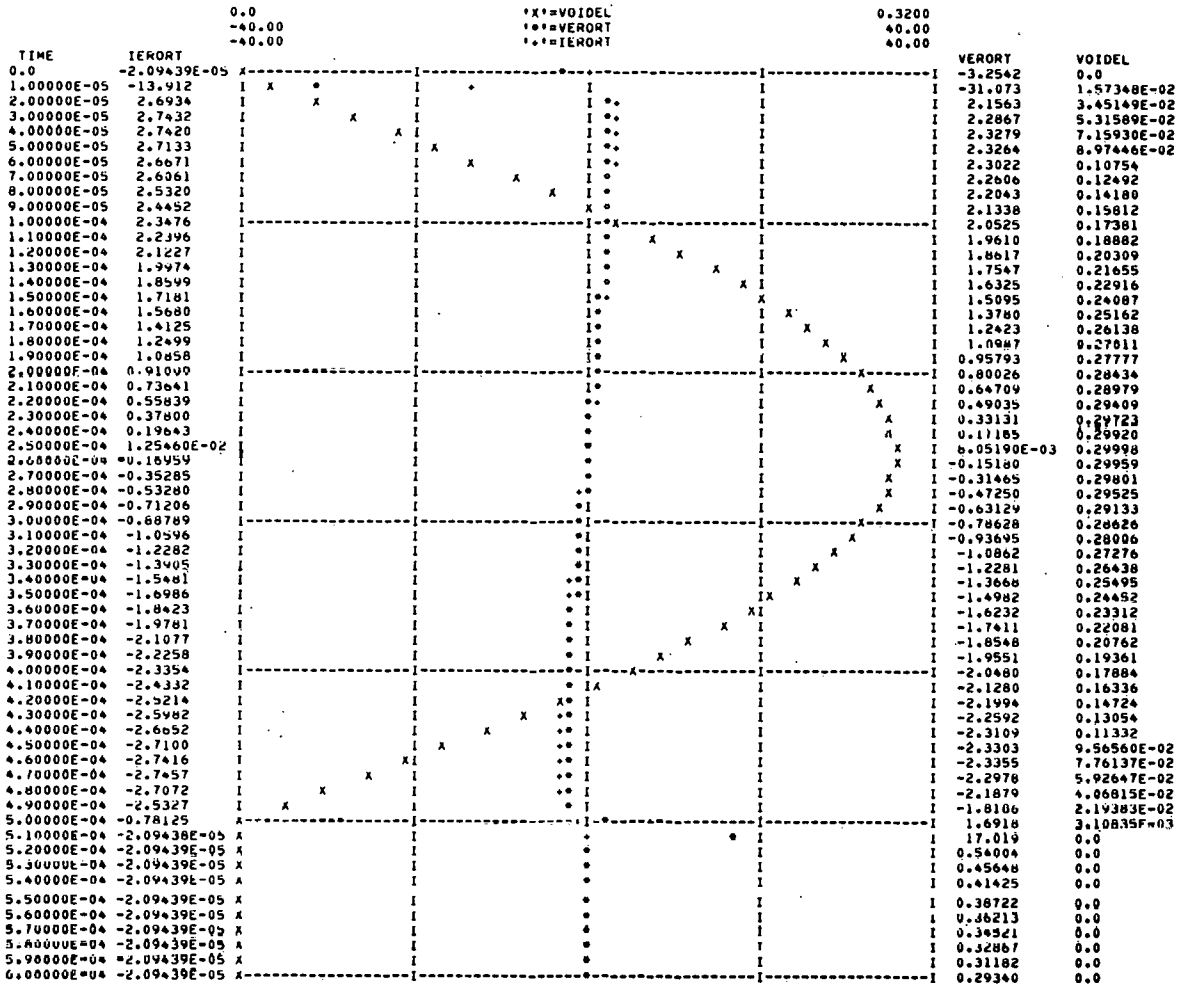

TIME	IERORT	VERORT	VOIDEL
0.0	-2.09439E-05	-3.2542	0.0
1.00000E-05	-13.912	-31.073	1.57348E-02
2.00000E-05	2.6934	2.1563	3.45149E-02
3.00000E-05	2.7432	2.2867	5.31589E-02
4.00000E-05	2.7420	2.3279	7.15930E-02
5.00000E-05	2.7133	2.3264	8.97446E-02
6.00000E-05	2.6671	2.3022	0.10754
7.00000E-05	2.6061	2.2606	0.12492
8.00000E-05	2.5320	2.2043	0.14180
9.00000E-05	2.4452	2.1338	0.15812
1.00000E-04	2.3476	2.0525	0.17381
1.10000E-04	2.2396	1.9610	0.18882
1.20000E-04	2.1227	1.8617	0.20309
1.30000E-04	1.9974	1.7547	0.21655
1.40000E-04	1.8599	1.6325	0.22916
1.50000E-04	1.7181	1.5095	0.24087
1.60000E-04	1.5680	1.3780	0.25162
1.70000E-04	1.4125	1.2423	0.26138
1.80000E-04	1.2499	1.0987	0.27011
1.90000E-04	1.0858	0.95793	0.27777
2.00000E-04	0.91099	0.80026	0.28434
2.10000E-04	0.73641	0.64709	0.28979
2.20000E-04	0.55839	0.49035	0.29409
2.30000E-04	0.37800	0.33131	0.29723
2.40000E-04	0.19643	0.17185	0.29920
2.50000E-04	1.25460E-02	6.05190E-03	0.29998
2.60000E-04	-0.16959	-0.15180	0.29959
2.70000E-04	-0.35285	-0.31465	0.29801
2.80000E-04	-0.53280	-0.47250	0.29525
2.90000E-04	-0.71206	-0.63129	0.29133
3.00000E-04	-0.88789	-0.78628	0.28626
3.10000E-04	-1.0596	-0.93695	0.28006
3.20000E-04	-1.2282	-1.0862	0.27276
3.30000E-04	-1.3905	-1.2281	0.26438
3.40000E-04	-1.5481	-1.3668	0.25495
3.50000E-04	-1.6986	-1.4982	0.24452
3.60000E-04	-1.8423	-1.6232	0.23312
3.70000E-04	-1.9781	-1.7411	0.22081
3.80000E-04	-2.1077	-1.8548	0.20762
3.90000E-04	-2.2258	-1.9551	0.19361
4.00000E-04	-2.3354	-2.0480	0.17884
4.10000E-04	-2.4332	-2.1280	0.16336
4.20000E-04	-2.5214	-2.1994	0.14724
4.30000E-04	-2.5982	-2.2592	0.13054
4.40000E-04	-2.6652	-2.3109	0.11332
4.50000E-04	-2.7100	-2.3303	9.56560E-02
4.60000E-04	-2.7416	-2.3355	7.76137E-02
4.70000E-04	-2.7457	-2.2978	5.92647E-02
4.80000E-04	-2.7072	-2.1879	4.06815E-02
4.90000E-04	-2.5327	-1.8106	2.19383E-02
5.00000E-04	-0.78125	1.6918	3.10835E-03
5.10000E-04	-2.09438E-05	17.019	0.0
5.20000E-04	-2.09439E-05	0.54004	0.0
5.30000E-04	-2.09439E-05	0.45648	0.0
5.40000E-04	-2.09439E-05	0.41425	0.0
5.50000E-04	-2.09439E-05	0.38722	0.0
5.60000E-04	-2.09439E-05	0.36213	0.0
5.70000E-04	-2.09439E-05	0.34521	0.0
5.80000E-04	-2.09439E-05	0.32867	0.0
5.90000E-04	-2.09439E-05	0.31182	0.0
6.00000E-04	-2.09439E-05	0.29340	0.0

(c) VOIDEL, VERORT, and IERORT with SR = 0.5 V/μsec.

Figure 30 (continued)

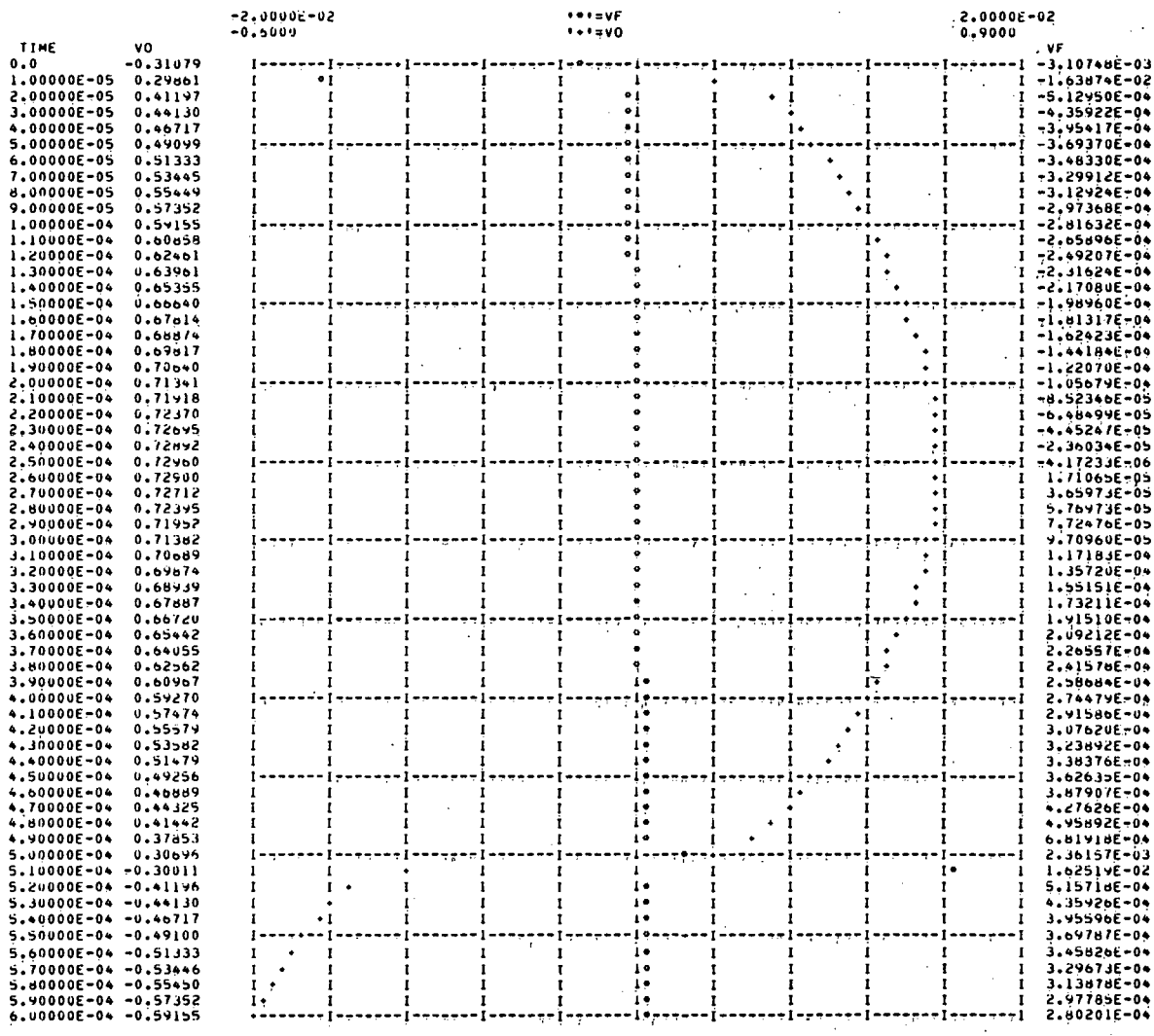

(d) VF and VO with SR = 0.5 V/μsec.

Figure 30 (continued)

the recovery behavior of the amplifier is included in the analysis. That is, once D1 is turned off, V_f remains above the limiting value for a period of time: the amplifier remains overloaded. A measure of this recovery time is known as the settling time (the time required for the output of an opamp to reach a value within a specified error bound of its final value with a step input signal). This overload phenomenon also is known as transient intermodulation distortion.[66] The recovery behavior of the opamp depends on the open-loop frequency response of the opamp and the feedback network. For more information on slew rate recovery see References 66, 67, 68, and 69. Figure 31 shows the effects of settling time on rectifier waveforms. The test apparatus employed to photograph rectifier waveforms is shown in Figure 32.

Figure 29(b), (c), and (d) on pages 141 and 142 graph the peak errors computed by the delay method. Note that these errors are much less than those shown in Figure 27(c) on page 126. This is due to the phase of VF with respect to ID1 and VR1: for a circuit with no frequency response limitations, VF is out of phase with the rectifier output, but it is in quadrature with the output for ω_o TOL >> 1. Since VF is approximately zero when the output and input of the rectifier are at their peak excursions for the latter case, the peak error must be approximately zero (see Figure 30). But in the former, VF is at a local peak; therefore, considerable peak error can exist.

The method of integrating, integration step size, and TDELAY can influence the results of the CSMP simulation. Choosing TDELAY too small will increase the CPU time of the program. Also, choosing a step size too large can cause the integration routine to diverge, while

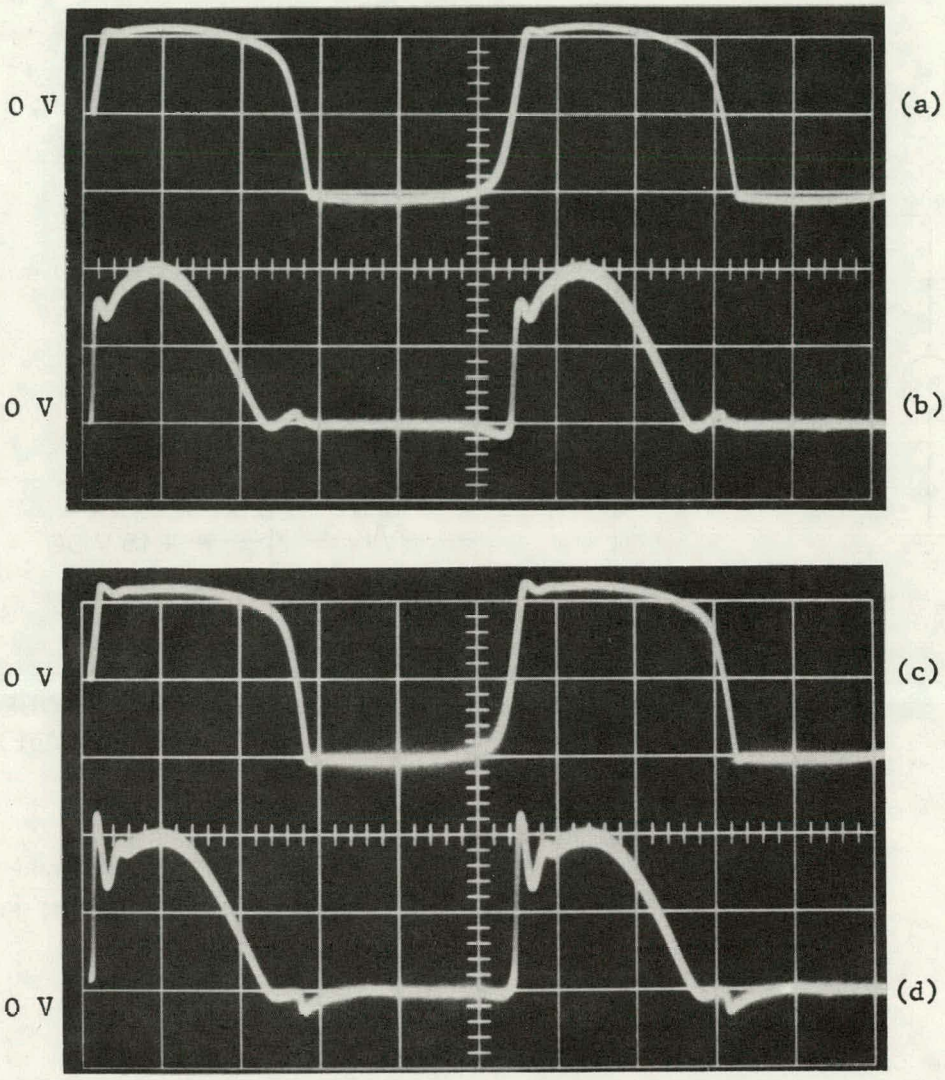

Figure 31. Effects of opamp settling time on 0.1 V_p 100 KHz waveforms of a FD300 diode rectifier with R_2 = 0Ω, R_1 = R_3 = 2 KΩ, C_3 = 0.2 μF, and an AD528JH opamp. (a) V_o with settling time compensation; (b) V_{R1} with settling time compensation; (c) V_o without settling time compensation; (d) V_{R1} without settling time compensation. Typical settling time to 0.1%: 800 ns [curves (a) and (b)]; 2 μs [curves (c) and (d)]. Horizontal scale: 2 μs/div. Vertical scale: 0.5 V/div [curves (a) and (c)]; 0.05 V/div [curves (b) and (d)].

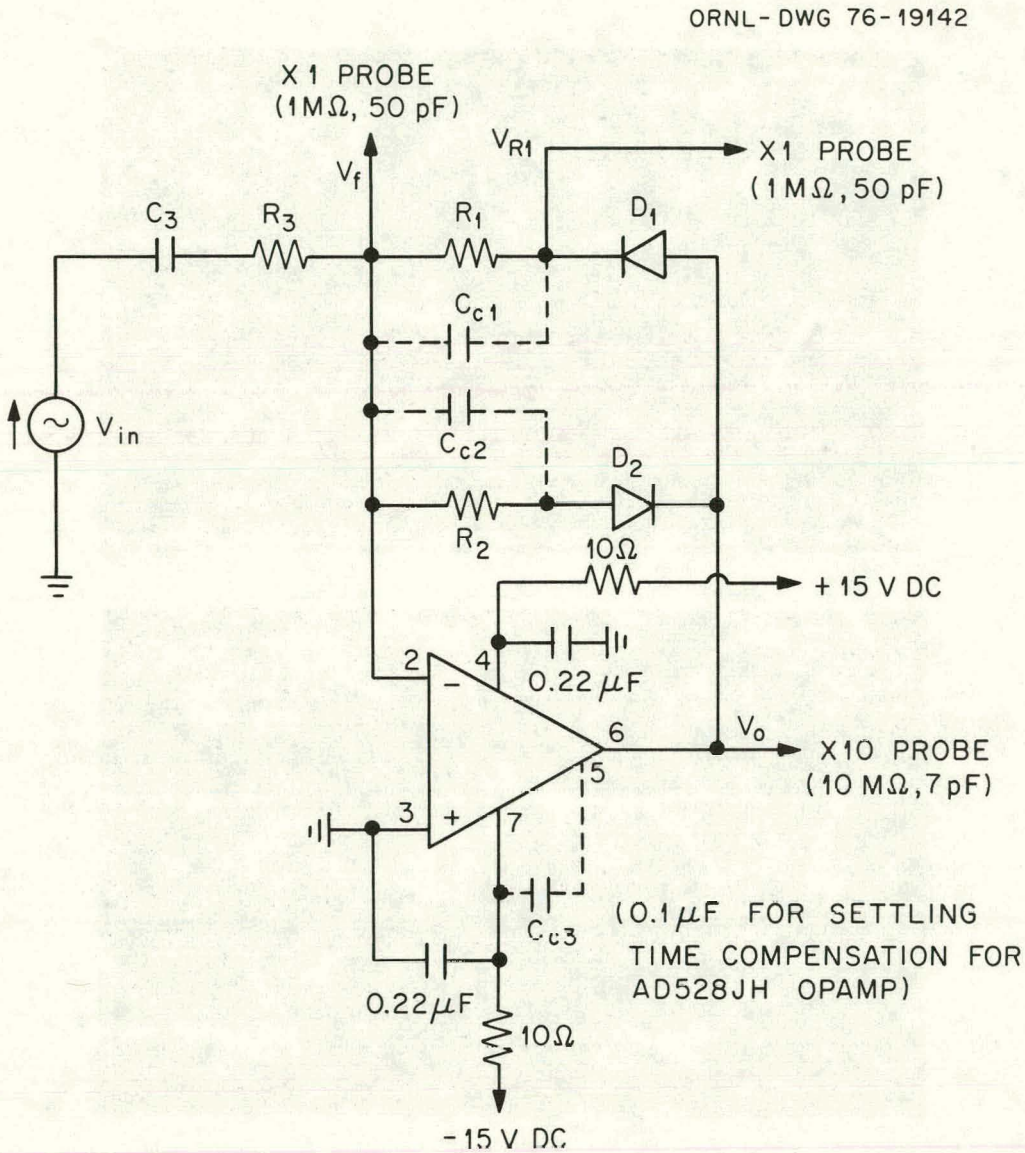

Figure 32. Test apparatus employed to photograph rectifier waveforms. A Tektronix 535A oscilloscope with a 54/53C plug-in dual channel amplifier was employed for oscilloscope photographs. The X1 probe was disconnected from V_f while V_{R1} and V_o were being photographed. R_1, R_2, and R_3 are wirewound resistors (Daven type 1350). Circuit was breadboarded on a Continental Specialties Proto Board® model 103. C_{c1} and C_{c2} are 22 pF for AD528JH opamp, and 0 pF otherwise.

choosing a step size too small can result in round-off error or excessive CPU time. CSMP offers several fixed step and variable step integration routines, and the author tried several of these routines. Because of the high degree of nonlinearity of the system, fixed step integration is impractical. STIFF is by far the best integration routine that is offered in IBM's CSMP III.[64,65] STIFF integration is designed for systems having widely separated poles and in this system, has much lower sensitivity to maximum step size and much faster CPU time than Runge Kutta integration. Unfortunately, only Runge Kutta is available as a canned double precision routine. For average rectifier errors below 0.3%, round-off error becomes significant for STIFF integration. But for Runge Kutta to converge to an accuracy equal to STIFF integration requires step sizes orders of magnitude smaller than that used with STIFF in Figure 29 on pages 140-142. The maximum step size is equal to the output interval (PRDEL) which was chosen as 0.5% of the period of the input signal, except for the case where a slew rate limit was assumed in which a PRDEL of 0.1% of the input signal period was employed to better resolve the spikes of VF.

In the variable step integration routine, two convergence criteria may be chosen for each integrator: ABSERR and RELERR. In this method, a complementary integration routine is employed to estimate the integral (Y_e). The step size is reduced until the computed integral (Y_c) meets the following requirements or the step size reaches the lower limit:

$$|Y_c - Y_e| \leq \text{ABSERR} + \text{RELERR}\ |Y_c| \ . \tag{189}$$

Because of the nonlinearity of the system, these error criteria must be chosen with care. For instance, the desired computational accuracy of the diode currents are directly given by RELERR and ABSERR of IF1 and IF2, but the accuracy of VO is exponentially related to the accuracy of the diode currents. For instance, if VR1 and VR2 are assumed zero, then the error in VO (ΔVO) causes a relative error in IFi of

$$\frac{\Delta IFi}{IFi} = \frac{\Delta VO}{VTi} . \tag{190}$$

Specifying ABSERR of VO (ΔVO) determines the relative error of IFi. However, as shown previously, the actual error of IFi can be expected to consist largely of both a scale factor and a DC error. Choosing RELERR does not help significantly since VO is approximately related to IFi logarithmically. Good choices for ABSERR of VO are VTi P_{ce}IFi max/$\overline{IFi}$ and VTi P_{cp} where P_{ce} and P_{cp} are the desired relative average and peak accuracies of the simulation, respectively. RELERR may then be set to zero. Note that increasing the desired accuracy reduces the CPU time up to a point, beyond which the results begin to diverge and the CPU time increases.

In addition to affecting integrator accuracies, the output interval limits resolution of peak values of rectifier outputs. For example, if V_{in} is sinusoidal and the output interval is PRDEL, then the maximum resolution error is

$$\begin{aligned} P_{rp} &= 100\% \ (\cos(\omega_o \frac{PRDEL}{2}) - 1) \\ &\simeq -12.5\% \ (\omega_o \ PRDEL)^2 . \end{aligned} \tag{191}$$

Since the integration step size will normally be less than PRDEL, a procedural subroutine can be placed in the CSMP program to hold the maximum computed values for outputs, thereby substantially improving P_{rp}. This was not done for any of the computer results presented in this dissertation since the result of primary interest is the average error. Peak errors, however, are presented since they will be of interest to some readers.

Figures 30 (pages 144-147) and 33 show rectifier waveforms computed by the delay method, while Figures 34, 35, and 36 show measured rectifier waveforms. The FD300 diodes have characteristics similar to those modeled in the computer analysis. Moreover, the AD506LH opamp is an FET input opamp having input bias currents less than 5 pA and input offset voltages less than 1.0 mV to minimize offset errors. Other characteristics of the AD506LH also closely approximate the computer model (i.e., AOL = 120,000 and GBWP = 1 MHz with a single pole). Furthermore, slew rate errors are zero since SR > 3V/μsec. Comparing Figure 33(a) and (c) with Figure 34, Figure 33(d) and (f) with Figure 35, and Figure 33(i), (k), (l), and (n) with Figure 36 shows that the computer simulation accurately predicts the rectifier waveforms at moderate input signal levels. Note that the relative phase between traces on any of the oscilloscope pictures presented in this dissertation cannot be compared since the triggering on each trace is independent. For example, in Figure 36, the phase relations among traces C, D, E, and F are approximately correct, but these traces are approximately out of phase with A and B. Note especially the spikes on VF and VR1 that are predicted with good accuracy in the computer results. Note also that these spikes increase in amplitude as either the gain or

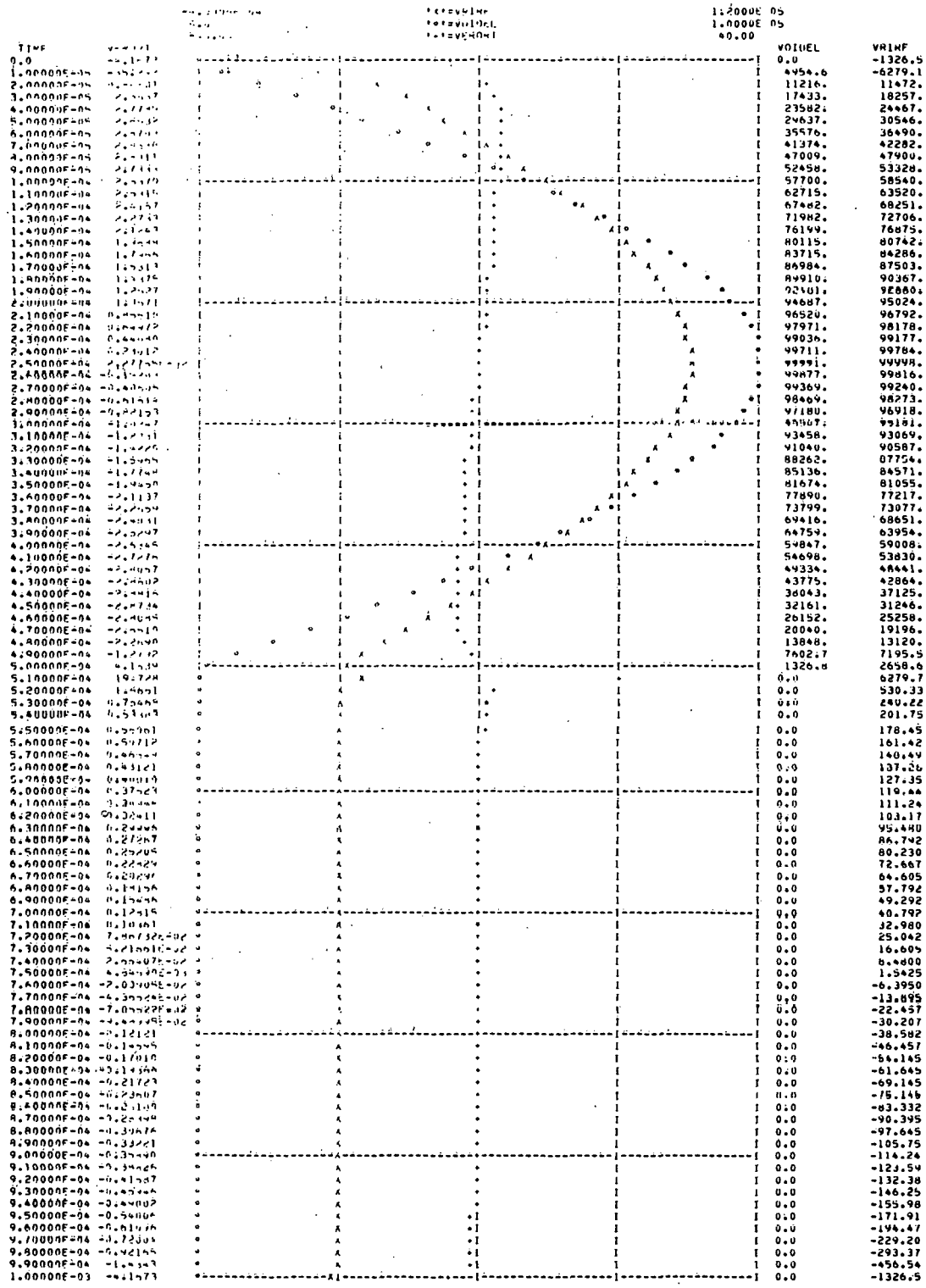

(a) VR1RF, VOIDEL, and VERORT at 1 KHz with R_2 = 2 KΩ.

Figure 33. Performance of precision rectifiers computed by delay method for A_{o1} = 2 × 10^5, GBWP = 1 MHz, R_1 = R_2 = 2 KΩ, and matched diodes. All voltages in μV.

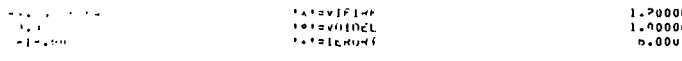

TIME		VOIDEL	VIF1RF
0.0		0.0	0.0
1.00000E-05		4954.6	-1.90941E-02
2.00000E-05		11216.	12003.
3.00000E-05		17433.	18498.
4.00000E-05		23582.	24668.
5.00000E-05		29637.	30724.
6.00000E-05		35576.	36651.
7.00000E-05		41374.	42430.
8.00000E-05		47009.	48038.
9.00000E-05		52458.	53455.
1.00000E-04		57700.	58659.
1.10000E-04		62715.	63631.
1.20000E-04		67482.	68353.
1.30000E-04		71982.	72801.
1.40000E-04		76199.	76963.
1.50000E-04		80115.	80822.
1.60000E-04		83715.	84360.
1.70000E-04		86984.	87567.
1.80000E-04		89910.	90425.
1.90000E-04		92481.	92929.
2.00000E-04		94687.	95065.
2.10000E-04		96520.	96825.
2.20000E-04		97971.	98204.
2.30000E-04		99036.	99194.
2.40000E-04		99711.	99793.
2.50000E-04		99991.	99999.
2.60000E-04		99877.	99809.
2.70000E-04		99369.	99226.
2.80000E-04		98469.	98251.
2.90000E-04		97180.	96888.
3.00000E-04		95507.	95143.
3.10000E-04		93456.	93023.
3.20000E-04		91040.	90535.
3.30000E-04		88262.	87692.
3.40000E-04		85136.	84502.
3.50000E-04		81674.	80979.
3.60000E-04		77890.	77134.
3.70000E-04		73794.	72987.
3.80000E-04		69416.	68553.
3.90000E-04		64759.	63848.
4.00000E-04		59847.	58893.
4.10000E-04		54698.	53706.
4.20000E-04		49334.	48308.
4.30000E-04		43775.	42721.
4.40000E-04		38043.	36969.
4.50000E-04		32161.	31074.
4.60000E-04		26152.	25064.
4.70000E-04		20040.	18967.
4.80000E-04		13846.	12827.
4.90000E-04		7502.7	6737.4
5.00000E-04		1326.8	1329.4
5.10000E-04		0.0	0.40431
5.20000E-04		0.0	-2.00000E-02
5.30000E-04		0.0	-2.00000E-02
5.40000E-04		0.0	-2.00000E-02
5.50000E-04		0.0	-2.00000E-02
5.60000E-04		0.0	-2.00000E-02
5.70000E-04		0.0	-2.00000E-02
5.80000E-04		0.0	-2.00000E-02
5.90000E-04		0.0	-2.00000E-02
6.00000E-04		0.0	-2.00000E-02
6.10000E-04		0.0	-2.00000E-02
6.20000E-04		0.0	-2.00000E-02
6.30000E-04		0.0	-2.00000E-02
6.40000E-04		0.0	-2.00000E-02
6.50000E-04		0.0	-2.00000E-02
6.60000E-04		0.0	-2.00000E-02
6.70000E-04		0.0	-2.00000E-02
6.80000E-04		0.0	-2.00000E-02
6.90000E-04		0.0	-2.00000E-02
7.00000E-04		0.0	-2.00000E-02
7.10000E-04		0.0	-2.00000E-02
7.20000E-04		0.0	-2.00000E-02
7.30000E-04		0.0	-2.00000E-02
7.40000E-04		0.0	-2.00000E-02
7.50000E-04		0.0	-2.00000E-02
7.60000E-04		0.0	-2.00000E-02
7.70000E-04		0.0	-2.00000E-02
7.80000E-04		0.0	-2.00000E-02
7.90000E-04		0.0	-2.00000E-02
8.00000E-04		0.0	-2.00000E-02
8.10000E-04		0.0	-2.00000E-02
8.20000E-04		0.0	-2.00000E-02
8.30000E-04		0.0	-2.00000E-02
8.40000E-04		0.0	-2.00000E-02
8.50000E-04		0.0	-2.00000E-02
8.60000E-04		0.0	-2.00000E-02
8.70000E-04		0.0	-2.00000E-02
8.80000E-04		0.0	-2.00000E-02
8.90000E-04		0.0	-2.00000E-02
9.00000E-04		0.0	-2.00000E-02
9.10000E-04		0.0	-2.00000E-02
9.20000E-04		0.0	-2.00000E-02
9.30000E-04		0.0	-2.00000E-02
9.40000E-04		0.0	-2.00000E-02
9.50000E-04		0.0	-2.00000E-02
9.60000E-04		0.0	-2.00000E-02
9.70000E-04		0.0	-2.00000E-02
9.80000E-04		0.0	-2.00000E-02
9.90000E-04		0.0	-2.00000E-02
1.00000E-03		0.0	-1.99997E-02

(b) VIF1RF, VOIDEL, and IERORT at 1 KHz with R_2 = 2 KΩ.

Figure 33 (continued)

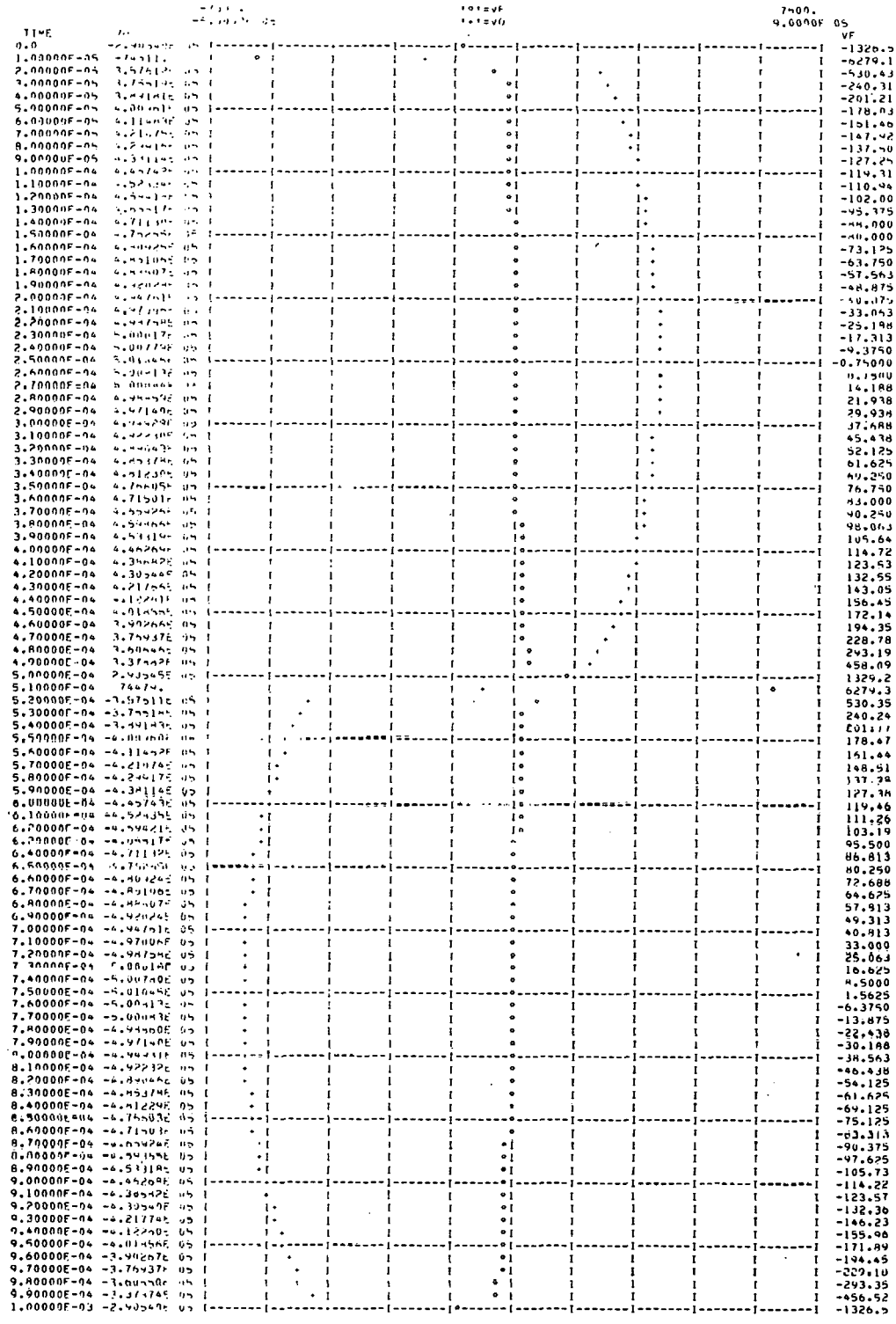

(c) VO and VF at 1 KHz with R_2 = 2 KΩ.

Figure 33 (continued)

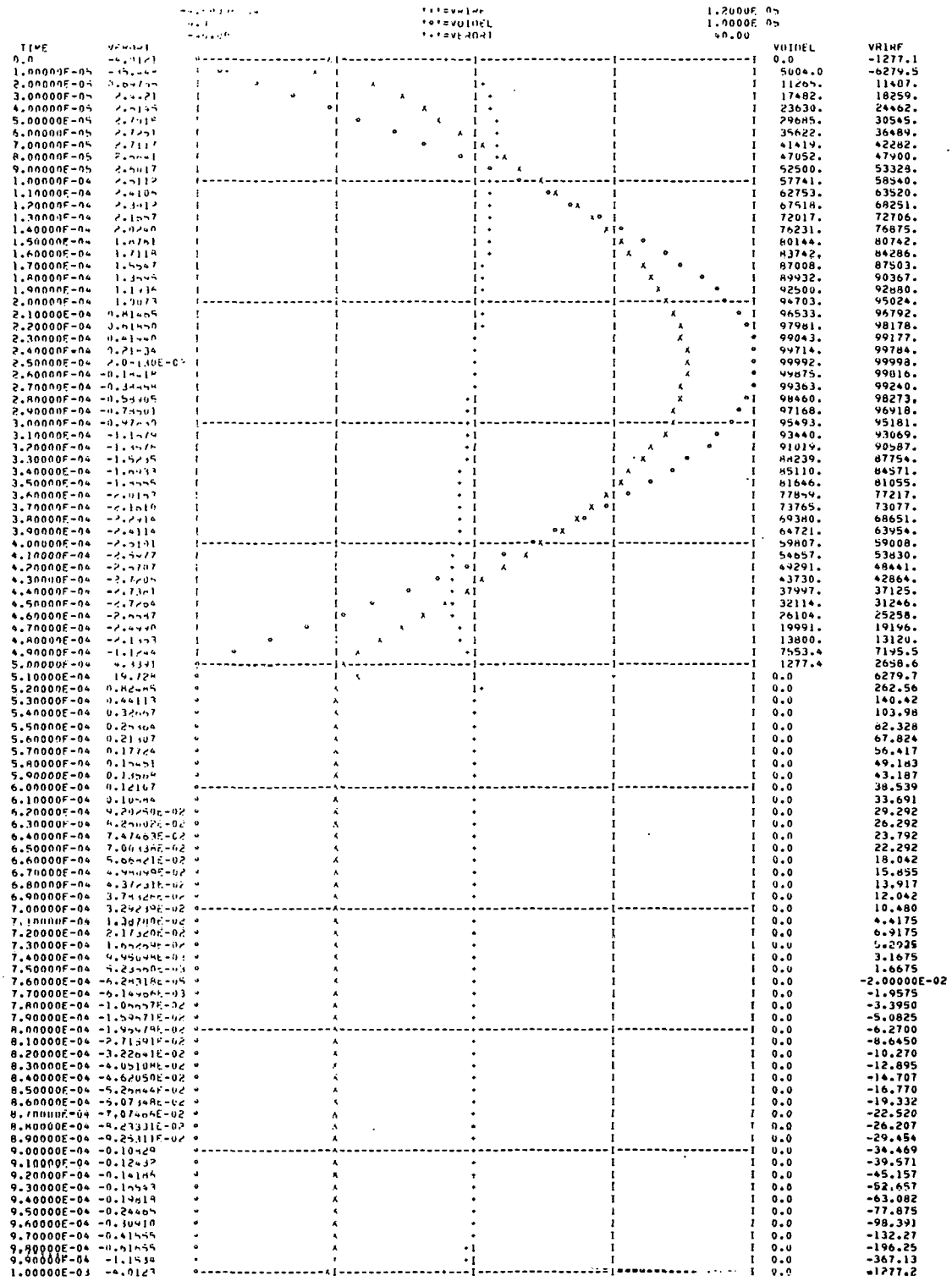

(d) VR1RF, VOIDEL, and VEROR T at 1 KHz with R_2 = 0Ω.

Figure 33 (continued)

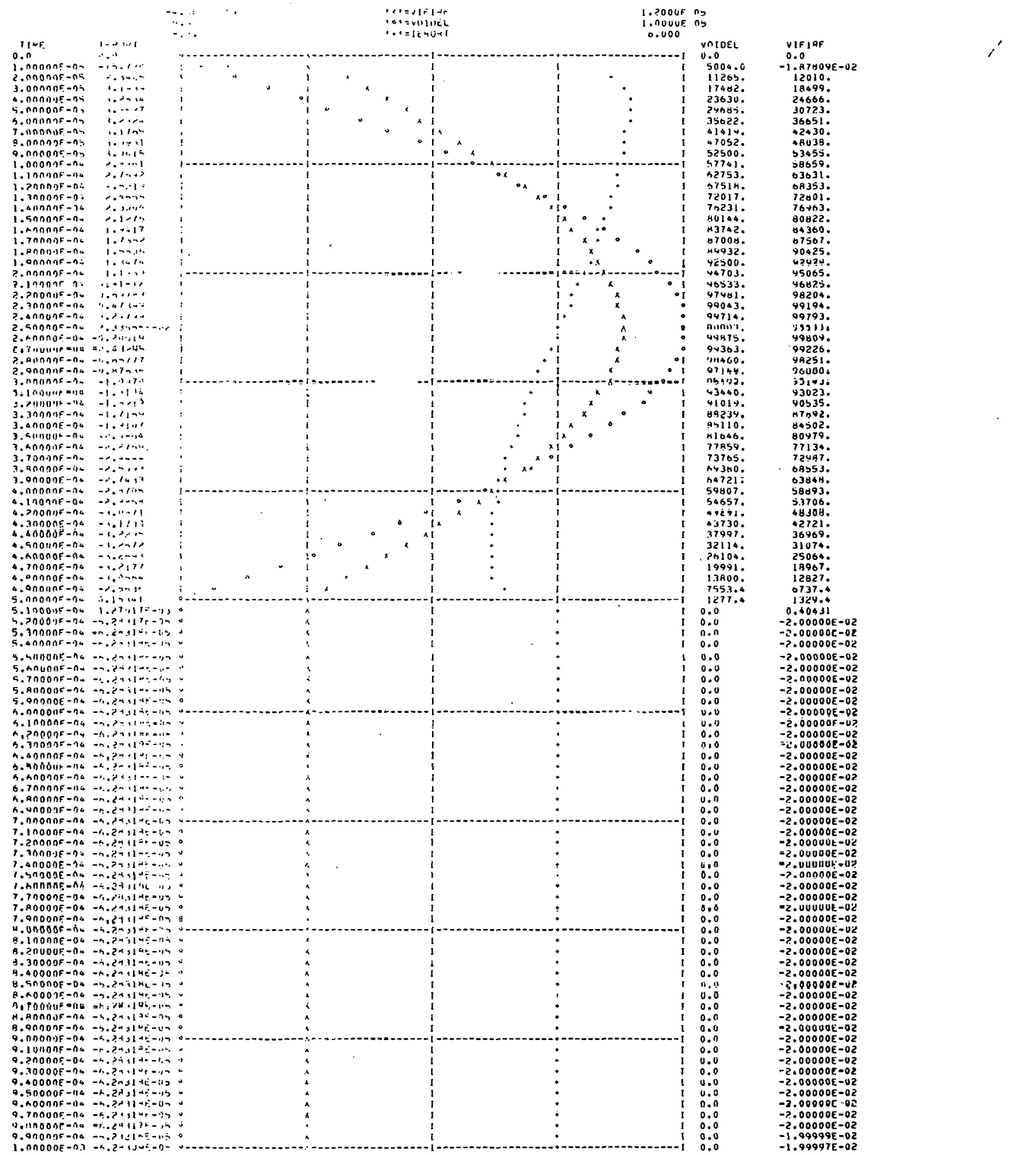

TIME		VOIDEL	VIF1RF
0.0		0.0	0.0
1.00000E-05		5004.6	-1.87809E-02
2.00000E-05		11265.	12010.
3.00000E-05		17482.	18499.
4.00000E-05		23630.	24666.
5.00000E-05		29685.	30723.
6.00000E-05		35622.	36651.
7.00000E-05		41414.	42430.
8.00000E-05		47052.	48038.
9.00000E-05		52500.	53455.
1.00000E-04		57741.	58659.
1.10000E-04		62753.	63631.
1.20000E-04		67514.	68353.
1.30000E-04		72017.	72801.
1.40000E-04		76231.	76963.
1.50000E-04		80144.	80822.
1.60000E-04		83742.	84360.
1.70000E-04		87008.	87567.
1.80000E-04		89932.	90425.
1.90000E-04		92500.	92929.
2.00000E-04		94703.	95065.
2.10000E-04		96533.	96825.
2.20000E-04		97981.	98204.
2.30000E-04		99043.	99194.
2.40000E-04		99714.	99793.
2.50000E-04		99991.	99999.
2.60000E-04		99875.	99809.
2.70000E-04		99363.	99226.
2.80000E-04		98460.	98251.
2.90000E-04		97149.	96880.
3.00000E-04		95492.	95192.
3.10000E-04		93440.	93023.
3.20000E-04		91019.	90535.
3.30000E-04		88239.	87692.
3.40000E-04		85110.	84502.
3.50000E-04		81646.	80979.
3.60000E-04		77859.	77134.
3.70000E-04		73765.	72987.
3.80000E-04		69380.	68553.
3.90000E-04		64721.	63848.
4.00000E-04		59807.	58893.
4.10000E-04		54657.	53706.
4.20000E-04		49291.	48308.
4.30000E-04		43730.	42721.
4.40000E-04		37997.	36969.
4.50000E-04		32114.	31074.
4.60000E-04		26104.	25064.
4.70000E-04		19991.	18967.
4.80000E-04		13800.	12827.
4.90000E-04		7553.4	6737.4
5.00000E-04		1277.4	1329.4
5.10000E-04		0.0	0.40431
5.20000E-04		0.0	-2.00000E-02
5.30000E-04		0.0	-2.00000E-02
5.40000E-04		0.0	-2.00000E-02
5.50000E-04		0.0	-2.00000E-02
5.60000E-04		0.0	-2.00000E-02
5.70000E-04		0.0	-2.00000E-02
5.80000E-04		0.0	-2.00000E-02
5.90000E-04		0.0	-2.00000E-02
6.00000E-04		0.0	-2.00000E-02
6.10000E-04		0.0	-2.00000E-02
6.20000E-04		0.0	-2.00000E-02
6.30000E-04		0.0	-2.00000E-02
6.40000E-04		0.0	-2.00000E-02
6.50000E-04		0.0	-2.00000E-02
6.60000E-04		0.0	-2.00000E-02
6.70000E-04		0.0	-2.00000E-02
6.80000E-04		0.0	-2.00000E-02
6.90000E-04		0.0	-2.00000E-02
7.00000E-04		0.0	-2.00000E-02
7.10000E-04		0.0	-2.00000E-02
7.20000E-04		0.0	-2.00000E-02
7.30000E-04		0.0	-2.00000E-02
7.40000E-04		0.0	-2.00000E-02
7.50000E-04		0.0	-2.00000E-02
7.60000E-04		0.0	-2.00000E-02
7.70000E-04		0.0	-2.00000E-02
7.80000E-04		0.0	-2.00000E-02
7.90000E-04		0.0	-2.00000E-02
8.00000E-04		0.0	-2.00000E-02
8.10000E-04		0.0	-2.00000E-02
8.20000E-04		0.0	-2.00000E-02
8.30000E-04		0.0	-2.00000E-02
8.40000E-04		0.0	-2.00000E-02
8.50000E-04		0.0	-2.00000E-02
8.60000E-04		0.0	-2.00000E-02
8.70000E-04		0.0	-2.00000E-02
8.80000E-04		0.0	-2.00000E-02
8.90000E-04		0.0	-2.00000E-02
9.00000E-04		0.0	-2.00000E-02
9.10000E-04		0.0	-2.00000E-02
9.20000E-04		0.0	-2.00000E-02
9.30000E-04		0.0	-2.00000E-02
9.40000E-04		0.0	-2.00000E-02
9.50000E-04		0.0	-2.00000E-02
9.60000E-04		0.0	-2.00000E-02
9.70000E-04		0.0	-2.00000E-02
9.80000E-04		0.0	-2.00000E-02
9.90000E-04		0.0	-1.99999E-02
1.00000E-03		0.0	-1.99997E-02

(e) VIF1RF, VOIDEL, and IERORT at 1 KHz with $R_2 = 0\Omega$.

Figure 33 (continued)

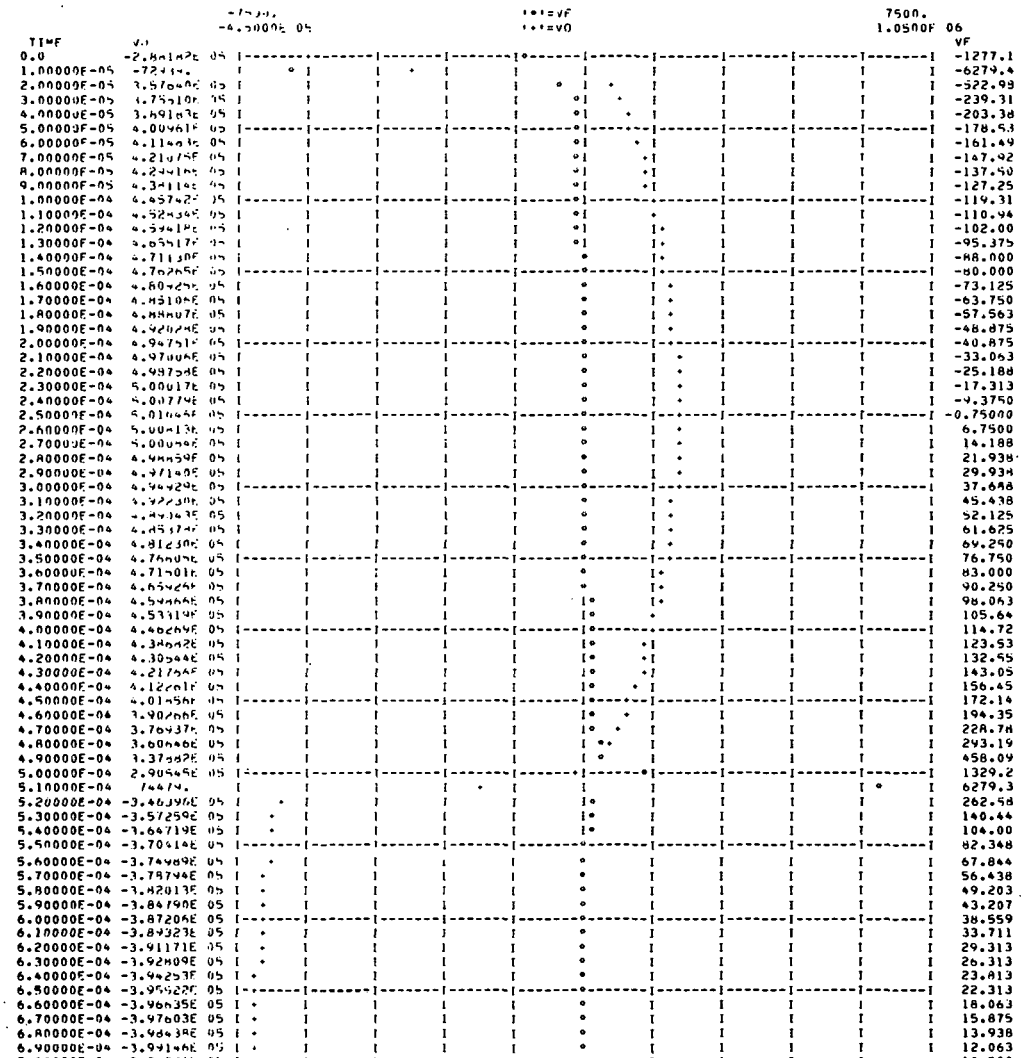

(f) VO and VF at 1 KHz with R_2 = 0Ω.

Figure 33 (continued)

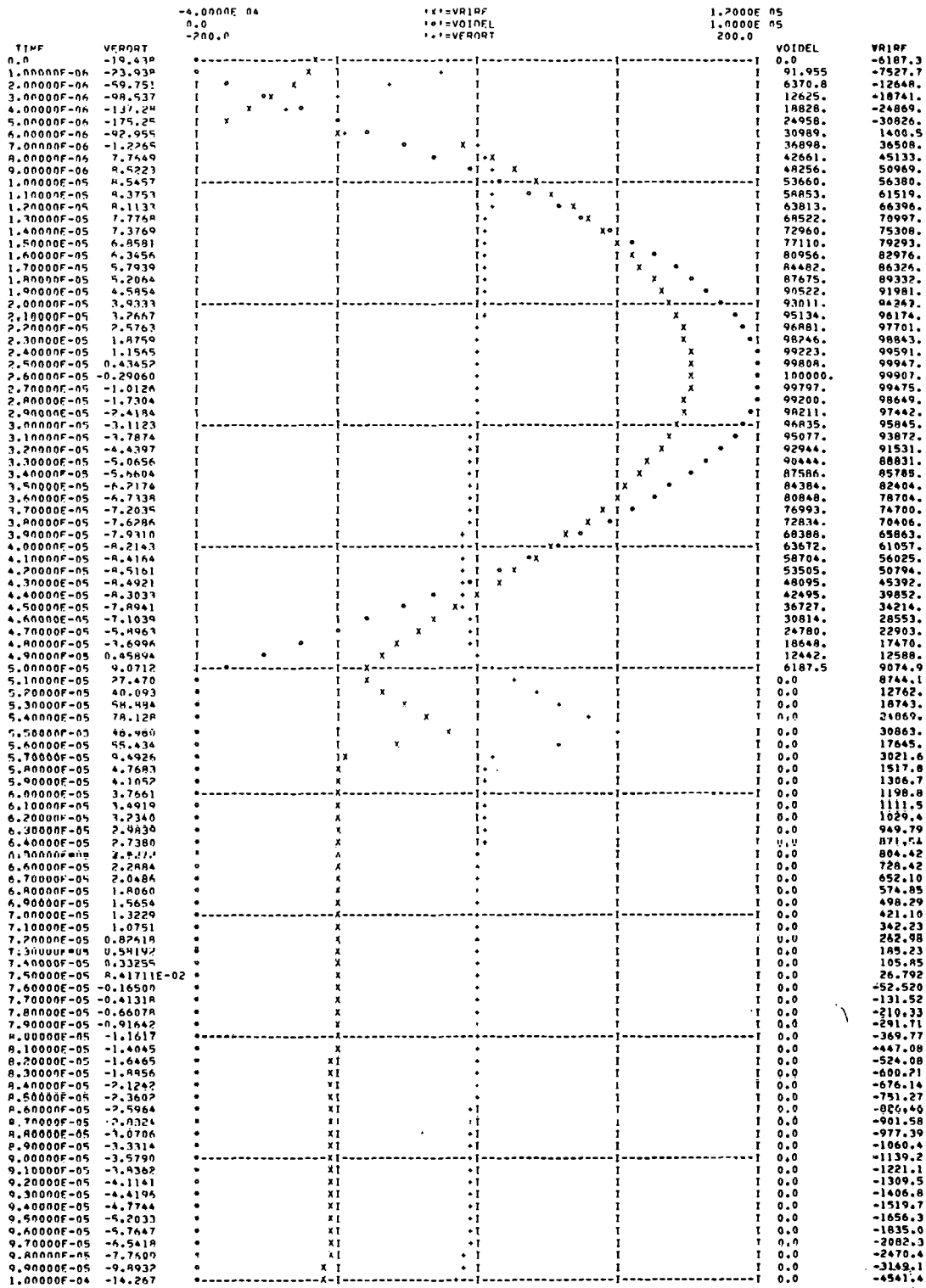

(g) VR1RF, VOIDEL, and VERORT at 10 KHz with R_2 = 2 KΩ.

Figure 33 (continued)

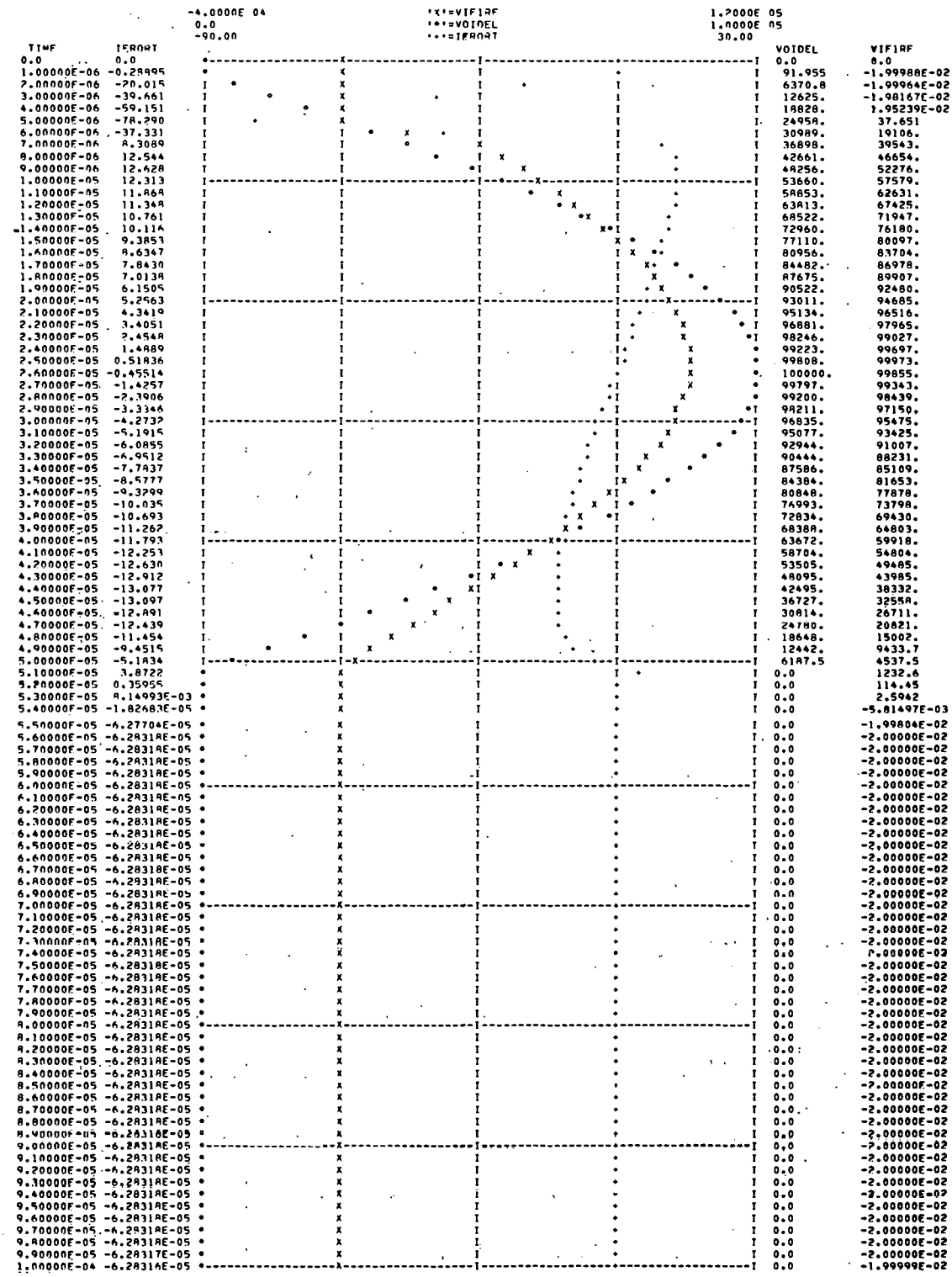

(h) VIF1RF, VOIDEL, and VERORT at 10 KHz with R_2 = 2 KΩ.

Figure 33 (continued)

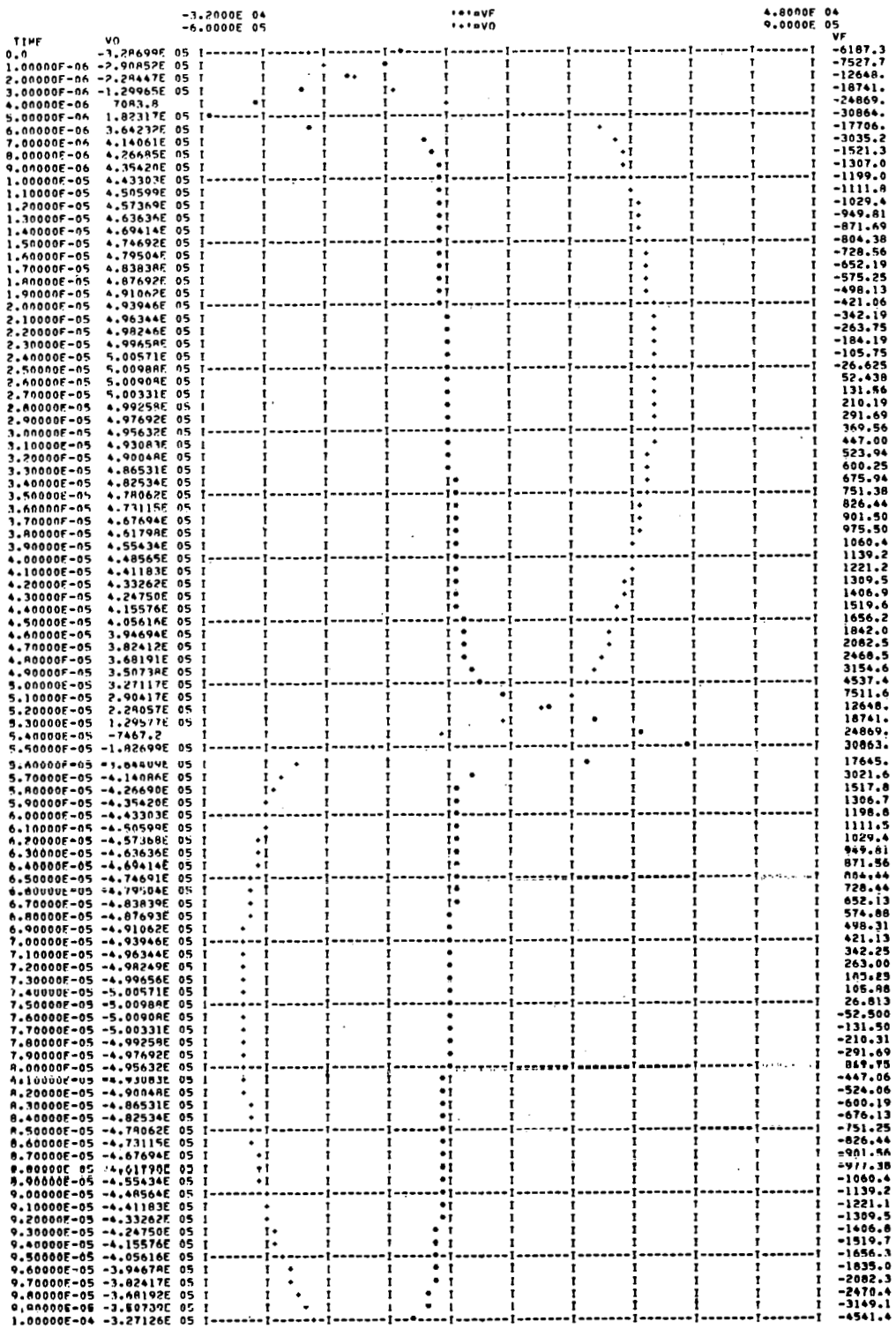

(i) VO and VF at 10 KHz with R_2 = 2 KΩ.

Figure 33 (continued)

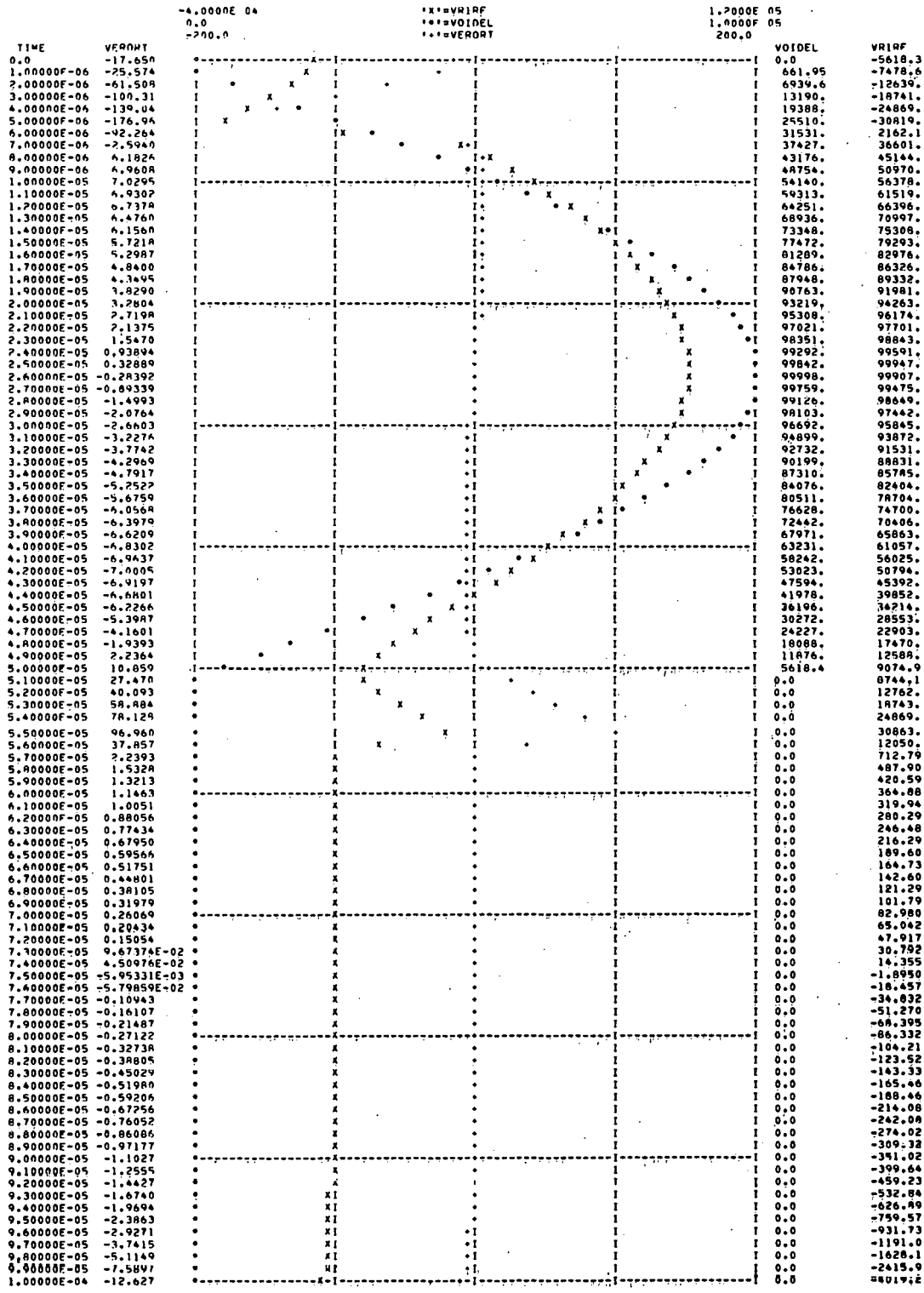

(j) VR1RF, VOIDEL, and VERORT at 10 KHz with $R_2 = 0\Omega$.

Figure 33 (continued)

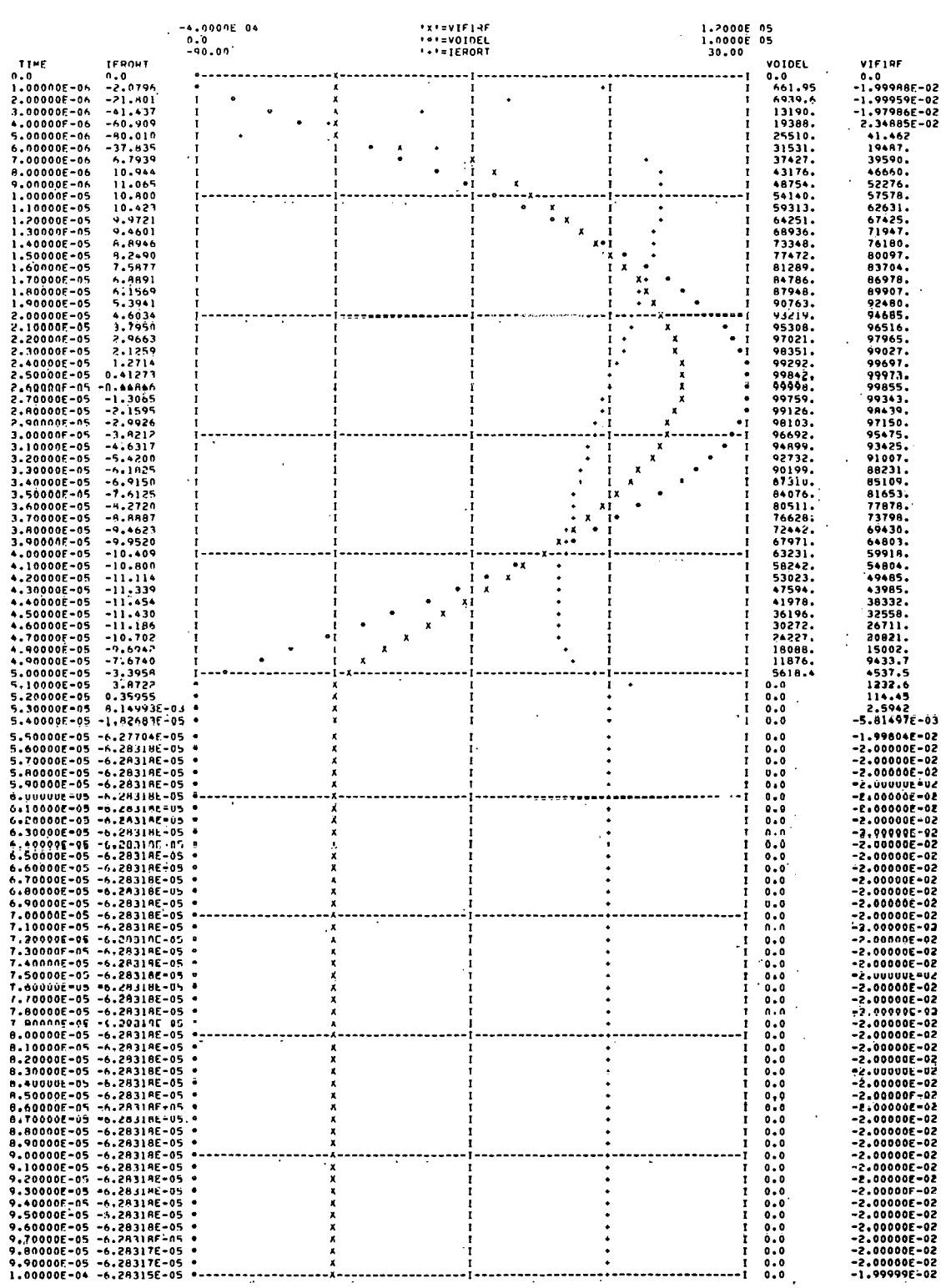

TIME	IEROUT	VOIDEL	VIF1RF
0.0	0.0	0.0	0.0
1.00000E-06	-2.0796	661.95	-1.99988E-02
2.00000E-06	-21.801	6939.6	-1.99959E-02
3.00000E-06	-41.437	13190.	-1.97986E-02
4.00000E-06	-60.909	19388.	2.34885E-02
5.00000E-06	-80.010	25510.	41.462
6.00000E-06	-37.835	31531.	19487.
7.00000E-06	6.7939	37427.	39590.
8.00000E-06	10.944	43176.	46660.
9.00000E-06	11.065	48754.	52276.
1.00000E-05	10.800	54140.	57578.
1.10000E-05	10.423	59313.	62631.
1.20000E-05	9.9721	64251.	67425.
1.30000E-05	9.4601	68936.	71947.
1.40000E-05	8.8946	73348.	76180.
1.50000E-05	8.2490	77472.	80097.
1.60000E-05	7.5877	81289.	83704.
1.70000E-05	6.8891	84786.	86978.
1.80000E-05	6.1569	87948.	89907.
1.90000E-05	5.3941	90763.	92480.
2.00000E-05	4.6034	93219.	94685.
2.10000E-05	3.7950	95308.	96516.
2.20000E-05	2.9663	97021.	97965.
2.30000E-05	2.1259	98351.	99027.
2.40000E-05	1.2714	99292.	99697.
2.50000E-05	0.41273	99842.	99973.
2.60000E-05	-0.44866	99998.	99855.
2.70000E-05	-1.3065	99759.	99343.
2.80000E-05	-2.1595	99126.	98439.
2.90000E-05	-2.9926	98103.	97150.
3.00000E-05	-3.8212	96692.	95475.
3.10000E-05	-4.6317	94899.	93425.
3.20000E-05	-5.4200	92732.	91007.
3.30000E-05	-6.1825	90199.	88231.
3.40000E-05	-6.9150	87310.	85109.
3.50000E-05	-7.6125	84076.	81653.
3.60000E-05	-8.2720	80511.	77878.
3.70000E-05	-8.8887	76628.	73798.
3.80000E-05	-9.4623	72442.	69430.
3.90000E-05	-9.9520	67971.	64803.
4.00000E-05	-10.409	63231.	59918.
4.10000E-05	-10.800	58242.	54804.
4.20000E-05	-11.114	53023.	49485.
4.30000E-05	-11.339	47594.	43985.
4.40000E-05	-11.454	41978.	38332.
4.50000E-05	-11.430	36196.	32558.
4.60000E-05	-11.186	30272.	26711.
4.70000E-05	-10.702	24227.	20821.
4.80000E-05	-9.6942	18088.	15002.
4.90000E-05	-7.6740	11876.	9433.7
5.00000E-05	-3.3958	5618.4	4537.5
5.10000E-05	3.8722	0.0	1232.6
5.20000E-05	0.35955	0.0	114.45
5.30000E-05	8.14993E-03	0.0	2.5942
5.40000E-05	-1.82683E-05	0.0	-5.81497E-03
5.50000E-05	-6.27704E-05	0.0	-1.99804E-02
5.60000E-05	-6.28318E-05	0.0	-2.00000E-02
5.70000E-05	-6.28318E-05	0.0	-2.00000E-02
5.80000E-05	-6.28318E-05	0.0	-2.00000E-02
5.90000E-05	-6.28318E-05	0.0	-2.00000E-02
6.00000E-05	-6.28318E-05	0.0	-2.00000E-02
6.10000E-05	-6.28318E-05	0.0	-2.00000E-02
6.20000E-05	-6.28318E-05	0.0	-2.00000E-02
6.30000E-05	-6.28318E-05	0.0	-2.00000E-02
6.40000E-05	-6.28318E-05	0.0	-2.00000E-02
6.50000E-05	-6.28318E-05	0.0	-2.00000E-02
6.60000E-05	-6.28318E-05	0.0	-2.00000E-02
6.70000E-05	-6.28318E-05	0.0	-2.00000E-02
6.80000E-05	-6.28318E-05	0.0	-2.00000E-02
6.90000E-05	-6.28318E-05	0.0	-2.00000E-02
7.00000E-05	-6.28318E-05	0.0	-2.00000E-02
7.10000E-05	-6.28318E-05	0.0	-2.00000E-02
7.20000E-05	-6.28318E-05	0.0	-2.00000E-02
7.30000E-05	-6.28318E-05	0.0	-2.00000E-02
7.40000E-05	-6.28318E-05	0.0	-2.00000E-02
7.50000E-05	-6.28318E-05	0.0	-2.00000E-02
7.60000E-05	-6.28318E-05	0.0	-2.00000E-02
7.70000E-05	-6.28318E-05	0.0	-2.00000E-02
7.80000E-05	-6.28318E-05	0.0	-2.00000E-02
7.90000E-05	-6.28318E-05	0.0	-2.00000E-02
8.00000E-05	-6.28318E-05	0.0	-2.00000E-02
8.10000E-05	-6.28318E-05	0.0	-2.00000E-02
8.20000E-05	-6.28318E-05	0.0	-2.00000E-02
8.30000E-05	-6.28318E-05	0.0	-2.00000E-02
8.40000E-05	-6.28318E-05	0.0	-2.00000E-02
8.50000E-05	-6.28318E-05	0.0	-2.00000E-02
8.60000E-05	-6.28318E-05	0.0	-2.00000E-02
8.70000E-05	-6.28318E-05	0.0	-2.00000E-02
8.80000E-05	-6.28318E-05	0.0	-2.00000E-02
8.90000E-05	-6.28318E-05	0.0	-2.00000E-02
9.00000E-05	-6.28318E-05	0.0	-2.00000E-02
9.10000E-05	-6.28318E-05	0.0	-2.00000E-02
9.20000E-05	-6.28318E-05	0.0	-2.00000E-02
9.30000E-05	-6.28318E-05	0.0	-2.00000E-02
9.40000E-05	-6.28318E-05	0.0	-2.00000E-02
9.50000E-05	-6.28318E-05	0.0	-2.00000E-02
9.60000E-05	-6.28318E-05	0.0	-2.00000E-02
9.70000E-05	-6.28318E-05	0.0	-2.00000E-02
9.80000E-05	-6.28317E-05	0.0	-2.00000E-02
9.90000E-05	-6.28317E-05	0.0	-2.00000E-02
1.00000E-04	-6.28315E-05	0.0	-1.99999E-02

(k) VIF1RF, VOIDEL, and VEROUT at 10 KHz with $R_2 = 0\Omega$.

Figure 33 (continued)

-3.2000E 04 '*'=VF 4.8000E 04
-4.5000E 05 '+'=VO 1.0500E 06

TIME	VO	VF
0.0	-3.26191E 05	-5618.3
1.00000E-06	-2.88236E 05	-7478.5
2.00000E-06	-2.26025E 05	-12639.
3.00000E-06	-1.27560E 05	-18741.
4.00000E-06	9488.2	-24869.
5.00000E-06	1.84720E 05	-30860.
6.00000E-06	3.65357E 05	-17325.
7.00000E-06	4.14173E 05	-2988.3
8.00000E-06	4.26696E 05	-1515.7
9.00000E-06	4.35421E 05	-1306.3
1.00000E-05	4.43300E 05	-1200.3
1.10000E-05	4.50599E 05	-1111.8
1.20000E-05	4.57369E 05	-1029.4
1.30000E-05	4.63636E 05	-949.81
1.40000E-05	4.69414E 05	-871.69
1.50000E-05	4.74692E 05	-804.38
1.60000E-05	4.79504E 05	-728.56
1.70000E-05	4.83838E 05	-652.19
1.80000E-05	4.87692E 05	-575.25
1.90000E-05	4.91062E 05	-498.13
2.00000E-05	4.93946E 05	-421.06
2.10000E-05	4.96344E 05	-342.19
2.20000E-05	4.98246E 05	-263.75
2.30000E-05	4.99658E 05	-184.19
2.40000E-05	5.00571E 05	-105.75
2.50000E-05	5.00988E 05	-26.625
2.60000E-05	5.00908E 05	52.438
2.70000E-05	5.00331E 05	131.56
2.80000E-05	4.99258E 05	210.19
2.90000E-05	4.97692E 05	291.69
3.00000E-05	4.95632E 05	369.56
3.10000E-05	4.93083E 05	447.00
3.20000E-05	4.90049E 05	523.94
3.30000E-05	4.86531E 05	600.25
3.40000E-05	4.82534E 05	675.94
3.50000E-05	4.78062E 05	751.38
3.60000E-05	4.73115E 05	826.44
3.70000E-05	4.67694E 05	901.50
3.80000E-05	4.61798E 05	975.50
3.90000E-05	4.55434E 05	1060.4
4.00000E-05	4.48565E 05	1139.2
4.10000E-05	4.41183E 05	1221.2
4.20000E-05	4.33262E 05	1309.5
4.30000E-05	4.24750E 05	1406.9
4.40000E-05	4.15576E 05	1519.6
4.50000E-05	4.05616E 05	1656.2
4.60000E-05	3.94694E 05	1842.0
4.70000E-05	3.82412E 05	2082.5
4.80000E-05	3.68191E 05	2468.5
4.90000E-05	3.50738E 05	3154.6
5.00000E-05	3.27117E 05	4537.4
5.10000E-05	2.90417E 05	7511.6
5.20000E-05	2.28057E 05	12648.
5.30000E-05	1.29577E 05	18741.
5.40000E-05	-7467.2	24869.
5.50000E-05	-1.82699E 05	30863.
5.60000E-05	-3.57363E 05	12050.
5.70000E-05	-3.78094E 05	712.81
5.80000E-05	-3.81608E 05	487.92
5.90000E-05	-3.84460E 05	420.61
6.00000E-05	-3.86931E 05	364.90
6.10000E-05	-3.89086E 05	319.96
6.20000E-05	-3.90980E 05	280.31
6.30000E-05	-3.92647E 05	246.50
6.40000E-05	-3.94114E 05	216.31
6.50000E-05	-3.95404E 05	189.63
6.60000E-05	-3.96534E 05	164.75
6.70000E-05	-3.97517E 05	142.63
6.80000E-05	-3.98365E 05	121.31
6.90000E-05	-3.99086E 05	101.81
7.00000E-05	-3.99687E 05	83.000
7.10000E-05	-4.00174E 05	65.063
7.20000E-05	-4.00550E 05	47.938
7.30000E-05	-4.00820E 05	30.813
7.40000E-05	-4.00985E 05	14.375
7.50000E-05	-4.01047E 05	-1.8750
7.60000E-05	-4.01006E 05	-18.438
7.70000E-05	-4.00862E 05	-34.813
7.80000E-05	-4.00614E 05	-51.250
7.90000E-05	-4.00259E 05	-68.375
8.00000E-05	-3.99796E 05	-86.313
8.10000E-05	-3.99220E 05	-104.19
8.20000E-05	-3.98527E 05	-123.50
8.30000E-05	-3.97709E 05	-143.31
8.40000E-05	-3.96759E 05	-165.44
8.50000E-05	-3.95666E 05	-188.44
8.60000E-05	-3.94419E 05	-214.06
8.70000E-05	-3.93003E 05	-242.06
8.80000E-05	-3.91397E 05	-274.00
8.90000E-05	-3.89578E 05	-309.30
9.00000E-05	-3.87514E 05	-351.00
9.10000E-05	-3.85163E 05	-399.63
9.20000E-05	-3.82472E 05	-459.21
9.30000E-05	-3.79364E 05	-532.82
9.40000E-05	-3.75730E 05	-626.88
9.50000E-05	-3.71419E 05	-759.55
9.60000E-05	-3.66159E 05	-931.71
9.70000E-05	-3.59541E 05	-1191.0
9.80000E-05	-3.50788E 05	-1628.1
9.90000E-05	-3.38359E 05	-2415.8
1.00000E-04	-3.18767E 05	-4019.2

(1) VO and VF at 10 KHz with R_2 = 0Ω.

Figure 33 (continued)

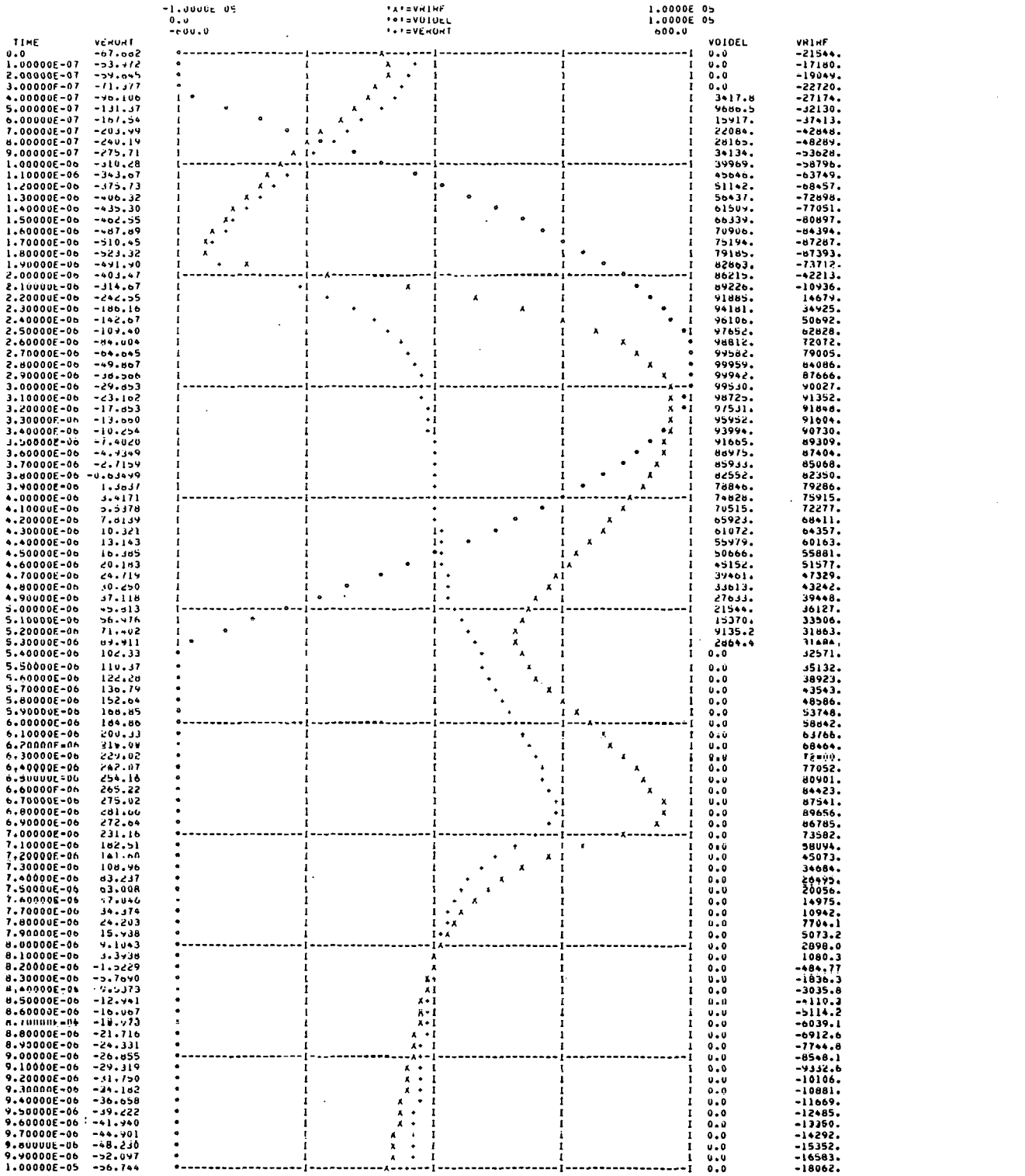

(m) VR1RF, VOIDEL, and VERORT at 100 KHz with R_2 = 2 KΩ.

Figure 33 (continued)

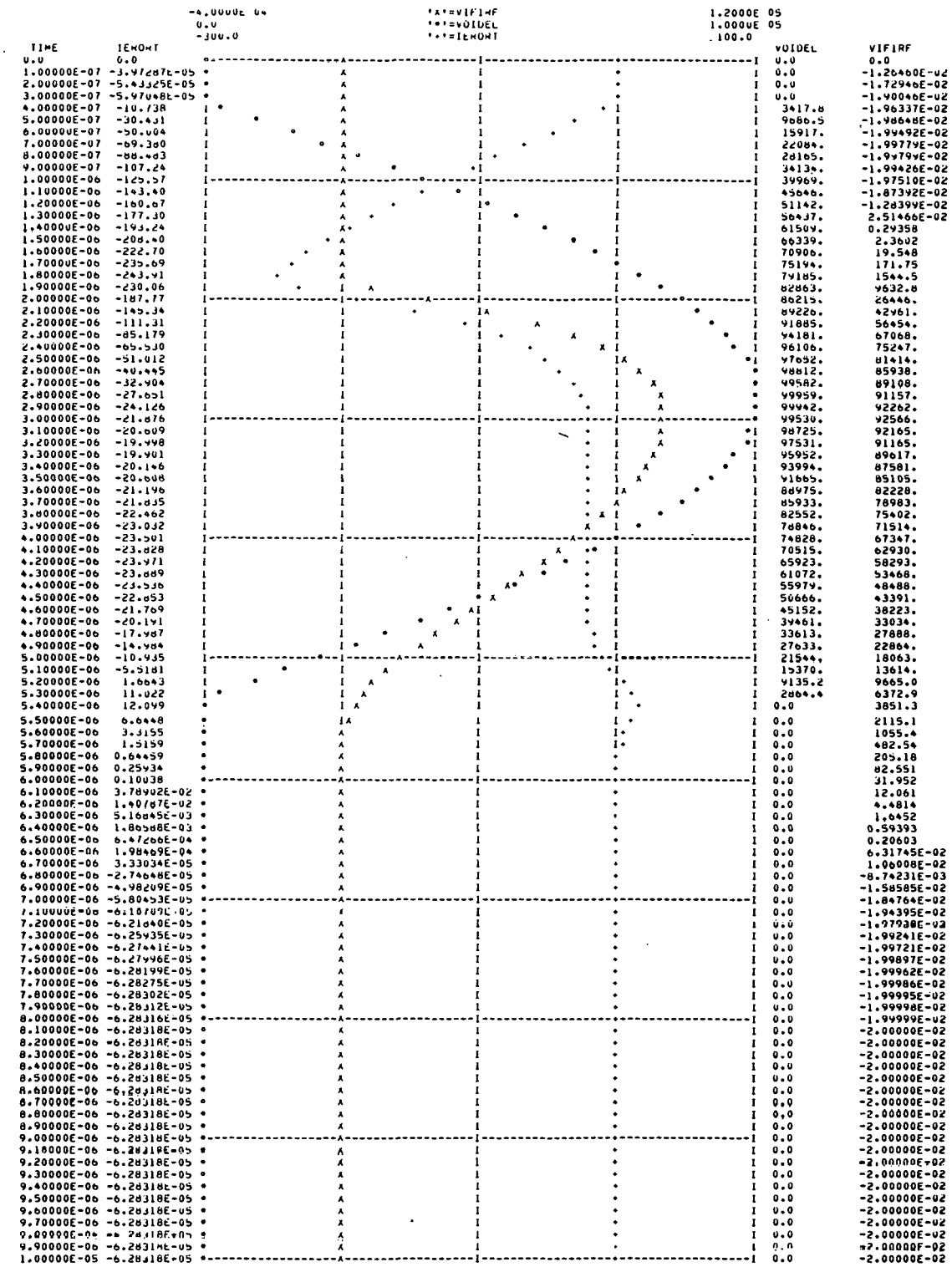

TIME	IEROUT	VOIDEL	VIF1RF
0.0	0.0	0.0	0.0
1.00000E-07	-3.97287E-05	0.0	-1.26460E-02
2.00000E-07	-5.43325E-05	0.0	-1.72946E-02
3.00000E-07	-5.97048E-05	0.0	-1.90046E-02
4.00000E-07	-10.738	3417.8	-1.96337E-02
5.00000E-07	-30.431	9686.5	-1.98648E-02
6.00000E-07	-50.604	15917.	-1.99492E-02
7.00000E-07	-69.380	22084.	-1.99779E-02
8.00000E-07	-88.483	28165.	-1.99799E-02
9.00000E-07	-107.24	34134.	-1.99426E-02
1.00000E-06	-125.57	39969.	-1.97510E-02
1.10000E-06	-143.40	45646.	-1.87392E-02
1.20000E-06	-160.67	51142.	-1.28399E-02
1.30000E-06	-177.30	56437.	2.51466E-02
1.40000E-06	-193.24	61509.	0.29358
1.50000E-06	-208.40	66339.	2.3602
1.60000E-06	-222.70	70906.	19.548
1.70000E-06	-235.69	75194.	171.75
1.80000E-06	-243.91	79185.	1544.5
1.90000E-06	-230.06	82863.	9632.8
2.00000E-06	-187.77	86215.	26446.
2.10000E-06	-145.34	89226.	42961.
2.20000E-06	-111.31	91885.	56454.
2.30000E-06	-85.179	94181.	67068.
2.40000E-06	-65.530	96106.	75247.
2.50000E-06	-51.012	97652.	81414.
2.60000E-06	-40.445	98812.	85938.
2.70000E-06	-32.904	99582.	89108.
2.80000E-06	-27.651	99959.	91157.
2.90000E-06	-24.126	99942.	92262.
3.00000E-06	-21.876	99530.	92566.
3.10000E-06	-20.609	98725.	92165.
3.20000E-06	-19.998	97531.	91165.
3.30000E-06	-19.901	95952.	89617.
3.40000E-06	-20.146	93994.	87581.
3.50000E-06	-20.608	91665.	85105.
3.60000E-06	-21.196	88975.	82228.
3.70000E-06	-21.835	85933.	78983.
3.80000E-06	-22.462	82552.	75402.
3.90000E-06	-23.032	78846.	71514.
4.00000E-06	-23.501	74828.	67347.
4.10000E-06	-23.828	70515.	62930.
4.20000E-06	-23.971	65923.	58293.
4.30000E-06	-23.889	61072.	53468.
4.40000E-06	-23.536	55979.	48488.
4.50000E-06	-22.853	50666.	43391.
4.60000E-06	-21.769	45152.	38223.
4.70000E-06	-20.191	39461.	33034.
4.80000E-06	-17.987	33613.	27888.
4.90000E-06	-14.984	27633.	22864.
5.00000E-06	-10.935	21544.	18063.
5.10000E-06	-5.5181	15370.	13614.
5.20000E-06	1.6643	9135.2	9665.0
5.30000E-06	11.022	2864.4	6372.9
5.40000E-06	12.099	0.0	3851.3
5.50000E-06	6.6448	0.0	2115.1
5.60000E-06	3.3155	0.0	1055.4
5.70000E-06	1.5159	0.0	482.54
5.80000E-06	0.64459	0.0	205.18
5.90000E-06	0.25934	0.0	82.551
6.00000E-06	0.10038	0.0	31.952
6.10000E-06	3.78902E-02	0.0	12.061
6.20000E-06	1.40787E-02	0.0	4.4814
6.30000E-06	5.16845E-03	0.0	1.6452
6.40000E-06	1.86588E-03	0.0	0.59393
6.50000E-06	6.47266E-04	0.0	0.20603
6.60000E-06	1.98469E-04	0.0	6.31745E-02
6.70000E-06	3.33034E-05	0.0	1.06008E-02
6.80000E-06	-2.74648E-05	0.0	-8.74231E-03
6.90000E-06	-4.98209E-05	0.0	-1.58585E-02
7.00000E-06	-5.80453E-05	0.0	-1.84764E-02
7.10000E-06	-6.10709E-05	0.0	-1.94395E-02
7.20000E-06	-6.21640E-05	0.0	-1.97938E-02
7.30000E-06	-6.25935E-05	0.0	-1.99241E-02
7.40000E-06	-6.27441E-05	0.0	-1.99721E-02
7.50000E-06	-6.27996E-05	0.0	-1.99897E-02
7.60000E-06	-6.28199E-05	0.0	-1.99962E-02
7.70000E-06	-6.28275E-05	0.0	-1.99986E-02
7.80000E-06	-6.28302E-05	0.0	-1.99995E-02
7.90000E-06	-6.28312E-05	0.0	-1.99998E-02
8.00000E-06	-6.28316E-05	0.0	-1.99999E-02
8.10000E-06	-6.28318E-05	0.0	-2.00000E-02
8.20000E-06	-6.28318E-05	0.0	-2.00000E-02
8.30000E-06	-6.28318E-05	0.0	-2.00000E-02
8.40000E-06	-6.28318E-05	0.0	-2.00000E-02
8.50000E-06	-6.28318E-05	0.0	-2.00000E-02
8.60000E-06	-6.28318E-05	0.0	-2.00000E-02
8.70000E-06	-6.28318E-05	0.0	-2.00000E-02
8.80000E-06	-6.28318E-05	0.0	-2.00000E-02
8.90000E-06	-6.28318E-05	0.0	-2.00000E-02
9.00000E-06	-6.28318E-05	0.0	-2.00000E-02
9.10000E-06	-6.28318E-05	0.0	-2.00000E-02
9.20000E-06	-6.28318E-05	0.0	-2.00000E-02
9.30000E-06	-6.28318E-05	0.0	-2.00000E-02
9.40000E-06	-6.28318E-05	0.0	-2.00000E-02
9.50000E-06	-6.28318E-05	0.0	-2.00000E-02
9.60000E-06	-6.28318E-05	0.0	-2.00000E-02
9.70000E-06	-6.28318E-05	0.0	-2.00000E-02
9.80000E-06	-6.28318E-05	0.0	-2.00000E-02
9.90000E-06	-6.28318E-05	0.0	-2.00000E-02
1.00000E-05	-6.28318E-05	0.0	-2.00000E-02

(n) VIF1RF, VOIDEL, and IEROUT at 100 KHz with R_2 = 2 KΩ.

Figure 33 (continued)

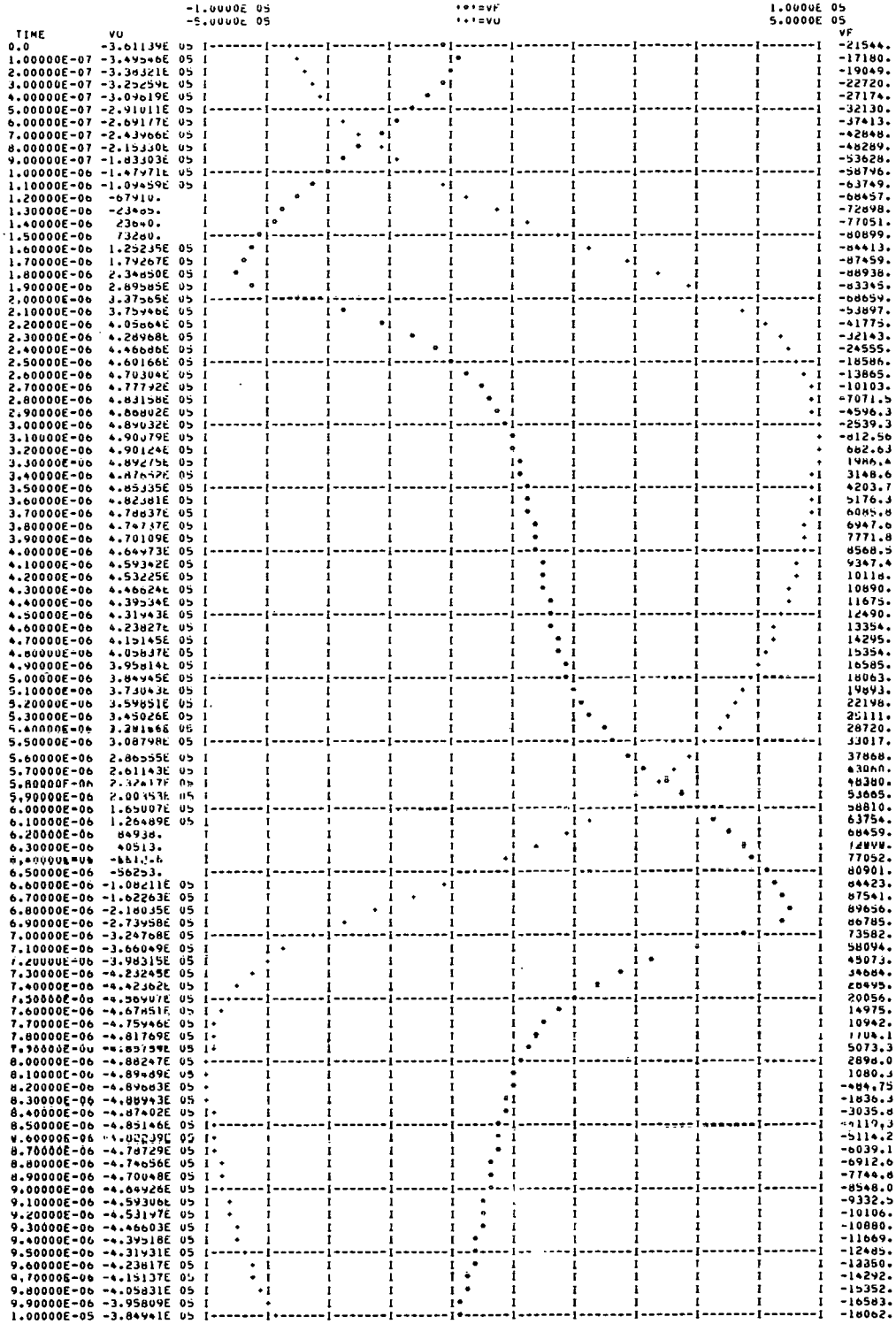

(o) VO and VF at 100 KHz with R_2 = 2 KΩ.

Figure 33 (continued)

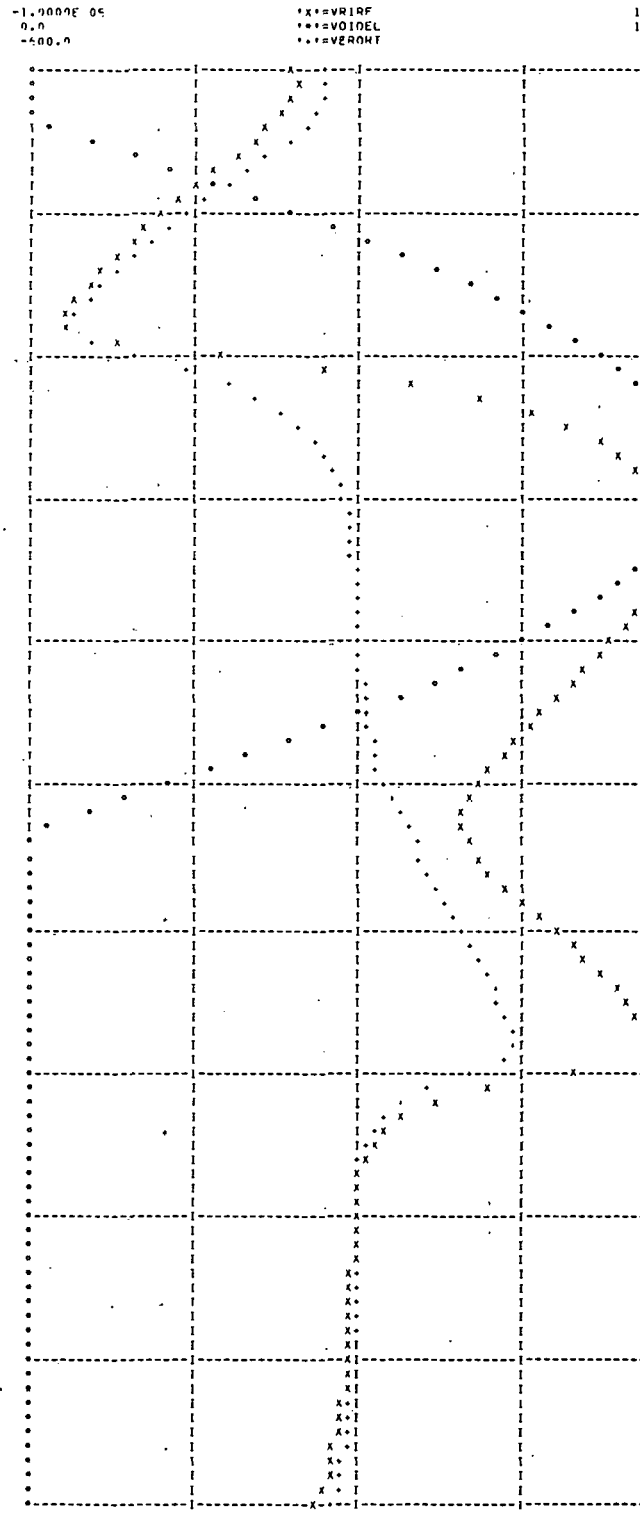

TIME	VERORT	VOIDEL	VR1RF
0.0	-67.688	0.0	-21546.
1.00000E-07	-59.059	0.0	-19053.
2.00000E-07	-63.756	0.0	-20294.
3.00000E-07	-73.206	0.0	-23302.
4.00000E-07	-96.742	3415.9	-27391.
5.00000E-07	-131.57	9684.5	-32194.
6.00000E-07	-167.57	15915.	-37426.
7.00000E-07	-203.99	22083.	-42849.
8.00000E-07	-240.18	28163.	-48288.
9.00000E-07	-275.71	34132.	-53627.
1.00000E-06	-310.27	39967.	-58796.
1.10000E-06	-343.67	45644.	-63749.
1.20000E-06	-375.73	51141.	-68457.
1.30000E-06	-406.31	56436.	-72898.
1.40000E-06	-435.29	61508.	-77051.
1.50000E-06	-462.55	66337.	-80896.
1.60000E-06	-487.87	70905.	-84389.
1.70000E-06	-510.32	75193.	-87249.
1.80000E-06	-522.32	79184.	-87075.
1.90000E-06	-487.85	82862.	-72424.
2.00000E-06	-398.49	86214.	-40631.
2.10000E-06	-310.53	89225.	-9620.5
2.20000E-06	-239.31	91884.	15710.
2.30000E-06	-183.68	94181.	35714.
2.40000E-06	-140.79	96106.	51290.
2.50000E-06	-107.98	97651.	63281.
2.60000E-06	-82.924	98811.	72416.
2.70000E-06	-63.817	99582.	79268.
2.80000E-06	-49.265	99959.	84277.
2.90000E-06	-38.116	99942.	87809.
3.00000E-06	-29.551	99530.	90124.
3.10000E-06	-22.920	98725.	91430.
3.20000E-06	-17.684	97531.	91902.
3.30000E-06	-13.535	95952.	91644.
3.40000E-06	-10.164	93995.	90759.
3.50000E-06	-7.3386	91666.	89330.
3.60000E-06	-4.8826	88976.	87421.
3.70000E-06	-2.6743	85934.	85083.
3.80000E-06	-0.60449	82553.	82360.
3.90000E-06	1.4033	78847.	79293.
4.00000E-06	3.4306	74829.	75921.
4.10000E-06	5.5455	70516.	72281.
4.20000E-06	7.8204	65925.	68414.
4.30000E-06	10.324	61073.	64359.
4.40000E-06	13.144	55981.	60165.
4.50000E-06	16.383	50667.	55882.
4.60000E-06	20.181	45154.	51578.
4.70000E-06	24.717	39462.	47330.
4.80000E-06	30.246	33615.	43243.
4.90000E-06	37.114	27635.	39449.
5.00000E-06	45.808	21546.	36127.
5.10000E-06	56.971	15372.	33506.
5.20000E-06	71.397	9137.1	31863.
5.30000E-06	89.905	2866.3	31484.
5.40000E-06	102.33	0.0	32572.
5.50000E-06	110.37	0.0	35132.
5.60000E-06	122.28	0.0	38923.
5.70000E-06	136.79	0.0	43543.
5.80000E-06	152.64	0.0	48586.
5.90000E-06	168.85	0.0	53748.
6.00000E-06	184.86	0.0	58842.
6.10000E-06	200.33	0.0	63766.
6.20000E-06	215.09	0.0	68464.
6.30000E-06	229.02	0.0	72900.
6.40000E-06	242.07	0.0	77052.
6.50000E-06	254.16	0.0	80901.
6.60000E-06	265.22	0.0	84423.
6.70000E-06	275.02	0.0	87541.
6.80000E-06	281.61	0.0	89641.
6.90000E-06	269.99	0.0	85942.
7.00000E-06	204.63	0.0	65136.
7.10000E-06	126.01	0.0	40109.
7.20000E-06	73.730	0.0	23469.
7.30000E-06	42.684	0.0	13587.
7.40000E-06	24.536	0.0	7810.1
7.50000E-06	13.913	0.0	4428.7
7.60000E-06	7.6244	0.0	2426.9
7.70000E-06	3.8134	0.0	1213.9
7.80000E-06	1.4435	0.0	459.48
7.90000E-06	-0.14968	0.0	-47.645
8.00000E-06	-1.2973	0.0	-412.96
8.10000E-06	-2.1884	0.0	-696.58
8.20000E-06	-2.9545	0.0	-940.46
8.30000E-06	-3.6594	0.0	-1164.8
8.40000E-06	-4.3498	0.0	-1384.6
8.50000E-06	-5.0537	0.0	-1608.6
8.60000E-06	-5.7916	0.0	-1843.5
8.70000E-06	-6.5795	0.0	-2094.3
8.80000E-06	-7.4354	0.0	-2366.8
8.90000E-06	-8.3779	0.0	-2666.8
9.00000E-06	-9.4274	0.0	-3000.8
9.10000E-06	-10.615	0.0	-3378.8
9.20000E-06	-11.972	0.0	-3810.9
9.30000E-06	-13.549	0.0	-4312.8
9.40000E-06	-15.403	0.0	-4902.9
9.50000E-06	-17.619	0.0	-5608.3
9.60000E-06	-20.307	0.0	-6463.8
9.70000E-06	-23.613	0.0	-7516.4
9.80000E-06	-27.736	0.0	-8828.7
9.90000E-06	-32.428	0.0	-10481.
1.00000E-05	-39.492	0.0	-12571.

(p) VR1RF, VOIDEL, and VERORT at 100 KHz with $R_2 = 0\Omega$.

Figure 33 (continued)

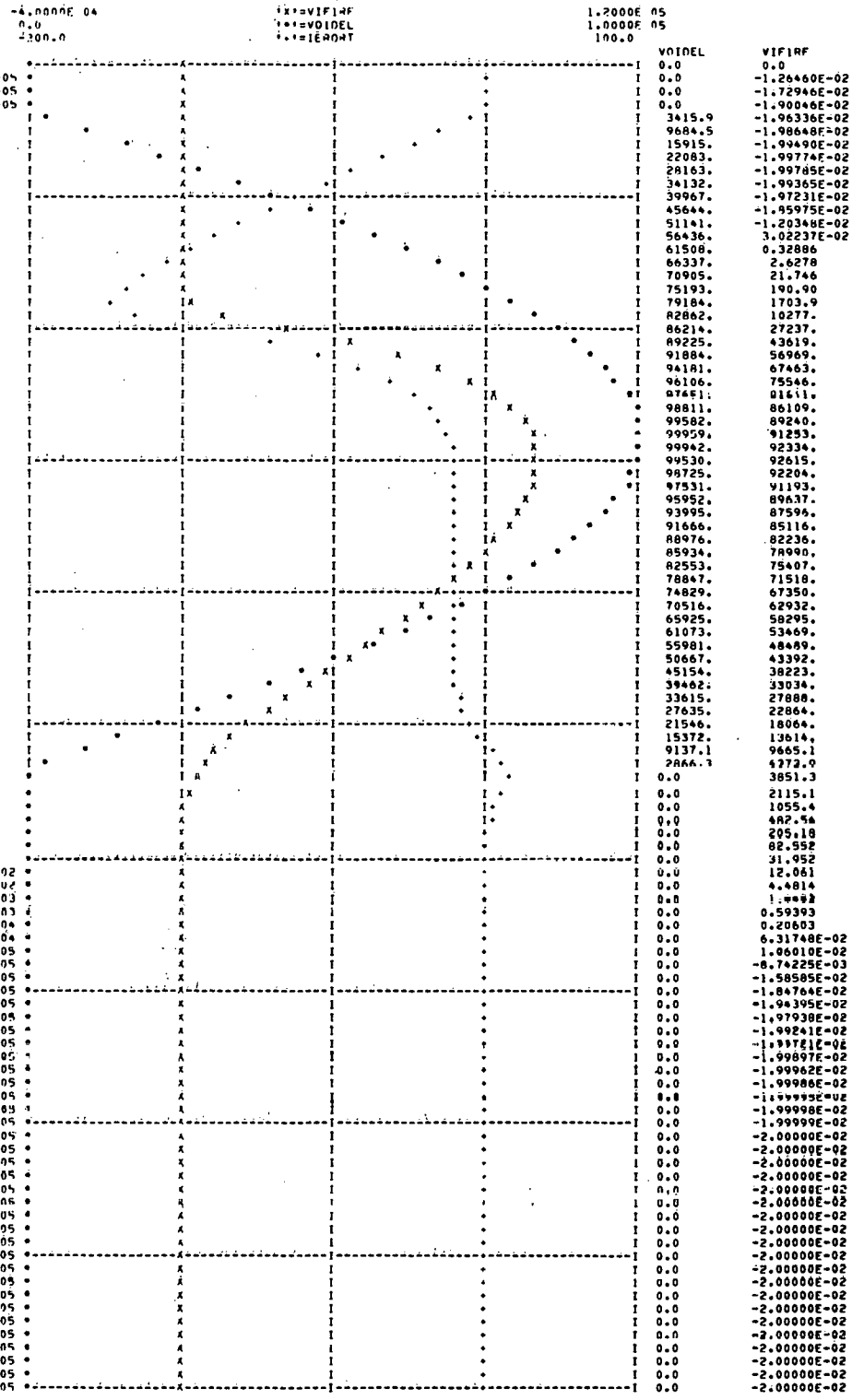

TIME	IERORT	VOIDEL	VIF1RF
0.0	0.0	0.0	0.0
1.00000E-07	-3.97287E-05	0.0	-1.26460E-02
2.00000E-07	-5.43325E-05	0.0	-1.72946E-02
3.00000E-07	-5.97048E-05	0.0	-1.90046E-02
4.00000E-07	-10.731	3415.9	-1.96336E-02
5.00000E-07	-30.425	9684.5	-1.98648E-02
6.00000E-07	-49.998	15915.	-1.99490E-02
7.00000E-07	-69.374	22083.	-1.99774E-02
8.00000E-07	-88.477	28163.	-1.99785E-02
9.00000E-07	-107.23	34132.	-1.99365E-02
1.00000E-06	-125.58	39967.	-1.97231E-02
1.10000E-06	-143.39	45644.	-1.85975E-02
1.20000E-06	-160.65	51141.	-1.20348E-02
1.30000E-06	-177.30	56436.	3.02237E-02
1.40000E-06	-193.23	61508.	0.32886
1.50000E-06	-208.40	66337.	2.6278
1.60000E-06	-222.69	70905.	21.746
1.70000E-06	-235.62	75193.	190.90
1.80000E-06	-243.41	79184.	1703.9
1.90000E-06	-228.03	82862.	10277.
2.00000E-06	-185.28	86214.	27237.
2.10000E-06	-143.28	89225.	43619.
2.20000E-06	-109.69	91884.	56969.
2.30000E-06	-83.937	94181.	67463.
2.40000E-06	-64.589	96106.	75546.
2.50000E-06	-50.299	97651.	81611.
2.60000E-06	-40.005	98811.	86109.
2.70000E-06	-32.490	99582.	89240.
2.80000E-06	-27.350	99959.	91253.
2.90000E-06	-23.901	99942.	92334.
3.00000E-06	-21.725	99530.	92615.
3.10000E-06	-20.488	98725.	92204.
3.20000E-06	-19.914	97531.	91193.
3.30000E-06	-19.839	95952.	89637.
3.40000E-06	-20.102	93995.	87596.
3.50000E-06	-20.578	91666.	85116.
3.60000E-06	-21.172	88976.	82236.
3.70000E-06	-21.816	85934.	78990.
3.80000E-06	-22.450	82553.	75407.
3.90000E-06	-23.024	78847.	71518.
4.00000E-06	-23.497	74829.	67350.
4.10000E-06	-23.828	70516.	62932.
4.20000E-06	-23.970	65925.	58295.
4.30000E-06	-23.890	61073.	53469.
4.40000E-06	-23.539	55981.	48489.
4.50000E-06	-22.858	50667.	43392.
4.60000E-06	-21.773	45154.	38223.
4.70000E-06	-20.195	39462.	33034.
4.80000E-06	-17.998	33615.	27888.
4.90000E-06	-14.989	27635.	22864.
5.00000E-06	-10.940	21546.	18064.
5.10000E-06	-5.5236	15372.	13614.
5.20000E-06	1.6586	9137.1	9665.1
5.30000E-06	11.018	2866.3	4272.9
5.40000E-06	12.099	0.0	3851.3
5.50000E-06	6.6448	0.0	2115.1
5.60000E-06	3.3155	0.0	1055.4
5.70000E-06	1.5159	0.0	482.56
5.80000E-06	0.64460	0.0	205.18
5.90000E-06	0.25934	0.0	82.552
6.00000E-06	0.1003B	0.0	31.952
6.10000E-06	3.78904E-02	0.0	12.061
6.20000E-06	1.40787E-02	0.0	4.4814
6.30000E-06	5.1684E-03	0.0	1.[illegible]
6.40000E-06	1.06509E-03	0.0	0.59393
6.50000E-06	6.4726E-04	0.0	0.20603
6.60000E-06	1.98470E-04	0.0	6.31748E-02
6.70000E-06	3.33039E-05	0.0	1.06010E-02
6.80000E-06	-2.74646E-05	0.0	-8.74225E-03
6.90000E-06	-4.98208E-05	0.0	-1.58585E-02
7.00000E-06	-5.80457E-05	0.0	-1.84764E-02
7.10000E-06	-6.10709E-05	0.0	-1.94395E-02
7.20000E-06	-6.21840E-05	0.0	-1.97938E-02
7.30000E-06	-6.25935E-05	0.0	-1.99241E-02
7.40000E-06	-6.27441E-05	0.0	-1.99761E-02
7.50000E-06	-6.27994E-05	0.0	-1.99897E-02
7.60000E-06	-6.28199E-05	0.0	-1.99962E-02
7.70000E-06	-6.28274E-05	0.0	-1.99986E-02
7.80000E-06	-6.28302E-05	0.0	-1.99995E-02
7.90000E-06	-6.28810E-05	0.0	-1.99998E-02
8.00000E-06	-6.28316E-05	0.0	-1.99999E-02
8.10000E-06	-6.28317E-05	0.0	-2.00000E-02
8.20000E-06	-6.28318E-05	0.0	-2.00000E-02
8.30000E-06	-6.28318E-05	0.0	-2.00000E-02
8.40000E-06	-6.28318E-05	0.0	-2.00000E-02
8.50000E-06	-6.28318E-05	0.0	-2.00000E-02
8.60000E-06	-6.28318E-05	0.0	-2.00000E-02
8.70000E-06	-6.28318E-05	0.0	-2.00000E-02
8.80000E-06	-6.28318E-05	0.0	-2.00000E-02
8.90000E-06	-6.28318E-05	0.0	-2.00000E-02
9.00000E-06	-6.28318E-05	0.0	-2.00000E-02
9.10000E-06	-6.28318E-05	0.0	-2.00000E-02
9.20000E-06	-6.28318E-05	0.0	-2.00000E-02
9.30000E-06	-6.28318E-05	0.0	-2.00000E-02
9.40000E-06	-6.28318E-05	0.0	-2.00000E-02
9.50000E-06	-6.28318E-05	0.0	-2.00000E-02
9.60000E-06	-6.28318E-05	0.0	-2.00000E-02
9.70000E-06	-6.28318E-05	0.0	-2.00000E-02
9.80000E-06	-6.28318E-05	0.0	-2.00000E-02
9.90000E-06	-6.28317E-05	0.0	-2.00000E-02
1.00000E-05	-6.28317E-05	0.0	-2.00000E-02

(q) VIF1RF, VOIDEL, and VERORT at 100 KHz with $R_2 = 0\Omega$.

Figure 33 (continued)

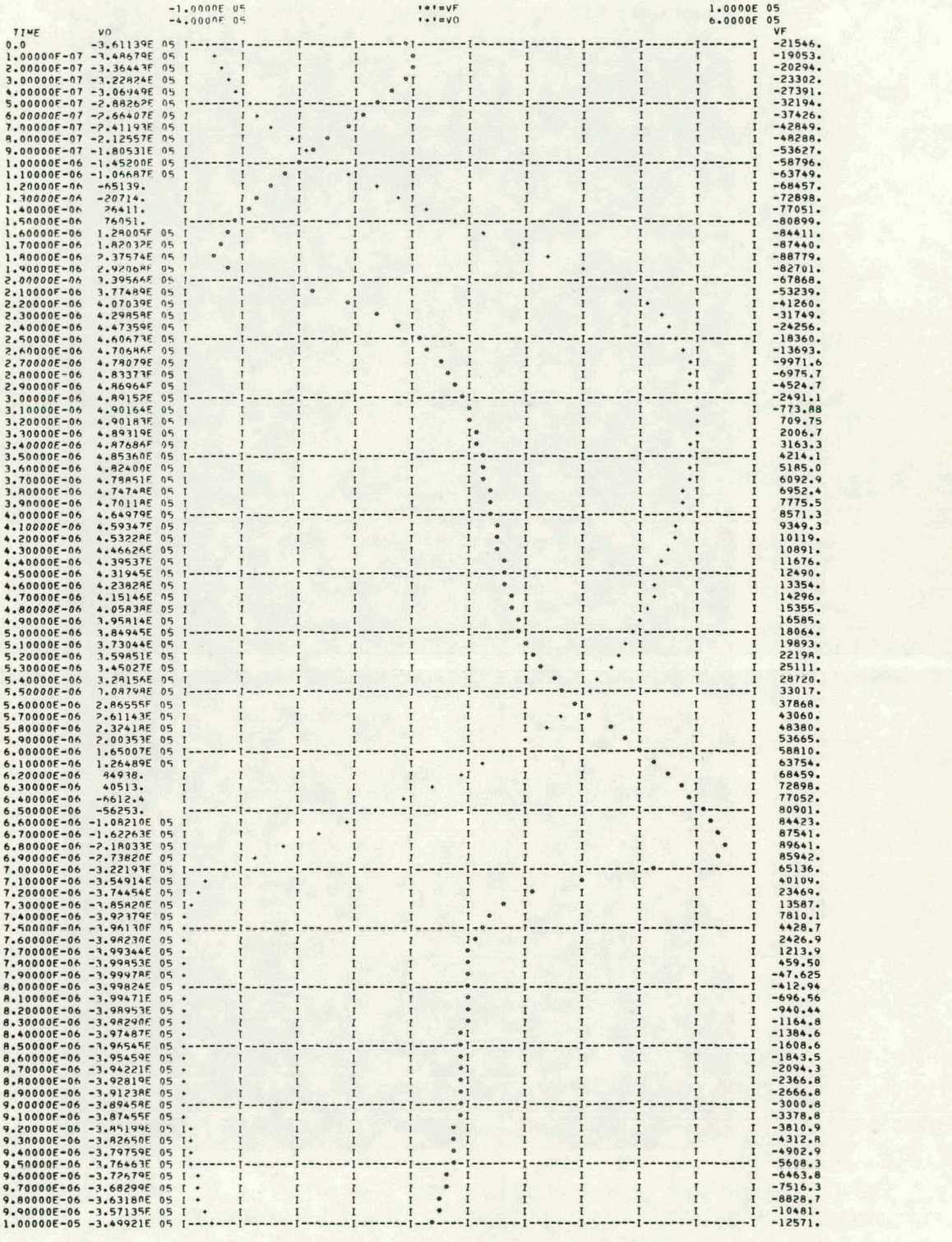

(r) VO and VF at 100 KHz with R_2 = 0Ω.

Figure 33 (continued)

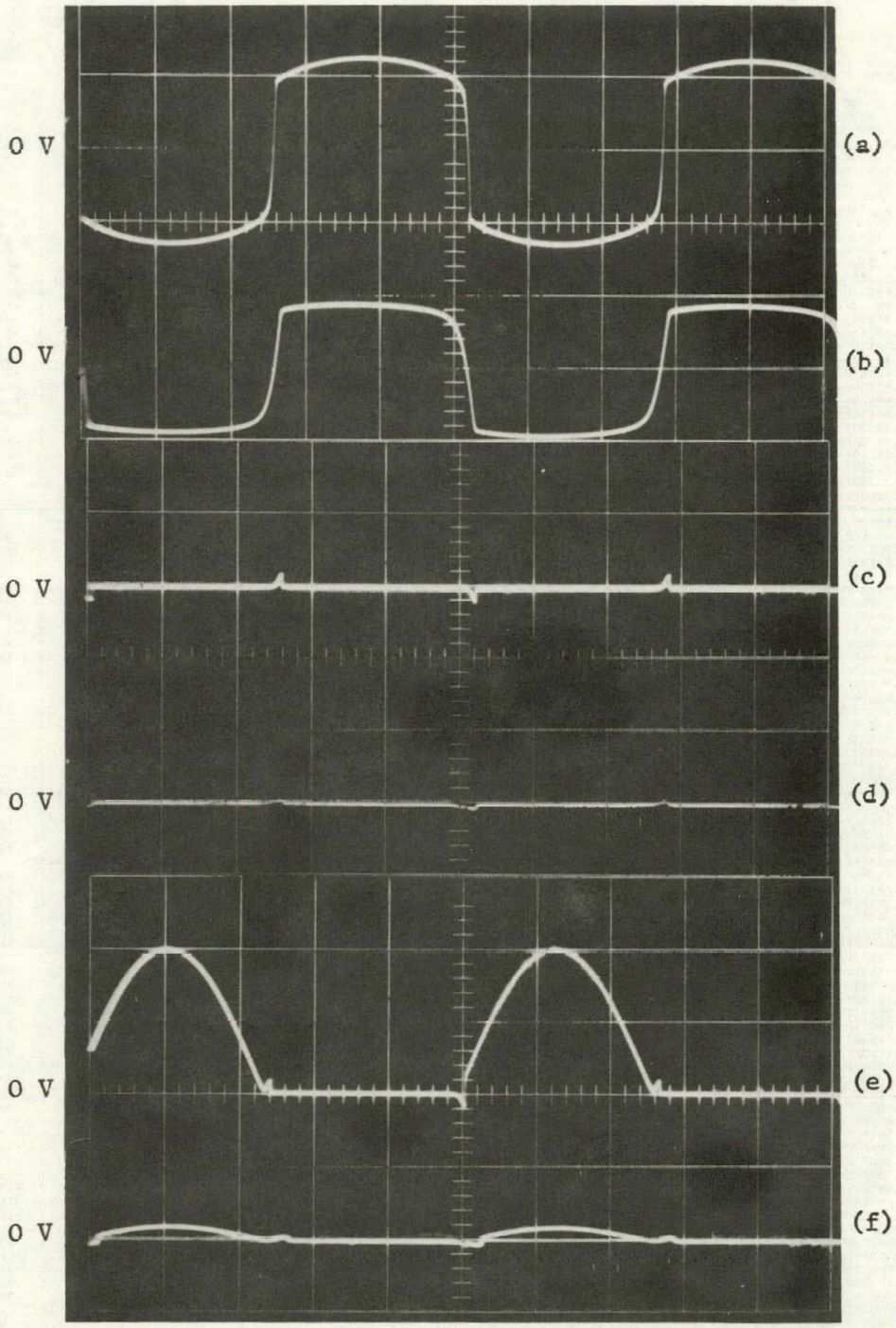

Figure 34. Experimental 1 KHz waveforms of a FD300 diode rectifier with $R_1 = R_2 = R_3 = 2\ K\Omega$, $C_3 = 2\ \mu F$, and an AD506LH opamp. (a) V_o with $V_{inp} = 0.1$ V; (b) V_o with $V_{inp} = 10$ mV; (c) V_f with $V_{inp} = 0.1$ V; (d) V_f with $V_{inp} = 10$ mV; (e) V_{R1} with $V_{inp} = 0.1$ V; (f) V_{R1} with $V_{inp} = 10$ mV. Horizontal scale: 0.2 ms/div. Vertical scale: 0.5 V/div [curves (a) and (b)]; 0.5 V/div [curves (c), (d), (e), and (f)].

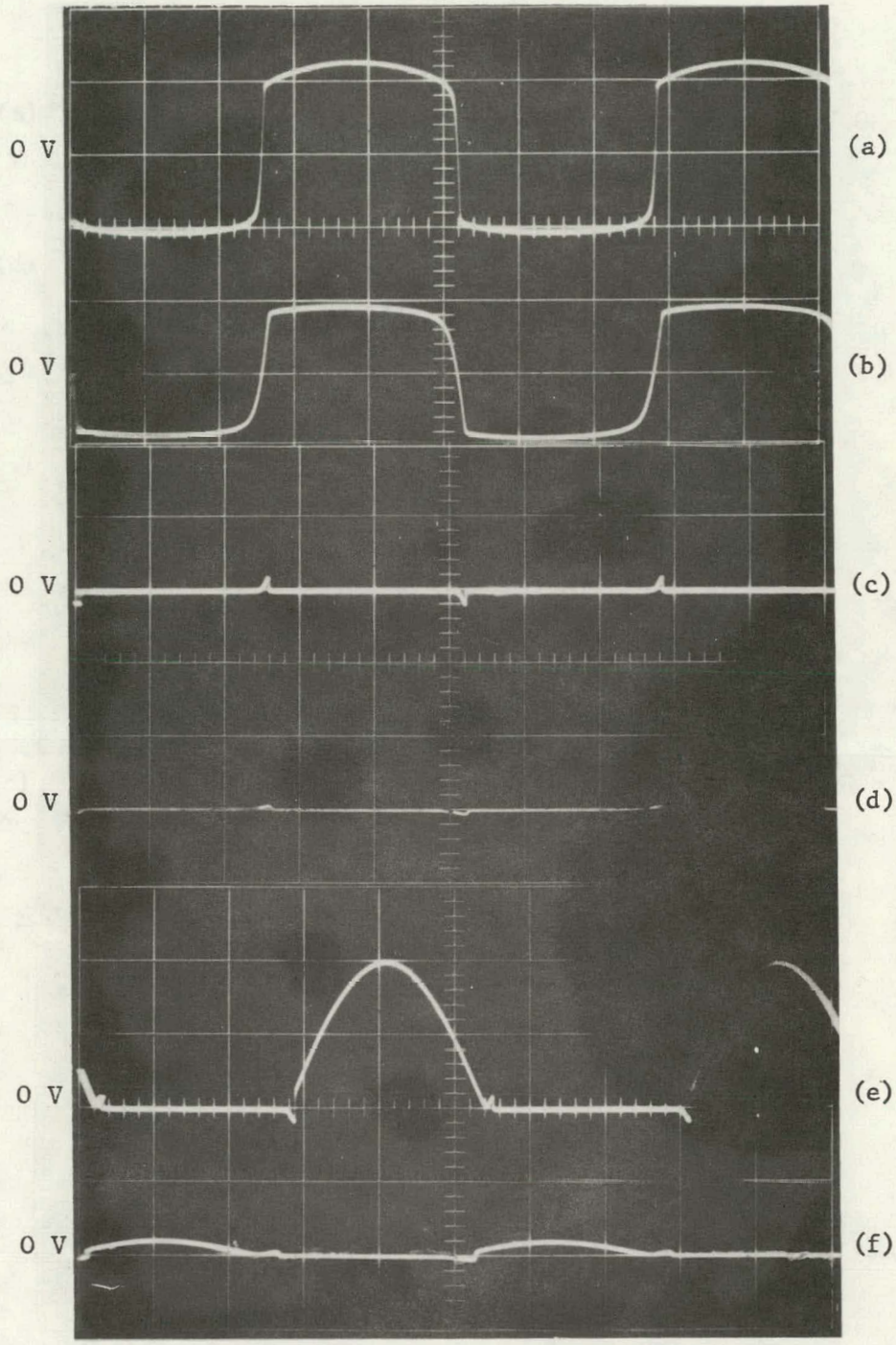

Figure 35. Experimental 1 KHz waveforms of a FD300 diode rectifier with $R_1 = R_3 = 2$ KΩ, $R_2 = 0$, $C_3 = 2$ μF, and an AD506LH opamp. (a) V_o with $V_{inp} = 0.1$ V; (b) V_o with $V_{inp} = 10$ mV; (c) V_f with $V_{inp} = 0.1$ V; (d) V_f with $V_{inp} = 10$ mV; (e) V_{R1} with $V_{inp} = 0.1$ V; (f) V_{R1} with $V_{inp} = 10$ mV. Horizontal scale: 0.2 ms/div. Vertical scale: 0.5 V/div [curves (a) and (b)]; 0.05 V/div [curves (c), (d), (e), and (f)].

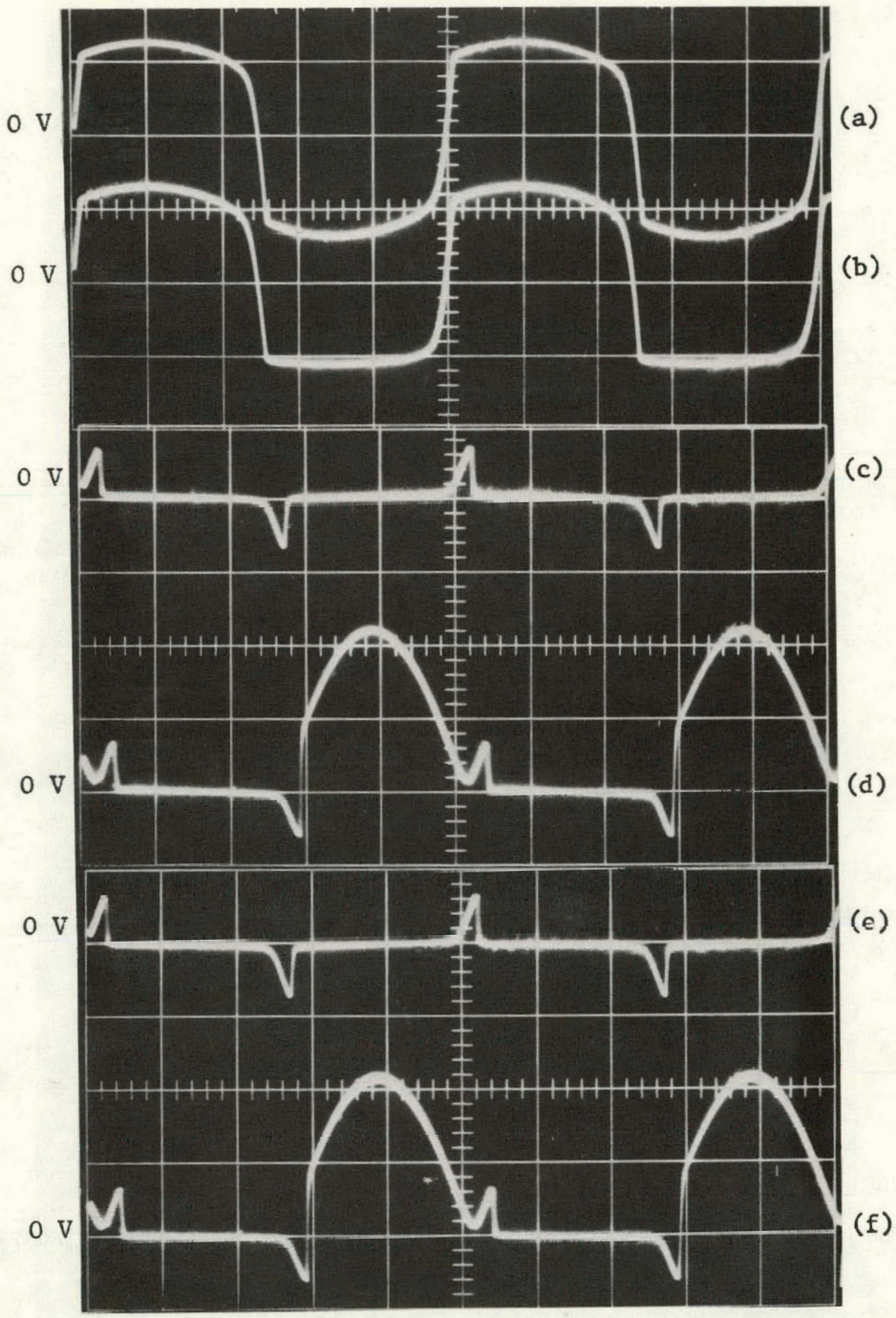

Figure 36. Experimental 10 KHz waveforms of a FD300 diode rectifier with $R_1 = R_3 = 2$ KΩ, $C_3 = 2$ μF, $V_{inp} = 0.1$ V, and an AD506LH opamp. (a) V_o with $R_2 = 2$ KΩ; (b) V_o with $R_2 = 0\Omega$; (c) V_f with $R_2 = 2$ KΩ; (d) V_f with $R_2 = 2$ KΩ; (e) V_{R1} with $R_2 = 0\Omega$; (f) V_{R1} with $R_2 = 0\Omega$; Horizontal scale: 20 μs/div. Vertical scale: 0.5 V/div [curves (a) and (b)]; 0.05 V/div [durves (c), (d), (e), and (f)].

frequency is increased, and that the ratio of spike amplitude to peak output signal increases as the input signal level decreases. Therefore, for very low signal levels, very high frequencies or very low opamp gain, the spike can exceed the desired peak signal output thereby causing large error for peak detectors. The computer simulation and measurements show in Figures 30 (pages 144-147), 33 (pages 154-171), and 37 that spikes in the rectifier output are substantially reduced, if not eliminated, with a current output rectifier.

Computed and experimental waveforms for an asymmetrical rectifier are pictured in Figures 33, 35, 36, and 37 for comparison with a symmetrical rectifier as shown in Figures 33, 34, and 36. For the asymmetrical rectifier, R2 = 0. These pictures show that the waveforms for the asymmetrical and symmetrical circuits are essentially identical, except for V_o where a flattening of the negative swing is evident for the asymmetrical circuit.

As shown in Figure 21(d) on page 91, both R1 and R2 may be set to zero when transistors are used as the rectifying elements. Assuming ideal transistors with $\alpha = 1$, the delay method may be utilized to compute rectifier performance. Figure 38 shows the average error for R1 = R2 = 0Ω. Note that for input voltages below 0.1 V_p the error is essentially identical to that with R1 = R2 = 2 KΩ just as predicted by the iteration method. Although Figure 38 shows lower error at high input voltages, the results are in doubt due to round-off error. Round-off accuracy can be substantially improved by the direct solution of a differential equation to be discussed next.

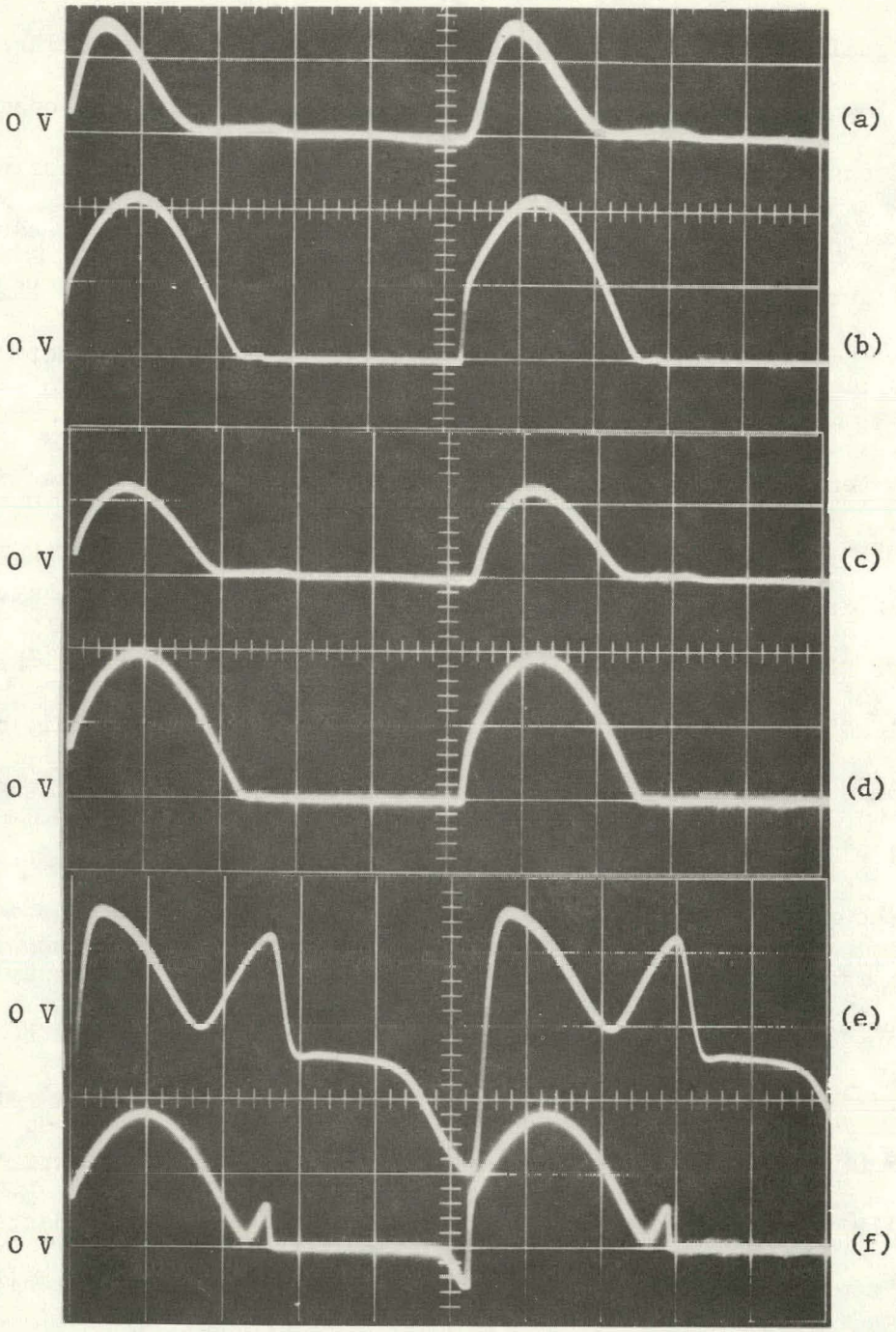

Figure 37. Experimental comparison of 10 KHz and 100 KHz 0.1 V_p waveforms of 2N5087 Darlington transistor and FD300 diode rectifiers with R_3 = 2 KΩ and an AD506LH opamp. (a) 100 KHz V_{IF1RF} for transistor rectifier with no R; (b) same as (a) but 10 KHz; (c) same as (a) but R = 14.7 KΩ; (d) same as (c) but 10 KHz; (e) 100 KHz V_{R1} for diode rectifier with R_2 = 0Ω; (f) same as (e) but 10 KHz. Horizontal scale: 2 μs/div [curves (a), (c), and (e)]; 20 μs/div [curves (b), (d), and (f). Vertical scale: 0.5 V/div.

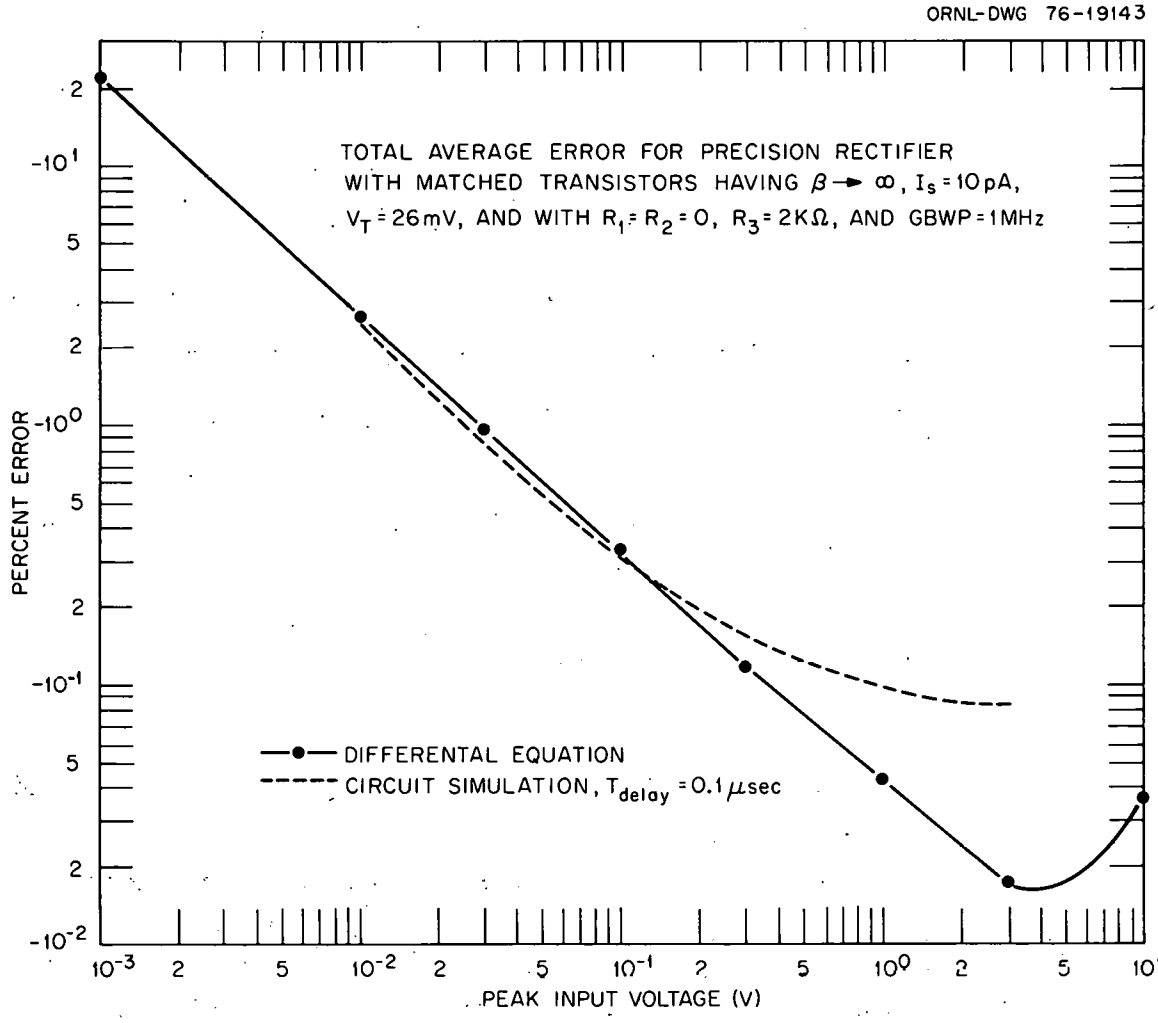

Figure 38. Computed average error for ideal-transistor rectifier with I_s = 10 pA, A_{ol} = 2 × 10^5, and GBWP = 1 MHz.

Computer Simulation by Differential Equation

Computer simulation by the delay method employs two extra integrators to enable simulation of the transcendental equation. However, these extra integrators increase CPU time and round-off error. But for a symmetrical circuit at FINPUT > $(2\pi\ \mathrm{TOL})^{-1}$, a first-order, nonlinear differential equation may be written to find ID1 and ID2. Using the circuit simplification shown in Figure 26(b) on page 118 where the reverse diode currents are neglected, R1 = R2, and assuming matched diodes, the following procedure can be employed to derive a differential equation. From Equation (120) on page on page 89,

$$\mathrm{VO} - \mathrm{VR1} = V_{D1} = \mathrm{VT}\ \sinh^{-1}\left(\frac{\mathrm{VF} - \mathrm{VIN}}{2\ \mathrm{R3}\ \mathrm{IS}}\right) , \tag{192}$$

where I_{in} = (VF - VIN)/R3. Differentiating the above equation, one obtains

$$\dot{\mathrm{VO}} - \dot{\mathrm{VR1}} = \mathrm{VT}\ \dot{Z}/(1 + Z^2)^{1/2} , \tag{193}$$

where Z = (VF - VIN)/(2 R3 IS). Using the high frequency approximation of $\frac{\mathrm{AOL}}{1 + \mathrm{TOL}j\omega} \simeq \frac{\mathrm{AOL}}{\mathrm{TOL}j\omega}$, $\dot{\mathrm{VO}} \simeq \frac{\mathrm{AOL\ VF}}{\mathrm{TOL}}$. Substituting $\mathrm{VR1} = \frac{(\mathrm{R3} + \mathrm{R1})}{\mathrm{R3}}\ \mathrm{VF} - \frac{\mathrm{R1}}{\mathrm{R3}}\mathrm{VIN}$ and the above approximation for $\dot{\mathrm{VO}}$ into Equation (193) and collecting terms, the following differential equation results:

$$\dot{Z}\left(\frac{\mathrm{VT}}{(1 + Z^2)^{1/2}} + 2(\mathrm{R3} + \mathrm{R1})\ \mathrm{IS}\right) + Z\ \frac{\mathrm{AOL}}{\mathrm{TOL}}\ 2\ \mathrm{R3}\ \mathrm{IS} = -\mathrm{VIN}\ \frac{\mathrm{AOL}}{\mathrm{TOL}}$$

$$- \dot{\mathrm{VIN}}\ \frac{\mathrm{R3} + \mathrm{R1}}{\mathrm{R3}} . \tag{194}$$

This equation is easily solved with CSMP by the following expression:

3

$$Z = VIFRF/K \ ,$$

$$DVIFRF = \frac{-K(VIFRF + VIN + VIN2 \frac{TOL\ (R3 + R1)}{AOL\ R3})\ AOL\ SQRTZ}{TOL\ (VT + 2\ (R3 + R1)\ IS\ SQRTZ)} \ ,$$

$$SQRTZ = (1 + Z^2)^{1/2} \ , \tag{195}$$

and

$$VIFRF = \int_0^t DVIFRF\ dX + VIFRFI \ ,$$

where K = 2 R3 IS, VIFRFI = VIFRF at t = 0, VIN2 = $\dot{VIN}$, and VIFRF = VIF1RF and VIF2RF when VIFRF is positive and negative, respectively. VF, VO, and VR1 are easily obtained using the following expressions:

$$VF = VIN + VIFRF$$

$$VR1 = VF + VIF1RF\ \ R1/R3 \tag{196}$$

and

$$VO = VF + VIFRF \frac{R1}{R3} + VT\ \ln\ (Z + SQRTZ) \ .$$

For large $|Z|$ ($|Z| > 1000$), replacing Z + SQRTZ with $Z + |Z| + 0.5/|Z|$ will result in improved accuracy particularly if $Z << 0$. A computer program using these equations is listed in Appendix C.

The average error of a transistor rectifier with R1 = 0 and $\alpha = 1$ as computed by the differential equation method is graphed in Figure 38 on page 177 along with the error as computed by the delay method for comparison. This graph shows that both techniques give essentially the same results for rectifier errors above 0.3%, but for lower errors, the differential technique yields superior results. In fact, the differential method gives accurate results down to rectifier errors of

0.03% beyond which round-off error becomes significant (both graphs were computed with STIFF integration). Moreover, double-precision Runge Kutta integration can be used since there is only one pole. To discover the effects of the integration routine and step size on computed rectifier accuracy, stiff, double-precision Runge Kutta (DKSDP), and single-precision Runge Kutta (RKS) integration were used to simulate the 1 KHz 0.3 Vp performance. With PRDEL = 5 μsec, IERORA is -0.1174%, -0.04188%, and -0.02609% for STIFF, RKS, and RKSDP integration, respectively. With PRDEL = 2.5 μsec, IERORA is -0.1182% and -0.08264% with stiff and RKS integration. Reducing PRDEL further to 1 μsec causes IERORA to be -0.09675% with RKSDP integration. This indicates that a larger PRDEL can be used with stiff integration without changing the results significantly. Also, PRDEL should be less than 1 μsec when RKSDP integration is employed. Surprisingly, the CPU time was essentially independent of PRDEL for both STIFF and RKSDP integration, RKSDP taking about 30% more CPU time than STIFF.

Figure 39 shows the rectifier waveforms for a 0.1 V_p input signal as computed by both delay and differential equation methods. This shows that there is little difference between the waveforms computed by these two methods. Comparing Figure 39 with Figure 33(a), (b), and (c) on pages 154, 155, and 156 where R1 = R2 = 2 KΩ show them to be very similar except the estimate for PHASE was poorer for the former causing a cosinusoidal component of IERORT.

Error Analysis of the Darlington Transistor Rectifier Circuit

The Darlington rectifier, as shown in Figure 21(e) on page 91, is a modification of Figure 21(d) on page 91 which the author designed to

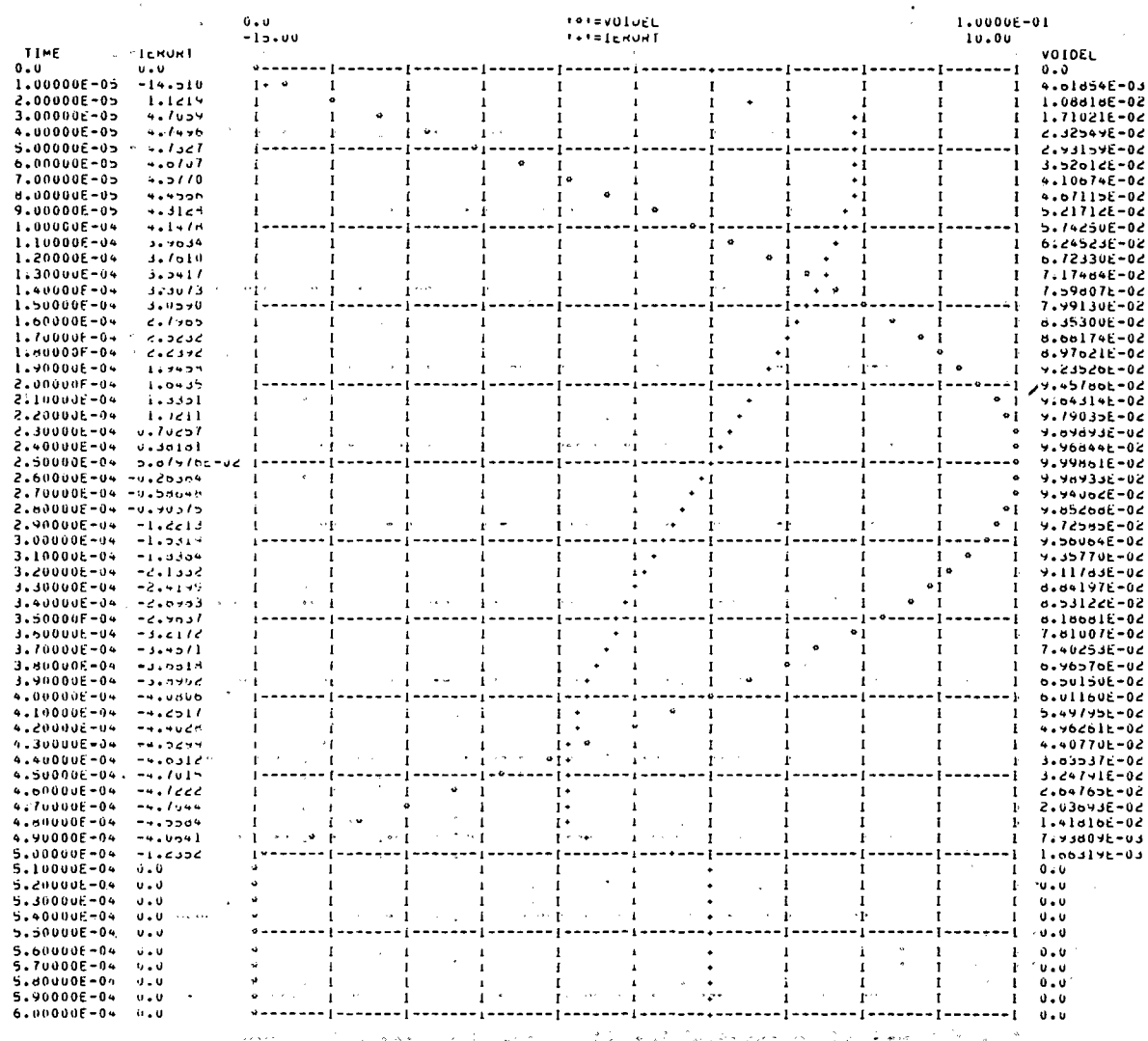

(a) VOIDEL and IEROUT computed by differential equation method.

Figure 39. Performance of ideal-transistor rectifier with $A_{o1} = 2 \times 10^5$, GBWP = 1 MHz, $R_1 = R_2 = 0\Omega$, and $R_3 = 2\ K\Omega$.

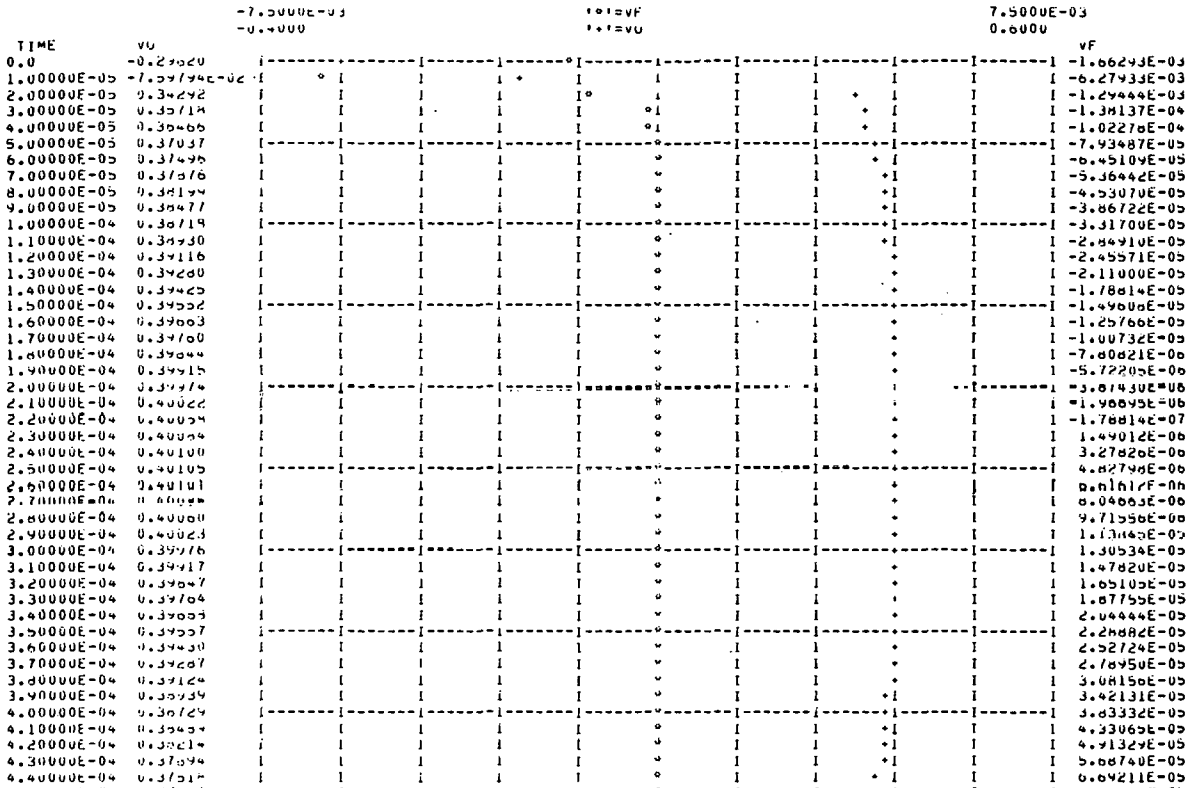

(b) VF and VO computed by differential equation method.

Figure 39 (continued)

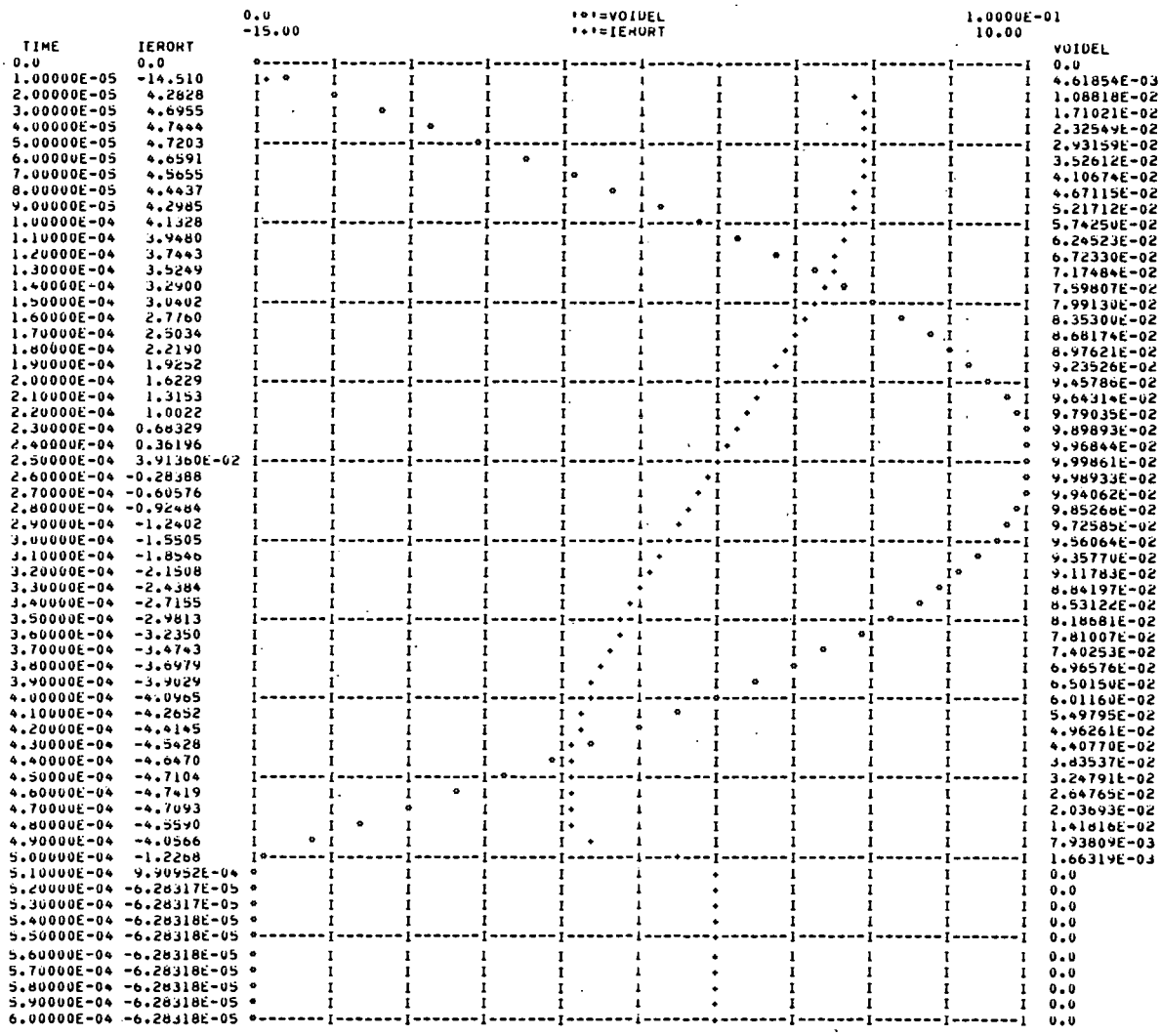

(c) VOIDEL and IEROUT computed by delay method.

Figure 39 (continued)

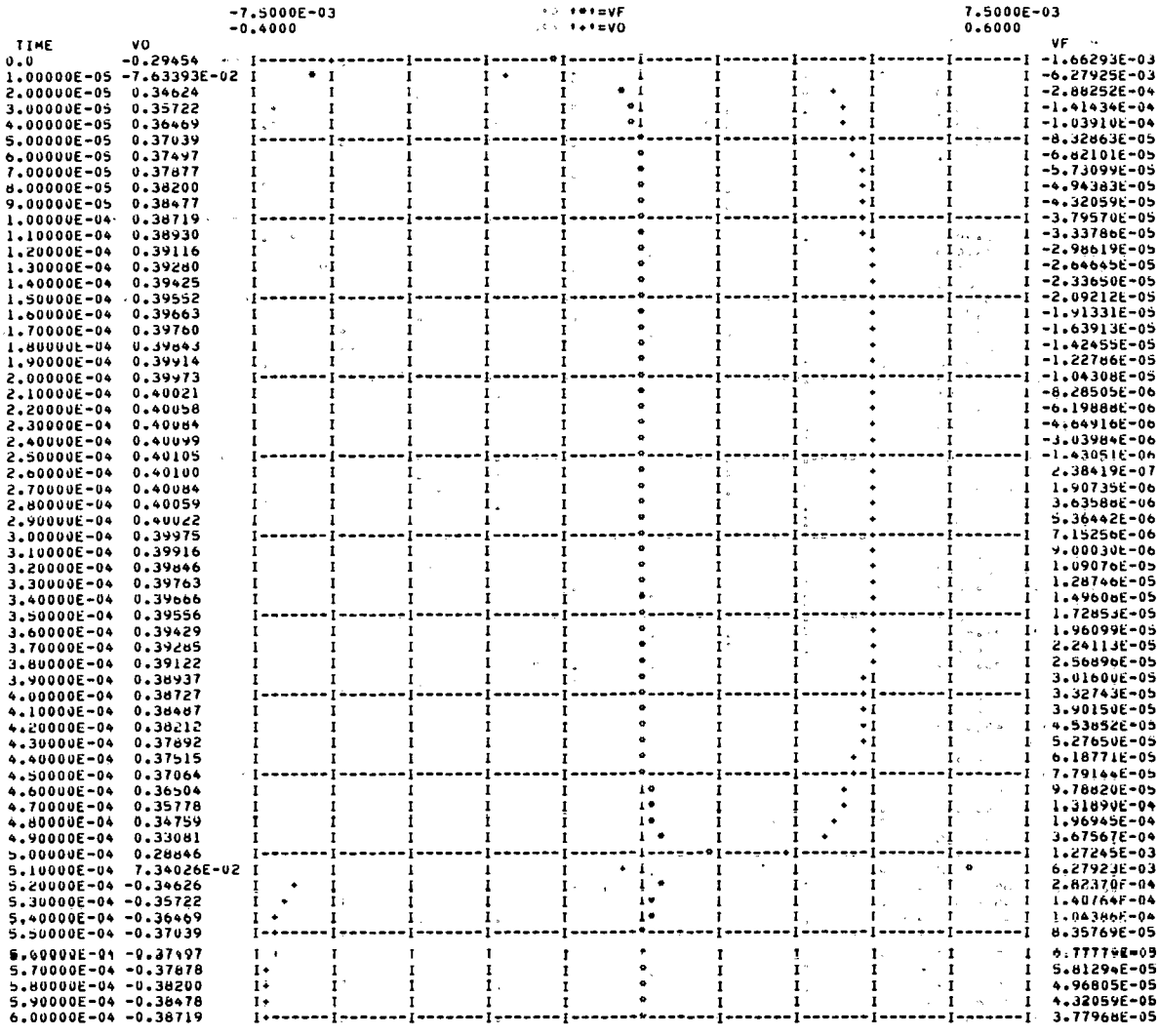

TIME	VO	VF
0.0	-0.29454	-1.66293E-03
1.00000E-05	-7.63393E-02	-6.27925E-03
2.00000E-05	0.34624	-2.88252E-04
3.00000E-05	0.35722	-1.41434E-04
4.00000E-05	0.36469	-1.03910E-04
5.00000E-05	0.37039	-8.32863E-05
6.00000E-05	0.37497	-6.82101E-05
7.00000E-05	0.37877	-5.73099E-05
8.00000E-05	0.38200	-4.94383E-05
9.00000E-05	0.38477	-4.32059E-05
1.00000E-04	0.38719	-3.79570E-05
1.10000E-04	0.38930	-3.33786E-05
1.20000E-04	0.39116	-2.98619E-05
1.30000E-04	0.39280	-2.64645E-05
1.40000E-04	0.39425	-2.33650E-05
1.50000E-04	0.39552	-2.09212E-05
1.60000E-04	0.39663	-1.91331E-05
1.70000E-04	0.39760	-1.63913E-05
1.80000E-04	0.39843	-1.42455E-05
1.90000E-04	0.39914	-1.22786E-05
2.00000E-04	0.39973	-1.04308E-05
2.10000E-04	0.40021	-8.28505E-06
2.20000E-04	0.40058	-6.19888E-06
2.30000E-04	0.40084	-4.64916E-06
2.40000E-04	0.40099	-3.03984E-06
2.50000E-04	0.40105	-1.43051E-06
2.60000E-04	0.40100	2.38419E-07
2.70000E-04	0.40084	1.90735E-06
2.80000E-04	0.40059	3.63588E-06
2.90000E-04	0.40022	5.36442E-06
3.00000E-04	0.39975	7.15256E-06
3.10000E-04	0.39916	9.00030E-06
3.20000E-04	0.39846	1.09076E-05
3.30000E-04	0.39763	1.28746E-05
3.40000E-04	0.39666	1.49606E-05
3.50000E-04	0.39556	1.72853E-05
3.60000E-04	0.39429	1.96099E-05
3.70000E-04	0.39285	2.24113E-05
3.80000E-04	0.39122	2.56896E-05
3.90000E-04	0.38937	3.01600E-05
4.00000E-04	0.38727	3.32743E-05
4.10000E-04	0.38487	3.90150E-05
4.20000E-04	0.38212	4.53852E-05
4.30000E-04	0.37892	5.27650E-05
4.40000E-04	0.37515	6.18771E-05
4.50000E-04	0.37064	7.79144E-05
4.60000E-04	0.36504	9.78820E-05
4.70000E-04	0.35778	1.31890E-04
4.80000E-04	0.34759	1.96945E-04
4.90000E-04	0.33081	3.67567E-04
5.00000E-04	0.28846	1.27245E-03
5.10000E-04	7.34026E-02	6.27923E-03
5.20000E-04	-0.34626	2.82370E-04
5.30000E-04	-0.35722	1.40764E-04
5.40000E-04	-0.36469	1.04386E-04
5.50000E-04	-0.37039	8.35769E-05
5.60000E-04	-0.37497	6.77779E-05
5.70000E-04	-0.37878	5.81294E-05
5.80000E-04	-0.38200	4.96805E-05
5.90000E-04	-0.38478	4.32059E-05
6.00000E-04	-0.38719	3.77968E-05

(d) VF and VO computed by delay method.

Figure 39 (continued)

overcome the error limitations imposed by the current dependence of α for real transistors. Three different computer simulations will be presented: the first using the delay method and a simple power law model for HFE(I), the second using the base-emitter capacitance of Q_2 to write a differential equation, and the third using a three-term power-law model for HFE(I) and includes all hybrid-pi transistor capacitances and reverse saturation collector currents.

Delay method. The delay method can readily be applied to the Darlington rectifier if R is neglected. The simplified expression for HFE(I) is utilized as follows:

$$HFE(I) = HFE_o(I/I_o)^M . \tag{197}$$

To simulate the Darlington rectifier, two quantities must be known: the composite base emitter voltage and collector current (I_c) as a function of IF1P. From Figure 40(a), the composite collector current is derived in the following manner:

$$I_c = I_{c1} + I'_{c1} = IF1P\ \alpha_{1D} , \tag{198}$$

where

$$\alpha_{1D} = (\alpha_1 + \frac{\alpha_1'}{1 + HFE1}) = \frac{HFE1 + \frac{HFE1'}{1 + HFE1'}}{1 + HFE1} .$$

An expression can be derived for IF1P as follows: first equations are written for IF1P and IF1P′ (′ applies to Q1′) in terms of their respective base-emitter voltages:

ORNL-DWG 76-19144

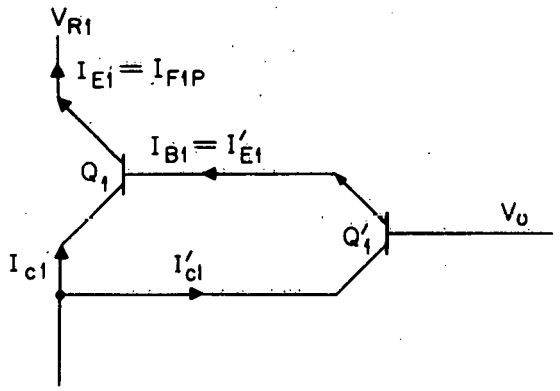

(a) Simple Darlington transistor used in delay method simulation.

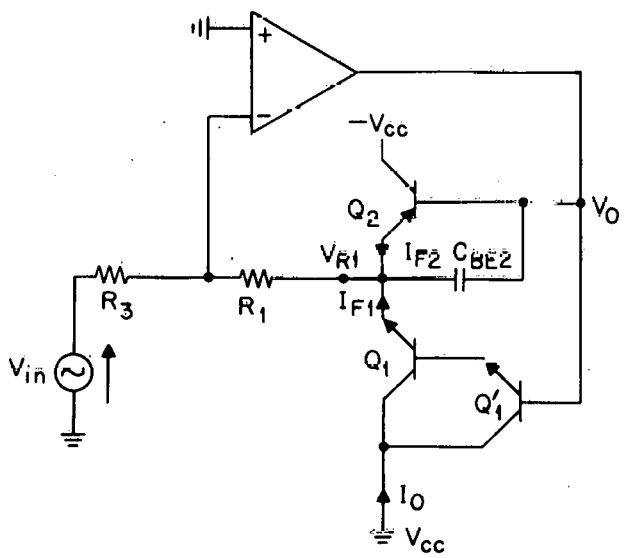

(b) Circuit used to simulate Darlington transistor rectifier by C_{BE2} differential equation method.

Figure 40. Circuit models used to simulate the Darlington transistor rectifier.

ORNL-DWG 76-19145

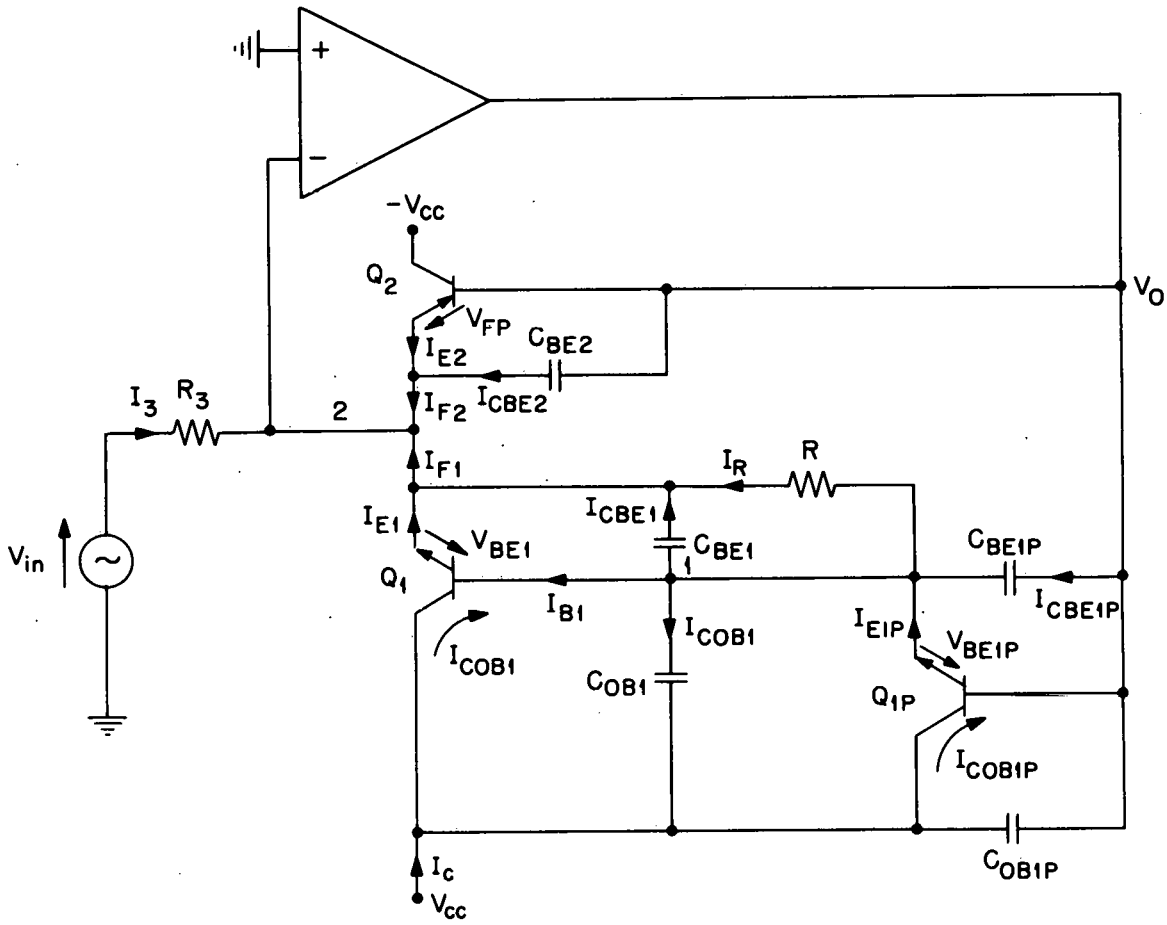

(c) Circuit used in advanced simulation.

Figure 40 (continued)

$$IF1P = IS1(\exp(VBE1/VT1) - 1)$$

and (199)

$$IF1P' = IS1'(\exp(VBE1'/VT1') - 1) = IF1P/(1 + HFE1) .$$

Solving the above expressions for base-emitter voltages and assuming matched transistors, VO - VR1 is

$$VO - VR1 = VT1 \ln\left(\left(\frac{IF1P}{IS1} + 1\right)\left(\frac{IF1P}{IS1\ (HFE1 + 1)} + 1\right)\right) , \tag{200}$$

or

$$\left(\frac{IF1P}{IS1} + 1\right)^2 + HFE1\left(\frac{IF1P}{IS1} + 1\right) = (HFE1 + 1)\exp\left(\frac{VO - VR1}{VT1}\right) .$$

Because IF1P/IS1 >>1 except when Q1 is turned off, the second term of the above expression can be neglected. Substituting Equation (197) for HFE1 where I is IF1P + IS1 and HFE1 >> 1, the following expression for IF1P results:

$$IF1P \simeq \left(IS1^2\ HFE_o(IF1P_o + IS1)^{-M}\right)^{\left(\frac{1}{2-M}\right)} \exp\left(\frac{VO - VR1}{(2-M)VT1}\right) - IS1 . \tag{201}$$

Since Equation (201) is strictly valid only for IF1P >> IS1, it must be modified to approximate IF1P down to -IS1. The arbitrary modifications to Equations (198) and (201) chosen for the simulation were:

$$HFE1 = BETA1 = HFE_o\left(\frac{IF1P + 2\ IS1DAR}{I_o}\right)^M ,$$

$$HFE1' = BETA1P = HFE_o\left(\frac{IF1 + 2\ IS1DAR}{I_o(BETA1 + 1)}\right)^M , \tag{202}$$

and

$$IF1P = IS1DAR\left(\exp\left(\frac{VO - VR1}{(2-M)VT1}\right) - 1\right) ,$$

where $IS1DAR = \left(IS1^2 HFE_o(I_o)^{-M}\right)^{\left(\frac{1}{2-M}\right)}$.

A CSMP program was written using expressions (120) to compute the average error of a 2N5087 Darlington transistor rectifier. This program is listed in Appendix C. To determine the constants of HFE(I), HFE at 0.01 and 0.1 MA were obtained from the typical HFE curve for a 2N5087 transistor as shown in Figure 41. $HFE_o\ I_o^{-M}$ was determined to be 8400 while M was found to be 0.301. Figure 42 graphs the average error as computed by this program. Comparing this graph with Figure 38 on page 177 shows that the Darlington rectifier has approximately 40% more error than a single transistor rectifier with $\alpha = 1$ at input signals below 0.1 V_p; however, the delay method gives lower error values for the Darlington rectifier at input signals above 1 V_p. Comparing the rectifier waveforms for the Darlington rectifier in Figure 43(c) and (d) with those for the single transistor rectifier shown in Figure 39 on page 181 shows that IEROR has a larger negative spike of longer duration for the Darlington rectifier. Also, VO and VF are asymmetrical for the Darlington rectifier. Symmetry can be restored, of course, by making Q2 a Darlington transistor.

<u>CBE2 differential equation method</u>. A limitation of the delay method is that it does not accurately represent the stray reactances of the circuit. If R1 and R2 are combined as one resistor as was done in the differential method on page 178, both delay poles may be replaced by CBE2, as shown in Figure 40(b) on page 186. A simple differential node equation describes the effect of CBE2 as follows:

$$\frac{VF - VIN}{R3} = IF1 + IF2 + CBE2\ (\dot{V}O - \dot{V}R1)\ . \qquad (203)$$

Substituting VF = VR1 - R1 (IF1 + IF2) and solving Equation (203) for VR1 yields the following solution:

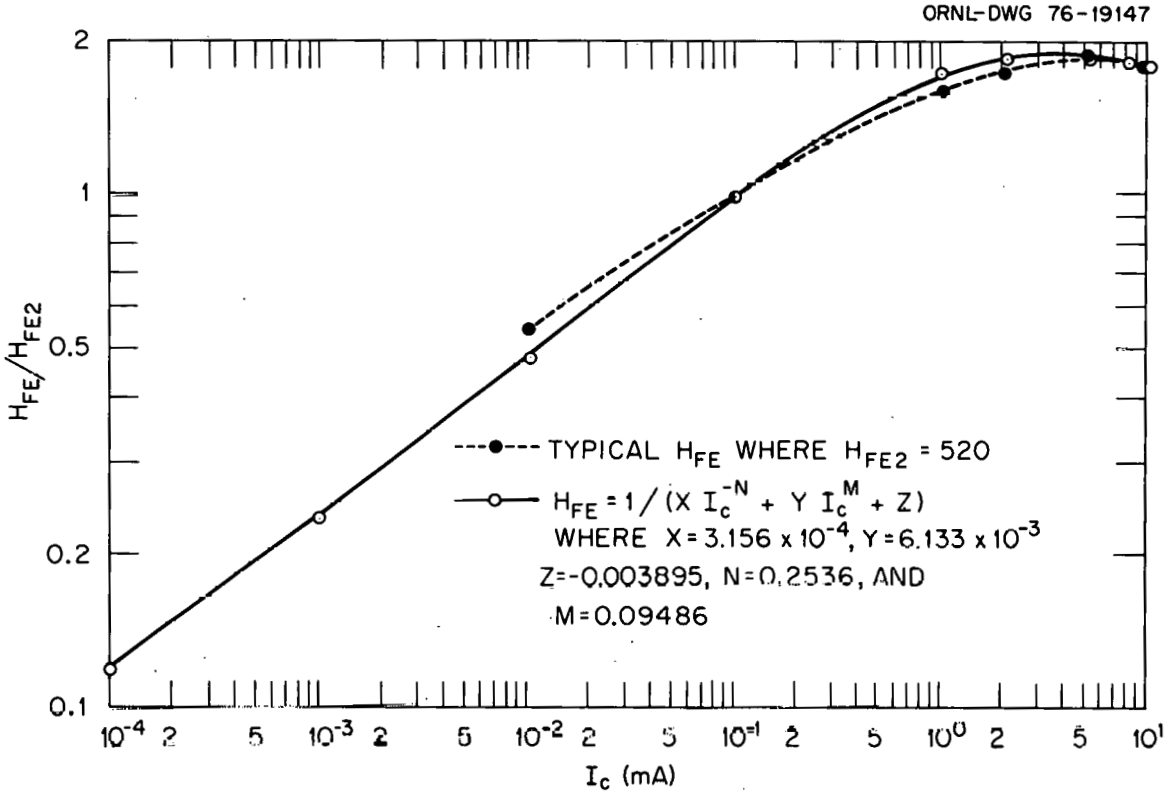

Figure 41. Typical H_{FE} for a 2N5087 transistor.

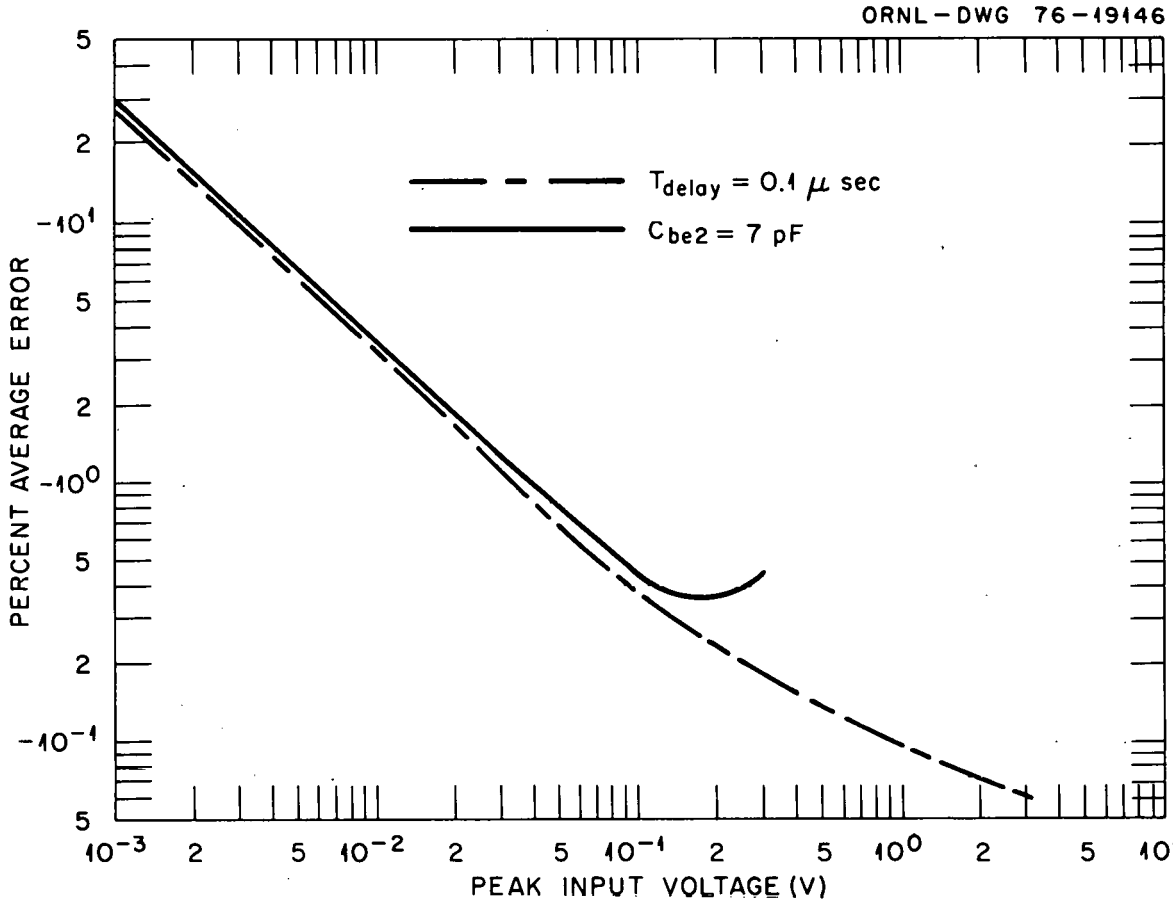

Figure 42. Computed average error of Darlington transistor rectifier with approximate H_{FE} for 2N5087, $A_{o1} = 2 \times 10^5$, GBWP = 1 MHz, $R_1 = R_2 = 0\Omega$, and $R_3 = 2K\Omega$.

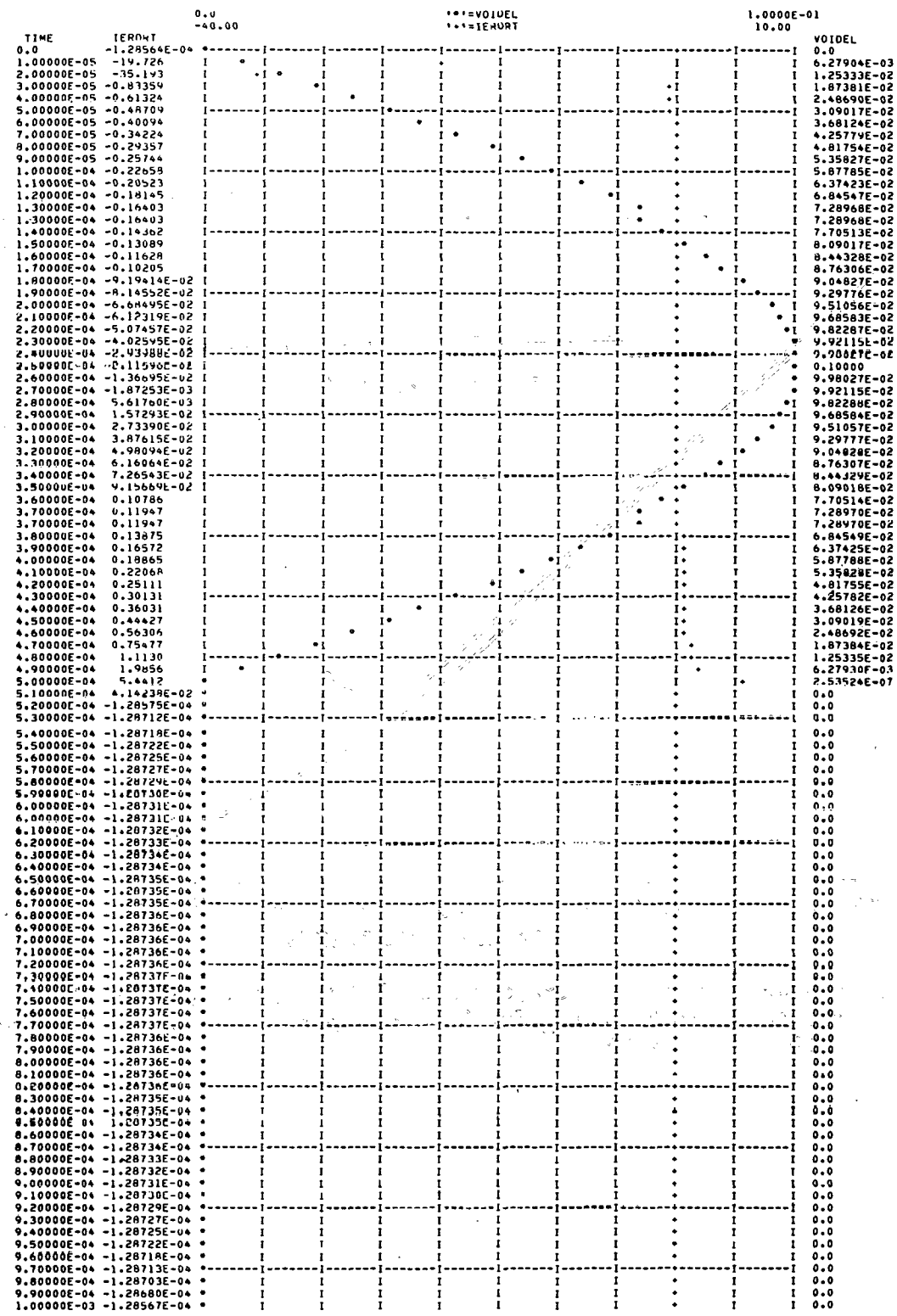

(a) VOIDEL and IEROUT with CBE2 = 7 pF.

Figure 43. Computed performance of a Darlington rectifier with approximate H_{FE} for 2N5087, $A_{o1} = 2 \times 10^5$, GBWP = 1 MHz, $R_1 = R_2 = 0\Omega$, and $R_3 = 2\ K\Omega$.

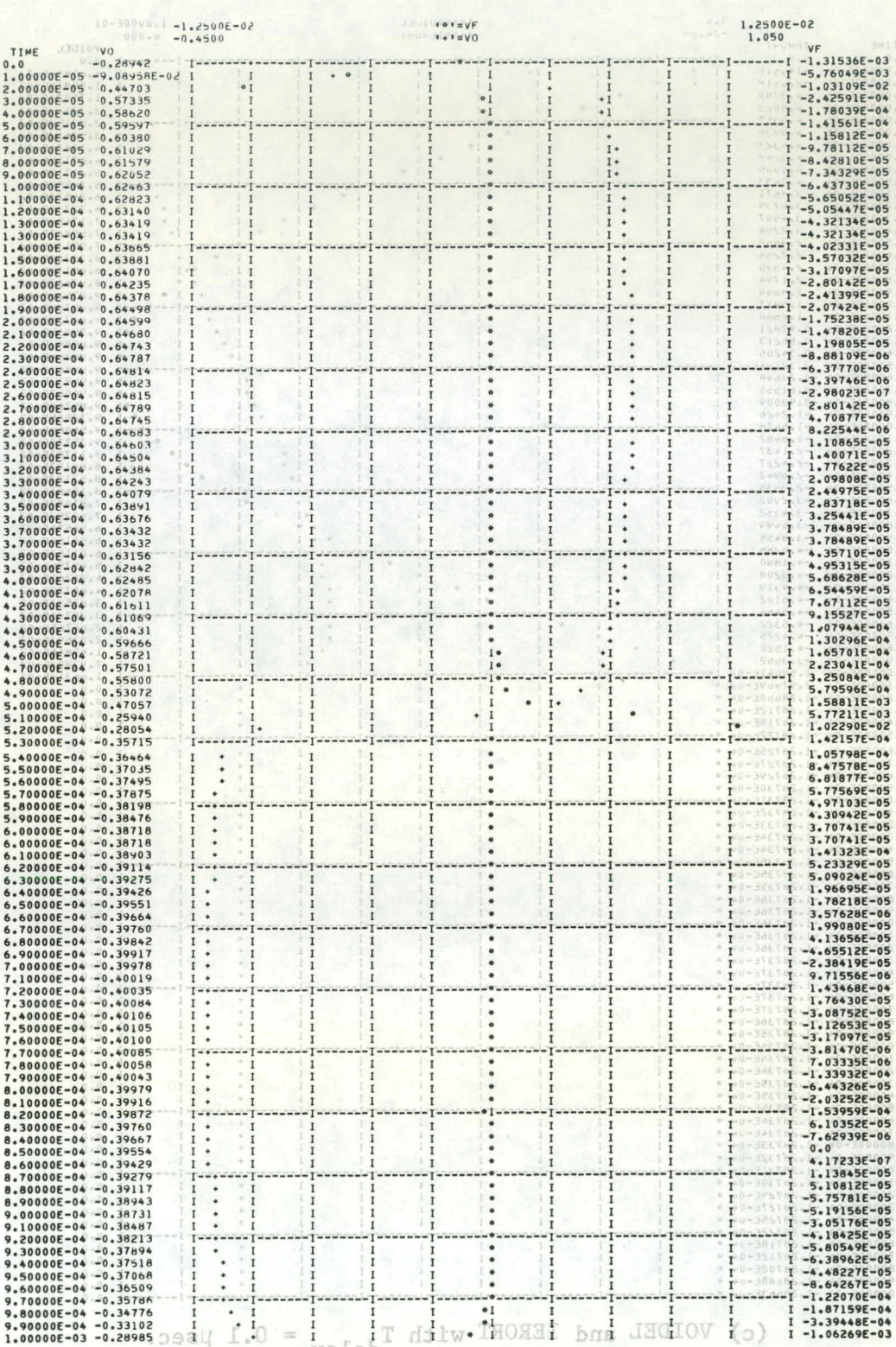

TIME	VO	VF
0.0	-0.28942	-1.31536E-03
1.00000E-05	-9.08958E-02	-5.76049E-03
2.00000E-05	0.44703	-1.03109E-02
3.00000E-05	0.57335	-2.42591E-04
4.00000E-05	0.58620	-1.78039E-04
5.00000E-05	0.59597	-1.41561E-04
6.00000E-05	0.60380	-1.15812E-04
7.00000E-05	0.61029	-9.78112E-05
8.00000E-05	0.61579	-8.42810E-05
9.00000E-05	0.62052	-7.34329E-05
1.00000E-04	0.62463	-6.43730E-05
1.10000E-04	0.62823	-5.65052E-05
1.20000E-04	0.63140	-5.05447E-05
1.30000E-04	0.63419	-4.32134E-05
1.30000E-04	0.63419	-4.32134E-05
1.40000E-04	0.63665	-4.02331E-05
1.50000E-04	0.63881	-3.57032E-05
1.60000E-04	0.64070	-3.17097E-05
1.70000E-04	0.64235	-2.80142E-05
1.80000E-04	0.64378	-2.41399E-05
1.90000E-04	0.64498	-2.07424E-05
2.00000E-04	0.64599	-1.75238E-05
2.10000E-04	0.64680	-1.47820E-05
2.20000E-04	0.64743	-1.19805E-05
2.30000E-04	0.64787	-8.88109E-06
2.40000E-04	0.64814	-6.37770E-06
2.50000E-04	0.64823	-3.39746E-06
2.60000E-04	0.64815	-2.98023E-07
2.70000E-04	0.64789	2.80142E-06
2.80000E-04	0.64745	4.70877E-06
2.90000E-04	0.64683	8.22544E-06
3.00000E-04	0.64603	1.10865E-05
3.10000E-04	0.64504	1.40071E-05
3.20000E-04	0.64384	1.77622E-05
3.30000E-04	0.64243	2.09808E-05
3.40000E-04	0.64079	2.44975E-05
3.50000E-04	0.63891	2.83718E-05
3.60000E-04	0.63676	3.25441E-05
3.70000E-04	0.63432	3.78489E-05
3.70000E-04	0.63432	3.78489E-05
3.80000E-04	0.63156	4.35710E-05
3.90000E-04	0.62842	4.95315E-05
4.00000E-04	0.62485	5.68628E-05
4.10000E-04	0.62078	6.54459E-05
4.20000E-04	0.61611	7.67112E-05
4.30000E-04	0.61069	9.15527E-05
4.40000E-04	0.60431	1.07944E-04
4.50000E-04	0.59666	1.30296E-04
4.60000E-04	0.58721	1.65701E-04
4.70000E-04	0.57501	2.23041E-04
4.80000E-04	0.55800	3.25084E-04
4.90000E-04	0.53072	5.79596E-04
5.00000E-04	0.47057	1.58811E-03
5.10000E-04	0.25940	5.77211E-03
5.20000E-04	-0.28054	1.02290E-02
5.30000E-04	-0.35715	1.42157E-04
5.40000E-04	-0.36464	1.05798E-04
5.50000E-04	-0.37035	8.47578E-05
5.60000E-04	-0.37495	6.81877E-05
5.70000E-04	-0.37875	5.77569E-05
5.80000E-04	-0.38198	4.97103E-05
5.90000E-04	-0.38476	4.30942E-05
6.00000E-04	-0.38718	3.70741E-05
6.00000E-04	-0.38718	3.70741E-05
6.10000E-04	-0.38903	1.41323E-04
6.20000E-04	-0.39114	5.23329E-05
6.30000E-04	-0.39275	5.09024E-05
6.40000E-04	-0.39426	1.96695E-05
6.50000E-04	-0.39551	1.78218E-05
6.60000E-04	-0.39664	3.57628E-06
6.70000E-04	-0.39760	1.99080E-05
6.80000E-04	-0.39842	4.13656E-05
6.90000E-04	-0.39917	-4.65512E-05
7.00000E-04	-0.39978	-2.38419E-05
7.10000E-04	-0.40019	9.71556E-06
7.20000E-04	-0.40035	1.43468E-04
7.30000E-04	-0.40084	1.76430E-05
7.40000E-04	-0.40106	-3.08752E-05
7.50000E-04	-0.40105	-1.12653E-05
7.60000E-04	-0.40100	-3.17097E-05
7.70000E-04	-0.40085	-3.81470E-06
7.80000E-04	-0.40058	7.03335E-06
7.90000E-04	-0.40043	-1.33932E-04
8.00000E-04	-0.39979	-6.44326E-05
8.10000E-04	-0.39916	-2.03252E-05
8.20000E-04	-0.39872	-1.53959E-04
8.30000E-04	-0.39760	6.10352E-05
8.40000E-04	-0.39667	-7.62939E-06
8.50000E-04	-0.39554	0.0
8.60000E-04	-0.39429	4.17233E-07
8.70000E-04	-0.39279	1.13845E-05
8.80000E-04	-0.39117	5.10812E-05
8.90000E-04	-0.38943	-5.75781E-05
9.00000E-04	-0.38731	-5.19156E-05
9.10000E-04	-0.38487	-3.05176E-05
9.20000E-04	-0.38213	-4.18425E-05
9.30000E-04	-0.37894	-5.80549E-05
9.40000E-04	-0.37518	-6.38962E-05
9.50000E-04	-0.37068	-4.48227E-05
9.60000E-04	-0.36509	-8.64267E-05
9.70000E-04	-0.35786	-1.22070E-04
9.80000E-04	-0.34776	-1.87159E-04
9.90000E-04	-0.33102	-3.39448E-04
1.00000E-03	-0.28985	-1.06269E-03

(b) VF and VO with CBE2 = 7 pF.

Figure 43 (continued)

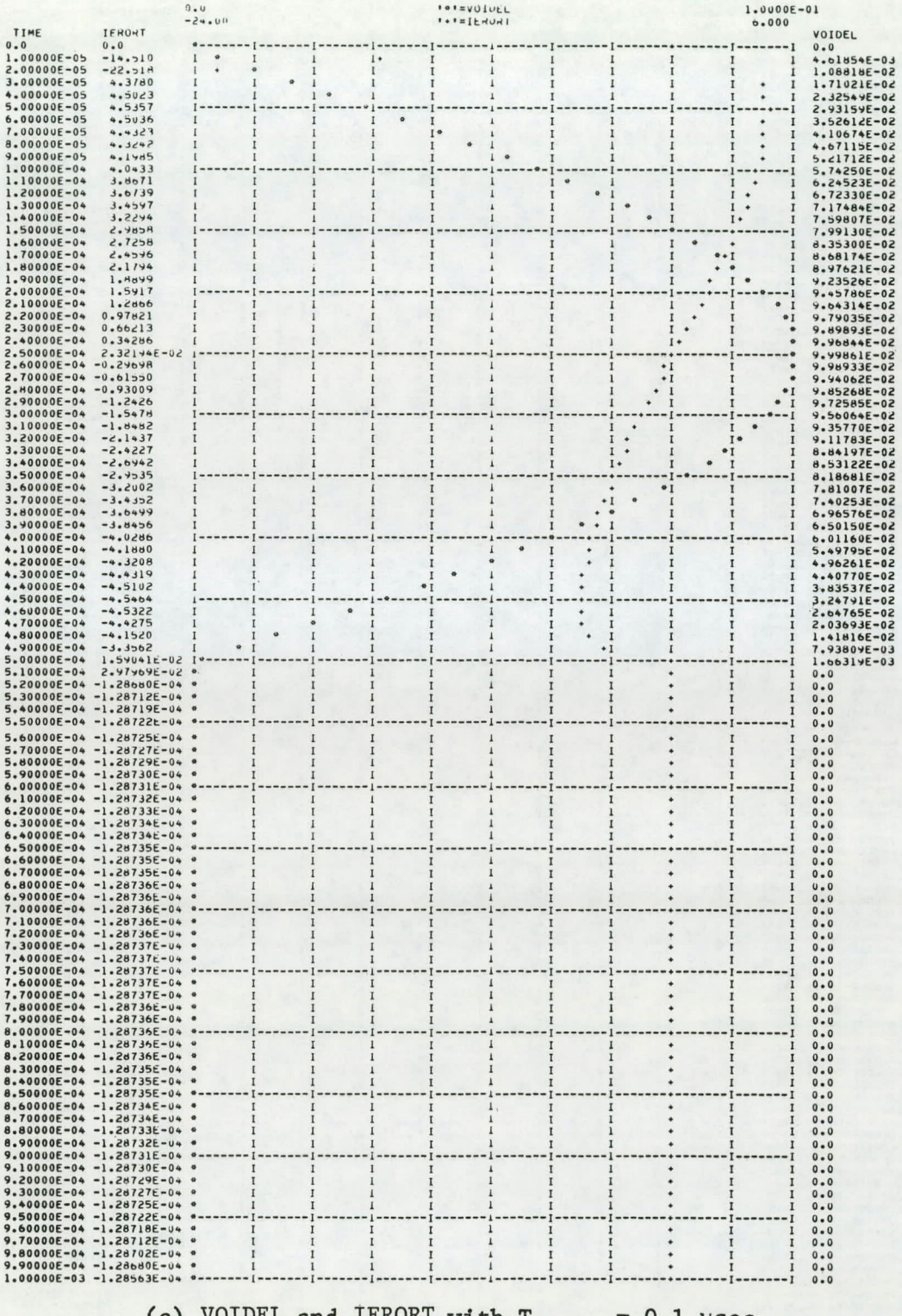

TIME	IEROR1	VOIDEL
0.0	0.0	0.0
1.00000E-05	-14.510	4.61854E-03
2.00000E-05	-22.518	1.08818E-02
3.00000E-05	4.3780	1.71021E-02
4.00000E-05	4.5023	2.32549E-02
5.00000E-05	4.5357	2.93159E-02
6.00000E-05	4.5036	3.52612E-02
7.00000E-05	4.4323	4.10674E-02
8.00000E-05	4.3242	4.67115E-02
9.00000E-05	4.1985	5.21712E-02
1.00000E-04	4.0433	5.74250E-02
1.10000E-04	3.8671	6.24523E-02
1.20000E-04	3.6739	6.72330E-02
1.30000E-04	3.4597	7.17484E-02
1.40000E-04	3.2294	7.59807E-02
1.50000E-04	2.9858	7.99130E-02
1.60000E-04	2.7258	8.35300E-02
1.70000E-04	2.4596	8.68174E-02
1.80000E-04	2.1794	8.97621E-02
1.90000E-04	1.8899	9.23526E-02
2.00000E-04	1.5917	9.45786E-02
2.10000E-04	1.2866	9.64314E-02
2.20000E-04	0.97821	9.79035E-02
2.30000E-04	0.66213	9.89893E-02
2.40000E-04	0.34286	9.96844E-02
2.50000E-04	2.32194E-02	9.99861E-02
2.60000E-04	-0.29698	9.98933E-02
2.70000E-04	-0.61550	9.94062E-02
2.80000E-04	-0.93009	9.85268E-02
2.90000E-04	-1.2426	9.72585E-02
3.00000E-04	-1.5478	9.56064E-02
3.10000E-04	-1.8482	9.35770E-02
3.20000E-04	-2.1437	9.11783E-02
3.30000E-04	-2.4227	8.84197E-02
3.40000E-04	-2.6942	8.53122E-02
3.50000E-04	-2.9535	8.18681E-02
3.60000E-04	-3.2002	7.81007E-02
3.70000E-04	-3.4352	7.40253E-02
3.80000E-04	-3.6499	6.96576E-02
3.90000E-04	-3.8456	6.50150E-02
4.00000E-04	-4.0286	6.01160E-02
4.10000E-04	-4.1880	5.49795E-02
4.20000E-04	-4.3208	4.96261E-02
4.30000E-04	-4.4319	4.40770E-02
4.40000E-04	-4.5102	3.83537E-02
4.50000E-04	-4.5464	3.24791E-02
4.60000E-04	-4.5322	2.64765E-02
4.70000E-04	-4.4275	2.03693E-02
4.80000E-04	-4.1520	1.41816E-02
4.90000E-04	-3.3562	7.93809E-03
5.00000E-04	1.59041E-02	1.66319E-03
5.10000E-04	2.97969E-02	0.0
5.20000E-04	-1.28680E-04	0.0
5.30000E-04	-1.28712E-04	0.0
5.40000E-04	-1.28719E-04	0.0
5.50000E-04	-1.28722E-04	0.0
5.60000E-04	-1.28725E-04	0.0
5.70000E-04	-1.28727E-04	0.0
5.80000E-04	-1.28729E-04	0.0
5.90000E-04	-1.28730E-04	0.0
6.00000E-04	-1.28731E-04	0.0
6.10000E-04	-1.28732E-04	0.0
6.20000E-04	-1.28733E-04	0.0
6.30000E-04	-1.28734E-04	0.0
6.40000E-04	-1.28734E-04	0.0
6.50000E-04	-1.28735E-04	0.0
6.60000E-04	-1.28735E-04	0.0
6.70000E-04	-1.28735E-04	0.0
6.80000E-04	-1.28736E-04	0.0
6.90000E-04	-1.28736E-04	0.0
7.00000E-04	-1.28736E-04	0.0
7.10000E-04	-1.28736E-04	0.0
7.20000E-04	-1.28736E-04	0.0
7.30000E-04	-1.28737E-04	0.0
7.40000E-04	-1.28737E-04	0.0
7.50000E-04	-1.28737E-04	0.0
7.60000E-04	-1.28737E-04	0.0
7.70000E-04	-1.28737E-04	0.0
7.80000E-04	-1.28736E-04	0.0
7.90000E-04	-1.28736E-04	0.0
8.00000E-04	-1.28736E-04	0.0
8.10000E-04	-1.28736E-04	0.0
8.20000E-04	-1.28736E-04	0.0
8.30000E-04	-1.28735E-04	0.0
8.40000E-04	-1.28735E-04	0.0
8.50000E-04	-1.28735E-04	0.0
8.60000E-04	-1.28734E-04	0.0
8.70000E-04	-1.28734E-04	0.0
8.80000E-04	-1.28733E-04	0.0
8.90000E-04	-1.28732E-04	0.0
9.00000E-04	-1.28731E-04	0.0
9.10000E-04	-1.28730E-04	0.0
9.20000E-04	-1.28729E-04	0.0
9.30000E-04	-1.28727E-04	0.0
9.40000E-04	-1.28725E-04	0.0
9.50000E-04	-1.28722E-04	0.0
9.60000E-04	-1.28718E-04	0.0
9.70000E-04	-1.28712E-04	0.0
9.80000E-04	-1.28702E-04	0.0
9.90000E-04	-1.28680E-04	0.0
1.00000E-03	-1.28563E-04	0.0

(c) VOIDEL and IEROR1 with T_{delay} = 0.1 μsec.

Figure 43 (continued)

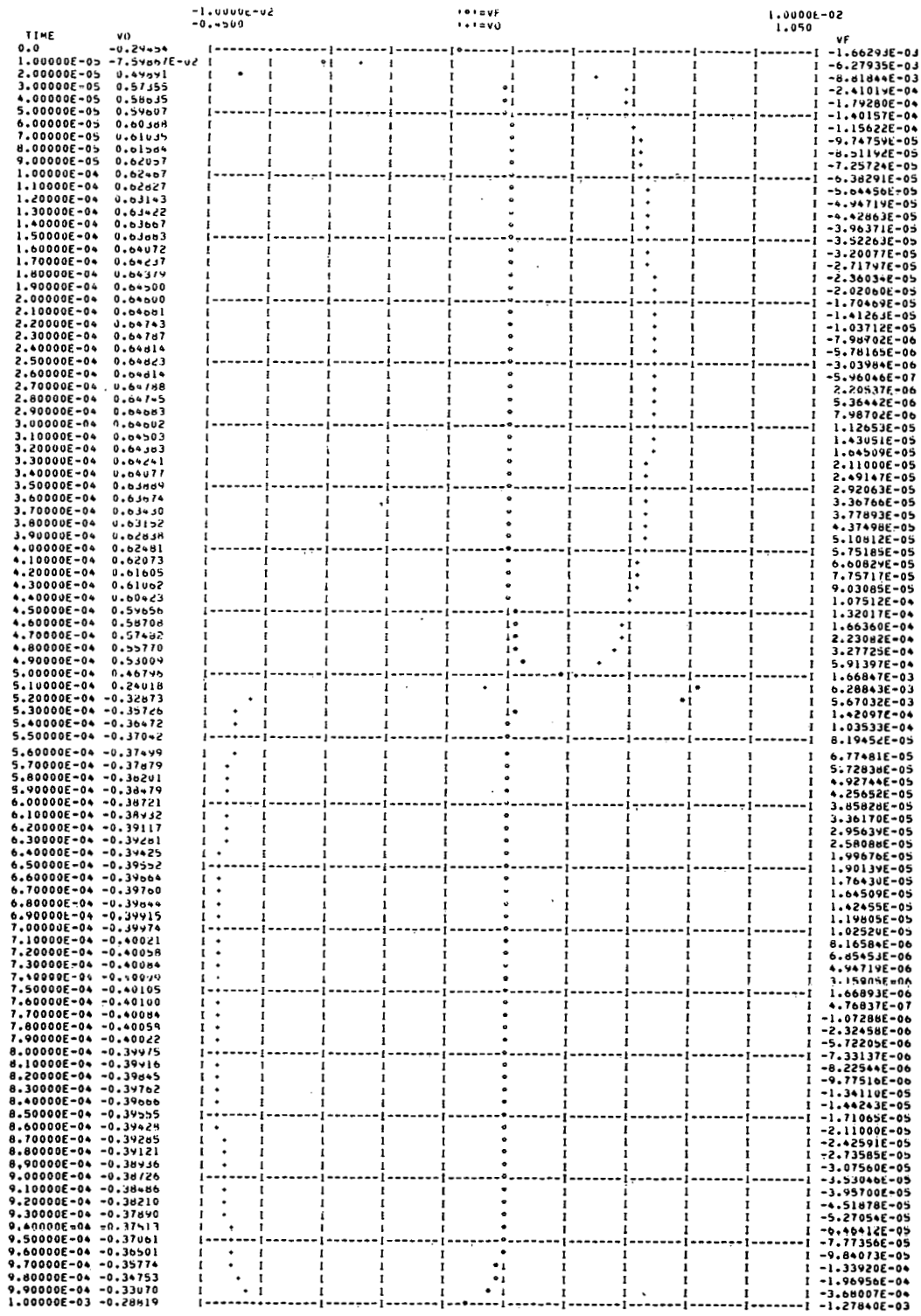

(d) VF and VO with T_{delay} = 0.1 μsec.

Figure 43 (continued)

$$VR1 = VO + VRP \ ,$$

$$VRP = \int_0^t DVR \, dt + VRPIC \ , \tag{204}$$

$$DVR = (VIN - VR1 + (IF1 + IF2)\ (R1 + R3))/(R3\ CBE2) \ ,$$

and

$$VRPIC = (IF2IC - IS1DAR)\ (R1 + R3) - VOIC \ .$$

These equations can readily be applied to either diode, transistor, or Darlington transistor rectifier circuits. A CSMP computer program using the above equations to simulate a Darlington rectifier is listed in Appendix C.

The average error and rectifier waveforms for a Darlington rectifier as computed by Equation (204) are shown in Figures 42 and 43(a) and (b). From Figure 42 it is shown that using CBE2 gives slightly higher error than the delay simulation. Also, round-off error occurs more abruptly for CBE2 differental method. The waveforms for both techniques are essentially the same at 10 mV peak input signal.

Advanced analysis. The differential equation technique can be expanded to include all hybrid-pi capacitances as well as complex models for HFE(I). The complete circuit to be simulated is shown in Figure 40(c) on page 187 (CSMP program listed in Appendix C).

In the computer simulation, differential equations are written to include the effects of transistor capacitances. First, a node equation is written for node number 1:

$$IE1P = IR + IB1 + ICOB1 + ICBE1 - ICBE1P \ ,$$

where

$$IE1P = IS1P\ (\exp(\frac{VBE1P}{VT1P}) - 1)\ ,$$

$$IR = VBE1/R\ ,$$

$$IB1 = IE1/(HFE1 + 1) - ICBO1\ ,$$

$$IE1 = IS1\ (\exp(\frac{VBE1}{VT1}) - 1)\ , \tag{205}$$

$$ICOB1 = COB1\ (\dot{VBE1} + \dot{VF})\ ,$$

$$ICBE1 = CBE1\ \dot{VBE1}\ ,$$

and

$$ICBE1P = CBE1P\ \dot{VBE1P}\ .$$

Making use of the fact that VBE1P = VO - VF - VBE1, Equation (205) can be solved for VBE1:

$$VBE1 = VVBE1 + (CBE1P\ VO - (COB1 + CBE1P)\ VF)/SUMC\ ,$$

where

$$VVBE1 = \int DIE1P\ dt\ ,$$

$$DIE1P = \frac{DIE1PP}{SUMC} = \frac{IE1P - IB1 - IR}{SUMC}\ , \tag{206}$$

and

$$SUMC = CBE1 + CBE1P + COB1\ .$$

Next a node equation for node number 2 can be written:

$$I3 + IF1 + IF2 = 0\ ,$$

where

$$I3 = (VIN - VF)/R3 \ ,$$

$$IF1 = IE1 + ICBE1 + IR \ ,$$

$$IF2 = IE2 + ICBE2 \ , \tag{207}$$

$$IE2 = -IS2 \ (\exp(\frac{VFP}{VT2}) - 1) \ ,$$

$$VFP = VF - VO \ ,$$

and

$$ICBE2 = -CBE2 \ \dot{V}FP \ .$$

Finally, the output current (IC) is given by the following expression:

$$IC = IE1 \ \alpha_1 + IE1P \ \alpha_{1P} + ICBO1 + ICBO1P - ICOB1 - ICOB1P \ ,$$

where (208)

$$ICOB1P = COB1P \ \dot{V}O \ .$$

In this simulation a fourth-order exponential equation is employed to model H_{FE}; i.e.,

$$H_{FE} = 1/(X \ I^{-N} + Y \ I^{M} + Z) \ . \tag{209}$$

A computer program designed to compute the constants of the above expression as written by Bernstein[70] was incorporated in the CSMP simulation. To compute these five constants, five data points of the form (I_i, B_i) are specified on two parameter cards. B_i is H_{FE} at collector current I_i. The five data points are defined as follows:

1. I_1 is the minimum current of interest.
2. I_2 is a current less than I_p but greater than I_1.
3. I_p is the current at which H_{FE} is maximum.

4. I_3 is a current greater than I_p but less than I_4.

5. I_4 is the maximum current of interest.

Usually better results are obtained when I_1 and I_4 are widely separated from I_p. Finally, I and I_i must be nonnegative to insure a real H_{FE}. Data points taken from the typical curve of a 2N5087 transistor as graphed in Figure 41 on page 190 were used in this simulation. The data points chosen are listed in the program in Appendix C. The resultant equation and its curve may also be found in Figure 41. Note that the equation fits the data to within 15%.

The results of the advanced simulation for a 1 KHz input signal and GBWP = 1 MHz are shown in Figures 44 and 45. In this simulation, as in all the advanced simulations of Darlington transistors presented in this work, all transistor capacitances are assumed to be 7 pF. Figure 44(a) and (b) depict the average error for R = 1 GΩ and 14.7 KΩ. Note that the average error changes polarity with input voltage for R = 1 GΩ. The positive error at low input voltages is due to charge storage in CBE1. When Q1P is turned off, CBE1 must discharge through the high resistances of the base of Q1 and the reverse-biased base-emitter junction of Q1. This behavior is illustrated by both computed waveforms (Figure 45) and experimental waveforms (Figure 46) of V_{BE1}. Test apparatus used to measure Darlington rectifier performance is illustrated in Figure 47. This charge storage effect also causes the peak rectifier error to change polarity twice as the input increases (Figure 44(c) and (d)) when R = 1 GΩ. Letting R = 14.7 KΩ provides a discharge path for CBE1. As shown in both computed and experimental waveforms (Figures 48 and 49), VBE1 goes to zero when Q1P is turned off; i.e., CBE1 is discharged. Note

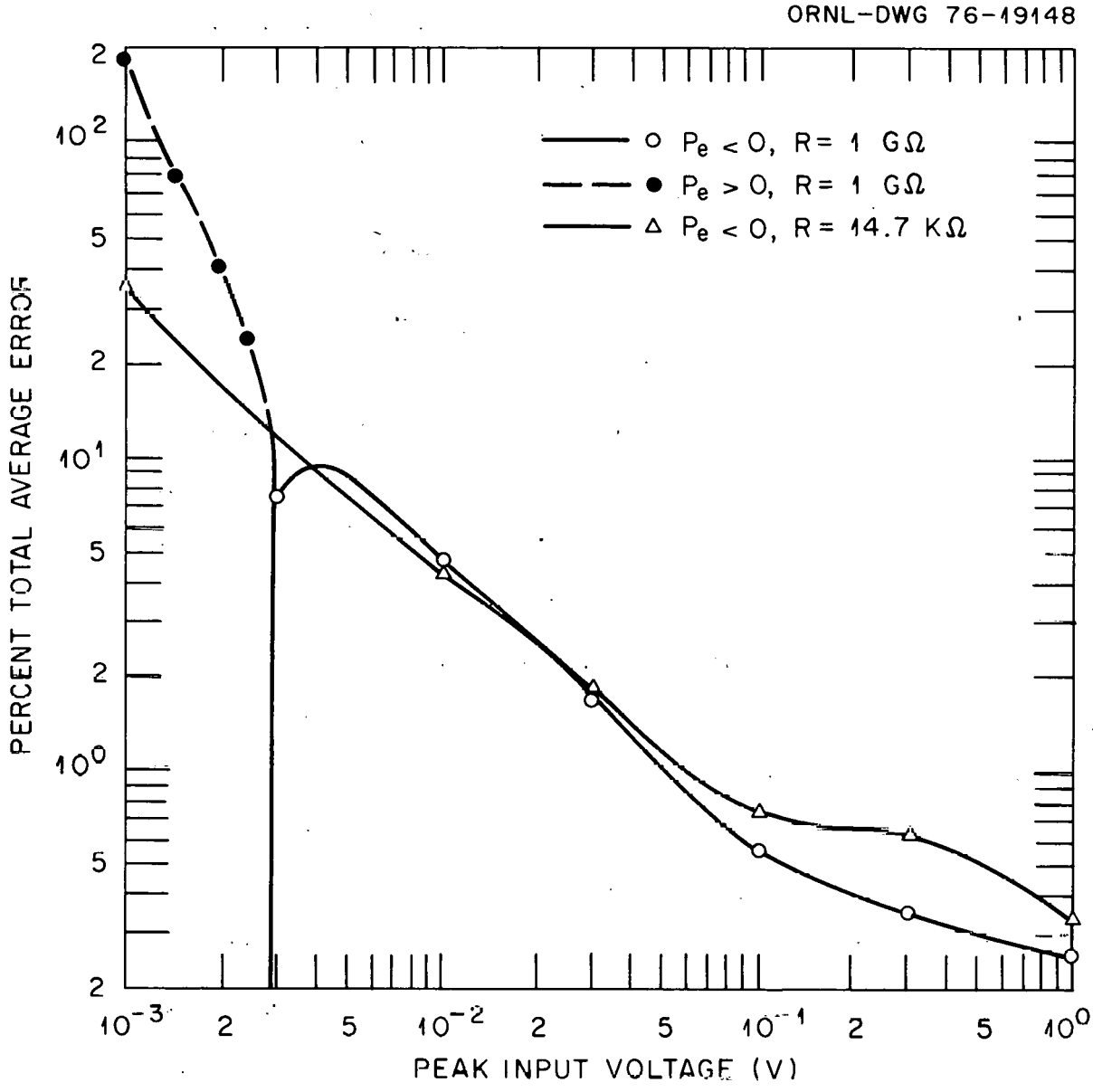

(a) Logarithmic plot of total theoretical average error.

Figure 44. The 1 KHz performance of Darlington 2N5087 transistor rectifier with $A_{o1} = 2 \times 10^5$, GBWP = 1 MHz, $R_1 = R_2 = 0\Omega$, and $R_3 = 2\ K\Omega$.

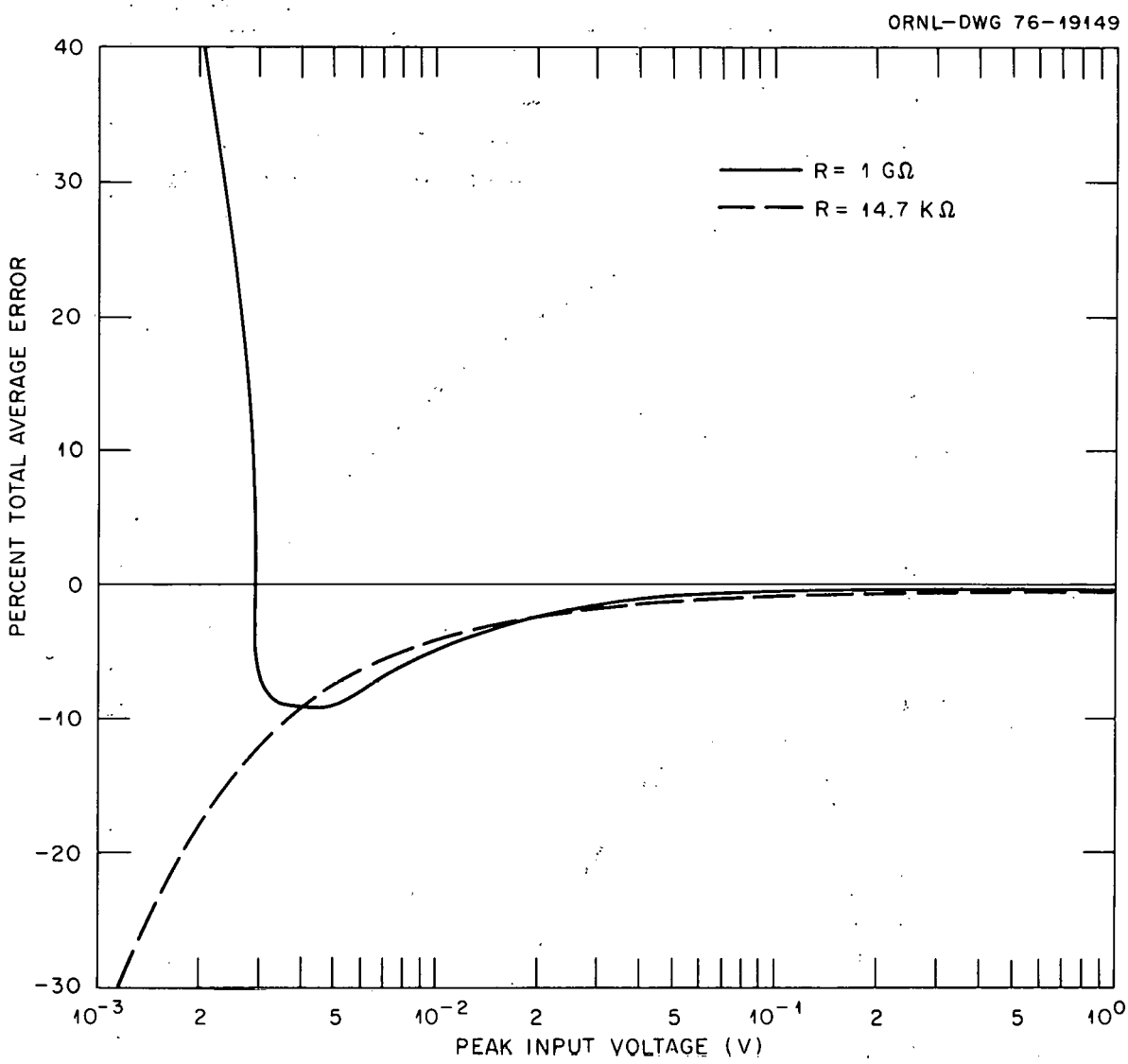

(b) Linear plot of total theoretical average error.

Figure 44 (continued)

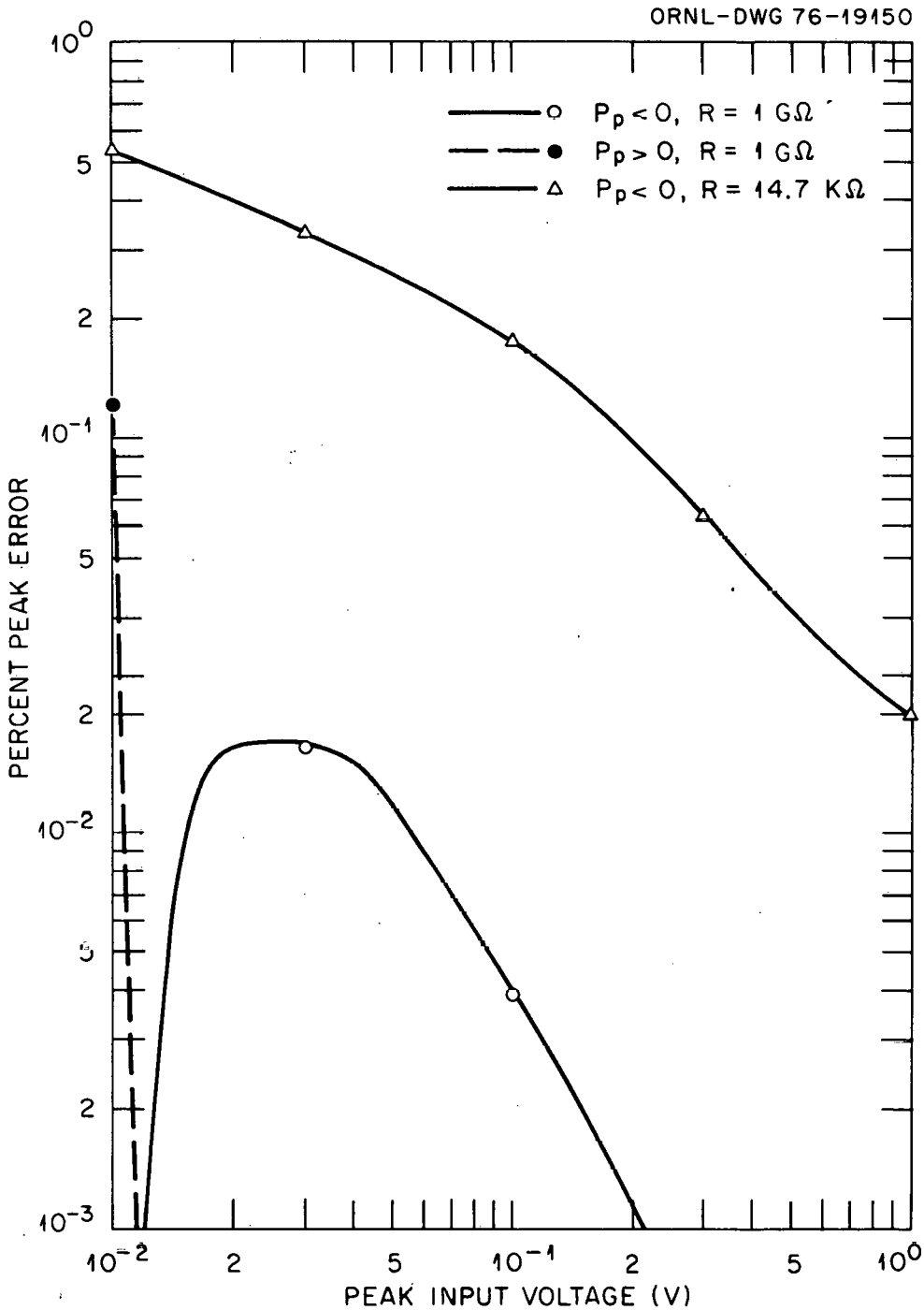

(c) Logarithmic plot of total theoretical peak error.

Figure 44 (continued)

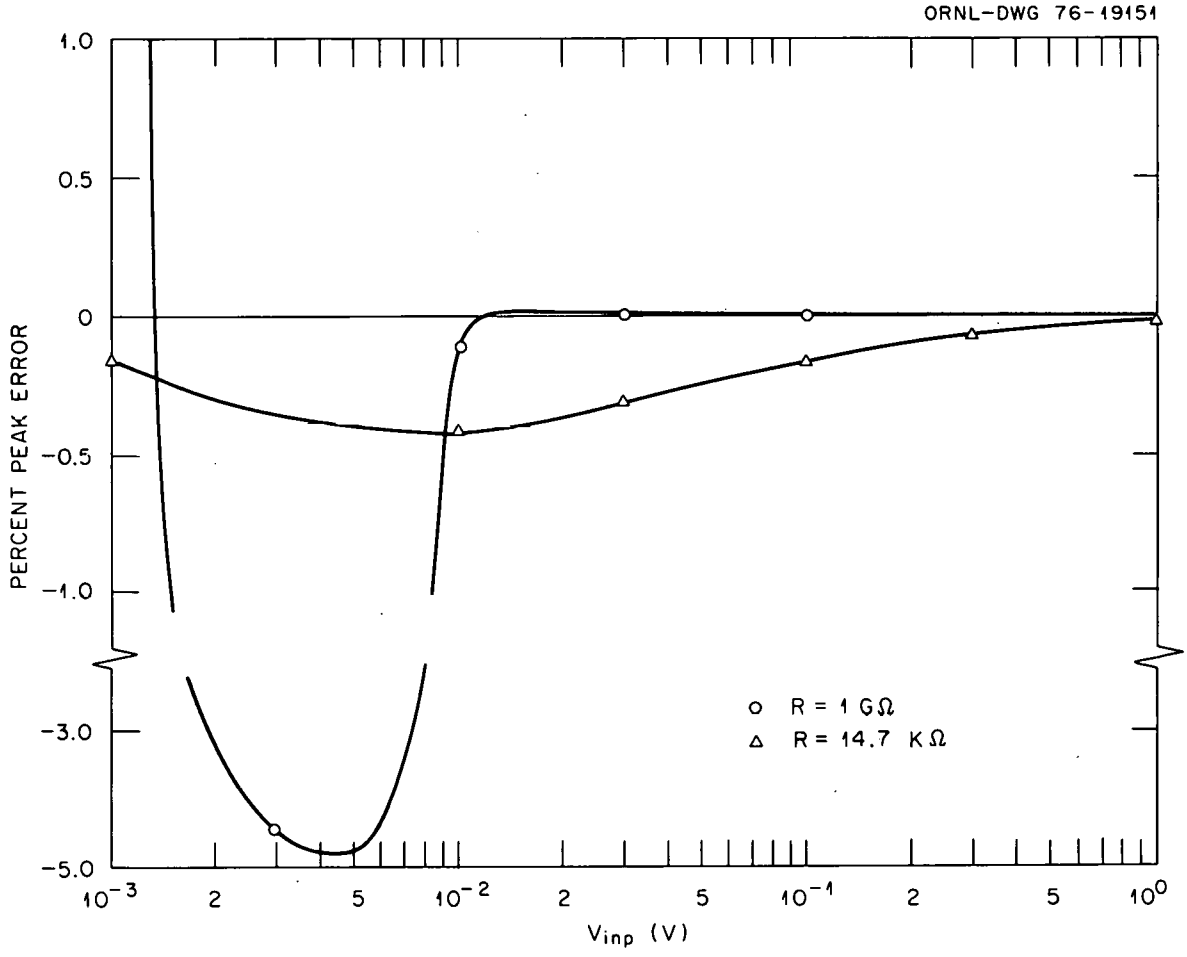

(d) Linear plot of total theoretical peak error.

Figure 44 (continued)

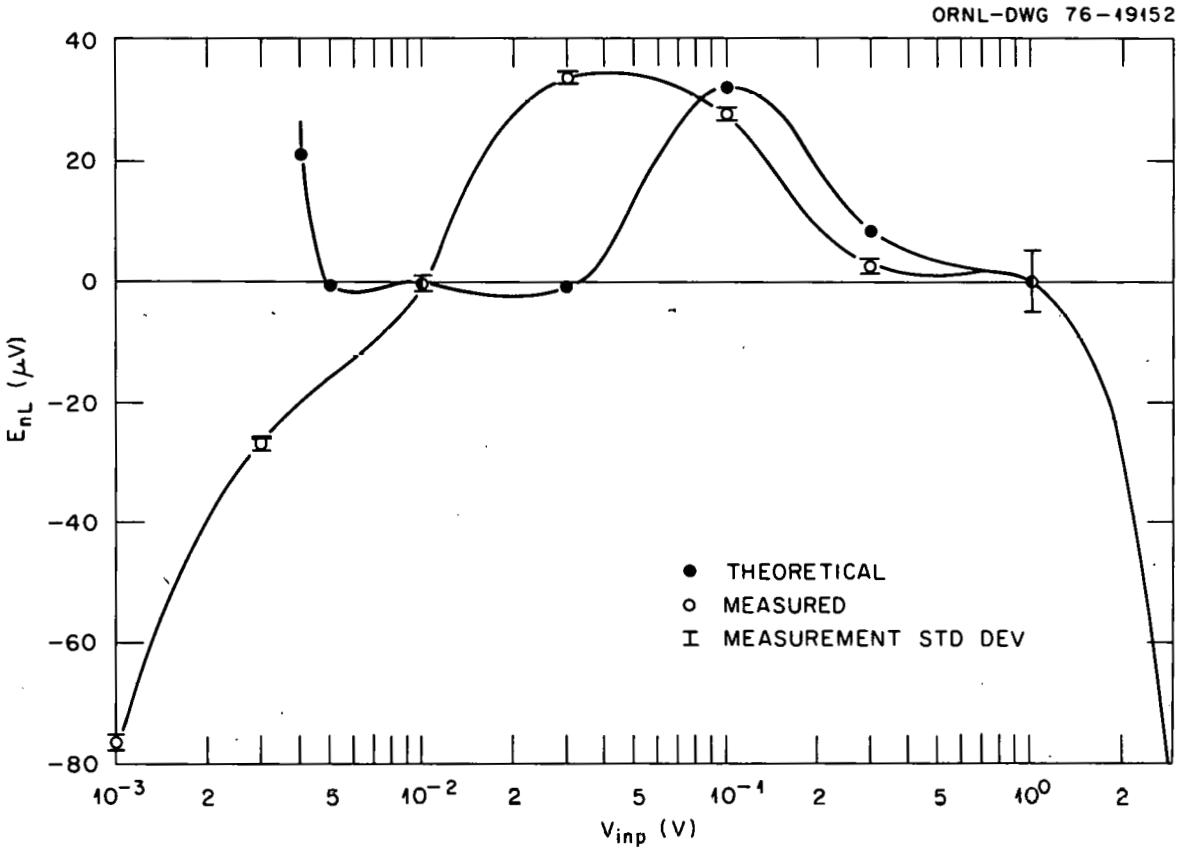

(e) Nonlinear error voltage with R = 1 GΩ.

Figure 44 (continued)

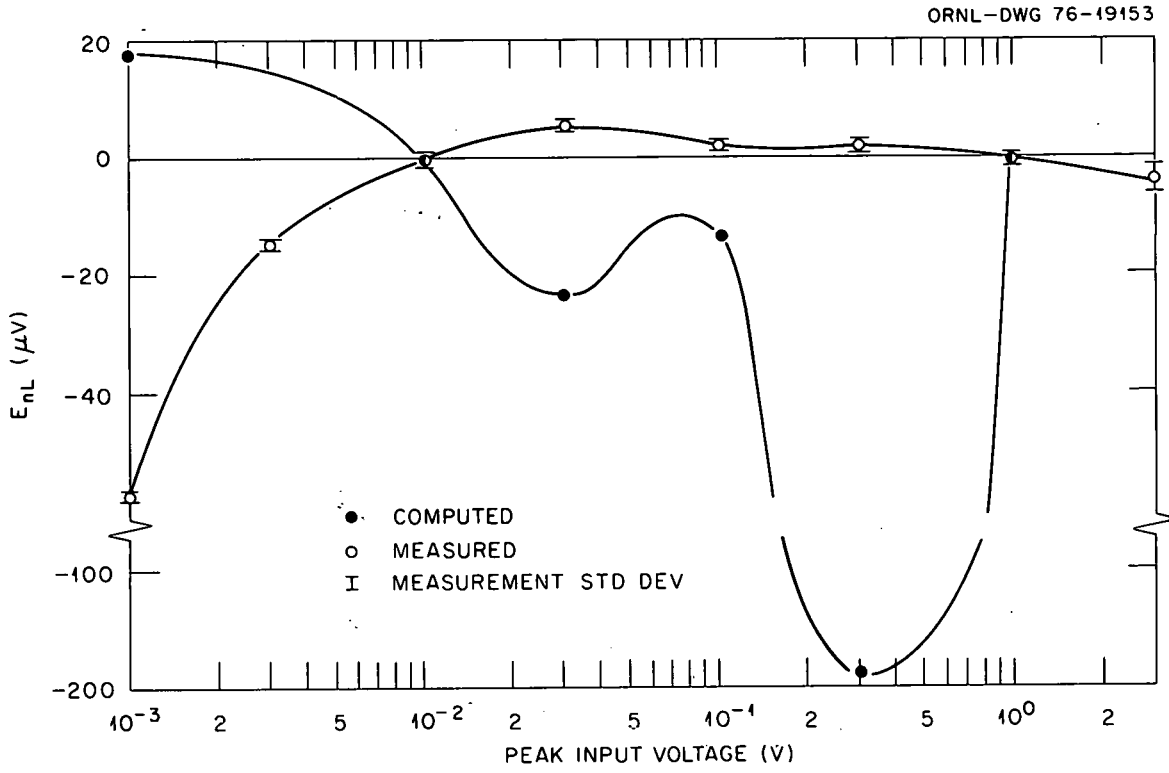

(f) Nonlinear error voltage with R = 14.7 KΩ.

Figure 44 (continued)

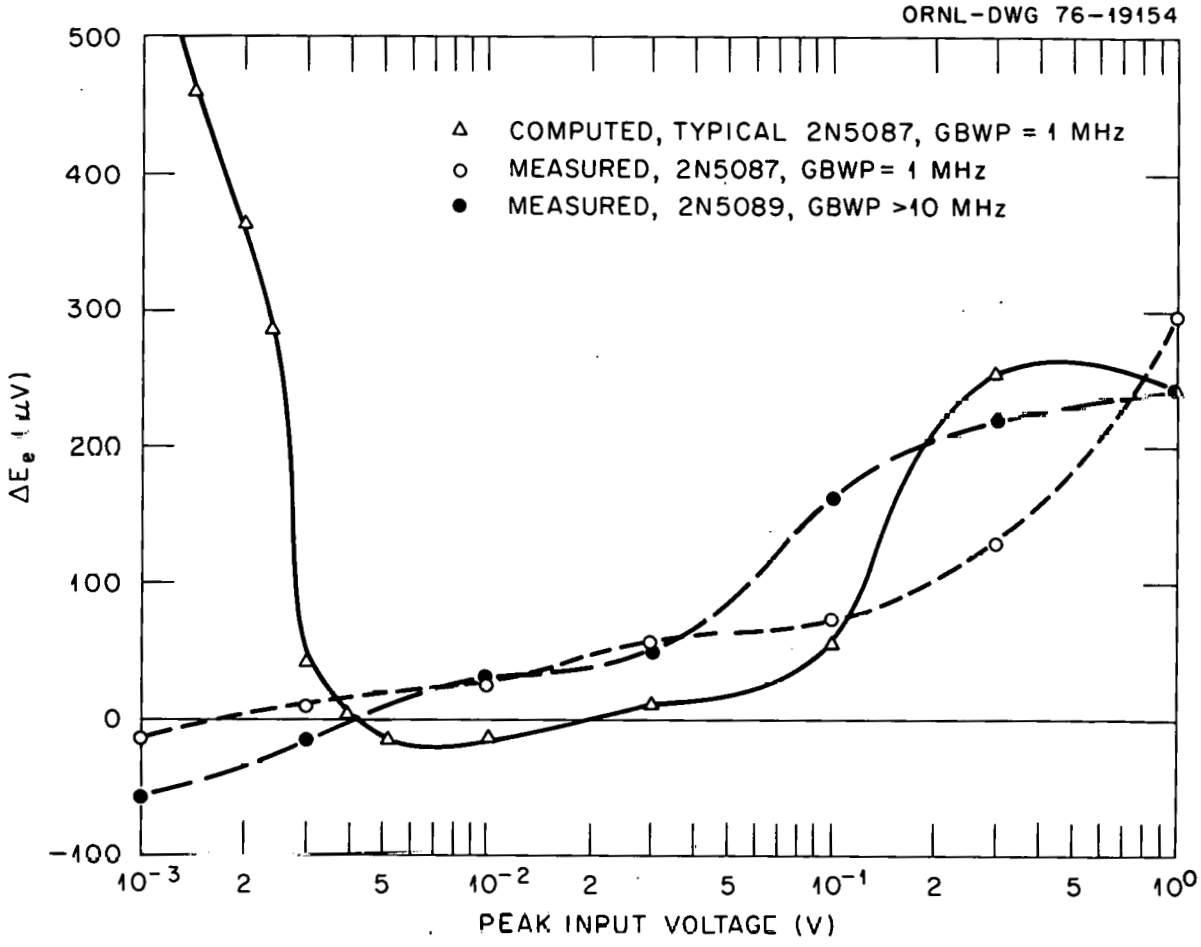

(g) The change in total average error voltage when R is increased from 14.7 KΩ to 1 GΩ.

Figure 44 (continued)

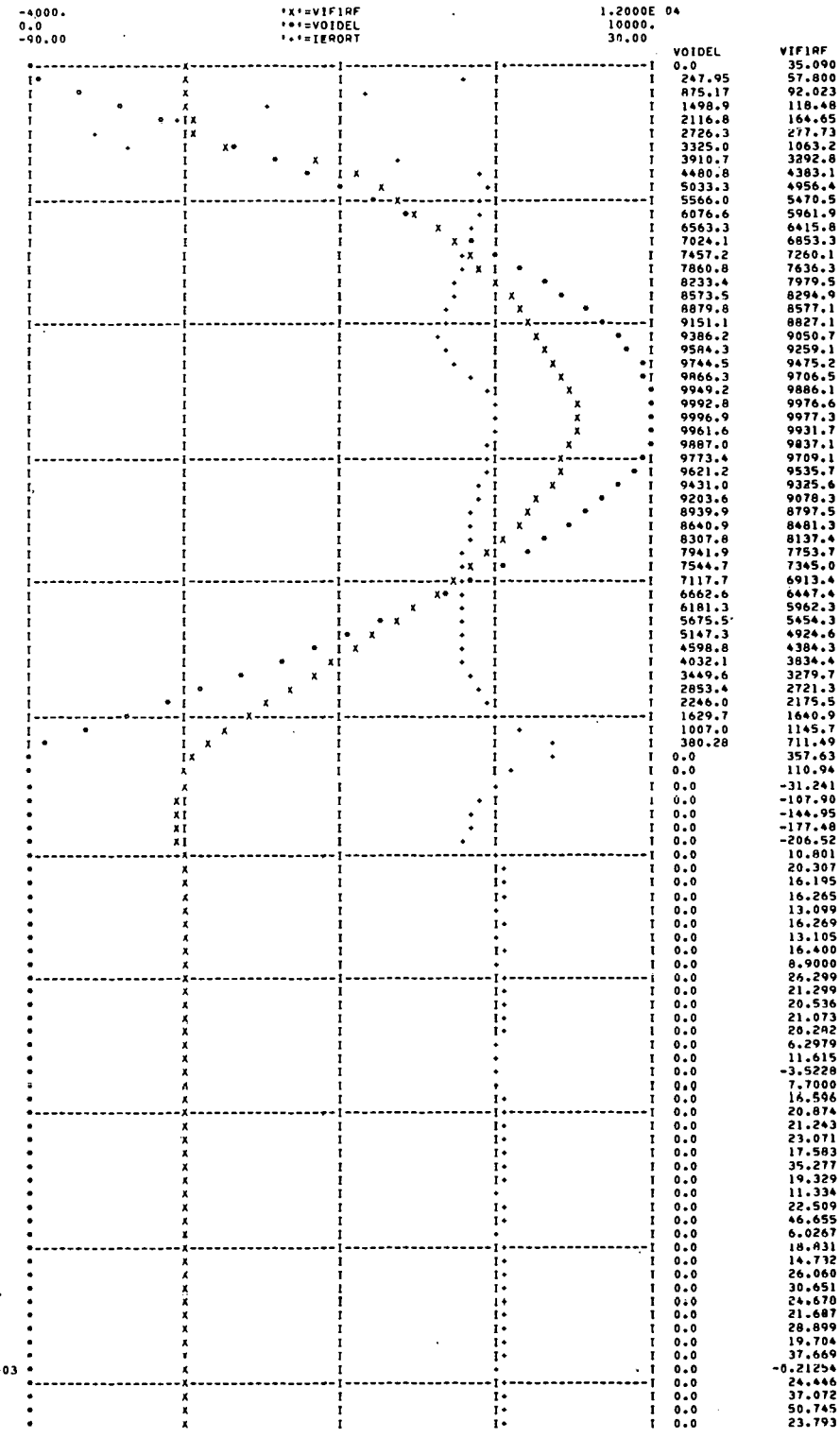

TIME	IERORT	VOIDEL	VIF1RF
0.0	1.1024	0.0	35.090
1.00000E-05	-5.9738	247.95	57.800
2.00000E-05	-24.603	875.17	92.023
3.00000E-05	-43.369	1498.9	118.48
4.00000E-05	-61.328	2116.8	164.65
5.00000E-05	-76.924	2726.3	277.73
6.00000E-05	-71.058	3325.0	1063.2
7.00000E-05	-19.410	3910.7	3292.8
8.00000E-05	-3.0702	4480.8	4383.1
9.00000E-05	-2.4158	5033.3	4956.4
1.00000E-04	-2.9986	5566.0	5470.5
1.10000E-04	-3.6056	6076.6	5961.9
1.20000E-04	-4.6352	6563.3	6415.8
1.30000E-04	-5.3657	7024.1	6853.3
1.40000E-04	-6.1923	7457.2	7260.1
1.50000E-04	-7.0519	7860.8	7636.3
1.60000E-04	-7.9768	8233.4	7979.5
1.70000E-04	-8.7536	8573.5	8294.9
1.80000E-04	-9.5097	8879.8	8577.1
1.90000E-04	-10.176	9151.1	8827.1
2.00000E-04	-10.541	9386.2	9050.7
2.10000E-04	-10.217	9584.3	9259.1
2.20000E-04	-8.4609	9744.5	9475.2
2.30000E-04	-5.0215	9866.3	9706.5
2.40000E-04	-1.9828	9949.2	9886.1
2.50000E-04	-0.50879	9992.8	9976.6
2.60000E-04	-0.61654	9996.9	9977.3
2.70000E-04	-0.94076	9961.6	9931.7
2.80000E-04	-1.5676	9887.0	9837.1
2.90000E-04	-2.0203	9773.4	9709.1
3.00000E-04	-2.6862	9621.2	9535.7
3.10000E-04	-3.3124	9431.0	9325.6
3.20000E-04	-3.9383	9203.6	9078.3
3.30000E-04	-4.4741	8939.9	8797.5
3.40000E-04	-5.0150	8640.9	8481.3
3.50000E-04	-5.3537	8307.8	8137.4
3.60000E-04	-5.9140	7941.9	7753.7
3.70000E-04	-6.2750	7544.7	7345.0
3.80000E-04	-6.4190	7117.7	6913.4
3.90000E-04	-6.7620	6662.6	6447.4
4.00000E-04	-6.8779	6181.3	5962.3
4.10000E-04	-6.9486	5675.5	5454.3
4.20000E-04	-6.9969	5147.3	4924.6
4.30000E-04	-6.7397	4598.8	4384.3
4.40000E-04	-6.2123	4032.1	3834.4
4.50000E-04	-5.3383	3449.6	3279.7
4.60000E-04	-4.1525	2853.4	2721.3
4.70000E-04	-2.2135	2246.0	2175.5
4.80000E-04	0.35295	1629.7	1640.9
4.90000E-04	4.3567	1007.0	1145.7
5.00000E-04	10.405	380.28	711.49
5.10000E-04	11.235	0.0	357.63
5.20000E-04	3.4853	0.0	110.94
5.30000E-04	-0.98145	0.0	-31.241
5.40000E-04	-3.3897	0.0	-107.90
5.50000E-04	-4.5536	0.0	-144.95
5.60000E-04	-5.5758	0.0	-177.48
5.70000E-04	-6.4881	0.0	-206.52
5.80000E-04	0.33931	0.0	10.801
5.90000E-04	0.63795	0.0	20.307
6.00000E-04	0.50877	0.0	16.195
6.10000E-04	0.51098	0.0	16.265
6.20000E-04	0.41151	0.0	13.099
6.30000E-04	0.51112	0.0	16.269
6.40000E-04	0.41171	0.0	13.105
6.50000E-04	0.51523	0.0	16.400
6.60000E-04	0.27968	0.0	8.9000
6.70000E-04	0.82620	0.0	26.299
6.80000E-04	0.66911	0.0	21.299
6.90000E-04	0.64517	0.0	20.536
7.00000E-04	0.66204	0.0	21.073
7.10000E-04	0.63718	0.0	20.282
7.20000E-04	0.19785	0.0	6.2979
7.30000E-04	0.36489	0.0	11.615
7.40000E-04	-0.11067	0.0	-3.5228
7.50000E-04	0.24140	0.0	7.7000
7.60000E-04	0.52137	0.0	16.596
7.70000E-04	0.65579	0.0	20.874
7.80000E-04	0.66736	0.0	21.243
7.90000E-04	0.72480	0.0	23.071
8.00000E-04	0.55238	0.0	17.583
8.10000E-04	1.1082	0.0	35.277
8.20000E-04	0.60723	0.0	19.329
8.30000E-04	0.35606	0.0	11.334
8.40000E-04	0.70715	0.0	22.509
8.50000E-04	1.4657	0.0	46.655
8.60000E-04	0.18933	0.0	6.0267
8.70000E-04	0.59160	0.0	18.831
8.80000E-04	0.46283	0.0	14.732
8.90000E-04	0.81870	0.0	26.060
9.00000E-04	0.96292	0.0	30.651
9.10000E-04	0.77527	0.0	24.670
9.20000E-04	0.68131	0.0	21.687
9.30000E-04	0.90789	0.0	28.899
9.40000E-04	0.61902	0.0	19.704
9.50000E-04	1.1034	0.0	37.669
9.60000E-04	-6.67713E-03	0.0	-0.21254
9.70000E-04	0.76799	0.0	24.446
9.80000E-04	1.1647	0.0	37.072
9.90000E-04	1.5942	0.0	50.745
1.00000E-03	0.74748	0.0	23.793

(a) VIF1RF, VOIDEL, and IERORT with V_{inp} = 10 mV.

Figure 45. Computed 1 KHz waveforms of a Darlington 2N5087 transistor rectifier with $R_1 = R_2 = 0\Omega$, $R_3 = 2\ K\Omega$, $R = 1\ G\Omega$, $A_{o1} = 2 \times 10^5$, and GBWP = 1 MHz. All voltages in μV unless specified otherwise.

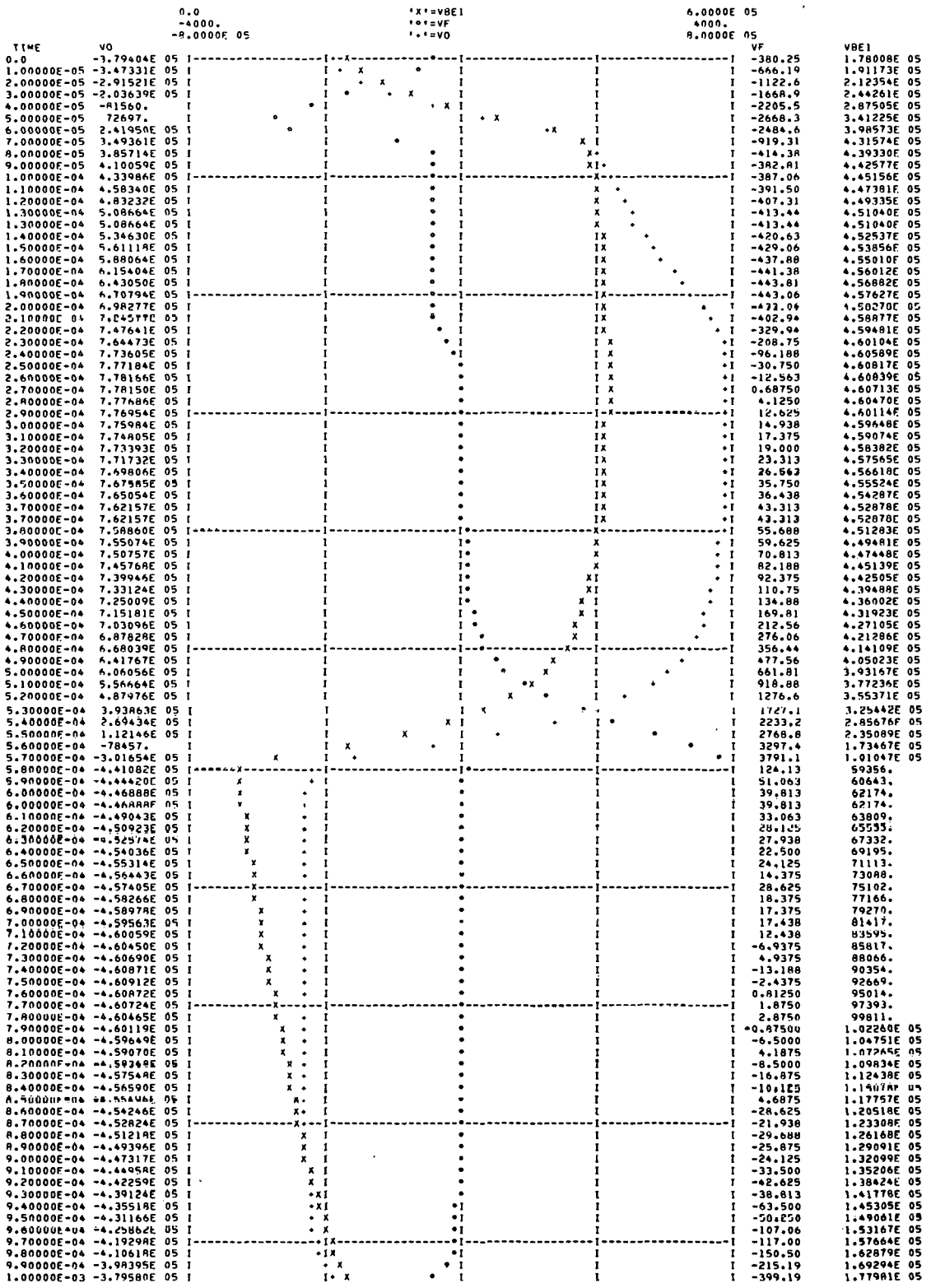

TIME	VO	VF	VBE1
0.0	-3.79404E 05	-380.25	1.78008E 05
1.00000E-05	-3.47331E 05	-666.19	1.91173E 05
2.00000E-05	-2.91521E 05	-1122.6	2.12354E 05
3.00000E-05	-2.03639E 05	-1668.9	2.44261E 05
4.00000E-05	-81560.	-2205.5	2.87505E 05
5.00000E-05	72697.	-2668.3	3.41225E 05
6.00000E-05	2.41950E 05	-2484.6	3.98573E 05
7.00000E-05	3.49361E 05	-919.31	4.31574E 05
8.00000E-05	3.85714E 05	-414.38	4.39330E 05
9.00000E-05	4.10059E 05	-382.81	4.42577E 05
1.00000E-04	4.33986E 05	-387.06	4.45156E 05
1.10000E-04	4.58340E 05	-391.50	4.47381E 05
1.20000E-04	4.83232E 05	-407.31	4.49335E 05
1.30000E-04	5.08664E 05	-413.44	4.51040E 05
1.30000E-04	5.08664E 05	-413.44	4.51040E 05
1.40000E-04	5.34630E 05	-420.63	4.52537E 05
1.50000E-04	5.61118E 05	-429.06	4.53856E 05
1.60000E-04	5.88064E 05	-437.88	4.55010E 05
1.70000E-04	6.15404E 05	-441.38	4.56012E 05
1.80000E-04	6.43050E 05	-443.81	4.56882E 05
1.90000E-04	6.70794E 05	-443.06	4.57627E 05
2.00000E-04	6.98277E 05	-421.04	4.50270E 05
2.10000E 04	7.24577E 05	-402.94	4.58877E 05
2.20000E-04	7.47641E 05	-329.94	4.59481E 05
2.30000E-04	7.64473E 05	-208.75	4.60104E 05
2.40000E-04	7.73605E 05	-96.188	4.60589E 05
2.50000E-04	7.77184E 05	-30.750	4.60817E 05
2.60000E-04	7.78166E 05	-12.563	4.60839E 05
2.70000E-04	7.78150E 05	0.68750	4.60713E 05
2.80000E-04	7.77686E 05	4.1250	4.60470E 05
2.90000E-04	7.76954E 05	12.625	4.60114E 05
3.00000E-04	7.75984E 05	14.938	4.59648E 05
3.10000E-04	7.74805E 05	17.375	4.59074E 05
3.20000E-04	7.73393E 05	19.000	4.58382E 05
3.30000E-04	7.71732E 05	23.313	4.57565E 05
3.40000E-04	7.69806E 05	26.563	4.56610E 05
3.50000E-04	7.67585E 05	35.750	4.55524E 05
3.60000E-04	7.65054E 05	36.438	4.54287E 05
3.70000E-04	7.62157E 05	43.313	4.52878E 05
3.70000E-04	7.62157E 05	43.313	4.52878E 05
3.80000E-04	7.58860E 05	55.688	4.51283E 05
3.90000E-04	7.55074E 05	59.625	4.49481E 05
4.00000E-04	7.50757E 05	70.813	4.47448E 05
4.10000E-04	7.45768E 05	82.188	4.45139E 05
4.20000E-04	7.39946E 05	92.375	4.42505E 05
4.30000E-04	7.33124E 05	110.75	4.39488E 05
4.40000E-04	7.25009E 05	134.88	4.36002E 05
4.50000E-04	7.15181E 05	169.81	4.31923E 05
4.60000E-04	7.03096E 05	212.56	4.27105E 05
4.70000E-04	6.87828E 05	276.06	4.21286E 05
4.80000E-04	6.68039E 05	356.44	4.14109E 05
4.90000E-04	6.41767E 05	477.56	4.05023E 05
5.00000E-04	6.06056E 05	661.81	3.93167E 05
5.10000E-04	5.56664E 05	918.88	3.77236E 05
5.20000E-04	4.87976E 05	1276.6	3.55371E 05
5.30000E-04	3.93863E 05	1727.1	3.25442E 05
5.40000E-04	2.69434E 05	2233.2	2.85676E 05
5.50000E-04	1.12146E 05	2768.8	2.35089E 05
5.60000E-04	-78457.	3297.4	1.73467E 05
5.70000E-04	-3.01654E 05	3791.1	1.01047E 05
5.80000E-04	-4.41082E 05	124.13	59356.
5.90000E-04	-4.44420E 05	51.063	60643.
6.00000E-04	-4.46888E 05	39.813	62174.
6.00000E-04	-4.46888E 05	39.813	62174.
6.10000E-04	-4.49043E 05	33.063	63809.
6.20000E-04	-4.50923E 05	28.125	65535.
6.30000E-04	-4.52574E 05	27.938	67332.
6.40000E-04	-4.54036E 05	22.500	69195.
6.50000E-04	-4.55314E 05	24.125	71113.
6.60000E-04	-4.56443E 05	14.375	73088.
6.70000E-04	-4.57405E 05	28.625	75102.
6.80000E-04	-4.58266E 05	18.375	77166.
6.90000E-04	-4.58978E 05	17.375	79270.
7.00000E-04	-4.59563E 05	17.438	81417.
7.10000E-04	-4.60059E 05	12.438	83595.
7.20000E-04	-4.60450E 05	-6.9375	85817.
7.30000E-04	-4.60690E 05	4.9375	88066.
7.40000E-04	-4.60871E 05	-13.188	90354.
7.50000E-04	-4.60912E 05	-2.4375	92669.
7.60000E-04	-4.60872E 05	0.81250	95014.
7.70000E-04	-4.60724E 05	1.8750	97393.
7.80000E-04	-4.60465E 05	2.8750	99811.
7.90000E-04	-4.60119E 05	-0.87500	1.02260E 05
8.00000E-04	-4.59649E 05	-6.5000	1.04751E 05
8.10000E-04	-4.59070E 05	4.1875	1.07265E 05
8.20000E-04	-4.58249E 05	-8.5000	1.09834E 05
8.30000E-04	-4.57549E 05	-16.875	1.12438E 05
8.40000E-04	-4.56590E 05	-10.125	1.15078E 05
8.50000E-04	-4.55496E 05	4.6875	1.17757E 05
8.60000E-04	-4.54246E 05	-28.625	1.20518E 05
8.70000E-04	-4.52824E 05	-21.938	1.23308E 05
8.80000E-04	-4.51218E 05	-29.688	1.26168E 05
8.90000E-04	-4.49396E 05	-25.875	1.29091E 05
9.00000E-04	-4.47317E 05	-24.125	1.32099E 05
9.10000E-04	-4.44958E 05	-33.500	1.35206E 05
9.20000E-04	-4.42259E 05	-42.625	1.38424E 05
9.30000E-04	-4.39124E 05	-38.813	1.41778E 05
9.40000E-04	-4.35518E 05	-63.500	1.45305E 05
9.50000E-04	-4.31166E 05	-50.250	1.49061E 05
9.60000E-04	-4.25862E 05	-107.06	1.53167E 05
9.70000E-04	-4.19298E 05	-117.00	1.57664E 05
9.80000E-04	-4.10618E 05	-150.50	1.62879E 05
9.90000E-04	-3.98395E 05	-215.19	1.69294E 05
1.00000E-03	-3.79580E 05	-399.19	1.77981E 05

(b) VO, VF, and VBE1 with V_{inp} = 10 mV.

Figure 45 (continued)

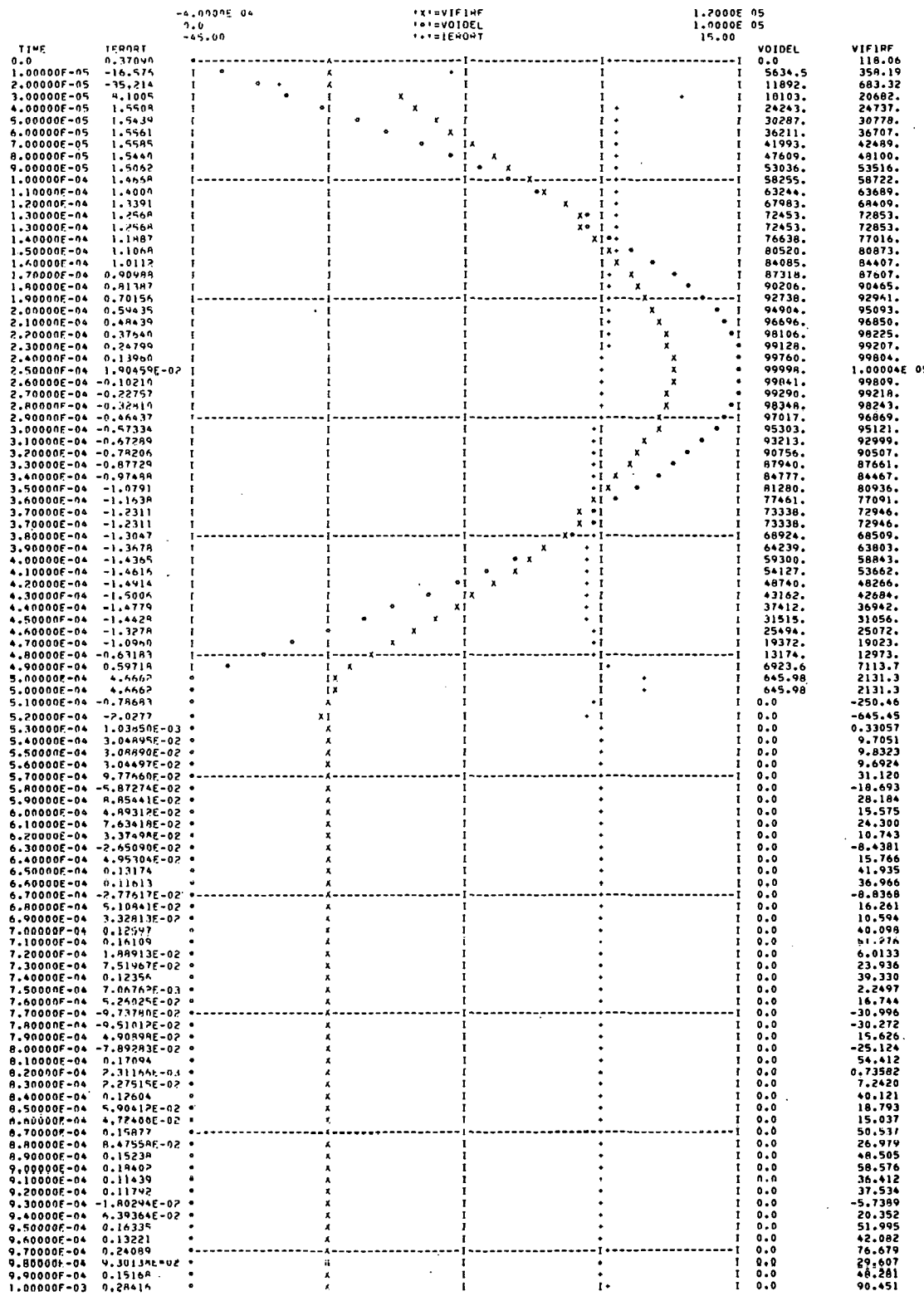

(c) VIF1RF, VOIDEL, and IERORT with V_{inp} = 0.1 V.

Figure 45 (continued)

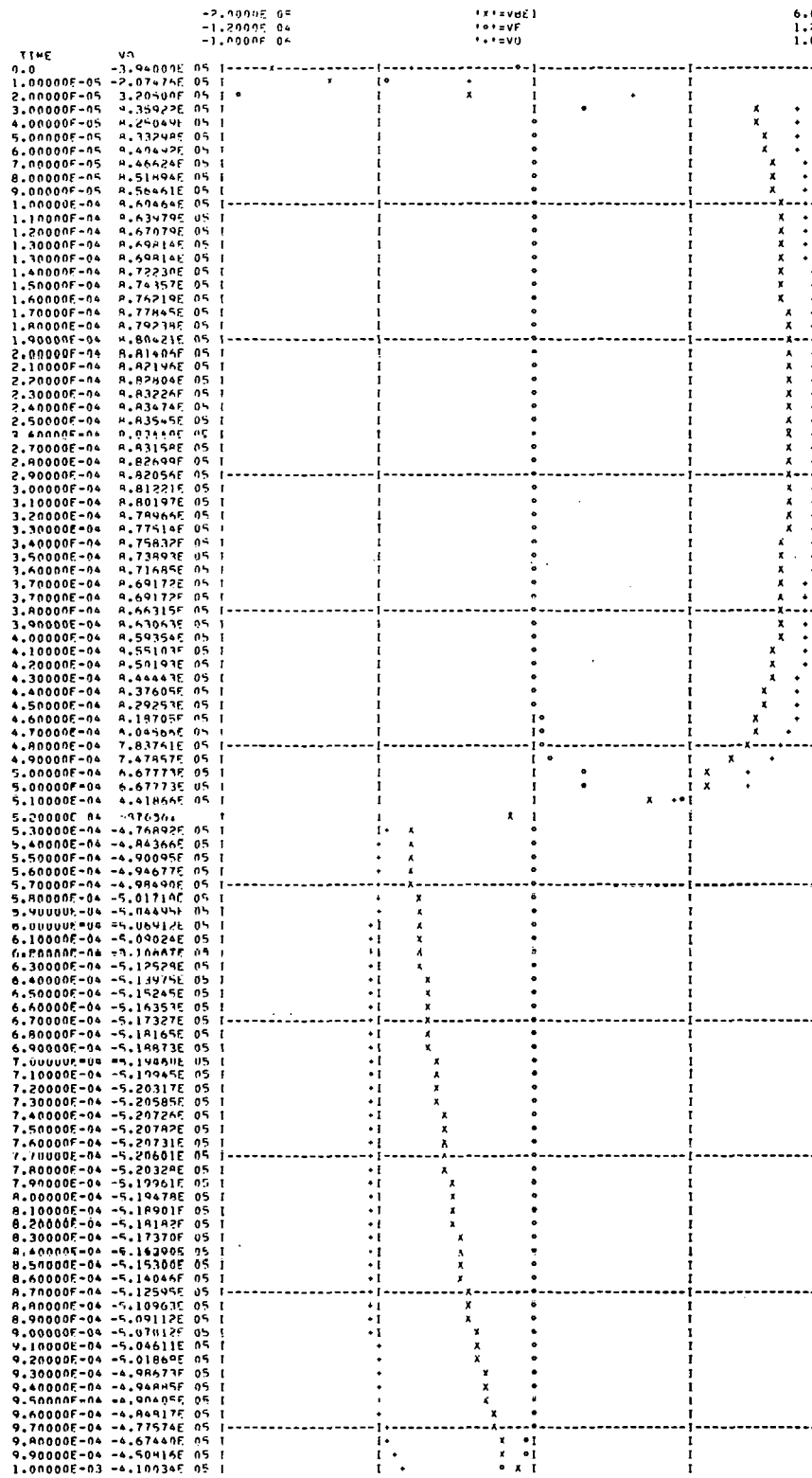

TIME	VO	VF	VBE1
0.0	-3.94000E 05	-645.69	-1.30903E 05
1.00000E-05	-2.07476E 05	-5595.0	-62998.
2.00000E-05	3.20500E 05	-11196.	1.19109E 05
3.00000E-05	4.35922E 05	1920.4	4.79836E 05
4.00000E-05	4.25049E 05	-138.56	4.84439E 05
5.00000E-05	4.33298E 05	-127.81	4.90127E 05
6.00000E-05	4.40442E 05	-110.31	4.94712E 05
7.00000E-05	4.46626E 05	-94.313	4.98518E 05
8.00000E-05	4.51494E 05	-80.875	5.01744E 05
9.00000E-05	4.56461E 05	-73.250	5.04520E 05
1.00000E-04	4.60466E 05	-62.813	5.06934E 05
1.10000E-04	4.63479E 05	-59.125	5.09050E 05
1.20000E-04	4.67079E 05	-52.125	5.10909E 05
1.30000E-04	4.69214E 05	-49.313	5.12548E 05
1.30000E-04	4.69214E 05	-49.313	5.12548E 05
1.40000E-04	4.72230E 05	-41.313	5.13990E 05
1.50000E-04	4.74357E 05	-34.875	5.15260E 05
1.60000E-04	4.76219E 05	-32.188	5.16372E 05
1.70000E-04	4.77845E 05	-29.875	5.17342E 05
1.80000E-04	4.79238E 05	-24.750	5.18175E 05
1.90000E-04	4.80421E 05	-23.063	5.18884E 05
2.00000E-04	4.81406E 05	-18.750	5.19473E 05
2.10000E-04	4.82196E 05	-15.063	5.19948E 05
2.20000E-04	4.82804E 05	-9.8750	5.20313E 05
2.30000E-04	4.83226E 05	-11.250	5.20576E 05
2.40000E-04	4.83474E 05	-5.0000	5.20729E 05
2.50000E-04	4.83545E 05	-3.0625	5.20782E 05
2.60000E-04	4.83440E 05	-1.1250	5.20731E 05
2.70000E-04	4.83158E 05	-0.81250	5.20579E 05
2.80000E-04	4.82699E 05	6.3125	5.20319E 05
2.90000E-04	4.82056E 05	3.3125	5.19958E 05
3.00000E-04	4.81221E 05	6.9375	5.19483E 05
3.10000E-04	4.80197E 05	13.875	5.18894E 05
3.20000E-04	4.78966E 05	17.063	5.18199E 05
3.30000E-04	4.77514E 05	21.938	5.17356E 05
3.40000E-04	4.75832E 05	25.313	5.16392E 05
3.50000E-04	4.73893E 05	26.438	5.15283E 05
3.60000E-04	4.71685E 05	30.875	5.14019E 05
3.70000E-04	4.69172E 05	39.063	5.12580E 05
3.70000E-04	4.69172E 05	39.063	5.12580E 05
3.80000E-04	4.66315E 05	43.688	5.10950E 05
3.90000E-04	4.63063E 05	51.188	5.09099E 05
4.00000E-04	4.59354E 05	55.000	5.06999E 05
4.10000E-04	4.55103E 05	67.438	5.04598E 05
4.20000E-04	4.50193E 05	79.375	5.01845E 05
4.30000E-04	4.44443E 05	92.750	4.98651E 05
4.40000E-04	4.37605E 05	115.88	4.94892E 05
4.50000E-04	4.29253E 05	139.38	4.90387E 05
4.60000E-04	4.18705E 05	185.44	4.84826E 05
4.70000E-04	4.04566E 05	263.75	4.77652E 05
4.80000E-04	7.83741E 05	409.69	4.67715E 05
4.90000E-04	7.47857E 05	782.44	4.52248E 05
5.00000E-04	6.67773E 05	2002.2	4.22104E 05
5.00000E-04	6.67773E 05	2002.2	4.22104E 05
5.10000E-04	4.41866E 05	5672.9	3.44609E 05
5.20000E-04	-97636.	11194.	1.66552E 05
5.30000E-04	-4.76892E 05	134.56	46509.
5.40000E-04	-4.84366E 05	112.13	46386.
5.50000E-04	-4.90095E 05	80.750	46851.
5.60000E-04	-4.94677E 05	70.250	47685.
5.70000E-04	-4.98490E 05	64.125	48771.
5.80000E-04	-5.01710E 05	50.563	50064.
5.90000E-04	-5.04495E 05	48.563	51486.
6.00000E-04	-5.06912E 05	38.563	53038.
6.10000E-04	-5.09024E 05	37.813	54686.
6.20000E-04	-5.10887E 05	30.125	56421.
6.30000E-04	-5.12529E 05	20.500	58232.
6.40000E-04	-5.13975E 05	23.313	60099.
6.50000E-04	-5.15245E 05	27.813	62019.
6.60000E-04	-5.16353E 05	29.500	63994.
6.70000E-04	-5.17327E 05	12.375	66024.
6.80000E-04	-5.18165E 05	14.813	68086.
6.90000E-04	-5.18873E 05	13.125	70194.
7.00000E-04	-5.19488E 05	20.125	72336.
7.10000E-04	-5.19945E 05	14.250	74520.
7.20000E-04	-5.20317E 05	-6.25000E-02	76748.
7.30000E-04	-5.20585E 05	-3.9375	78999.
7.40000E-04	-5.20726E 05	10.125	81280.
7.50000E-04	-5.20782E 05	-1.3750	83607.
7.60000E-04	-5.20731E 05	1.9375	85950.
7.70000E-04	-5.20601E 05	-27.688	88356.
7.80000E-04	-5.20329E 05	-16.813	90775.
7.90000E-04	-5.19961E 05	-4.9375	93224.
8.00000E-04	-5.19478E 05	-8.1250	95715.
8.10000E-04	-5.18901E 05	1.0000	98228.
8.20000E-04	-5.18182E 05	-2.3125	1.00797E 05
8.30000E-04	-5.17370E 05	-16.000	1.03404E 05
8.40000E-04	-5.16390E 05	3.0000	1.06044E 05
8.50000E-04	-5.15300E 05	-19.063	1.08747E 05
8.60000E-04	-5.14046E 05	-30.063	1.11496E 05
8.70000E-04	-5.12595E 05	-13.188	1.14289E 05
8.80000E-04	-5.10963E 05	-19.750	1.17157E 05
8.90000E-04	-5.09112E 05	-15.375	1.20092E 05
9.00000E-04	-5.07012E 05	-16.125	1.23112E 05
9.10000E-04	-5.04611E 05	-25.563	1.26237E 05
9.20000E-04	-5.01869E 05	-39.438	1.29475E 05
9.30000E-04	-4.98673E 05	-61.000	1.32870E 05
9.40000E-04	-4.94885E 05	-42.813	1.36432E 05
9.50000E-04	-4.90405E 05	-63.188	1.40250E 05
9.60000E-04	-4.84917E 05	-88.188	1.44437E 05
9.70000E-04	-4.77574E 05	-99.813	1.49165E 05
9.80000E-04	-4.67440E 05	-193.38	1.54909E 05
9.90000E-04	-4.50416E 05	-354.25	1.62856E 05
1.00000E-03	-4.10034E 05	-1198.9	1.79306E 05

(d) VO, VF, and VBE1 with V_{inp} = 0.1 V.

Figure 45 (continued)

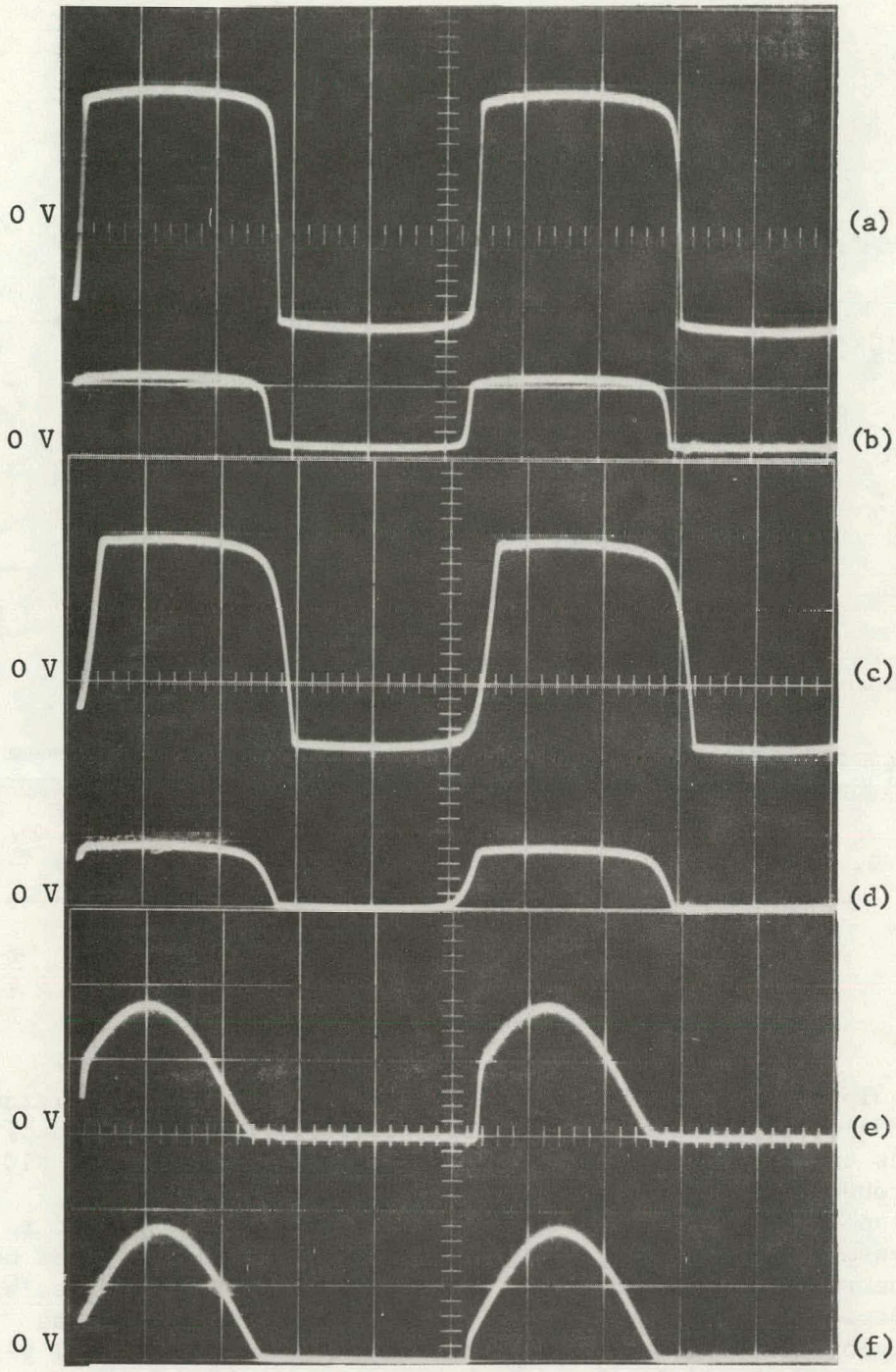

Figure 46. Experimental 1 KHz waveforms of a Darlington 2N5087 transistor rectifier with R_1 and R_2 = 0Ω, R_3 = 2 KΩ, C_3 = 0.15 μF, no R, and an AD506LH opamp. (a) $\overline{V_f} - V_o$ with V_{inp} = 0.1 V; (b) $\overline{V_f} - V_{BE1}$ with V_{inp} = 0.1 V; (c) $\overline{V_f} - V_o$ with V_{inp} = 10 mV; (d) $\overline{V_f} - V_{BE1}$ with V_{inp} = 10 mV; (e) V_{IF1RF} with V_{inp} = 10 mV; (f) V_{IF1RF} with V_{inp} = 0.1 V. Horizontal scale: 0.2 mε/div. Vertical scale: 0.5 V/div [curves (a), (b), (c), and (d)]; 0.05 V/div [curve (f)]; 0.005 V/div [curve (e)].

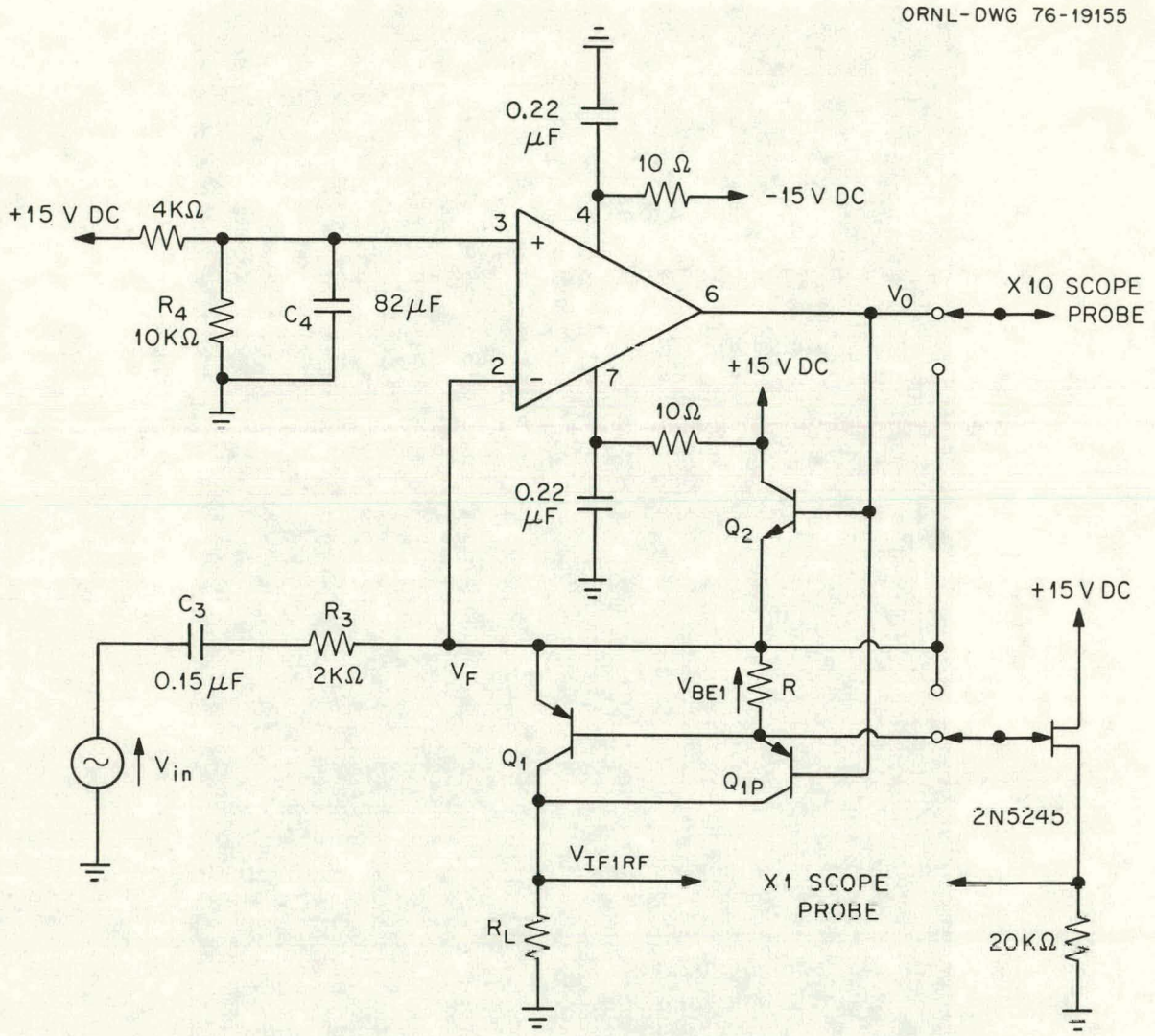

(a) Equipment used to make oscilloscope photographs. A Tektronix 535A oscilloscope with a 54/53C plug-in, dual-channel amplifier was employed for oscilloscope photographs. The X1 and X10 probes present loads of 1 MΩ - 50 pF and 10 MΩ - 7 pF respectively. The FET common drain buffer was utilized to measure VBE1 without loading the circuit and is not part of the rectifier circuit. R_3, R_4, and R_5 are wirewound resistors (Daven type 1350), while R is metal film. R_L = 2 KΩ was employed except where V_{inp} = 10 mV, R_L = 20 KΩ was employed to overcome the limitation of the oscilloscope's low sensitivity. Although the circuit was constructed on a double sided PC board, waveforms are unchanged when the circuit is breadboarded on a Continental Specialties Proto Board®.

Figure 47. Test apparatus used to measure the performance of a Darlington transistor rectifier.

ORNL-DWG 76-19156

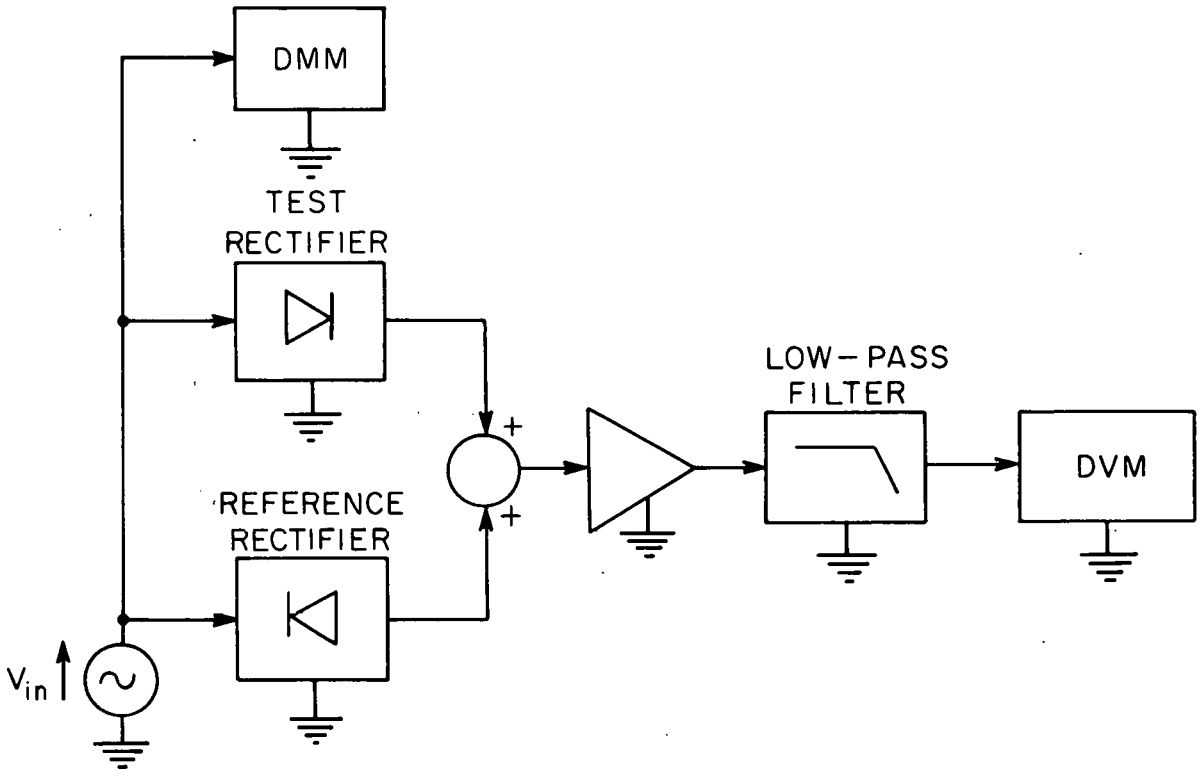

(b) Equipment employed to measure rectifier accuracy. The reference rectifier is a Darlington 2N5089 transistor rectifier with an AD528JH opamp, while the test rectifier is a Darlington 2N5087 transistor rectifier with an AD506LH opamp. No R is used with the reference rectifier. A Kiethley digital voltmeter (model 180) was used to measure the error voltage, while a Hewlett-Packard digital multimeter (model 3490A) monitored the input voltage. In order to reduce errors due to noise, twenty consecutive readings were taken with the Kiethley DVM set for longest integration period (∿5 sec). These twenty data points were then averaged using the HP45 calculator's averaging program.

Figure 47 (continued)

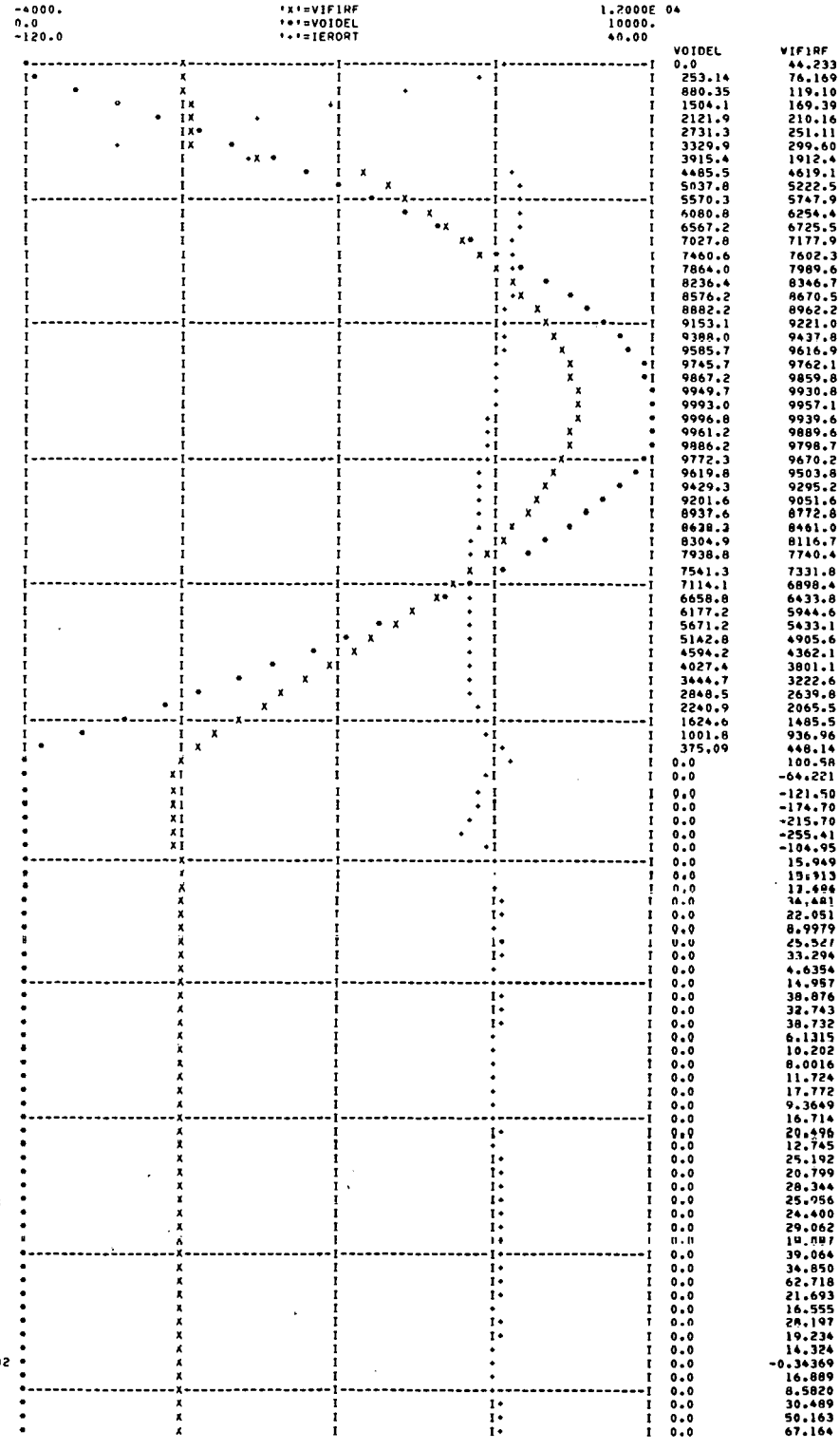

TIME	IEROUT	VOIDEL	VIFIRF
0.0	1.3896	0.0	44.233
1.00000E-05	-5.5598	253.14	76.169
2.00000E-05	-23.915	880.35	119.10
3.00000E-05	-41.930	1504.1	169.39
4.00000E-05	-60.058	2121.9	210.16
5.00000E-05	-77.917	2731.3	251.11
6.00000E-05	-95.201	3329.9	299.60
7.00000E-05	-62.926	3915.4	1912.4
8.00000E-05	4.1975	4485.5	4619.1
9.00000E-05	5.8026	5037.8	5222.5
1.00000E-04	5.5803	5570.3	5747.9
1.10000E-04	5.4540	6080.8	6254.4
1.20000E-04	4.9728	6567.2	6725.5
1.30000E-04	4.7137	7027.8	7177.9
1.40000E-04	4.4511	7460.6	7602.3
1.50000E-04	3.9443	7864.0	7989.6
1.60000E-04	3.4674	8236.4	8346.7
1.70000E-04	2.9624	8576.2	8670.5
1.80000E-04	2.5129	8882.2	8962.2
1.90000E-04	2.1320	9153.1	9221.0
2.00000E-04	1.5656	9388.0	9437.8
2.10000E-04	0.97770	9585.7	9616.9
2.20000E-04	0.51615	9745.7	9762.1
2.30000E-04	-0.23059	9867.2	9859.8
2.40000E-04	-0.59469	9949.7	9930.8
2.50000E-04	-1.1278	9993.0	9957.1
2.60000E-04	-1.7966	9996.8	9939.6
2.70000E-04	-2.2481	9961.2	9889.6
2.80000E-04	-2.7511	9886.2	9798.7
2.90000E-04	-3.2087	9772.3	9670.2
3.00000E-04	-3.6430	9619.8	9503.8
3.10000E-04	-4.2128	9429.3	9295.2
3.20000E-04	-4.7125	9201.6	9051.6
3.30000E-04	-5.1777	8937.6	8772.8
3.40000E-04	-5.5708	8638.3	8461.0
3.50000E-04	-5.9152	8304.9	8116.7
3.60000E-04	-6.2339	7938.8	7740.4
3.70000E-04	-6.5831	7541.3	7331.8
3.80000E-04	-6.7765	7114.1	6898.4
3.90000E-04	-7.0683	6658.8	6433.8
4.00000E-04	-7.3058	6177.2	5944.6
4.10000E-04	-7.4801	5671.2	5433.1
4.20000E-04	-7.4543	5142.8	4905.6
4.30000E-04	-7.2908	4594.2	4362.1
4.40000E-04	-7.1107	4027.4	3801.1
4.50000E-04	-6.9785	3444.7	3222.6
4.60000E-04	-6.5561	2848.5	2639.8
4.70000E-04	-5.5128	2240.9	2065.5
4.80000E-04	-4.3696	1624.6	1485.5
4.90000E-04	-2.0375	1001.8	936.96
5.00000E-04	2.2949	375.09	448.14
5.10000E-04	3.1600	0.0	100.58
5.20000E-04	-2.0176	0.0	-64.221
5.30000E-04	-3.8169	0.0	-121.50
5.40000E-04	-5.4884	0.0	-174.70
5.50000E-04	-6.7763	0.0	-215.70
5.60000E-04	-8.0240	0.0	-255.41
5.70000E-04	-3.2970	0.0	-104.95
5.80000E-04	0.50105	0.0	15.949
5.90000E-04	0.49991	0.0	15.913
6.00000E-04	0.42998	0.0	13.694
6.10000E-04	1.0832	0.0	34.481
6.20000E-04	0.69274	0.0	22.051
6.30000E-04	0.28268	0.0	8.9979
6.40000E-04	0.80197	0.0	25.527
6.50000E-04	1.0459	0.0	33.294
6.60000E-04	0.14563	0.0	4.6354
6.70000E-04	0.46988	0.0	14.957
6.80000E-04	1.2213	0.0	38.876
6.90000E-04	1.0287	0.0	32.743
7.00000E-04	1.2168	0.0	38.732
7.10000E-04	0.19263	0.0	6.1315
7.20000E-04	0.32049	0.0	10.202
7.30000E-04	0.25138	0.0	8.0016
7.40000E-04	0.36831	0.0	11.724
7.50000E-04	0.55834	0.0	17.772
7.60000E-04	0.29421	0.0	9.3649
7.70000E-04	0.52509	0.0	16.714
7.80000E-04	0.64390	0.0	20.496
7.90000E-04	0.40039	0.0	12.745
8.00000E-04	0.79144	0.0	25.192
8.10000E-04	0.65341	0.0	20.799
8.20000E-04	0.89044	0.0	28.344
8.30000E-04	0.81544	0.0	25.956
8.40000E-04	0.76654	0.0	24.400
8.50000E-04	0.91302	0.0	29.062
8.60000E-04	0.59904	0.0	19.067
8.70000E-04	1.2272	0.0	39.064
8.80000E-04	1.0948	0.0	34.850
8.90000E-04	1.9703	0.0	62.718
9.00000E-04	0.68149	0.0	21.693
9.10000E-04	0.52010	0.0	16.555
9.20000E-04	0.88584	0.0	28.197
9.30000E-04	0.60424	0.0	19.234
9.40000E-04	0.44999	0.0	14.324
9.50000E-04	-1.07973E-02	0.0	-0.34369
9.60000E-04	0.53060	0.0	16.889
9.70000E-04	0.26961	0.0	8.5820
9.80000E-04	0.95784	0.0	30.489
9.90000E-04	1.5759	0.0	50.163
1.00000E-03	2.1100	0.0	67.164

(a) VIFIRF, VOIDEL, and IEROUT with V_{inp} = 10 mV.

Figure 48. Computed 1 KHz waveforms of a Darlington 2N5087 transistor rectifier with $R_1 = R_2 = 0\Omega$, $R_3 = 2\ K\Omega$, $R = 14.7\ K\Omega$, $A_{o1} = 2 \times 10^5$, and GBWP = 1 MHz. All voltages in μV unless specified otherwise.

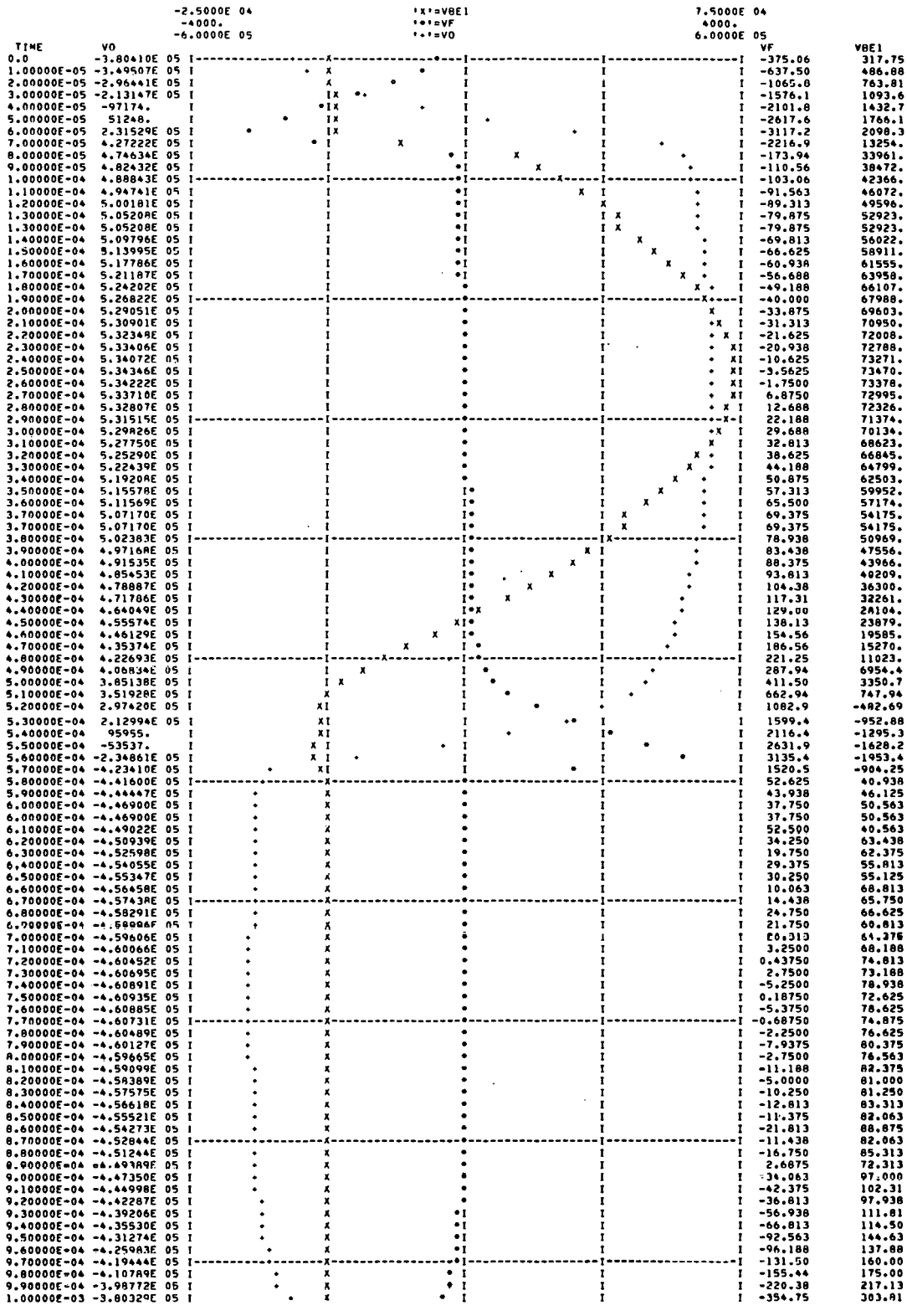

TIME	VO	VF	VBE1
0.0	-3.80410E 05	-375.06	317.75
1.00000E-05	-3.49507E 05	-637.50	486.88
2.00000E-05	-2.96441E 05	-1065.8	763.81
3.00000E-05	-2.13147E 05	-1576.1	1093.6
4.00000E-05	-97174.	-2101.8	1432.7
5.00000E-05	51248.	-2617.6	1766.1
6.00000E-05	2.31529E 05	-3117.2	2098.3
7.00000E-05	4.27222E 05	-2216.9	13254.
8.00000E-05	4.74634E 05	-173.94	33961.
9.00000E-05	4.82432E 05	-110.56	38472.
1.00000E-04	4.88843E 05	-103.06	42366.
1.10000E-04	4.94741E 05	-91.563	46072.
1.20000E-04	5.00181E 05	-89.313	49596.
1.30000E-04	5.05208E 05	-79.875	52923.
1.30000E-04	5.05208E 05	-79.875	52923.
1.40000E-04	5.09796E 05	-69.813	56022.
1.50000E-04	5.13995E 05	-66.625	58911.
1.60000E-04	5.17786E 05	-60.938	61555.
1.70000E-04	5.21187E 05	-56.688	63958.
1.80000E-04	5.24202E 05	-49.188	66107.
1.90000E-04	5.26822E 05	-40.000	67988.
2.00000E-04	5.29051E 05	-33.875	69603.
2.10000E-04	5.30901E 05	-31.313	70950.
2.20000E-04	5.32348E 05	-21.625	72008.
2.30000E-04	5.33406E 05	-20.938	72788.
2.40000E-04	5.34072E 05	-10.625	73271.
2.50000E-04	5.34346E 05	-3.5625	73470.
2.60000E-04	5.34222E 05	-1.7500	73378.
2.70000E-04	5.33710E 05	6.8750	72995.
2.80000E-04	5.32807E 05	12.688	72326.
2.90000E-04	5.31515E 05	22.188	71374.
3.00000E-04	5.29826E 05	29.688	70134.
3.10000E-04	5.27750E 05	32.813	68623.
3.20000E-04	5.25290E 05	38.625	66845.
3.30000E-04	5.22439E 05	44.188	64799.
3.40000E-04	5.19209E 05	50.875	62503.
3.50000E-04	5.15578E 05	57.313	59952.
3.60000E-04	5.11569E 05	65.500	57174.
3.70000E-04	5.07170E 05	69.375	54175.
3.70000E-04	5.07170E 05	69.375	54175.
3.80000E-04	5.02383E 05	78.938	50969.
3.90000E-04	4.97168E 05	83.438	47556.
4.00000E-04	4.91535E 05	88.375	43966.
4.10000E-04	4.85453E 05	93.813	40209.
4.20000E-04	4.78887E 05	104.38	36300.
4.30000E-04	4.71786E 05	117.31	32261.
4.40000E-04	4.64049E 05	129.00	28104.
4.50000E-04	4.55574E 05	138.13	23879.
4.60000E-04	4.46129E 05	154.56	19585.
4.70000E-04	4.35374E 05	186.56	15270.
4.80000E-04	4.22693E 05	221.25	11023.
4.90000E-04	4.08834E 05	287.94	6954.4
5.00000E-04	3.85138E 05	411.50	3350.7
5.10000E-04	3.51928E 05	662.94	747.94
5.20000E-04	2.97420E 05	1082.9	-482.69
5.30000E-04	2.12994E 05	1599.4	-952.88
5.40000E-04	95955.	2116.4	-1295.3
5.50000E-04	-53537.	2631.9	-1628.2
5.60000E-04	-2.34861E 05	3135.4	-1953.4
5.70000E-04	-4.23410E 05	1520.5	-904.25
5.80000E-04	-4.41600E 05	52.625	40.938
5.90000E-04	-4.44447E 05	43.938	46.125
6.00000E-04	-4.46900E 05	37.750	50.563
6.00000E-04	-4.46900E 05	37.750	50.563
6.10000E-04	-4.49022E 05	52.500	40.563
6.20000E-04	-4.50939E 05	34.250	63.438
6.30000E-04	-4.52598E 05	19.750	62.375
6.40000E-04	-4.54055E 05	29.375	55.813
6.50000E-04	-4.55347E 05	30.250	55.125
6.60000E-04	-4.56458E 05	10.063	68.813
6.70000E-04	-4.57438E 05	14.438	65.750
6.80000E-04	-4.58291E 05	24.750	66.625
6.90000E-04	-4.58998E 05	21.750	60.813
7.00000E-04	-4.59606E 05	60.313	64.375
7.10000E-04	-4.60066E 05	3.2500	68.188
7.20000E-04	-4.60452E 05	0.43750	74.813
7.30000E-04	-4.60695E 05	2.7500	73.188
7.40000E-04	-4.60891E 05	-5.2500	78.938
7.50000E-04	-4.60935E 05	0.18750	72.625
7.60000E-04	-4.60885E 05	-5.3750	78.625
7.70000E-04	-4.60731E 05	-0.68750	74.875
7.80000E-04	-4.60489E 05	-2.2500	76.625
7.90000E-04	-4.60127E 05	-7.9375	80.375
8.00000E-04	-4.59665E 05	-2.7500	76.563
8.10000E-04	-4.59099E 05	-11.188	82.375
8.20000E-04	-4.58389E 05	-5.0000	81.000
8.30000E-04	-4.57575E 05	-10.250	81.250
8.40000E-04	-4.56618E 05	-12.813	83.313
8.50000E-04	-4.55521E 05	-11.375	82.063
8.60000E-04	-4.54273E 05	-21.813	88.875
8.70000E-04	-4.52844E 05	-11.438	82.063
8.80000E-04	-4.51244E 05	-16.750	85.313
8.90000E-04	-4.49389E 05	2.6875	72.313
9.00000E-04	-4.47350E 05	-34.063	97.000
9.10000E-04	-4.44998E 05	-42.375	102.31
9.20000E-04	-4.42287E 05	-36.813	97.938
9.30000E-04	-4.39206E 05	-56.938	111.81
9.40000E-04	-4.35530E 05	-66.813	114.50
9.50000E-04	-4.31274E 05	-92.563	144.63
9.60000E-04	-4.25983E 05	-96.188	137.88
9.70000E-04	-4.19444E 05	-131.50	160.00
9.80000E-04	-4.10789E 05	-155.44	175.00
9.90000E-04	-3.98772E 05	-220.38	217.13
1.00000E-03	-3.80329E 05	-354.75	303.81

(b) VO, VF, and VBE1 with V_{inp} = 10 mV.

Figure 48 (continued)

TIME	IERORT	VOIDEL	VIF1RF
0.0	6.41360E-02	0.0	20.415
1.00000E-05	-14.365	5072.5	500.06
2.00000E-05	-32.542	11333.	974.89
3.00000E-05	0.19180	17550.	17611.
4.00000E-05	0.80393	23697.	23953.
5.00000E-05	0.81955	29750.	30011.
6.00000E-05	0.79249	35686.	35938.
7.00000E-05	0.77464	41481.	41728.
8.00000E-05	0.76276	47113.	47356.
9.00000E-05	0.86514	52558.	52834.
1.00000E-04	1.1997	57797.	58178.
1.10000E-04	1.5327	62807.	63294.
1.20000E-04	1.6034	67569.	68079.
1.30000E-04	1.6684	72064.	72595.
1.30000E-04	1.6684	72064.	72595.
1.40000E-04	1.5771	76275.	76777.
1.50000E-04	1.4728	80185.	80654.
1.60000E-04	1.2961	83779.	84192.
1.70000E-04	1.1418	87042.	87405.
1.80000E-04	0.92324	89962.	90255.
1.90000E-04	0.77342	92526.	92772.
2.00000E-04	0.57080	94725.	94907.
2.10000E-04	0.33419	96551.	96657.
2.20000E-04	0.13725	97995.	98039.
2.30000E-04	-8.16814E-02	99053.	99027.
2.40000E-04	-0.28099	99720.	99630.
2.50000E-04	-0.53819	99993.	99821.
2.60000E-04	-0.74613	99871.	99634.
2.70000E-04	-0.97802	99356.	99044.
2.80000E-04	-1.1773	98448.	98073.
2.90000E-04	-1.3878	97152.	96710.
3.00000E-04	-1.6226	95472.	94956.
3.10000E-04	-1.8300	93416.	92833.
3.20000E-04	-2.0269	90991.	90346.
3.30000E-04	-2.2136	88206.	87502.
3.40000E-04	-2.3692	85074.	84320.
3.50000E-04	-2.5009	81606.	80810.
3.60000E-04	-2.6321	77816.	76978.
3.70000E-04	-2.7037	73719.	72858.
3.70000E-04	-2.7037	73719.	72858.
3.80000E-04	-2.7010	69331.	68471.
3.90000E-04	-2.5980	64669.	63842.
4.00000E-04	-2.3397	59752.	59007.
4.10000E-04	-2.0341	54599.	53952.
4.20000E-04	-1.7242	49231.	48682.
4.30000E-04	-1.5960	43669.	43160.
4.40000E-04	-1.5402	37934.	37443.
4.50000E-04	-1.4914	32049.	31574.
4.60000E-04	-1.3906	26038.	25595.
4.70000E-04	-1.2578	19924.	19524.
4.80000E-04	-1.0227	13732.	13406.
4.90000E-04	-0.53526	7484.9	7314.5
5.00000E-04	1.5368	1208.7	1697.9
5.00000E-04	1.5368	1208.7	1697.9
5.10000E-04	-1.4507	0.0	-461.76
5.20000E-04	-2.9224	0.0	-930.23
5.30000E-04	4.59525E-02	0.0	14.500
5.40000E-04	9.9100BE-02	0.0	31.545
5.50000E-04	9.46005E-02	0.0	30.112
5.60000E-04	-5.62768E-02	0.0	-17.913
5.70000E-04	6.08758E-02	0.0	19.314
5.80000E-04	2.42703E-02	0.0	7.7256
5.90000E-04	1.54712E-02	0.0	4.9246
6.00000E-04	2.76620E-02	0.0	8.8051
6.10000E-04	0.10595	0.0	33.724
6.20000E-04	9.23809E-02	0.0	29.406
6.30000E-04	6.17587E-02	0.0	19.658
6.40000E-04	0.11249	0.0	35.807
6.50000E-04	5.95906E-02	0.0	18.968
6.60000E-04	0.17421	0.0	55.452
6.70000E-04	4.46610E-02	0.0	14.216
6.80000E-04	7.32477E-02	0.0	23.315
6.90000E-04	0.16980	0.0	53.790
7.00000E-04	6.38795E-02	0.0	20.333
7.10000E-04	3.33640E-02	0.0	10.620
7.20000E-04	0.10142	0.0	32.282
7.30000E-04	-2.37309E-02	0.0	-7.5538
7.40000E-04	0.10929	0.0	34.787
7.50000E-04	1.48302E-02	0.0	4.7206
7.60000E-04	6.40754E-02	0.0	20.650
7.70000E-04	-0.13959	0.0	-44.434
7.80000E-04	8.46475E-02	0.0	26.944
7.90000E-04	4.83221E-02	0.0	15.381
8.00000E-04	0.13532	0.0	43.075
8.10000E-04	2.76404E-02	0.0	8.7984
8.20000E-04	2.34718E-02	0.0	7.4713
8.30000E-04	0.11381	0.0	36.226
8.40000E-04	7.60705E-03	0.0	2.4851
8.50000E-04	3.56207E-02	0.0	11.338
8.60000E-04	4.01358E-02	0.0	12.776
8.70000E-04	-6.30901E-02	0.0	-20.082
8.80000E-04	8.10364E-02	0.0	25.795
8.90000E-04	0.10655	0.0	33.917
9.00000E-04	0.14661	0.0	46.667
9.10000E-04	0.20530	0.0	65.348
9.20000E-04	0.30343	0.0	96.583
9.30000E-04	4.54934E-02	0.0	14.481
9.40000E-04	0.11377	0.0	36.215
9.50000E-04	0.15710	0.0	50.006
9.60000E-04	0.11488	0.0	36.568
9.70000E-04	0.13121	0.0	41.764
9.80000E-04	7.94151E-02	0.0	25.279
9.90000E-04	0.19581	0.0	62.327
1.00000E-03	0.51758	0.0	164.75

(c) VIF1RF, VOIDEL, and IERORT with V_{inp} = 0.1 V.

Figure 48 (continued)

-2.0000E 05 'X'=VBE1 6.0000E 05
-1.2000E 04 '*'=VF 1.2000E 04
-6.0000E 05 '+'=VO 1.8000E 06

TIME	VO	VF	VBE1
0.0	-4.09640E 05	-1208.5	859.00
1.00000E-05	-2.25823E 05	-5314.7	3513.3
2.00000E-05	2.75665E 05	-10628.	6985.2
3.00000E-05	6.03446E 05	-1048.9	1.28804E 05
4.00000E-05	6.58571E 05	-827.06	1.75707E 05
5.00000E-05	7.0911BE 05	-788.88	2.20353E 05
6.00000E-05	7.57512E 05	-759.69	2.64031E 05
7.00000E-05	8.03903E 05	-722.69	3.06519E 05
8.00000E-05	8.47969E 05	-681.38	3.47305E 05
9.00000E-05	8.88182E 05	-595.81	3.84778E 05
1.00000E-04	9.20956E 05	-444.88	4.15419E 05
1.10000E-04	9.43820E 05	-297.75	4.36833E 05
1.20000E-04	9.58986E 05	-200.94	4.51076E 05
1.30000E-04	9.69481E 05	-145.88	4.60947E 05
1.30000E-04	9.69481E 05	-145.88	4.60947E 05
1.40000E-04	9.77155E 05	-109.50	4.68181E 05
1.50000E-04	9.83006E 05	-86.750	4.73700E 05
1.60000E-04	9.87586E 05	-71.563	4.78029E 05
1.70000E-04	9.91243E 05	-61.813	4.81485E 05
1.80000E-04	9.94183E 05	-43.625	4.84260E 05
1.90000E-04	9.96544E 05	-39.313	4.86492E 05
2.00000E-04	9.98428E 05	-32.188	4.88272E 05
2.10000E-04	9.99904E 05	-18.313	4.89663E 05
2.20000E-04	1.00100E 06	-20.188	4.90702E 05
2.30000E-04	1.00177E 06	-2.3125	4.91420E 05
2.40000E-04	1.00223E 06	-9.8125	4.91858E 05
2.50000E-04	1.00238E 06	-10.000	4.92007E 05
2.60000E-04	1.00224E 06	-1.6875	4.91864E 05
2.70000E-04	1.00181E 06	2.9375	4.91446E 05
2.80000E-04	1.00106E 06	9.6875	4.90728E 05
2.90000E-04	9.99971E 05	12.563	4.89695E 05
3.00000E-04	9.98528E 05	18.063	4.88323E 05
3.10000E-04	9.96676E 05	27.375	4.86559E 05
3.20000E-04	9.94356E 05	36.625	4.84351E 05
3.30000E-04	9.91469E 05	45.688	4.81606E 05
3.40000E-04	9.87890E 05	58.563	4.78201E 05
3.50000E-04	9.83419E 05	80.063	4.73947E 05
3.60000E-04	9.77745E 05	92.250	4.68561E 05
3.70000E-04	9.70385E 05	128.88	4.61563E 05
3.70000E-04	9.70385E 05	128.88	4.61563E 05
3.80000E-04	9.60505E 05	175.31	4.52176E 05
3.90000E-04	9.46672E 05	252.56	4.39042E 05
4.00000E-04	9.26624E 05	383.94	4.20032E 05
4.10000E-04	8.97957E 05	522.94	3.92974E 05
4.20000E-04	8.60844E 05	637.13	3.58172E 05
4.30000E-04	8.18339E 05	703.31	3.18654E 05
4.40000E-04	7.72896E 05	737.31	2.76847E 05
4.50000E-04	7.25367E 05	768.94	2.33710E 05
4.60000E-04	6.75884E 05	800.69	1.89649E 05
4.70000E-04	6.24163E 05	839.88	1.44918E 05
4.80000E-04	5.69359E 05	905.81	99810.
4.90000E-04	5.08913E 05	1034.9	54909.
5.00000E-04	4.31010E 05	1606.6	13246.
5.00000E-04	4.31010E 05	1606.6	13246.
5.10000E-04	2.36663E 05	5330.9	-3357.3
5.20000E-04	-2.65514E 05	10641.	-6808.9
5.30000E-04	-4.76883E 05	145.00	-18.875
5.40000E-04	-4.84380E 05	115.25	0.31250
5.50000E-04	-4.90096E 05	90.000	16.813
5.60000E-04	-4.94721E 05	35.625	53.000
5.70000E-04	-4.98492E 05	59.125	36.875
5.80000E-04	-5.01700E 05	60.500	44.188
5.90000E-04	-5.04507E 05	34.750	52.813
6.00000E-04	-5.06916E 05	33.188	50.438
6.10000E-04	-5.09031E 05	37.125	51.125
6.20000E-04	-5.10889E 05	33.875	53.125
6.30000E-04	-5.12532E 05	26.250	58.063
6.40000E-04	-5.13976E 05	26.938	57.688
6.50000E-04	-5.15245E 05	23.063	60.250
6.60000E-04	-5.16363E 05	25.438	58.750
6.70000E-04	-5.17325E 05	20.250	61.875
6.80000E-04	-5.18151E 05	27.688	56.688
6.90000E-04	-5.18877E 05	19.063	63.000
7.00000E-04	-5.19466E 05	11.563	67.625
7.10000E-04	-5.19994E 05	-30.938	96.625
7.20000E-04	-5.20332E 05	-5.8125	79.313
7.30000E-04	-5.20595E 05	-16.750	86.500
7.40000E-04	-5.20728E 05	8.0625	69.750
7.50000E-04	-5.20784E 05	-1.7500	76.188
7.60000E-04	-5.20734E 05	0.75000	74.688
7.70000E-04	-5.20611E 05	-36.188	99.563
7.80000E-04	-5.20312E 05	8.8750	69.063
7.90000E-04	-5.19962E 05	-5.5625	78.813
8.00000E-04	-5.19484E 05	3.0000	72.813
8.10000E-04	-5.18902E 05	-8.6250	80.813
8.20000E-04	-5.18185E 05	-2.6875	76.875
8.30000E-04	-5.17370E 05	-8.8750	80.750
8.40000E-04	-5.16403E 05	-15.625	85.438
8.50000E-04	-5.15299E 05	-19.188	87.625
8.60000E-04	-5.14031E 05	-17.563	86.375
8.70000E-04	-5.12616E 05	-43.750	103.81
8.80000E-04	-5.10969E 05	-23.500	90.313
8.90000E-04	-5.09123E 05	-26.625	92.250
9.00000E-04	-5.07024E 05	-27.000	92.563
9.10000E-04	-5.04617E 05	-18.250	86.375
9.20000E-04	-5.01871E 05	-22.000	88.688
9.30000E-04	-4.98680E 05	-55.625	110.94
9.40000E-04	-4.94924E 05	-59.563	108.00
9.50000E-04	-4.90401E 05	-62.750	115.19
9.60000E-04	-4.84843E 05	-97.750	138.69
9.70000E-04	-4.77603E 05	126.25	149.43
9.80000E-04	-4.67473E 05	-200.13	204.50
9.90000E-04	-4.50909E 05	-351.94	302.38
1.00000E-03	-4.10737E 05	-1138.4	815.13

(d) VO, VF, VBE1 with V_{inp} = 0.1 V.

Figure 48 (continued)

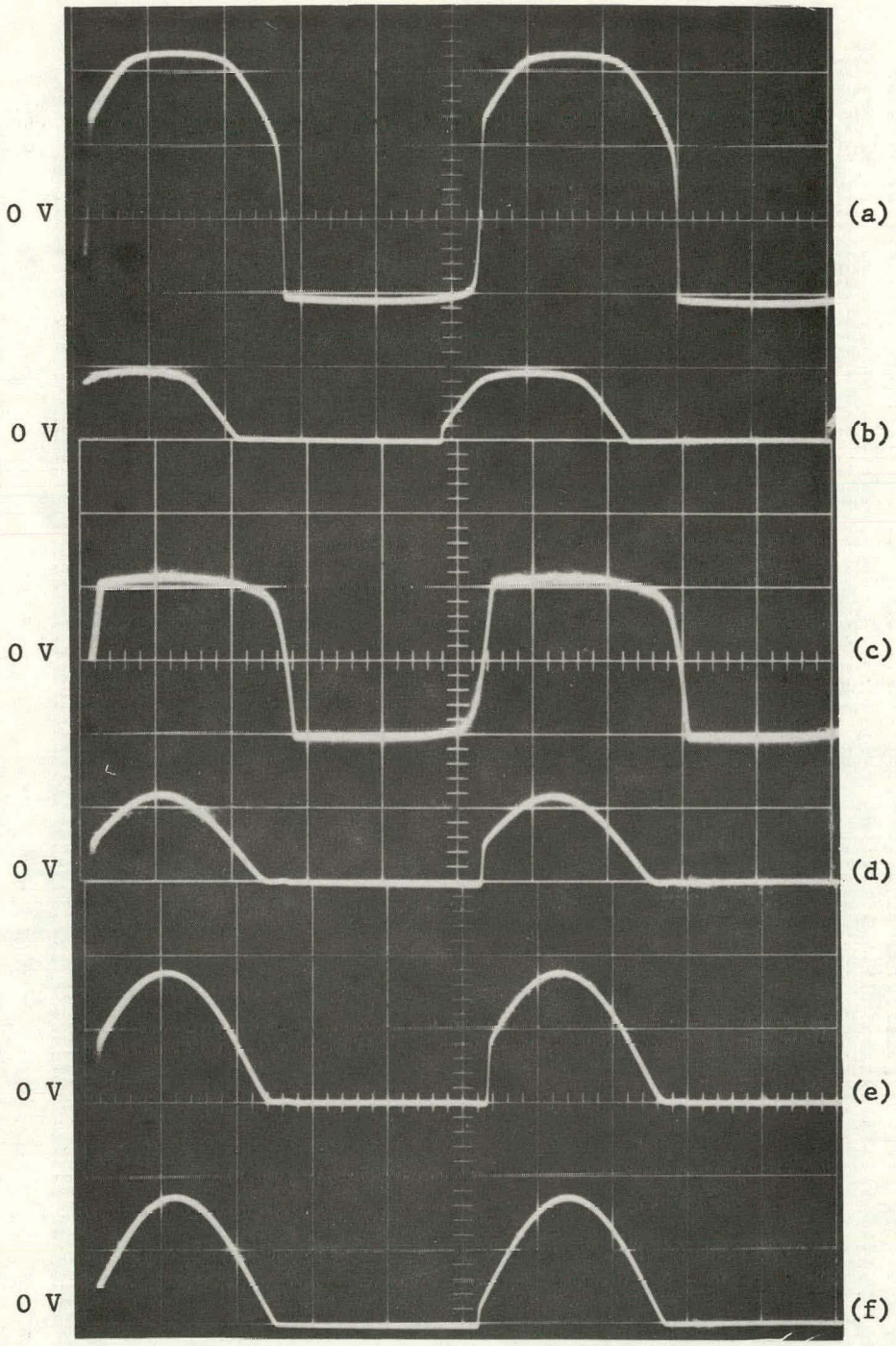

Figure 49. Experimental 1 KHz waveforms of a Darlington 2N5087 transistor rectifier with $R_1 = R_2 = 0\Omega$, $R_3 = 2\ K\Omega$, $C = 0.15\ \mu F$, $R = 14.7\ K\Omega$, and an AD506LH opamp. (a) $\overline{V_f} - V_o$ with $V_{inp} = 0.1\ V$; (b) $\overline{V_f} - V_{BE1}$ with $V_{inp} = 0.1\ V$; (c) $\overline{V_f} - V_o$ with $V_{inp} = 10\ mV$; (d) $\overline{V_f} - V_{BE1}$ with $V_{inp} = 10\ mV$; (e) V_{IF1RF} with $V_{inp} = 10\ mV$; (f) V_{IF1RF} with $V_{inp} = 0.1\ V$. Horizontal scale: 0.2 ms/div. Vertical scale: 0.5 V/div [curves (a), (b), and (c)]; 0.05 V/div [curves (d) and (f)]; 0.005 V/div [curve (e)].

that except for V_o where R = 1 GΩ and 10 mV input, the agreement between experimental and calculated waveforms is very good. The discrepancy is expected for two reasons. First, CBE of real transistors is dependent on emitter current, while a constant CBE was used in the simulations. Secondly, typical values were used for H_{FE} and capacitances, instead of measuring them for the actual transistors used. Probably a more appropriate value of C_{ob} would be 2 or 3 pF instead of the worst case value of 7 pF. The values of C_{ob} and C_{BE} determine where the errors change polarities.

As a further investigation of the accuracy of the simulation, the nonlinearity of the average output was both measured and computed. Figure 47(b) shows the measurement scheme. Because an AC voltmeter having sufficient accuracy (0.005% or better at 1 volt peak) was not available, another Darlington rectifier was employed as a voltmeter. An assumption was made that increasing the opamp gain increases the accuracy of the rectifier. Hence the output of a rectifier having an AD506LH opamp and a 2N5087 Darlington transistor was compared with that of a rectifier having an AD528JH opamp and a Darlington 2N5089 transistor. An absolute calibration was not made because of the 0.5% tolerance of the resistors (Daven wirewound resistors, series 1350). Instead the DC difference in the outputs of the two rectifiers was recorded versus input voltage at 1 KHz (THD < 0.15%). Then the nonlinear error (E_{nl}) was arbitrarily assumed zero for peak input voltages of 10 mV and 1 V for both experimental and calculated errors causing E_{nl} as shown in Figure 44 on pages 204 and 205 to have a linear component. The error voltage referred to the input is given by

$$DELVIF = E_L + E_{NL} ,$$

where (210)

$$E_L = M\,V_{inp} + B .$$

Given two pairs of values of E_{Li} and V_{inp_i} (i=1,2), M and B are found to be

$$B = \frac{E_{L1}\,V_{inp2} - E_{L2}\,V_{inp1}}{V_{inp2} - V_{inp1}}$$

and (211)

$$M = \frac{E_{Li} - B}{V_{inpi}} .$$

Using Equations (210) and (211) with V_{inp1} and V_{inp2} of 10 mV and 1 V, respectively, E_{NL} was obtained for R = 1 GΩ (Figure 44(e) on page 204) and R = 14.7 KΩ (Figure 44(f) on page 205). Note that for inputs between 10 mV and 1 V, the computed and measured E_{NL} agree surprisingly well for R = 1 GΩ, but poorly for R = 14.7 KΩ.

The poor agreement for R = 14.7 KΩ can be explained in the following manner. From Figures 48 and 49, VBE1 shows that at low currents almost all of the output current goes through R and Q1P, while at high current most of the output current is supplied by Q1. This indicates that R may reduce the increase in H_{FE} obtainable by the Darlington configuration. Indeed, this is verified by Figure 50 which shows the 10 mV_p, 1 KHz average error versus GBWP. This graph depicts an approach to a minimum error for R = 14.7 KΩ as GBWP approaches 10 MHz, while the error for R = 1 GΩ shows no sign of approaching a minimum error. A further indication of the higher H_{FE} dependence of rectifier error with R = 14.7 KΩ

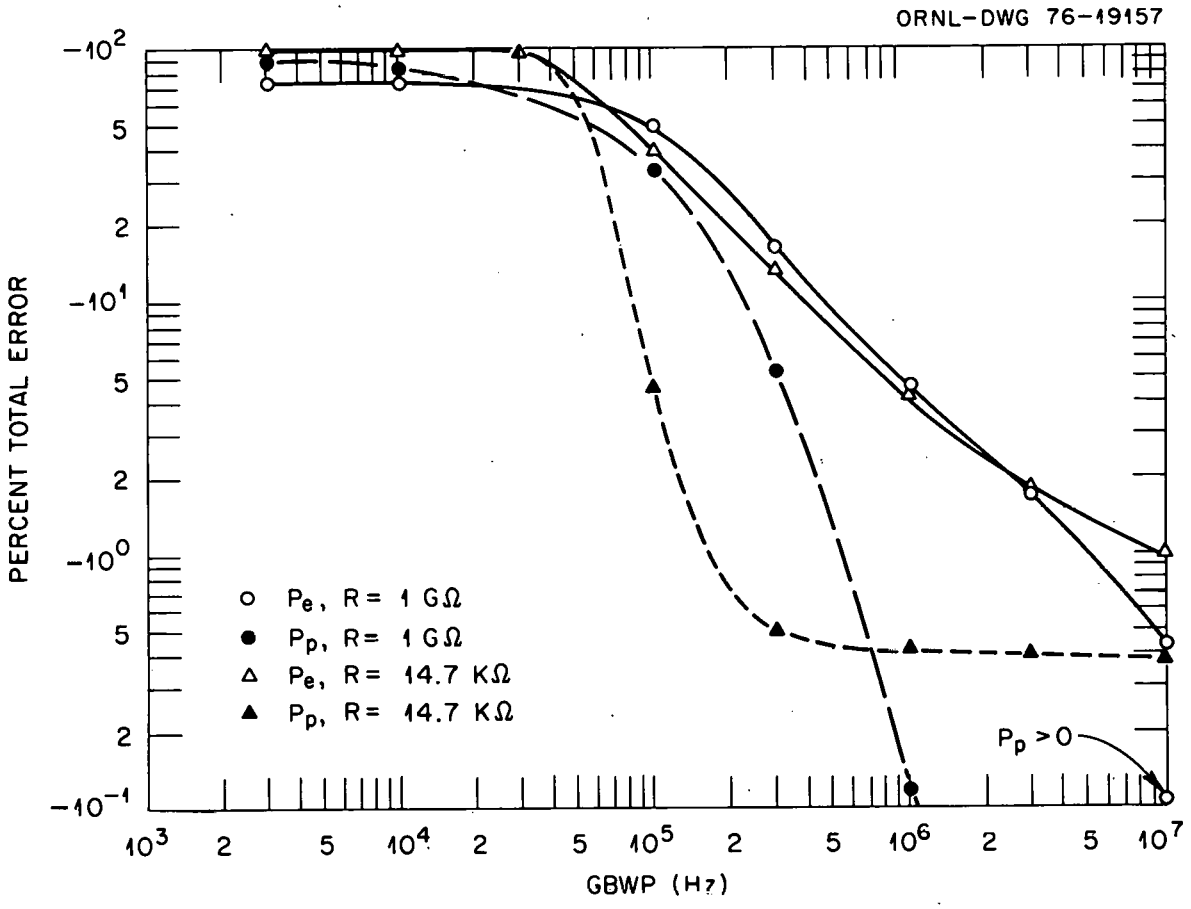

Figure 50. Computed 1 KHz accuracy of a Darlington 2N5087 transistor rectifier versus GBWP with $A_{ol} = 2 \times 10^5$, $R_1 = R_2 = 0\Omega$, and $R_3 = 2$ KΩ.

is the increase in measured E_{NL} of more than 100 μV for V_{inp} between 0.1 V and 0.3 V when R is reduced to 14.7 KΩ on the reference rectifier.

The change in rectifier error voltage when R is increased from 14.7 KΩ to 1 GΩ is shown in Figure 44(g) on page 206. The agreement between the computed change and the measured changes with both 2N5087 and 2N5089 transistors is fairly good for input voltages above 10 mV_p. Discrepancies at low input voltages is, of course, due to actual capacitance and H_{FE} values not matching those employed in the simulation. An additional cause for deviation of measured and computed results at low voltage levels is the change in exponential slope of the base-emitter current-voltage characteristic (see Figure 20 on page 86).

The change in rectifier error with frequency due to transistor capacitances is illustrated in Figure 51. This figure depicts the inferior high frequency accuracy when R = 14.7 KΩ. Although one might think the faster turn off times when R is included would lead to lower errors, this slower turn off results in an increase in the average output current which reduces the magnitude of the negative error. In fact, both computed waveforms at 10 KHz and measured waveforms (Figures 52, 53, 54, and 55) show little or no advantage in waveform accuracy for R = 14.7 KΩ. Note that the agreement between measured and computed waveforms is very good. Also comparing these waveforms with those of the diode rectifier (Figures 33, 36, and 37 on pages 160-165, 174, and 176) illustrates the superiority of the transistor rectifier.

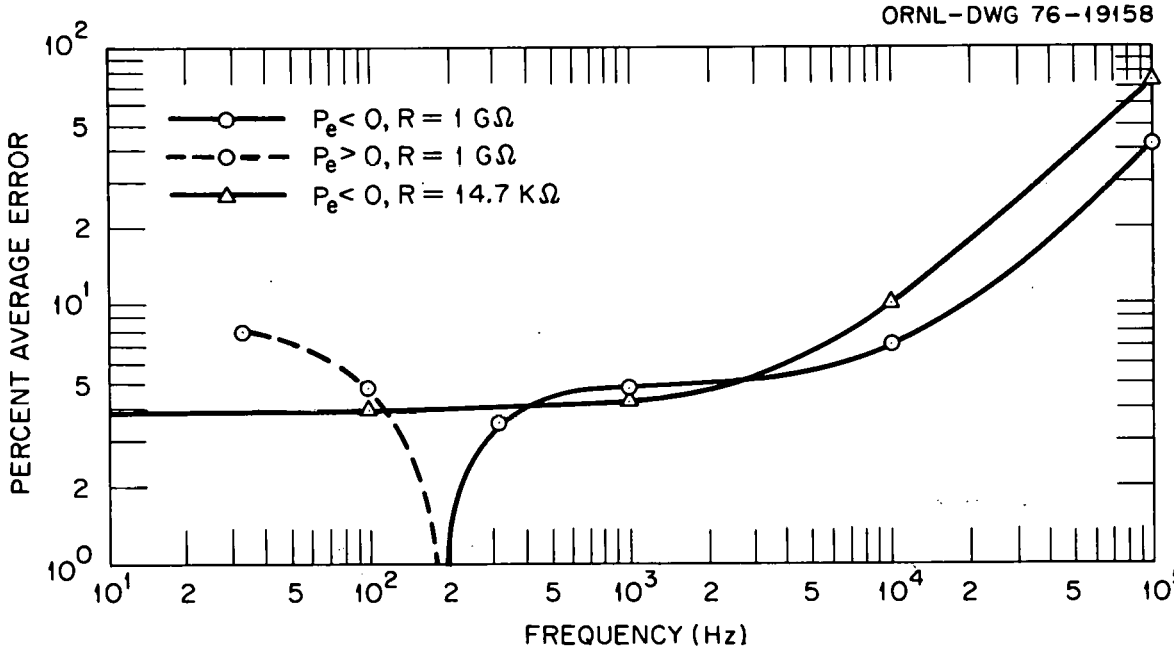

(a) Total average error with GBWP = 1000 f_{in}.

Figure 51. Computed frequency dependence of Darlington 2N5087 transistor rectifier duc to transistor capacitances.

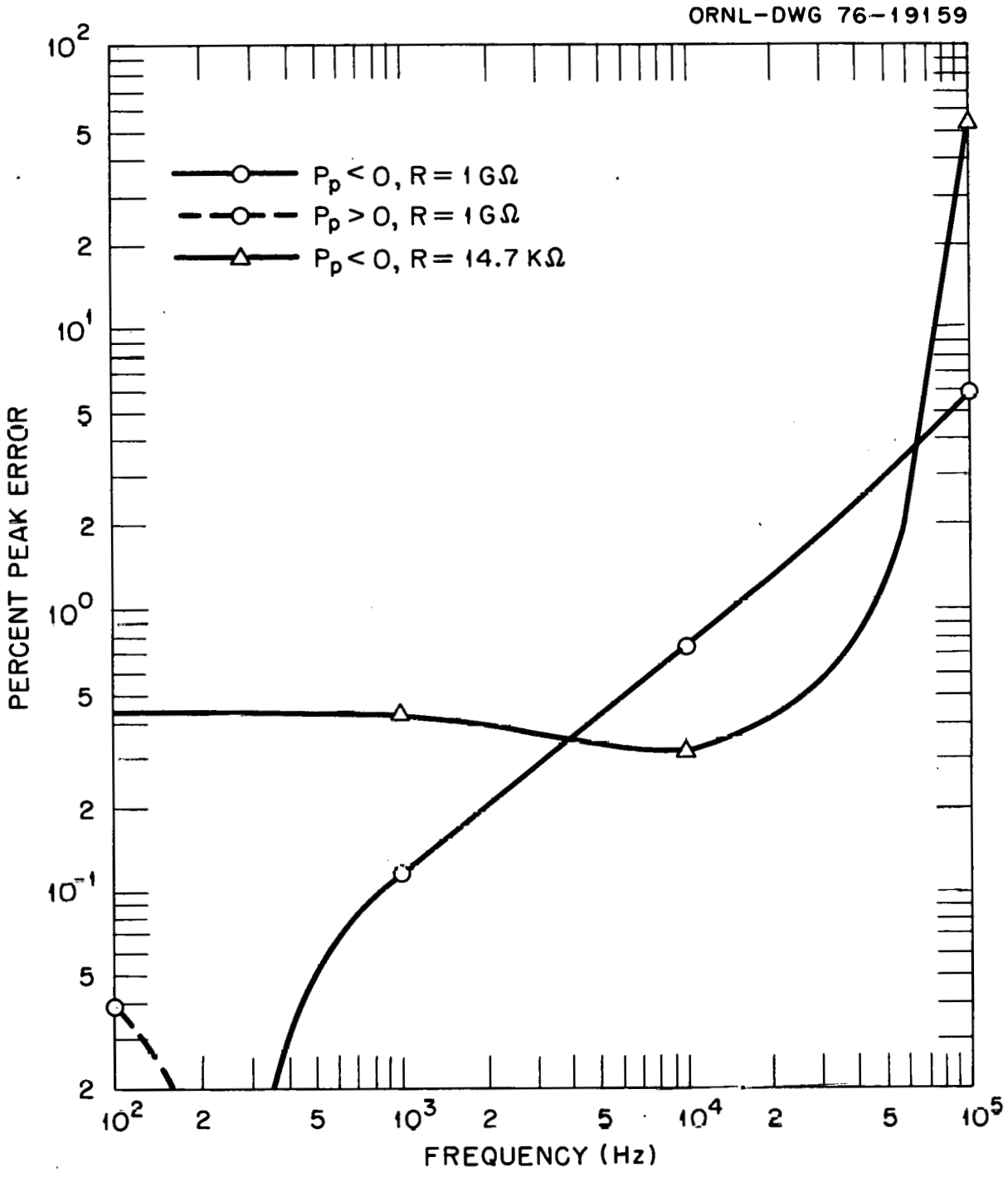

(b) Total peak error with GBWP = 1000 f_{in}.

Figure 51 (continued)

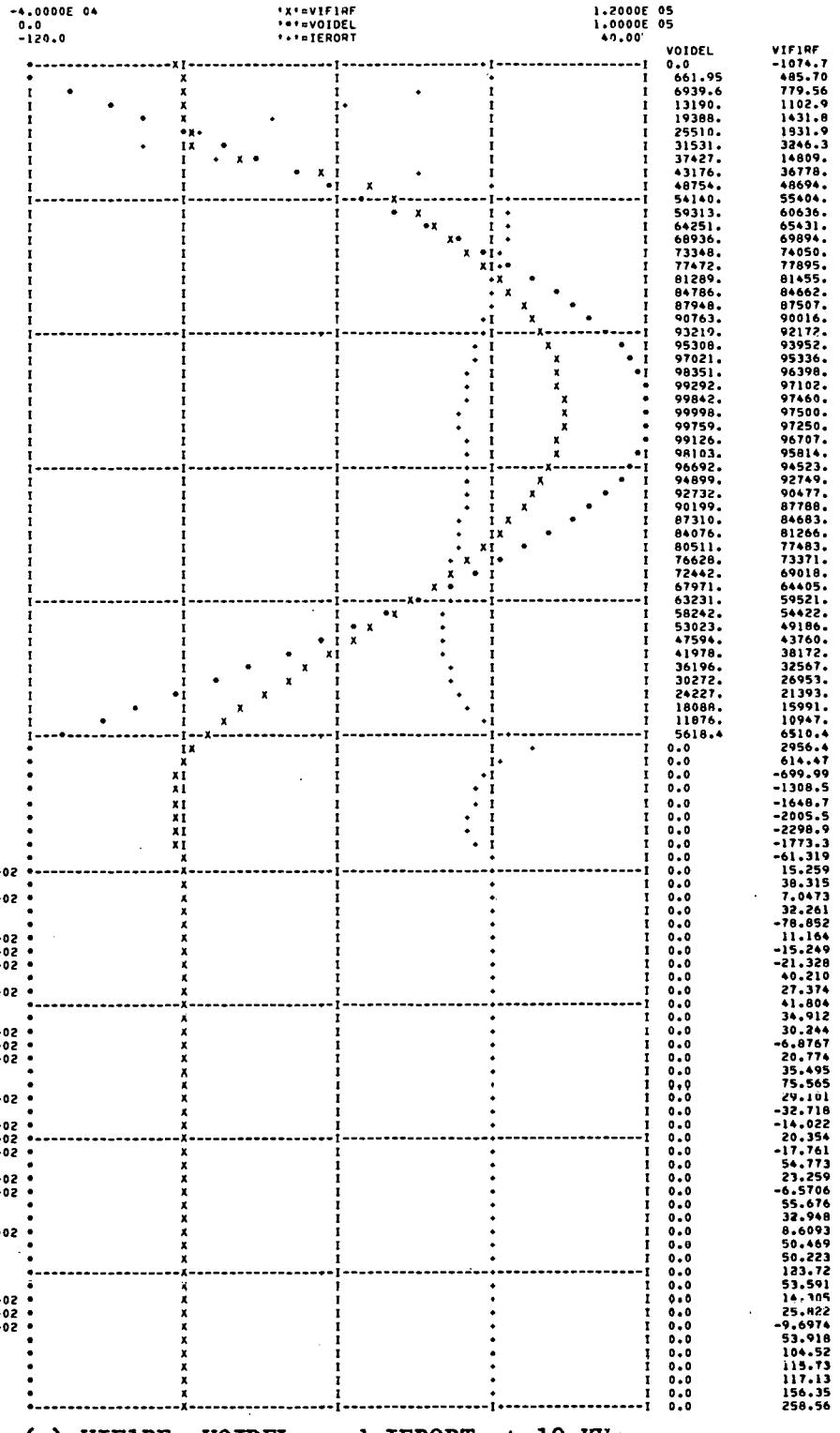

TIME	IERORT	VOIDEL	VIF1RF
0.0	-3.3761	0.0	-1074.7
1.00000E-06	-0.55372	661.95	485.70
2.00000E-06	-19.352	6939.6	779.56
3.00000E-06	-37.972	13190.	1102.9
4.00000E-06	-56.411	19388.	1431.8
5.00000E-06	-74.386	25510.	1931.9
6.00000E-06	-88.858	31531.	3246.3
7.00000E-06	-71.058	37427.	14809.
8.00000E-06	-20.100	43176.	36778.
9.00000E-06	-0.18999	48754.	48694.
1.00000E-05	3.9681	54140.	55404.
1.10000E-05	4.1571	59313.	60636.
1.20000E-05	3.7056	64251.	65431.
1.30000E-05	3.0118	68936.	69894.
1.40000E-05	2.2028	73348.	74050.
1.50000E-05	1.3289	77472.	77895.
1.60000E-05	0.52268	81289.	81455.
1.70000E-05	-0.38700	84786.	84662.
1.80000E-05	-1.3837	87948.	87507.
1.90000E-05	-2.3466	90763.	90016.
2.00000E-05	-3.2912	93219.	92172.
2.10000E-05	-4.2614	95308.	93952.
2.20000E-05	-5.2944	97021.	95336.
2.30000E-05	-6.1338	98351.	96398.
2.40000E-05	-6.8799	99292.	97102.
2.50000E-05	-7.4825	99842.	97460.
2.60000E-05	-7.8485	99998.	97500.
2.70000E-05	-7.8805	99759.	97250.
2.80000E-05	-7.6021	99126.	96707.
2.90000E-05	-7.1897	98103.	95814.
3.00000E-05	-6.8125	96692.	94523.
3.10000E-05	-6.7560	94899.	92749.
3.20000E-05	-7.0837	92732.	90477.
3.30000E-05	-7.5744	90199.	87788.
3.40000E-05	-8.2534	87310.	84683.
3.50000E-05	-8.8298	84076.	81266.
3.60000E-05	-9.5114	80511.	77483.
3.70000E-05	-10.231	76628.	73371.
3.80000E-05	-10.756	72442.	69018.
3.90000E-05	-11.201	67971.	64405.
4.00000E-05	-11.655	63231.	59521.
4.10000E-05	-12.002	58242.	54422.
4.20000E-05	-12.053	53023.	49186.
4.30000E-05	-12.046	47594.	43760.
4.40000E-05	-11.957	41978.	38172.
4.50000E-05	-11.402	36196.	32567.
4.60000E-05	-10.424	30272.	26953.
4.70000E-05	-8.9044	24227.	21393.
4.80000E-05	-6.5877	18088.	15991.
4.90000E-05	-2.9204	11876.	10947.
5.00000E-05	2.8021	5618.4	6510.4
5.10000E-05	9.2879	0.0	2956.4
5.20000E-05	1.9304	0.0	614.47
5.30000E-05	-2.1991	0.0	-699.99
5.40000E-05	-4.1107	0.0	-1308.5
5.50000E-05	-5.1796	0.0	-1648.7
5.60000E-05	-6.3006	0.0	-2005.5
5.70000E-05	-7.2221	0.0	-2298.9
5.80000E-05	-5.5711	0.0	-1773.3
5.90000E-05	-0.19264	0.0	-61.319
6.00000E-05	4.79369E-02	0.0	15.259
6.10000E-05	0.12037	0.0	38.315
6.20000E-05	2.21398E-02	0.0	7.0473
6.30000E-05	0.10135	0.0	32.261
6.40000E-05	-0.24772	0.0	-78.852
6.50000E-05	3.50739E-02	0.0	11.164
6.60000E-05	-4.79063E-02	0.0	-15.249
6.70000E-05	-6.70031E-02	0.0	-21.328
6.80000E-05	0.12632	0.0	40.210
6.90000E-05	8.59993E-02	0.0	27.374
7.00000E-05	0.13133	0.0	41.804
7.10000E-05	0.10968	0.0	34.912
7.20000E-05	9.50141E-02	0.0	30.244
7.30000E-05	-2.16037E-02	0.0	-6.8767
7.40000E-05	6.52627E-02	0.0	20.774
7.50000E-05	0.11151	0.0	35.495
7.60000E-05	0.23739	0.0	75.565
7.70000E-05	9.14233E-02	0.0	29.101
7.80000E-05	-0.10279	0.0	-32.718
7.90000E-05	-4.40510E-02	0.0	-14.022
8.00000E-05	6.39430E-02	0.0	20.354
8.10000E-05	-5.57971E-02	0.0	-17.761
8.20000E-05	0.17208	0.0	54.773
8.30000E-05	7.30692E-02	0.0	23.259
8.40000E-05	-2.06421E-02	0.0	-6.5706
8.50000E-05	0.17491	0.0	55.676
8.60000E-05	0.10351	0.0	32.948
8.70000E-05	2.70468E-02	0.0	8.6093
8.80000E-05	0.15855	0.0	50.469
8.90000E-05	0.15778	0.0	50.223
9.00000E-05	0.38868	0.0	123.72
9.10000E-05	0.16836	0.0	53.591
9.20000E-05	4.49412E-02	0.0	14.305
9.30000E-05	8.11208E-02	0.0	25.822
9.40000E-05	-3.04653E-02	0.0	-9.6974
9.50000E-05	0.16939	0.0	53.918
9.60000E-05	0.32836	0.0	104.52
9.70000E-05	0.36358	0.0	115.73
9.80000E-05	0.36797	0.0	117.13
9.90000E-05	0.49119	0.0	156.35
1.00000E-04	0.81229	0.0	258.56

(a) VIF1RF, VOIDEL, and IERORT at 10 KHz.

Figure 52. Computed high frequency waveforms of a Darlington 2N5087 transistor rectifier with $R_1 = R_2 = 0\Omega$, $R_3 = 2\ K\Omega$, $R = 1\ G\Omega$, $V_{inp} = 0.1$ V, $A_{o1} = 2 \times 10^5$, and GBWP = 1 MHz. All voltages in μV unless specified otherwise.

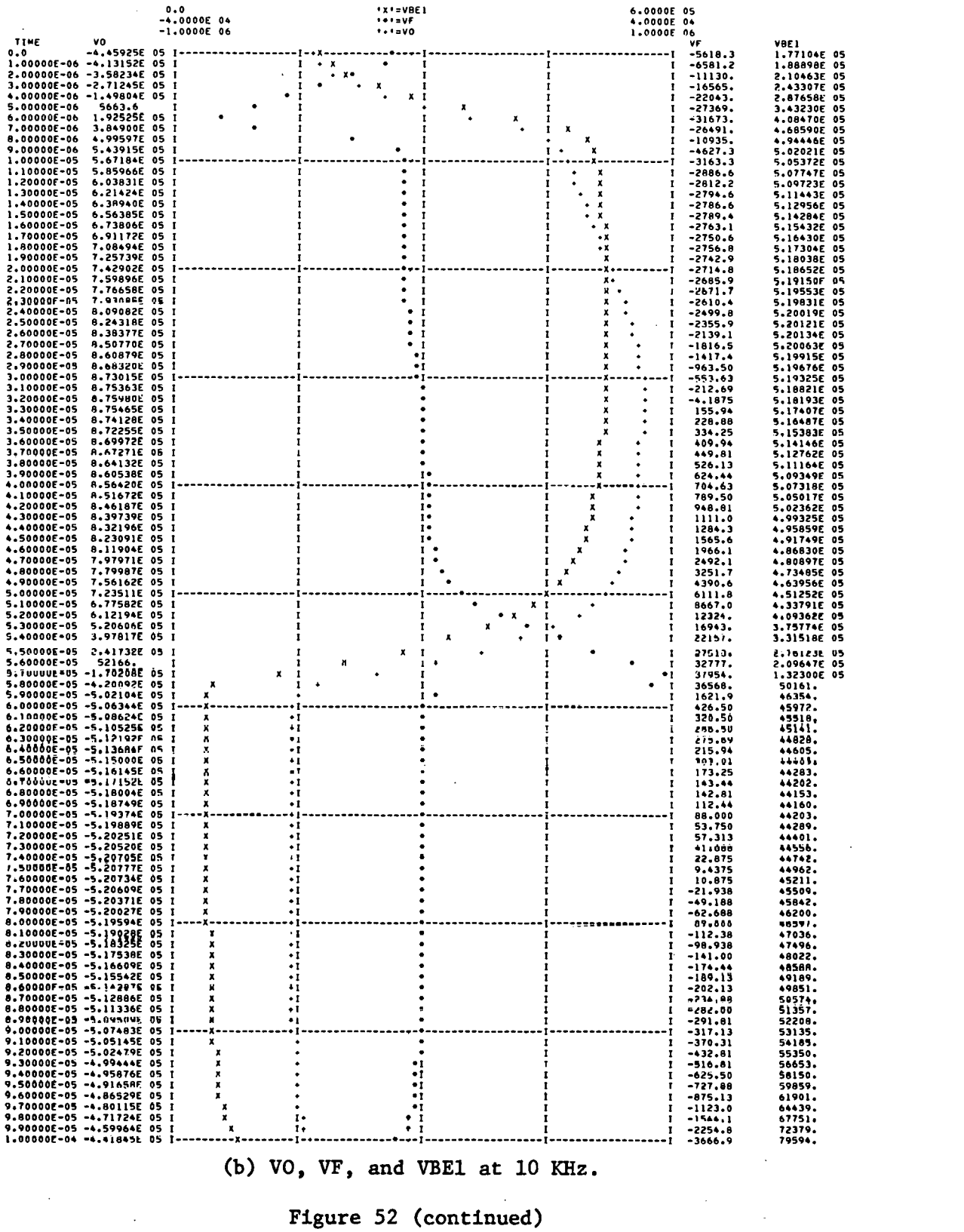

(b) VO, VF, and VBE1 at 10 KHz.

Figure 52 (continued)

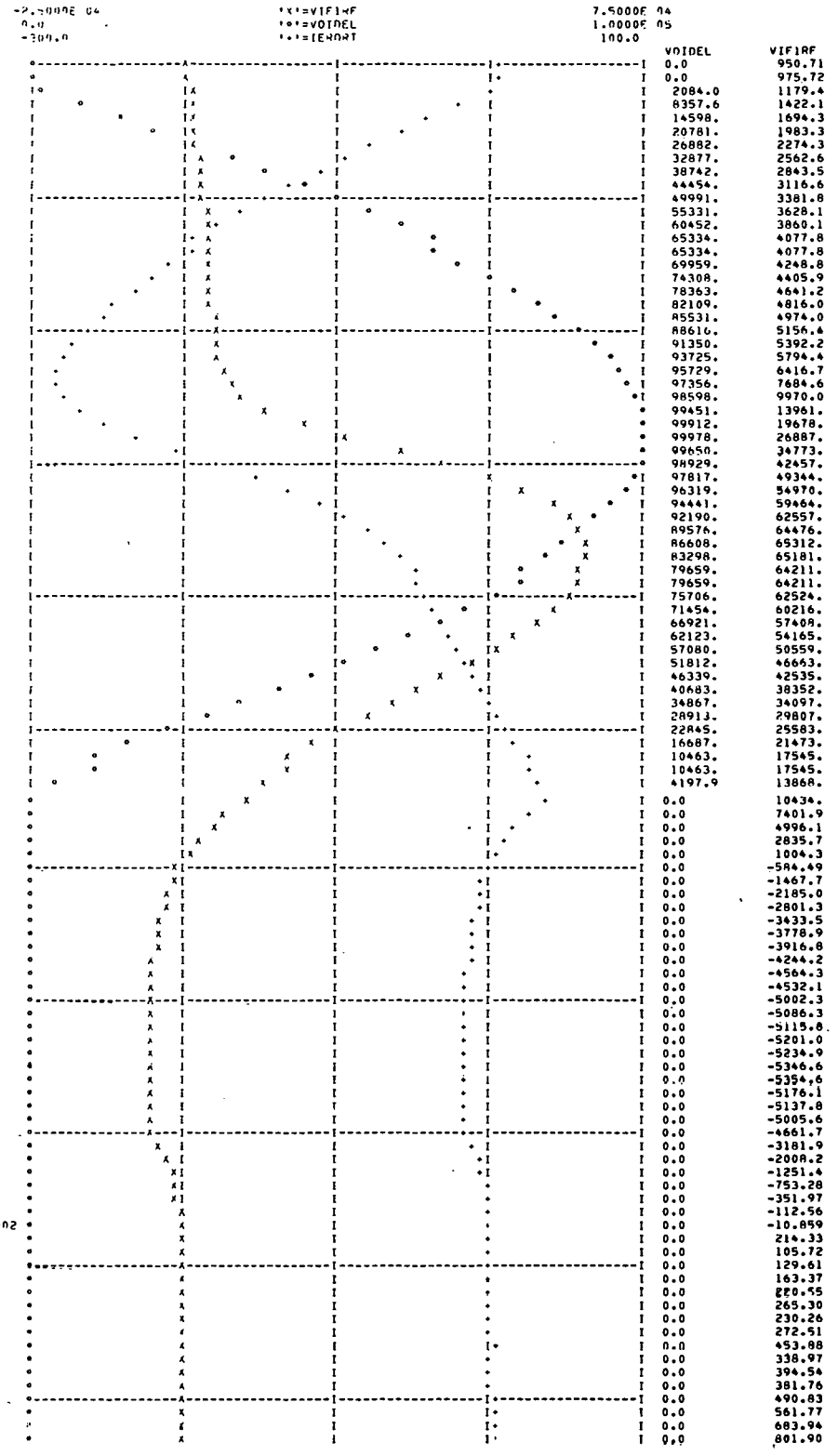

TIME	IERORT	VOIDEL	VIF1RF
0.0	2.9657	0.0	950.71
1.00000E-07	3.0553	0.0	975.72
2.00000E-07	-2.8421	2084.0	1179.4
3.00000E-07	-21.749	8357.6	1422.1
4.00000E-07	-40.539	14598.	1694.3
5.00000E-07	-59.055	20781.	1983.3
6.00000E-07	-77.308	26882.	2274.3
7.00000E-07	-95.235	32877.	2562.6
8.00000E-07	-112.79	38742.	2843.5
9.00000E-07	-129.87	44454.	3116.6
1.00000E-06	-146.43	49991.	3381.8
1.10000E-06	-162.43	55331.	3628.1
1.20000E-06	-177.79	60452.	3860.1
1.30000E-06	-192.44	65334.	4077.8
1.30000E-06	-192.44	65334.	4077.8
1.40000E-06	-206.43	69959.	4248.8
1.50000E-06	-219.60	74308.	4405.9
1.60000E-06	-231.60	78363.	4641.2
1.70000E-06	-242.82	82109.	4816.0
1.80000E-06	-253.08	85531.	4974.0
1.90000E-06	-262.19	88616.	5156.4
2.00000E-06	-270.05	91350.	5392.2
2.10000E-06	-276.24	93725.	5794.4
2.20000E-06	-280.58	95729.	6416.7
2.30000E-06	-281.71	97356.	7684.6
2.40000E-06	-278.43	98598.	9970.0
2.50000E-06	-268.57	99451.	13961.
2.60000E-06	-252.06	99912.	19678.
2.70000E-06	-229.62	99978.	26887.
2.80000E-06	-201.82	99650.	34773.
2.90000E-06	-177.41	98929.	42457.
3.00000E-06	-152.28	97817.	49344.
3.10000E-06	-129.40	96319.	54970.
3.20000E-06	-109.40	94441.	59464.
3.30000E-06	-93.095	92190.	62557.
3.40000E-06	-78.054	89576.	64476.
3.50000E-06	-66.903	86608.	65312.
3.60000E-06	-56.917	83298.	65181.
3.70000E-06	-48.532	79659.	64211.
3.70000E-06	-48.532	79659.	64211.
3.80000E-06	-41.414	75706.	62524.
3.90000E-06	-35.308	71454.	60216.
4.00000E-06	-29.586	66921.	57408.
4.10000E-06	-24.249	62123.	54165.
4.20000E-06	-20.464	57080.	50559.
4.30000E-06	-16.176	51812.	46663.
4.40000E-06	-11.949	46339.	42535.
4.50000E-06	-7.3224	40683.	38352.
4.60000E-06	-2.4171	34867.	34097.
4.70000E-06	2.8093	28913.	29807.
4.80000E-06	8.6020	22845.	25583.
4.90000E-06	15.035	16687.	21473.
5.00000E-06	22.247	10463.	17545.
5.00000E-06	22.247	10463.	17545.
5.10000E-06	30.379	4197.9	13868.
5.20000E-06	32.779	0.0	10434.
5.30000E-06	23.254	0.0	7401.9
5.40000E-06	15.696	0.0	4996.1
5.50000E-06	8.9085	0.0	2835.7
5.60000E-06	3.1552	0.0	1004.3
5.70000E-06	-1.8362	0.0	-584.49
5.80000E-06	-4.6109	0.0	-1467.7
5.90000E-06	-6.8644	0.0	-2185.0
6.00000E-06	-8.8007	0.0	-2801.3
6.10000E-06	-10.787	0.0	-3433.5
6.20000E-06	-11.872	0.0	-3778.9
6.30000E-06	-12.305	0.0	-3916.8
6.40000E-06	-13.334	0.0	-4244.2
6.50000E-06	-14.339	0.0	-4564.3
6.60000E-06	-14.238	0.0	-4532.1
6.70000E-06	-15.715	0.0	-5002.3
6.80000E-06	-15.979	0.0	-5086.3
6.90000E-06	-16.072	0.0	-5115.8
7.00000E-06	-16.339	0.0	-5201.0
7.10000E-06	-16.466	0.0	-5234.9
7.20000E-06	-16.797	0.0	-5346.6
7.30000E-06	-16.822	0.0	-5354.6
7.40000E-06	-16.261	0.0	-5176.1
7.50000E-06	-16.141	0.0	-5137.8
7.60000E-06	-15.725	0.0	-5005.6
7.70000E-06	-14.665	0.0	-4661.7
7.80000E-06	-9.9964	0.0	-3181.9
7.90000E-06	-6.3091	0.0	-2008.2
8.00000E-06	-3.9314	0.0	-1251.4
8.10000E-06	-2.3665	0.0	-753.28
8.20000E-06	-1.1057	0.0	-351.97
8.30000E-06	-0.35367	0.0	-112.56
8.40000E-06	-3.41153E-02	0.0	-10.859
8.50000E-06	0.67333	0.0	214.33
8.60000E-06	0.33213	0.0	105.72
8.70000E-06	0.40710	0.0	129.61
8.80000E-06	0.51324	0.0	163.37
8.90000E-06	0.64289	0.0	220.55
9.00000E-06	0.83346	0.0	265.30
9.10000E-06	0.72339	0.0	230.26
9.20000E-06	0.85611	0.0	272.51
9.30000E-06	1.4259	0.0	453.88
9.40000E-06	1.0649	0.0	338.97
9.50000E-06	1.2395	0.0	394.54
9.60000E-06	1.1993	0.0	381.76
9.70000E-06	1.5420	0.0	490.83
9.80000E-06	1.7649	0.0	561.77
9.90000E-06	2.1480	0.0	683.94
1.00000E-05	2.5192	0.0	801.90

(c) VIF1RF, VOIDEL, and IERORT at 100 KHz.

Figure 52 (continued)

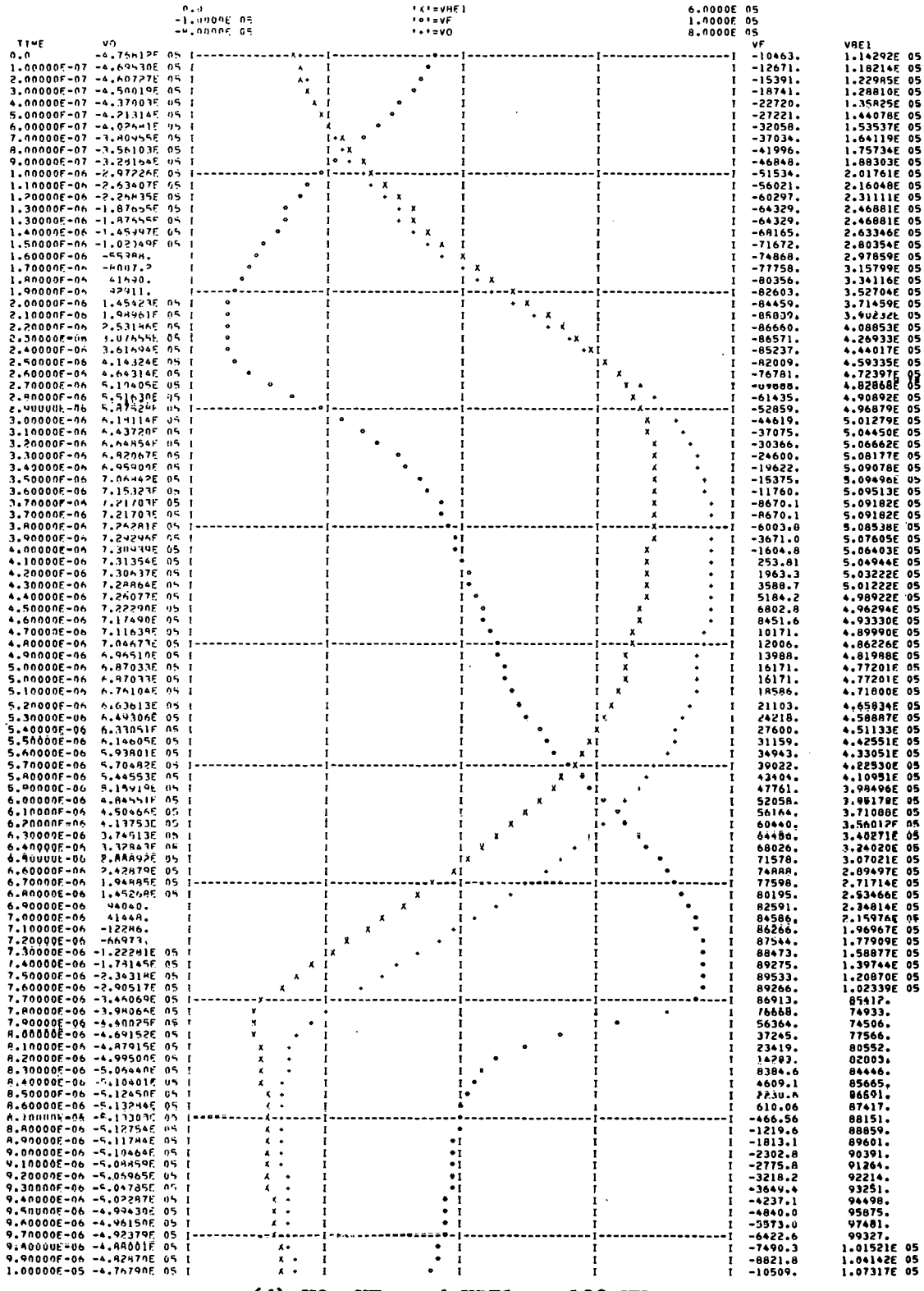

(d) VO, VF, and VBE1 at 100 KHz.

Figure 52 (continued)

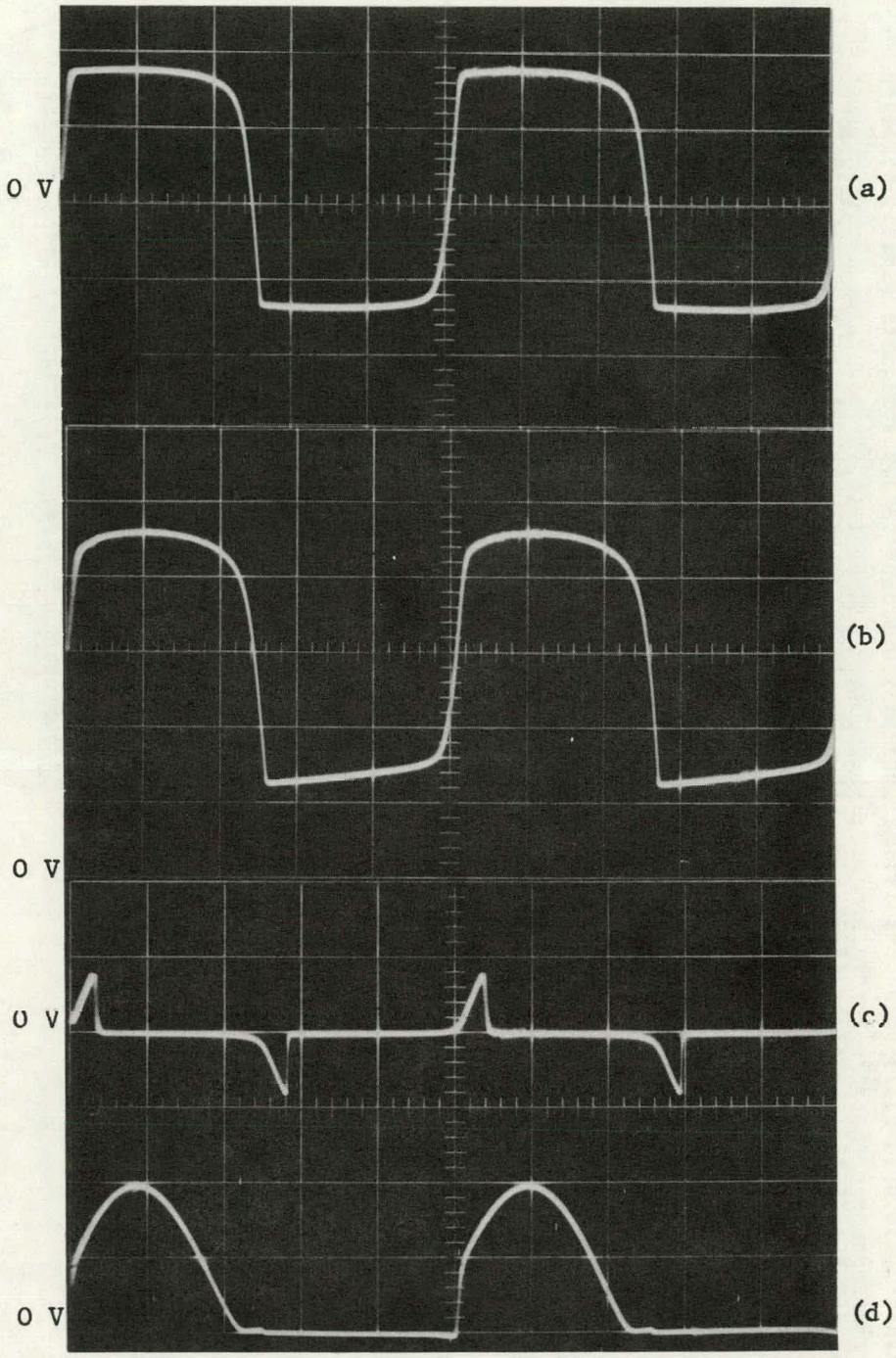

Figure 53. Experimental 10 KHz waveforms of a Darlington 2N5087 transistor rectifier with $R_1 = R_2 = 0\Omega$, $R_3 = 2\ K\Omega$, $C_3 = 0.15\ \mu F$, no R, $V_{inp} = 0.1$ V, and an AD506LH opamp. (a) $\overline{V_f} - V_o$; (b) $\overline{V_f} - V_{BE1}$; (c) $\overline{V_f} - V_f$; (d) V_{IF1RF}. Horizontal scale: 20 μs/div. Vertical scale: 0.5 V/div [curve (a)]; 0.1 V/div [curve (b)]; 0.05 V/div [curves (c) and (d)].

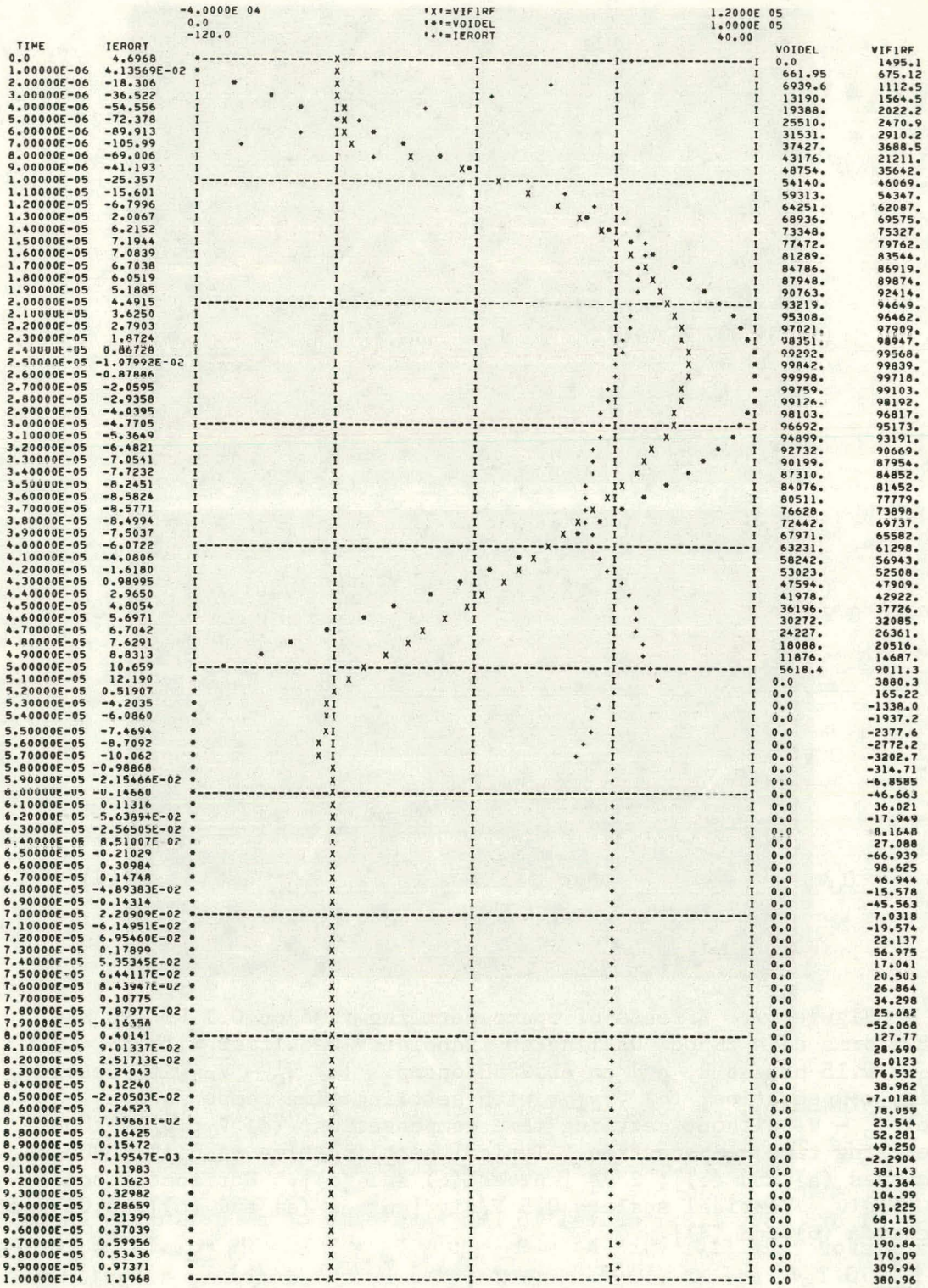

TIME	IERORT	VOIDEL	VIF1RF
0.0	4.6968	0.0	1495.1
1.00000E-06	4.13569E-02	661.95	675.12
2.00000E-06	-18.306	6939.6	1112.5
3.00000E-06	-36.522	13190.	1564.5
4.00000E-06	-54.556	19388.	2022.2
5.00000E-06	-72.378	25510.	2470.9
6.00000E-06	-89.913	31531.	2910.2
7.00000E-06	-105.99	37427.	3688.5
8.00000E-06	-69.006	43176.	21211.
9.00000E-06	-41.193	48754.	35642.
1.00000E-05	-25.357	54140.	46069.
1.10000E-05	-15.601	59313.	54347.
1.20000E-05	-6.7996	64251.	62087.
1.30000E-05	2.0067	68936.	69575.
1.40000E-05	6.2152	73348.	75327.
1.50000E-05	7.1944	77472.	79762.
1.60000E-05	7.0839	81289.	83544.
1.70000E-05	6.7038	84786.	86919.
1.80000E-05	6.0519	87948.	89874.
1.90000E-05	5.1885	90763.	92414.
2.00000E-05	4.4915	93219.	94649.
2.10000E-05	3.6250	95308.	96462.
2.20000E-05	2.7903	97021.	97909.
2.30000E-05	1.8724	98351.	98947.
2.40000E-05	0.86728	99292.	99568.
2.50000E-05	-1.07992E-02	99842.	99839.
2.60000E-05	-0.87886	99998.	99718.
2.70000E-05	-2.0595	99759.	99103.
2.80000E-05	-2.9358	99126.	98192.
2.90000E-05	-4.0395	98103.	96817.
3.00000E-05	-4.7705	96692.	95173.
3.10000E-05	-5.3649	94899.	93191.
3.20000E-05	-6.4821	92732.	90669.
3.30000E-05	-7.0541	90199.	87954.
3.40000E-05	-7.7232	87310.	84852.
3.50000E-05	-8.2451	84076.	81452.
3.60000E-05	-8.5824	80511.	77779.
3.70000E-05	-8.5771	76628.	73898.
3.80000E-05	-8.4994	72442.	69737.
3.90000E-05	-7.5037	67971.	65582.
4.00000E-05	-6.0722	63231.	61298.
4.10000E-05	-4.0806	58242.	56943.
4.20000E-05	-1.6180	53023.	52508.
4.30000E-05	0.98995	47594.	47909.
4.40000E-05	2.9650	41978.	42922.
4.50000E-05	4.8054	36196.	37726.
4.60000E-05	5.6971	30272.	32085.
4.70000E-05	6.7042	24227.	26361.
4.80000E-05	7.6291	18088.	20516.
4.90000E-05	8.8313	11876.	14687.
5.00000E-05	10.659	5618.4	9011.3
5.10000E-05	12.190	0.0	3880.3
5.20000E-05	0.51907	0.0	165.22
5.30000E-05	-4.2035	0.0	-1338.0
5.40000E-05	-6.0860	0.0	-1937.2
5.50000E-05	-7.4694	0.0	-2377.6
5.60000E-05	-8.7092	0.0	-2772.2
5.70000E-05	-10.062	0.0	-3202.7
5.80000E-05	-0.98868	0.0	-314.71
5.90000E-05	-2.15466E-02	0.0	-8.8585
6.00000E-05	-0.14660	0.0	-46.663
6.10000E-05	0.11316	0.0	36.021
6.20000E-05	5.63894E-02	0.0	-17.949
6.30000E-05	-2.56505E-02	0.0	8.1648
6.40000E-05	8.51007E-02	0.0	27.088
6.50000E-05	-0.21029	0.0	-66.939
6.60000E-05	0.30984	0.0	98.625
6.70000E-05	0.14748	0.0	46.944
6.80000E-05	-4.89383E-02	0.0	-15.578
6.90000E-05	-0.14314	0.0	-45.563
7.00000E-05	2.20909E-02	0.0	7.0318
7.10000E-05	-6.14951E-02	0.0	-19.574
7.20000E-05	6.95460E-02	0.0	22.137
7.30000E-05	0.17899	0.0	56.975
7.40000E-05	5.35345E-02	0.0	17.041
7.50000E-05	6.44117E-02	0.0	20.503
7.60000E-05	8.43947E-02	0.0	26.864
7.70000E-05	0.10775	0.0	34.298
7.80000E-05	7.87977E-02	0.0	25.082
7.90000E-05	-0.16358	0.0	-52.068
8.00000E-05	0.40141	0.0	127.77
8.10000E-05	9.01337E-02	0.0	28.690
8.20000E-05	2.51713E-02	0.0	8.0123
8.30000E-05	0.24043	0.0	76.532
8.40000E-05	0.12240	0.0	38.962
8.50000E-05	-2.20503E-02	0.0	-7.0188
8.60000E-05	0.24523	0.0	78.059
8.70000E-05	7.39661E-02	0.0	23.544
8.80000E-05	0.16425	0.0	52.281
8.90000E-05	0.15472	0.0	49.250
9.00000E-05	-7.19547E-03	0.0	-2.2904
9.10000E-05	0.11983	0.0	38.143
9.20000E-05	0.13623	0.0	43.364
9.30000E-05	0.32982	0.0	104.99
9.40000E-05	0.28659	0.0	91.225
9.50000E-05	0.21399	0.0	68.115
9.60000E-05	0.37039	0.0	117.90
9.70000E-05	0.59956	0.0	190.84
9.80000E-05	0.53436	0.0	170.09
9.90000E-05	0.97371	0.0	309.94
1.00000E-04	1.1968	0.0	380.96

(a) VIF1RF, VOIDEL, and IERORT at 10 KHz.

Figure 54. Computed high frequency waveforms of a Darlington 2N5087 transistor rectifier with $R_1 = R_2 = 0\Omega$, $R_3 = 2\ K\Omega$, $R = 14.7\ K\Omega$, $V_{inp} = 0.1$ V, $A_{o1} = 2 \times 10^5$, and GBWP = 1 MHz. All voltages in μV unless specified otherwise.

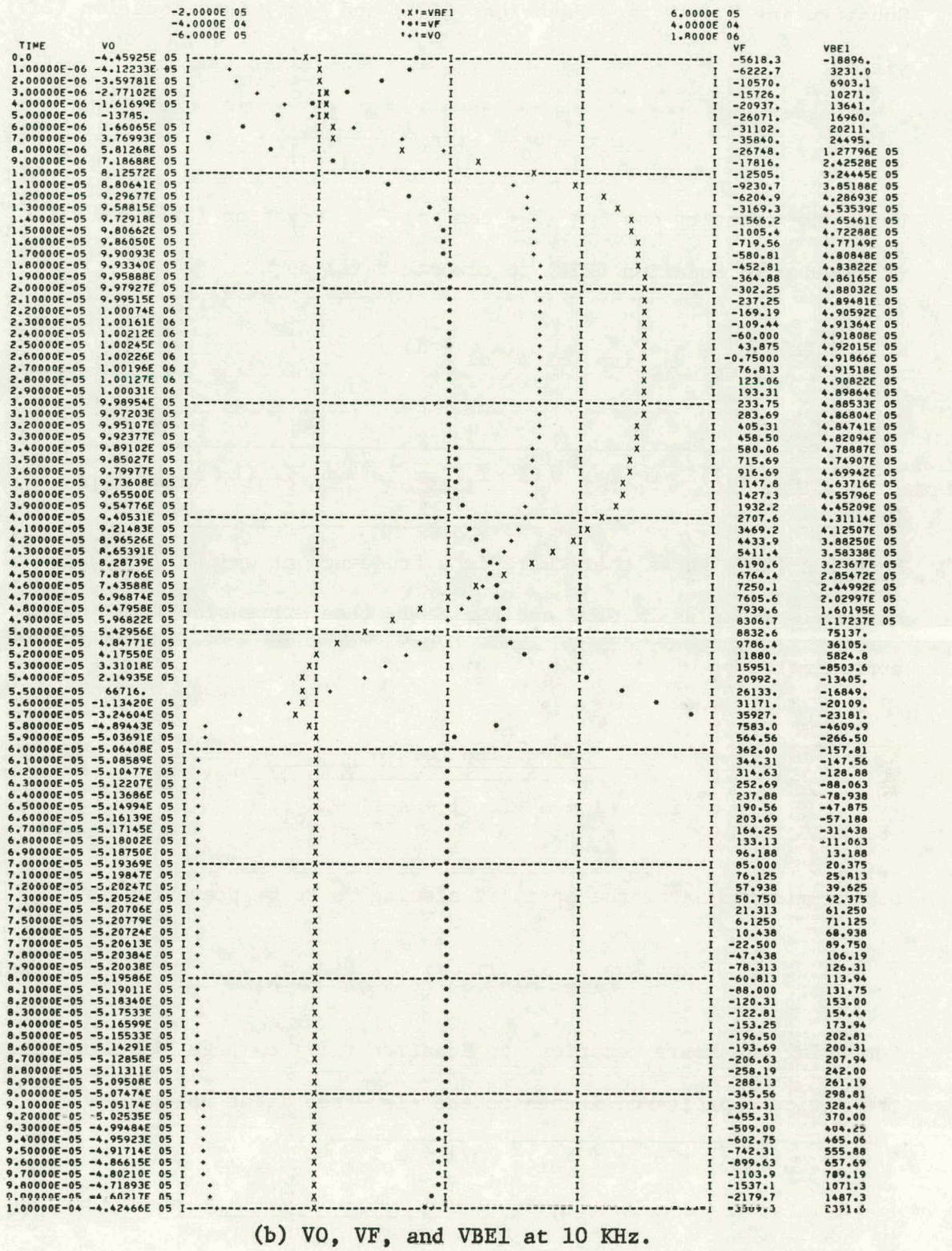

TIME	VO	VF	VBE1
0.0	-4.45925E 05	-5618.3	-18896.
1.00000E-06	-4.12233E 05	-6222.7	3231.0
2.00000E-06	-3.59781E 05	-10570.	6903.1
3.00000E-06	-2.77102E 05	-15726.	10271.
4.00000E-06	-1.61699E 05	-20937.	13641.
5.00000E-06	-13785.	-26071.	16960.
6.00000E-06	1.66065E 05	-31102.	20211.
7.00000E-06	3.76993E 05	-35840.	24495.
8.00000E-06	5.81268E 05	-26748.	1.27796E 05
9.00000E-06	7.18688E 05	-17816.	2.42528E 05
1.00000E-05	8.12572E 05	-12505.	3.24445E 05
1.10000E-05	8.80641E 05	-9230.7	3.85188E 05
1.20000E-05	9.29677E 05	-6204.9	4.28693E 05
1.30000E-05	9.58815E 05	-3169.3	4.53539E 05
1.40000E-05	9.72918E 05	-1566.2	4.65461E 05
1.50000E-05	9.80662E 05	-1005.4	4.72288E 05
1.60000E-05	9.86050E 05	-719.56	4.77149E 05
1.70000E-05	9.90093E 05	-580.81	4.80848E 05
1.80000E-05	9.93340E 05	-452.81	4.83822E 05
1.90000E-05	9.95888E 05	-364.88	4.86165E 05
2.00000E-05	9.97927E 05	-302.25	4.88032E 05
2.10000E-05	9.99515E 05	-237.25	4.89481E 05
2.20000E-05	1.00074E 06	-169.19	4.90592E 05
2.30000E-05	1.00161E 06	-109.44	4.91364E 05
2.40000E-05	1.00212E 06	-60.000	4.91808E 05
2.50000E-05	1.00245E 06	43.875	4.92015E 05
2.60000E-05	1.00226E 06	-0.75000	4.91866E 05
2.70000E-05	1.00196E 06	76.813	4.91518E 05
2.80000E-05	1.00127E 06	123.06	4.90822E 05
2.90000E-05	1.00031E 06	193.31	4.89864E 05
3.00000E-05	9.98954E 05	233.75	4.88533E 05
3.10000E-05	9.97203E 05	283.69	4.86804E 05
3.20000E-05	9.95107E 05	405.31	4.84741E 05
3.30000E-05	9.92377E 05	458.50	4.82094E 05
3.40000E-05	9.89102E 05	580.06	4.78887E 05
3.50000E-05	9.85027E 05	715.69	4.74907E 05
3.60000E-05	9.79977E 05	916.69	4.69942E 05
3.70000E-05	9.73608E 05	1147.8	4.63716E 05
3.80000E-05	9.65500E 05	1427.3	4.55796E 05
3.90000E-05	9.54776E 05	1932.2	4.45209E 05
4.00000E-05	9.40531E 05	2707.6	4.31114E 05
4.10000E-05	9.21483E 05	3469.2	4.12507E 05
4.20000E-05	8.96526E 05	4433.9	3.88250E 05
4.30000E-05	8.65391E 05	5411.4	3.58338E 05
4.40000E-05	8.28739E 05	6190.6	3.23677E 05
4.50000E-05	7.87766E 05	6764.4	2.85472E 05
4.60000E-05	7.43588E 05	7250.1	2.44992E 05
4.70000E-05	6.96874E 05	7605.6	2.02997E 05
4.80000E-05	6.47958E 05	7939.6	1.60195E 05
4.90000E-05	5.96822E 05	8306.7	1.17237E 05
5.00000E-05	5.42956E 05	8832.6	75137.
5.10000E-05	4.84771E 05	9786.4	36105.
5.20000E-05	4.17550E 05	11880.	5824.8
5.30000E-05	3.31018E 05	15951.	-8503.6
5.40000E-05	2.14935E 05	20992.	-13405.
5.50000E-05	66716.	26133.	-16849.
5.60000E-05	-1.13420E 05	31171.	-20109.
5.70000E-05	-3.24604E 05	35927.	-23181.
5.80000E-05	-4.89443E 05	7583.0	-4609.9
5.90000E-05	-5.03691E 05	564.56	-266.50
6.00000E-05	-5.06408E 05	362.00	-157.81
6.10000E-05	-5.08589E 05	344.31	-147.56
6.20000E-05	-5.10477E 05	314.63	-128.88
6.30000E-05	-5.12207E 05	252.69	-88.063
6.40000E-05	-5.13686E 05	237.88	-78.938
6.50000E-05	-5.14994E 05	190.56	-47.875
6.60000E-05	-5.16139E 05	203.69	-57.188
6.70000E-05	-5.17145E 05	164.25	-31.438
6.80000E-05	-5.18002E 05	133.13	-11.063
6.90000E-05	-5.18750E 05	96.188	13.188
7.00000E-05	-5.19369E 05	85.000	20.375
7.10000E-05	-5.19847E 05	76.125	25.813
7.20000E-05	-5.20247E 05	57.938	39.625
7.30000E-05	-5.20524E 05	50.750	42.375
7.40000E-05	-5.20706E 05	21.313	61.250
7.50000E-05	-5.20779E 05	6.1250	71.125
7.60000E-05	-5.20724E 05	10.438	68.938
7.70000E-05	-5.20613E 05	-22.500	89.750
7.80000E-05	-5.20384E 05	-47.438	106.19
7.90000E-05	-5.20038E 05	-78.313	126.31
8.00000E-05	-5.19586E 05	-60.813	113.94
8.10000E-05	-5.19011E 05	-88.000	131.75
8.20000E-05	-5.18340E 05	-120.31	153.00
8.30000E-05	-5.17533E 05	-122.81	154.44
8.40000E-05	-5.16599E 05	-153.25	173.94
8.50000E-05	-5.15533E 05	-196.50	202.81
8.60000E-05	-5.14291E 05	-193.69	200.31
8.70000E-05	-5.12858E 05	-206.63	207.94
8.80000E-05	-5.11311E 05	-258.19	242.00
8.90000E-05	-5.09508E 05	-288.13	261.19
9.00000E-05	-5.07474E 05	-345.56	298.81
9.10000E-05	-5.05174E 05	-391.31	328.44
9.20000E-05	-5.02535E 05	-455.31	370.00
9.30000E-05	-4.99484E 05	-509.00	404.25
9.40000E-05	-4.95923E 05	-602.75	465.06
9.50000E-05	-4.91714E 05	-742.31	555.88
9.60000E-05	-4.86615E 05	-899.63	657.69
9.70000E-05	-4.80210E 05	-1103.9	789.19
9.80000E-05	-4.71893E 05	-1537.1	1071.3
9.90000E-05	-4.60217E 05	-2179.7	1487.3
1.00000E-04	-4.42466E 05	-3509.3	2391.6

(b) VO, VF, and VBE1 at 10 KHz.

Figure 54 (continued)

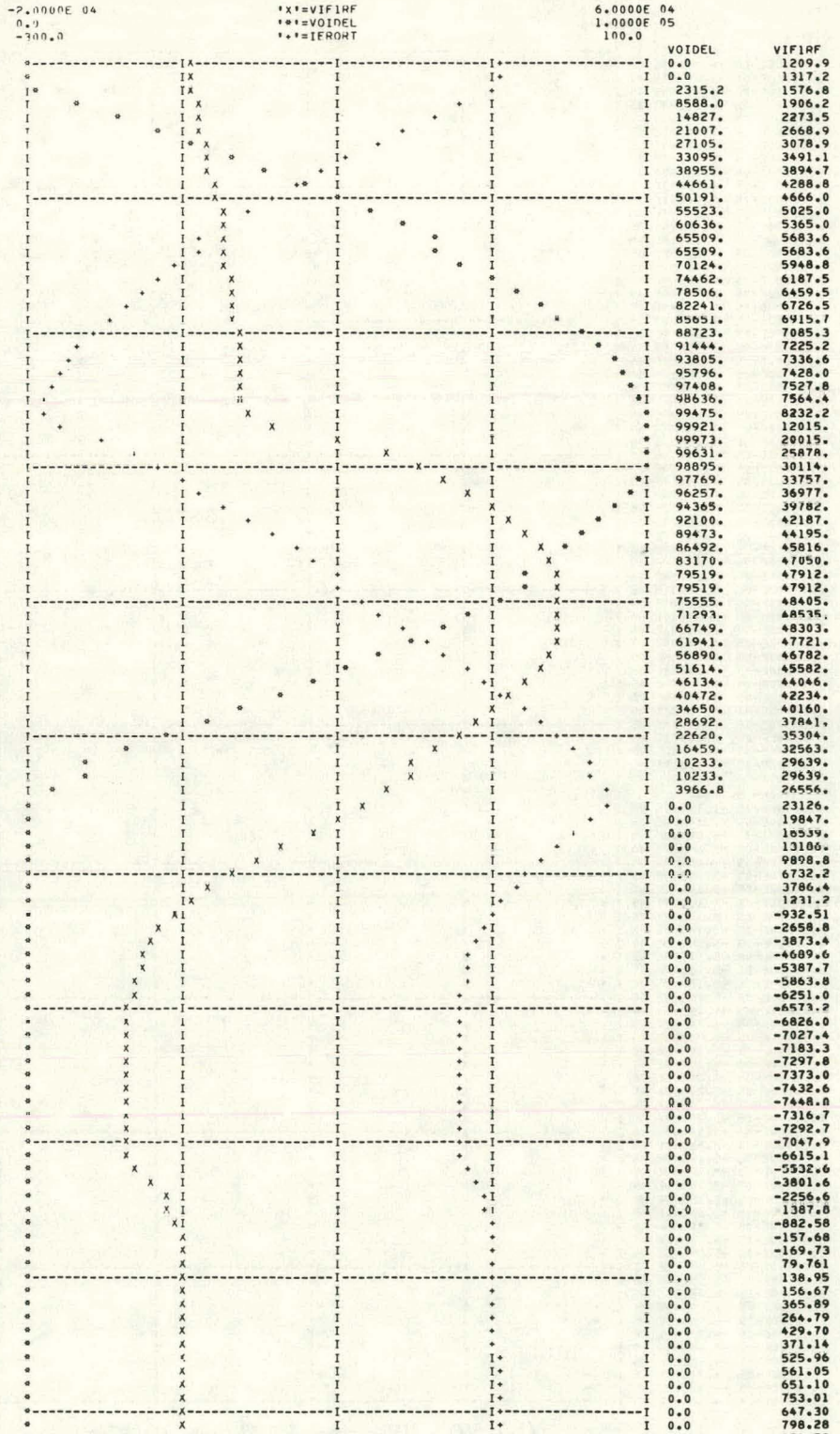

TIME	IERORT	VOIDEL	VIF1RF
0.0	3.8010	0.0	1209.9
1.00000E-07	4.1382	0.0	1317.2
2.00000E-07	-2.3199	2315.2	1576.8
3.00000E-07	-20.992	8588.0	1906.2
4.00000E-07	-39.438	14827.	2273.5
5.00000E-07	-57.612	21007.	2668.9
6.00000E-07	-75.480	27105.	3078.9
7.00000E-07	-93.004	33095.	3491.1
8.00000E-07	-110.15	38955.	3894.7
9.00000E-07	-126.43	44661.	4288.8
1.00000E-06	-143.02	50191.	4666.0
1.10000E-06	-158.64	55523.	5025.0
1.20000E-06	-173.64	60636.	5365.0
1.30000E-06	-187.95	65509.	5683.6
1.30000E-06	-187.95	65509.	5683.6
1.40000E-06	-201.61	70124.	5948.8
1.50000E-06	-214.49	74462.	6187.5
1.60000E-06	-226.34	78506.	6459.5
1.70000E-06	-237.24	82241.	6726.5
1.80000E-06	-247.35	85651.	6915.7
1.90000E-06	-256.47	88723.	7085.3
2.00000E-06	-264.58	91444.	7225.2
2.10000E-06	-271.65	93805.	7336.6
2.20000E-06	-277.61	95796.	7428.0
2.30000E-06	-282.37	97408.	7527.8
2.40000E-06	-286.11	98636.	7564.4
2.50000E-06	-286.65	99475.	8232.2
2.60000E-06	-276.16	99921.	12015.
2.70000E-06	-251.20	99973.	20015.
2.80000E-06	-231.70	99631.	25878.
2.90000E-06	-216.08	98895.	30114.
3.00000E-06	-201.10	97769.	33757.
3.10000E-06	-186.23	96257.	36977.
3.20000E-06	-171.48	94365.	39782.
3.30000E-06	-156.81	92100.	42187.
3.40000E-06	-142.24	89473.	44195.
3.50000E-06	-127.79	86492.	45816.
3.60000E-06	-113.47	83170.	47050.
3.70000E-06	-99.298	79519.	47912.
3.70000E-06	-99.298	79519.	47912.
3.80000E-06	-85.294	75555.	48405.
3.90000E-06	-71.494	71293.	48535.
4.00000E-06	-57.948	66749.	48303.
4.10000E-06	-44.675	61941.	47721.
4.20000E-06	-31.755	56890.	46782.
4.30000E-06	-18.948	51614.	45582.
4.40000E-06	-6.5594	46134.	44046.
4.50000E-06	5.5379	40472.	42234.
4.60000E-06	17.310	34650.	40160.
4.70000E-06	28.745	28692.	37841.
4.80000E-06	39.847	22620.	35304.
4.90000E-06	50.592	16459.	32563.
5.00000E-06	60.965	10233.	29639.
5.00000E-06	60.965	10233.	29639.
5.10000E-06	70.966	3966.8	26556.
5.20000E-06	72.653	0.0	23126.
5.30000E-06	62.352	0.0	19847.
5.40000E-06	51.960	0.0	16539.
5.50000E-06	41.424	0.0	13186.
5.60000E-06	31.098	0.0	9898.8
5.70000E-06	21.150	0.0	6732.2
5.80000E-06	11.895	0.0	3786.4
5.90000E-06	3.8680	0.0	1231.2
6.00000E-06	-2.9296	0.0	-932.51
6.10000E-06	-8.3530	0.0	-2658.8
6.20000E-06	-12.169	0.0	-3873.4
6.30000E-06	-14.733	0.0	-4689.6
6.40000E-06	-16.926	0.0	-5387.7
6.50000E-06	-18.422	0.0	-5863.8
6.60000E-06	-19.638	0.0	-6251.0
6.70000E-06	-20.650	0.0	-6573.2
6.80000E-06	-21.444	0.0	-6826.0
6.90000E-06	-22.077	0.0	-7027.4
7.00000E-06	-22.567	0.0	-7183.3
7.10000E-06	-22.927	0.0	-7297.8
7.20000E-06	-23.163	0.0	-7373.0
7.30000E-06	-23.350	0.0	-7432.6
7.40000E-06	-23.399	0.0	-7448.0
7.50000E-06	-22.306	0.0	-7316.7
7.60000E-06	-22.911	0.0	-7292.7
7.70000E-06	-22.142	0.0	-7047.9
7.80000E-06	-20.782	0.0	-6615.1
7.90000E-06	-17.381	0.0	-5532.6
8.00000E-06	-11.943	0.0	-3801.6
8.10000E-06	-7.0893	0.0	-2256.6
8.20000E-06	-4.3599	0.0	1387.8
8.30000E-06	-2.7727	0.0	-882.58
8.40000E-06	-0.49537	0.0	-157.68
8.50000E-06	-0.53321	0.0	-169.73
8.60000E-06	0.25059	0.0	79.761
8.70000E-06	0.43652	0.0	138.95
8.80000E-06	0.49219	0.0	156.67
8.90000E-06	1.1495	0.0	365.89
9.00000E-06	0.83186	0.0	264.79
9.10000E-06	1.3499	0.0	429.70
9.20000E-06	1.1660	0.0	371.14
9.30000E-06	1.6524	0.0	525.96
9.40000E-06	1.7626	0.0	561.05
9.50000E-06	2.0455	0.0	651.10
9.60000E-06	2.3657	0.0	753.01
9.70000E-06	2.0336	0.0	647.30
9.80000E-06	2.5079	0.0	798.28
9.90000E-06	2.9893	0.0	951.53
1.00000E-05	3.4977	0.0	1113.4

(c) VIF1RF, VOIDEL, and IERORT at 100 KHz.

Figure 54 (continued)

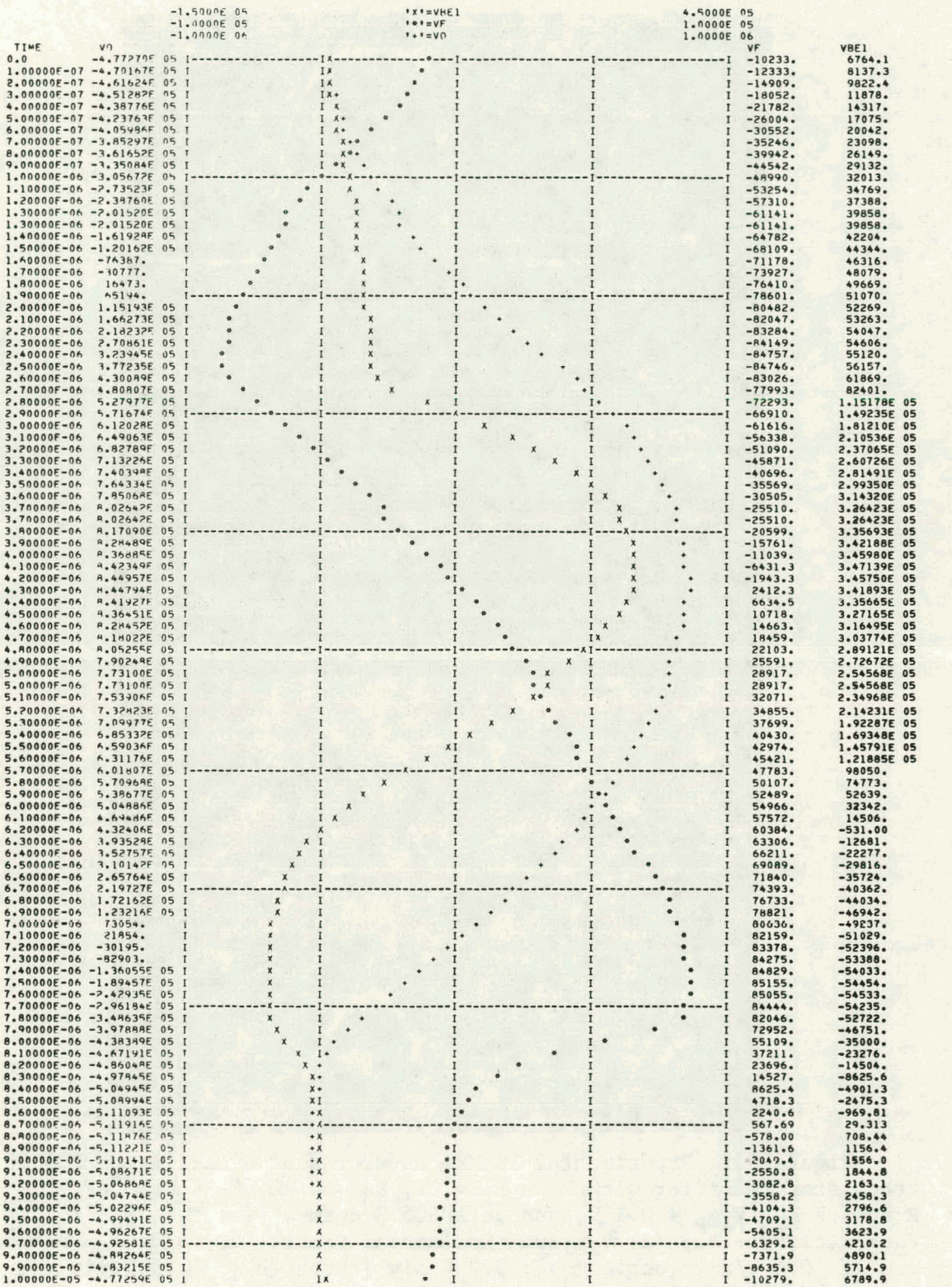

TIME	VO	VF	VBE1
0.0	-4.77270E 05	-10233.	6764.1
1.00000E-07	-4.70167E 05	-12333.	8137.3
2.00000E-07	-4.61624E 05	-14909.	9822.4
3.00000E-07	-4.51282E 05	-18052.	11878.
4.00000E-07	-4.38776E 05	-21782.	14317.
5.00000E-07	-4.23763E 05	-26004.	17075.
6.00000E-07	-4.05986E 05	-30552.	20042.
7.00000E-07	-3.85297E 05	-35246.	23098.
8.00000E-07	-3.61652E 05	-39942.	26149.
9.00000E-07	-3.35084E 05	-44542.	29132.
1.00000E-06	-3.05672E 05	-48990.	32013.
1.10000E-06	-2.73523E 05	-53254.	34769.
1.20000E-06	-2.38760E 05	-57310.	37388.
1.30000E-06	-2.01520E 05	-61141.	39858.
1.30000E-06	-2.01520E 05	-61141.	39858.
1.40000E-06	-1.61928E 05	-64782.	42204.
1.50000E-06	-1.20162E 05	-68109.	44344.
1.60000E-06	-76387.	-71178.	46316.
1.70000E-06	-30777.	-73927.	48079.
1.80000E-06	16473.	-76410.	49669.
1.90000E-06	65194.	-78601.	51070.
2.00000E-06	1.15193E 05	-80482.	52269.
2.10000E-06	1.66273E 05	-82047.	53263.
2.20000E-06	2.18232E 05	-83284.	54047.
2.30000E-06	2.70861E 05	-84149.	54606.
2.40000E-06	3.23945E 05	-84757.	55120.
2.50000E-06	3.77235E 05	-84746.	56157.
2.60000E-06	4.30089E 05	-83026.	61869.
2.70000E-06	4.80807E 05	-77993.	82401.
2.80000E-06	5.27977E 05	-72293.	1.15178E 05
2.90000E-06	5.71674E 05	-66910.	1.49235E 05
3.00000E-06	6.12028E 05	-61616.	1.81210E 05
3.10000E-06	6.49063E 05	-56338.	2.10536E 05
3.20000E-06	6.82789E 05	-51090.	2.37065E 05
3.30000E-06	7.13226E 05	-45871.	2.60726E 05
3.40000E-06	7.40398E 05	-40696.	2.81491E 05
3.50000E-06	7.64334E 05	-35569.	2.99350E 05
3.60000E-06	7.85068E 05	-30505.	3.14320E 05
3.70000E-06	8.02642E 05	-25510.	3.26423E 05
3.70000E-06	8.02642E 05	-25510.	3.26423E 05
3.80000E-06	8.17090E 05	-20599.	3.35693E 05
3.90000E-06	8.28489E 05	-15761.	3.42188E 05
4.00000E-06	8.36885E 05	-11039.	3.45980E 05
4.10000E-06	8.42349E 05	-6431.3	3.47139E 05
4.20000E-06	8.44957E 05	-1943.3	3.45750E 05
4.30000E-06	8.44794E 05	2412.3	3.41893E 05
4.40000E-06	8.41927E 05	6634.5	3.35665E 05
4.50000E-06	8.36451E 05	10718.	3.27165E 05
4.60000E-06	8.28452E 05	14663.	3.16495E 05
4.70000E-06	8.18022E 05	18459.	3.03774E 05
4.80000E-06	8.05255E 05	22103.	2.89121E 05
4.90000E-06	7.90288E 05	25591.	2.72672E 05
5.00000E-06	7.73100E 05	28917.	2.54568E 05
5.00000E-06	7.73100E 05	28917.	2.54568E 05
5.10000E-06	7.53906E 05	32071.	2.34968E 05
5.20000E-06	7.32823E 05	34855.	2.14231E 05
5.30000E-06	7.09977E 05	37699.	1.92287E 05
5.40000E-06	6.85332E 05	40430.	1.69348E 05
5.50000E-06	6.59036E 05	42974.	1.45791E 05
5.60000E-06	6.31176E 05	45421.	1.21885E 05
5.70000E-06	6.01807E 05	47783.	98050.
5.80000E-06	5.70968E 05	50107.	74773.
5.90000E-06	5.38677E 05	52489.	52639.
6.00000E-06	5.04886E 05	54966.	32342.
6.10000E-06	4.69486E 05	57572.	14506.
6.20000E-06	4.32406E 05	60384.	-531.00
6.30000E-06	3.93528E 05	63306.	-12681.
6.40000E-06	3.52757E 05	66211.	-22277.
6.50000E-06	3.10142E 05	69089.	-29816.
6.60000E-06	2.65764E 05	71840.	-35724.
6.70000E-06	2.19727E 05	74393.	-40362.
6.80000E-06	1.72162E 05	76733.	-44034.
6.90000E-06	1.23216E 05	78821.	-46942.
7.00000E-06	73054.	80636.	-49237.
7.10000E-06	21854.	82159.	-51029.
7.20000E-06	-30195.	83378.	-52396.
7.30000E-06	-82903.	84275.	-53388.
7.40000E-06	-1.36055E 05	84829.	-54033.
7.50000E-06	-1.89457E 05	85155.	-54454.
7.60000E-06	-2.42935E 05	85055.	-54533.
7.70000E-06	-2.96184E 05	84444.	-54235.
7.80000E-06	-3.48635E 05	82046.	-52722.
7.90000E-06	-3.97888E 05	72952.	-46751.
8.00000E-06	-4.38389E 05	55109.	-35000.
8.10000E-06	-4.67191E 05	37211.	-23276.
8.20000E-06	-4.86048E 05	23696.	-14504.
8.30000E-06	-4.97845E 05	14527.	-8625.6
8.40000E-06	-5.04945E 05	8625.4	-4901.3
8.50000E-06	-5.08994E 05	4718.3	-2475.3
8.60000E-06	-5.11093E 05	2240.6	-969.81
8.70000E-06	-5.11916E 05	567.69	29.313
8.80000E-06	-5.11876E 05	-578.00	708.44
8.90000E-06	-5.11221E 05	-1361.6	1156.4
9.00000E-06	-5.10141E 05	-2049.4	1556.0
9.10000E-06	-5.08671E 05	-2550.8	1844.8
9.20000E-06	-5.06868E 05	-3082.8	2163.1
9.30000E-06	-5.04744E 05	-3558.2	2458.3
9.40000E-06	-5.02296E 05	-4104.3	2796.6
9.50000E-06	-4.99491E 05	-4709.1	3178.8
9.60000E-06	-4.96267E 05	-5405.1	3623.9
9.70000E-06	-4.92581E 05	-6329.2	4210.2
9.80000E-06	-4.88264E 05	-7371.9	4890.1
9.90000E-06	-4.83215E 05	-8635.3	5714.9
1.00000E-05	-4.77259E 05	-10279.	6789.9

(d) VO, VF, and VBE1 at 100 KHz.

Figure 54 (continued)

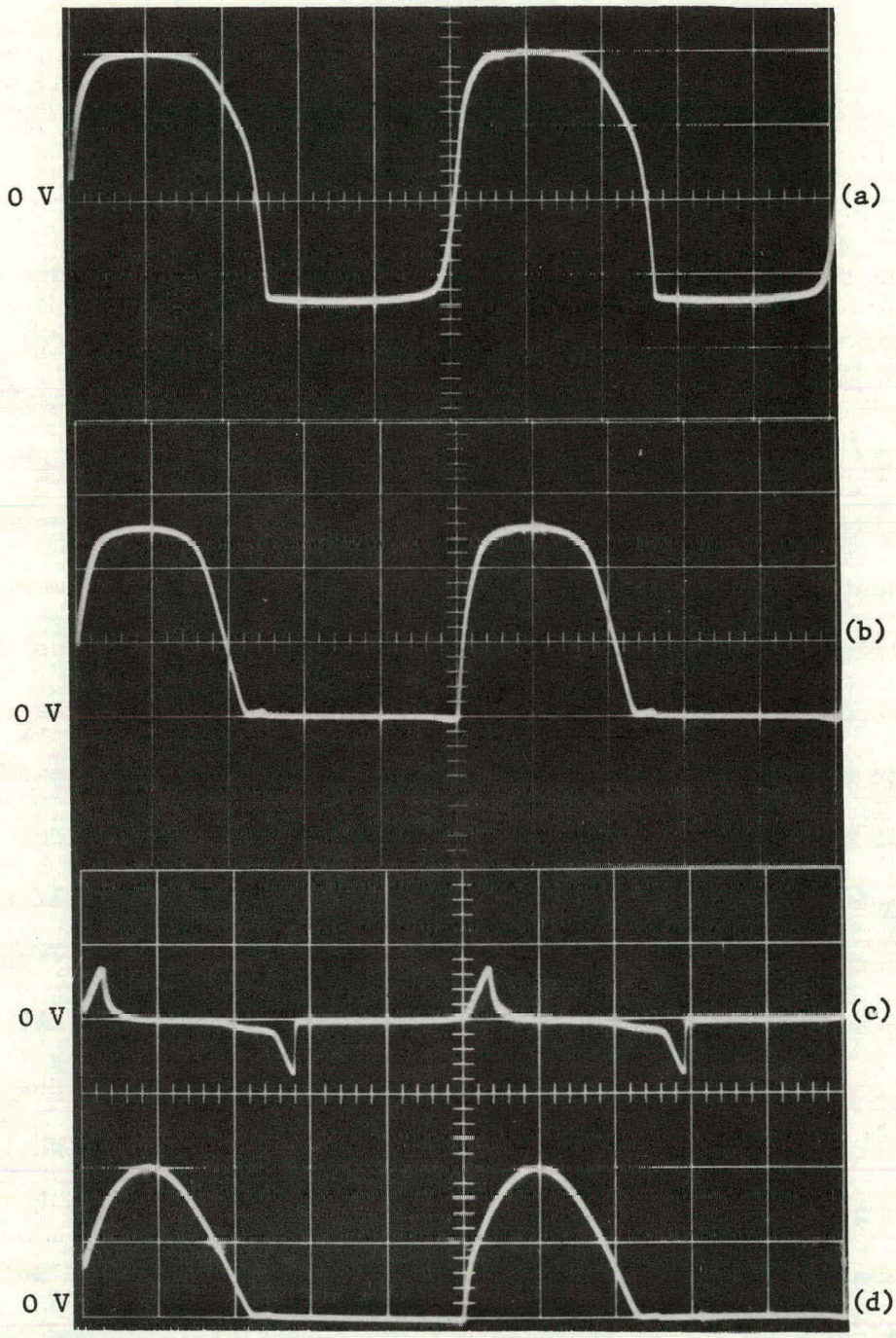

Figure 55. Experimental 10 KHz waveforms of a Darlington 2N5087 transistor rectifier with $R_1 = R_2 = 0\Omega$, $R_3 = 2\ K\Omega$, $C_3 = 0.15\ \mu F$, $R = 14.7\ K\Omega$, $V_{inp} = 0.1$ V, and an AD506LH opamp. (a) $\overline{V_f} - V_o$; (b) $\overline{V_f} - V_{BE1}$; (c) $\overline{V_f} - V_f$; (d) V_{IF1RF}. Horizontal scale: 20 μs/div. Vertical scale: 0.5 V/div [curve (a)]; 0.2 V/div [curve (b)]; 0.05 V/div [curves (c) and (d)].

III. PRACTICAL ACCURACY LIMITATIONS OF PRECISION RECTIFIER CIRCUITS

In addition to the fundamental accuracy limitations discussed in the preceding section, other accuracy limitations include electronic component noise, DC offset, amplifier gain stability and linearity, and passive component drift. These limitations tend to be less severe with transistor rectifiers.

Electronic Component Noise

Electronic component noise cannot be treated in the same manner as narrow-band input noise (see page 73) because narrow-band approximations are invalid for the broad-band noise of electrical components. To analyze such noise, the equivalent noise sources are shown in Figure 56 for both diode and transistor rectifier circuits. Unless stated otherwise, all noise sources will be considered as white. Resistive noise sources are Johnson noise and are given by Equation (19) on page 31. $\overline{i_c^2}$, $\overline{i_b^2}$, and $\overline{i_D^2}$ are shot noises given by

$$\overline{i_c^2} = 2\,q\,\overline{I_c}\,,$$

$$\overline{i_b^2} = 2\,q\,\overline{I_B}\,, \tag{212}$$

and

$$\overline{i_D^2} = 2\,q\,\overline{I_D}\,,$$

where q is the magnitude of the charge of an electron. Chenette's three noise source model is used to simulate bipolar transistor noise.[71]

In the analysis of rectifier noise, the assumption that the opamp open-loop gain is infinite and the common-base current gain (α) is

ORNL-DWG 76-19160

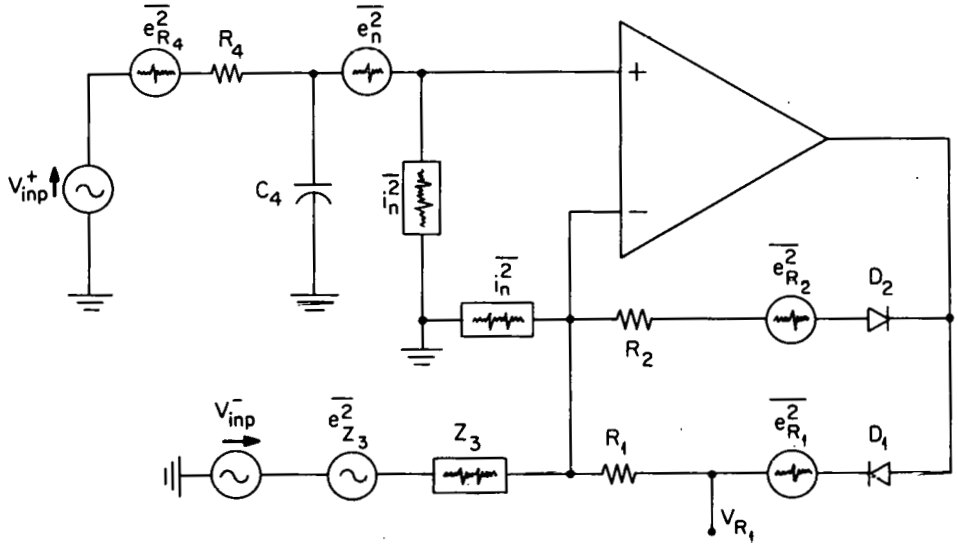

(a) Diode rectifier.

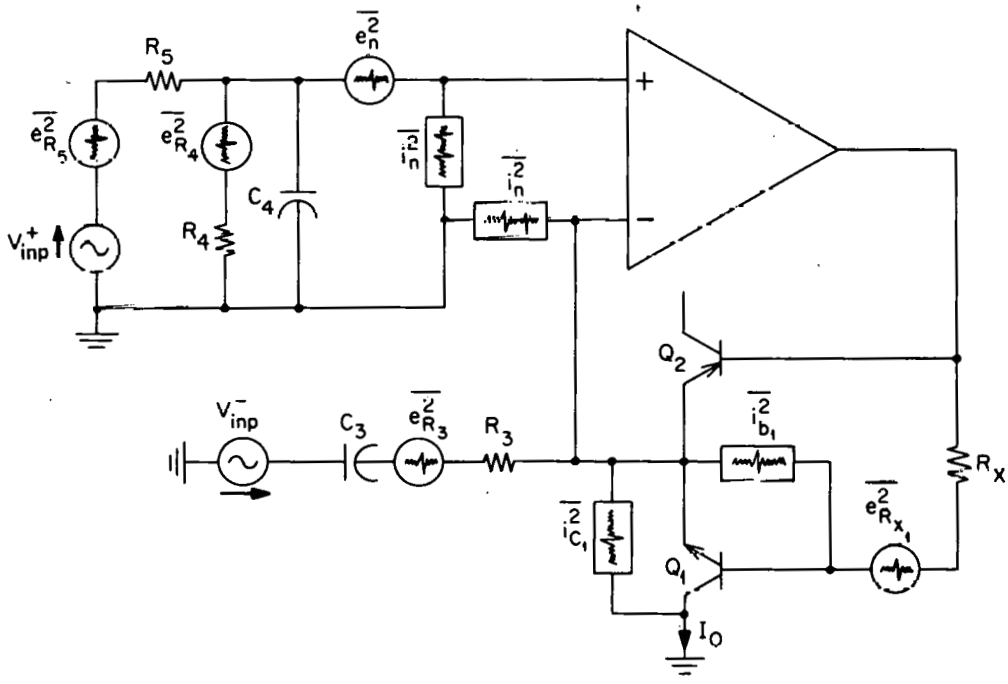

(b) Transistor rectifier.

Figure 56. Circuits used for noise analysis of rectifiers.

independent of I_c will be made; i.e., rectification is essentially perfect. Thomas[22] has shown that for a perfect half-wave rectifier

$$R_y(\tau) = C^2 \left[\frac{R_x(\tau)}{4} + \frac{R_x(0)}{2\pi} \left[\frac{R_x(\tau)}{R_x(0)} \sin^{-1} \left(\frac{R_x(\tau)}{R_x(0)}\right) + \left(1 - \left(\frac{R_x(\tau)}{R_x(0)}\right)^2\right)^{1/2}\right]\right], \tag{213}$$

where $R_x(\tau)$ and $R_y(\tau)$ are the autocorrelation functions of the rectifier input and output, respectively, and C is the rectifier gain. Note that the above expression is valid only for a stationary gaussian input. Since $R_g(0) = \overline{g^2}$, Equation (213) gives the noise gain as $C^2/4$. Fortunately, the power gain of a half-wave rectifier for a sinusoidal input is also $C^2/4$. Therefore, the output noise of a diode rectifier is

$$\overline{e_{n1}^2} \simeq \frac{R1^2}{4} \left[\overline{i_n^2} + \frac{\overline{e_{R1}^2}}{R_1^2} + \frac{R_1^2\, \overline{e_{R3}^2} + (R_3 + Z_3)^2 [Z_4^2\, \overline{i_n^2} + \overline{e_n^2} + \overline{e_{Z4}^2}]}{R_1^2 Z_3^2}\right], \tag{214}$$

if diode shot noise is neglected and the noise sources are uncorrelated. To include the diode noise requires the solution of transcendental equations. Note that the thermal noise of R_1 is not rectified, hence it is not multiplied by 1/4 in Equation (214). The signal output is

$$\overline{V_{R1}^2} = \frac{1}{4}\left((V_{inp}^+)^2 \left(\frac{R_1 + Z_3}{Z_3}\right)^2 + (V_{inp}^-)^2 \left(\frac{R_1}{Z_3}\right)^2 + 2\gamma\, V_{inp}^+\, V_{inp}^- \left|\left(\frac{R_1 + Z_3}{Z_3}\right) \cdot \frac{R_1}{Z_3}\right|\right), \tag{215}$$

where γ is the correlation coefficient between V^+_{inp} and V^-_{inp}. The presence of signal and noise together will affect the results; nevertheless, the ratio of $\overline{V^2_{R1}}$ to $\overline{e^2_{n1}}$ as given by Equations (214) and (215) can be used to estimate the signal-to-noise ratio of the detector.

The transistor rectifier noise and signal performance is particularly interesting. The output noise current is

$$\overline{i^2_{no}} \simeq \frac{(C_3\ \omega\ \alpha_1)^2}{1 + T_3{}^2\omega^2} \left[\frac{\left(\frac{R_4}{R_4 + R_5}\right)^2 (\overline{e^2_{ns}} + R_5^2\ \overline{i^2_n}) + 4KT(R_4||R_5)}{4(1 + (T\ \omega)^2)} + \frac{\overline{e^2_n} + \overline{e^2_{R3}}}{4} \right] + \left(\frac{\overline{i^2_n}}{4} + \overline{i^2_{b1}}\right) \alpha_1{}^2 + \overline{i^2_{c1}}(HFE + 1)^{-2} \tag{216}$$

where $T_3 = R_3\ C_3$, $T = (R_4||R_5)\ C_4$, and the base-spreading resistance (r_x) of Q1 is assumed zero (i.e., $\overline{e^2_{r_x}} = 0$). Note that $\overline{i^2_{c1}}$ and $\overline{i^2_{b1}}$ are signal dependent; i.e., they are proportional to $\overline{I_o}$. The signal output is

$$\overline{I^2_o} = 1/4 \frac{(\alpha_1\ C_3\omega_o)^2}{(1 + (T_3\omega_o)^2)} \left(V^-_{inp}{}^2 + V^+_{inp}{}^2 \left(\frac{R_4}{R_4 + R_5}\right)^2 (1 + (T\ \omega_o)^2)^{-1}\right)$$

$$+ \frac{\gamma V^+_{inp}\ V^-_{inp}}{2} \left(\frac{R_4}{R_4 + R_5}\right) \frac{\alpha_1{}^2 (C_3\omega)^2}{(1 + (T_3\omega_o)^2)(1 + (T\ \omega_o{}^2)^{1/2}} . \tag{217}$$

Inspection of Equation (216) shows that although the transistor rectifier is sensitive to power supply noise ($\overline{e^2_{ns}}$), the noise is easily suppressed since the transfer function is a band-pass filter. For example if C_4 = 82 μF, R_4 = 10 KΩ, R_5 = 4 KΩ, R_3 = 2 KΩ, and C_3 = 0.15 μF (as used

in the Oak Ridge apparatus); then $T_4 = 0.23$ sec and $T_3 = 0.3$ msec. The noise spectrum is attenuated by 60 dB relative to V^-_{in} at midband of the band-pass filter, and the filter has corner frequencies of 0.69 and 690 Hz.

To compare the noise performance of these two types of rectifiers, assume that $V^+_{inp} = 0$. Then the signal-to-noise ratio of the diode rectifier as obtained from Equations (214) and (215) is

$$\frac{S}{N} \simeq \frac{V_{R1}^2}{\int_0^{\Delta f_n} \overline{e_{n1}^2}\, df} \simeq \frac{[C_3\omega_o V^-_{inp}]^2}{[1+(T_3\omega_o)^2]} \Bigg/ \Bigg((\overline{i_n^2} + 4KTR_1)\Delta f_n + \int_0^{\Delta f_n} \frac{(R_1C_3\omega)^2\, 4KTR_3 + [(R_1+R_3)^2(C_3\omega)^2+1]\left(\overline{e_n^2} + \frac{4KTR_4 + R_4^2\, \overline{i_n^2}}{1+(T_4\omega)^2}\right)}{R_1^2(1+(T_3\omega)^2)}\, df \Bigg) \tag{218}$$

where Δf is the noise bandwidth of the measurement system which is assumed much less than the closed-loop bandwidth of the rectifier circuit, Z_3 is the series combination of R_3 and C_3, Z_4 is the parallel combination of R_4 and C_4, and $T_4 = R_4C_4$. The signal-to-noise ratio of the transistor rectifier as obtained from Equations (216) and (217) is

$$\frac{S}{N} \simeq \frac{\overline{I_o^2}}{\int_0^{\Delta f_n} \overline{i_{no}^2}\, df} \simeq \frac{V^-_{inp}\, C_3\omega_o)^2}{(1+(T_3\omega_o)^2)} \Bigg/ \Bigg(\left(\overline{i_n^2} + \frac{8Q\, V^-_{inp}C_3\omega_o}{\pi\sqrt{1+(T_3\omega_o)^2}\, HFE}\right)\Delta f_n + \int_0^{\Delta f_n} \left(\frac{(C_3\omega)^2}{1+(T_3\omega)^2}\right)\left(\overline{e_n^2} + 4KTR_3 + \frac{4KT(R_4||R_5) + (\frac{R_4}{R_4+R_5})^2(\overline{e_{ns}^2}+R_5^2\, \overline{i_n^2})}{1 + T^2\omega^2}\right) df \Bigg) \tag{219}$$

or neglecting the noise contributed by Q1 and assuming $R_5 >> R_4$,

$$\frac{S}{N} \simeq \frac{\bar{V}_{inp}^{2}(C_3\omega_o)^2}{(1+(T_3\omega_o)^2)} \Bigg/ \left[\overline{i_n^2}\,\Delta f_n + \int_0^{\Delta f_n}\left(\frac{(C_3\omega)^2}{1+(T_3\omega)^2}\right)\left(\overline{e_n^2} + 4KTR_3 + \frac{4KTR_4+R_4^2\,\overline{i_n^2}}{1+(T_4\omega)^2}\right)df\right] \tag{220}$$

Comparing expressions (218) with (220) indicates that the transistor rectifier has potentially higher S/N since it has no thermal noise due to R_1 and the noise due to $\overline{e_n^2}$ and R_4 is reduced by a factor of $(R_1C_3\omega)^2/(1 + (R_1+R_3)^2(C_3\omega)^2)$. Note that since the feedback controls the emitter current of Q1, the noise currents $\overline{i_{c1}^2}$ and $\overline{i_{b1}^2}$ must go through the emitter of Q1. Therefore, $\overline{i_{c1}^2}$ circulates largely within Q1, thereby reducing the output noise current due to $\overline{i_{c1}^2}$ by $(HFE1 + 1)^{-1}$. This indicates that the inferior low-frequency noise of MOSFET devices will largely be cancelled by negative feedback in the circuit shown in Figure 21(f) on page 91.

The accuracy of a rectifier can influence the output noise of the rectifier. Since practical rectifier circuits usually have a dead-band (i.e., a range of input signals to which there is essentially on output response) signals below a threshold level yield rectifier outputs significantly less than the ideal level. If the dead-band is greater than the input noise to the rectifier, the noise output will be reduced. But if a signal greater than the dead-band is also applied to the rectifier input, rectifier accuracy will improve; hence, the output noise will increase.

This noise threshold effect was observed by the author when measuring the linearity of the rectifier bridge detector. For instance,

with both Darlington rectifiers in Figure 47(b) on page 213 employing AD528JH opamps and no R, the peak-to-peak variation in DVM readings increased from 60 μV for $V_{inp} = 0$, to a constant 200 μV for V_{inp} between 10 mV and 8 V. When using AD506LH opamps, the peak-to-peak variation was less than 14 μV for inputs below 15 mV_p but increased to 400 μV with peak inputs between 20 mV and 70 mV and to 300 μV for peak input signals from 140 mV to 750 mV. Since the noise threshold is lower for the AD528JH opamp (below 10 mV), which has approximately twenty times more gain at the input frequency of 1 KHz, this verifies the hypothesis that the lower the dead-band, the lower the noise threshold.

DC Offset

An important benefit of the transistor rectifier is in its lower DC offset. Using the terminology of Figure 56 on page 236, the DC offset of the opamp will be multiplied by $(R_1 + R_3)/R_1$ unless C_3 is included, in which case the DC offset passes directly to the output. But in the transistor rectifier, the DC offset gain is the same as the signal gain $(1/R_3)$ unless C_3 is included, in which case the DC offset gain is zero. Assume that the input bias currents are I_B^+ and I_B^- at noninverting and inverting inputs of the opamp, respectively. Then, for a diode rectifier, the offset induced by input bias currents is

$$V_{Rloff} = (R_4\ I_B^+ - R_1||R_3\ I_B^-)\left(\frac{R_1 + R_3}{R_3}\right) \tag{221}$$

or if C_3 is included,

$$V_{Rloff} = R_4\ I_B^+ - R_1\ I_B^- .$$

Similarly, the offset induced by input bias currents for transistor rectifier is

$$I_{o_{off}} = -\frac{R_4}{R_3} I_B^+ + I_B^-$$

or if C_3 is included, (222)

$$I_{o_{off}} = + I_B^- .$$

Note that if I_B^+ and I_B^- thermally track each other, the offset due to input bias currents can be set to zero by appropriate choices of R_4, except for the case where C_3 is included in a transistor rectifier. A good opamp for the transistor rectifier is the opamp with an FET input stage since I_B is very small ($\sim$ pA). The higher offset voltage typical of FET opamps is not important with transistor rectifiers with C_3.

Another cause of DC offset is I_{CBO} of the transistor with transistor rectifiers. This is minimized by choosing transistors with low I_{CBO}. Transistors with $I_{CBO} < 10$ nA are available. Since the offset current due to I_{CBO} is I_{CBO} itself, the offset due to a Darlington transistor is the sum of I_{CBO}'s of the two transistors.

Passive Component Drift

Since the passive components largely determine the rectifier gain, it is important to choose stable components such as bulk metal or wire-wound (noninductive) resistors. Assuming infinite opamp gain, the output of a diode rectifier is

$$V_{R1} = V_{inp}^+ \left(\frac{R_1 + Z_3}{Z_3}\right) - V_{inp}^- \frac{R_1}{Z_3}$$

while the output of a transistor rectifier is (223)

$$I_0 = -(V^+_{inp} - V^-_{inp})\alpha_1/Z_3$$

regardless of R_1 or R_2. Since the positive and negative gains are identical in magnitude for the transistor rectifier, forming a fullwave rectifier is simplified. While a diode fullwave rectifier normally requires the matching of at least three resistors, a transistor fullwave rectifier requires matching of only two resistors to insure symmetry. In fact, if a current mirror is employed with the transistor rectifier, no resistor matching is necessary for a fullwave rectifier. Another advantage of the transistor rectifier is that a balanced line can be connected directly to the inputs without the need for an instrumentation amplifier or transformer. Additionally, the common mode rejection is independent of passive components. Furthermore, the + input is high impedance. The current output facilitates summation of rectifier outputs since the outputs can be directly connected to the current summing input of an opamp with shunt feedback without the need for additional summing resistors. Clearly, the gain flexibility of the transistor rectifier is one of its strongest advantages.

Gain Stability and Linearity

While the sensitivity of both types of rectifiers to gain stability and linearity is similar, the opamp gain stability and linearity can be improved using a transistor rectifier. The sensitivity of rectifier gain to opamp gain is $(1 + A\,(\frac{Z_3}{R_1 + Z_3}))^{-1}$. Since R1 can be made zero, the transistor rectifier can have a lower sensitivity with internally compensated opamps. The opamp gain drift is less with a transistor rectifier because the opamp drives the high impedance load of a

transistor instead of R_1 and R_2. The low current output together with the low voltage swing makes the power dissipation of the opamp minimal. This low power dissipation results in a more uniform temperature of the opamp with low signal dependence of open-loop gain due to thermal feedback. This lowering of thermal feedback substantially reduces low-frequency distortion of the open-loop gain. Thermal feedback can cause distortion due to the temperature dependence of the opamp gain.[68,69] Typically, thermal feedback distortion becomes significant for frequencies below 100 Hz.

The low current drain of the transistor rectifier can also improve amplifier accuracy at all frequencies by reducing or eliminating crossover distortion. Most modern opamps have class AB output stages. If the load current is less than the bias current of the output stage, the output stage will operate in class A mode.

Load current is minimized by choosing high H_{FE} transistors or MOSFET's with low capacitances. The capacitance current is important during the switching time.

As mentioned earlier, settling time and slew rate limit of the opamp is important to high frequency performance. Figures 57 and 58 illustrate the effects of reducing settling time from 2 μsec to 800 nsec on the 100 KHz waveforms of a Darlington transistor rectifier. Note that reducing the settling time improves the output waveforms only slightly for both R = 14.7 KΩ and no R as opposed to the substantial effect on a diode rectifier (see Figure 31 on page 149). Note that settling time is also a measure of the overshoot behavior of an opamp, whether there is slewing or not. For both types of rectifiers, the question of whether or not an opamp will slew is complicated by the device capacitances.

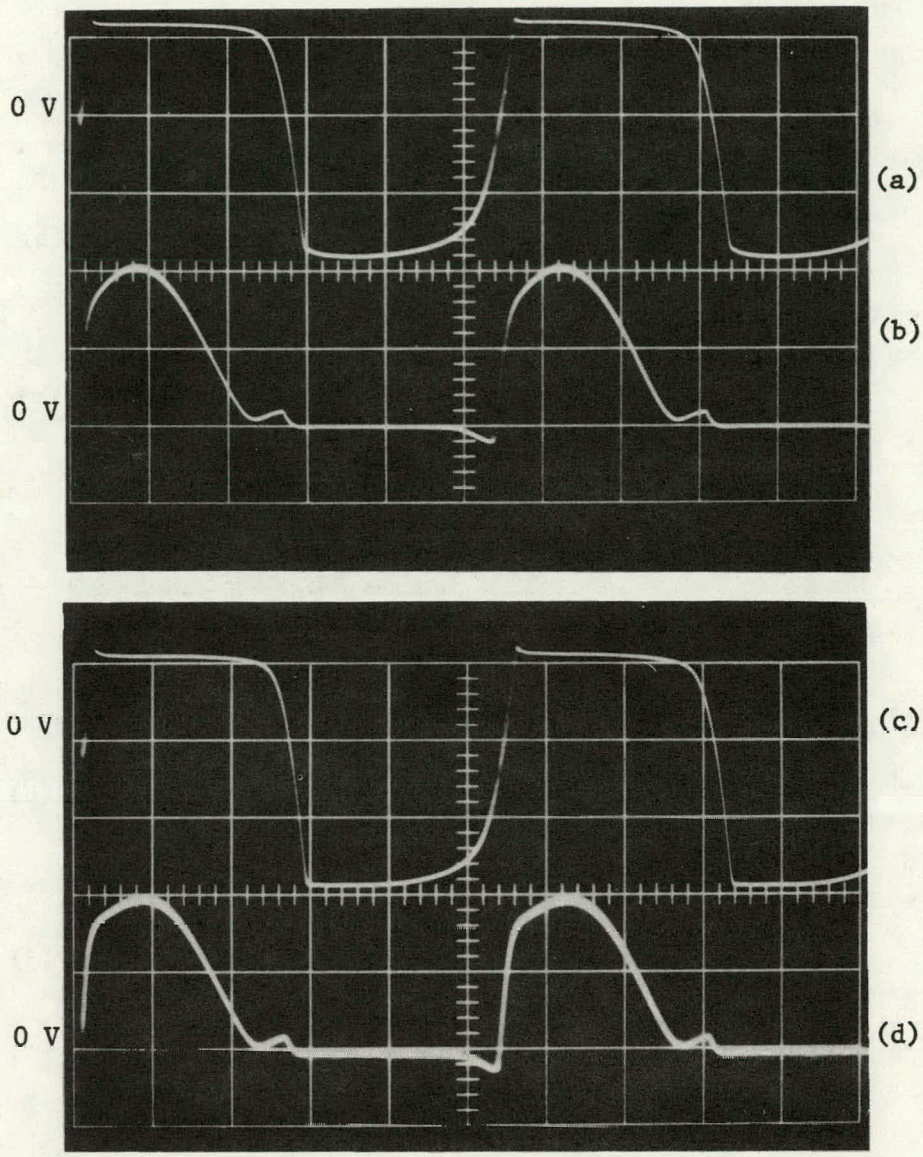

Figure 57. Effects of opamp settling time on 0.1 V_p 100 KHz waveforms of a 2N5087 Darlington transistor rectifier with R_3 = 2 KΩ, C_3 = 0.15 μF, no R, and an AD528JH opamp. (a) $V_o - \overline{V_f}$ with settling time compensation; (b) V_{IF1RF} with settling time compensation; (c) $V_o - \overline{V_f}$ without settling time compensation; (d) V_{IF1RF} without settling time compensation. Typical settling time to 0.1%: 800 ns [curves (a) and (b)]; 2 μs [curves (c) and (d)]. Horizontal scale: 2 μs/div. Vertical scale: 0.5 V/div [curves (a) and (c)]; 0.05 V/div [curves (b) and (d)].

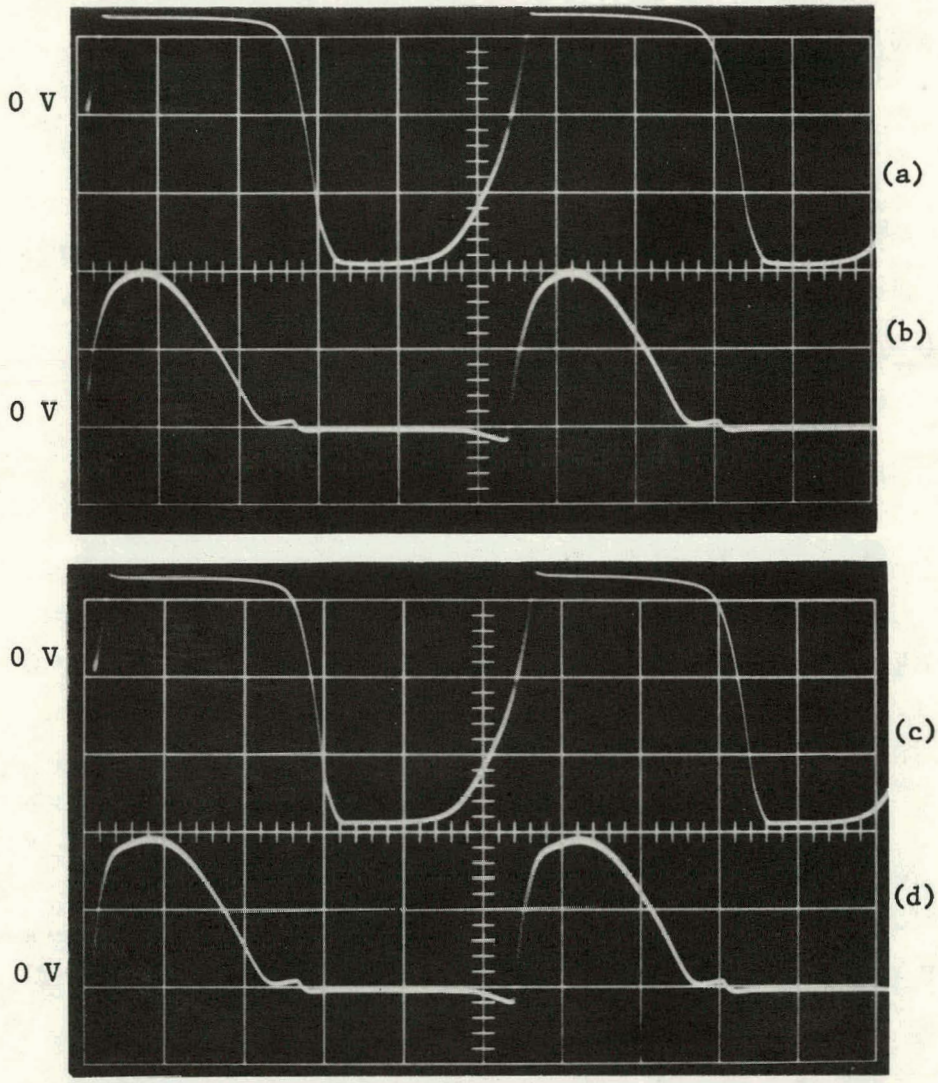

Figure 58. Effects of opamp settling time on 0.1 V_p 100 KHz waveforms of a 2N5087 Darlington transistor rectifier with R_3 = 2 KΩ, C_3 = 0.15 μF, R = 14.7 KΩ, and an AD528JH opamp. (a) $V_o - \overline{V_f}$ with settling time compensation; (b) V_{IF1RF} with settling time compensation; (c) $V_o - \overline{V_f}$ without settling time compensation; (d) V_{IF1RF} without settling time compensation. Typical settling time to 0.1%: 800 ns [curves (a) and (b)]; 2 μs [curves (c) and (d)]. Horizontal scale factor: 2 μs/div. Vertical scale: 0.5 V/div [curves (a) and (c)]; 0.05 V/div [curves (b) and (d)].

Whereas the calculations on page 139 can predict whether an opamp will slew if the capacitances are neglected, the capacitances can actually prevent slewing.

Slewing conditions with device capacitance can be determined for a single pole opamp in the following manner. Assume that both diodes or transistors are off. Then the Fourier transform of the output of the opamp ($\hat{V}_o(j\omega)$) is

$$\hat{V}_o(j\omega) = \frac{-\hat{V}_{in}(j\omega)\ A(j\omega)\ B(j\omega)}{(1 + A(j\omega)\ B(j\omega))\ T_3\ j\omega}\ , \tag{224}$$

where $A(j\omega)$ is the transfer function of the opamp, $B(j\omega)$ is $T_3\ j\omega/(1 + T_3\ j\omega)$, $\hat{V}_{in}(j\omega)$ is the Fourier transform of the input signal, and T_3 is $R_3\ C_{BE}$. If $V_{in}(t)$ is $V_{inp}\ \sin\omega_o t$, then Equation (224) gives $V_o(t)$ as follows:

$$V_o(t) = \frac{-A_{o1}\ V_{inp}\ \sin(\omega_o t + \theta_o)}{\sqrt{(1 + T_3\ T_{o1}\omega_o^2)^2 + \omega_o^2\ (T_3\ (1 + A_{o1}) + T_{o1})^2}}\ ,$$

where (225)

$$\theta_o = -\tan^{-1}\left(\frac{\omega_o(T_3\ (1 + A_{o1}) + T_{o1})}{1 + T_3\ T_{o1}\omega_o^2}\right)\ .$$

Therefore $\dot{V}_o(t)$ is given by

$$\dot{V}_o(t) = \frac{-\omega_o A_{o1}\ V_{inp}\ \cos(\omega_o t + \theta_o)}{\sqrt{(1 + T_3\ T_{o1}\omega_o^2)^2 + \omega_o^2(T_3\ (1 + A_{o1}) + T_{o1})^2}}\ . \tag{226}$$

$\dot{V}_o$ where $V_o = V_f$ is easily found by noting that

$$V_f = -\frac{V_o + T_{o1}\ \dot{V}_o}{A_{o1}}\ . \tag{227}$$

Substituting $V_f = V_o$ and Equations (225) and (226) into Equation (227) yields

$$\omega_o t + \theta_o = -\tan^{-1}\left(\frac{\omega_o T_{o1}}{A_{o1} + 1}\right) . \tag{228}$$

Using the identity $\cos\phi = (1 + \tan^2\phi)^{-1/2}$, Equation (228) can be utilized with Equation (226) to compute $\dot{V}_o(t)$ as

$$\dot{V}_o(t)\Big|_{V_o=V_f} = -V_{inp} A_{o1}\omega_o(A_{o1} + 1) \Big/ \sqrt{(A_{o1} + 1)^2 + \omega_o^2 T_{o1}^2}\sqrt{(1 + T_3 T_{o1}\omega_o^2)^2 + \omega_o^2(T_3(1 + A_{o1}) + T_{o1})^2} . \tag{229}$$

Equation (229) shows that there is a frequency at which $|\dot{V}_o(t)|$ is maximum. If $\omega_o << 2\pi$ GBWP and $A_{o1} >> 1$, then expression (229) may be approximated by

$$\dot{V}_o(t)\Big|_{V_o=V_f} \simeq -\frac{-V_{inp} A_{o1} \omega_o}{\sqrt{1 + \omega_o^2(T_3 (1 + A_{o1}) + T_{o1})^2}} , \tag{230}$$

or the minimum SR of the opamp if slewing is to be prevented is

$$SR \simeq V_{inp} A_{o1}/(T_3 (1 + A_{o1}) + T_{o1}) . \tag{231}$$

Comparing the above equations to Equation (187) on page 143 shows that the device capacitance increases the slew-free input voltage by $\sqrt{(1 + \omega_o(T_3 (1 + A_{o1}) + T_{o1})^2} / \sqrt{1 + (\omega_o T_{o1})^2}$.

CHAPTER V

THE TEMPERATURE CONTROL SYSTEM

I. HOW THE CONTROL SYSTEM FUNCTIONS

The temperature control system designed for the Oak Ridge irradiation creep experiment is a partially linearized, three-mode control system employing a modified AC Kelvin bridge to measure sample resistance (see Figure 12 on page 56) and a phase-insensitive averaging detector. A block diagram of the system is drawn in Figure 59. In this system, the 1 KHz heating current (THD < 0.6%) functions as the measurement current to maximize the S/N. The two bridge signals (V_R and V_s) pass through two instrumentation amplifiers (each formed with two sections of a Raytheon RC4136 quad opamp) having common-mode rejection ratios greater than 105 dB at 1 KHz (typically 110 dB) to prevent ground loop noise. The remaining noise is filtered by mains rejection notch filters (60 Hz) and second-order 1 KHz band-pass filters with Q=3.54. The filtered signals are passed through precision half-wave rectifiers (Darlington 2N5087 and 2N5089 transistors with AD528JH opamps). Since the two rectifiers are complementary (one has a positive DC output while the other a negative DC output), the current outputs are summed by an opamp with shunt feedback. This opamp also functions as a single pole low-pass filter. An active second-order low-pass filter further reduces the ripple of the error signal.

Figure 60 pictures the temperature control system. On the front panel are located the following controls:

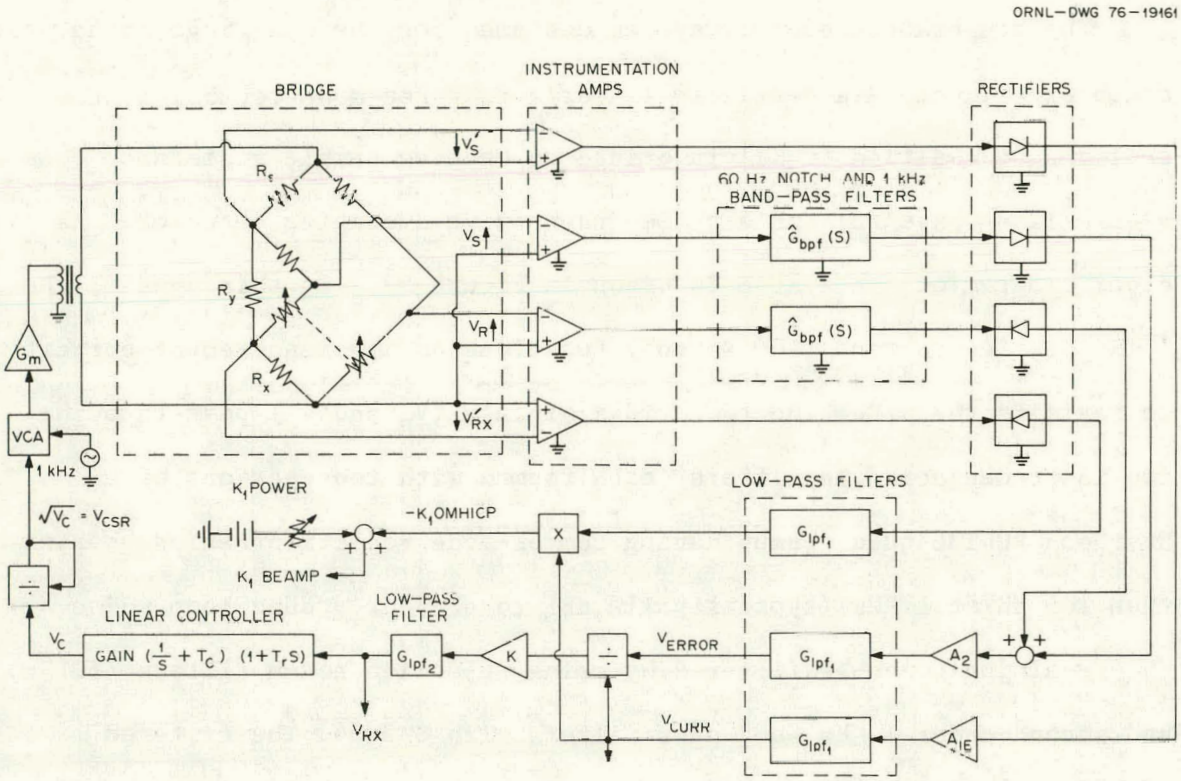

Figure 59. Block diagram of temperature control system.

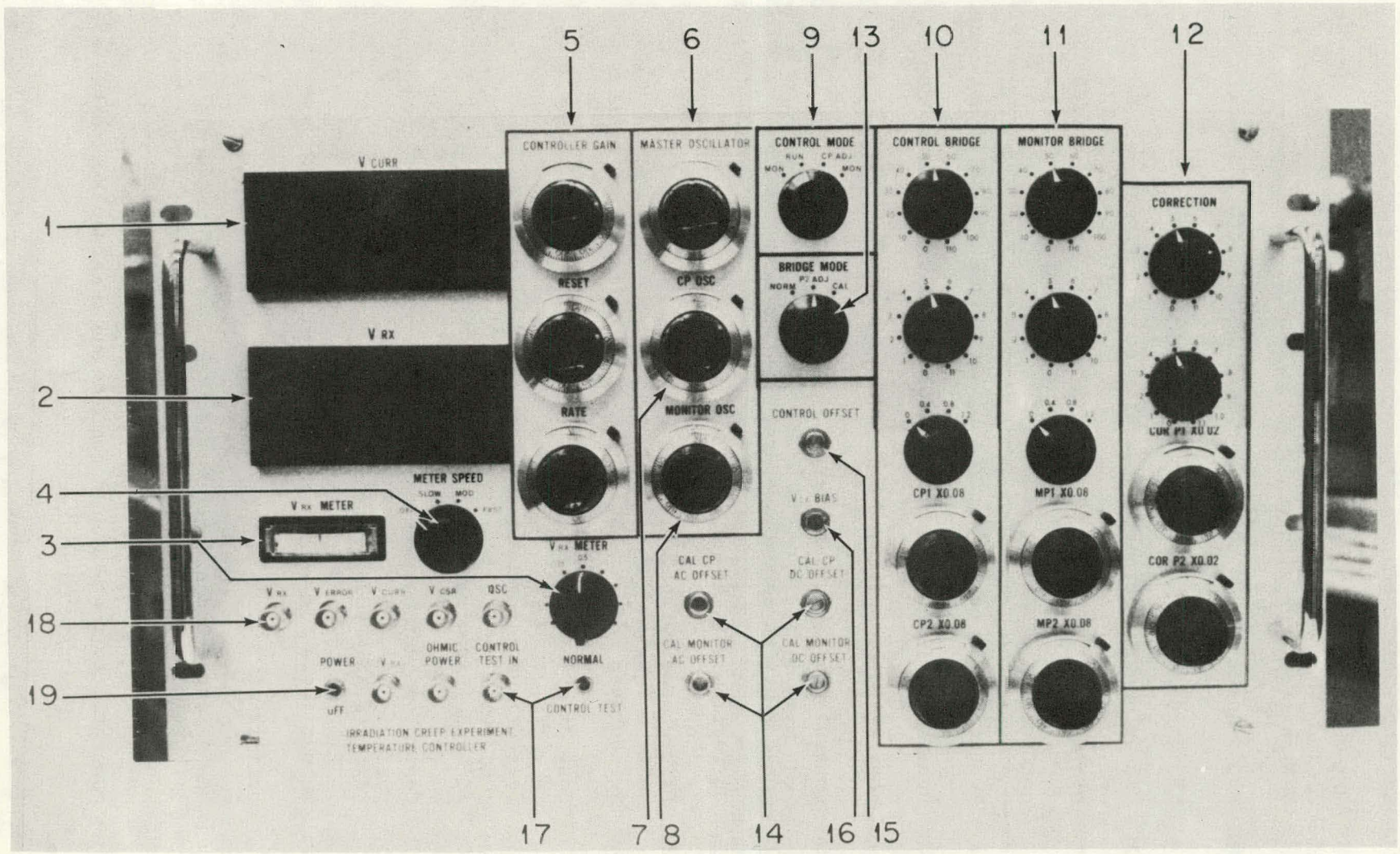

Figure 60. Front panel of temperature controller.

1. Current monitor DPM,
2. VRX monitor DPM,
3. VRX analog meter with scale factor switch,
4. Meter speed switch to average readings of both VRX meters for measuring noisy signals,
5. Linear control parameters adjustment potentiometers,
6. Master oscillator output control to limit heating current in control and CP adjust mode,
7. CP oscillator output control to set current in CP adjust mode,
8. Monitor oscillator output control to set monitor current,
9. Mode selector switch,
10. Control bridge potentiometers,
11. Monitor bridge potentiometers,
12. Correction potentiometers,
13. Bridge mode switch,
14. Screwdriver adjustments for AC and DC offsets for monitor and control bridge detectors,
15. Screwdriver adjustment for controller offset,
16. VCA bias screwdriver adjustment,
17. Control adjustment switch to connect external input to simulate beam power perturbations,
18. Output jacks for monitoring VRX, VERROR, VCURR, VC, and oscillator.

The mode selector and bridge mode switches are of particular interest. When the mode selector switch is in monitor mode, the monitor bridge is connected to the bridge detectors and a manually adjustable

current less than 1 A (adjusted via the monitor oscillator potentiometer) is delivered to the sample. Also the gain of the instrumentation amplifiers is increased and the gain of the summing amplifier is decreased by the same factor to maintain a constant scale factor on VRX (within 1%), while simultaneously increasing the signal level at the rectifiers to improve linearity. When in the CP ADJ mode, the current may be adjusted by both the master and CP oscillator controls. Also the control bridge is connected to the bridge detectors. The bridge mode switch is employed to balance the two arms of the Kelvin bridge via MP2 and CP2. The CAL position shorts the bridge error signal to zero so that the rectifier gains and offsets may be adjusted. Note that for the temperature controller to control the specimen temperature, both controller mode and bridge mode switches must be in RUN and NORMAL positions respectively. If the bridge mode switch is not in NORMAL mode then VC is held close to zero to prevent uncontrolled heating currents. Likewise, VC is held close to zero unless controller is in run mode to improve turn on behavior.

RXSET may be read directly from the bridge potentiometers as the sum of the control potentiometers excluding CP2 (CP) plus the correction potentiometers excluding COR P2 (CORRP). CP + CORRP can be used to obtain RX within 0.02% via the following expression:

$$RX = RS\ (CP + CORRP)/100.00\ . \tag{232}$$

Similarly, the monitor value of RX is obtained via the following expression:

$$RX = RS\ (MP + CORRP)/100.00\ . \tag{233}$$

Initially, V_{error} was employed as the controlled signal; however, V_{error} is proportional to the product of heating current and the deviation of sample resistance from set point (ΔR_x). The system is highly nonlinear, i.e., the loop gain is proportional to the heating current, thereby causing the system to have very poor transient characteristics. To linearize the system, V_{error} must be divided by a signal proportional to the average magnitude of the heating current. This is accomplished by measuring the voltage drop across the standard resistor (R_s) with an instrumentation amplifier whose output is rectified and filtered identically to V_{error} (V_{curr}). A precision two-quadrant divider (AD436B) is employed to take the quotient of V_{error}/V_{curr}. This quotient is filtered further to reduce noise and ripple (V_{R_x}) and is proportional to ΔR_x.

The error signal, V_{R_x}, is fed to a three-mode controller. This controller has integration (or reset action), proportional gain, and rate action. That is, the output of the controller is (ideally) given by the sum of $\int_0^t V_{R_x}\,dT$, V_{R_x}, and $\frac{d\,V_{R_x}}{dt}$, each term multiplied by adjustable constants. The frequency response of such a controller is depicted in Figure 61. The integration insures that the average value of V_{R_x} is zero. The proportional gain is adjusted so that the zero (T_c) is approximately equal to the dominant thermal pole of the specimen (T_t). The rate action can be used to cancel other poles in the system or compensate for delays. However, it was found experimentally, that rate action in this system is unnecessary.

The output of the linear controller is passed through a square-root circuit to linearize the system. This linearized control voltage (V_{cl})

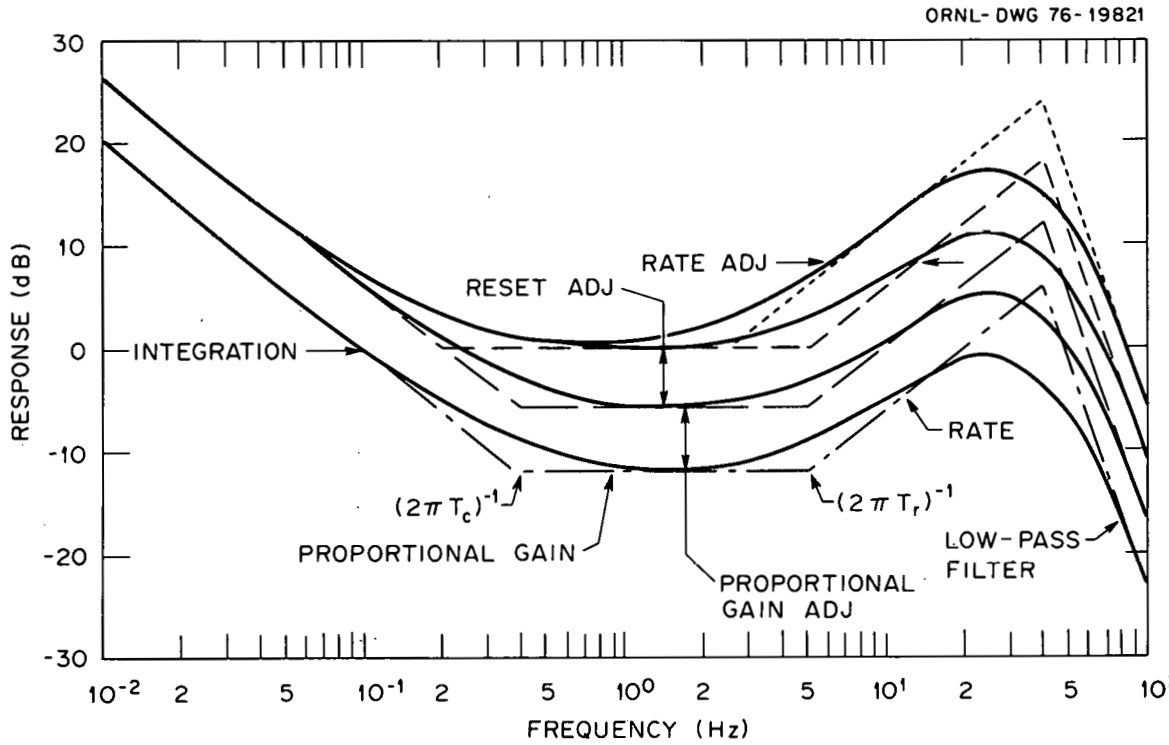

Figure 61. Frequency response of a linear three-mode controller.

is employed to control the heating current by a voltage controlled amplifier (VCA). The output of a Wien-bridge oscillator is passed through the VCA to a 100 W transconductance power amplifier which supplies the heating current to the bridge. In order to maintain loop gain at all times, the VCA has a gain proportional to $(1 + K_1 V_{c1} 0$, where K is approximately $(.053)^{-1}$. Therefore one obtains a minimum heating current greater than zero allowing measurement of R_x.

In operation of the system, VERROR and VRX are less than zero when the sample is too hot. This causes V_c to decrease thereby reducing the heating current. This causes the sample temperature to decrease. If the sample is too cool, VRX becomes positive causing V_c and the heating current to increase. Thus, the specimen becomes hotter. When there are no beam perturbations and the controller is properly adjusted, the sample temperature will be well within 0.05 °C of set point. With beam perturbations, the sample temperature will alternately be slightly too cold or hot such that the average sample temperature is within 0.05 °C of set point.

II. APPROXIMATE ANALYSIS OF SYSTEM PERFORMANCE

The loop gain of the linearized system may be approximated as follows. The temperature of the specimen is

$$\text{TEMP} = \text{TMPSET} + \text{ERRTMP} , \tag{234}$$

where

$$\text{ERRTMP} = H_t * \Delta\text{POWER},$$

TMPSET is the desired specimen temperature, H_t is the small signal thermal impulse response of the specimen, and ΔPOWER is the deviation in total

heating power from that required to maintain TEMP = TMPSET. The total heating power is

$$\text{POWER} = \text{OHMICP} + \text{BEAMP} \ , \tag{235}$$

where BEAMP is the effective heating power of the beam and OHMICP is the ohmic heating power (R_x CURENT^2 where CURENT is the RMS value of the heating current). VERROR is given by the following expression:

$$\text{VERROR} = ((\text{CURENT DELRX}) * G_{lpf1} * G_{bpf})/((1 + \text{AR CP})\ A_2), \tag{236}$$

where DELRX = RX - RXSET, RXSET is RX at TEMP = TMPSET, AR CP = RXSET/RS, A_2 is a constant, and G_{lpf} and G_{bpf} are the impulse responses of the low-pass and band-pass filters, respectively. The heating current monitor voltage is

$$\text{VCURR} = \frac{\text{RS CURENT} * G_{lpf1}}{\text{AIER}} \ , \tag{237}$$

where AIER is a constant. The filtered output of the divider is given by

$$\text{VRX} = \left(\frac{\text{VERROR}}{\text{VCURR K}}\right) * G_{lpf1} \ ,$$

$$= \left(\frac{(\text{CURENT DELRX}) * G_{lpf1} * G_{bpf} \quad \text{AIER}}{\text{K RS } A_2\ (1 + \text{AR CP})\ \text{CURENT} * G_{lpf1}}\right) * G_{lpf2} \ . \tag{238}$$

OHMICP is approximately given by

$$\text{OHMICP} \simeq \text{RXSET CURENT}^2$$

$$\simeq \text{RXSET VC } (10.9/5.3)^2/\text{RS} \ , \tag{239}$$

where $VC = A_{1c} * VRX$ and A_{1c} is the impulse response of the linear controller.

Equation (239) is difficult to interpret. If both CURENT and DELRX are functions of time, then the Laplace transform of VRX does not have a linear relation to RX and CURENT. For a fixed CURENT, VRX simplifies to

$$VRX = \frac{DELRX * G_{1pf1} * G_{bpf} * G_{1pf2}\ AIER}{K\ RS\ A2(1 + AR\ CP)}, \tag{240}$$

where $G_{1pf}\Big|_{S = 0} = 1$. On the other hand, if DELRX is fixed, then VRX can be simplified to

$$VRX = \frac{DELRX\ AIER}{K\ RS\ A(1 + AR\ CP)}, \tag{241}$$

if $\hat{G}_{bpf} = 1$ (note that the Laplace transform of a function (X) will be indicated by $\hat{X}$) and all filters have unity gain for S = 1. Note that for both of the above expressions, VRX is independent of CURENT.

The errors associated with neglecting the frequency response of the band-pass filter are small if the low-pass filters dominate. Treating the bridge signals as amplitude modulated 1 KHz sinewaves, the Fourier transform of the AM signal when passed through a second-order 1 KHz band-pass filter is

$$\hat{V}(j\omega) = \pi(\delta(\omega-\omega_o) + \delta(\omega+\omega_o)) + \frac{1}{2}\hat{M}(j\omega-j\omega_o)\ \hat{G}_{bpf}(j\omega)$$

$$+ \frac{1}{2}\hat{M}(j\omega+j\omega_o)\ \hat{G}_{bpf}(j\omega), \tag{242}$$

where $V(t) = (1 + M(t)) \cos \omega_o t$ and $\omega_o = 1$ KHz. Upon demodulation the envelope of V(t) is recovered as

$$\hat{V}_{det}(j\omega) = \frac{\hat{M}(j\omega)[\hat{G}_{bpf}(j\omega+j\omega_o) + \hat{G}_{bpf}(j\omega-j\omega_o)]}{2} . \tag{243}$$

Since

$$\hat{G}_{bpf}(j\omega) = \frac{j\omega}{\omega_o}/[Q(1+\frac{j\omega}{Q\omega_o} - (\frac{\omega}{\omega_0})^2)] ,$$

$$\hat{G}_{bpf}(j(\omega\pm\omega_o)) = \frac{(\frac{\omega}{\omega_o} \pm 1)}{\left[\frac{1}{Q}(\frac{\omega}{\omega_o} \pm 1) + \frac{j\omega}{\omega_o}(\frac{\omega}{\omega_o} \pm 2)\right]Q} . \tag{244}$$

Therefore, for $|\omega| < \omega_o$, $\hat{V}_{det}(\omega)$ is

$$\hat{V}_{det}(j\omega) = \frac{\hat{M}(j\omega)}{Q}\left[\frac{-j(\frac{\omega}{\omega_o})^3 - \frac{1}{Q}(\frac{\omega}{\omega_o})^2 + \frac{2j\omega}{\omega_o} + \frac{1}{Q}}{(\frac{\omega}{\omega_o})^4 - \frac{2j}{Q}(\frac{\omega}{\omega_o})^3 - (\frac{1}{Q^2} + 4)(\frac{\omega}{\omega_o})^2 + \frac{4j\omega}{Q^2\omega_o} + \frac{1}{Q^2}}\right] \tag{245}$$

The effective transfer function of the band-pass filter is that of a low-pass filter. This is plotted in Figure 62 for Q = 3.54. Note that the 3 dB point occurs at 140 Hz and that the slope between 300 Hz and 10 KHz is approximately 5 dB/octave. Therefore, the effect of the band-pass filter is negligible if G_{lpf1} is a single pole filter followed by a second-order Butterworth filter and G_{lpf2} is a second-order Butterworth filter, all having corner frequencies of 40 Hz since the loop transmission will have to be down over -70 dB at 140 Hz if the system is to be stable. Even if the low-pass filters' corner frequencies were increased to 80 Hz, the loop transmission would be down at least -30 dB at 140 Hz; i.e., the loop transmission would have to be less than 1 at 40 Hz due to phase shift.

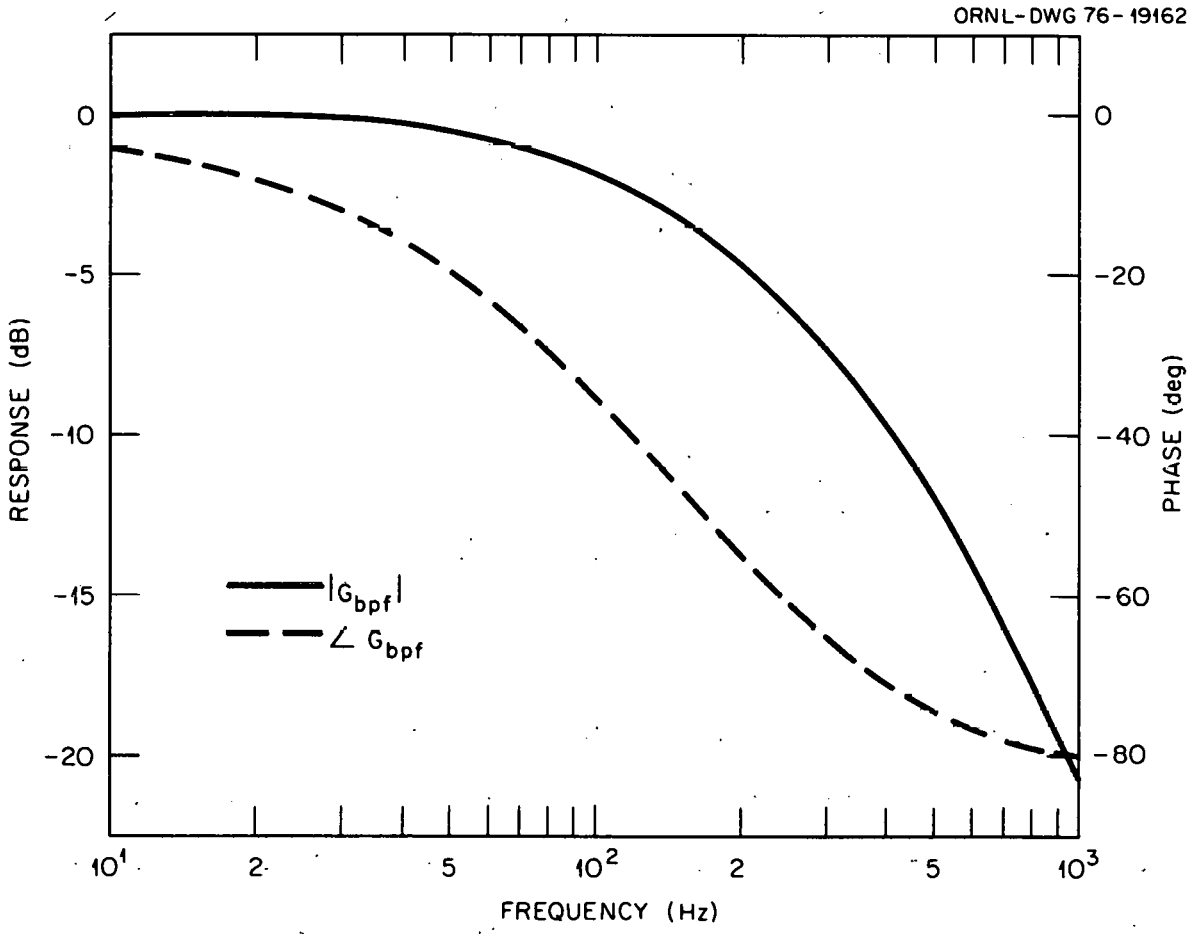

Figure 62. Effective frequency response of a second-order 1 KHz band-pass filter with a Q of 3.54 on a demodulated AM signal.

Using Equations (239) through (240) the loop transmission can now be approximated. Assuming a test $ERRTMP_t$, this will cause a DELRX of RXSET α_T $ERRTMP_t$. Employing Equations (239) and (240), the change in ohmic heating power is

$$\hat{OHMICP} \simeq \frac{RXSET^2 AIER\ (10.9)^2\ \alpha_T\ \hat{ERRTMP}_t \hat{G}_{1pf1} \hat{G}_{1pf2} \hat{A}_{1c}}{K\ RS^2 A2 (1 + \frac{RXSET}{RS})(5.3)^2} . \tag{246}$$

The resultant ERRTMP due to $ERRTMP_t$ can be found from Equation (234). Therefore, the small signal loop transmission is

$$\hat{T}_{system} = \frac{\hat{ERRTMP}}{\hat{ERRTMP}_t} \simeq \frac{(10.9)^2\ RXSET\ AIER\ \alpha_T\ \hat{G}_{1pf1} \hat{G}_{1pf2} \hat{A}_{1c} \hat{H}_t}{K\ RS\ A2\ (\frac{RS}{RXSET} + 1)(5.3)^2} . \tag{247}$$

Setting ERRTMP = $ERRTMP_t$ in Equation (234), ERRTMP due to ΔBEAMP is shown to be

$$\hat{ERRTMP} = \hat{H}_t\ \Delta\hat{BEAMP}/(1 - \hat{T}_{system}) . \tag{248}$$

If the G_{1pf1} and G_{1pf2} are neglected, and if $H_t = H_{to}/(1 + T_t\ S)$ and $A_{1c} = GAIN\ (\frac{1 + T_c S}{S})$, then ERRTMP is

$$\hat{ERRTMP} = \frac{\Delta\hat{BEAMP}\ H_{to}\ S}{GAINP\ [\frac{T_t\ S^2}{GAINP} + (\frac{1}{GAINP} + T_c)\ S + 1]} . \tag{249}$$

where

$$GAINP = - \frac{(10.9)^2 RXSET\ AIER\ \alpha_T\ GAIN\ H_{to}}{K\ R_S\ A_2\ (\frac{R_S}{RXSET} + 1)(5.3)^2} .$$

If $T_t = T_c$, then

$$\hat{ERRTMP} = \frac{\Delta\hat{BEAMP}\ H_{to}\ S}{GAINP\ (1 + T_t\ S)(\frac{S}{GAINP} + 1)} . \tag{250}$$

Therefore, for a unit step change in beam power,

$$ERRTMP = \frac{H_{to}(\exp(-t/T_t) - \exp(-t\ GAINP))\ U(t)}{GAINP\ T_t - 1} \tag{251}$$

where $T_t = T_c$. Without temperature control, ERRTMP would be

$$ERRTMP = (H_{to}\ (1 - \exp(-t/T_t)) . \tag{252}$$

An example of the improvement in temperature stability can be appreciated by the following computation. Typically, $T_t = 0.4$, $H_t = 52$, and GAINP = 56 at TMPSET = 150 °C. For a 3.6 W step increase in beam power at t = 0 such as would occur when the beam is turned on, ERRTMP increases from zero to a maximum of about 7 °C at t = 0.06 sec, then decays toward zero with a time constant of 0.4 sec. Without control, ERRTMP increases from zero toward 190 °C with a time constant of 0.4 sec. Thus a substantial improvement in temperature stability may be obtained.

III. COMPUTER SIMULATION OF TEMPERATURE CONTROL SYSTEM

In the preceding analysis, several assumptions were made that limit the accuracy of the computations. First, a small signal model was employed. Secondly, VRX was assumed independent of CURENT. In addition, the ohmic power was assumed to be proportional to RXSET instead of RX.

To study the large signal properties of the system, a CSMP program was written (see Appendix D). In this model, equations for RX and heating power as functions of temperature obtained from the curve fitting program listed in Appendix A, were utilized to improve the accuracy of the simulation. All filters, except the band-pass, were included in the simulation. Secondary filtering due to AC coupling capacitors was also neglected. Finally, DC offsets, rectifier accuracy, AC offsets, electrical noise, and temperature ripple due to the AC heating current were not considered.

Figure 63 graphs the results for a 3 mil stainless steel sample at TMPSET - 150 °C and a 3.6 W beam which is turned off at t = 0.1 sec and back on at t = 3.0 sec. Part (a) shows the temperature with GAIN = 0 (no control), part (b) shows the temperature with GAIN = 1 and all filters adjusted for 40 Hz cutoff frequencies and $T_t = T_c = 0.4$ sec. These graphs illustrate that without control, turning the beam off causes the temperature to drop from 150 to 42.666 °C in only 0.4 sec, while after 2.9 seconds, the temperature drops to -22.787 °C. This amounts to a change in temperature of 173 °C as opposed to the 190 °C change predicted by the approximate analysis. With control the peak change in temperature is -9.68 and 9.50 °C 0.04 sec after the beam is turned off and on respectively. Within 0.4 seconds after the beam transient the sample temperature is within 3.19 °C of 150 °C, and within 2.15 sec, the temperature error is only 0.05 °C. Comparing these figures with the approximate analysis shows slightly larger peak errors. This discrepancy is partly due to the overshoot in heating current caused by the filters. This overshoot may be eliminated by either reducing GAIN or increasing

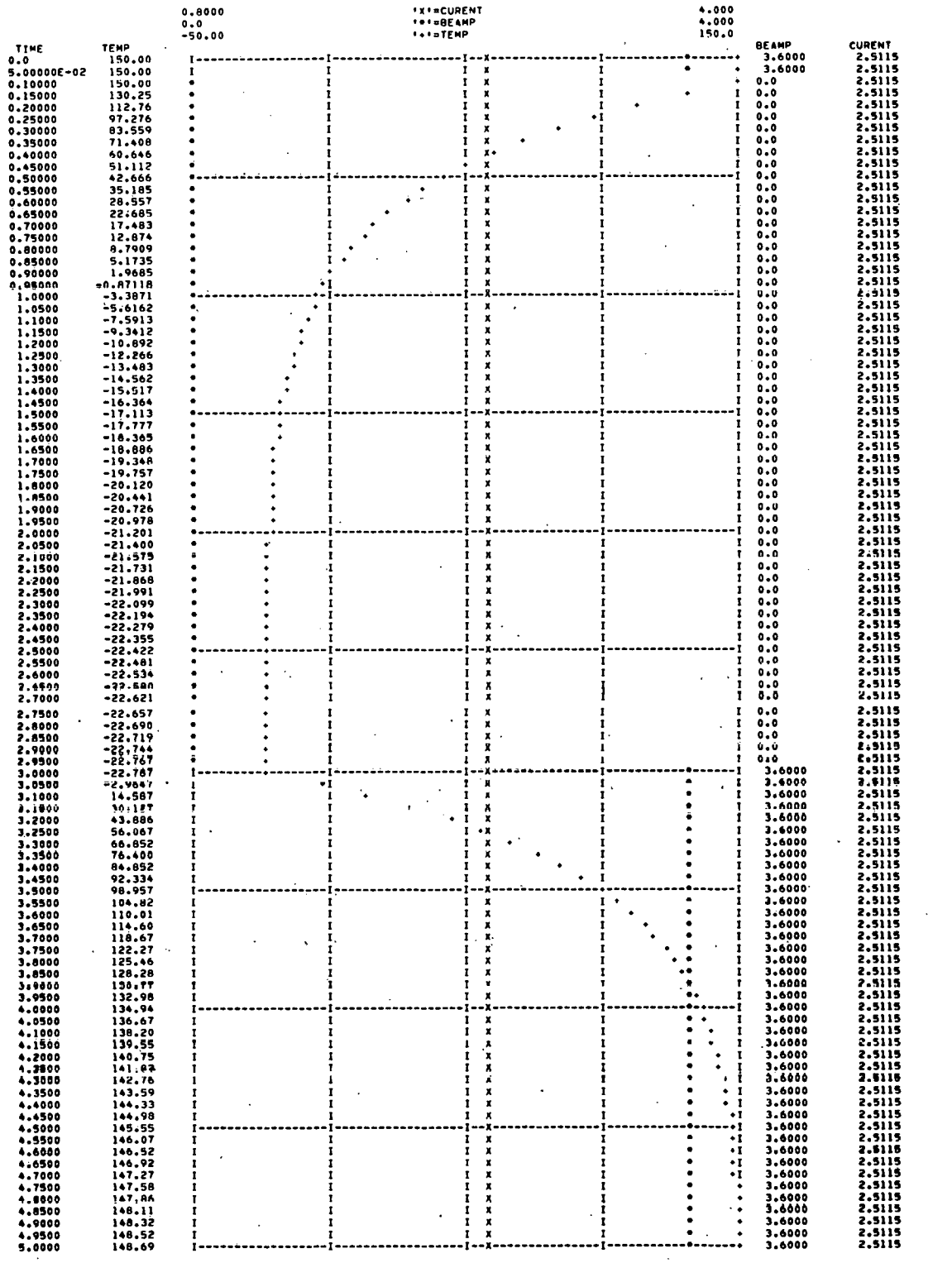

TIME	TEMP	BEAMP	CURENT
0.0	150.00	3.6000	2.5115
5.00000E-02	150.00	3.6000	2.5115
0.10000	150.00	0.0	2.5115
0.15000	130.25	0.0	2.5115
0.20000	112.76	0.0	2.5115
0.25000	97.276	0.0	2.5115
0.30000	83.559	0.0	2.5115
0.35000	71.408	0.0	2.5115
0.40000	60.646	0.0	2.5115
0.45000	51.112	0.0	2.5115
0.50000	42.666	0.0	2.5115
0.55000	35.185	0.0	2.5115
0.60000	28.557	0.0	2.5115
0.65000	22.685	0.0	2.5115
0.70000	17.483	0.0	2.5115
0.75000	12.874	0.0	2.5115
0.80000	8.7909	0.0	2.5115
0.85000	5.1735	0.0	2.5115
0.90000	1.9685	0.0	2.5115
0.95000	-0.87118	0.0	2.5115
1.0000	-3.3871	0.0	2.5115
1.0500	-5.6162	0.0	2.5115
1.1000	-7.5913	0.0	2.5115
1.1500	-9.3412	0.0	2.5115
1.2000	-10.892	0.0	2.5115
1.2500	-12.266	0.0	2.5115
1.3000	-13.483	0.0	2.5115
1.3500	-14.562	0.0	2.5115
1.4000	-15.517	0.0	2.5115
1.4500	-16.364	0.0	2.5115
1.5000	-17.113	0.0	2.5115
1.5500	-17.777	0.0	2.5115
1.6000	-18.365	0.0	2.5115
1.6500	-18.886	0.0	2.5115
1.7000	-19.348	0.0	2.5115
1.7500	-19.757	0.0	2.5115
1.8000	-20.120	0.0	2.5115
1.8500	-20.441	0.0	2.5115
1.9000	-20.726	0.0	2.5115
1.9500	-20.978	0.0	2.5115
2.0000	-21.201	0.0	2.5115
2.0500	-21.400	0.0	2.5115
2.1000	-21.575	0.0	2.5115
2.1500	-21.731	0.0	2.5115
2.2000	-21.868	0.0	2.5115
2.2500	-21.991	0.0	2.5115
2.3000	-22.099	0.0	2.5115
2.3500	-22.194	0.0	2.5115
2.4000	-22.279	0.0	2.5115
2.4500	-22.355	0.0	2.5115
2.5000	-22.422	0.0	2.5115
2.5500	-22.481	0.0	2.5115
2.6000	-22.534	0.0	2.5115
2.6500	-22.580	0.0	2.5115
2.7000	-22.621	0.0	2.5115
2.7500	-22.657	0.0	2.5115
2.8000	-22.690	0.0	2.5115
2.8500	-22.719	0.0	2.5115
2.9000	-22.744	0.0	2.5115
2.9500	-22.767	0.0	2.5115
3.0000	-22.787	3.6000	2.5115
3.0500	-2.9847	3.6000	2.5115
3.1000	14.587	3.6000	2.5115
3.1500	30.127	3.6000	2.5115
3.2000	43.886	3.6000	2.5115
3.2500	56.067	3.6000	2.5115
3.3000	66.852	3.6000	2.5115
3.3500	76.400	3.6000	2.5115
3.4000	84.852	3.6000	2.5115
3.4500	92.334	3.6000	2.5115
3.5000	98.957	3.6000	2.5115
3.5500	104.82	3.6000	2.5115
3.6000	110.01	3.6000	2.5115
3.6500	114.60	3.6000	2.5115
3.7000	118.67	3.6000	2.5115
3.7500	122.27	3.6000	2.5115
3.8000	125.46	3.6000	2.5115
3.8500	128.28	3.6000	2.5115
3.9000	130.77	3.6000	2.5115
3.9500	132.98	3.6000	2.5115
4.0000	134.94	3.6000	2.5115
4.0500	136.67	3.6000	2.5115
4.1000	138.20	3.6000	2.5115
4.1500	139.55	3.6000	2.5115
4.2000	140.75	3.6000	2.5115
4.2500	141.82	3.6000	2.5115
4.3000	142.76	3.6000	2.5115
4.3500	143.59	3.6000	2.5115
4.4000	144.33	3.6000	2.5115
4.4500	144.98	3.6000	2.5115
4.5000	145.55	3.6000	2.5115
4.5500	146.07	3.6000	2.5115
4.6000	146.52	3.6000	2.5115
4.6500	146.92	3.6000	2.5115
4.7000	147.27	3.6000	2.5115
4.7500	147.58	3.6000	2.5115
4.8000	147.86	3.6000	2.5115
4.8500	148.11	3.6000	2.5115
4.9000	148.32	3.6000	2.5115
4.9500	148.52	3.6000	2.5115
5.0000	148.69	3.6000	2.5115

(a) Gain = 0, T_c = 0.4 sec, and 40 Hz filters.

Figure 63. Computed performance of temperature controller with a temperature setpoint of 150°C.

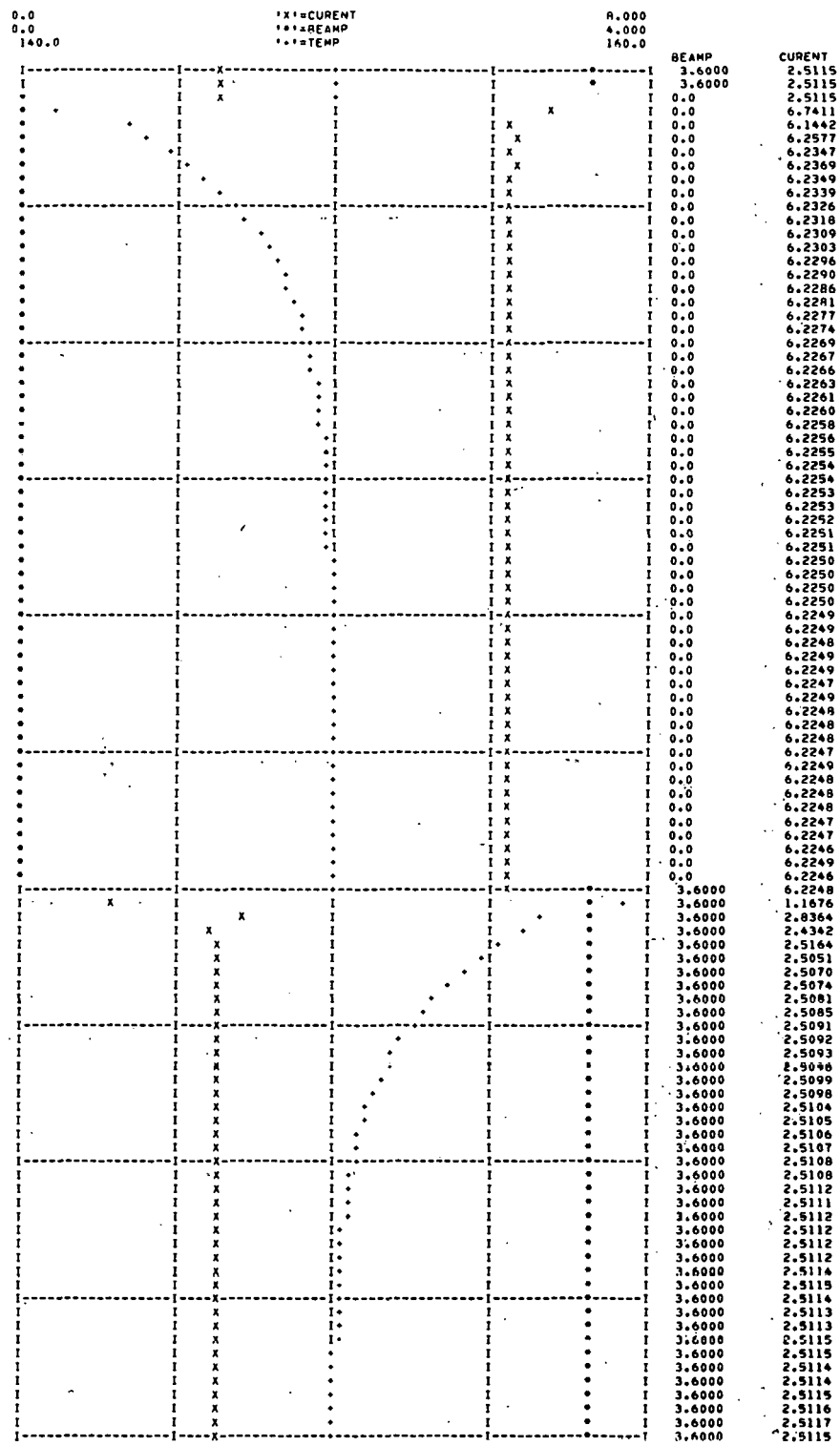

TIME	TEMP	BEAMP	CURENT
0.0	150.00	3.6000	2.5115
5.00000E-02	150.00	3.6000	2.5115
0.10000	150.00	0.0	2.5115
0.15000	141.10	0.0	6.7411
0.20000	143.49	0.0	6.1442
0.25000	144.06	0.0	6.2577
0.30000	144.79	0.0	6.2347
0.35000	145.40	0.0	6.2369
0.40000	145.95	0.0	6.2349
0.45000	146.43	0.0	6.2339
0.50000	146.85	0.0	6.2326
0.55000	147.22	0.0	6.2318
0.60000	147.55	0.0	6.2309
0.65000	147.84	0.0	6.2303
0.70000	148.09	0.0	6.2296
0.75000	148.32	0.0	6.2290
0.80000	148.52	0.0	6.2286
0.85000	148.69	0.0	6.2281
0.90000	148.85	0.0	6.2277
0.95000	148.98	0.0	6.2274
1.0000	149.10	0.0	6.2269
1.0500	149.21	0.0	6.2267
1.1000	149.30	0.0	6.2266
1.1500	149.39	0.0	6.2263
1.2000	149.46	0.0	6.2261
1.2500	149.52	0.0	6.2260
1.3000	149.58	0.0	6.2258
1.3500	149.63	0.0	6.2256
1.4000	149.67	0.0	6.2255
1.4500	149.71	0.0	6.2254
1.5000	149.75	0.0	6.2254
1.5500	149.78	0.0	6.2253
1.6000	149.80	0.0	6.2253
1.6500	149.83	0.0	6.2252
1.7000	149.85	0.0	6.2251
1.7500	149.86	0.0	6.2251
1.8000	149.88	0.0	6.2250
1.8500	149.89	0.0	6.2250
1.9000	149.91	0.0	6.2250
1.9500	149.92	0.0	6.2250
2.0000	149.93	0.0	6.2249
2.0500	149.94	0.0	6.2249
2.1000	149.94	0.0	6.2248
2.1500	149.95	0.0	6.2249
2.2000	149.96	0.0	6.2249
2.2500	149.96	0.0	6.2247
2.3000	149.97	0.0	6.2249
2.3500	149.97	0.0	6.2248
2.4000	149.97	0.0	6.2248
2.4500	149.98	0.0	6.2248
2.5000	149.98	0.0	6.2247
2.5500	149.98	0.0	6.2249
2.6000	149.98	0.0	6.2248
2.6500	149.99	0.0	6.2248
2.7000	149.99	0.0	6.2248
2.7500	149.99	0.0	6.2247
2.8000	149.99	0.0	6.2247
2.8500	149.99	0.0	6.2246
2.9000	149.99	0.0	6.2249
2.9500	149.99	0.0	6.2246
3.0000	149.99	3.6000	6.2248
3.0500	159.07	3.6000	1.1676
3.1000	156.62	3.6000	2.8364
3.1500	155.98	3.6000	2.4342
3.2000	155.27	3.6000	2.5164
3.2500	154.64	3.6000	2.5051
3.3000	154.10	3.6000	2.5070
3.3500	153.61	3.6000	2.5074
3.4000	153.19	3.6000	2.5081
3.4500	152.81	3.6000	2.5085
3.5000	152.48	3.6000	2.5091
3.5500	152.19	3.6000	2.5092
3.6000	151.93	3.6000	2.5093
3.6500	151.70	3.6000	2.5096
3.7000	151.50	3.6000	2.5099
3.7500	151.33	3.6000	2.5098
3.8000	151.17	3.6000	2.5104
3.8500	151.03	3.6000	2.5105
3.9000	150.91	3.6000	2.5106
3.9500	150.80	3.6000	2.5107
4.0000	150.71	3.6000	2.5108
4.0500	150.63	3.6000	2.5108
4.1000	150.55	3.6000	2.5112
4.1500	150.49	3.6000	2.5111
4.2000	150.43	3.6000	2.5112
4.2500	150.38	3.6000	2.5112
4.3000	150.33	3.6000	2.5112
4.3500	150.29	3.6000	2.5112
4.4000	150.26	3.6000	2.5114
4.4500	150.23	3.6000	2.5115
4.5000	150.20	3.6000	2.5114
4.5500	150.18	3.6000	2.5113
4.6000	150.16	3.6000	2.5113
4.6500	150.14	3.6000	2.5115
4.7000	150.12	3.6000	2.5115
4.7500	150.11	3.6000	2.5114
4.8000	150.09	3.6000	2.5114
4.8500	150.08	3.6000	2.5115
4.9000	150.07	3.6000	2.5116
4.9500	150.07	3.6000	2.5117
5.0000	150.06	3.6000	2.5115

(b) Gain = 1, T_c = 0.4 sec, and 40 Hz filters.

Figure 63 (continued)

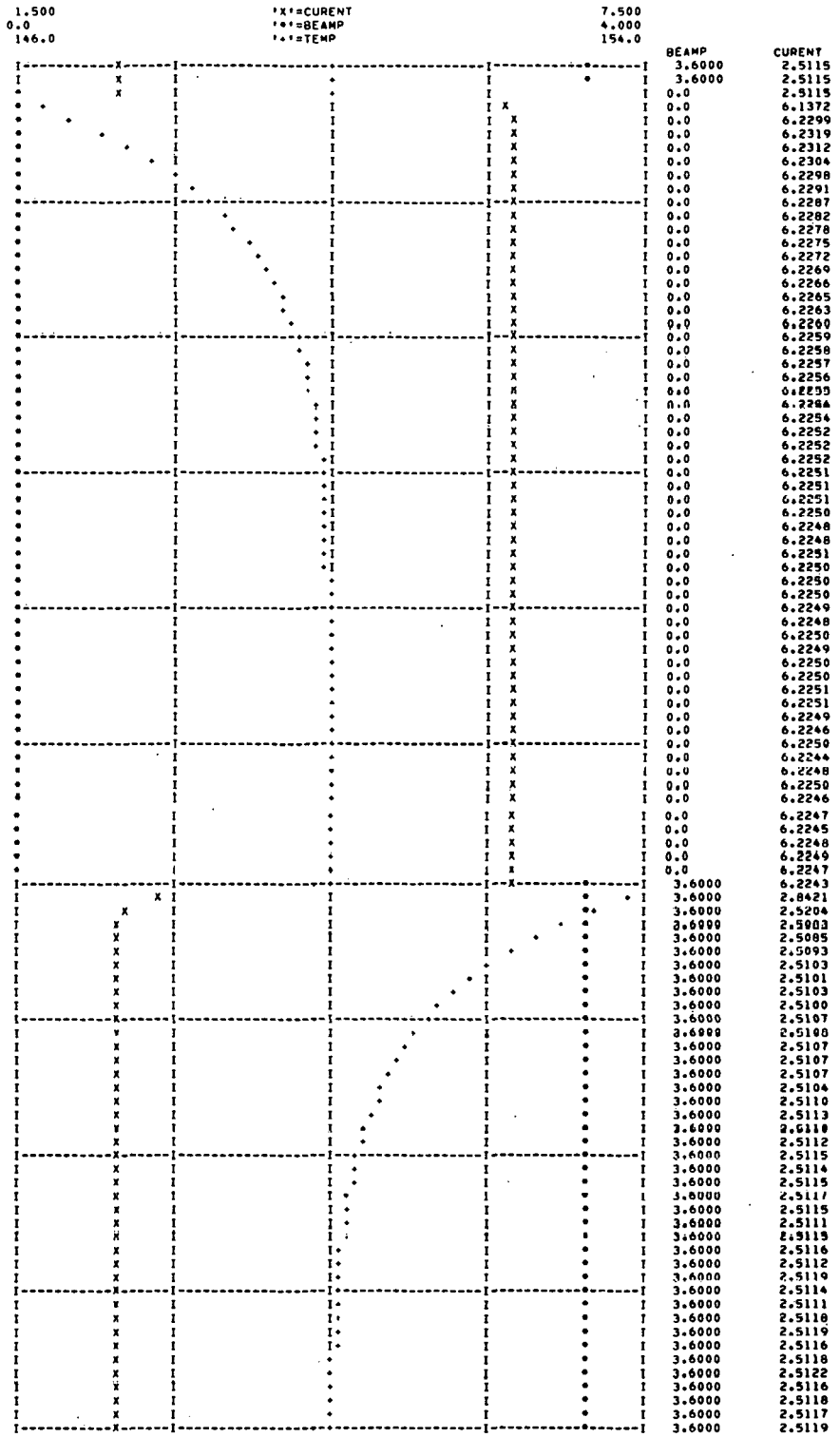

TIME	TEMP	BEAMP	CURENT
0.0	150.00	3.6000	2.5115
5.00000E-02	150.00	3.6000	2.5115
0.10000	150.00	0.0	2.5115
0.15000	146.32	0.0	6.1372
0.20000	146.67	0.0	6.2299
0.25000	147.06	0.0	6.2319
0.30000	147.41	0.0	6.2312
0.35000	147.72	0.0	6.2304
0.40000	147.98	0.0	6.2298
0.45000	148.22	0.0	6.2291
0.50000	148.43	0.0	6.2287
0.55000	148.62	0.0	6.2282
0.60000	148.78	0.0	6.2278
0.65000	148.92	0.0	6.2275
0.70000	149.05	0.0	6.2272
0.75000	149.16	0.0	6.2269
0.80000	149.26	0.0	6.2266
0.85000	149.35	0.0	6.2265
0.90000	149.42	0.0	6.2263
0.95000	149.49	0.0	6.2260
1.0000	149.55	0.0	6.2259
1.0500	149.61	0.0	6.2258
1.1000	149.65	0.0	6.2257
1.1500	149.69	0.0	6.2256
1.2000	149.72	0.0	6.2255
1.2500	149.76	0.0	6.2254
1.3000	149.79	0.0	6.2254
1.3500	149.81	0.0	6.2252
1.4000	149.84	0.0	6.2252
1.4500	149.85	0.0	6.2252
1.5000	149.87	0.0	6.2251
1.5500	149.89	0.0	6.2251
1.6000	149.90	0.0	6.2251
1.6500	149.91	0.0	6.2250
1.7000	149.92	0.0	6.2248
1.7500	149.93	0.0	6.2248
1.8000	149.94	0.0	6.2251
1.8500	149.95	0.0	6.2250
1.9000	149.95	0.0	6.2250
1.9500	149.96	0.0	6.2250
2.0000	149.96	0.0	6.2249
2.0500	149.97	0.0	6.2248
2.1000	149.97	0.0	6.2250
2.1500	149.97	0.0	6.2249
2.2000	149.98	0.0	6.2250
2.2500	149.98	0.0	6.2250
2.3000	149.98	0.0	6.2251
2.3500	149.98	0.0	6.2251
2.4000	149.99	0.0	6.2249
2.4500	149.99	0.0	6.2246
2.5000	149.99	0.0	6.2250
2.5500	149.99	0.0	6.2244
2.6000	149.99	0.0	6.2248
2.6500	149.99	0.0	6.2250
2.7000	149.99	0.0	6.2246
2.7500	149.99	0.0	6.2247
2.8000	149.99	0.0	6.2245
2.8500	150.00	0.0	6.2248
2.9000	150.00	0.0	6.2249
2.9500	150.00	0.0	6.2247
3.0000	150.00	3.6000	6.2243
3.0500	153.71	3.6000	2.8421
3.1000	153.34	3.6000	2.5204
3.1500	152.95	3.6000	2.5003
3.2000	152.60	3.6000	2.5085
3.2500	152.29	3.6000	2.5093
3.3000	152.02	3.6000	2.5103
3.3500	151.79	3.6000	2.5101
3.4000	151.58	3.6000	2.5103
3.4500	151.39	3.6000	2.5100
3.5000	151.23	3.6000	2.5107
3.5500	151.08	3.6000	2.5108
3.6000	150.96	3.6000	2.5107
3.6500	150.84	3.6000	2.5107
3.7000	150.74	3.6000	2.5107
3.7500	150.66	3.6000	2.5104
3.8000	150.58	3.6000	2.5110
3.8500	150.51	3.6000	2.5113
3.9000	150.45	3.6000	2.5110
3.9500	150.40	3.6000	2.5112
4.0000	150.35	3.6000	2.5115
4.0500	150.31	3.6000	2.5114
4.1000	150.27	3.6000	2.5115
4.1500	150.24	3.6000	2.5117
4.2000	150.21	3.6000	2.5115
4.2500	150.19	3.6000	2.5111
4.3000	150.16	3.6000	2.5115
4.3500	150.15	3.6000	2.5116
4.4000	150.13	3.6000	2.5112
4.4500	150.11	3.6000	2.5119
4.5000	150.10	3.6000	2.5114
4.5500	150.09	3.6000	2.5111
4.6000	150.08	3.6000	2.5118
4.6500	150.07	3.6000	2.5119
4.7000	150.06	3.6000	2.5116
4.7500	150.05	3.6000	2.5118
4.8000	150.05	3.6000	2.5122
4.8500	150.04	3.6000	2.5116
4.9000	150.04	3.6000	2.5118
4.9500	150.03	3.6000	2.5117
5.0000	150.03	3.6000	2.5119

(c) Gain = 2, T_c = 0.4 sec, and 80 Hz filters.

Figure 63 (continued)

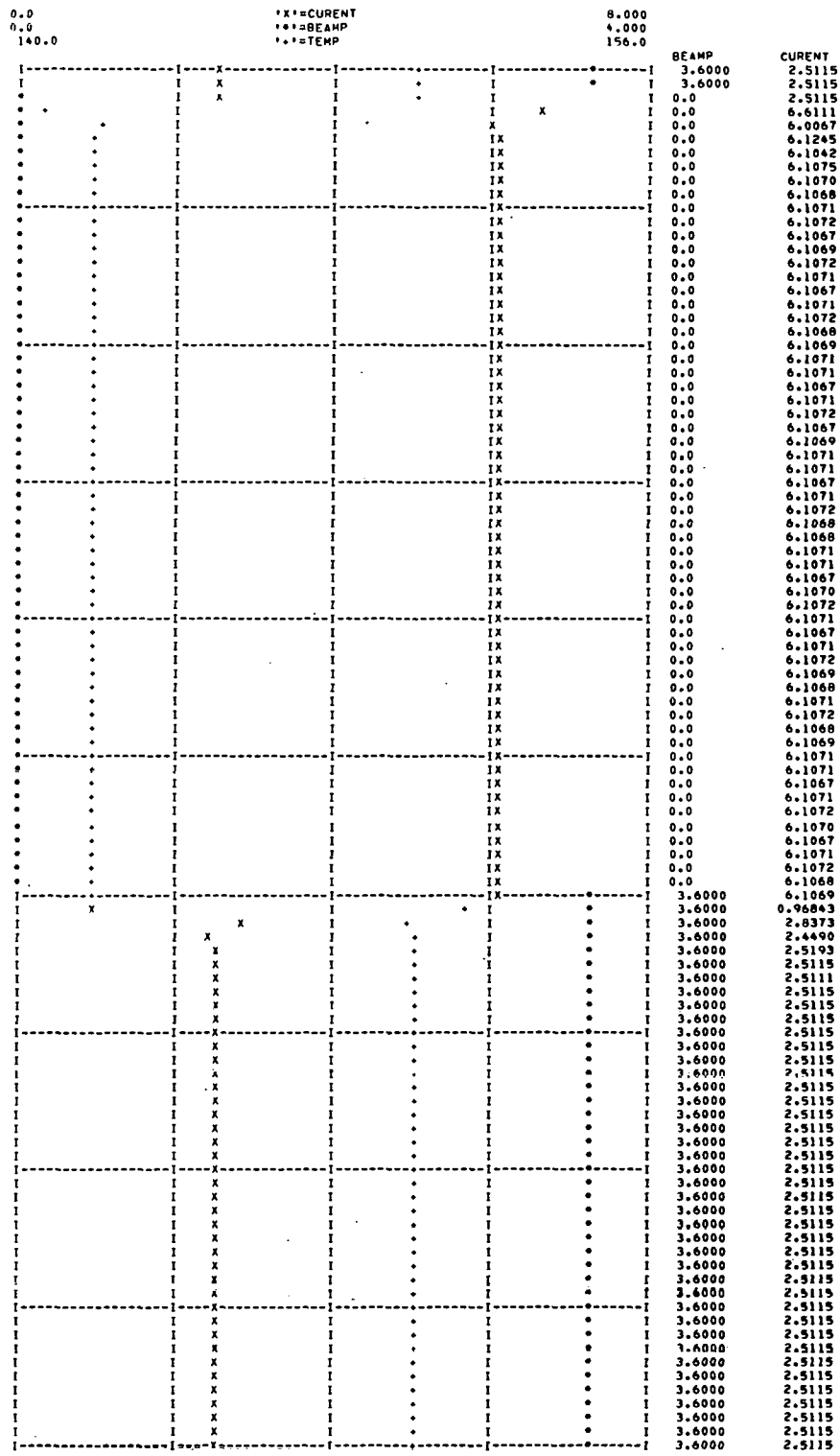

TIME	TEMP	BEAMP	CURENT
0.0	150.00	3.6000	2.5115
5.00000E-02	150.00	3.6000	2.5115
0.10000	150.00	0.0	2.5115
0.15000	140.82	0.0	6.6111
0.20000	142.09	0.0	6.0067
0.25000	141.93	0.0	6.1245
0.30000	141.94	0.0	6.1042
0.35000	141.94	0.0	6.1075
0.40000	141.94	0.0	6.1070
0.45000	141.94	0.0	6.1068
0.50000	141.94	0.0	6.1071
0.55000	141.94	0.0	6.1072
0.60000	141.94	0.0	6.1067
0.65000	141.94	0.0	6.1069
0.70000	141.94	0.0	6.1072
0.75000	141.94	0.0	6.1071
0.80000	141.94	0.0	6.1067
0.85000	141.94	0.0	6.1071
0.90000	141.94	0.0	6.1072
0.95000	141.94	0.0	6.1068
1.0000	141.94	0.0	6.1069
1.0500	141.94	0.0	6.1071
1.1000	141.94	0.0	6.1071
1.1500	141.94	0.0	6.1067
1.2000	141.94	0.0	6.1071
1.2500	141.94	0.0	6.1072
1.3000	141.94	0.0	6.1067
1.3500	141.94	0.0	6.1069
1.4000	141.94	0.0	6.1071
1.4500	141.94	0.0	6.1071
1.5000	141.94	0.0	6.1067
1.5500	141.94	0.0	6.1071
1.6000	141.94	0.0	6.1072
1.6500	141.94	0.0	6.1068
1.7000	141.94	0.0	6.1068
1.7500	141.94	0.0	6.1071
1.8000	141.94	0.0	6.1071
1.8500	141.94	0.0	6.1067
1.9000	141.94	0.0	6.1070
1.9500	141.94	0.0	6.1072
2.0000	141.94	0.0	6.1071
2.0500	141.94	0.0	6.1067
2.1000	141.94	0.0	6.1071
2.1500	141.94	0.0	6.1072
2.2000	141.94	0.0	6.1069
2.2500	141.94	0.0	6.1068
2.3000	141.94	0.0	6.1071
2.3500	141.94	0.0	6.1072
2.4000	141.94	0.0	6.1068
2.4500	141.94	0.0	6.1069
2.5000	141.94	0.0	6.1071
2.5500	141.94	0.0	6.1071
2.6000	141.94	0.0	6.1067
2.6500	141.94	0.0	6.1071
2.7000	141.94	0.0	6.1072
2.7500	141.94	0.0	6.1070
2.8000	141.94	0.0	6.1067
2.8500	141.94	0.0	6.1071
2.9000	141.94	0.0	6.1072
2.9500	141.94	0.0	6.1068
3.0000	141.94	3.6000	6.1069
3.0500	151.24	3.6000	0.96843
3.1000	149.88	3.6000	2.8373
3.1500	150.00	3.6000	2.4490
3.2000	150.01	3.6000	2.5193
3.2500	150.00	3.6000	2.5115
3.3000	150.00	3.6000	2.5111
3.3500	150.00	3.6000	2.5115
3.4000	150.00	3.6000	2.5115
3.4500	150.00	3.6000	2.5115
3.5000	150.00	3.6000	2.5115
3.5500	150.00	3.6000	2.5115
3.6000	150.00	3.6000	2.5115
3.6500	150.00	3.6000	2.5115
3.7000	150.00	3.6000	2.5115
3.7500	150.00	3.6000	2.5115
3.8000	150.00	3.6000	2.5115
3.8500	150.00	3.6000	2.5115
3.9000	150.00	3.6000	2.5115
3.9500	150.00	3.6000	2.5115
4.0000	150.00	3.6000	2.5115
4.0500	150.00	3.6000	2.5115
4.1000	150.00	3.6000	2.5115
4.1500	150.00	3.6000	2.5115
4.2000	150.00	3.6000	2.5115
4.2500	150.00	3.6000	2.5115
4.3000	150.00	3.6000	2.5115
4.3500	150.00	3.6000	2.5115
4.4000	150.00	3.6000	2.5115
4.4500	150.00	3.6000	2.5115
4.5000	150.00	3.6000	2.5115
4.5500	150.00	3.6000	2.5115
4.6000	150.00	3.6000	2.5115
4.6500	150.00	3.6000	2.5115
4.7000	150.00	3.6000	2.5115
4.7500	150.00	3.6000	2.5115
4.8000	150.00	3.6000	2.5115
4.8500	150.00	3.6000	2.5115
4.9000	150.00	3.6000	2.5115
4.9500	150.00	3.6000	2.5115
5.0000	150.00	3.6000	2.5115

(d) Gain = 1, 40 Hz filters, and no integration.

Figure 63 (continued)

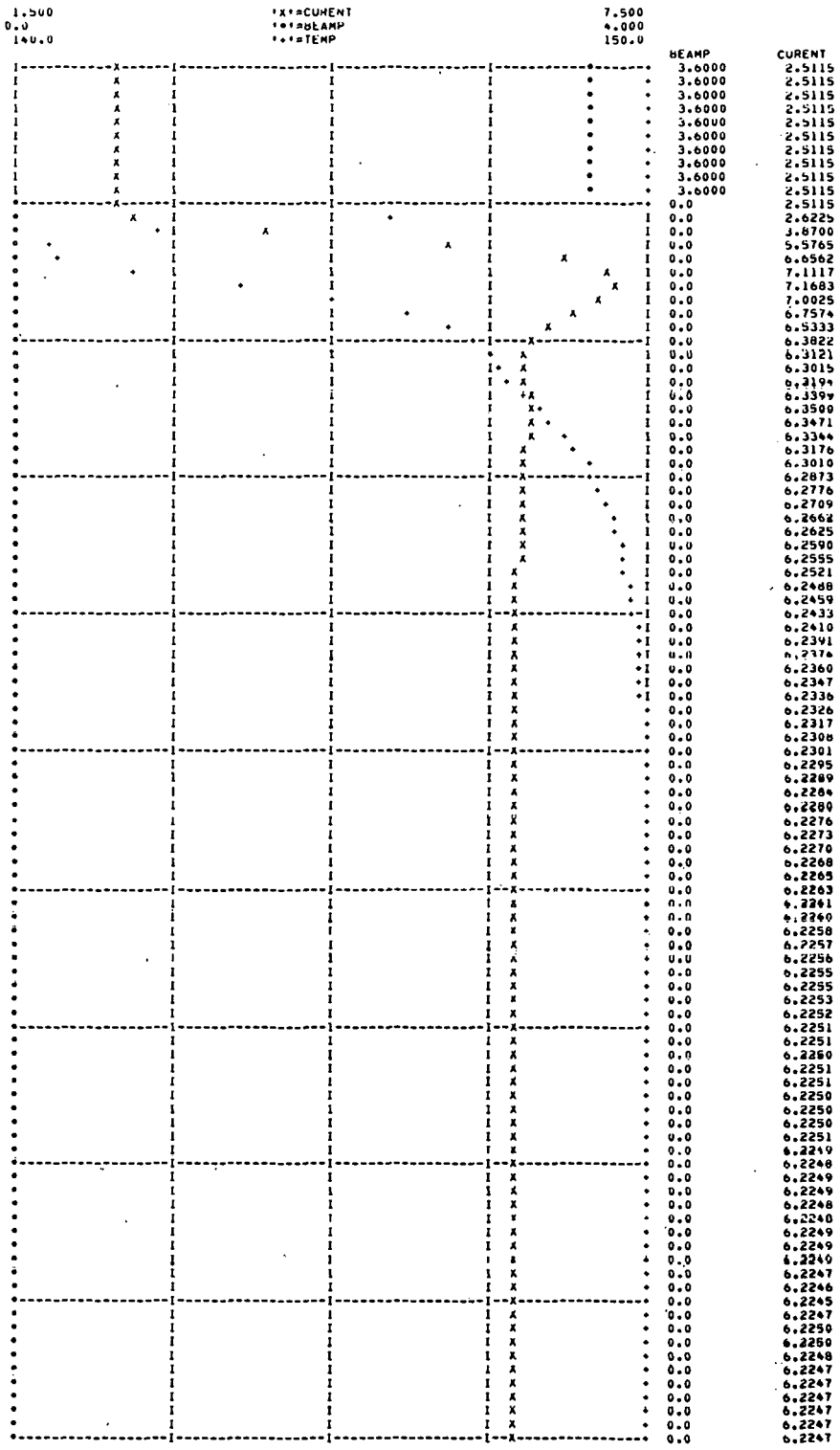

TIME	TEMP	BEAMP	CURENT
0.0	150.00	3.6000	2.5115
1.00000E-02	150.00	3.6000	2.5115
2.00000E-02	150.00	3.6000	2.5115
3.00000E-02	150.00	3.6000	2.5115
4.00000E-02	150.00	3.6000	2.5115
5.00000E-02	150.00	3.6000	2.5115
6.00000E-02	150.00	3.6000	2.5115
7.00000E-02	150.00	3.6000	2.5115
8.00000E-02	150.00	3.6000	2.5115
9.00000E-02	150.00	3.6000	2.5115
0.10000	150.00	0.0	2.5115
0.11000	145.87	0.0	2.6225
0.12000	142.33	0.0	3.8700
0.13000	140.55	0.0	5.5765
0.14000	140.69	0.0	6.6562
0.15000	141.44	0.0	7.1117
0.16000	143.55	0.0	7.1683
0.17000	145.02	0.0	7.0025
0.18000	146.11	0.0	6.7574
0.19000	146.82	0.0	6.5333
0.20000	147.22	0.0	6.3822
0.21000	147.45	0.0	6.3121
0.22000	147.62	0.0	6.3015
0.23000	147.79	0.0	6.3194
0.24000	147.99	0.0	6.3397
0.25000	148.21	0.0	6.3500
0.26000	148.44	0.0	6.3471
0.27000	148.64	0.0	6.3344
0.28000	148.82	0.0	6.3176
0.29000	148.97	0.0	6.3010
0.30000	149.09	0.0	6.2873
0.31000	149.20	0.0	6.2776
0.32000	149.28	0.0	6.2709
0.33000	149.36	0.0	6.2662
0.34000	149.44	0.0	6.2625
0.35000	149.50	0.0	6.2590
0.36000	149.56	0.0	6.2555
0.37000	149.61	0.0	6.2521
0.38000	149.66	0.0	6.2488
0.39000	149.70	0.0	6.2459
0.40000	149.73	0.0	6.2433
0.41000	149.76	0.0	6.2410
0.42000	149.79	0.0	6.2391
0.43000	149.81	0.0	6.2374
0.44000	149.84	0.0	6.2360
0.45000	149.86	0.0	6.2347
0.46000	149.87	0.0	6.2336
0.47000	149.89	0.0	6.2326
0.48000	149.90	0.0	6.2317
0.49000	149.91	0.0	6.2308
0.50000	149.92	0.0	6.2301
0.51000	149.93	0.0	6.2295
0.52000	149.94	0.0	6.2289
0.53000	149.95	0.0	6.2284
0.54000	149.95	0.0	6.2280
0.55000	149.96	0.0	6.2276
0.56000	149.96	0.0	6.2273
0.57000	149.97	0.0	6.2270
0.58000	149.97	0.0	6.2268
0.59000	149.97	0.0	6.2265
0.60000	149.98	0.0	6.2263
0.61000	149.98	0.0	6.2261
0.62000	149.98	0.0	6.2260
0.63000	149.98	0.0	6.2258
0.64000	149.99	0.0	6.2257
0.65000	149.99	0.0	6.2256
0.66000	149.99	0.0	6.2255
0.67000	149.99	0.0	6.2255
0.68000	149.99	0.0	6.2253
0.69000	149.99	0.0	6.2252
0.70000	149.99	0.0	6.2251
0.71000	149.99	0.0	6.2251
0.72000	149.99	0.0	6.2250
0.73000	149.99	0.0	6.2251
0.74000	150.00	0.0	6.2251
0.75000	150.00	0.0	6.2250
0.76000	150.00	0.0	6.2250
0.77000	150.00	0.0	6.2250
0.78000	150.00	0.0	6.2251
0.79000	150.00	0.0	6.2249
0.80000	150.00	0.0	6.2248
0.81000	150.00	0.0	6.2249
0.82000	150.00	0.0	6.2249
0.83000	150.00	0.0	6.2248
0.84000	150.00	0.0	6.2250
0.85000	150.00	0.0	6.2249
0.86000	150.00	0.0	6.2249
0.87000	150.00	0.0	6.2250
0.88000	150.00	0.0	6.2247
0.89000	150.00	0.0	6.2246
0.90000	150.00	0.0	6.2245
0.91000	150.00	0.0	6.2247
0.92000	150.00	0.0	6.2250
0.93000	150.00	0.0	6.2250
0.94000	150.00	0.0	6.2248
0.95000	150.00	0.0	6.2247
0.96000	150.00	0.0	6.2247
0.97000	150.00	0.0	6.2247
0.98000	150.00	0.0	6.2247
0.99000	150.00	0.0	6.2247
1.0000	150.00	0.0	6.2247

(e) Gain = 4, 40 Hz filters, and T_c = 0.1 sec. Note different time scale.

Figure 63 (continued)

the corner frequencies of the filters. Figure 63(c) shows the same beam transient with GAIN = 2 and the filter corner frequencies increased to 80 Hz. As expected, the peak temperature errors are reduced by a factor of two (5.0 °C within 0.02 sec and 0.05 °C within 1.88 sec). Figure 63(d) illustrates the effect of removing the integration from the controller. With GAIN = 1 and 40 Hz filters the temperature overshoot is clearly visible. When the beam is cut off the temperature error drops to -9.80 at 0.03 sec after the beam transient and settles to a constant error of -8.06 °C. The temperature overshoots 1.56 °C at 0.04 sec after the beam is turned on. Finally, Figure 63(e) illustrates that increasing the reset action by reducing T_c can reduce the recovery time. However, increasing the reset action too much will cause temperature overshoot during recovery.

Figure 64 shows the transient performance with TMPSET = 500 °C. The GAIN was increased to 1.67 with filter corner frequencies set to 40 Hz to compensate for the lower sample resistance coefficient at 500 °C. Peak temperature deviations are 8.0 °C 0.04 sec after the beam is switched on or off. Recovery behavior is similar to that at 150 °C.

Figure 65 shows the turn on behavior of the system. Part (a) shows that if the sample temperature is approximately at TMPSET before the control is switched on, the temperature undershoot is about 10 °C. Due to the nonlinear nature of the resistance temperature coefficient, control turn on with initial temperatures substantially below TMPSET can lead to overshoot. For instance, if the initial temperature without beam is 0 °C and the controller and beam are switched on simultaneously as shown in Figure 65(c) the computer program predicts a temperature overshoot in

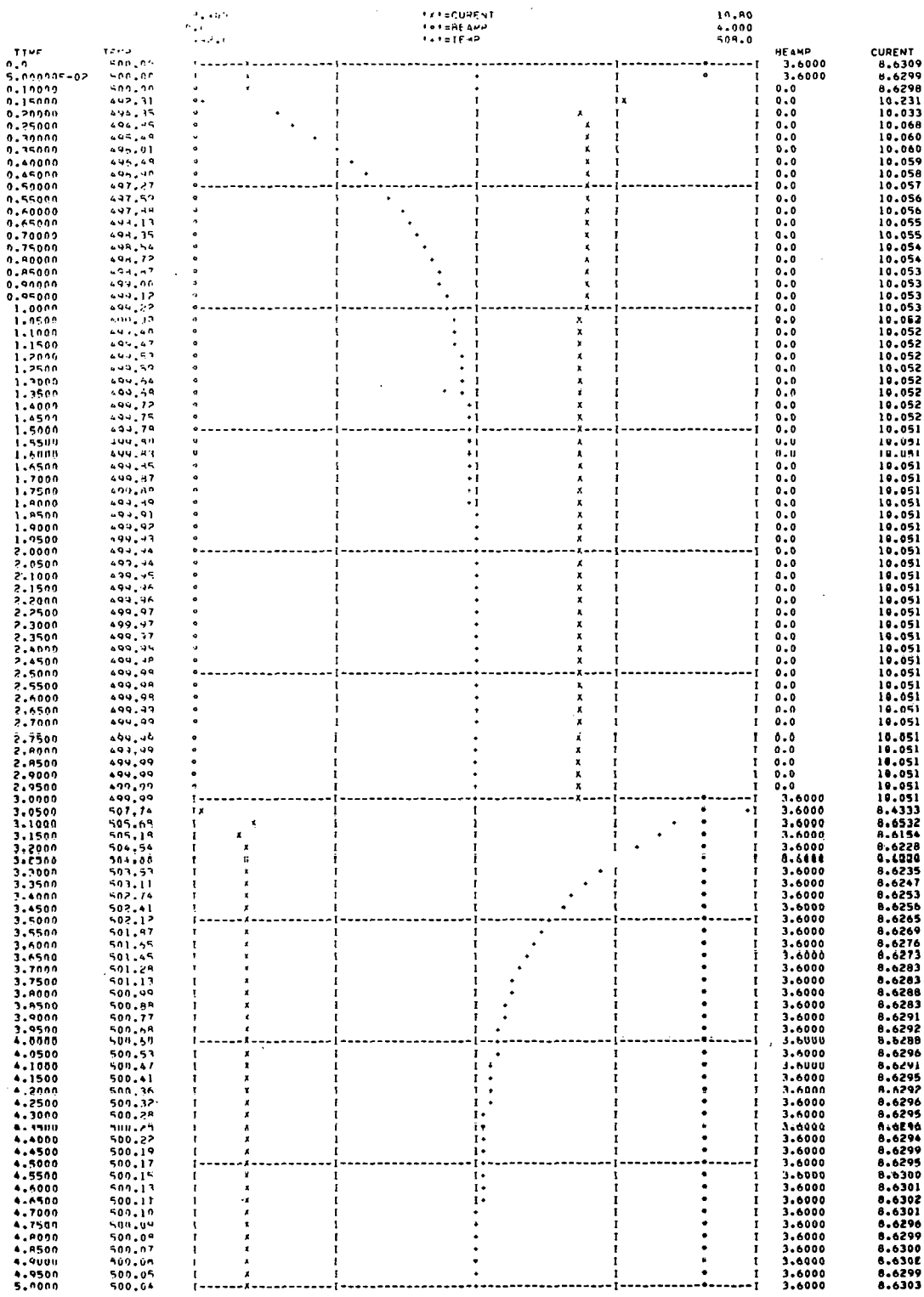

Figure 64. Computed performance of temperature controller at temperature setpoint of 500°C. Gain = 1.67, T_c = 0.4 sec, and 40 Hz. filters.

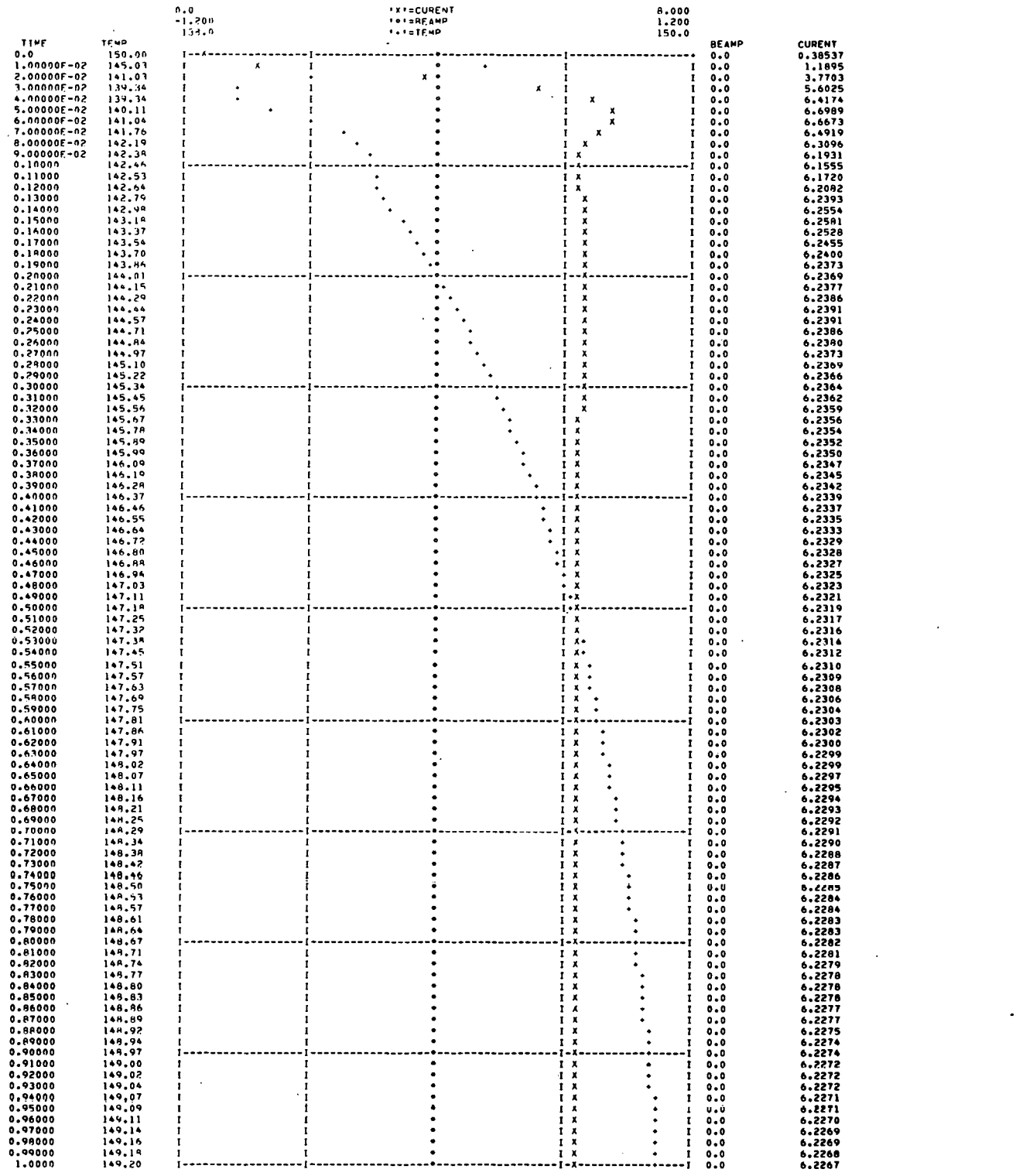

TIME	TEMP	BEAMP	CURENT
0.0	150.00	0.0	0.38537
1.00000E-02	145.03	0.0	1.1895
2.00000E-02	141.03	0.0	3.7703
3.00000E-02	139.34	0.0	5.6025
4.00000E-02	139.34	0.0	6.4174
5.00000E-02	140.11	0.0	6.6989
6.00000E-02	141.04	0.0	6.6673
7.00000E-02	141.76	0.0	6.4919
8.00000E-02	142.19	0.0	6.3096
9.00000E-02	142.38	0.0	6.1931
0.10000	142.46	0.0	6.1555
0.11000	142.53	0.0	6.1720
0.12000	142.64	0.0	6.2082
0.13000	142.79	0.0	6.2393
0.14000	142.98	0.0	6.2554
0.15000	143.18	0.0	6.2581
0.16000	143.37	0.0	6.2528
0.17000	143.54	0.0	6.2455
0.18000	143.70	0.0	6.2400
0.19000	143.86	0.0	6.2373
0.20000	144.01	0.0	6.2369
0.21000	144.15	0.0	6.2377
0.22000	144.29	0.0	6.2386
0.23000	144.44	0.0	6.2391
0.24000	144.57	0.0	6.2391
0.25000	144.71	0.0	6.2386
0.26000	144.84	0.0	6.2380
0.27000	144.97	0.0	6.2373
0.28000	145.10	0.0	6.2369
0.29000	145.22	0.0	6.2366
0.30000	145.34	0.0	6.2364
0.31000	145.45	0.0	6.2362
0.32000	145.56	0.0	6.2359
0.33000	145.67	0.0	6.2356
0.34000	145.78	0.0	6.2354
0.35000	145.89	0.0	6.2352
0.36000	145.99	0.0	6.2350
0.37000	146.09	0.0	6.2347
0.38000	146.19	0.0	6.2345
0.39000	146.28	0.0	6.2342
0.40000	146.37	0.0	6.2339
0.41000	146.46	0.0	6.2337
0.42000	146.55	0.0	6.2335
0.43000	146.64	0.0	6.2333
0.44000	146.72	0.0	6.2329
0.45000	146.80	0.0	6.2328
0.46000	146.88	0.0	6.2327
0.47000	146.94	0.0	6.2325
0.48000	147.03	0.0	6.2323
0.49000	147.11	0.0	6.2321
0.50000	147.18	0.0	6.2319
0.51000	147.25	0.0	6.2317
0.52000	147.32	0.0	6.2316
0.53000	147.38	0.0	6.2314
0.54000	147.45	0.0	6.2312
0.55000	147.51	0.0	6.2310
0.56000	147.57	0.0	6.2309
0.57000	147.63	0.0	6.2308
0.58000	147.69	0.0	6.2306
0.59000	147.75	0.0	6.2304
0.60000	147.81	0.0	6.2303
0.61000	147.86	0.0	6.2302
0.62000	147.91	0.0	6.2300
0.63000	147.97	0.0	6.2299
0.64000	148.02	0.0	6.2299
0.65000	148.07	0.0	6.2297
0.66000	148.11	0.0	6.2295
0.67000	148.16	0.0	6.2294
0.68000	148.21	0.0	6.2293
0.69000	148.25	0.0	6.2292
0.70000	148.29	0.0	6.2291
0.71000	148.34	0.0	6.2290
0.72000	148.38	0.0	6.2288
0.73000	148.42	0.0	6.2287
0.74000	148.46	0.0	6.2286
0.75000	148.50	0.0	6.2285
0.76000	148.53	0.0	6.2284
0.77000	148.57	0.0	6.2284
0.78000	148.61	0.0	6.2283
0.79000	148.64	0.0	6.2283
0.80000	148.67	0.0	6.2282
0.81000	148.71	0.0	6.2281
0.82000	148.74	0.0	6.2279
0.83000	148.77	0.0	6.2278
0.84000	148.80	0.0	6.2278
0.85000	148.83	0.0	6.2278
0.86000	148.86	0.0	6.2277
0.87000	148.89	0.0	6.2277
0.88000	148.92	0.0	6.2275
0.89000	148.94	0.0	6.2274
0.90000	148.97	0.0	6.2274
0.91000	149.00	0.0	6.2272
0.92000	149.02	0.0	6.2272
0.93000	149.04	0.0	6.2272
0.94000	149.07	0.0	6.2271
0.95000	149.09	0.0	6.2271
0.96000	149.11	0.0	6.2270
0.97000	149.14	0.0	6.2269
0.98000	149.16	0.0	6.2269
0.99000	149.18	0.0	6.2268
1.0000	149.20	0.0	6.2267

(a) No beam with initial temperature = final temperature = 150°C and no VRX limit.

Figure 65. Computed turn on behavior of temperature control system. Gain = 1, T_c = 0.4 sec, and 40 Hz filters.

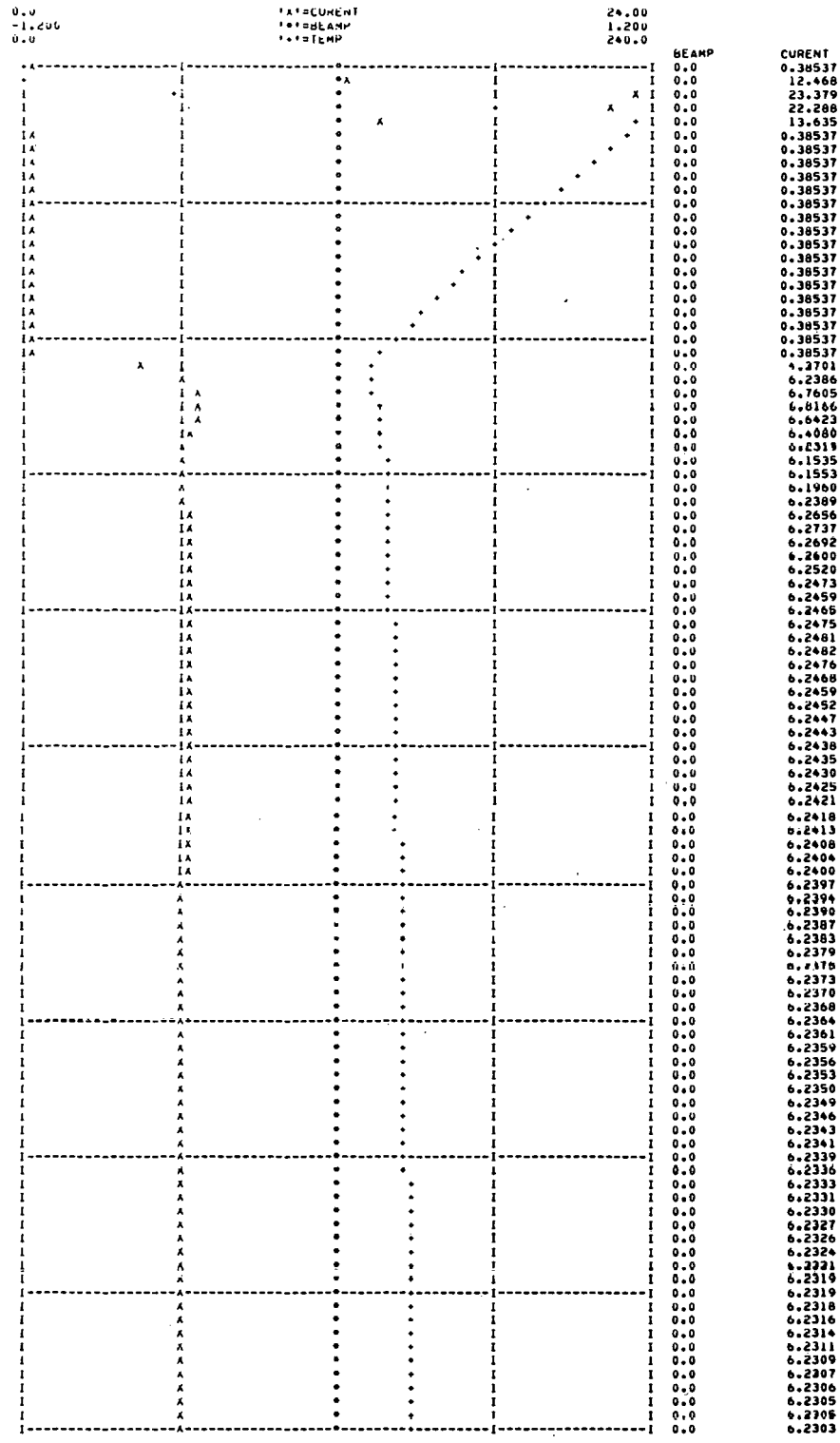

TIME	TEMP	BEAMP	CURENT
0.0	0.0	0.0	0.38537
1.00000E-02	2.2164	0.0	12.468
2.00000E-02	58.543	0.0	23.379
3.00000E-02	178.27	0.0	22.288
4.00000E-02	232.00	0.0	13.635
5.00000E-02	230.59	0.0	0.38537
6.00000E-02	223.55	0.0	0.38537
7.00000E-02	216.72	0.0	0.38537
8.00000E-02	210.06	0.0	0.38537
9.00000E-02	203.57	0.0	0.38537
0.10000	197.23	0.0	0.38537
0.11000	191.05	0.0	0.38537
0.12000	185.03	0.0	0.38537
0.13000	179.15	0.0	0.38537
0.14000	173.42	0.0	0.38537
0.15000	167.83	0.0	0.38537
0.16000	162.38	0.0	0.38537
0.17000	157.06	0.0	0.38537
0.18000	151.87	0.0	0.38537
0.19000	146.81	0.0	0.38537
0.20000	141.88	0.0	0.38537
0.21000	137.06	0.0	0.38537
0.22000	133.42	0.0	4.2701
0.23000	132.75	0.0	6.2386
0.24000	133.61	0.0	6.7605
0.25000	134.84	0.0	6.8166
0.26000	135.93	0.0	6.6423
0.27000	136.87	0.0	6.4080
0.28000	137.09	0.0	6.2319
0.29000	137.29	0.0	6.1535
0.30000	137.45	0.0	6.1553
0.31000	137.54	0.0	6.1960
0.32000	137.90	0.0	6.2389
0.33000	138.20	0.0	6.2656
0.34000	138.51	0.0	6.2737
0.35000	138.83	0.0	6.2692
0.36000	139.12	0.0	6.2600
0.37000	139.40	0.0	6.2520
0.38000	139.66	0.0	6.2473
0.39000	139.91	0.0	6.2459
0.40000	140.15	0.0	6.2466
0.41000	140.39	0.0	6.2475
0.42000	140.63	0.0	6.2481
0.43000	140.86	0.0	6.2482
0.44000	141.09	0.0	6.2476
0.45000	141.31	0.0	6.2468
0.46000	141.53	0.0	6.2459
0.47000	141.74	0.0	6.2452
0.48000	141.94	0.0	6.2447
0.49000	142.14	0.0	6.2443
0.50000	142.34	0.0	6.2438
0.51000	142.53	0.0	6.2435
0.52000	142.71	0.0	6.2430
0.53000	142.89	0.0	6.2425
0.54000	143.07	0.0	6.2421
0.55000	143.24	0.0	6.2418
0.56000	143.41	0.0	6.2413
0.57000	143.57	0.0	6.2408
0.58000	143.73	0.0	6.2404
0.59000	143.89	0.0	6.2400
0.60000	144.04	0.0	6.2397
0.61000	144.19	0.0	6.2394
0.62000	144.33	0.0	6.2390
0.63000	144.47	0.0	6.2387
0.64000	144.61	0.0	6.2383
0.65000	144.74	0.0	6.2379
0.66000	144.87	0.0	6.2376
0.67000	145.00	0.0	6.2373
0.68000	145.12	0.0	6.2370
0.69000	145.24	0.0	6.2368
0.70000	145.36	0.0	6.2364
0.71000	145.48	0.0	6.2361
0.72000	145.59	0.0	6.2359
0.73000	145.70	0.0	6.2356
0.74000	145.81	0.0	6.2353
0.75000	145.91	0.0	6.2350
0.76000	146.01	0.0	6.2349
0.77000	146.11	0.0	6.2346
0.78000	146.21	0.0	6.2343
0.79000	146.30	0.0	6.2341
0.80000	146.39	0.0	6.2339
0.81000	146.48	0.0	6.2336
0.82000	146.57	0.0	6.2333
0.83000	146.66	0.0	6.2331
0.84000	146.74	0.0	6.2330
0.85000	146.82	0.0	6.2327
0.86000	146.90	0.0	6.2326
0.87000	146.98	0.0	6.2324
0.88000	147.05	0.0	6.2321
0.89000	147.13	0.0	6.2319
0.90000	147.20	0.0	6.2319
0.91000	147.27	0.0	6.2318
0.92000	147.33	0.0	6.2316
0.93000	147.40	0.0	6.2314
0.94000	147.46	0.0	6.2311
0.95000	147.62	0.0	6.2309
0.96000	147.59	0.0	6.2307
0.97000	147.65	0.0	6.2306
0.98000	147.71	0.0	6.2305
0.99000	147.76	0.0	6.2304
1.0000	147.82	0.0	6.2303

(b) No beam with initial temperature = 0°C, final temperature = 150°C, and no VRX limit.

Figure 65 (continued)

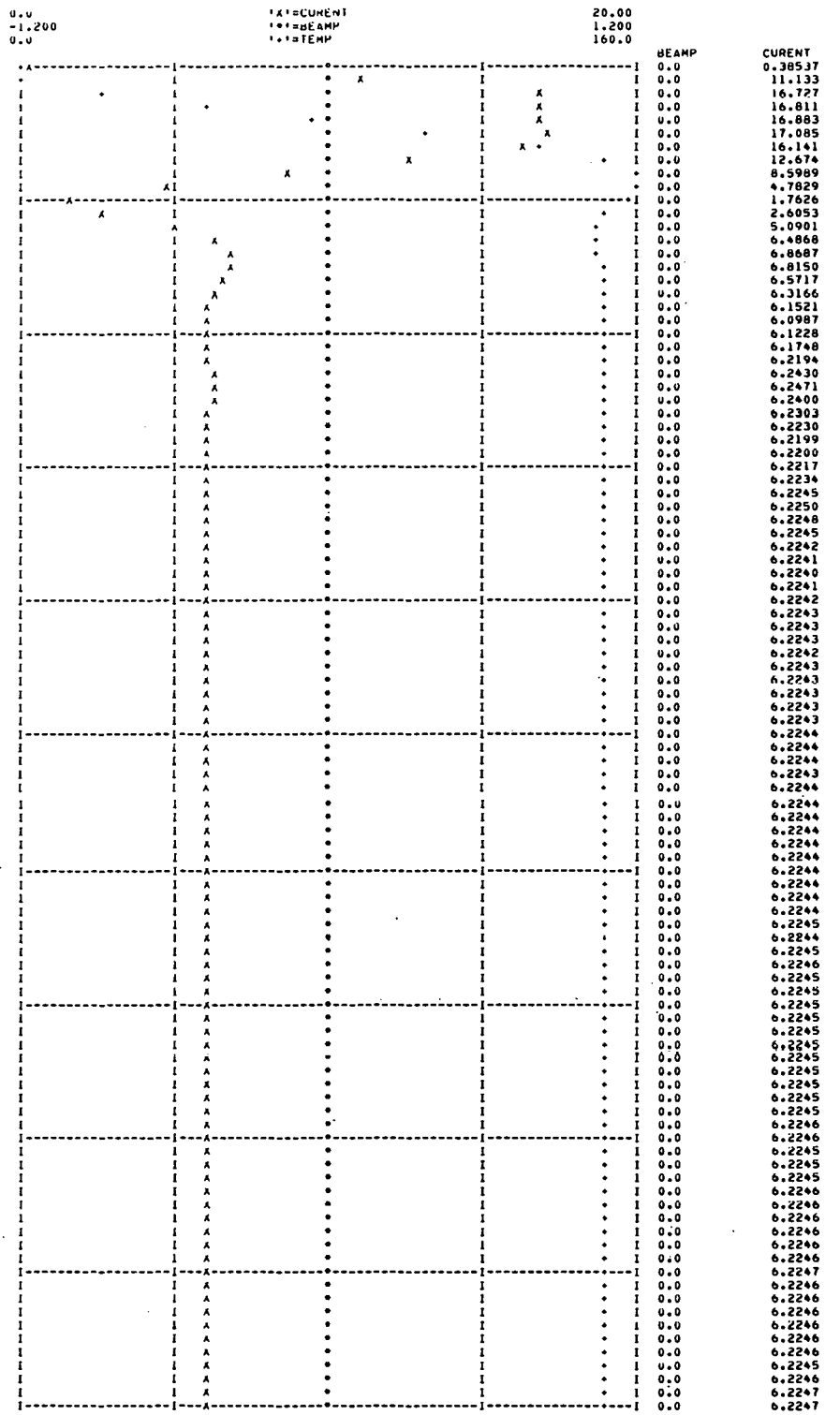

TIME	TEMP	BEAMP	CURENT
0.0	0.0	0.0	0.38537
1.00000E-02	1.9370	0.0	11.133
2.00000E-02	22.247	0.0	16.727
3.00000E-02	49.255	0.0	16.811
4.00000E-02	76.485	0.0	16.883
5.00000E-02	104.96	0.0	17.085
6.00000E-02	133.27	0.0	16.141
7.00000E-02	151.48	0.0	12.674
8.00000E-02	159.26	0.0	8.5989
9.00000E-02	159.78	0.0	4.7829
0.10000	156.00	0.0	1.7626
0.11000	151.29	0.0	2.6053
0.12000	148.35	0.0	5.0901
0.13000	147.95	0.0	6.4868
0.14000	148.75	0.0	6.8687
0.15000	149.75	0.0	6.8150
0.16000	150.47	0.0	6.5717
0.17000	150.78	0.0	6.3166
0.18000	150.76	0.0	6.1521
0.19000	150.58	0.0	6.0987
0.20000	150.40	0.0	6.1228
0.21000	150.28	0.0	6.1748
0.22000	150.24	0.0	6.2194
0.23000	150.24	0.0	6.2430
0.24000	150.27	0.0	6.2471
0.25000	150.29	0.0	6.2400
0.26000	150.30	0.0	6.2303
0.27000	150.30	0.0	6.2230
0.28000	150.28	0.0	6.2199
0.29000	150.27	0.0	6.2200
0.30000	150.26	0.0	6.2217
0.31000	150.25	0.0	6.2234
0.32000	150.24	0.0	6.2245
0.33000	150.24	0.0	6.2250
0.34000	150.23	0.0	6.2248
0.35000	150.23	0.0	6.2245
0.36000	150.22	0.0	6.2242
0.37000	150.22	0.0	6.2241
0.38000	150.21	0.0	6.2240
0.39000	150.21	0.0	6.2241
0.40000	150.20	0.0	6.2242
0.41000	150.20	0.0	6.2243
0.42000	150.19	0.0	6.2243
0.43000	150.19	0.0	6.2243
0.44000	150.18	0.0	6.2242
0.45000	150.18	0.0	6.2243
0.46000	150.17	0.0	6.2243
0.47000	150.17	0.0	6.2243
0.48000	150.16	0.0	6.2243
0.49000	150.16	0.0	6.2243
0.50000	150.16	0.0	6.2244
0.51000	150.15	0.0	6.2244
0.52000	150.15	0.0	6.2244
0.53000	150.15	0.0	6.2243
0.54000	150.14	0.0	6.2244
0.55000	150.14	0.0	6.2244
0.56000	150.13	0.0	6.2244
0.57000	150.13	0.0	6.2244
0.58000	150.13	0.0	6.2244
0.59000	150.12	0.0	6.2244
0.60000	150.12	0.0	6.2244
0.61000	150.12	0.0	6.2244
0.62000	150.12	0.0	6.2244
0.63000	150.11	0.0	6.2244
0.64000	150.11	0.0	6.2245
0.65000	150.11	0.0	6.2244
0.66000	150.10	0.0	6.2245
0.67000	150.10	0.0	6.2246
0.68000	150.10	0.0	6.2245
0.69000	150.10	0.0	6.2245
0.70000	150.09	0.0	6.2245
0.71000	150.09	0.0	6.2245
0.72000	150.09	0.0	6.2245
0.73000	150.09	0.0	6.2245
0.74000	150.09	0.0	6.2245
0.75000	150.08	0.0	6.2245
0.76000	150.08	0.0	6.2245
0.77000	150.08	0.0	6.2245
0.78000	150.08	0.0	6.2245
0.79000	150.08	0.0	6.2246
0.80000	150.07	0.0	6.2246
0.81000	150.07	0.0	6.2245
0.82000	150.07	0.0	6.2245
0.83000	150.07	0.0	6.2245
0.84000	150.07	0.0	6.2246
0.85000	150.06	0.0	6.2246
0.86000	150.06	0.0	6.2246
0.87000	150.06	0.0	6.2246
0.88000	150.06	0.0	6.2246
0.89000	150.06	0.0	6.2246
0.90000	150.06	0.0	6.2247
0.91000	150.06	0.0	6.2246
0.92000	150.05	0.0	6.2246
0.93000	150.05	0.0	6.2246
0.94000	150.05	0.0	6.2246
0.95000	150.05	0.0	6.2246
0.96000	150.05	0.0	6.2246
0.97000	150.05	0.0	6.2245
0.98000	150.05	0.0	6.2246
0.99000	150.04	0.0	6.2247
1.0000	150.04	0.0	6.2247

(c) No beam with initial temperature = 0°C, final temperature = 150°C, and $|VRX| \leq 12$ V.

Figure 65 (continued)

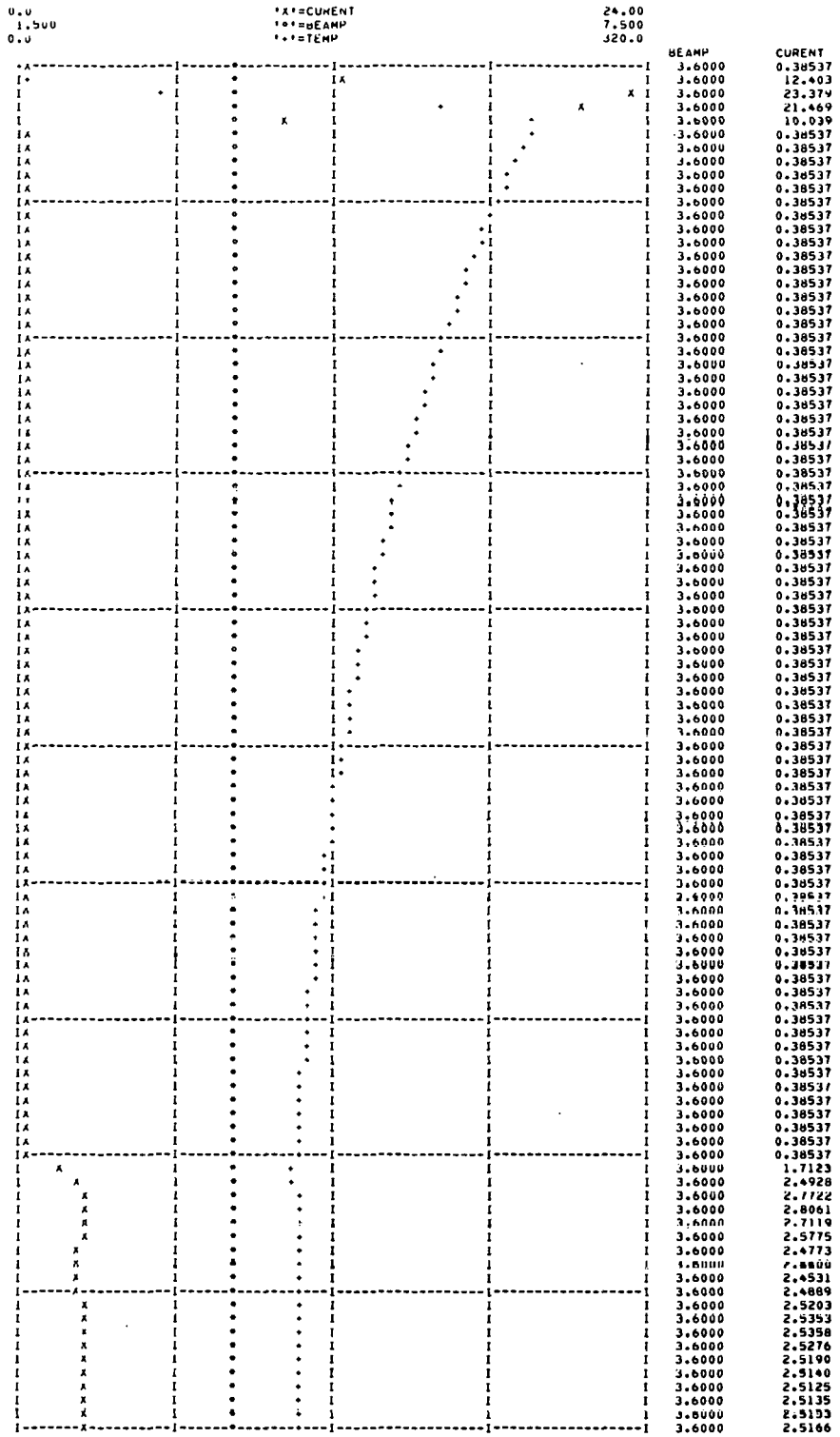

TIME	TEMP	BEAMP	CURENT
0.0	0.0	3.6000	0.38537
1.00000E-02	6.0619	3.6000	12.403
2.00000E-02	71.817	3.6000	23.379
3.00000E-02	212.72	3.6000	21.469
4.00000E-02	261.30	3.6000	10.039
5.00000E-02	259.18	3.6000	0.38537
6.00000E-02	255.74	3.6000	0.38537
7.00000E-02	252.40	3.6000	0.38537
8.00000E-02	249.14	3.6000	0.38537
9.00000E-02	245.95	3.6000	0.38537
0.10000	242.85	3.6000	0.38537
0.11000	239.82	3.6000	0.38537
0.12000	236.87	3.6000	0.38537
0.13000	233.99	3.6000	0.38537
0.14000	231.19	3.6000	0.38537
0.15000	228.45	3.6000	0.38537
0.16000	225.78	3.6000	0.38537
0.17000	223.17	3.6000	0.38537
0.18000	220.63	3.6000	0.38537
0.19000	218.15	3.6000	0.38537
0.20000	215.74	3.6000	0.38537
0.21000	213.38	3.6000	0.38537
0.22000	211.08	3.6000	0.38537
0.23000	208.84	3.6000	0.38537
0.24000	206.65	3.6000	0.38537
0.25000	204.52	3.6000	0.38537
0.26000	202.44	3.6000	0.38537
0.27000	200.41	3.6000	0.38537
0.28000	198.43	3.6000	0.38537
0.29000	196.50	3.6000	0.38537
0.30000	194.62	3.6000	0.38537
0.31000	192.78	3.6000	0.38537
0.32000	190.98	3.6000	0.38537
0.33000	189.24	3.6000	0.38537
0.34000	187.54	3.6000	0.38537
0.35000	185.88	3.6000	0.38537
0.36000	184.26	3.6000	0.38537
0.37000	182.68	3.6000	0.38537
0.38000	181.14	3.6000	0.38537
0.39000	179.63	3.6000	0.38537
0.40000	178.17	3.6000	0.38537
0.41000	176.74	3.6000	0.38537
0.42000	175.34	3.6000	0.38537
0.43000	173.98	3.6000	0.38537
0.44000	172.65	3.6000	0.38537
0.45000	171.36	3.6000	0.38537
0.46000	170.10	3.6000	0.38537
0.47000	168.87	3.6000	0.38537
0.48000	167.67	3.6000	0.38537
0.49000	166.49	3.6000	0.38537
0.50000	165.35	3.6000	0.38537
0.51000	164.24	3.6000	0.38537
0.52000	163.15	3.6000	0.38537
0.53000	162.09	3.6000	0.38537
0.54000	161.06	3.6000	0.38537
0.55000	160.05	3.6000	0.38537
0.56000	159.07	3.6000	0.38537
0.57000	158.11	3.6000	0.38537
0.58000	157.17	3.6000	0.38537
0.59000	156.26	3.6000	0.38537
0.60000	155.37	3.6000	0.38537
0.61000	154.50	2.4000	0.38537
0.62000	153.66	3.6000	0.38537
0.63000	152.83	3.6000	0.38537
0.64000	152.03	3.6000	0.38537
0.65000	151.24	3.6000	0.38537
0.66000	150.48	3.6000	0.38537
0.67000	149.73	3.6000	0.38537
0.68000	149.00	3.6000	0.38537
0.69000	148.29	3.6000	0.38537
0.70000	147.60	3.6000	0.38537
0.71000	146.92	3.6000	0.38537
0.72000	146.26	3.6000	0.38537
0.73000	145.62	3.6000	0.38537
0.74000	144.99	3.6000	0.38537
0.75000	144.38	3.6000	0.38537
0.76000	143.79	3.6000	0.38537
0.77000	143.20	3.6000	0.38537
0.78000	142.64	3.6000	0.38537
0.79000	142.08	3.6000	0.38537
0.80000	141.54	3.6000	0.38537
0.81000	141.14	3.6000	1.7123
0.82000	141.16	3.6000	2.4928
0.83000	141.47	3.6000	2.7722
0.84000	141.85	3.6000	2.8061
0.85000	142.21	3.6000	2.7119
0.86000	142.47	3.6000	2.5775
0.87000	142.66	3.6000	2.4773
0.88000	142.80	3.6000	2.4600
0.89000	142.94	3.6000	2.4531
0.90000	143.08	3.6000	2.4889
0.91000	143.25	3.6000	2.5203
0.92000	143.42	3.6000	2.5353
0.93000	143.59	3.6000	2.5358
0.94000	143.76	3.6000	2.5276
0.95000	143.92	3.6000	2.5190
0.96000	144.07	3.6000	2.5140
0.97000	144.21	3.6000	2.5125
0.98000	144.35	3.6000	2.5135
0.99000	144.49	3.6000	2.5153
1.0000	144.63	3.6000	2.5166

(d) Beam turned on at TIME = 0 with initial temperature = 0°C, final temperature = 150°C, and no VRX limit.

Figure 65 (continued)

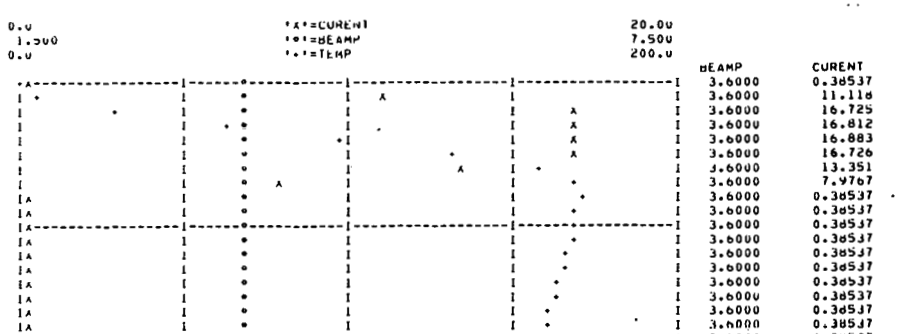

TIME	TEMP	BEAMP	CURENT
0.0	0.0	3.6000	0.38537
1.00000E-02	5.8007	3.6000	11.118
2.00000E-02	30.312	3.6000	16.725
3.00000E-02	63.054	3.6000	16.812
4.00000E-02	96.337	3.6000	16.883
5.00000E-02	131.10	3.6000	16.726
6.00000E-02	157.22	3.6000	13.351
7.00000E-02	166.48	3.6000	7.9767
8.00000E-02	167.95	3.6000	0.38537
9.00000E-02	166.72	3.6000	0.38537
0.10000	167.53	3.6000	0.38537
0.11000	166.35	3.6000	0.38537
0.12000	165.27	3.6000	0.38537
0.13000	164.11	3.6000	0.38537
0.14000	163.02	3.6000	0.38537
0.15000	161.97	3.6000	0.38537
0.16000	160.94	3.6000	0.38537
0.17000	159.93	3.6000	0.38537
0.18000	158.95	3.6000	0.38537
0.19000	158.06	3.6000	0.38537
0.20000	157.08	3.6000	0.38537
0.21000	156.15	3.6000	0.38537
0.22000	155.27	3.6000	0.38537
0.23000	154.40	3.6000	0.38537
0.24000	153.56	3.6000	0.38537
0.25000	152.74	3.6000	0.38537
0.26000	152.19	3.6000	2.0456
0.27000	152.07	3.6000	2.6473
0.28000	152.17	3.6000	2.7924
0.29000	152.28	3.6000	2.7541
0.30000	152.34	3.6000	2.6337
0.31000	152.32	3.6000	2.5124
0.32000	152.24	3.6000	2.4437
0.33000	152.14	3.6000	2.4356
0.34000	152.05	3.6000	2.4644
0.35000	151.99	3.6000	2.4999
0.36000	151.94	3.6000	2.5219
0.37000	151.90	3.6000	2.5285
0.38000	151.86	3.6000	2.5236
0.39000	151.82	3.6000	2.5150
0.40000	151.78	3.6000	2.5077
0.41000	151.73	3.6000	2.5051
0.42000	151.69	3.6000	2.5058
0.43000	151.64	3.6000	2.5079
0.44000	151.60	3.6000	2.5095
0.45000	151.56	3.6000	2.5108
0.46000	151.53	3.6000	2.5108
0.47000	151.49	3.6000	2.5106
0.48000	151.45	3.6000	2.5107
0.49000	151.42	3.6000	2.5104
0.50000	151.38	3.6000	2.5099
0.51000	151.35	3.6000	2.5100
0.52000	151.31	3.6000	2.5099
0.53000	151.28	3.6000	2.5100
0.54000	151.25	3.6000	2.5100
0.55000	151.22	3.6000	2.5100
0.56000	151.19	3.6000	2.5104
0.57000	151.16	3.6000	2.5107
0.58000	151.13	3.6000	2.5110
0.59000	151.10	3.6000	2.5110
0.60000	151.07	3.6000	2.5104
0.61000	151.05	3.6000	2.5102
0.62000	151.02	3.6000	2.5103
0.63000	151.00	3.6000	2.5103
0.64000	150.97	3.6000	2.5102
0.65000	150.95	3.6000	2.5105
0.66000	150.92	3.6000	2.5107
0.67000	150.90	3.6000	2.5107
0.68000	150.88	3.6000	2.5108
0.69000	150.86	3.6000	2.5108
0.70000	150.84	3.6000	2.5109
0.71000	150.82	3.6000	2.5108
0.72000	150.80	3.6000	2.5107
0.73000	150.78	3.6000	2.5106
0.74000	150.76	3.6000	2.5108
0.75000	150.74	3.6000	2.5109
0.76000	150.72	3.6000	2.5110
0.77000	150.70	3.6000	2.5107
0.78000	150.68	3.6000	2.5107
0.79000	150.67	3.6000	2.5108
0.80000	150.65	3.6000	2.5108
0.81000	150.63	3.6000	2.5108
0.82000	150.62	3.6000	2.5109
0.83000	150.60	3.6000	2.5108
0.84000	150.59	3.6000	2.5110
0.85000	150.57	3.6000	2.5110
0.86000	150.56	3.6000	2.5109
0.87000	150.55	3.6000	2.5109
0.88000	150.53	3.6000	2.5110
0.89000	150.52	3.6000	2.5111
0.90000	150.51	3.6000	2.5112
0.91000	150.49	3.6000	2.5114
0.92000	150.48	3.6000	2.5113
0.93000	150.47	3.6000	2.5110
0.94000	150.46	3.6000	2.5109
0.95000	150.45	3.6000	2.5110
0.96000	150.44	3.6000	2.5110
0.97000	150.43	3.6000	2.5111
0.98000	150.41	3.6000	2.5112
0.99000	150.40	3.6000	2.5111
1.0000	150.39	3.6000	2.5111

(e) Beam turned on at TIME = 0 with initial temperature = 0°C, final temperature = 150°C, and $|VRX| \leq 12$ V.

Figure 65 (continued)

excess of 100 °C due to severe overshoot in the heating current. Fortunately, the real controller has adjustable current limitations to prevent severe overshoots. First, the rate of current increase and decrease is limited by the ±12 V limit on VRX. No such limit was placed on VRX for the simulations shown in Figure 65(a), (b), and (c), but the results are shown in Figure 65(d) and (e) for a limited VRX. These figures show that the overshoot is reduced to less than 20 °C by limiting $|VRX| \leq 12$ V. This agrees well with measured overshoots. Secondly, the maximum current limit is adjustable.

While the preceding computations show good behavior for large signal beam transients, the most common beam perturbations are random noise with short term standard deviations of about 3%. Additionally, turbulence in the He atmosphere causes substantial temperature noise. To simulate beam and He induced noise, Gaussian noise was assumed for the beam power. This was accomplished by using the CSMP Gaussian random number generator with an average value of 1 and a standard deviation of 0.1. This noisy signal was then squared and multiplied by the steady state beam power. The square of ERRTMP was integrated for 1 second to obtain the variance in temperature. The standard deviation was obtained by taking the square root of the variance. For a mean temperature of 150 °C with a mean beam power of 3.6 W, the standard deviation was 0.559, 0.205, 0.188, and 0.195 °C for GAIN equal 0, 0.7, 1, and 1.4, respectively. Peak deviation in temperature (output interval = 10 msec) was 1.25, 0.51, 0.43, and 0.44 °C for GAIN equal 0, 0.7, 1, and 1.4, respectively. Since the bandwidth of this simulated noise depends on the integration step size, which is variable,

it was difficult to predetermine noise spectrum. Probably, the spectrum is relatively flat to a frequency beyond the filter cutoff frequencies. In addition, the noise spectrum of the actual beam is unknown.

IV. MEASURED TEMPERATURE CONTROLLER PERFORMANCE

Figure 66 shows the measured performance of the temperature control system. The filter corner frequencies were set for 37 Hz. Temperature error was computed from VRX. VRX, VCURR, and other data were monitored by fast sampling A-D converters (grounded) and processed by a minicomputer. Data sampling rates were 24 sec^{-1} and 1 sec^{-1}. Ground loops and RF noise pickup on the cables caused some random fluctuations in the indicated temperature. This problem has been solved in the present design by employing integrating A-D converters with differential inputs (4-1/2 digit panel meters with BCD output). Note that turning the 3.3 W off caused a drop in temperature of only 4.2 °C about 80 msec after the beam transient. Within 2.2 sec, the temperature returned to the set point temperature of 150 °C to within 0.05 °C. Note that the peak error is less than half that predicted by the computer simulation. This results from the fact that the simulation assumed an instantaneous change in beam power, whereas the actual beam has a finite rise (fall) time.

Figure 66 also depicts standard deviations in temperature. Average temperature and standard deviations were calculated on an HP45 calculator from ten consecutive data points. Note that the standard deviations are only slightly higher with beam than without beam. This fluctuation in temperature is largely due to turbulence in the He

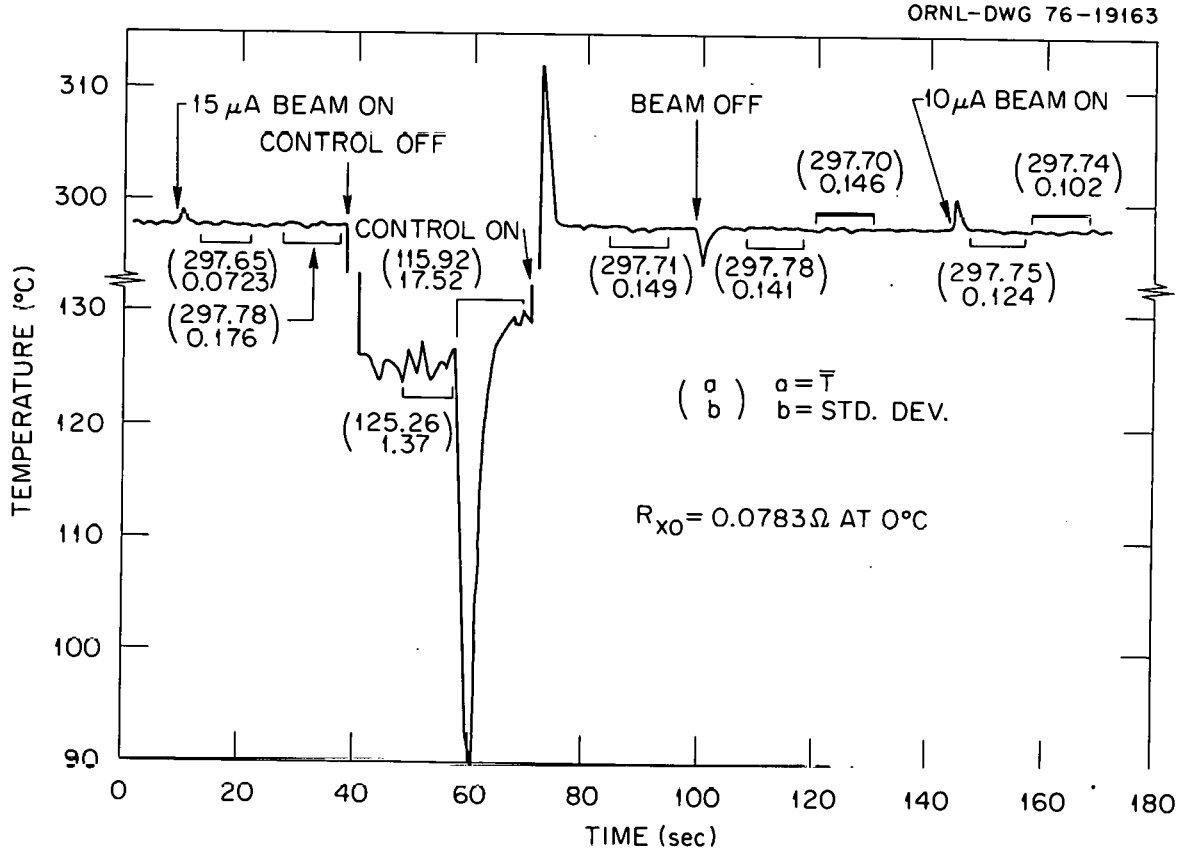

(a) Long-term response with 316 stainless steel sample.

Figure 66. Measured temperature control at 150°C.

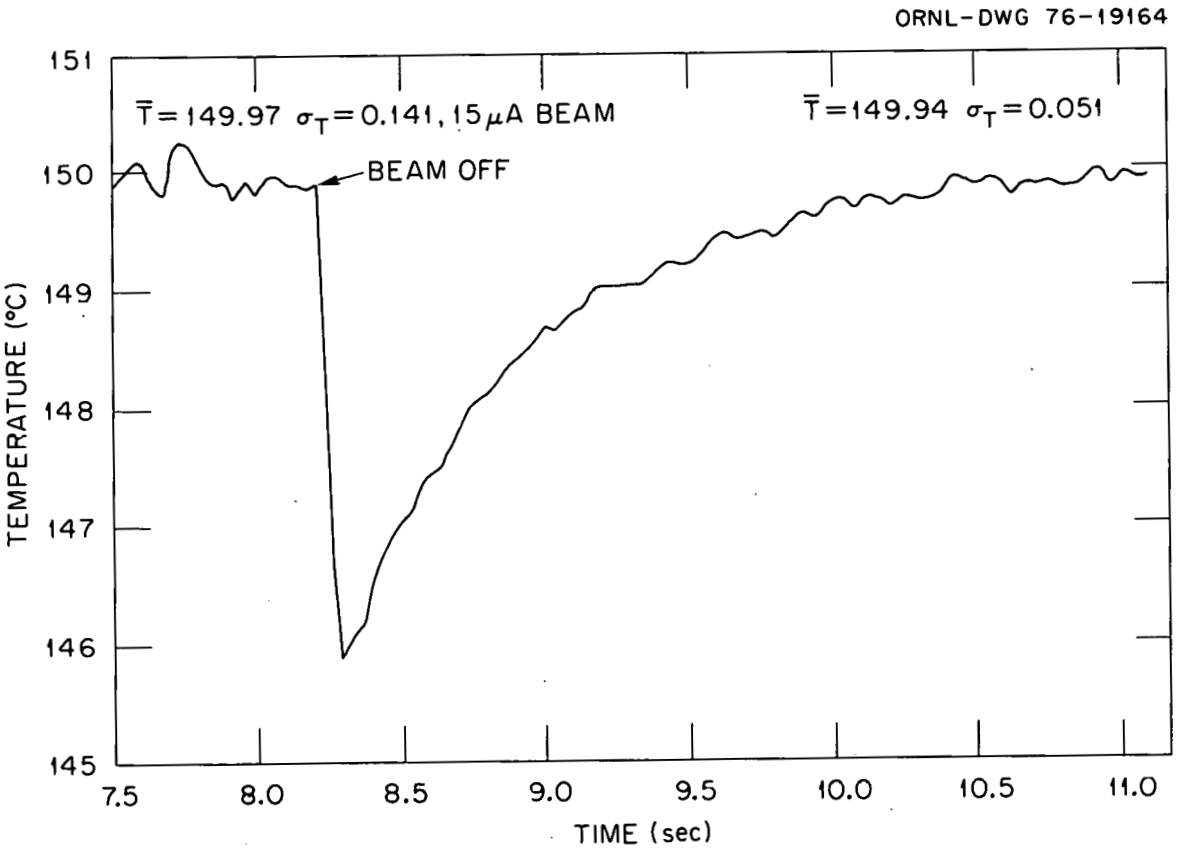

(b) Transient response with 316 stainless steel sample.

Figure 66 (continued)

atmosphere caused by the circulating fan: without beam and a constant heating current of less than 0.33 A, the fluctuation in sample temperature was twenty-five times higher in circulated He than in a vacuum. Note that without control, the standard deviation is about ten times higher ignoring the times when the beam is momentarily lost as shown in Figure 66. Note also that the turn on overshoot is only 14 °C due to the slew rate limit of the controller. Note also that this overshoot decays within 2 seconds.

Temperature controller performance was also measured at different temperatures and He pressures. For 1 at. pressure and 150 °C as shown in Figure 66, 24 sec measurement periods yielded typical standard deviations of 0.06 and 0.15 °C without and with a 3.3 W beam, respectively. Reducing the He pressure to 1/2 at. gave standard deviations of 0.07 and 0.12 °C for 10 sec measurement periods without and with a 3.3 W beam respectively. At TMPSET of 500 °C with 1 at. He, standard deviations of 0.05 and 0.12 °C were obtained for 10 second measurement periods without and with a 3.3 W beam, respectively.

Figure 67 illustrates the system error due to rectifier and linearity errors. A Keithley model 180 DVM was used to measure VERROR while a Hewlett-Packard model 3490A DMM was used to measure VCURR. RXSET = RS = 0.1 was assumed to compute ΔRX = DELRX. Peak error due to noise is shown in Figure 67. Darlington 2N5087 and 2N5089 transistor rectifiers were employed. Note that with an AD528JH opamp, ΔRX is held to within 30 ppm for currents ranging from 200 mA to above 30 A. If noise is included, then a peak error of 30 ppm is obtained for a current range of 2 A to 30 A. Excluding noise, an AD506LH opamp gives a typical

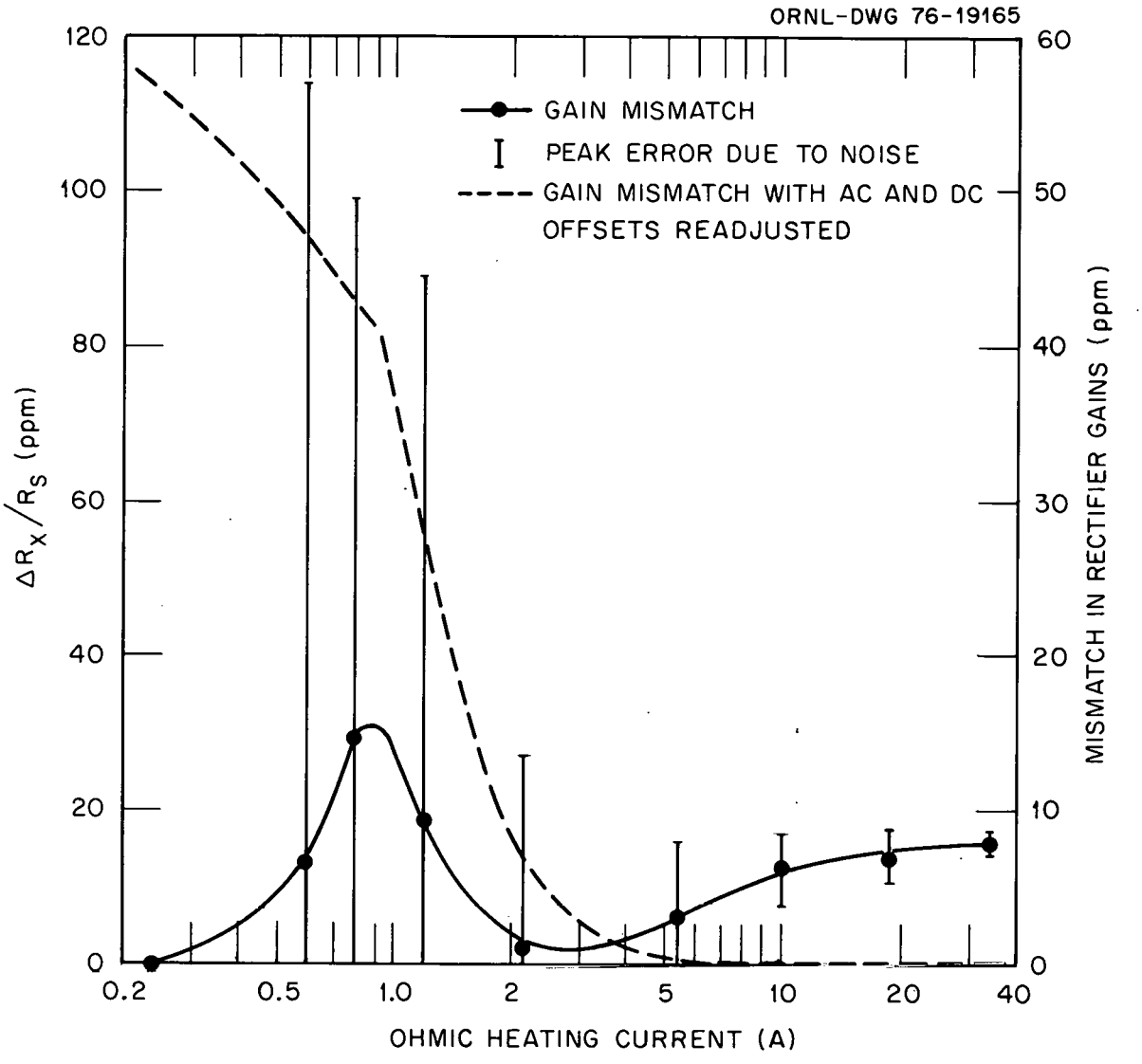

(a) AD528JH rectifier opamps.

Figure 67. Effect of rectifier linearity on control system accuracy. $R_x = R_s = 0.08\Omega$ and $r_y = 0\Omega$.

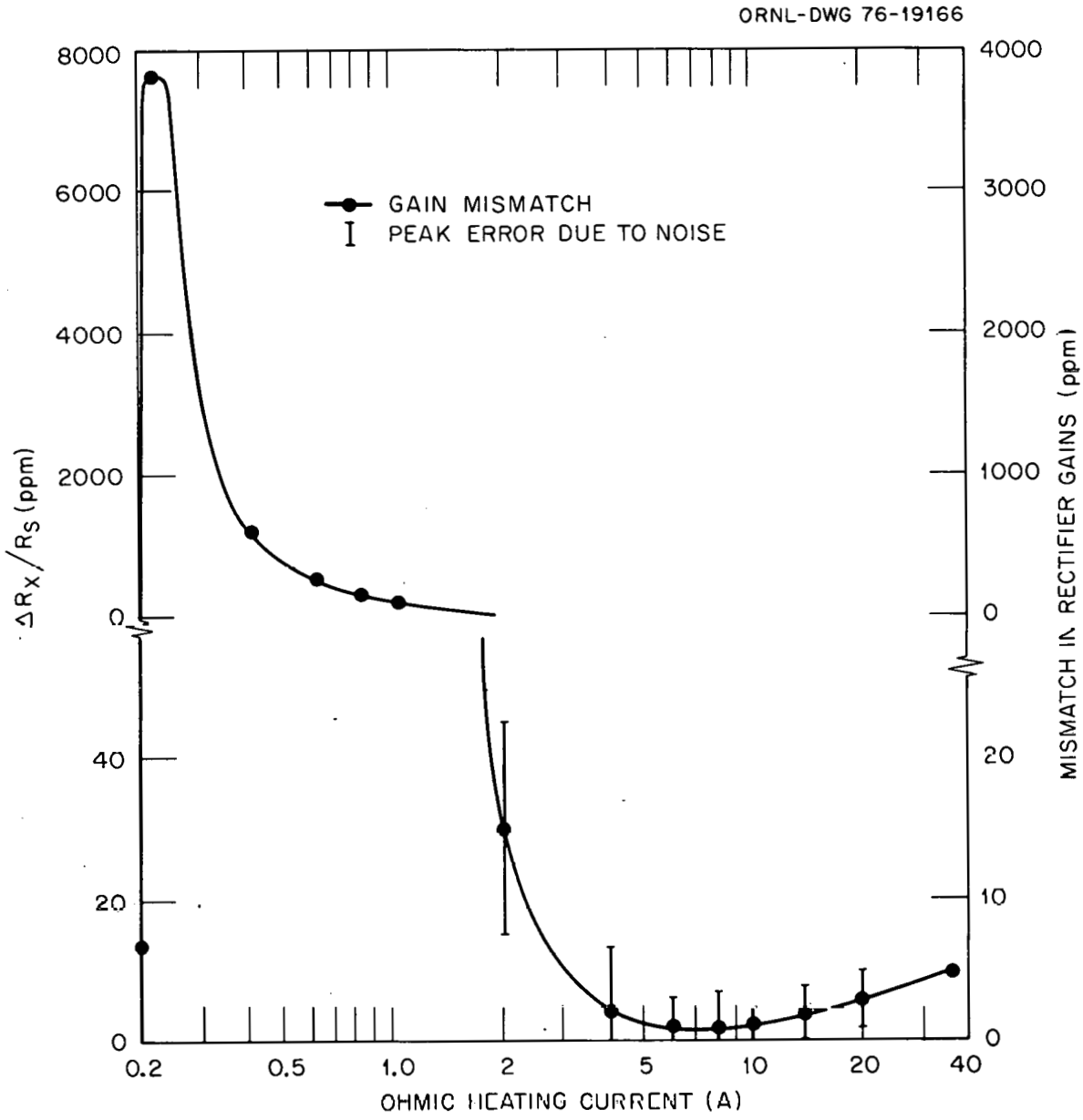

(h) AD506LH rectifier opamps.

Figure 67 (continued)

error of 30 ppm in R_x for a current greater than 2 A. Also note that for AD528JH opamps, the AC and DC offset controls can be adjusted to reduce the error to less than 10 ppm for currents above 3 A. This indicates that the PID can measure resistance with sufficient accuracy to enable outstanding temperature measurement accuracies; i.e., accuracies range from 0.005 °C at 150 °C for zirconium to 0.2 °C at 700 °C with Hastelloy F for a 10 ppm resistance accuracy. Moreover, the noise voltage contributed by the rectifiers is less than a fourth of the noise of the instrumentation amplifiers. Hence by redesign of these amplifiers, a resistance measurement accuracy of 2 ppm may be obtained.

CHAPTER VI

CONCLUSIONS

I. DISCUSSION OF RESULTS

It was shown that temperature control for an irradiation experiment is very complex. Although a constant average specimen temperature averaged along the width and length of the sample to within 0.05 °C is necessary for some materials to prevent 1 ppm thermal expansion, the temperature profile must also be fairly constant. This is required because of the nonlinear nature of thermal expansion versus temperature and nonlinearity of the temperature measurement system. Moreover, temperature dependence of the total sample creep rate may require a uniform sample temperature.

It has also been shown that accurate measurement of the specimen temperature in the environment of the cyclotron is difficult; however, a technique has been described by which the sample resistance can be utilized to measure and control specimen temperature.

A new modification of a Kelvin bridge was designed to allow compensation for resistance drift. The bridge is designed to allow two switchable balance conditions: one at operating temperature, and the other at ambient temperature. A correction potentiometer is in series so that it changes the balance condition for the sample by the same amount on both balance conditions. Thus, by periodically rebalancing the bridge with the specimen at a constant ambient temperature with the correction potentiometers, the operating set point is automatically compensated for resistance drift.

A new phase-insensitive method of detecting the bridge error signal was presented in Chapter III. It was shown that by detecting the magnitudes of two bridge signals before taking the difference, the errors caused by reactances in the bridge were substantially reduced. However, the PID is sensitive to gain drift and linearity in the AC to DC converters. In addition, the type of detector influences the transient response and noise rejection of the PID. The S/N gain for both the peak and average magnitude detector is 3 dB, but for an rms detector, the S/N gain is dependent on the input S/N. For high input S/N, the S/N gain can be substantial for an rms detector. Unfortunately, rms detectors with sufficient accuracy are too slow in response time to be used as the primary detector. Because of the low sensitivity of the average magnitude detector to phase shift of distortion products and its fast response, the average detector was deemed the best choice.

Chapter IV presented a detailed study of rectifier accuracy limitations. It was shown that current driving diodes or transistors resulted in almost perfect rectification. Furthermore, it was shown that putting diodes or transistors in the feedback path of an opamp simulated a current source drive. Neglecting frequency response limitations, an approximate analysis of the performance of the rectifier was made assuming a piecewise-linear diode model. A more accurate analysis was completed assuming an exponential diode model via an iterative technique. It was shown that for a wide range of input voltages, the computations converge in one iteration. Thus, it was possible to write an expression for the rectifier error. This technique proved much easier to use than the piecewise-linear results besides

being more accurate. Both methods showed an improvement in accuracy for both peak and average detection with an increase in opamp gain or input signal. Furthermore, it was shown that the errors were composed of three terms, a constant scale factor error, a DC offset error, and a nonlinear error. At low input voltages, the DC and nonlinear components dominate, while at high input voltages, the scale factor error dominates. Provided the gain of the opamp is constant over the frequency range of interest, the error can substantially be reduced by nulling the linear error.

To include second order effects such as device capacitance, opamp slew rate limitations and frequency response, CSMP simulations were written. These showed that for a given loop gain at the input frequency, a single pole roll off in the opamp gain can actually improve the rectifier accuracy because the error signal is shifted in phase with respect to the output.

Both computer and hand analysis showed that a transistor rectifier is potentially superior to a diode rectifier because the output is proportional (ideally) to the feedback current. Hence a transistor rectifier's error is that of the feedback current. The diode rectifier has the same error component in addition to that due to the feedback voltage. The scale factor error can be reduced substantially by making the feedback unity for the transistor rectifier.

However, the common base current gain nonlinearity can substantially reduce the accuracy of a transistor rectifier. It was illustrated that increasing H_{FE}, choosing a device with a constant H_{FE} versus collector current, or using a MOSFET could reduce or eliminate this error. The

effects of using a Darlington transistor to increase H_{FE} were examined. In the analysis including transistor capacitances, leakage currents, and H_{FE} versus collector current, some strange errors occurred. In a pure Darlington with no R, the error changed polarity at low input signals or frequency. However, for moderate to large input signals and for frequencies above 300 Hz, the error for the pure Darlington rectifier was lower than that for Darlington rectifier with R = 14.7 KΩ

Experimental waveforms and measurements were compared with calculated results. The most severe error occurred at low input voltages where the transistor model may not have been accurate. Since the computed polarity change in error for the Darlington transistor is due to device capacitance, error in capacitance values is the likely cause of the error, particularly since device capacitances (CBE) can be current dependent. Agreement between measured results and computed results was particularly good for the diode rectifier. Differences between the delay method and the differential method were small.

The temperature control system was analyzed approximately by hand in addition to elaborate CSMP simulation. Agreement of results was excellent. The effects of the filters were a small overshoot in the temperature when the beam was turned on or off. Actual system performance proved to be better than predicted since the beam cannot be manually turned on or off instantaneously. Short term temperature control (~ 10 sec) was demonstrated to be approximately 0.14 to 0.05 °C with the long term temperature control (~ 10 min) being 0.03 °C.

II. SUGGESTIONS FOR FURTHER STUDY

Several aspects of the computer simulation of rectifier accuracy could be improved. The two basic problems with the CSMP simulation were round off error and excessive execution time. The round off error might be approached in two ways. First, a signal that closely approaches that to be integrated could be subtracted from that signal. Thus the computer would have to integrate a smaller signal to the same absolute error. If the reference signal's integral is known explicitly, then it may be added to the integral of the difference signal resulting in better overall accuracy and possibly a saving in computer time. A second approach would be to investigate other numerical integration methods and incorporate them into the CSMP library via the CENTRAL integration routine in double precision. Furthermore, different computer programs might give better results (see References 72, 73, and 74 for suggested programs). In addition, accuracy could be improved by incorporating more exact models for the rectifying devices.

Effects of temperature profile on the irradiation creep experiment should be analyzed in more detail. Furthermore, resistance drift versus fluence and temperature needs to be studied in greater detail.

LIST OF REFERENCES

LIST OF REFERENCES

1. J. R. Saltvold, "A Survey of Temperature Measurement," Atomic Energy of Canada Ltd., Whiteshell Nuclear Research Establishment Technical Report No. AECL-5394.

2. F. L. Vook, "Effects of Radiation on Materials," Physics Today, Vol. 28, pp. 34-40, Sept. 1975.

3. J. H. Gittus, Creep, Viscoelasticity, and Creep Fracture. New York: John Wiley and Sons, 1975.

4. P. L. Hendrick, "Ion-Simulated Irradiation-Induced Creep," Dissertation (unpublished), Massachusetts Institute of Technology, 1975.

5. W. G. Wolfer, M. Ashkin, and A. Boltax, "Creep and Swelling Deformation in Structural Materials During Fast-Neutron Irradiation," Properties of Reactor Structural Alloys after Neutron or Particle Irradiation, ASTM STP 570. Philadelphia: ASTM, 1975, pp. 233-258.

6. Proceedings of Conference on "Fundamental Aspects of Radiation Damage in Metals," sponsored by ERDA, NSF and ORNL, Gatlinburg, Tennessee, Oct. 6-10, 1975.

7. E. R. Gilbert, "Dependence of Irradiation Creep on Temperature and Atom Displacements in 20% Cold Worked 316 Stainless Steel," International Colloquium on Measurement of Irradiation Enhanced Creep in Nuclear Materials, May 6, 1976, Petten, Netherlands.

8. R. V. Hesketh, Proceedings of Conference on "Irradiation Embrittlement and Creep in Fuel Cladding and Core Components," BNES, London, 1973, p. 221.

9. K. Hershback and K. Mueller, "Apparatus to Study Irradiation-Induced Creep with a Cyclotron," Conference on Radiation Effects and Tritium Technology for Fusion Reactors, ORNL, ERDA, ANS, AIME, Gatlinburg, Tennessee, Oct. 1976, Vol. 2, pp. 118-121.

10. R. J. McElroy, J. A. Hudson, and R. J. Frances, "Irradiation Creep Under Proton Bombardment," AERE Harwell Publication No. AERE-R 7998, 1976. A condensed version of the above paper is "Irradiation Creep During 4 MeV Proton Irradiation," Conference on Radiation Effects and Tritium Technology for Fusion Reactors, ORNL, ERDA, ANS, AIME, Gatlinburg, Tennessee, Oct. 1976, Vol. 2, pp. 72-83.

11. Y. S. Touloukia, Thermophysical Properties of High Temperature Solid Materials. New York: Macmillan Co., 1967.

12. T. Lyman, H. E. Boyer, P. M. Unterweiser, J. E. Foster, J. P. Hontas, and H. Lawton, Metals Handbook, Metals Park: ASM, 1961.

13. K. K. Chipley, Oak Ridge National Laboratory, Experimental Engineering Division, Intralaboratory correspondence.

14. T. G. Kollie, K. R. Carr, J. L. Horton, M. B. Herskovitz, and C. A. Mossman, "Temperature Measurement Errors with Type K (Chromel vs Alumel) Thermocouples Due to Short-Ranged Ordering in Chromel," ORNL Report No. ORNL-TM-4962.

15. M. Lucot, "Aging of Thermocouples by Nuclear Radiation," French Atomic Energy Report, Saclay Nuclear Research Center Report No. DPE/SPE/69-253, ML/JL, April 1967 (in French), English trans.: ORNL Tech. Report No. ORNL-tr-2854.

16. Y. S. Touloukia, D. P. Dewitt, and R. S. Hernicz, Thermophysical Properties of Matter, Vol. 9. New York: IFI Plenum Data Corp., 1972.

17. H. E. Bennett and W. F. Koehler, "Precision Measurement of Absolute Specular Reflectance with Minimized Errors," J. Opt. Soc. Am., Vol. 50, pp. 1-6, Jan. 1960.

18. D. L. Styris, R. H. Jones, O. K. Harling, G. L. Kulcinaki, and R. P. Marshall, "Some Experimental Considerations Regarding Ion Beam Simulation of Neutron Irradiation for Mechanical Property Measurements," Battelle Pacific NW Lab. Report No. BNWL-1961, 1975.

19. D. P. DeWitt and H. Kunz, "Theory and Technique for Surface Temperature Determinations by Measuring the Radiance Temperatures and the Absorptance Ratio for Two Wavelengths," in Temperature: Its Measurement and Control in Science and Industry, ed. H. H. Plumb, Pittsburg: Instrument Society of America, 1972, pp. 599-610.

20. T. P. Murray, "The Polarized Radiation Method of Radiation Thermometry," in Temperature: Its Measurement and Control in Science and Industry, ed. H. H. Plumb. Pittsburg: Instrument Society of America, 1972, pp. 619-623.

21. C. J. Borkowski and T. V. Blalock, "A New Method of Johnson Noise Thermometry," Rev. of Sci. Instrum., Vol. 45, pp. 151-162, Feb. 1974.

22. J. B. Thomas, An Introduction to Statistical Communication. New York: John Wiley and Sons, Inc., 1959.

23. M. G. Duncan, "Design Criteria of a Universal Compandor for the Elimination of Audible Noise in Tape, Disc, and Broadcast Systems," Master's Thesis (unpublished) University of Tennessee, 1973; M. G. Duncan, D. Rosenberg, and G. W. Hoffman, "Design Criteria of a Universal Compandor for the Elimination of Audible Noise in Tape, Disc, and Broadcast Systems," J. Aud. Eng. Soc., Vol. 23, pp. 610-622, Oct. 1975; "Correction to ...," Vol. 24, p. 121, Mar. 1976.

24. E. F. McClain, Jr., "Intermodulation Distortion Produced by Out-of-Band Program Components," J. Aud. Eng. Soc., Vol. 24, pp. 103-106, Mar. 1976.

25. J. J. Hill, "Platinum-Resistance Thermometry Using an AC Inductive Ratio Bridge," ISA Transactions, Vol. 7, pp. 101-107, 1968.

26. G. C. Stauffer and M. A. Hunter, "Alloys of Iron and Nickel in Resistance Thermometry," in Temperature: Its Measurement and Control in Science and Industry. New York: Reinhold Publishing Corp., 1941, pp. 1236-1323.

27. F. J. Weaver and D. L. McElroy, ORNL Intralaboratory correspondence, Oct. 1, 1975; H. E. McCoy, Jr. and D. L. McElroy, "Electrical Resistivity Anomaly in Nickel-Base Alloys," Trans. of the ASM, Vol. 61, pp. 729-741, 1968.

28. G. J. Dienes and G. H. Vineyard, Radiation Effects in Solids. New York: Interscience Publishers Inc., 1957.

29. A. J. Dekker, Solid State Physics. Englewood Cliffs: Prentice-Hall, Inc., 1957.

30. J. D. Cobine, Gaseous Conductor. New York: Dover, 1958, p. 123.

31. L. G. Christophorou, Atomic and Molecular Radiation Physics. London: John Wiley and Sons Ltd., 1971, p. 236.

32. P. P. B. Brooks, Calibration Procedures for Direct-Current Resistance Apparatus, NBS Monogram 39. Washington, D.C.: U.S. Government Printing Office, 1962.

33. "Standard Method of Test for Temperature-Resistance Constants of Alloy Wires for Precision Resistors," B-84, 1958 Book of ASTM Standards, 1958, III, pp. 466-471.

34. "Standard Method of Test for Temperature-Resistance Constants of Sheet Materials for Shunts and Precision Resistors," B114, 1958 Book of ASTM Standards, 1958, III, pp. 472-476.

35. "Standard Method of Test for Resistivity of Electrical Conductor Materials," B193, 1958 Book of ASTM Standards, 1958, III, pp. 455-459.

36. T. D. Towers, "D.C. and A.C. Bridges," Wireless World, Vol. 75, pp. i-iv, Feb. 1969.

37. D. K. Cheng, Analysis of Linear Systems. Massachusetts: Addison-Wesley Pub. Co., Inc., 1959.

38. J. J. Blum, Introduction to Analog Computations. New York: Harcourt, Brace and World, Inc., 1969.

39. Signetics Digital, Linear, and MOS Applications. Sunnyvale: Signetics, 1974.

40. W. Weyhman, "Thermometry at Ultralow Temperatures," in Methods of Experimental Physics: Solid State Physics, ed. L. Marton and R. V. Coleman. New York: Academic Press, 1974, pp. 489-501.

41. C. G. Kirby, "The Use of Operational Amplifiers to Generate Precise Current Ratios for Platinum Resistance Thermometry," in Temperature: Its Measurement and Control in Science and Industry, ed. H. H. Plumb. Pittsburg: Instrument Society of America, 1972, pp. 1511-1519.

42. K. L. Smith, "The Ubiquitous Phase Sensitive Detector," Wireless World, Vol. 78, pp. 367-370, Aug. 1972.

43. D. H. Sheingold, Nonlinear Circuits Handbook, Designing with Analog Function Modules and IC's. Norwood: Analog Devices, Inc., 1976.

44. "New Product Applications: Multijunction Thermal Converter Features 1-ppm AC/DC Transfer Difference," IEEE Spectrum, Vol. 11, p. 72, Dec. 1974.

45. W. E. Ott, "A New Technique of Thermal RMS Measurement," IEEE Journal of Solid-State Circuits, Vol. SC-9, pp. 374-380, Dec. 1974.

46. H. Handler, "True RMS Voltage Conversion," Electronic Design, Vol. 4, pp. 66-72, Feb. 1974.

47. M. Wind, Handbook of Electronic Measurements. New York: Polytechnic Press, 1956, Ch. 2.

48. D. K. Mee, "An RMS Converter for Application in a Johnson Noise Thermometer," Master's Thesis (unpublished), University of Tennessee, 1976.

49. A. S. Grove, Physics and Technology of Semiconductor Devices. New York: John Wiley and Sons, Inc., 1967.

50. J. F. Pierce and T. J. Paulus, Applied Electronics. Columbus: Charles E. Merrill Pub. Co., 1972.

51. J. J. Ebers and J. L. Moll, "Large-Signal Behavior of Junction Transistors," Proc. IRE, Vol. 42, pp. 1761-1772, Dec. 1954.

52. M. Abramowitz and I. A. Stegun, Handbook of Mathematical Functions with Formulas, Graphs, and Mathematical Tables. NBS Applied Math Series 55. Washington, D.C.: U.S. Government Printing Office, 1970.

53. V. A. Thomason, "A Study of an A.C. to D.C. Conversion Instrument," Master's Thesis (unpublished), University of Tennessee, 1971.

54. M. J. Chien and E. S. Kuh, "Solving Piecewise-Linear Equations for Resistive Networks," Intl. J. Circuit Theory and Appl., Vol. 4, pp. 3-24.

55. L. O. Chau, "Efficient Computer Algorithms for Piecewise-Linear Analysis of Resistive Nonlinear Networks," IEEE Trans. Circuit Theory, Vol. CT-18, pp. 73-85, Jan. 1971.

56. T. Fujisawa, E. S. Kuh, and T. Ohtsuki, "A Sparse Matrix Method for Analysis of Piecewise-Linear Resistive Networks," IEEE Trans. Circuit Theory, Vol. CT-19, pp. 572-584, Nov. 1972.

57. E. S. Kuh and I. N. Hajj, Nonlinear Circuit Theory: Resistive Networks," Proc. IEEE, Vol. 59, pp. 340-355, Mar. 1971.

58. M. J. Chien, "Conditions for a Piecewise-Linear Resistive Network Function to be Homeomorphic," Proc. Eighth Annual Southeastern Symposium Syst., IEEE, Apr. 26-27, 1976.

59. T. Ohtsuki and N. Yoshida, "DC Analysis of Nonlinear Networks Based on Generalized Piecewise-Linear Characterization," IEEE Trans. Circuit Theory, Vol. CT-18, pp. 146-152, Jan. 1971.

60. R. A. Schaefer, "Production of Harmonics and Distortion in P-N-Junctions," J. Aud. Eng. Soc., Vol. 19, pp. 759-768, Oct. 1971.

61. W. M. C. Sansen and R. G. Meyer, "Distortion in Bipolar Transistor Variable-Gain Amplifiers," IEEE J. Solid-State Circuits, Vol. SC-8, pp. 275-282, Aug. 1973.

62. S. M. Perlow, "Intermodulation Distortion in Resistive Mixers," RCA Review, Vol. 35, pp. 25-47, Mar. 1974.

63. T. R. Williams, Programming Notes: PCAP 3. Princeton: Trustees of Princeton University, 1970.

64. W. L. Green and F. H. Speckhart. A User's Guide to CSMP—The Continuous System Modeling Program. Englewood Cliffs: Prentice-Hall, 1976.

65. Continuous System Modeling Program III (CSMP III) Program Reference Manual. Ontario: International Business Machines Corp., 1972.

66. M. Otala, "Circuit Design Modifications for Minimizing Transient Intermodulation Distortion in Audio Amplifiers," Jour. Aud. Eng. Soc., Vol. 20, pp. 296-299, June 1972.

67. R. J. Apfel and P. R. Gray, "A Fast-Settling Monolithic Operational Amplifier Using Doublet Compression Techniques," IEEE J. Solid-State Circuits, Vol. SC-9, pp. 332-340, Dec. 1974.

68. J. G. Graeme, Applications of Operational Amplifiers. New York: McGraw-Hill Book Co., 1973.

69. J. E. Solomon, "The Monolithic Op Amp: A Tutorial Study," IEEE J. Solid-State Circuits, Vol. SC-9, pp. 314-332, Dec. 1974.

70. S. Bernstein, "Represent Transistor Beta Variations," Electronic Design, Vol. 19, pp. 146-148, Sept. 13, 1974.

71. R. D. Thorton, D. DeWitt, E. R. Chenette, and P. E. Gray, Characteristics and Limitations of Transistors. New York: John Wiley and Sons, Inc., 1966, Ch. 4.

72. F. H. Branin, Jr., G. R. Rogsett, R. L. Lunde, and L. E. Kugel, "ECAP-II—A New Electronic Circuit Analysis Program," IEEE J. Solid-State Circuits, Vol. SC-6, pp. 146-166, Aug. 1971.

73. L. Nagel and R. Rohrer, "Computer Analysis of Nonlinear Circuits, Excluding Radiation (CANCER)," IEEE J. Solid-State Circuits, Vol. SC-6, pp. 166-182, Aug. 1971.

74. F. S. Jenkins and S. P. Fan, "TIME—A Nonlinear DC and Time-Domain Circuit-Simulation Program," IEEE J. Solid-State Circuits, Vol. SC-6, pp. 182-188, Aug. 1971.

THIS PAGE

WAS INTENTIONALLY

LEFT BLANK

APPENDIXES

APPENDIX A

COMPUTER PROGRAMS TO FIT POLYNOMIAL EQUATIONS TO SPECIMEN RESISTANCE AND LENGTH VERSUS TEMPERATURE DATA POINTS AND TO CALCULATE PARAMETERS OF THE TEMPERATURE CONTROL SYSTEM

The following program will fit polynomial equations of the form $Y(X) = \sum_{j=1}^{N} A_j X^{j-1}$ to M data points, (X,Y) where $N \leq M \leq 20$. Moreover, the program also provides a polynomial equation for X(Y). Optionally, Y(X)/Y(0) and X(Y/Y(0)) may be computed. Usage and description of the program are given on the next page.

```
C  CURVE FITTING PROGRAM WRITTEN BY MICHAEL G. DUNCAN ON JANUARY 2, 1976
C
C  ******************************************************************
C
C
C  PURPOSE
C     TO FIT A POLYNOMIAL EQUATION OF ORDER LESS THAN M TO M DATA POINTS
C     ROUTINE GIVES BOTH Y(X) AND X(Y).
C
C  DESCRIPTION OF PARAMETERS
C     NTRCHG IS EMPLOYED TO INTERCHANGE X & Y SO AS TO GIVE Y(X) & X(Y).
C     WHEN NTRCHG IS 1, X & Y ARE EQUAL TO THEIR ORIGINAL VALUES, BUT
C     WHEN NTRCHG IS 2, X & Y ARE EQUAL TO THE ORIGINAL VALUES OF Y & X,
C     RESPECTIVELY.
C     X IS THE VARIABLE DESCRIBED BY NAMEX AND NAMEY WHEN NTRCHG IS 1 &
C     RESPECTIVELY.
C     Y  IS THE VARIABLE DESCRIBED BY NAMEY & NAMEX WHEN NTRCHG IS 1 & 2
C     RESPECTIVELY.  Y IS A FUNCTION OF X.
C     METAL = TYPE OF METAL.
C     M = NUMBER OF DATA POINTS (X,Y).
C     YERROR = RMS ERROR; THAT IS, SQROOT(SUM OF ((YCAL - Y) ** 2) / M).
C     XERROR = RMS ERROR; THAT IS, SQROOT(SUM OF ((XCAL - X) ** 2) / M).
C     NODATA = NUMBER OF DATA SETS.
C
C  INSTRUCTIONS FOR USE OF PROGRAM.
C     ON THE FIRST CARD TYPE THE NUMBER OF DATA SETS IN THE FIRST TWO
C     COLUMNS,AND IN THE THIRD COLUMN TYPE THE NUMBER 1 IF NORMALIZATION
C     IS DESIRED.  LEAVE IT BLANK OTHERWISE.  NORMALIZATION WILL GIVE
C     X(Y/Y0) WHERE X(1) = 0.  OTHERWISE Y0 = 1. ON THE NEXT  DATA CARD
C     TYPE THE NAME OF THE METAL IN THE FIRST TWENTY COLUMNS, NAMEX IN
C     THE NEXT TWENTY COLUMNS, NAMEY IN THE FOLLOWING TWENTY COLUMNS,
C     XSRROR IN THE NEXT NINE COLUMNS, YERROR IN THE FOLLOWING NINE
C     COLUMNS, AND THE NUMBER OF DATA POINTS IN THE LAST TWO COLUMNS.
C     ON THE NEXT CARD TYPE THE DATA POINTS, (X,Y),IN CONSECUTIVE ORDER
C     ACROSS THE CARD ALLOWING TEN SPACES PER NUMBER.  FOR INSTANCE,
C     IF M = 5, THEN ONE DATA CARD WOULD HOLD  THE FOLLOWING: X1,Y1,X2,
C     Y2,X3,Y3,X4,Y4, AND THE NEXT CARD WOULD HOLD THE FIFTH DATA POINT.
C     UP TO TWENTY DATA POINTS CAN BE HANDLED WITHOUT PROGRAM MODIFI-
C     THE METAL ETC. ON THE NEXT CARD.  UP TO 99 DATA SETS CAN BE
C     HANDLED.
C
C  REMARKS
C     PROGRAM USES LEAST SQUARE ERROR CRITERIA.
C     PROGRAM CALLS SUBROUTINE DGELG TO SOLVE SIMULTANEOUS LINEAR
C     EQUATIONS.
C     PRINTS ERROR MESSAGES IF NODATA = 0, M LESS THAN 2 OR GREATER THAN
C     20, OR X OR Y TOO LARGE FOR A GIVEN M.
C
C  ******************************************************************
C
C
      DIMENSION NAMEX(5), NAMEY(5), METAL(5)
      DOUBLE PRECISION X(20), Y(20), A(20), CONST(20), YCAL(20),
     1  LSQCA(400), SUMATX(39), ABSERR(20), XSTORE(20), YSTORE(20),
     2 SUMSQ, XO, DSQRT, DABS
      READ 1000, NODATA, NORM
```

```
C
C  PRINTS ERROR MESSAGE IF NODATA =0.
C
      IF (NODATA.EQ.0) PRINT 1010
C
C  DO LOOP TO HANDLE NODATA NUMBER OF DATA SETS.
C
      DO 280 NUMRUN = 1, NODATA
      READ 1020, METAL, NAMEX, NAMEY, XERROR, YERROR, M
C
C  PRINTS ERROR MESSAGE IF M .GT. 20 .OR. M .LT. 2.
C
      IF (M .GT. 20 .OR. M .LT. 2) PRINT 1030
      READ 1040, (X(KLM), Y(KLM), KLM = 1, M)
C
C  THE MAXIMUM ORDER OF THE EQUATION IS M - 1.
C
      MLS1 = M - 1
      MLS1X2 = 2 * MLS1 + 1
      SUMATX(1) = FLOAT(M)
C
C  DO LOOP TO INTERCHANGE X & Y SO AS TO GIVE Y(X) & X(Y).
C
      DO 280 NTRCHG = 1, 2
C
C  SET UP OF COEFFICIENT MATRIX FOR SUBROUTINE DGELG.
C
      DO 30  K = 2, MLS1X2
      SUMATX(K) = 0.0
C
C  NOTE THAT THE DO LOOP ON CARD 10 MAY BE DO 20 OR DO 30 TO ALTER THE
C  CPU TIME AND ERROR PRINTOUT EFFICIENCY.  IF DO 20, CPU TIME IS FASTER
C  BUT OVERFLOW MAY TERMINATE EXECUTION BEFORE ERROR MESSAGE IS PRINTED.
C  IF DO THE ERROR MESSAGE WILL BE PRINTED BEFORE OR AFTER OVERFLOW.
C  CPU TIME MAY BE SLIGHTLY LONGER, HOWEVER.
C
   10 DO 30 KA = 1, M
   20 SUMATX(K) = SUMATX(K) + X(KA)**(K - 1)
C
C  PRINTS WARNING STATEMENT IF SUMATX(K) .GT. 7E75 AND LIMITS THE
C  MAXIMUM ORDER OF THE POLYNOMIAL TO LESS THAN M-1 TO PREVENT OVERFLOW.
C
      IF (SUMATX(K) .GT. 7.0E75)  GOTO 40
   30 CONTINUE
      MPRIME = M
      GO TO 80
   40 IF (NTRCHG - 1) 50, 50, 60
   50 PRINT 1050
      GO TO 70
   60 PRINT 1060
   70 MPRIME = K / 2
   80 MPRLS1 = MPRIME - 1
C
C  SET UP OF CONSTANT VECTOR FOR SUBROUTINE DGELG.
C
      DO 110  JK = 1,  MPRIME
      CONST(JK) = 0.0
      DO 110  LK = 1, M
      IF (JK - 1) 90, 90, 100
   90 CONST(JK) = Y(LK) + CONST(JK)
      GO TO 110
  100 CONST(JK) = CONST(JK) + Y(LK) * X(LK)**(JK - 1)
  110 CONTINUE
```

```
C  DO LOOP TRIES TO FIT LINEAR EQUATION FIRST.  IF ERROR IS TOO HIGH, IT
C  INCREASES THE ORDER OF THE EQUATION UNTIL ERROR REQUIREMENTS ARE MET
C  OR THE ORDER REACHES MPRIME - 1.
C
      DO 250  N = 1, MPRLS1
      NPLUS1 = N + 1
C
C  CONST IS USED FOR STORAGE OF CONSTANT VECTOR.  A IS SET EQUIVALENT TO
C  CONST BEFORE EXECUTION OF DGELG.  DGELG RETURNS RESULTANT VECTOR AS
C  VECTOR A.
C
      DO 120  JKL = 1, NPLUS1
      A(JKL) = CONST(JKL)
      DO 120  LKJ = 1, NPLUS1
  120 LSQCA((LKJ - 1) * NPLUS1 + JKL) = SUMATX(LKJ + JKL - 1)
      CALL DGELG(A, LSQCA, NPLUS1, 1, 1.0E-14, IER)
C
C  CALCULATION OF Y(X) AND ERROR TEST.
C
      SUMSQ = 0.0
      DO 150 IC = 1, M
      YCAL(IC) = A(NPLUS1)
      DO 140  LC = 1, N
  140 YCAL(IC) = YCAL(IC) * X(IC) + A(NPLUS1 - LC)
      ABSERR(IC) =    Y(IC) - YCAL(IC)
  150 SUMSQ = SUMSQ + (ABSERR(IC)) ** 2
C
C  CONVERTS SUM SQUARE ERROR TO RMS ERROR.
C
      SUMSQ = DSQRT(SUMSQ / SUMATX(1))
C
C  EXCHANGE OF X AND Y HEADINGS WHEN NTRCHG = 2.
C
      IF ( NTRCHG - 1) 160, 160, 220
C
C  XO = Y(0) WHEN NTRCHG = 1
C
  160 IF (NORM - 1) 170, 180, 170
  170 XO = 1.0
      PRINT 1080, METAL, NAMEX, NAMEY, (L, X(L), Y(L), YCAL(L),
     1 ABSERR(L), L = 1, M)
      PRINT 1090, NAMEY, NAMEX, METAL, A(1), (A(KOUNT+1), KOUNT, KOUNT =
     1 1, N)
      PRINT 1100, XO
      GO TO 210
C
C  NORMALIZATION OF Y.    Y IS DIVIDED BY Y(0).
C
  180 XO = A(1)
      DO 190 MGD = 2, NPLUS1
  190 A(MGD) = A(MGD) / A(1)
      PRINT 1080, METAL, NAMEX, NAMEY, (L, X(L), Y(L), YCAL(L),
     1 ABSERR(L), L = 1, M)
  200 PRINT 1110, NAMEY, NAMEX, METAL, A(1), (A(KOUNT+1), KOUNT, KOUNT =
     1 1, N)
  210 PRINT 1120, SUMSQ
      IF (IER .NE. 0) PRINT 1070, IER
      IF (SUMSQ .LE. YERROR) GO TO 270
      GO TO 250
```

```
C
C  Y(X) IS NORMALIZED TO Y(X/XO).
C
  220 DO 230 MGD = 2, NPLUS1
  230 A(MGD) = A(MGD) * (XO ** (MGD - 1))
      PRINT 1080, METAL, NAMEY, NAMEX, (L, X(L), Y(L), YCAL(L),
     1 ABSERR(L), L = 1, M)
  240 PRINT 1090, NAMEX, NAMEY, METAL, A(1), (A(KOUNT+1), KOUNT, KOUNT =
     1 1, N)
      PRINT 1100, XO
      PRINT 1120, SUMSQ
      IF (IER .NE. 0) PRINT 1070, IER
      IF (SUMSQ .LE. XERROR) GO TO 280
  250 CONTINUE
C
C
C  PRINT WARNING IF ERROR REQUIREMENT NOT MET.
C
  260 PRINT 1130
  270 CONTINUE
C
C  THIS ROUTINE INTERCHANGES X AND Y.
C
      DO 275 IC = 1, M
      XSTORE(IC) = X(IC)
      YSTORE(IC) = Y(IC)
      Y(IC) = XSTORE(IC)
  275 X(IC) = YSTORE(IC)
  280 CONTINUE
 1000 FORMAT (I2, I1)
 1010 FORMAT (1H1, ' *** ERROR *** NODATA (THE NUMBER OF DATA SETS) IS S
     1PECIFIED AS ZERO.')
 1020 FORMAT ( 15A4, 2E5.2, I2)
 1030 FORMAT (1H0, ' *** ERROR *** M .GT. 20 .OR. M .LT. 2.')
 1040 FORMAT ( 8F10.8)
 1050 FORMAT (1H1, ' *** WARNING *** SUM OF X**(2*M-1) .GT. 7E75, MAXIMU
     1M ORDER OF THE POLYNOMIAL HAS BEEN  LIMITED .LT. M-1.')
 1060 FORMAT (1H1, ' *** WARNING *** SUM OF Y**(2*M-1) .GT. 7E75.  MAXIM
     1UM ORDER OF THE POLYNOMIAL HAS BEEN LIMITED .LT. M-1')
 1070 FORMAT (1H0, 60X, 'IER = ', I3)
 1080 FORMAT (1H1, 44X,'DATA POINTS AND RESULTS FOR ', 5A4, //, 18X,
     1 'L', 8X,'X = ',  5A4, 2X, 'Y = ', 5A4, 10X, 'YCAL(L)', 15X,
     2 'Y(L) - YCAL(L)', //, (17X, I2, 13X, 1PD13.6, 13X, 1PD13.6, 13X,
     3 1PD13.6, 13X, 1PD13.6, /))
 1090 FORMAT (1H0, 24X, 5A4, ' AS A FUNCTION OF ', 5A4, ' FOR ', 5A4,
     1 //, 46X, 'Y =      ', 1PD13.6, /, (/, 50X, ' + (', 1PD13.6
     2, ') * (X / XO) ** ', I2))
 1100 FORMAT (1H0, /, 54X,'WHERE XO = ', 1PD13.6)
 1110 FORMAT (1H0, 24X, 5A4, ' AS A FUNCTION OF ', 5A4, ' FOR ', 5A4,
     1 //, 43X, 'Y / (', 1PD13.6, ') = 1.0' /, (/, 60X, ' + (', 1PD13.6
     2, ') * X ** ', I2))
 1120 FORMAT (1H0, /, 47X, 'ROOT MEAN SQUARE ERROR = ', 1PE13.6)
 1130 FORMAT (1H1, '*** WARNING *** XERROR OR YERROR REQUIREMENTS HAVE
     1NOT BEEN MET')
      STOP
      END
```

```
C     ..................................................................
C
C        SUBROUTINE DGELG
C
C        PURPOSE
C           TO SOLVE A GENERAL SYSTEM OF SIMULTANEOUS LINEAR EQUATIONS.
C
C        USAGE
C           CALL DGELG(R,A,M,N,EPS,IER)
C
C        DESCRIPTION OF PARAMETERS
C           R       - DOUBLE PRECISION M BY N RIGHT HAND SIDE MATRIX
C                     (DESTROYED). ON RETURN R CONTAINS THE SOLUTIONS
C                     OF THE EQUATIONS.
C           A       - DOUBLE PRECISION M BY M COEFFICIENT MATRIX
C                     (DESTROYED).
C           M       - THE NUMBER OF EQUATIONS IN THE SYSTEM.
C           N       - THE NUMBER OF RIGHT HAND SIDE VECTORS.
C           EPS     - SINGLE PRECISION INPUT CONSTANT WHICH IS USED AS
C                     RELATIVE TOLERANCE FOR TEST ON LOSS OF
C                     SIGNIFICANCE.
C           IER     - RESULTING ERROR PARAMETER CODED AS FOLLOWS
C                     IER=0  - NO ERROR,
C                     IER=-1 - NO RESULT BECAUSE OF M LESS THAN 1 OR
C                              PIVOT ELEMENT AT ANY ELIMINATION STEP
C                              EQUAL TO 0.
C                     IER=K  - WARNING DUE TO POSSIBLE LOSS OF SIGNIFI-
C                              CANCE INDICATED AT ELIMINATION STEP K+1,
C                              WHERE PIVOT ELEMENT WAS LESS THAN OR
C                              EQUAL TO THE INTERNAL TOLERANCE EPS TIMES
C                              ABSOLUTELY GREATEST ELEMENT OF MATRIX A.
C
C        REMARKS
C           INPUT MATRICES R AND A ARE ASSUMED TO BE STORED COLUMNWISE
C           IN M*N RESP. M*M SUCCESSIVE STORAGE LOCATIONS. ON RETURN
C           SOLUTION MATRIX R IS STORED COLUMNWISE TOO.
C           THE PROCEDURE GIVES RESULTS IF THE NUMBER OF EQUATIONS M IS
C           GREATER THAN 0 AND PIVOT ELEMENTS AT ALL ELIMINATION STEPS
C           ARE DIFFERENT FROM 0. HOWEVER WARNING IER=K - IF GIVEN -
C           INDICATES POSSIBLE LOSS OF SIGNIFICANCE. IN CASE OF A WELL
C           SCALED MATRIX A AND APPROPRIATE TOLERANCE EPS, IER=K MAY BE
C           INTERPRETED THAT MATRIX A HAS THE RANK K. NO WARNING IS
C           GIVEN IN CASE M=1.
C
C        SUBROUTINES AND FUNCTION SUBPROGRAMS REQUIRED
C           NONE
C
C        METHOD
C           SOLUTION IS DONE BY MEANS OF GAUSS-ELIMINATION WITH
C           COMPLETE PIVOTING.
C
C     ..................................................................
C
      SUBROUTINE DGELG(R,A,M,N,EPS,IER)
C
C
      DIMENSION A(400),R(20)
      DOUBLE PRECISION R,A,PIV,TB,TOL,PIVI, DABS
      IF(M)230,230,10
```

```
C       SEARCH FOR GREATEST ELEMENT IN MATRIX A
   10 IER=0
      PIV=0.D0
      MM=M*M
      NM=N*M
      DO 30 L=1,MM
      TB=DABS(A(L))
      IF(TB-PIV)30,30,20
   20 PIV=TB
      I=L
   30 CONTINUE
      TOL=EPS*PIV
C     A(I) IS PIVOT ELEMENT. PIV CONTAINS THE ABSOLUTE VALUE OF A(I).
C
C
C     START ELIMINATION LOOP
      LST=1
      DO 170 K=1,M
C
C     TEST ON SINGULARITY
      IF(PIV)230,230,40
   40 IF(IER)70,50,70
   50 IF(PIV-TOL)60,60,70
   60 IER=K-1
   70 PIVI=1.D0/A(I)
      J=(I-1)/M
      I=I-J*M-K
      J=J+1-K
C     I+K IS ROW-INDEX, J+K COLUMN-INDEX OF PIVOT ELEMENT
C
C     PIVOT ROW REDUCTION AND ROW INTERCHANGE IN RIGHT HAND SIDE R
      DO 80 L=K,NM,M
      LL=L+I
      TB=PIVI*R(LL)
      R(LL)=R(L)
   80 R(L)=TB
C
C     IS ELIMINATION TERMINATED
      IF(K-M)90,180,180
C
C     COLUMN INTERCHANGE IN MATRIX A
   90 LEND=LST+M-K
      IF(J)120,120,100
  100 II=J*M
      DO 110 L=LST,LEND
      TB=A(L)
      LL=L+II
      A(L)=A(LL)
  110 A(LL)=TB
C
C     ROW INTERCHANGE AND PIVOT ROW REDUCTION IN MATRIX A
  120 DO 130 L=LST,MM,M
      LL=L+I
      TB=PIVI*A(LL)
      A(LL)=A(L)
  130 A(L)=TB
C
C     SAVE COLUMN INTERCHANGE INFORMATION
      A(LST)=J
```

```
C
C     ELEMENT REDUCTION AND NEXT PIVOT SEARCH
      PIV=0.D0
      LST=LST+1
      J=0
      DO 160 II=LST,LEND
      PIVI=-A(II)
      IST=II+M
      J=J+1
      DO 150 L=IST,MM,M
      LL=L-J
      A(L)=A(L)+PIVI*A(LL)
      TB=DABS(A(L))
      IF(TB-PIV)150,150,140
  140 PIV=TB
      I=L
  150 CONTINUE
      DO 160 L=K,NM,M
      LL=L+J
  160 R(LL)=R(LL)+PIVI*R(L)
  170 LST=LST+M
C     END OF ELIMINATION LOOP
C
C
C     BACK SUBSTITUTION AND BACK INTERCHANGE
  180 IF(M-1)230,220,190
  190 IST=MM+M
      LST=M+1
      DO 210 I=2,M
      II=LST-I
      IST=IST-LST
      L=IST-M
      L=A(L)+.5D0
      DO 210 J=II,NM,M
      TB=R(J)
      LL=J
      DO 200 K=IST,MM,M
      LL=LL+1
  200 TB=TB-A(K)*R(LL)
      K=J+L
      R(J)=R(K)
  210 R(K)=TB
  220 RETURN
C
C
C     ERROR RETURN
  230 IER=-1
      RETURN
      END
```

The next program takes normalized equations for $R_x(T)$ and $L(T)$, as provided by the previous program, to compute the following parameters at six temperatures: given the resistivity of the sample at T = 0 °C, $R_x(T)$ and $R_x'(T)$ for one or two sample thicknesses and a gauge length of 2 cm, the temperature and resistance control for 1 ppm thermal expansion, the thermal expansion for 0.05 °C temperature control, V_{error} due to specimen temperature changes of 0.05 °C and that which causes 1 ppm thermal expansion both with and without beam power, V_{R_x} (V_{error} normalized with respect to heating current) for 0.05 °C temperature change and that which results in 1 ppm thermal expansion, ohmic heating current and the current monitor voltage (V_{Rx}) with and without beam power, the sample temperature deviations from set point that will cause V_{error} and V_{Rx} to be 10 V, and the bridge potentiometer settings (CP). All of the above are calculated for three values of R_s. If a given parameter cannot be computed for a given condition, the value of zero is assigned. A sample printout is also provided.

```
C IRRADIATION CREEP TEMPERATURE CONTROL PARAMETER LIMITS PROGRAM WRITTEN
C BY MICHAEL G. DUNCAN ON JANUARY 14, 1976.
C
C*********************************************************************
C
C
C  PURPOSE
C     TO FIND PARAMETER LIMITS OF SAMPLE TEMPERATURE CONTROL SYSTEM FOR
C     IRRADIATION CREEP EXPERIMENT.   PROGRAM FINDS THE FOLLOWING
C     PARAMETERS AT SIX OPERATING TEMPERATURES, WITH AND WITHOUT BEAM,
C     AND FOR 3 AND 5 MIL SAMPLES:  RX AND ITS TEMPERATURE COEFFICIENT,
C     BOTH ERROR MONITOR VOLTAGES FOR 0.05 C TEMPERATURE ERROR AND THE
C     TEMPERATURE ERROR THAT WOULD CAUSE 1 MICROSTRAIN ERROR, TEMPERA-
C     TURE DEVIATION LIMITS FOR BOTH ERROR VOLTAGES, HEATING CURRENT AND
C     ITS MONITOR VOLTAGE, AND STRAIN ACCURACY FOR 0.05 C TEMPERATURE
C     CONTROL ACCURACY.  UNITS ARE MKS UNLESS SPECIFIED OTHERWISE.
C
C  DESCRIPTION OF PARAMETERS
C     NODATA = NUMBER OF DATA SETS.
C     RX = SAMPLE RESISTANCE.
C     RS = STANDARD RESISTANCE.
C     CURR = OHMIC HEATING CURRENT.
C     VCURR = CURRENT MONITOR VOLTAGE.
C     SET POINT VALUE OF RX = AR * RS * CP.
C     AIER * VCURR = CURR * RS.
C     RESIST = SAMPLE RESISTIVITY IN MICROOHMS-CM.
C     VERROR = BRIDGE ERROR VOLTAGE MONITOR.
C     A2 = SCALE FACTOR ON VERROR.
C     VRX = RX DEVIATION MONITOR VOLTAGE.
C     DTMAX = TEMPERAURE DEVIATION FROM SETPOINT WITH 10 VOLT ERROR
C     SIGNAL (VERROR OR VRX) DIVIDED BY THE TEMPERATURE DERIVATIVE
C     OF THE ERROR SIGNAL AT TEMPERATURE SET POINT.
C     THICKN = SAMPLE THICKNESS IN MILS.
C     THICK IS THICKN ROUNDED OFF TO ONE DIGIT.
C     BEAMP = BEAM POWER ABSORBED BY SAMPLE.
C     RX / RXO = SUM OF ARX(I) * TEMP ** (I - 1).
C     MR - 1 = THE ORDER OF THE POLYNOMIAL EQUATION OF RX.
C     LENGTH OF SAMPLE / LENGTH AT A TEMP OF 0 = SUM OF AT(I) * TEMP **
C     (I - 1).
C     MT - 1 = THE ORDER OF THE POLYNOMIAL EQUATION OF SAMPLE LENGTH.
C     POWER ABSORBED BY 3-MIL SAMPLE AS A FUNCTION OF TEMPERATURE IS
C     GIVEN BY THE SUM OF AP(I) * TEMP ** (I - 1).
C     MP - 1 = THE ORDER OF THE POLYNOMIAL EQUATION OF POWER.
C     PWRMAX IS EMPLOYED TO SET OHMIC POWER TO A CONSTANT FOR TEMPERA-
C     TURES LESS THAN TMAX.  IF PWRMAX IS GREATER THAN 0.0 AND TEMP IS
C     LESS THAN TMAX, OHMIC POWER = PWRMAX.  OTHERWISE, OHMIC POWER IS
C     SET BY AP.
C
C  USEAGE
C     ON THE FIRST DATA CARD TYPE AR, AIER, A2, AND K BEGINNING ON
C     COLUMNS 1, 21, 41, & 61, RESPECTIVELY.  ON THE SECOND CARD TYPE
C     RS(1), RS(2), & RS(3) BEGINNING IN COLUMNS 1, 21, & 41,
C     RESPECTIVELY.  13 COLUMNS ARE ALLOWED FOR EACH OF THE ABOVE
C     CONSTANTS.  ON THE THIRD CARD TYPE MP IN THE FIRST TWO COLUMNS.
C     ON THE FOURTH CARD TYPE AP(I) BEGINNING IN COLUMNS 1, 21, 41, ETC.
C     13 COLUMNS ARE ALLOWED FOR EACH COEFFICIENT.   ON THE NEXT CARD
C     TYPE PWRMAX AND TMAX BEGINNING IN COLUMNS 1 AND 21 RESPECTIVLY,
C     ALLOWING 13 COLUMNS FOR EACH.  THEN ON THE THE FOLLOWING CARD
C     TYPE THE NUMBER OF DATA SETS IN THE FIRST TWO COLUMNS.    FOR THE
C     FIRST DATA SET TYPE THE NAME OF THE METAL IN COLUMNS 1 THROUGH 20,
```

```
C     THE RESISTIVITY OF THE METAL IN THE NEXT 20 COLUMNS, AND MR AND MT
C     ALLOWING 2 COLUMNS EACH.  ON THE NEXT CARD TYPE ARX(I) IN A MANNER
C     SIMILAR TO AP(I).  THEN ON THE NEXT CARD TYPE AT(I) IN A LIKE
C     MANNER.   ON THE FOLLOWING CARD TYPE TEMP(I) IN A SIMILAR MANNER.
C     IN COLUMNS 1 THROUGH 13 AND 21 THROUGH 33 TYPE THE TWO SAMPLE
C     THICKNESS LIMITS.  LEAVE THE CARD BLANK IF 3 AND 5 MIL SAMPLE
C     THICKNESS LIMITS ARE DESIRED.  IF THE PARAMETERS FOR A SINGLE
C     THICKNESS ARE DESIRED,  TYPE A VALUE ONLY FOR THE FIRST THICKNESS
C     LIMIT.  IF MORE THAN ONE DATA SET IS TO BE HANDLED, BEGIN
C     WITH THE NAME OF THE NEXT METAL, ETC. ON THE NEXT CARD.
C
C  REMARKS
C     MAXIMUM TEMPERATURE DEVIATION (PLUS OR MINUS) ARE BASED ON
C     ERROR VOLTAGE SENSITIVITY AT SET POINT TEMPERARURE.  THAT IS THE
C     THE ERROR VOLTAGE SENSITIVITY IS ASSUMED CONSTANT AT A GIVEN
C     SET POINT TEMPERATURE. SOME ERROR WILL RESULT DUE TO THE NONLINEAR
C     RELATION OF RESISTANCE WITH TEMPERATURE CAUSING VERROR SENSITIVITY
C     TO BE TEMPERATURE DEPENDENT.
C
C*********************************************************************
C
      DOUBLE PRECISION ARX(20), RS(3), METAL(5), AT(20), AP(20),
     1 RX(6, 2), RXTC(6,6), DXPAND(6), VCURR(6,4), VERROR(6, 4, 2),
     2 CP(6, 2), TEMP(6), RLDW(2), CURR(6,4), DTMAX(6,6), TSTRAN(6),
     3 RSTRAN(6,2), VRX(6,2, 2), DT(2), THICKN(2), AR, AIER, A2, K,
     4 DSQRT, DABS, POLY, DRVPLY, PWRMAX, TMAX
      DIMENSION THICK(2)
      COMMON TEMP
      INTEGER THICK
      LOGICAL NEGPWR
      READ 1000, AR, AIER, A2, K, (RS(I), I = 1,3)
      DT(1) = 0.05
      READ 1010, MP
      DO 10 I = 1, 20
   10 AP(I) = 0.0
      READ 1000,  (AP(I), I = 1, MP)
      READ 1000, PWRMAX, TMAX
      READ 1010, NODATA
      DO 280 NUMRUN = 1, NODATA
      READ 1020, METAL, RESIST, MR, MT
      DO 20 I = 1, 20
      ARX(I) = 0.0
   20 AT(I) = 0.0
      READ 1000, (ARX(I), I = 1, MR)
      READ 1000,  (AT(I), I = 1, MT)
      READ 1000, (TEMP(I), I = 1, 6)
      READ 1000, THICKN
      M = MR
      IF (M .LT. MP) M = MP
      IF (M .LT. MT) M = MT
      PRINT 1070 , METAL
      PRINT 1030, AR, AIER, A2, K, (RS(I), I = 1, 3)
      PRINT 1080, RESIST
      PRINT 1065, PWRMAX, TMAX
      PRINT 1060
      DO 30 I = 1, 2
   30 THICK(I) = (2 * THICKN(I) + 1) / 2.0
      IF ( THICK(2) .EQ. 0) ITHIKM = 1
      IF (THICK(1) .EQ. 0) GO TO 40
      GO TO 50
   40 ITHIKM = 2
```

```
      THICK(1) = 5
      THICKN(1) = 5.0
      THICK(2) = 3
      THICKN(2) = 3.0
50    PRINT 1040, THICKN
      PRINT 1050, (I, ARX(I), AT(I), AP(I), I = 1, M)
      DO 280 ISTD = 1, 3
      DO 110 ITEMP = 1, 6
C  CALCULATES THERMAL EXPANSION COEFFICIENT IN PPM / C.
      DXPAND(ITEMP) = 1.0E6 * DRVPLY(AT, MT, ITEMP)
      DT(2) = 1.0 / DXPAND(ITEMP)
      DXPAND(ITEMP) = DXPAND(ITEMP) * DT(1)
      TSTRAN(ITEMP) = DT(2)
C  SAMPLE THICKNESS IS 5 AND 3 MILS WHEN ITHICK IS 1 & 2 RESPECTIVLY.
      DO 110 ITHICK = 1, ITHIKM
C  CALCULATION OF BEAM POWER ABSORBED BY SAMPLE
C  BEAMP3 = BEAM POWER ABSORBED BY 3-MIL SAMPLE.
      BEAMP3 = 2.73
      BEAMP = BEAMP3 * THICKN(ITHICK) / 3.0
      NEGPWR = .FALSE.
C  CALCULATION OF SAMPLE RESISTANCE AND CP.
      RLDW(ITHICK) = 2.0 * RESIST * 1.0E-6/ (0.2 * 2.54 * 1.0E-3 *
     1 THICKN(ITHICK))
      RX(ITEMP, ITHICK) = POLY(ARX, MR, ITEMP) * RLDW(ITHICK)
      CP(ITEMP, ITHICK) = RX(ITEMP, ITHICK) / (AR * RS(ISTD))
C  CALCULATION OF RESISTANCE TEMPERATURE COEFFICIENT.
      RXTC(ITEMP, ITHICK) = DRVPLY(ARX,MR, ITEMP) * RLDW(ITHICK)
      RSTRAN (ITEMP, ITHICK) = RXTC(ITEMP, ITHICK) * DT(2)
C  IF RX IS OUT OF RANGE FOR GIVEN RS, PROGRAM SETS CONTROL PARAMETERS
C  TO ZERO.
      IF (RX(ITEMP, ITHICK) .GT. 0.1* RS(ISTD) .AND. RX(ITEMP, ITHICK)
     1 .LT. 1.272 * RS(ISTD)) GO TO 70
      CP(ITEMP, ITHICK) = 0.0
      CURR(ITEMP, ITHICK) = 0.0
      VCURR(ITEMP, ITHICK) = 0.0
      DTMAX(ITEMP, ITHICK) = 0.0
      DTMAX(ITEMP, ITHICK + 4) = 0.0
      VERROR(ITEMP, ITHICK, 1) = 0.0
      VERROR(ITEMP, ITHICK, 2) = 0.0
      VRX(ITEMP, ITHICK, 1) = 0.0
      VRX(ITEMP, ITHICK, 2) = 0.0
   60 CURR(ITEMP, ITHICK + 2) = 0.0
      VCURR(ITEMP, ITHICK + 2) = 0.0
      DTMAX(ITEMP, ITHICK + 2) = 0.0
      VERROR(ITEMP, ITHICK + 2, 1) = 0.0
      VERROR(ITEMP, ITHICK + 2, 2) = 0.0
      GO TO 110
C  CURR(ITEMP, I):  WHEN I IS 3 & 4, CURR IS LIKE CURR WITH I = 1 & 2
C  RESPECTIVELY, BUT WITH BEAM ON.
   70 CURR(ITEMP, ITHICK) = POLY(AP, MP, ITEMP) / RX(ITEMP, ITHICK)
      IF (TEMP(ITEMP) .LT. TMAX .AND. PWRMAX .GT. 0.0) CURR(ITEMP, ITHIC
     1K) = PWRMAX / RX(ITEMP, ITHICK)
      CURR(ITEMP, ITHICK + 2) = CURR(ITEMP, ITHICK) - BEAMP/ RX(ITEMP,
     1 ITHICK)
      CURR(ITEMP,ITHICK) = DSQRT(CURR(ITEMP,ITHICK))
C  IF TEMP IS NOT ATTAINABLE WITH BEAM ON BECAUSE THE REQUIRED OHMIC
C  HEATING POWER IS NEGATIVE, PROGRAM SET THE CORRESPONDING PARAMETERS
C  TO ZERO.
      IF (CURR(ITEMP, ITHICK + 2) .LE. 0.0) GO TO 80
      CURR(ITEMP,ITHICK + 2) = DSQRT(CURR(ITEMP, ITHICK + 2))
      GO TO 90
```

```
   80 CURR(ITEMP, ITHICK + 2) = 1.0
      NEGPWR = .TRUE.
   90 VCURR(ITEMP, ITHICK)= RS(ISTD) * CURR(ITEMP, ITHICK) / AIER
      VCURR(ITEMP, ITHICK + 2) = RS(ISTD) * CURR(ITEMP, ITHICK + 2) /
     1 AIER
      DO 100 I2 = 1, 2
C  VERROR(ITEMP, I, I2):  WHEN I = 3 & 4,VERROR IS LIKE THE CASE WHERE
C  I = 1 & 2, BUT WITH BEAM ON.  WHEN I2 = 1, DT = 0.05C, BUT WITH
C  I2 = 2, DT IS THAT WHICH RESULTS IN 1 MICROSTRAIN ERROR.
      VERROR(ITEMP, ITHICK, I2) = RXTC(ITEMP, ITHICK) * DT(I2) * CURR(IT
     1EMP, ITHICK) / ((1.0 + AR * CP(ITEMP, ITHICK)) * A2)
      VERROR(ITEMP, ITHICK + 2, I2) = RXTC(ITEMP, ITHICK) * DT(I2) * CUR
     1R(ITEMP, ITHICK + 2) / ((1.0 + AR * CP(ITEMP, ITHICK)) * A2)
  100 VRX(ITEMP, ITHICK , I2) = VERROR(ITEMP, ITHICK, I2) /
     1 (VCURR(ITEMP, ITHICK) * K)
C  DTMAX IS THE MAXIMUM DEVIATION OF TEMPERATURE. THIS OCCURS WHEN THE
C  VOLTAGE IS PLUS OR MINUS TEN VOLTS.
      DTMAX(ITEMP, ITHICK)  = DABS(0.500 / VERROR(ITEMP,ITHICK, 1))
      DTMAX(ITEMP, ITHICK + 2)  = DABS(0.500 / VERROR(ITEMP,ITHICK+2,1))
      DTMAX(ITEMP, ITHICK + 4) = DABS(0.500 / VRX(ITEMP, ITHICK, 1))
      IF (NEGPWR) GO TO 60
  110 CONTINUE
      PRINT 1090, METAL, RS(ISTD)
      PRINT 1310
      PRINT 1100, TEMP
      PRINT 1310
      DO 115 I = 1, ITHIKM
      PRINT 1110, THICK(I)
  115 PRINT 1120, (RX(ISTEP, I), ISTEP = 1, 6)
      PRINT 1310
      DO 120 I = 1, ITHIKM
      PRINT 1130 , THICK(I)
  120 PRINT 1120, (CP(ISTEP,I), ISTEP = 1, 6)
      PRINT 1310
      DO 130 I = 1, ITHIKM
      PRINT 1140, THICK(I)
  130 PRINT 1120, (RXTC(ISTEP, I), ISTEP = 1, 6)
      PRINT 1310
      DO 140 I = 1, ITHIKM
      PRINT 1240, THICK(I)
  140 PRINT 1120, (RSTRAN(ISTEP, I), ISTEP = 1, 6)
      PRINT 1310
      PRINT 1230
      PRINT 1120, TSTRAN
      PRINT 1310
      PRINT 1250
      PRINT 1120, DXPAND
      PRINT 1310
      DO 150 I = 1, ITHIKM
      PRINT 1150     , THICK(I)
  150 PRINT 1120, (VERROR(ISTEP, I, 1), ISTEP = 1, 6)
      PRINT 1310
      DO 160 I = 1, ITHIKM
      PRINT 1270, THICK(I)
  160 PRINT 1120, (VERROR(ISTEP, I + 2, 1), ISTEP = 1, 6)
      PRINT 1310
      DO 170 I = 1, ITHIKM
      PRINT 1160, THICK(I)
  170 PRINT 1120, (VERROR(ISTEP, I, 2), ISTEP = 1, 6)
      PRINT 1310
```

```
      DO 180 I = 1, ITHIKM
      PRINT 1290, THICK(I)
  180 PRINT 1120, (VERROR(ISTEP, I + 2, 2), ISTEP = 1, 6)
      PRINT 1310
      DO 190 I = 1, ITHIKM
      PRINT 1260, THICK(I)
  190 PRINT 1120, (VRX(ISTEP, I, 1), ISTEP  = 1, 6)
      PRINT 1310
      DO 200 I = 1, ITHIKM
      PRINT 1280, THICK(I)
  200 PRINT 1120, (VRX(ISTEP, I, 2), ISTEP  = 1, 6)
      PRINT 1310
      DO 210 I = 1, ITHIKM
      PRINT 1170, THICK(I)
  210 PRINT 1120, (CURR(ISTEP, I), ISTEP = 1, 6)
      PRINT 1310
      DO 220 I = 1, ITHIKM
      PRINT 1190, THICK(I)
  220 PRINT 1120, (CURR(ISTEP, I + 2), ISTEP = 1, 6)
      PRINT 1310
      DO 230 I = 1, ITHIKM
      PRINT 1190, THICK(I)
  230 PRINT 1120, (VCURR(ISTEP, I), ISTEP = 1, 6)
      PRINT 1310
      DO 240 I = 1, ITHIKM
      PRINT 1200, THICK(I)
  240 PRINT 1120, (VCURR(ISTEP, I + 2), ISTEP = 1, 6)
      PRINT 1310
      DO 250 I = 1, ITHIKM
      PRINT 1210, THICK(I)
  250 PRINT 1120, (DTMAX(ISTEP, I), ISTEP = 1, 6)
      PRINT 1310
      DO 260 I = 1, ITHIKM
      PRINT 1220, THICK(I)
  260 PRINT 1120, (DTMAX(ISTEP, I + 2), ISTEP = 1, 6)
      PRINT 1310
      DO 270 I = 1, ITHIKM
      PRINT 1300, THICK(I)
  270 PRINT 1120, (DTMAX(ISTEP, I + 4), ISTEP = 1, 6)
  280 CONTINUE
 1000 FORMAT (4(F13.11, 7X))
 1010 FORMAT (I2)
 1020 FORMAT (5A4, F13.11, 7X, 2I2)
 1030 FORMAT (1H0, 20X, '  AR = ',1PD13.6,   10H     AIER =   , 1PD13.6,
     1 10H       A2 = , 1PD13.6  , 10H       K =   , 1PD13.6,//,23X,14HX1 R
     2S (OHMS) =   , 1PD13.6, 17H   X2 RS (OHMS) =   , 1PD13.6, 17H   X4 R
     3S (OHMS) = , 1PD13.6)
 1040 FORMAT (1H0, 45X, (1P5D20.6, /))
 1050 FORMAT (1H0, /, 30X, 70HI                          ARX(I)                AT
     1(I)                  AP(I)          , //, (29X, I2, 10X,1P3D20.6,//))
 1060 FORMAT (1H0, /, 55X, 'SAMPLE THICKNESS LIMITS (MILS)')
 1065 FORMAT (1H0, 43X, 'PWRMAX = ', 1PD13.6, 7X, 'TMAX = ', 1PD13.6)
 1070 FORMAT (1H1, 15X, 'INPUT DATA UTILIZED TO CALCULATE IRRADIATION TE
     1MPERATURE CONTROL PARAMETER LIMITS FOR ', 5A4)
 1080 FORMAT (1H0, 43X, 'SAMPLE RESISTIVITY (MICROOHM-CM) = ', 1PE13.6)
 1090 FORMAT (1H1, 5(/), 10X, 'IRRADIATION CREEP TEMPERATURE CONTROL SYS
     1TEM PARAMETER LIMITS FOR ', 5A4, ' WITH RS = ', 1PD13.6, ' OHMS',
     2 /)
 1100 FORMAT (1H , 'PARAMETERS', 18X, 'I', 45X, 'TEMPERATURE (C)', /,
     1 29X, 'I', /, 29X, 'I', 1X, 6(F10.3, 7X), /, 29X, 'I', /, 1X, 28('
     1-'), 'I', 103('-'))
```

```
1110 FORMAT  (  ' RX (OHMS) FOR ', I1, '-MIL SAMPLE  I')
1120 FORMAT (1H+, 28X, 1P6U17.6, /, 29X, 'I')
1130 FORMAT (' CP FOR ', I1, ' MIL SAMPLE          I')
1140 FORMAT ( ' RESISTIVE TEMP COEFFICIENT  I', /, ' FOR ', I1, '-MIL S
    1AMPLE (OHMS / C) I')
1150 FORMAT ( ' VERROR DUE TO T CHANGE OF   I', /, ' 0.05C FOR ', I1, '
    1-MIL SAMPLE       I', /, ' WITHOUT BEAM      (VOLTS)     I')
1160 FORMAT (          ' VERROR DUE TO TEMP. CHANGE  I', /, ' EQUIV. TO 1
    1-MICROSTRAIN FOR I', /, 1X, I1, '-MIL SAMPLE WITHOUT BEAM(V)I')
1170 FORMAT ( ' CURRENT WITH NO BEAM FOR A  I', /, 1X, I1,  '-MIL SAMPL
    1E        (AMPS)    I')
1180 FORMAT ( ' CURRENT WITH 15 MICROAMP    I', /, ' BEAM FOR ', I1, '-
    1MIL SAMPLE (AMPS)I')
1190 FORMAT (  ' VCURR WITH NO BEAM FOR A    I', /, 1X, I1, '-MIL SAMPL
    1E        (VOLTS)    I')
1200 FORMAT ( ' VCURR WITH 15 MICROAMP BEAM I', /, ' FOR A ', I1, '-MIL
    1 SAMPLE (VOLTS)  I')
1210 FORMAT ( ' MAX. TEMP DEVIATION FROM    I', /, ' VERROR WITH ', I1,
    1'-MIL SAMPLE     I', /, ' WITHOUT BEAM          (C)    I')
1220 FORMAT ( ' MAX. TEMP DEVIATION FROM    I', /, ' VERROR WITH ', I1,
    1'-MIL SAMPLE     I', /, ' AND 15 MICROAMP BEAM  (C)    I')
1230 FORMAT(          ' TEMP CONTROL NEEDED FOR      I', / , ' 1MICROSTRAI
    1N ACCURACY  (C)  I')
1240 FORMAT ( ' RX CONTROL NEEDED FOR       I', /, ' 1MICROSTRAIN ACCUR
    1ACY FOR   I', /, 1X, I1, '-MIL SAMPLE        (OHMS)    I')
1250 FORMAT (' STRAIN ACCURACY FOR 0.05 C  I', /, ' CONTROL ACCURACY (U
    1STRAIN)  I')
1260 FORMAT ( ' VRX DUE TO TEMP. CHANGE OF  I', /, ' .05 C FOR ', I1, '
    1-MIL SAMPLE (V)  I')
1270 FORMAT ( ' VERROR DUE TO T CHANGE OF   I', /, ' 0.05C FOR ', I1, '
    1-MIL SAMPLE WITH I', /, ' 15 MICROAMP BEAM    (VOLTS) I')
1280 FORMAT ( ' VRX DUE TO TEMP. CHANGE     I', /, ' EQUIV. TO 1-MICROS
    1TRAIN FOR I', /, 1X, I1, '-MIL SAMPLE          (V)    I')
1290 FORMAT ( ' VERROR DUE TO TEMP. CHANGE  I', /, ' EQUIV. TO 1-MICROS
    1TRAIN FOR I', /, 1X, I1, '-MIL SAMPLE , 15UA BEAM (V)I')
1300 FORMAT ( ' MAX. TEMP DEVIATION FROM    I', /, ' VRX FOR ', I1, '-M
    1IL SAMPLE   (C)  I')
1310 FORMAT(1H , 28('-'), 'I', 103('-'), /, 29X, 'I')
     STOP
     END
     FUNCTION POLY(A, M, I)
     DOUBLE PRECISION A(20), TEMP(6), POLY
     COMMON TEMP
     POLY = A(M)
     MLS1 = M - 1
     DO 10 IPOLY = 1, MLS1
  10 POLY = POLY * TEMP(I) + A(M - IPOLY)
     RETURN
     END
     FUNCTION DRVPLY(A, M, I)
     DOUBLE PRECISION A(20), TEMP(6), DRVPLY
     COMMON TEMP
     DRVPLY = A(M) * FLOAT(M-1)
     IF (M .LE. 2) GO TO 20
     MLS2 = M - 2
     DO 10 IDERIV = 1, MLS2
  10 DRVPLY = DRVPLY * TEMP(I) + A(M - IDERIV) * FLOAT(M - 1- IDERIV)
  20 CONTINUE
     RETURN
     END
```

INPUT DATA UTILIZED TO CALCULATE IRRADIATION TEMPERATURE CONTROL PARAMETER LIMITS FOR 316 STAINLESS STEEL

AR = 2.000000D-02 AIER = 3.294000D-01 A2 =-8.980000D-03 K = 1.000000D-01

X1 RS (OHMS) = 4.000000D-02 X2 RS (OHMS) = 8.000000D-02 X4 RS (OHMS) = 1.600000D-01

SAMPLE RESISTIVITY (MICROOHM-CM) = 7.400000E 01

PWRMAX = 1.000000D-02 TMAX = 5.000000D 01

SAMPLE THICKNESS LIMITS (MILS)

3.000000D 00 0.0

I	ARX(I)	AT(I)	AP(I)
1	1.000000D 00	1.000000D 00	1.039113D 00
2	1.019505D-03	1.540559D-05	1.994726D-02
3	-4.519260D-07	5.673796D-09	1.245214D-05
4	0.0	0.0	-3.370553D-09

TABLE 4

IRRADIATION CREEP TEMPERATURE CONTROL SYSTEM PARAMETER LIMITS FOR 316 STAINLESS STEEL WITH RS = 8.0000000-02 OHMS

PARAMETERS	TEMPERATURE (C) 0.0	26.460	150.000	300.000	500.000	700.000
RX (OHMS) FOR 3-MIL SAMPLE	9.7112320-02	9.9721150-02	1.1097640-01	1.2286500-01	1.3564440-01	1.449127D-01
CP FOR 3 MIL SAMPLE	6.0495610 01	6.2325720 01	6.9360240 01	7.6740630 01	8.4777730 01	9.0570430 01
RESISTIVE TEMP COEFFICIENT FOR 3-MIL SAMPLE (OHMS / C)	9.9007000-05	9.6666900-05	8.5840660-05	7.2674320-05	5.511919D-05	3.756407D-05
RX CONTROL NEEDED FOR 1MICROSTRAIN ACCURACY FOR 3-MIL SAMPLE (OHMS)	6.4766930-06	6.1539460-06	5.0176540-06	3.8636270-06	2.614839D-06	1.608815D-06
TEMP CONTROL NEEDED FOR 1MICROSTRAIN ACCURACY (C)	6.4911500-02	6.3661350-02	5.845311D-02	5.3163590-02	4.743971D-02	4.282856D-02
STRAIN ACCURACY FOR 0.05 C CONTROL ACCURACY (USTRAIN)	7.7027950-01	7.8540560-01	8.553864D-01	9.4049330-01	1.053969D 00	1.167445D 00
VERROR DUE TO T CHANGE OF 0.05C FOR 3-MIL SAMPLE WITHOUT BEAM (VOLTS)	-7.9902670-05	-7.5869740-05	-1.246281D-03	-1.2916780-03	-1.144402D-03	-8.728406D-04
VERROR DUE TO T CHANGE OF 0.05C FOR 3-MIL SAMPLE WITH 15 MICROAMP BEAM (VOLTS)	0.0	0.0	-7.530634D-04	-1.0503180-03	-1.024092D-03	-8.109162D-04
VERROR DUE TO TEMP. CHANGE EQUIV. TO 1-MICROSTRAIN FOR 3-MIL SAMPLE WITHOUT BEAM(V)	-1.037320D-04	-9.659942D-05	-1.456980D-03	-1.3736180-03	-1.085802D-03	-7.476502D-04
VERROR DUE TO TEMP. CHANGE EQUIV. TO 1-MICROSTRAIN FOR 3-MIL SAMPLE + 15UA BEAM (V)	0.0	0.0	-8.803780D-04	-1.1167730-03	-9.716529D-04	-6.946076D-04
VRX DUE TO TEMP. CHANGE OF .05 C FOR 3-MIL SAMPLE (V)	-1.0252580-02	-9.8649720-03	-8.243860D-03	-6.5703880-03	-4.687939D-03	-3.063204D-03
VRX DUE TO TEMP. CHANGE EQUIV. TO 1-MICROSTRAIN FOR 3-MIL SAMPLE (V)	-1.3310210-02	-1.2560350-02	-9.637586D-03	-6.9861080-03	-4.447890D-03	-2.623853D-03
CURRENT WITH NO BEAM FOR A 3-MIL SAMPLE (AMPS)	3.2089410-01	3.1666960-01	6.2247070 00	8.0958820 00	1.005148D 01	1.173255D 01
CURRENT WITH 15 MICROAMP BEAM FOR 3-MIL SAMPLE (AMPS)	0.0	0.0	3.761270D 00	6.5820820 00	8.994783D 00	1.090018D 01
VCURR WITH NO BEAM FOR A 3-MIL SAMPLE (VOLTS)	7.7934210-02	7.6908220-02	1.511769D 00	1.9662130 00	2.441161D 00	2.849437D 00
VCURR WITH 15 MICROAMP BEAM FOR A 3-MIL SAMPLE (VOLTS)	0.0	0.0	9.134839D-01	1.5985630 00	2.184525D 00	2.647281D 00
MAX. TEMP DEVIATION FROM VERROR WITH 3-MIL SAMPLE WITHOUT BEAM (C)	6.2576130 03	6.5902420 03	4.011937D 02	3.8703340 02	4.369096D 02	5.728423D 02
MAX. TEMP DEVIATION FROM VERROR WITH 3-MIL SAMPLE AND 15 MICROAMP BEAM (C)	0.0	0.0	5.639548D 02	4.7604640 02	4.882373D 02	6.165865D 02
MAX. TEMP DEVIATION FROM VRX FOR 3-MIL SAMPLE (C)	4.8763210 01	5.0664340 01	6.063120D 01	7.6099000 01	1.066567D 02	1.632278D 02

APPENDIX B

DERIVATION OF KELVIN BRIDGE ERRORS DUE TO STRAY RESISTANCE AND CAPACITANCE

The circuit used to compute bridge voltages is shown in Figure 18 on page 73. Simplification of this circuit can be accomplished using equivalent Thevenin voltage sources. As shown in Figure 68(a), the equivalent voltage sources at nodes 1 through 4 are

$$V_1 = V_{cm} - V_g/2 \ ,$$

$$V_2 = V_{cm} - V_g \ (1/2 - R_x/R_\Sigma) \ , \tag{253}$$

$$V_3 = V_{cm} + V_g \ (1/2 - R_s/R_\Sigma) \ ,$$

and

$$V_4 = V_{cm} + V_g/2 \ ,$$

where $R_\Sigma = R_x + R_y + R_s$. The Thevenen equivalent resistances are

$$R_1 = 0 \ ,$$

$$R_2 = R_x || (R_y + R_s) \ , \tag{254}$$

$$R_3 = (R_x + R_y) || R_s \ ,$$

and

$$R_4 = 0 \ .$$

ORNL-DWG 76-19167

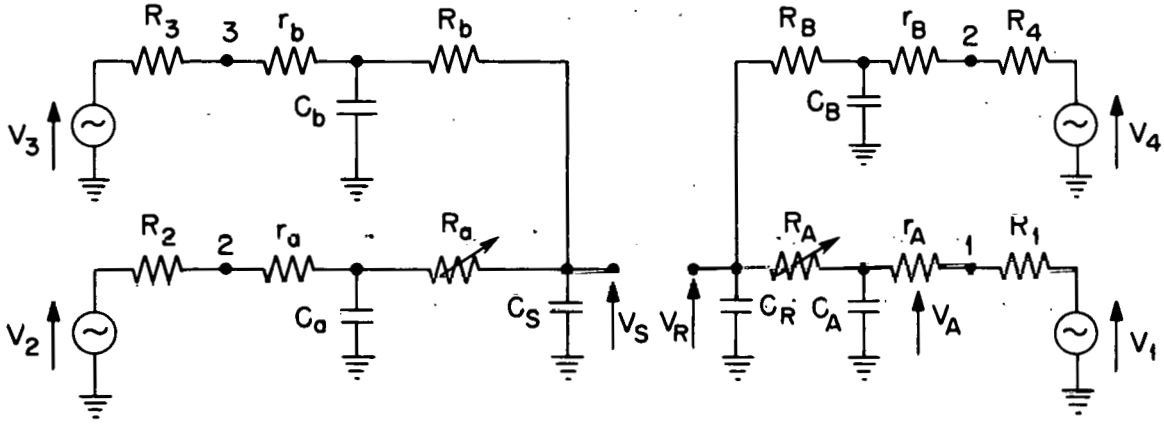

(a) Equivalent circuit of bridge simplified by Thevenin sources.

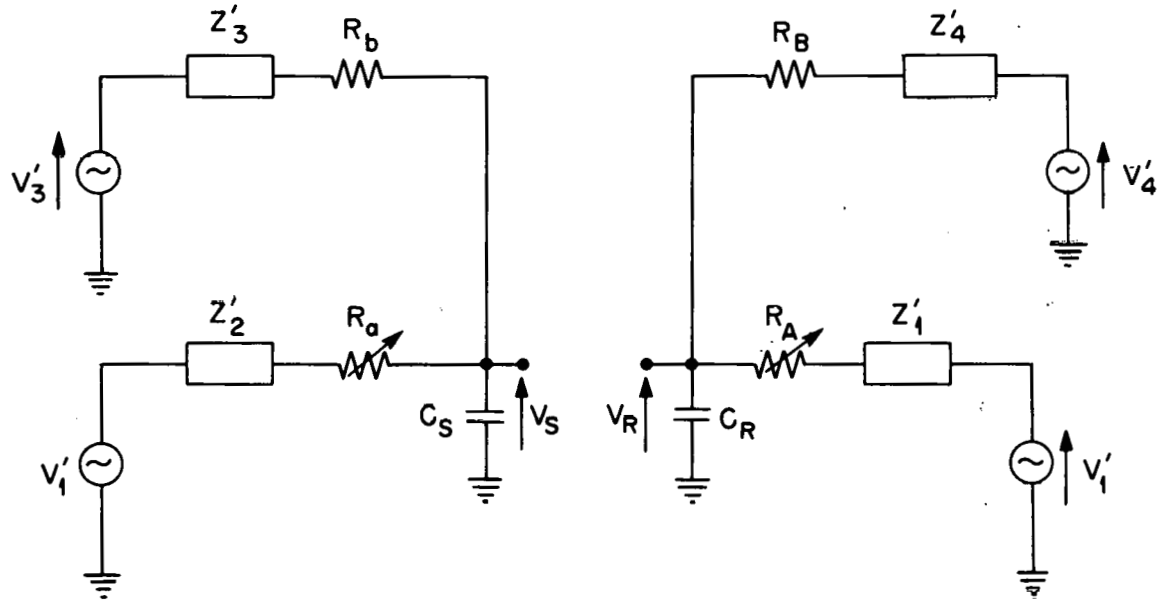

(b) Further simplification.

Figure 68. Simplification of bridge circuit.

As shown in Figure 68(b), the circuit may be simplified further by equivalent Thevenin voltage sources at nodes 1′ through 4′ where the open-circuit Thevenin voltages are

$$V_1' = \frac{V_1}{1 + T_A\, j\omega} ,$$

$$V_2' = \frac{V_2}{1 + T_a\, j\omega} , \tag{255}$$

$$V_3' = \frac{V_3}{1 + T_b\, j\omega} ,$$

and

$$V_4' = \frac{V_4}{1 + T_B\, j\omega}$$

and the Thevenin impedances are

$$Z_1' = r_A/(1 + T_A\, j\omega) ,$$

$$Z_2' = (R_2 + r_2)/(1 + T_a\, j\omega) , \tag{256}$$

$$Z_3' = (R_3 + r_b)/(1 + T_b\, j\omega) ,$$

and

$$Z_4' = r_B/(1 + T_B\, j\omega) ,$$

where T_A, T_B, T_a, and T_b are $r_A\, C_A$, $r_B\, C_B$, $(R_2 + r_a)\, C_a$, and $(R_3 + r_b)\, C_b$. From this equivalent circuit, V_R and V_S are shown to be given by the following expressions:

$$V_R = \frac{(R_B + Z_4')\ V_1' + (R_A + Z_1')\ V_4'}{(R_A + Z_1' + R_B + Z_4')(1 + ((R_A + Z_1')||(R_B + Z_4'))C_R j\omega)}$$

and (257)

$$V_S = \frac{(R_b + Z_3')\ V_2' + (R_a + Z_2')\ V_3'}{(R_a + Z_2' + R_b + Z_3')(1 + ((R_a + Z_2')||(R_b + Z_3'))C_S\ j\omega)} .$$

V_A is given by

$$V_A = \frac{V_R\ Z_1' + R_A\ V_1'}{R_A + Z_1'} . \tag{258}$$

The expressions derived here may be used to compute the performance of both the PSD and PID. Further simplification of the above equations are difficult to obtain without making approximations. One useful approximation is that $R_B + Z_4'$, $R_A + Z_1'$, $R_b + Z_3'$, and $R_a + Z_2'$ are $R_B + r_B$, $R_A + r_A$, $R_B + R_3 + r_b'$, and $R_a + R_2 + r_a'$, respectively. This assumption causes approximately 0.001 ppm error in the phase of V_R and V_S at 1 KHz for the component values shown in Figure 18 on page 73 while simplifying the computations significantly.

APPENDIX C

RECTIFIER SIMULATIONS

```
*************************************************************
*
*  SIMULATION OF PRECISION RECTIFIER BY DELAY METHOD
*
*  PARAMETERS
*     FINPUT = FREQUENCY IN HERTZ OF THE INPUT SIGNAL
*     TIMEF = THE PERIOD OF THE INPUT SIGNAL
*     VINPK = NEGATIVE PEAK INPUT VOLTAGE
*     AOL = OPEN-LOOP OPAMP VOLTAGE GAIN AT LOW FREQUENCIES
*     GBWP = THE GAIN-BANDWIDTH PRODUCT OF THE OPAMP
*     SR = SLEW RATE OF OPAMP IN VOLTS / MICROSEC
*     TOL = DOMINENT POLE TIME CONSTANT OF OPAMP
*     PHASE = NOMINAL PHASE SHIFT OF PRECISION RECTIFIER
*     VT, VT2, IS1, AND IS2 ARE PARAMETERS USED TO MODEL
*    THE PN JUNCTIONS OF DIODES D1 AND D2 RESPECTIVELY
*
*  VARIABLES
*     VF = VOLTAGE AT INVERTING INPUT OF OPAMP
*     VO = OUTPUT VOLTAGE OF OPAMP
*     VR1 = VOLTAGE AT NODE WHICH JOINS R1 AND D1
*     VR2 = VOLTAGE AT NODE WHICH JOINS R2 AND D2
*     VR1RF = VR1 REFERRED TO THE INPUT
*     VERORA = PERCENT ERROR OF VOA
*     VERORT = PERCENT ERROR OF VR1RF AS A FUNCTION OF TIME
*     VOA = AVERAGE VALUE OF VR1RF
*     IF1 AND IF2 ARE THE CURRENTS THROUGH D1 AND D2
*       RESPECTIVELY
*     VIF1RF = IF1 REFERRED TO THE INPUT
*     IERORA = PERCENT ERROR OF IOA
*     IERORT = PERCENT ERROR OF VIF1RF AS A FUNCTION OF TIME
*     IOA = AVERAGE VALUE OF VIF1RF
*     DELVIF = IOA - VIF1RF
*     VOIDEL = OUTPUT OF IDEAL HALF-WAVE RECTIFIER
*     VOIDLA = AVERAGE VALUE OF VOIDEL
*
*************************************************************
*
INITIAL
*  INPUT PARAMETERS
PARAMETER FINPUT = 1.0E3, PHASEI = 0.0, VINPK = -0.10E6
*  INITIAL CONDITIONS
      IOAIC = 0.0
*  DIODE PARAMETERS
PARAMETER VT1 = 26.0E3, VT2 = 26.0E3
PARAMETER IS1 = 1.0E-5, IS2 = 1.0E-5
PARAMETER TDELAY = 0.1E-6
*  RESISTANCE PARAMETERS
PARAMETER R1 = 2.0E3, R2 = 0.0  , R3 = 2.0E3
*  OPAMP PARAMETERS
PARAMETER AOL = 2.0E5, GBWP = 1.0E6
PARAMETER SRRISE = 70.0E6, SRFALL = 70.0E6
```

```
      TWOPI = 6.283185308
      OMEGAI = TWOPI * FINPUT
      TIMEF =  1.0 / FINPUT
      TOL = AOL / (TWOPI * GBWP)
NOSORT
      IF (VFIC .EQ. 0.0 .AND. VOIC .EQ. 0.0) GO TO 1010
      GO TO 1020
*  ITERATION LOOP TO FIND INITIAL CONDITIONS OF VO AND IF2
1010  IF2IC1 = -1.0E-1
      DO 1000 I = 1, 50
      FCL = (AOL * R3 / (R3 + R2 - VT2 / IF2IC1) + 1.0) /...
      (TOL * TWOPI)
      PHASE = ATAN(-FINPUT / FCL) + PHASEI
      IF2IC = -SIN(PHASE) * VINPK / R3
      CNVRG = ABS(IF2IC / IF2IC1 - 1.0)
      IF (CNVRG .LT. 1.0E-3) GO TO 1001
1000  IF2IC1 = (IF2IC1 + IF2IC) / 2.0
1001  VOIC = -VT2 * ALOG(1.0 - IF2IC / IS2)
      VFIC = R3 * (IF2IC - IS1)
      GO TO 1030
1020  IF2IC = IS1 + VFIC / R3
      PHASE = -ATAN(1. / SQRT(-1. + (VINPK/(R3*IF2IC))**2))
1030  VIFRFI = IF2IC * R3
      VFPIC = VFIC - VOIC
SORT
      SLEWR = SRRISE * TOL / AOL
      SLEWF = SRFALL * TOL / AOL
      VOIDLA = -VINPK * 2.0 / TWOPI
DYNAMIC
      VIN1 = SINE(0.0, OMEGAI, PHASEI)
      VIN = VIN1 * VINPK
*  OPAMP MODEL
*  FOR SLEW-RATE LIMIT, REMOVE * FROM COL. 1 OF V1 = LIMIT
*  ... CARD AND INSERT * IN COL. 1 OF V1 = VF CARD
*     V1 = LIMIT(-SLEWR, SLEWF, VF)
      V1 = VF
      V2 = -AOL * V1
      VO = REALPL(VOIC, TOL, V2)
      VF = VIN + (IF1 + IF2) * R3
      VR1 = VF + IF1 * R1
      VR2 = VF + IF2 * R2
*  DIODE FEEDBACK MODEL
      U1P = (VO - VR1) / VT1
      IF1P = IS1 * (EXP(U1P) - 1.0)
      IF1 = REALPL(-IS1, TDELAY, IF1P)
      U2P = (VR2 - VO) / VT2
      IF2P = -IS2 * (EXP(U2P) - 1.0)
      IF2 = REALPL(IF2IC, TDELAY, IF2P)
NOSORT
*  PERCENT ERROR CALCULATIONS
*  OMIT VR1RF, VOT, VOA, AND VERORA WHEN R1 = 0.0
```

```
      VOT = VR1RF / TIMEF
      VR1RF = VR1 * R3 / R1
      VIND = SINE(0.0, OMEGAI, PHASE)
      VINDLY = VINPK * VIND
      IF(VINDLY) 4, 5, 5
4     VOIDEL = -VINDLY
      GO TO 6
5     VOIDEL = 0.0
6     CONTINUE
SORT
      VOA = INTGRL(0.0, VOT)
      VIF1RF = IF1 * R3
      VIF1RT = VIF1RF / TIMEF
      IOA = INTGRL(IOAIC, VIF1RT)
      IERORT = (VIF1RF - VOIDEL) * 100.0 / VOIDLA
      VERORT = (VR1RF - VOIDEL) * 100.0 / VOIDLA
      DELVIF = IOA - VOIDLA
      IERORA = DELVIF * 100.0 / VOIDLA
      VERORA = (VOA - VOIDLA) * 100.0 / VOIDLA
PRINT VOIDEL,VIF1RF,IERORT,IERORA,DELVIF,VO,VF,VERORT,VERORA
OUTPUT  VERORT, VOIDEL, VR1RF
OUTPUT  IERORT, VOIDEL, VIF1RF
OUTPUT VO, VF
METHOD STIFF
TIMER FINTIM = 1.0E-3, PRDEL = 5.0E-6, OUTDEL = 10.0E-6
ABSERR VO=2.6,IF1=1.5E-2,IF26=1.5E-2,IOA=3.0E1,VOA=3.0E1
END
STOP
```

```
*************************************************************
*
*  SIMULATION OF PRECISION RECTIFIER BY DIFFERENTIAL
*    EQUATION METHOD
*
*  PARAMETERS
*     FINPUT = FREQUENCY IN HERTZ OF THE INPUT SIGNAL
*     TIMEF = THE PERIOD OF THE INPUT SIGNAL
*     VINPK = NEGATIVE PEAK INPUT VOLTAGE
*     AOL = OPEN-LOOP OPAMP VOLTAGE GAIN AT LOW FREQUENCIES
*     GBWP = THE GAIN-BANDWIDTH PRODUCT OF THE OPAMP
*     SR = SLEW RATE OF OPAMP IN VOLTS / MICROSEC
*     TOL = DOMINENT POLE TIME CONSTANT OF OPAMP
*     PHASE = NOMINAL PHASE SHIFT OF PRECISION RECTIFIER
*     VT, VT2, IS1, AND IS2 ARE PARAMETERS USED TO MODEL
*       THE PN JUNCTIONS OF DIODES D1 AND D2 RESPECTIVELY
*
*  VARIABLES
*     VF = VOLTAGE AT INVERTING INPUT OF OPAMP
*     VO = OUTPUT VOLTAGE OF OPAMP
*     VR1 = VOLTAGE AT NODE WHICH JOINS R1 AND D1
*     VR2 = VOLTAGE AT NODE WHICH JOINS R2 AND D2
*     VR1RF = VR1 REFERRED TO THE INPUT
*     VERORA = PERCENT ERROR OF VOA
*     VERORT = PERCENT ERROR OF VR1RF AS A FUNCTION OF TIME
*     VOA = AVERAGE VALUE OF VR1RF
*     IF1 AND IF2 ARE THE CURRENTS THROUGH D1 AND D2
*       RESPECTIVELY
*     VIF1RF = IF1 REFERRED TO THE INPUT
*     IERORA = PERCENT ERROR OF IOA
*     IERORT = PERCENT ERROR OF VIF1RF AS A FUNCTION OF TIME
*     IOA = AVERAGE VALUE OF VIF1RF
*     DELVIF = IOA - VIF1RF
*     VOIDEL = OUTPUT OF IDEAL HALF-WAVE RECTIFIER
*     VOIDLA = AVERAGE VALUE OF VOIDEL
*
*************************************************************
*
INITIAL
*  INPUT PARAMETERS
PARAMETER FINPUT = 1.0E3, PHASE1 = 0.0, VINPK = -0.1E6
*  INITIAL CONDITIONS
      IOATC = 0.0
*  DIODE PARAMETERS
PARAMETER VT1 = 26.0E3, VT2 = 26.0E3
PARAMETER IS1 = 1.0E-5, IS2 = 1.0E-5
PARAMETER TDELAY = 0.1E-5
*  RESISTANCE PARAMETERS
PARAMETER R1 = 2.0E3, R2 = 2.0E3, R3 = 2.0E3
*  OPAMP PARAMETERS
PARAMETER AOL = 2.0E5, GBWP = 1.0E6
PARAMETER SRRISE = 70.0E6, SRFALL = 70.0E6
      TWOPI = 6.283185306
```

```
      OMEGAI = TWOPI * FINPUT
      TIMEF =  1.0 / FINPUT
      TOL = AOL / (TWOPI * GBWP)
NOSORT
      IF (VFIC .EQ. 0.0 .AND. VOIC .EQ. 0.0) GO TO 1010
      GO TO 1020
*  ITERATION LOOP TO FIND INITIAL CONDITIONS OF VO AND IF2
1010  IF2IC1 = -1.0E-1
      DO 1000 I = 1, 50
      FCL = (AOL * R3 / (R3 + R2 - VT2 / IF2IC1) + 1.0) /...
      (TOL * TWOPI)
      PHASE = ATAN(-FINPUT / FCL) + PHASEI
      IF2IC = -SIN(PHASE) * VINPK / R3
      CNVRG = ABS(IF2IC / IF2IC1 - 1.0)
      IF (CNVRG .LT. 1.0E-3) GO TO 1001
1000  IF2IC1 = (IF2IC1 + IF2IC) / 2.0
1001  VOIC = -VT2 * ALOG(1.0 - IF2IC / IS2)
      VFIC = R3 * (IF2IC - IS1)
      GO TO 1030
1020  IF2IC = IS1 + VFIC / R3
      PHASE = -ATAN(1. / SQRT(-1. + (VINPK/(R3*IF2IC))**2))
1030  VIFRFI = IF2IC * R3
      VFPIC = VFIC - VOIC
SORT
      SLEWR = SRRISE * TOL / AOL
      SLEWF = SRFALL * TOL / AOL
      VOIDLA = -VINPK * 2.0 / TWOPI
      K = 2.0 * R3 * IS1
DYNAMIC
      VIN1 = SINE(0.0, OMEGAI, PHASEI)
      VIN = VIN1 * VINPK
      VIN2P = SINE(0.0, OMEGAI, 1.570796327)
      VIN2 = VINPK * OMEGAI * VIN2P
      SQRTZ = SQRT(1.0 + Z * Z)
      DVIFRF = -K * (VIFRF + VIN + VIN2 * (1.0 + R1 / R3)...
      * TOL / AOL) * AOL * SQRTZ / ((VT1 + K * SQRTZ) * TOL)
      VIFRF = INTGRL(VIFRFI, DVIFRF)
      Z = VIFRF / K
      VF = VIN + VIFRF
NOSORT
      IF(VIFRF) 14, 15, 15
14    VIF1RF = 0.0
      AZ = -Z
      GO TO 16
15    VIF1RF = VIFRF
      AZ = Z
16    CONTINUE
      VR1 = VF + VIF1RF * R1 / R3
      IF(AZ .GT. 1000.0) GO TO 26
      VO = VF + VIFRF * R1 / R3 + VT1 * ALOG(Z + SQRTZ)
      GO TO 27
26    VO = VF + VIFRF * R1 / R3 + VT1 * ALOG((Z + AZ) + 0.5 / AZ)
27    CONTINUE
```

```
*   PERCENT ERROR CALCULATIONS
*   OMIT VR1RF, VOT, VOA, AND VERORA WHEN R1 = 0.0
        VOT = VR1RF / TIMEF
        VR1RF = VR1 * R3 / R1
        VIND = SINE(0.0, OMEGA1, PHASE)
        VINDLY = VINPK * VIND
        IF(VINDLY) 4, 5, 5
4       VOIDEL = -VINDLY
        GO TO 6
5       VOIDEL = 0.0
6       CONTINUE
SORT
        VOA = INTGRL(0.0, VOT)
        VIF1RT = VIF1RF / TIMEF
        IOA = INTGRL(IOAIC, VIF1RT)
        IERORT = (VIF1RF - VOIDEL) * 100.0 / VOIDLA
        VERORT = (VR1RF - VOIDEL) * 100.0 / VOIDLA
        DELVIF = IOA - VOIDLA
        IERORA = DELVIF * 100.0 / VOIDLA
        VERORA = (VOA - VOIDLA) * 100.0 / VOIDLA
PRINT VOIDEL,VIF1RF,IERORT,IERORA,DELVIF,VO,VF,VERORT,VERORA
OUTPUT  VERORT, VOIDEL, VR1RF
OUTPUT  IERORT, VOIDEL, VIF1RF
OUTPUT VO, VF
METHOD STIFF
TIMER FINTIM = 1.0E-3, PRDEL = 5.0E-6, OUTDEL = 10.0E-6
ABSERR VIFRF = 50., IOA = 20.
RELERR VIFRF = 0.0, IOA = 0.0
END
STOP
```

```
*************************************************************************
*
*  SIMULATION OF APPROXIMATE DARLINGTON 2N5087 TRANSISTOR
*    RECTIFIER BY DELAY METHOD
*
*  PARAMETERS
*     FINPUT = FREQUENCY IN HERTZ OF THE INPUT SIGNAL
*     TIMEF = THE PERIOD OF THE INPUT SIGNAL
*     VINPK = NEGATIVE PEAK INPUT VOLTAGE
*     AOL = OPEN-LOOP OPAMP VOLTAGE GAIN AT LOW FREQUENCIES
*     GBWP = THE GAIN-BANDWIDTH PRODUCT OF THE OPAMP
*     SR = SLEW RATE OF OPAMP
*     TOL = DOMINENT POLE TIME CONSTANT OF OPAMP
*     PHASE = NOMINAL PHASE SHIFT OF PRECISION RECTIFIER
*     VT, VT2, IS1, AND IS2 ARE PARAMETERS USED TO MODEL
*       THE PN JUNCTIONS OF TRANSISTORS Q1 AND Q2 RESPECTIVELY
*
*  VARIABLES
*     VF = VOLTAGE AT INVERTING INPUT OF OPAMP
*     VO = OUTPUT VOLTAGE OF OPAMP
*     VR1 = VOLTAGE AT EMITTER OF Q1
*     VR2 = VOLTAGE AT EMITTER OF Q2
*     VR1RF = VR1 REFERRED TO THE INPUT
*     VERORA = PERCENT ERROR OF VOA
*     VERORT = PERCENT ERROR OF VR1RF AS A FUNCTION OF TIME
*     VOA = AVERAGE VALUE OF VR1RF
*     IF1 AND IF2 ARE THE EMITTER CURRENTS OF TRANSISTORS
*       Q1 AND Q2 RESPECTIVELY
*     VIF1RF = IF1 REFERRED TO THE INPUT
*     IERORA = PERCENT ERROR OF IOA
*     IERORT = PERCENT ERROR OF VIF1RF AS A FUNCTION OF TIME
*     IOA = AVERAGE VALUE OF VIF1RF
*     DELVIF = IOA - VIF1RF
*     VOIDEL = OUTPUT OF IDEAL HALF-WAVE RECTIFIER
*     VOIDLA = AVERAGE VALUE OF VOIDEL
*
*************************************************************************
*
INITIAL
PARAMETER FINPUT = 1.0E3, VINPK = -1.0E-2
PARAMETER IS1 = 1.0E-11, IS2 = 1.0E-11, VT1 = 26.0E-3, VT2 = 26.0E-3
PARAMETER  AOL = 2.0E5, GBWP = 1.0E6, SRRISE = 70.0E6, SRFALL = 70.0E6
PARAMETER R1 = 0.0, R2 = 0.0, R3 = 2.0E3, TDELAY = 0.10E-6
      TIMEF =  1.0 / FINPUT
      TWOPI = 6.283185308
      OMEGAI = TWOPI * FINPUT
      TOL = AOL / (TWOPI * GBWP)
      IS1DAR = 204.0 * (IS1 ** 1.18)
NOSORT
*  ITERATION LOOP TO FIND INITIAL CONDITIONS OF VO AND IF2
      IF2IC1 = -1.0E-7
      DO 1000 I = 1, 50
      FCL = (AOL * R3 / (R3 + R2 - VT2 / IF2IC1) + 1.0) / (TOL * TWOPI)
      PHASE = ATAN(-FINPUT / FCL)
      IF2IC = -SIN(PHASE) * VINPK / R3
      CNVRG = ABS(IF2IC / IF2IC1 - 1.0)
      IF (CNVRG .LT. 1.0E-3) GO TO 1001
1000  IF2IC1 = (IF2IC1 + IF2IC) / 2.0
1001  VOIC = -VT2 * ALOG(1.0 - IF2IC / IS2)
SORT
```

```
      SLEWR = SRRISE * TOL / AOL
      SLEWF = SRFALL * TOL / AOL
      VOIDLA = -VINPK * 2.0 / TWOPI
DYNAMIC
      VIN1 = SINE(0.0, OMEGAI, 0.0)
      VIN = VIN1 * VINPK
*  OPAMP MODEL
*  FOR SLEW-RATE LIMIT, REMOVE * FROM COL. 1 OF V1 = LIMIT ... CARD AND
*  INSERT * IN COL. 1 OF V1 = VF CARD
*     V1 = LIMIT(-SLEWR, SLEWF, VF)
      V1 = VF
      V2 = -AOL * V1
      VO = REALPL(VOIC, TOL, V2)
      VF = VIN + (IF1 + IF2) * R3
      VR1 = VF + IF1 * R1
      VR2 = VF + IF2 * R2
*  DARLINGTON TRANSISTOR FEEDBACK MODEL
      U1P = (VO - VR1) / VT1
      U1DAR = U1P / 1.7
      IF1P = IS1DAR * (EXP(U1DAR) - 1.0)
      IF1 = REALPL(-IS1DAR, TDELAY, IF1P)
      BETA1 = 8400.0 * ((IF1  + 2.0 * IS1DAR)** 0.301)
      BETA1P = 8400.0 * (((IF1 + 2.0 * IS1DAR)/(BETA1 + 1.0)) ** 0.301)
      ALPHA1 = BETA1 / (BETA1 + 1.0)
      ALPHAP  = BETA1P / (BETA1P + 1.0)
      ALPHAD = ALPHA1 * (ALPHAP / BETA1 + 1.0)
      VIC1RF = R3 * ALPHAD * IF1
      U2P = (VR2 - VO) / VT2
      IF2P = -IS1 * (EXP(U2P) - 1.0)
      IF2 = REALPL(IF2IC, TDELAY, IF2P)
*
*  PERCENT ERROR CALCULATIONS
*  OMIT VR1RF, VOT, VOA, AND VERORA WHEN R1 = 0.0
*     VR1RF = VR1 * R3 / R1
      VIND = SINE(0.0, OMEGAI, PHASE)
      VINDLY = VINPK * VIND
PROCEDURE VOIDEL = RECT(VINDLY)
      IF(VINDLY) 4, 5, 5
4     VOIDEL = -VINDLY
      GO TO 6
5     VOIDEL = 0.0
6     CONTINUE
ENDPRO
*     VOT = VR1RF / TIMEF
*     VOA = INTGRL(0.0, VOT)
      VIF1RT = VIC1RF / TIMEF
      IOA = INTGRL(0.0, VIF1RT)
      IERORT = (VIC1RF - VOIDEL) * 100.0 / VOIDLA
      IERORA = (IOA - VOIDLA) * 100.0 / VOIDLA
LABEL PRECISION RECTIFIER WITH AOL=2E5, GBWP=1MHZ, NO SLEW LIMIT,...
 R1=2K, R2=0, & DARLINGTOM TRANSISTOR WITH IS=10PA & VT=0.026V
TITLE PRECISION RECTIFIER WITH AOL=2E5, GBWP=1MHZ, NO SLEW LIMIT,...
 R1=2K, R2=0, & DARLINGTOM TRANSISTOR WITH IS=10PA & VT=0.026V
PRINT  VOIDEL, VIC1RF, IERORT, IERORA, VO, VF, IF2, VR2
OUTPUT  IERORT, VOIDEL
OUTPUT VO, VF
METHOD STIFF
RELERR VO = 0.0, IF1 = 1.E-4, IF2 = 1.E-4, IOA = 1.E-4
ABSERR VO = 2.6E-6, IF1 = 1.5E-8, IF2 = 1.5E-8, IOA = 3.E-5
TIMER FINTIM = 1.0E-3, PRDEL = 5.0E-6, OUTDEL = 10.E-6
END
STOP
```

```
*****************************************************************
*
*  SIMULATION OF APPROXIMATE DARLINGTON 2N5087 TRANSISTOR
*       RECTIFIER WITH CREE
*
*  PARAMETERS
*     FINPUT = FREQUENCY IN HERTZ OF THE INPUT SIGNAL
*     TIMEF = THE PERIOD OF THE INPUT SIGNAL
*     VINPK = NEGATIVE PEAK INPUT VOLTAGE
*     AOL = OPEN-LOOP OPAMP VOLTAGE GAIN AT LOW FREQUENCIES
*     GBWP = THE GAIN-BANDWIDTH PRODUCT OF THE OPAMP
*     SR = SLEW RATE OF OPAMP
*     TOL = DOMINENT POLE TIME CONSTANT OF OPAMP
*     PHASE = NOMINAL PHASE SHIFT OF PRECISION RECTIFIER
*     VT, VT2, IS1, AND IS2 ARE PARAMETERS USED TO MODEL
*       THE PN JUNCTIONS OF TRANSISTORS Q1 AND Q2 RESPECTIVELY.
*
*  VARIABLES
*     VF = VOLTAGE AT INVERTING INPUT OF OPAMP
*     VO = OUTPUT VOLTAGE OF OPAMP
*     VR1 = VOLTAGE AT EMITTER OF Q1
*     VR2 = VOLTAGE AT EMITTER OF Q2
*     VR1RF = VR1 REFERRED TO THE INPUT
*     VERORA = PERCENT ERROR OF VOA
*     VERORT = PERCENT ERROR OF VR1RF AS A FUNCTION OF TIME
*     VOA = AVERAGE VALUE OF VR1RF
*     IE1 AND IE2 ARE THE EMITTER CURRENTS OF TRANSISTORS
*       Q1 AND Q2 RESPECTIVELY
*     VIE1RF = IE1 REFERRED TO THE INPUT
*     IERORA = PERCENT ERROR OF IOA
*     IERORT = PERCENT ERROR OF VIE1RF AS A FUNCTION OF TIME
*     IOA = AVERAGE VALUE OF VIE1RF
*     DELVIF = IOA - VIE1RF
*     VOIDEL = OUTPUT OF IDEAL HALF-WAVE RECTIFIER
*     VOIDLA = AVERAGE VALUE OF VOIDEL
*
*****************************************************************
*
INITIAL
PARAMETER FINPUT = 1.0E3, VINPK = -1.0E-2
PARAMETER IS1 = 1.0E-11, IS2 = 1.0E-11, VT1 = 26.0E-3, VT2 = 26.0E-3
PARAMETER  AOL = 2.0E5, GBWP = 1.0E6, SRRISE = 70.0E6, SRFALL = 70.0E6
PARAMETER R1 = 0.0, R2 = 0.0, R3 = 2.0E3, TDELAY = 0.05E-6
      TIMEF =  1.0 / FINPUT
      TWOPI = 6.283185308
      OMEGAI = TWOPI * FINPUT
      TOL  = AOL  / (TWOPI * GBWP)
      IS1DAR = 204.0 * (IS1 ** 1.18)
NOSORT
*  ITERATION LOOP TO FIND INITIAL CONDITIONS OF VO AND IF2
      IF2IC1 = -1.0E-7
      DO 1000 I = 1, 50
      FCL = (AOL * R3 / (R3 + R2 - VT2 / IF2IC1) + 1.0) / (TOL * TWOPI)
      PHASE = ATAN(-FINPUT / FCL)
      IF2IC = -SIN(PHASE) * VINPK / R3
      CNVRG = ABS(IF2IC / IF2IC1 - 1.0)
      IF (CNVRG .LT. 1.0E-3) GO TO 1001
1000  IF2IC1 = (IF2IC1 + IF2IC) / 2.0
1001  VOIC = -VT2 * ALOG(1.0 - IF2IC / IS2)
      VIFRFI = IF2IC * R3
```

```
      VFPIC = (-IS1DAR + IF2IC) * R3 - VOIC
      CBE = 7.0E-12
SORT
      SLEWR = SRRISE * TOL / AOL
      SLEWF = SRFALL * TOL / AOL
      VOIDLA = -VINPK * 2.0 / TWOPI
      K = 2.0 * R3 * IS1
DYNAMIC
      VIN1 = SINE(0.0, OMEGAI, 0.0)
      VIN = VIN1 * VINPK
*  OPAMP MODEL
*  FOR SLEW-RATE LIMIT, REMOVE * FROM COL. 1 OF V1 = LIMIT ... CARD AND
*  INSERT * IN COL. 1 OF V1 = VF CARD
*     V1 = LIMIT(-SLEWR, SLEWF, VF)
      V1 = VF
      V2 = -AOL * V1
      VO = REALPL(VOIC, TOL, V2)
      DVF = ((VIN - VF) / R3 + IF1 + IF2) / CBE
      VFP = INTGRL(VFPIC, DVF)
      VF = VO + VFP
*  DARLINGTON TRANSISTOR FEEDBACK MODEL
      U1P = -VFP / (1.7 * VT1)
      IF1 = IS1DAR * (EXP(U1P) - 1.0)
      BETA1 = 8400.0 * ((IF1  + 2.0 * IS1DAR)** 0.301)
      BETA1P = 8400.0 * (((IF1 + 2.0 * IS1DAR)/(BETA1 + 1.0)) ** 0.301)
      ALPHA1 = BETA1 / (BETA1 + 1.0)
      ALPHAP  = BETA1P / (BETA1P + 1.0)
      ALPHAD = ALPHA1 * (ALPHAP / BETA1 + 1.0)
      VIF1RF = R3 * ALPHAD * IF1
      U2P = VFP / VT2
      IF2 = -IS2 * (EXP(U2P) - 1.0)
NOSORT
*  PERCENT ERROR CALCULATIONS
*  OMIT VR1RF, VOT, VOA, AND VERORA WHEN R1 = 0.0
*     VR1RF = VR1 * R3 / R1
      VIND = SINE(0.0, OMEGAI, PHASE)
      VINDLY = VINPK * VIND
      IF(VINDLY) 4, 5, 5
4     VOIDEL = -VINDLY
      GO TO 6
5     VOIDEL = 0.0
6     CONTINUE
SORT
      VIF1RT = VIF1RF / TIMEF
*     VOT = VR1RF / TIMEF
*     VOA = INTGRL(0.0, VOT)
      IOA = INTGRL(0.0, VIF1RT)
      IERORT = (VIF1RF - VOIDEL) * 100.0 / VOIDLA
      DELVIF = IOA - VOIDLA
      IERORA = DELVIF * 100.0 / VOIDLA
TITLE PRECISION RECTIFIER WITH AOL=2E5, GBWP=1MHZ, NO SLEW LIMIT,...
 R1=R2=0, R3=2K, & DARLINGTON 2N5087 WITH IS = 10PA & VT = 0.026V
LABEL PRECISION RECTIFIER WITH AOL=2E5, GBWP=1MHZ, NO SLEW LIMIT,...
 R1=R2=0, R3=2K, & DARLINGTON 2N5087 WITH IS = 10PA & VT = 0.026V
PRINT  VOIDEL, VIF1RF, IERORT, IERORA, DELVIF, VO, VF, IF2, VR2
OUTPUT  IERORT, VOIDEL
OUTPUT VO, VF
METHOD STIFF
RELERR VO = 0.0, VFP = 0.0, IOA = 0.0
```

```
ABSERR VO = 2.6E-4, VFP = 2.6E-4, IOA = 1.0E-5
TIMER FINTIM = 1.3E-4, PRDEL = 5.0E-6, OUTDEL = 10.0E-6
END CONTINUE
TIMER FINTIM = 3.7E-4
ABSERR VO = 7.8E-5, VFP = 7.8E-5, IOA = 1.0E-5
END CONTINUE
ABSERR VO = 2.6E-4, VFP = 2.6E-4, IOA = 1.0E-5
TIMER FINTIM = 6.0E-4
END
STOP
```

```
*************************************************************
*
*  SIMULATION OF PRECISION RECTIFIER EMPLOYING DARLINGTON
*    2N5087 TRANSISTOR MODEL INCLUDING CBE, COB, AND HFE
*    VARITATONS WITH COLLECTOR CURRENT
*
*  PARAMETERS
*     VINPK = NEGATIVE PEAK INPUT VOLTAGE
*     FINPUT = FREQUENCY IN HERTZ OF THE INPUT SIGNAL
*     TIMEF = THE PERIOD OF THE INPUT SIGNAL
*     AOL = OPEN-LOOP OPAMP VOLTAGE GAIN AT LOW FREQUENCIES
*     TOL = DOMINENT POLE TIME CONSTANT OF OPAMP
*     GBWP = THE GAIN-BANDWIDTH PRODUCT OF THE OPAMP
*     PHASE = NOMINAL PHASE SHIFT OF PRECISION RECTIFIER
*     SR = SLEW RATE OF OPAMP IN VOLTS / MICROSEC
*     VT, VT1P, VT2, IS1, IS1P, IS2, ICBO1, ICBO1P, CBE1,
*       CBE1P, CBE2, COB1, AND COB1P ARE PARAMETERS USED TO
*       MODEL TRANSISTORS Q1, Q2, AND Q1P RESPECTIVELY
*     R1 AND R2 ARE ZERO
*     VOIC, VFIC, DVB1IC, AND VVB1IC ARE THE INITIAL VALUES
*       OF VO, VF, VBE1, AND VVBE1 RESPECTIVELY
*
*  VARIABLES
*     VF = VOLTAGE AT INVERTING INPUT OF OPAMP
*     VO = OUTPUT VOLTAGE OF OPAMP
*     IE1 AND IE2 ARE THE EMITTER CURRENTS OF Q1 AND Q2
*       NEGLECTING THE CURRENT COMPONENTS DUE TO BASE-EMIT-
*       TER CAPACITANCES (CBE1, CBE1P, AND CBE2)
*     VIF1RF = IF1 REFERRED TO THE INPUT
*     IERORT = PERCENT ERROR OF VIF1RF AS A FUNCTION OF TIME
*     IOA = AVERAGE VALUE OF VIF1RF
*     IERORA = PERCENT ERROR OF IOA
*     VOIDEL = OUTPUT OF IDEAL HALF-WAVE RECTIFIER
*     VOIDLA = AVERAGE VALUE OF VOIDEL
*
*************************************************************
*
INITIAL
*  INPUT PARAMETERS
PARAMETER FINPUT = 1.0E3, PHASEI = 0.0, VINPK = -0.010E6
*  INITIAL CONDITIONS
PARAMETER DVB1IC = 3.02E7  , VVB1IC = 1.33E5
      IOAIC = 0.0
*  TRANSISTOR PARAMETERS
PARAMETER VT1 = 26.0E3, VT2 = 26.0E3, VT1P = 26.0E3
PARAMETER IS1 = 1.0E-7, IS2 = 1.0E-7, IS1P = 1.0E-7
PARAMETER ICBO1 = 5.0E-3, ICBO1P = 5.0E-3
```

```
PARAMETER CBE1 = 7.0E-12, CBE2 = 7.0E-12, CBE1P = 7.0E-12
PARAMETER CCB1 = 7.0E-12, CCB1P = 7.0E-12
PARAMETER I1=10.. I2=100.. IP=5000.. I3=8000.. I4=1.E4
PARAMETER B1=290.. B2=520.. BP=990.. B3=960.. B4=940.
*  RESISTANCE PARAMETERS
PARAMETER  R3 = 2.0E3, R = 1.0E9
      R2 = 0.0
*  OPAMP PARAMETERS
PARAMETER AOL = 2.0E5, GBWP = 1.0E6
PARAMETER SRRISE = 70.0E6, SRFALL = 70.0E6
PARAMETER X71 = 0.0
      TWOPI = 6.283185308
      OMEGAI = TWOPI * FINPUT
      TIMEF =  1.0 / FINPUT
      TOL = AOL / (TWOPI * GBWP)
NOSCRT
      IF (VFIC .EQ. 0.0 .AND. VOIC .EQ. 0.0) GO TO 1010
      GO TO 1020
*  ITERATION LOOP TO FIND INITIAL CONDITIONS OF VO AND IF2
1010  IF2IC1 = -1.0E-1
      DO 1000 I = 1, 50
      FCL = (AOL * R3 / (R3 + R2 - VT2 / IF2IC1) + 1.0) /...
      (TOL * TWOPI)
      PHASE = ATAN(-FINPUT / FCL) + PHASEI
      IF2IC = -SIN(PHASE) * VINPK / R3
      CNVRG = ABS(IF2IC / IF2IC1 - 1.0)
      IF (CNVRG .LT. 1.0E-3) GO TO 1001
1000  IF2IC1 = (IF2IC1 + IF2IC) / 2.0
1001  VOIC = -VT2 * ALOG(1.0 - IF2IC / IS2)
      VFIC = R3 * (IF2IC - IS1)
      GO TO 1030
1020  IF2IC = IS1 + VFIC / R3
      PHASE = -ATAN(1. / SQRT(-1. + (VINPK/(R3*IF2IC))**2))
1030  VIERFI = IF2IC * R3
      VFPIC = VFIC - VOIC
*  COMPUTATION OF THE CONSTANTS OF HFE(I)
      N = ALOG(B2 / B1) / ALOG(I2 / I1)
      M = ALOG(B3 / B4) / ALOG(I4 / I3)
      MN = -N
      I2N = I2 ** MN
      IPN = IP ** MN
      I3N = I3 ** MN
      I2M = I2 ** M
      IPM = IP ** M
      I3M = I3 ** M
      B2 = 1.0 / B2
      BP = 1.0 / BP
      B3 = 1.0 / B3
      D = I2N*(IPM-I3M) + IPN*(I3M-I2M) + I3N*(I2M-IPM)
      X = (B2*(IPM-I3M) + BP*(I3M-I2M) + B3*(I2M-IPM)) / D
      Y = (I2N*(BP-B3) + IPN*(B3-B2) + I3N*(B2-BP)) / D
```

```
      Z = (I2N*(IPM*B3-I3M*BP) + IPN*(I3M*B2-I2M*B3) ...
          + I3N*(I2M*BP-IPM*B2)) / D
      WRITE (6,1100)
      WRITE (6,1101)
      WRITE (6,1102) X, N, Y
      WRITE (6,1105) M, Z
1100  FORMAT (1H1,'HFE OF TRANSISTOR Q1 AS A FCT OF IC')
1101  FORMAT(1H0,'HFE=1./(X*IC**(-N) + Y*IC**M + Z), WHERE')
1102  FORMAT(1H0,'X = ',E14.7,', N = ',E14.7,', Y = ',E14.7)
1105  FORMAT(1H0'M = ',E14.7,', AND Z = ', E14.7)
SORT
      SLEWR = SRRISE * TOL / AOL
      SLEWF = SRFALL * TOL / AOL
      VOIDLA = -VINPK * 2.0 / TWOPI
      SUMC = CBE1 + CBE1P + COB1
DYNAMIC
      VIN1 = SINE(0.0, OMEGAI, PHASEI)
      VIN = VIN1 * VINPK
*  OPAMP MODEL
*  FOR SLEW-RATE LIMIT, REMOVE * FROM COL. 1 OF V1 = LIMIT
*  ... CARD AND INSERT * IN COL. 1 OF V1 = VF CARD
*     V1 = LIMIT(-SLEWR, SLEWF, VF)
      V1 = VF
      V2 = -AOL * V1
      VO = REALPL(VOIC, TOL, V2)
      DIFP = ((VTN - VF) / R3 + IF1 + IE2) / CBE2
      VFP = INTGRL(VFPIC, DIFP)
      VF = VO + VFP
*  DARLINGTON TRANSISTOR FEEDBACK MODEL
      VBE1P = VO - VF - VBE1
      U1 = VBE1 / VT1
      U1P = VBE1P / VT1P
      IE1 = IS1 * (EXP(U1) - 1.0)
      IE1P = IS1P * (EXP(U1P) - 1.0)
      DIE1PP = IE1P + ICBO1 - IE1 / (HFE1 + 1.0) - VBE1 / R
      DIE1P = DIE1PP / SUMC
      VVBE1 = INTGRL(VVB1IC,DIE1P)
      VBE1 = VVBE1 + (CBE1P*VO - (CBE1P + COB1)*VF) / SUMC
      IF1 = IE1 + VBE1 / R + CBE1 * DVBE1
      IE1GO = IE1 + 2.0 * IS1
      IE1PGO = IE1P + 2.0 * IS1P
      HFE1P = 1.0 / (X * (IE1PGO**MN) + Y * (IE1PGO**M) + Z)
      HFE1 = 1.0 / (X * (IE1GO**MN) + Y * (IE1GO**M) + Z)
      ALPHA1 = HFE1 / (HFE1 + 1.0)
      ALPHAP  = HFE1P / (HFE1P + 1.0)
      DVO = (V1 - VO) / TOL
      DVBE1 = DERIV(DVB1IC, VBE1)
      DVF = DIFP + DVO
      DVBE1P = DVO - DVF - DVBE1
      VIF1R = R3 * (ALPHA1 * IE1 + ALPHAP * IE1P)
      VIF1X = R3 * (COB1 * (DVBE1P - DVO) - COB1P * DVO)
```

```
      VIF1DC = R3 * (ICBO1 + ICBO1P)
      VIF1RF = VTF1R + VIF1X + VIF1DC
      U2P = VFP / VT2
      IE2 = -IS2 * (EXP(U2P) - 1.0)
NOSORT
*  PERCENT ERROR CALCULATIONS
      VIND = SINE(0.0, OMEGAI, PHASE)
      VINDLY = VINPK * VIND
      IF(VINDLY) 4, 5, 5
4     VOIDEL = -VINDLY
      GO TO 6
5     VOIDEL = 0.0
6     CONTINUE
SORT
      VIF1RT = VIF1RF / TIMFF
      IOA = MODINT(IOAIC, XZ1,1.0,VIF1RT)
      IERORT = (VIF1RF - VOIDEL) * 100.0 / VOIDLA
      DELVIF = IOA - VOIDLA
      IERORA = DELVIF * 100.0 / VOIDLA
LABEL PRECISION RECTIFIER WITH AOL=2E5, GBWP=1MHZ, NO R,...
R1=R2=0, R3=2K, & DARLINGTON 2N5087 WITH IS=0.1PA & VT=.026V
TITLE PRECISION RECTIFIER WITH AOL=2E5, GBWP=1MHZ, NO R, ...
R1=R2=0, R3=2K, & DARLINGTON 2N5087 WITH IS=0.1PA & VT=.026V
PRINT  VOIDEL,VIF1RF,IERORT,IERORA,DELVIF,VO,VF,DVBE1,VVBE1
OUTPUT  IERORT, VOIDEL, VIF1RF
OUTPUT VO, VF, VBE1
METHOD STIFF
ABSERR VO = 410., VVBE1 = 410., VFP = 410., IOA = 5.0
TIMER FINTIM = 1.00E-3, PRDEL = 5.0E-6, OUTDEL = 10.0E-6
END CONTINUE
PARAMETER XZ1 = 1.0
ABSERR VO = 120., VVBE1 = 120., VFP = 120., IOA = 5.0
TIMER FINTIM = 1.13E-3
ABSERR VO = 41.0, VVBE1 = 41.0, VFP = 41.0, IOA = 5.0
TIMER FINTIM = 1.37E-3
END CONTINUE
ABSERR VO = 120., VVBE1 = 120., VFP = 120.
TIMER FINTIM = 1.5E-3
END CONTINUE
ABSERR VO = 410., VVBE1 = 410., VFP = 410.
TIMER FINTIM = 2.00E-3
END
STOP
```

APPENDIX D

SIMULATION OF TEMPERATURE CONTROL SYSTEM

```
*  SIMULATION OF TEMPERATURE CONTROL SYSTEM
*
STORAGE ARX(20), AP(20), ATP(20)
FIXED I, MR, MP, MT, MRLS, MPLS, MTLS
INITIAL
NOSORT
*  TMPSET AND TEMPIC ARE THE DESIRED TEMPERATURE AND
*     INITIAL TEMPERATURE RESPECTIVELY
PARAMETER TMPSET = 150.0, TEMPIC = 150.0
*  FOR TURN ON CONDITION, SET VC1IC .LT. 0.0
*  AMPLIFIER GAIN
PARAMETER AIER = 3.294E-1, A2 = -8.98E-3, K = 1.0E-1
PARAMETER GAIN = 1.0
*  LOW-PASS FILTER TIME CONSTANTS
PARAMETER TCURR = 4.0E-3, TEROR = 4.0E-3, TRX = 4.0E-3
      WCURR = 1.0 / TCURR
      WEROR = 1.0 / TEROR
      WRX = 1.0 / TRX
*  BMPIC = INITIAL BEAM POWER
PARAMETER BMPIC = 3.6
*  RS =  STANDARD RESISTANCE
PARAMETER RS = 0.08
*  THICK = SAMPLE THICKNESS IN MILS
PARAMETER THICK = 3.0
*  RESIST = SAMPLE RESISTIVITY IN MICROOHMS-CM
PARAMETER  RESIST = 7.4E1
      RLOW = 2.0 * RESIST * 1.0E-6 / (5.08E-4 * THICK)
*  ARX, AP, AND ATP ARE THE COEFFICENT MATRICIES OF
*     POLYNOMIAL EQUATIONS FOR RX(TEMP), POWER(TEMP), AND
*     TEMP(POWER) RESPECTIVELY
      READ (5,90) MR
      MRLS = MR - 1
      READ (5,100) (ARX(I), I = 1, MR)
      READ (5,90) MP
      MPLS = MP - 1
      READ (5,100) (AP(I), I = 1, MP)
      READ (5,90) MT
      MTLS = MT - 1
      READ (5,100) (ATP(I), I = 1, MT)
90    FORMAT (I2)
100   FORMAT(4F15.5)
      WRITE (6, 1000) (I, ARX(I), I = 1, MR)
      WRITE (6, 1010) (I, AP(I), I = 1, MP)
      WRITE (6, 1020) (I, ATP(I), I = 1, MT)
1000  FORMAT(1H1, 'I', 10X,' ARX(I)', //, (1X, I2, E20.5,/))
1010  FORMAT(1H0, 'I', 10X,' AP(I)', //, (1X, I2, E20.5,/))
1020  FORMAT(1H0, 'I', 10X,' ATP(I)', //, (1X, I2, E20.5,/))
*  RXIC AND RXSET ARE THE INITIAL AND DESIRED SAMPLE
*     RESISTANCES RESPECTIVIELY
      RXIC = ARX(MR)
      RXSET = ARX(MR)
```

```
      DO 10 I = 1, MRLS
      RXSET = RXSET * TMPSET + ARX(MR- I)
10    RXIC = RXIC * TEMPIC + ARX(MR - I)
      RXIC = RXIC * RLDW
      RXSET = RXSET * RLDW
SORT
*  CURRIC = INITIAL VALUE OF CURENT
NOSORT
      IF (VC1IC .LT. 0.0)  GO TO 200
      CURRIC = AP(MP)
      DO 30 I = 1, MPLS
30    CURRIC = CURRIC * TEMPIC + AP(MP - I)
      CURRIC = SQRT((CURRIC - BMPIC) / RXIC)
      VC1IC = (5.3E-2 * (CURRIC * SQRT(RS) / 0.109 - 1.))**2
      GO TO 210
200   CURRIC = 0.109 / SQRT(RS)
      VC1IC = 0.0
210   VCURRT = CURRIC * RS / AIER
DYNAMIC
*  BEAM POWER
      BMAVG = 1.0 - STEP(0.1) + STEP (3.0)
      BEAMP = BMPIC* BMAVG
*  INPUT2 = OSCILLATOR VOLTAGE.
      INPUT2 = 1.0
*  THE SAMPLE RESISTANCE, RX, IS A FUNCTION OF TEMPERATURE.
PROCEDURE RX = RXOFT(MRLS, ARX, TEMP, RLDW)
      RX = ARX(MR)
      DO 40 I = 1, MRLS
40    RX = RX * TEMP + ARX(MR - I)
      RX = RX * RLDW
ENDPROCEDURE
      VCURR1 = RS * CURENT / AIER
      VCURR2 = REALPL(VCURRI, TCURR, VCURR1)
      VCURR3 = VCURR2 * (WCURR ** 2)
      VCURR = CMPXPL(VCURRI, 0.0, 0.707, WCURR, VCURR3)
      DELRX = RX - RXSET
      VEROR1 = RS * DELRX * CURENT / ((RS + RXSET) * A2)
      VEROR2 = REALPL(0.0, TEROR, VEROR1)
      VEROR3 = VEROR2 * (WEROR ** 2)
      VERROR = CMPXPL(0.0, 0.0, 0.707, WEROR, VEROR3)
      VRX1 = VERROR / (VCURR * K)
      VRX2 = VRX1 * (WRX **2)
      VRX = CMPXPL(0.0, 0.0, 0.707, WRX, VRX2)
      VRXG =  VRX * GAIN
      VRXF = VRXG - 1000.0 * VC1F
      VC1 = INTGPL(VC1IC, VRXF)
      VC1F = DEADSP(-0.6, 10.0, VC1)
      VC = VC1 + 0.4 * VRXG
*  THE SQUARE ROOT OF THE CONTROL VOLTAGE (VC) IS USED TO
*    CONTROL THE OHMIC HEATING CURRENT
      VCP = LIMIT(0.0, 10.0, VC)
```

```
      VCSR = SQRT(VCP)
      FET = (10.0E3 * VCSR + 530.0) / 530.0
*  CURENT = THE OHMIC HEATING CURRENT.
      CURENT = 0.109 * FET / SQRT(RS)
*  THE TOTAL HEATING POWER IS COMPOSED OF BEAM POWER (BEAMP)
*  AND OHMIC HEATING POWER (OHMICP
      OHMICP = (CURENT **2) * RX
      POWER = OHMICP + BEAMP
NOSORT
*  THERMAL TRANSFER FUNCTION OF SAMPLE.
      TEMPSS = ATP(MT)
      DO 50 I = 1, MTLS
50    TEMPSS = TEMPSS * POWER + ATP(MT - I)
      TEMP = REALPL(TEMPIC,0.4,TEMPSS)
      ERRTMP = TEMP - TMPSET
PRINT TEMP, ERRTMP, VRX, DELRX, RX, VCURR, CURENT, BEAMP, VC
OUTPUT TEMP, BEAMP, CURENT
OUTPUT ERRTMP, VRX, DELRX
OUTPUT CURENT, VCURR
ABSERR VRX = 5.0E-3, VCURR = 5.0E-3, VCURR2 = 5.0E-3
ABSERR TEMP = 0.05, VERROR2 = 2.0E-4, VERROR = 2.0E-4
ABSERR VC1 = 1.0E-3
METHOD STIFF
TIMER FINTIM = 10.0, OUTDEL = 0.10, PRDEL = 1.0E-2
END
NOSORT
INPUT
 3
     1.00            1.019505E-3     -4.51926E-7
 4
   1.039113          1.994726E-2     1.245214E-5    -3.370553E-9
 4
    -5.339859E1      5.250829E1      -1.322550E0     3.215900E-2
ENDINPUT
STOP
```

INTERNAL DISTRIBUTION

1–2. Central Research Library
3. Document Reference Section
4–8. Laboratory Records Department
9. Laboratory Records, ORNL RC
10. ORNL Patent Office
11. R. L. Anderson
12. R. L. Auble
13. W. L. Bryant
14. J. E. Cunningham
15. F. L. Culler
16–25. M. G. Duncan
26. B. C. Duggins
27. W. W. Johnston
28. P. G. Jung
29–31. M. R. Hill
32. W. E. Lingan
33. C. J. McHargue
34. D. K. Mee
35. N. H. Packan
36–38. T. C. Reiley
39. K. Rush
40. M. J. Saltmarsh
41. J. O. Stiegler
42. L. H. Thacker
43. J. R. Weir, Jr.

EXTERNAL DISTRIBUTION

44. Argonne National Laboratory, 9700 South Cass Avenue, Argonne, IL 60439

45–47. Battelle Pacific Northwest Laboratories, P.O. Box 999, Richland, WA 99352

P. L. Hendrick
R. H. Jones
D. L. Styris

48. Hanford Engineering Development Laboratory, P.O. Box 1970, Richland, WA 99352

J. L. Straalsund

49. U.S. Naval Research Laboratory, Code 6396, Washington, DC 20375

D. J. Michel

50–55. USERDA, Division of Physical Research, Washington, DC 20545

J. S. Kane
L. C. Ianniello
D. Readey
D. K. Stevens
M. C. Wittels
S. Wolf

56–57. USERDA, Oak Ridge Operations Office, P.O. Box E, Oak Ridge, TN 37830

Director
Research and Technical Support Division

58–84. USERDA, Technical Information Center, Office of Information Services, P.O. Box 62, Oak Ridge, TN 37830

☆ U.S. GOVERNMENT PRINTING OFFICE: 1977-748-189/38